

Université de Lille1 - Sciences et Technologies (France)

Ecole Doctorale Biologie Santé

**University of Veterinary Medicine and Pharmacy in KOŠICE
(Slovakia)**

PhD THESIS

In fulfillment of the requirements for the degree of **Doctor in Science and Philosophy**
from the Université de Lille1 - Science et Technologies and the University of Veterinary
Medicine and Pharmacy in Kosice

Presented by

Stéphanie Devaux

**Spatio-temporal studies of the spinal cord injury through
OMICs and physiological approaches**

**International co-supervised PhD thesis under the direction of Pr Michel Salzet
and MVDr Dasa Cizkova, PhD, DrSc.**

Presented in Lille, 7th October 2016

Committee members:

Pr. Stephen McMahon	Reporter
Pr. Joost Verhaagen	Reporter
Pr. Serge Nataf	Examiner
Pr. Régis Bordet	Examiner
Ass. Pr Mangesh Bhide, PhD	Examiner
Ass. Pr Norbert Zilka, DrSc	Examiner
MVDr. Dasa Cizkova, PhD, DrSc	Co-Director
Pr. Michel Salzet	Co-Director

*” The future belongs to those who believe
in the beauty of their dreams.”*

— Eleanor Roosevelt

Acknowledgment

I would like to express a sincere thank you to everyone who has contributed to my work:

MVDr. Dasa Cizkova DrSc- my thesis adviser at the University of Veterinary Medicine and Pharmacy, in Kosice, Institute of Neurobiology, SAS- for having welcomed me to her institute, for her support in this co-supervised thesis, for her valuable guidance, enthusiasm and motivation, and for giving me the opportunity to learn from her expertise.

Pr. Michel Salzet- my thesis adviser at the Université de Lille1- for his continued support, for always being open, for all of his precious ideas, for guiding me through all these years of research.

Pr. Isabelle Fournier for her advice and her skills in proteomics.

My thesis reporters, Pr. Stephen McMahon and Pr. Joost Verhaagen for having kindly accepted to evaluate my work.

My thesis examiners, Pr. Serge Nataf, Pr Régis Bordet, Ass. Pr. Bhide Manges, PhD Ass. Pr. Norbert Zilka, DrSc, for accepting to judge my work.

Université de Lille 1, Conseil regional Nord-Pas-de-Calais and University of Veterinary Medicine and Pharmacy for giving me access to resources and funding for my PhD thesis, and also the Ecole Doctorale Biologie Santé de Lille.

Members of the laboratory in Lille for their availability and their assistance, Annie, Benoit, Maxence, Jean Pascal, Julien, Françoise, Christophe, Christelle, Céline, Pierre Eric, Franck, Jacopo, Lucie and especially to Jusal for his precious help with cryostat, “Patience is a virtue”.

Students or ex-students from Lille 1 laboratory, Antonella, Marie, Dounia, Philippe, Khalil, Adriana, Tanina, Vivian, Tony for keeping a cheerful atmosphere.

Members of Slovak laboratory, Marika, Lucia, Eva, Miriam for the warm welcome in Kosice, their precious advice, their sympathy, and especially to Juraj for his time and his patience when dealing with surgery, confocal microscopy and all “critical steps”.

My parents and my sister for their unfailing support and their encouragement throughout my way “C-C-C”, for always being there, as well as my family and my friends for listening to me when I needed it most. Kris for taking time to read and correct my manuscript.

And finally to Nicolas, for being present every day and for giving me strong motivation each step of the way.

Content

ACKNOWLEDGMENT	3
PUBLICATIONS	6
LIST OF FIGURES	8
ABBREVIATIONS	11
INTRODUCTION	13
1. SPINAL CORD ORGANIZATION	17
2. MODEL OF INJURY	18
3. PATHOPHYSIOLOGY	22
3.1. PRIMARY INJURY	22
3.2. SECONDARY INJURY	23
4. IMMUNE RESPONSE AFTER SCI	24
4.1. INNATE IMMUNE SYSTEM	25
4.1.1. <i>Neutrophils recruitment</i>	25
4.1.2. <i>Microglia cells</i>	26
4.1.3. <i>Astrocytes</i>	28
4.2. RELATION BETWEEN GLIAL CELLS AND NEURONS	29
4.2.1. <i>Cellular interactions</i>	30
4.2.2. <i>Molecular interactions</i>	30
4.3. T CELLS AND INNATE IMMUNE CELLS	33
5. TREATMENTS FOR SPINAL CORD INJURY	34
5.1. MYELIN NEURITE GROWTH INHIBITORS	35
5.2. PROTEOGLYCAN INHIBITOR	38
5.3. CELLULAR THERAPY	39
5.3.1. <i>Autologous Schwann cell transplantation</i>	39
5.3.2. <i>Olfactory ensheathing cells (OECs)</i>	40
5.3.3. <i>Human embryonic stem cells, induced pluripotent stem cells</i>	41
5.3.4. <i>Neural stem cells</i>	41
5.3.5. <i>Bone marrow stromal cells (BMSCs)</i>	42
5.4. PHARMACOTHERAPY	43
5.4.1. <i>Minocycline</i>	43
5.4.2. <i>Withanoside IV</i>	44
5.4.3. <i>Neuroimmunophilin ligand</i>	44

5.4.4. Estrogen	45
6. PROTEOMICS	47
6.1. PROTEOMIC APPROACH	47
PART 1: SPATIAL AND TEMPORAL ANALYSES AFTER SPINAL CORD INJURY	50
CHAPTER 1: SPATIAL AND TEMPORAL ANALYSES AFTER SPINAL CORD INJURY	50
<i>Article 1: Alterations of protein composition along the rostro-caudal axis after spinal cord injury: proteomic, in vitro and in vivo analyses</i>	<i>53</i>
<i>Article 2: Proteomic analysis of the spatio-temporal based molecular kinetics of acute spinal cord injury identifies a time- and segment-specific window for effective tissue repair.....</i>	<i>69</i>
CONCLUSION CHAPTER 1 & 2	100
IMMUNOGLOBULINS.....	100
MEMO1-RHOA-DIAPH1 signaling pathway.....	105
PART 2: MODULATION OF THE INFLAMMATION AND IMPROVEMENT OF THE REGENERATION	
PROCESS AND SPINAL CORD PLASTICITY: IN VITRO AND IN VIVO STUDIES	119
CHAPTER 2: PROPERTIES OF FACTORS RELEASED BY BONE MARROW STROMAL CELLS TO MODULATE MICROGLIA CELLS .	119
<i>Article 3: Modulation properties of factors released by bone marrow stromal cells on activated microglia: an in vitro study.....</i>	<i>122</i>
CONCLUSION CHAPTER 2	138
CHAPTER 3: ALGINATE BIOMATERIAL COUPLED WITH GROWTH FACTORS TO PROMOTE IN VIVO REGENERATION	140
<i>Article 4: Delivery of Alginate Scaffold Releasing Two Trophic Factors for Spinal Cord Injury Repair</i>	<i>144</i>
CONCLUSION CHAPTER 3	164
DISCUSSION	166
REFERENCES.....	169
ANNEX	194

Publications

Accepted Publications

Cizkova D., Le Marrec-Croq F., Franck J., Slovinska L., Grulova I., **Devaux S.**, Lefebvre C., Fournier I., Salzet M. **Alterations of protein composition along the rostro-caudal axis after spinal cord injury: proteomic, in vitro and in vivo analyses.** *Frontiers in Cell. Neurosci.* 2014, 8(105):1-15

Devaux S.*, Cizkova D.*, Le Marrec-Croq F., Franck J., Slovinska L., Rosocha J., Spakova T., Lefebvre C., Fournier I., Salzet M. **In vitro modulation properties of bone marrow stromal cells on BV2 microglia after spinal cord injury conditioned media activation.** *Scientific Reports* 2014, 4: 7514. * co-first authors

Slovinska L., Szekiova E., Blaško J., **Devaux S.**, Salzet M., Cizkova D. **Comparison of dynamic behavior and maturation of neural multipotent cells derived from different spinal cord developmental stages: an *in vitro* study.** *Acta Neurobiol Exp (Wars)* 2015; 75(1):107-14

Grulova I., Slovinska L., Blaško J., **Devaux S.**, Wisztorski M., Salzet M., Fournier I., Kryukov O., Cohen S., Cizkova D. **Functional improvement of injured spinal cord following injection of alginate scaffold releasing two trophic factors.** *Scientific Reports* 2015, 5:13702

Devaux S.*, Cizkova D.*, Quanico J., Franck J., Nataf S., Pays L., Hauberg-Lotte L., Mass P., Jobart J.H., Kobeissy F., Mériaux C., Wisztorski M., Slovinska L., Blasko J., Cigankova V., Fournier I., Salzet M. **Proteomic analysis of the spatio-temporal based molecular kinetics of acute spinal cord injury identifies a time- and segment-specific window for effective tissue repair.** *Molecular and Cellular Proteomics* (in Press). * co-first authors

Proceedings

Devaux S., Cizkova D., Slovinska L., Blasko J., Nagyova M., Lefebvre C., Fournier I., Salzet M. **Spatio-temporal proteins study of rat spinal cord injury and glial cells involvement.** *GLIA* (2015) 63, E414-E415

Salzet M., **Devaux S.**, Cizkova D., Quanico J., Franck J., Lotte L.H., Maass P., Wisztorski M., Slovinska L., Blasko J., Fournier I. **Spatial and temporal 3D MSI and proteomic studies of rat spinal cord injury: Evidence of caudal segment for possible therapy target.** *Journal of Biotechnology* (2015), 208, S10.

Adam A., Salzet M., **Devaux S.** **Profiling of Lipids Expression Along the Rostral and Caudal Axis After Spinal Cord Injury: Matrix Assisted Laser Desorption/Ionization Approach.** *The FASEB* (2015) *Journal* 29 (1 Supplement), 715.21

Oral communication

Devaux S., Cizkova D., Le Marrec-Croq F., Franck J., Slovinska L., Grulova I., Lefebvre C., Fournier I., Salzet M. **Proteomic analyses along the rostro-caudal axis of injured spinal cord.** EURON, 12-13th september 2013, Liège, Belgium

Devaux S., Cizkova D., Le Marrec-Croq F., Franck J., Slovinska L., Lefebvre C., Fournier I., Salzet M. **Proteomic analyses along the rostro-caudal axis of injured spinal cord.** Young club SFSM : Société Française de spectrométrie de masse 24-28th March 2014, Dieppe, France

Devaux S, Cizkova D, Le Marrec-Croq F, Franck J, Slovinska L, Lefebvre C, Fournier I, Salzet M. Traumatic injury spinal cord- Temporal and spatial change in proteome. Young club SFEAP : Société Française d'électrophorèse et d'analyse protéomique 14-16th May 2014, Toulouse, France.

Devaux S, Cizkova D, Wisztorski M, Slovinska L, Blasko J, Fournier I, Salzet M. Spatial and temporal MSI and proteomic studies of rat spinal cord injury: evidence of caudal segment for possible therapy target. 14th HUPO, 27-30th September 2015, Vancouver, Canada.

Poster

Devaux S, Cizkova D, Le Marrec-Croq F, Franck J, Slovinska L, Grulova I, Lefebvre C, Fournier I, Salzet M. Proteomic analyses along the rostro-caudal axis of injured spinal cord. 7th International Symposium on experimental and clinical neurobiology, June 2013, Kosice, Slovakia

Devaux S, Cizkova D, Le Marrec-Croq F, Franck J, Slovinska L, Blasko J, Nagyova M, Lefebvre C, Fournier I, Salzet M. Alterations of protein composition along the rostro-caudal axis after spinal cord injury: proteomic analyses. HUPO, 13th Annual World Congress of the Human Proteome Organization, Madrid, Spain, 5-8 October 2014 (Prize, Poster Award HUPO 2014)

Devaux S, Cigánkova V, Slovinska L, Blasko J, Lefebvre C, Fournier I, Salzet M, Cizkova D. Proteomic analysis of spinal cord injury: chemokines and neurotrophic factors. XVI. Celostátní conference biologické psychiatrie v Luhačovicích, 3-6th June 2015 Luhacovice, Czech Republic

Devaux S, Cizkova D, Slovinska L, Blasko J, Nagyova M, Lefebvre C, Fournier I, Salzet M. Spatio-temporal proteins study of rat spinal cord injury and glial cells involvement. Glia, XII European Meeting on Glial cells in Health and Disease, 15-18th July 2015, Bilbao, Spain.

Devaux S, Cizkova D, Wisztorski M, Slovinska L, Blasko J, Fournier I, Salzet M. Spatial and temporal MSI and proteomic studies of rat spinal cord injury: evidence of caudal segment for possible therapy target. 14th HUPO, 27-30th September 2015, Vancouver, Canada.

Devaux S, Cizkova D, Slovinska L, Blasko J, Fournier I, Salzet M. Spatio-temporal proteins study of rat spinal cord injury and immune cells involvement. FENS Featured Regional Meeting 2015, 7-10th October 2015, Thessaloniki, Greece.

Devaux S, Blasko J, Slovinska L, Cigankova V, Cizkova D, Salzet M. Immunomodulatory properties of bone marrow stromal cells on activated microglia for spinal cord injury therapy. 10th FENS Forum of Neuroscience, 2-6th July 2016, Copenhagen, Denmark.

Teaching

2015-2016: 64 hours practical courses in animal biology

Students supervision

Amna Adam, Bachelor degree, Internship 2 months 2014

Zahra Laou, Master degree, Internship 1 month 2016

Delphine Mansy, Master degree, Internship 4 months 2016

List of Figures

FIGURE 1: CONSEQUENCES OF THE LOCALIZATION OF THE LESION (ADAPTED MYHEALTH.ALBERTA.CA).....	17
FIGURE 2: A. CLIP COMPRESSION. B. AN INTRAOPERATIVE PICTURE SHOWING A CLIP COMPRESSING THE SPINAL CORD AT T2 TO CREATE THE INJURY (POON <i>ET AL.</i> 2007).....	20
FIGURE 3: BALLOON COMPRESSION MODEL. A. A PHOTOGRAPH REPRESENTING THE SIZE OF THE T9 VERTEBRA AND CATHETERS INFLATED WITH DIFFERENT VOLUMES OF SALINE 10, 15 AND 20 μ L RESPECTIVELY. B. LOCOMOTOR FUNCTION RECOVERY AFTER SCI GRADED ON AN EXPANDED SCALE (BBB SCORE). 21 IS NORMAL LOCOMOTOR FUNCTION, 0 REPRESENTS NO LOCOMOTOR FUNCTION. (ADAPTED FROM VANICKY <i>ET AL.</i> 2001).....	20
FIGURE 4: SCHEMA OF EVENTS FOLLOWING SPINAL CORD INJURY.....	22
FIGURE 5: TIME RECRUITMENT OF MICROGLIA, NEUTROPHILS, MONOCYTES/MACROPHAGES AND LYMPHOCYTES AFTER SCI (NEIRINCKX <i>ET AL.</i> 2014).....	25
FIGURE 6: MICROGLIA ARE THE ONLY HEMATOPOIETIC CELLS FOUND IN THE PARENCHYMA OF THE CNS (RANSOHOFF AND CARDONA 2010).....	26
FIGURE 7: MACROPHAGE POLARIZATION AFTER SCI. AT THE EARLY STAGE MACROPHAGES ARE PREDOMINANTLY M1 WITH THE PRESENCE OF PRO-INFLAMMATORY MOLECULES AND M1 WILL RELEASE PRO-INFLAMMATORY FACTORS. AT THE LATER STAGE THE RATIO M1/M2 EVOLVES TO HAVE AN ANTI-INFLAMMATORY RESPONSE AND THEN CYTOTOXIC EFFECTS (ADAPTED FROM DAVID & KRONER 2011).....	28
FIGURE 8: CX3CR1 RECEPTOR IN MICROGLIA AND ITS LIGAND CX3CL1 EXPRESSED BY A NEURON. A) FRACTALKINE COMPOSITION AND THE PROTEO CLEAVAGE BY ADAM10/17. B) DIFFERENT EFFECTS OF THE CLEAVAGE OF CX3CL1 ON MICROGLIA ACTIVITY (WOLF <i>ET AL.</i> 2013).....	32
FIGURE 9: RECRUITMENT OF INNATE IMMUNE CELLS AND ADAPTIVE IMMUNE CELLS AFTER SCI AND THE PROGRESSION TO THE CHRONIC PHASE (PHILLIP G. POPOVICH AND JONES 2003).....	33
FIGURE 10: SEVERAL PARAMETERS ARE INVOLVED IN SPINAL CORD REPAIR.....	35
FIGURE 11: MYELIN NEURITE GROWTH INHIBITORS NOGO-A, MAG AND OMGP AND THEIR DIFFERENT RECEPTORS NGR, p75. INHIBITION OF NOGO-A IS POSSIBLE BY THE DIFFERENT PROCESSES IN RED (MARTIN E SCHWAB 2004).....	36
FIGURE 12: THE MULTI-POTENTIALITY OF MSCs (UCCELLI <i>ET AL.</i> 2008).	42
FIGURE 13: FK506-FKBP COMPLEX INHIBITS NF-AT PATHWAY ELSEVIER IMAGE 29832.....	45
FIGURE 14: ANTI-INFLAMMATORY ROLE OF ESTROGEN AND ER AGONISTS IN CNS DISORDERS. INJURIES OF CNS INDUCE ACTIVATION OF MICROGLIA AND ASTROCYTES WHICH LEADS TO NEUROINFLAMMATION WITH THE RELEASE OF CYTOKINES AND CHEMOKINES PRO-INFLAMMATORY. ESTROGEN AND ER AGONISTS INDUCE ANTI-INFLAMMATORY EFFECTS AND THE ACTIVATION OF TH1/TH17 TO BLOCK NEUROINFLAMMATION (CHAKRABARTI <i>ET AL.</i> 2014).	46
FIGURE 15: PROTEOMIC STRATEGIES: THE BOTTOM-UP, THE SHOT-GUN AND THE TOP-DOWN APPROACHES.....	48
FIGURE 16: INFLAMMATION EXPANSION IN TIME DEPENDENT MANNER. BLUE CIRCLE CORRESPONDS TO THE INFLAMMATION SITE 10 MIN POST INJURY. THE RED CIRCLE CORRESPONDS TO THE SPREADING OF THE INFLAMMATION 24 HOURS AFTER SCI.	101
FIGURE 17: COMPARISON OF PROTEINS IDENTIFIED 24 HOURS AFTER INJURY. VENN DIAGRAM SHOWS THE COMMON AND THE EXCLUSIVE PROTEINS FOR THESE 5 CONDITIONS. 1681 PROTEINS ARE IN COMMON AND 114, 83, 121, 69 AND 126 EXCLUSIVES FOR R2, R1, L, C1 AND C2 RESPECTIVELY.	101

FIGURE 18: HEAT MAP FROM THE HIERARCHICAL CLUSTERING OF CONDITIONED MEDIA 24 HOURS AFTER INJURY. PROTEIN UNDER-EXPRESSION IS COLORED IN GREEN AND OVER-EXPRESSION IS IN RED. TABLE FOCUS ON THE CLUSTER SHOWN IN WHITE IN THE HEAT MAP, IN WHICH I_g AND COMPLEMENT FACTORS ARE EXPRESSED. 103

FIGURE 19: QUANTIFICATION OF SYNAPTOPHYSIN (SYN) AT THE LESION SITE (A) AND ROSTRAL-CAUDAL SEGMENTS (E) SHOWED SIGNIFICANT DECREASE OF SYN AFTER INJURY, WHILE RHOAi + FK506 TREATMENT INCREASED SYN EXPRESSION SIGNIFICANTLY AT LESION, BUT NOT IN ROSTRAL OR CAUDAL SEGMENTS (E), *P<0.05, ** P<0.001, *** P<0.0001 ONE-WAY ANOVA. REPRESENTATIVE IMAGES OF SYNAPTOPHYSIN IMMUNOREACTIVITY (SYN, GREEN) REVEALED INTENSELY STAINED SYNAPTIC VESICLES – PUNCTATE STRUCTURES WITHIN THE SPINAL CORD- LESION SITE IN CONTROL (B) AND TREATED GROUP (D), NOT IN SCI (C). CONFOCAL IMAGES WITH DOUBLE LABELING OF GAP-43 (RED) AND SYN(GREEN) ANTIBODIES, CONFIRMED ENHANCED GROWTH OF AXONS WITH DENSE SYNAPTIC VESICLES DISTRIBUTION AFTER RHOA INHIBITOR + FK506 TREATMENT (G). THE *IN VIVO* EXPERIMENTS DID NOT REVEALED SIGNIFICANT DIFFERENCES BETWEEN SCI AND TREATED RHOAi+ FK506 GROUPS IN GAP-43 IMMUNOREACTIVITY (I), OUTLINING GROWING AXONS WITHIN DAMAGED DORSAL AND LATERAL WHITE MATTER TRACTS (Ha, Hb). NOTE, HIGH NUMBER OF GAP-43 AXONS PENETRATING THE LESION SITE. SCALE BAR =25µM. BBB SCORE STUDY OF RAT WITH INJURY (SCI) AND AFTER TREATMENT WITH RHOAi + FK506 AT 0, 7, 14, 21, 28, 35, 42 AND 49 DAYS POST INJURY, REVEALS THAT WITH TREATMENT BBB SCORE REACHED TO 5, 14 DAYS AFTER SCI WHEREAS WITHOUT TREATMENT RATS NEED AROUND 30 DAYS TO GET SCORE AT 5. HOWEVER, THE SCORE DOES NOT INCREASE AFTER 14 DAYS (J). 107

FIGURE 20: ND7/23 DRG CELL LINE CULTURED FOR 24 HOURS IN 1/3 OF SCI-CM ROSTRAL (R1), LESION (L) OR CAUDAL (C1) OR DMEM AS CONTROL, THEN AN ADDITION OR NOT OF RHOA INHIBITOR WAS APPLIED FOR 24 HOURS (A). QUANTIFICATION OF NEURITE OUTGROWTH BY IMAGEJ DEMONSTRATES THE EFFECT OF RoAi ON NEURITE OUTGROWTH (B) (ONE WAY ANOVA FOLLOWED BY TUKEY-KRAMER TEST *P<0.05, **P<0.01, ***P<0.001, NS= NON-SIGNIFICANT). ARROWS INDICATE THE NEURITE OUTGROWTH 108

FIGURE 21: HEAT MAP OF PROTEINS FROM THE SECRETOME AFTER DIFFERENT STIMULATION OF ND7/23 DRG CELL LINE. CONTROL (DMEM) OR LESION (L), ROSTRAL (R1) OR CAUDAL (C1) CONDITIONED MEDIA FROM SPINAL CORD 3 DAYS AFTER INJURY WERE USED TO STIMULATE THE CELLS WITH OR WITHOUT STIMULATION OF RHOA INHIBITOR 24 HOURS AFTER CM STIMULATION (A). ZOOM OF THE CLUSTER SHOWING A DIFFERENCE BETWEEN SCI-CM MEDIA STIMULATION WITH LESION CM AND PROTEINS NAME EXPRESSED IN THIS CLUSTER (B). 109

FIGURE 22: IMMUNOGLOBULINS IN SPINAL CORD INJURY TISSUE FROM ROSTRAL, LESION AND CAUDAL SEGMENTS AFTER 3, 7 AND 10 DAYS POST INJURY. EXPRESSION OF HEAVY CHAIN OF I_gG (A) AND LIGHT CHAIN EXPRESSION (B) WERE ASSESSED BY WESTERN BLOT. HIGHER EXPRESSION OF I_gGs HEAVY OR LIGHT CHAIN WAS OBSERVED AT 3 DAYS POST SCI IN THE LESION SITE. 111

FIGURE 23: HEAT MAP OF PROTEINS SECRETED BY ND7/23 CELL LINE AFTER STIMULATION WITH OR WITHOUT RHOAi. CONTROL IS CELL IN DMEM WITH OR WITHOUT RHOAi, CELLS STIMULATED WITH CONDITIONED MEDIA FROM SCI AND RHOAi IS NAMED RHO AND WITHOUT RHOAi IS CALLED (NT). VENN DIAGRAM WITH THE TOTAL PROTEINS IDENTIFIED SHOW THE PRESENCE OF EXCLUSIVE AND COMMON PROTEINS FOR EACH CONDITIONS (A). HEAT MAP OF SECRETED PROTEINS FROM CONTROL VERSUS SCI-CM STIMULATION WITH OR WITHOUT RoAi TREATMENT (RHO VS NT) HAVE SHOWN DISTINCT CLUSTERS. 112

FIGURE 24: VENN DIAGRAM OF PROTEINS IDENTIFIED FROM THE CELLULAR PROTEIN EXTRACT (PE) OF ND7/23 CELL LINE. COMPARISON OF CONTROL (DMEM) WITH OR WITHOUT RHOAi AND PROTEIN EXTRACT FROM CELLS TREATED WITH SCI-CM WITH (RHOAi) OR NOT TREATED (NT). 115

FIGURE 25: EVIDENCE FOR PROTEIN-PROTEIN INTERACTION NETWORK OF THE ENRICHED TRANSCRIPTION FACTORS CONSTRUCTED BY
STRING..... 116

Abbreviations

ALG: alginate	IFN: interferon
ASC: adipocyte stem cell	IGF: insulin growth factor
BBB score: Basso, Beattie and Bresnahan	Ig: immunoglobulin
BBB: blood-brain-barrier	IL-: interleukin
BDNF: brain-derived neurotrophic factor	iPSC: induced pluripotent stem cells
BMSC: bone marrow stromal cell	KS: keratan sulfate
C5: cervical 5	LFA-1: Lymphocyte function-associated antigen 1
CD: cluster of differentiation	LPS: lipopolysaccharide
ChABC: chondroitinase ABC	MAC-1: macrophage-1 antigen
CINC-1: cytokine-induced neutrophil chemo-attractant 1	MAG: myelin associated glycoprotein
CNS: central nervous system	MALDI: matrix laser desorption ionization
CNTF: ciliary neurotrophic factor	MBP: myelin basic protein
CSF: cerebrospinal fluid	MHC: major histocompatibility complex
CSPG: chondroitin sulfate proteoglycans	MMPs: matrix metalloproteinases
DRG: dorsal root ganglia	MS: mass spectrometry
EGF: epidermal growth factor	MSC: mesenchymal stem cell
ER: estrogen receptor	MV: microvesicle
ESI: electrospray ionization	NCAM: Neural Cell Adhesion Molecule=CD56
FasL: Fas ligand	NG2: neuron-glia antigen 2
FcR β : Fc receptor β chain	NGF: nerve growth factor
FGF-2: fibroblast growth factor 2	NO: nitrite oxide
GAG: glycosaminoglycan	Nogo-66 receptor: NgR
G-CSF: granulocyte-colony stimulating factor	NPC: neural progenitor cell
GDNF: Glial cell-derived neurotrophic factor	OEC: Olfactory ensheathing cell
GF: growth factor	OMgp: oligodendrocyte myelin glycoprotein
hESC: human embryonic stem cell	PNS: peripheral nervous system
HMGB1: high-mobility group box 1	RAG: recombinant activating gene
ICAM-1: Intercellular Adhesion Molecule 1	
RAGE: Receptor for Advanced Glycation Endproducts	

RhoAi: RhoA inhibitor

ROCK: Rho kinase

SAL: saline

SCI: spinal cord injury

T12: thoracic 12

TF: transcription factor

TGF β : transforming growth factor β 1

TIMPs: metalloproteinase inhibitor

Introduction

Spinal cord injury (SCI) is one of the major traumas of the central nervous system (CNS). Traumatic SCI can lead to paralysis with complete or partial loss of neurological function below the injury site. The overall impact of SCI on both the patient and the society depends on a range of factors, including: the age of patient, the extent of the injury, the availability and timing of appropriate health care, services and the environment in which the person lives (physical, social, economic and attitudinal). Symptomatology treatment and physiotherapy care of patients with spinal cord injury requires high financial costs not only for the patient and his or her family but also for society. Statistics indicate that the U.S. has an annual growth of 11000 patients, which represents approximately 1.3 million people with a spinal cord injury. The economic costs of health care of a 25 years old patients are around \$3 mil U.S. In the European Union, there are about five hundred thousand people affected by SCI. The incidence of SCI in France is roughly 20 cases per million inhabitants per year or 934 cases per year (Albert and Ravaud 2005). In Europe the most commonly injured age group is 16-34 years olds (43%), followed by 31-45 years olds (28%).

Traumatic SCI can be the result of several different causes such as traffic accidents, falls, violence and sports injuries. SCI can be induced by non-traumatic causes involving communicable diseases such as tuberculosis and human immunodeficiency virus (HIV), and non-communicable diseases such as osteoarthritis leading to spinal stenosis, cardiovascular disease, nutritional deficiencies, neural tube defects, vitamin B12 deficiency and complication of medical care. The neurological outcomes depend on the range of damaged neuronal populations at the injury site, the level of disconnection of ascending and descending neuronal pathways, the secondary damage (edema, inflammation, ischemia) and the activation of regenerative processes (endogenous production of trophic factors, revascularization).

Currently there is no effective therapy available for patients with SCI. One of the approved clinical treatments for SCI is the administration of methylprednisolone in order to modulate inflammation. However, high-doses of this drug are often associated with severe immunosuppression and side effects, such as pulmonary or urinary tract infections. The central

nervous system has a limited regenerative capacity due to the inflammatory response, inhibitory molecules and scar tissue.

Different molecules and therapies have been used by many laboratories to preserve healthy tissue, to stimulate and reactivate spared tissue and to promote neuronal survival and axonal outgrowth. Injury to the spinal cord leads to an acute inflammatory response (Phillip G Popovich, Wei, and Stokes 1997). In parallel, immune response regulates the inflammation by the production of anti-inflammatory molecules (Riegger *et al.* 2007). Immune response is primordial to the preservation of tissue homeostasis.

Acute phase (hours to days after injury) is directly linked to the trauma and results in neurodegeneration along with cell death at the lesion site. After primary trauma, cellular and molecular inflammatory cascades are initiated causing activation of resident microglia and astrocytes, as well as infiltration of innate immune cells such as lymphocytes, monocytes. The local release of cytokines and chemokines by microglia, macrophages and neurons induces a particular environment that can be either neurotoxic or neurotrophic. During acute phase, macrophages phagocytose cell debris and glial scar protect healthy tissue.

Chronic inflammatory processes (weeks after trauma) lead to aberrant tissue remodeling and organ dysfunction. Among different mono-therapies, more complex-cellular therapy has several advantages targeting multiple aims: to bridge cavities or cysts, to replace dead cells, and to create a favorable environment allowing axonal regeneration (Rowland *et al.* 2008; Thuret, Moon, and Gage 2006). The transplantation of peripheral nerves, olfactory nervous system cells, embryonic CNS tissue, embryonic stem cells, adult stem cells (MSCs, NPCs), or activated macrophages (Thuret, Moon, and Gage 2006) has been studied to provide a solution to these aims.

Molecular therapy is used to protect neurons from secondary process, to promote axon growth and to enhance conduction. Different types of molecules are used such as erythropoietin and minocycline (neuroprotective effect), growth factors (BDNF, GDNF, NGF, NT-3), chondroitinase ABC to eliminate chondroitin sulfate proteoglycans (CSPG) with the major component NG2 which inhibits the regeneration of damaged axons (Bradbury *et al.* 2002), and nogo-A is one of several neurite growth inhibitory molecules. Thereby, Nogo neutralizing

antibodies or blockers of the post-receptors components RhoA are used to improve long-distance axon regeneration and sprouting (Martin E Schwab 2004). Rho pathway is important to control the neuronal response after CNS injury. A drug called cethrin that blocks activation of Rho is actually in phase I/IIa of clinical trials (Fehlings *et al.* 2011). However, among all these molecules and therapies currently used to ameliorate neuroprotection or neurite outgrowth, or to reduce inflammation, none of them allows a total understanding of the inflammation mechanism in the entire spinal cord to target specific segment at the appropriate time for SCI treatment. A lack of understanding of the molecular cross-talk occurring between cells at the lesion site and in the adjacent segments needs to be investigated. Such a study could give molecular targets taking into account both spatial and temporal data. Such an investigation could be performed by a proteomic approach which can be connected to cellular and physiological studies as well as to a global regeneration-activated gene (RAG) investigation. Mass spectrometry (MS) plays a central role among proteomic approaches. Several developments allow fast identification and relative quantification through label free quantification methods to thousands of proteins, allowing to identify such proteins of lower abundance as cytokines and chemokines (Meissner *et al.* 2013). MS is highly used in neuroscience to discover biomarker candidates and also to study the differential expressions of proteins at any given time in a proteome and they are then compared with the pattern of healthy ones (Singh *et al.* 2012).

Hypothesis

In the current biomedical research, it is important to understand the mechanisms of immune response, molecular and biological processes following injury to improve regeneration of nerve tissue, to promote axonal growth and to replace damaged nerve cells to create favorable conditions for regeneration. Therefore, it is crucial to the understanding of the physiopathology that occurs after SCI to use the strength of mass spectrometry in order to understand the microenvironment along the entire spinal cord throughout different stages of the injury evolution. It is necessary to find a new treatment that would better control:

i) the second process involving inflammation leading to the expansion of the central lesion which affects the rostro-caudal spinal segments that have not been damaged by the primary lesion

ii) the formation of the glial scar at the lesion representing a chemical and mechanical barrier for a number of molecules involved in axonal regrowth

iii) the production of trophic factors, both spatially and temporally to stimulate axonal growth, plasticity, and demyelination causing irreparable damage.

Objectives

My PhD thesis was divided into 2 main parts.

The first objective of my PhD thesis focuses on **the understanding of the biological process occurring after a spinal cord injury through a spatial and temporal point of view during the first stage of the injury**. Spatial and temporal analyses along the rostral-caudal axis were performed by mass spectrometry without preconditions. Based on *in vitro* and proteomics data, factors with immuno-modulatory efficiency on primary microglia and microglia cell line were characterized. Activation of microglial cells is carried out in the presence of the conditioned medium of the spinal cord to recreate the *in vivo* microenvironment. The switch M1 / M2 of microglial cells was studied to determine whether the phenotype would be pro or anti-inflammatory according to the position of the lesion site

The second part aims **to promote the regeneration *in vitro*** using cell therapy, followed by ***in vivo* stimulation of the regeneration process and spinal cord plasticity**. Bone marrow derived- mesenchymal stromal cells are known for their immuno-modulatory effects after injury. In this context, we analyze the BMSCs secreted factors by mass spectrometry to identify the molecules involved in the modulation of the microglia. *In vitro* studies on primary microglia and BV2 cell line confirmed the high modulatory potential on inflammation and microglia polarization. Then **the *in vivo* stimulation of the regeneration process and spinal cord plasticity** will be studied with the aim to increase the number of axons going through the lesion site which are able to create connections between each other. *In vivo*, the injection of alginate biomaterial, directly into the lesion site fills the cavity to produce a scaffold for the growth of neurons and axons. Alginate coupled with trophic growth factors (GF) such as Epidermal Growth Factor (EGF) and Fibroblast Growth Factor 2 (FGF2) significantly enhanced the sparing of spinal cord tissue and increased the number of surviving neurons.

1. Spinal cord organization

The spinal cord is part of the central nervous system which controls the voluntary movement of the limbs and trunk, and which receives sensory information from these regions. The spinal cord is located in the vertebral canal. In humans, the spinal cord is approximately 1cm thick and around 42 cm long and occupies the upper two-thirds of the vertebral canal. The spinal cord is cylindrical but also slightly flattened dorso-ventrally. The human spinal cord is composed of 31 segments in total: 8 cervical segments, 12 thoracic segments, 5 lumbar segments, 5 sacral segments and 1 coccygeal segment. Conversely, in rats, the spinal cord is made up of 34 segments: 8 cervical, 13 thoracic, 6 lumbar, 4 sacral, 3 coccygeal. The consequences of spinal cord injuries such as tetraplegia and paraplegia are dependent on the location of the trauma (Figure 1).

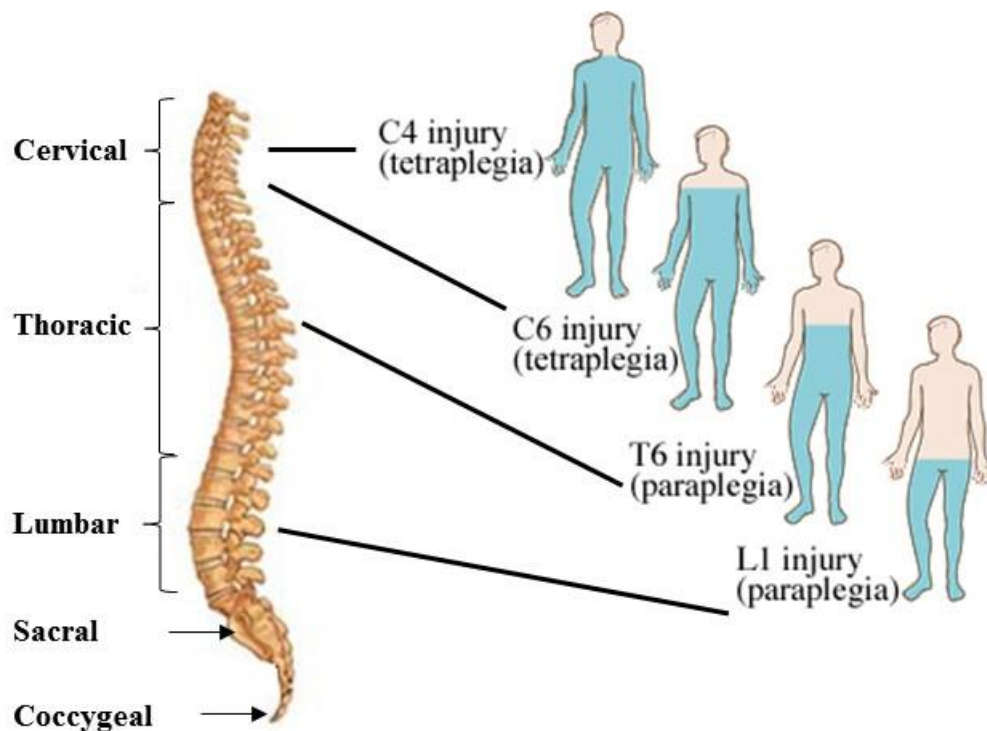


Figure 1: Consequences of the localization of the lesion (adapted myhealth.alberta.ca).

The spinal nerves run along the entire spinal cord- in humans there are 31 pairs of spinal nerves as supposed to 34 pairs in rats. The spinal nerves transmit sensory information from the target organs to the central nervous system, and send motor commands from the central nervous

system to muscles and target organs. Each spinal nerve is attached by a ventral and a dorsal root. One root is formed by six to eight rootlets. The ventral rootlets are made up of axons of motor neurons and the dorsal rootlets are made up of the axons of the sensory neurons. Each dorsal root bears an ovoid swelling named dorsal root ganglion (DRG) that contains primary sensory neurons. These neurons have pseudo-unipolar morphology with a single short axon that divides into a peripheral and central branch. The central branch enters the spinal cord via the dorsal roots and carries information from the cell body of the DRG neuron to the spinal cord. The peripheral branch conveys sensory information from the body to the DRG neuron. The spinal cord is composed of gray and white matter. A transverse section shows that the gray matter is arranged in the form of a butterfly which is surrounded by the white matter. The white matter is composed of longitudinally running axons and glial cells. The gray matter is made up of neuronal cell bodies, dendrites, axons and glial cells. The neurons are mostly multipolar, but vary greatly in size in different laminae. The laminae were first described by Rexed in 1954 in the cat. Afterwards, these were used to describe cyto architectonic boundaries in the spinal cord in rats by Molander in 1984. Ten laminae are described and these are organized in a series of layers from dorsal to ventral axis. The spinal cord is enclosed in the meninges and consists of three layers: the dura mater, the intermediate arachnoid mater and the pia mater. These membranes and the cerebrospinal fluid provide a protection and nourishment for the spinal cord and spinal nerve roots.

2. Model of injury

SCI can result from three main causes which lead to tissue damage: compression caused by spinal discs or bone material pressing against the cord, destruction from direct trauma, and reduction in blood flow from the initial damage (ischemia). The injuries can be divided in two main categories: complete and incomplete. According to the American Association of Spinal Cord Injury Nurses (AASCIN), complete SCI refers to no preservation of motor and/or sensory function that exists more than three segments below the level of injury, whereas as incomplete SCI refers to some preservation of motor or/and sensory function existing more than three segments below the level of the injury. Complete transection is clinically rare. Most injured spinal cords maintain some tissue continuity across the area of injury to create an environment more tractable for regeneration. Several animal models have been developed with the aim to

reproduce the complete or incomplete SCI in order to understand the anatomical and biological consequences. The rat model is widely used because the studies are inexpensive, the incidence of post-surgical infections are rare and rats are easy to care. Mouse models are also largely studied. Larger mammals such as dogs and cats are rarely used since they require expensive after care and housing, and due to the fact that stringent ethical restrictions are in place. Several animal models are used in research to mimic clinical human SCI.

The majority of human SCIs are due to motor vehicle accidents, falls and sport injuries, and involve a sudden compression of the spinal cord, usually as a result of vertebral column damage that allows bone or disc material to intrude on the spinal canal space. Compression injuries occur as a secondary consequence of injury or as a result of tumor growth. The laminectomy allows the exposition of the spinal cord by removing the bone.

Complete transection injury reflects clinical symptoms of complete SCI patients. This model is performed after laminectomy with spring scissors. It offers the advantage of complete damage to a given tract at a defined place and time. The complete transection model, when performed accurately, excludes the possibility that axonal sparing results in improved functional outcomes. However most of the traumas after injuries are not complete transections of the spinal cord.

Clip compression is processed with calibrated clip to exert a specific force- 50g for a severe response and 35g for a moderate response (Bruce, Oatway, and Weaver 2002) (Figure 2) but this method does not truly mimic the injury seen in humans.

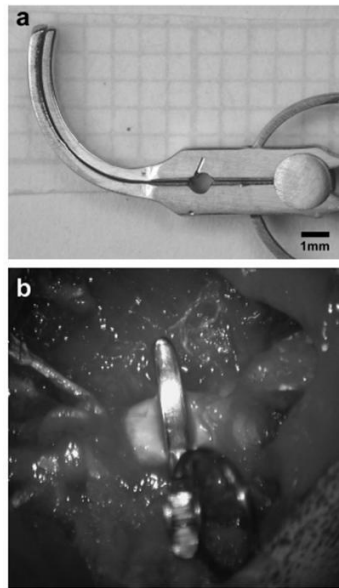


Figure 2: a. Clip compression. b. An intraoperative picture showing a clip compressing the spinal cord at T2 to create the injury (Poon *et al.* 2007).

The balloon compression model was first described by Tarlov in 1953 in dogs (Tarlov, Klinger, and Vitale 1953). The method uses different volumes to inflate the balloon and different compression durations in order to induce different grades of damage (Figure 3). After laminectomy, a 2-French Fogarty catheter is inserted into the dorsal epidural space through a small hole made in the T10 vertebral arch, which is then advanced cranially to the T8-9 spinal level and inflated for 5 min. A volume of 15 μ L of saline produced complete paraplegia followed by gradual recovery.

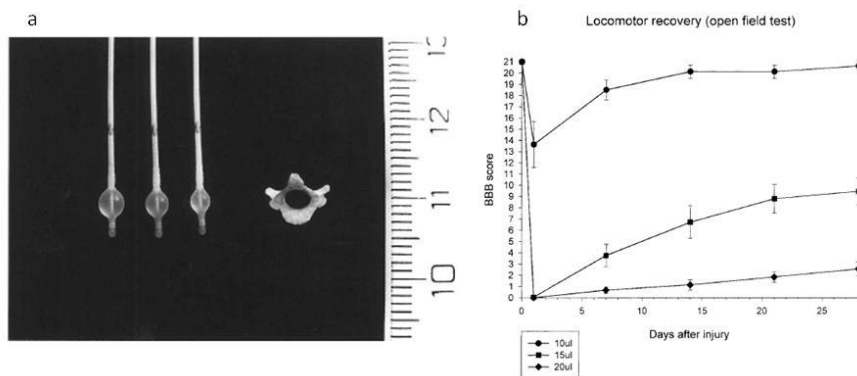


Figure 3: Balloon compression model. a. A photograph representing the size of the T9 vertebra and catheters inflated with different volumes of saline 10, 15 and 20 μ L respectively. b. Locomotor function recovery after SCI graded on an expanded scale (BBB score). 21 is normal locomotor function, 0 represents no locomotor function. (adapted from Vanicky *et al.* 2001)

Computer controlled contusion consists of an animal trap that reproducibly delivers a defined weight to the exposed spinal cord with a computer monitoring the dynamics impact (Stokes, Noyes, and Behrmann 1992). This method is reproducible but the equipment is expensive. The transaction model mimics a complete spinal transaction (rare in clinic) which is performed by using spring scissors following laminectomy, producing a laceration of the cord (Nakae *et al.* 2011).

The behavioral patterns are correlated with the severity of the injury and are evaluated in animals by using the BBB score, which is an open field locomotor activity test that was originally developed at the Ohio State University (Basso, Beattie, and Bresnahan 1995). The scale ranges from 0 to 21 with 0 indicating complete paraplegia and 21 indicating physiological locomotor movement (Table 1).

BBB score	Observations	
0	No movement	Movements only
1	Slight movement of 1-2 joints	
2	Extensive movement of 1 joint (+ slight movement of another)	
3	Extensive movement of 2 joints	
4	Slight movement of all 3 joints	
5	Slight movement of 2 joints AND extensive movement of 1	
6	Extensive movement of 2 joints AND slight movement of 1	
7	Extensive movement of all 3 joints	Plantar placement
8	Sweeping OR plantar placement (No weight support)	
9	Plantar placement (weight support in stance only) OR weight supporting dorsal stepping	Coordination
10	Occasional steps, No coordination	
11	Frequent-consistent steps, no coordination	
12	Frequent-consistent steps, occasional coordination	
13	Frequent-consistent steps, frequent coordination	
14	Consistent steps, consistent coordination, paw position rotated OR occasional stepping	Paw position, Toe clearance
15	Consistent steps, consistent coordination, No or occasional toe clearance	
16	Consistent steps, consistent coordination, frequent toe clearance, paw rotated at lift off	
17	Consistent steps, consistent coordination, frequent toe clearance, paw is predominantly parallel	
18	Consistent steps, consistent coordination, consistent toe clearance, paw is parallel at initial contact, and rotated at lift off	Tail, trunk stability
19	Consistent steps, consistent coordination, consistent toe clearance, paw is parallel at initial contact and at lift off tail is down part or all time	
20	Tail consistently up, trunk instability	
21	Trunk stability	

Table 1: The 21-point Basso, Beattie, Bresnahan locomotor rating scale (Adapted from Basso *et al.* 1995).

The BBB score evaluates the movements of the hind limb of an animal after injury to express a state of recovery. A method for gait analysis called catwalk is used to evaluate the paw position of the animal after injury and the improvement after treatment (Hamers *et al.* 2001). Each front and hind paw of animal that makes contact with the glass floor is automatically detected. The software registers footprints and calculates a wide range of parameters relative to the individual footprints (stand, print length), the relative positions of footprints (stride length, base of support), the time-based relationship between footprints (cadence), toe spread and paw angle.

3. Pathophysiology

Spinal cord injury is one of the major injuries of the central nervous system. The pathological mechanisms consist of two phases; the primary and the secondary phase (Figure 4). The most common form of acute SCI is a compressive type of injury in which displaced inter-vertebral discs and ligaments exert force on the cord causing immediate traumatic injury and often sustained compression (Sekhon and Fehlings 2001).

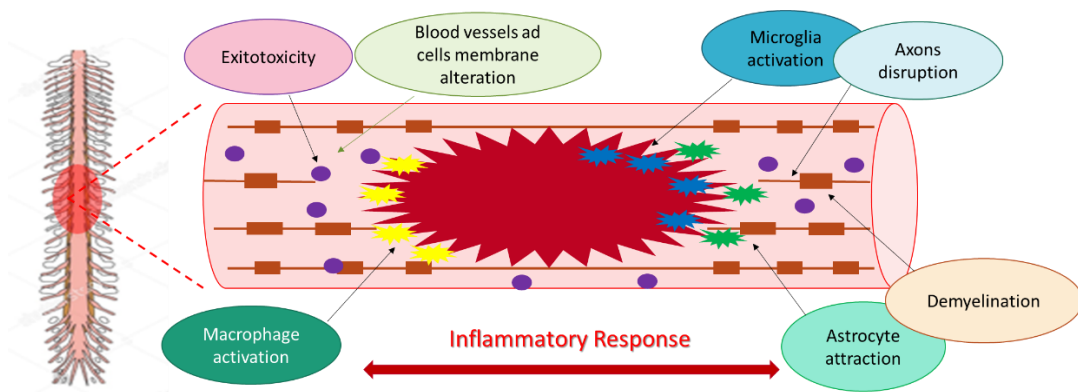


Figure 4: Schema of events following spinal cord injury

3.1. Primary injury

Primary injury is the result of the mechanical trauma which produces traction and compression forces. Primary mechanisms rarely transect or fully disrupt the anatomical continuity of the cord. Blood vessels are directly damaged and the axons are disrupted. Axons are present to traverse the lesion site with a demyelinated long tract axon. A few minutes after injury, micro-hemorrhages start to develop in the central grey matter and spread out radially

and axially over the next hours. The swelling of the spinal cord is observed at the injury site and it occupies the entire space of the spinal canal. Ischemia occurs when cord swelling exceeds venous blood pressure. Microglia cells are the first glial cells to be activated following injury, in less than two hours (Figure 4). These pathological events, such as damages to axons, cells and blood vessels, leads to the release of toxic chemicals and factors that attack intact neighboring cells within the early acute phase (after 48 hours).

3.2.Secondary injury

Secondary injury refers to the molecular and cellular cascade causing neuroinflammation (Donnelly and Popovich 2008), immune associated neurotoxicity which contributes to axonal and neuronal necrosis, edema, glutamate mediated excitotoxicity, ROS production and vascular dysfunction (Figure 4). The secondary phase results in tissue destruction whereas neurological deficits are present immediately following injury. Resident microglia respond immediately to the injury (Watanabe *et al.* 1999). Between 2 and 7 days most of the cells in the lesion are infiltrating macrophages (Phillip G Popovich, Wei, and Stokes 1997; Donnelly and Popovich 2008). This period of macrophages infiltration corresponds to the ascending sensory axon retraction. This process is not permanent, because when axons lost macrophages contact after retraction, they were able to extend (Horn *et al.* 2008).

Reactive astrocytes deposited proteoglycans (CSPGs), including neurocan and phosphacan, are major factors that inhibit regeneration by forming the glia scar within hours after injury. The glial scar serves to compact inflammatory cells to demarcate the injury site from the healthy tissue (Faulkner *et al.* 2004) and re-seal the blood brain barrier after the injury. Astrocytes become hypertrophic after moving away from the center of the lesion and dramatically upregulate the production of inhibitory chondroitin sulfate proteoglycans (CSPGs) that prevent regeneration (Silver and Miller 2004). But the glial scar seems to also have beneficial functions for stabilizing fragile CNS tissue by separating the injury from healthy tissue and preventing a cascading wave of uncontrolled tissue damage (Faulkner *et al.* 2004). Scar tissue together with CSPGs and NG2 are known for their inhibitory effect on axonal growth (Fidler *et al.* 1999; McKeon, R J *et al.* 1991; Smith-thomas *et al.* 1994). The degradation

of CSPGs by using inhibitors or specific enzymes shows an increase in axonal growth and regeneration (Caggiano *et al.* 2005; Smith-thomas *et al.* 1995; Tom and Houlé 2008).

After injury, neurons are exposed to a microenvironment that contains toxic factors, which results in neuronal loss and degeneration. Astrocytes have an important scavenging function, for example the regulation of excessive levels of glutamate. CSPGs produced by activated astrocytes in the lesion area create a diffusion barrier for molecules that are harmful to the healthy tissue and attenuate the spread of neurotoxicity (Roitbak and Syková 1999; Vorísek *et al.* 2002). Astrocytes provide trophic support at the injury site (White, Yin, and Jakeman 2008). Glial scar could be crucial for neuronal survival by filling the gaps in the lesion area, creating a scaffold for the vascularization network. Astrocytes are known to have a direct effect on the intensity of blood flow (Parri and Crunelli 2003).

Neuroinflammation is one of mechanisms involved after injury. An immune response is important to protect the organism but immune activity in the CNS could have deleterious effects by accelerating tissue damage. In the CNS, immune cells acquire diverse phenotypes depending on the microenvironment. Among glial cells, microglia cells, first to be recruited, are able to play a bifunctional role by secreting toxic factors and contributing to tissue damage, but they are also able to release neuroprotective and neurotrophic molecules to allow tissue repair (Aloisi 2001).

4. Immune response after SCI

The central nervous system has a highly specialized immune-modulatory microenvironment to protect itself from immune-mediated inflammation. The blood-brain-barrier (BBB) is a physiological and anatomical element to balance peripheral immune cells and molecules entry.

Immune response in the CNS is mediated by resident microglia and astrocytes, which are innate immune cells without direct counterparts in the periphery. However, microglia and astrocytes are able to engage a cross-talk with CNS-infiltrating T cells, neurons and other components of the innate immune system.

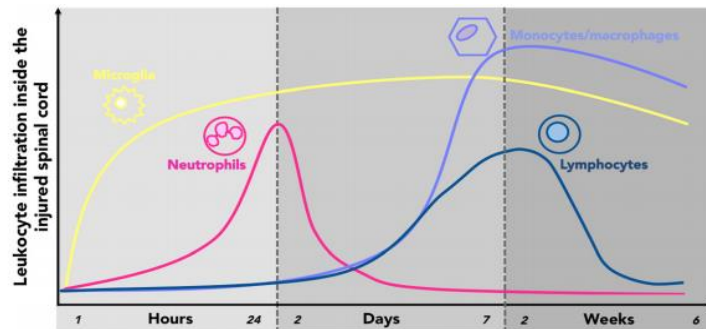


Figure 5: Time recruitment of microglia, neutrophils, monocytes/macrophages and lymphocytes after SCI (Neirinckx *et al.* 2014).

Inflammatory responses are the central point in the physiopathologic processes of acute and chronic phases of SCI. Neutrophils are the first inflammatory actors to invade the injury site with the peak appearing at 24h post injury. Circulating monocytes/macrophages are then recruited peaking at 7 days post-injury, with lymphocytes progressively invading the lesion epicenter thereafter. (Figure 5).

4.1. Innate immune system

After SCI, cells need restorative support, which is provided by inflammatory responses. However, excessive or chronic inflammation can become harmful. The micro-environment present at the lesion site confers this balance. This injured environment is composed of pro-inflammatory cytokines as tumor necrosis factor α (TNF α), interleukins IL-1 and IL-6 at the early phase of the inflammation but also some anti-inflammatory molecules are released as transforming growth factor β 1 (TGF β), IL-10.

4.1.1. Neutrophils recruitment

Neutrophils are considered the first inflammatory cells to arrive at the site of injury with a peak at 24 hours after injury (Means and Anderson 1983). They are rapidly mobilized from the bone marrow in response to signals from pro-inflammatory CXC (CXCL8) family chemokines, IL-8 and cytokine-induced neutrophil chemo-attractant 1 (CINC-1) to mediate pleiotropic functions in the immune-inflammatory response (Tonai *et al.* 2001).

Neutrophils adhere to post-capillary venules 6-12 hours post SCI and by 24h they migrate into the lesion site to phagocytose debris (Taoka *et al.* 1997). Neutrophils generate their

own cytokines after stimulation by pro-inflammatory mediators and produce proteases via the NF- κ B translocation pathway. Phagocytic activity can induce NF- κ B activation (McDonald and Cassatella 1997). Matrix metalloproteases (MMPs) as MMP-9 and cytokines TNF α , IL-1, IL-8 and TGF- β are these mediators (Cassatella 1995).

4.1.2. Microglia cells

Through the production of inflammatory factors, microglia cells represent the archetypal cells. Microglia are a unique myeloid cell population, derived from the yolk sac during a narrow time window before vascularization or definitive hematopoiesis in the embryo (Figure 6). Microglia cells, in the CNS parenchyma, are sustained by proliferation of resident progenitors, independent of blood cells.

Rio-Hortega was the first to use the term microglia in 1917. He observed that these cells were not stationary and were able to consume cellular debris. They scan the microenvironment with their branched processes to phagocyte cell and myelin debris. Microglia are small glial cells present in the brain and spinal cord. They have a small soma, little perinuclear cytoplasm and fine, branched processes.

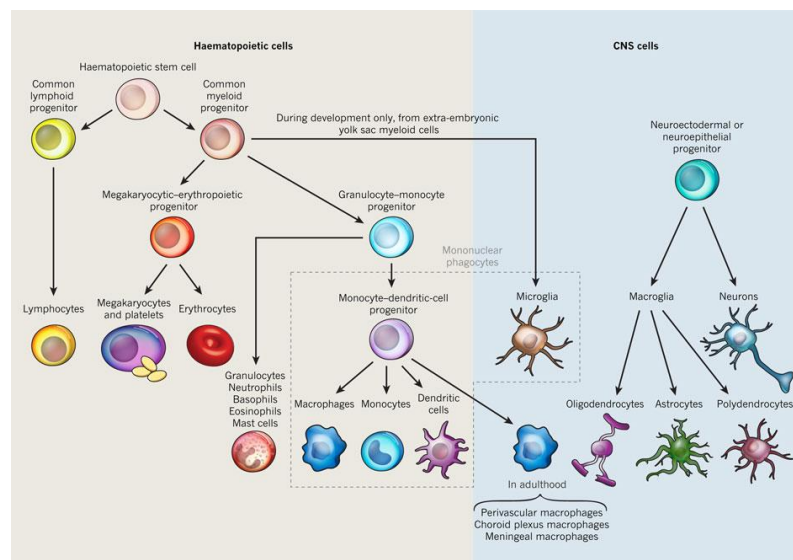


Figure 6: Microglia are the only hematopoietic cells found in the parenchyma of the CNS (Ransohoff and Cardona 2010).

Resident microglia cells express myeloid-monocytic markers such as Fc receptors-cluster of differentiation (CD32 and CD64), complement receptors CD11b and CD11c

integrins, major histocompatibility complex MHC class I and II, and CD45 (Tambuyzer, Ponsaerts, and Nouwen 2009). After injury, the resident ramified microglia morphologically transform into cells with retracted processes and enlarged cell bodies, and increase in number at the affected site. Microglia cells with this particular shape are generally referred to as “activated microglia or reactive microglia”. Even if macrophages and microglia have different origins, microglia are related to resident tissue macrophages.

Microglia response following pathological stimuli is characterized by an accumulation at the lesion site and the release of various bioactive molecules. Two categories of molecules are released- some are cytotoxic or pro-inflammatory, and others may aid survival and regeneration. Resident monocytes are the first cell types to respond after injury within 1-2 hours, which starts the initial acute inflammatory response accompanied by an expression of TNF α and IL-1 (M1 phenotype). This leads to the recruitment of other immune cells. M1 macrophages promote phagocytosis. 8 hours after of the injury, the production of pro-inflammatory cytokines is terminated, thus promoting the differentiation of macrophages into an anti-inflammatory M2 phenotype with the expression of arginase 1 and a mannose receptor (CD206). M2 macrophages promote angiogenesis and matrix remodeling while suppressing destructive immunity (Sica *et al.* 2006). The ratio M1/M2 varied in terms of microenvironment (Figure 7).

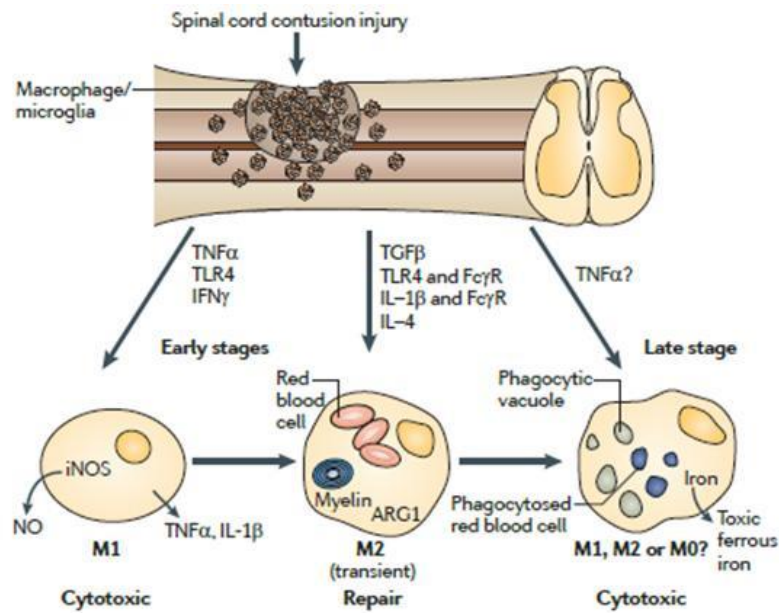


Figure 7: Macrophage polarization after SCI. At the early stage macrophages are predominantly M1 with the presence of pro-inflammatory molecules and M1 will release pro-inflammatory factors. At the later stage the ratio M1/M2 evolves to have an anti-inflammatory response and then cytotoxic effects (adapted from David & Kroner 2011).

4.1.3. Astrocytes

Reactive astrocytes are a prominent feature of the cellular response to SCI. They allow for an exchange in gene expression, hypertrophy, process extension and cell division (Eddleston and Mucke 1993). Reactive astrocytes are involved in scar tissue formation which prevents axonal regeneration (Rudge and Silver 1990). Therefore, they are often considered detrimental to the functional outcome after SCI. However, the action of reactive astrocytes is conserved throughout the vertebrate evolution (Larner *et al.* 1995), suggesting a beneficial role.

Astrocytes are able to clear glutamate and potassium ions from the extracellular space, representing a potential energy source and providing trophic support. All these factors are crucial for the survival of neurons located at the margins of the lesion site and are colocalized with the scar. Growth factors such as insulin growth factors (IGFs), nerve growth factor (NGF), brain-derived neurotrophic growth factor (BDNF) and neurotrophin-3 (NT-3), as well as metabolites including glucose and nutrients are produced by astrocytes to support the survival of the cells (Schwartz and Nishiyama 1994). It was shown that astrocytes can directly protect neurons from nitric oxide toxicity through a glutathione-dependent mechanism (Y. Chen *et al.* 2001). Although astrocytes produce CSPGs in the lesion area, this molecule creates a diffusion

barrier for molecules that are potentially harmful to the spared tissue (Roitbak and Syková 1999) and thereby attenuates the spread of neurotoxicity and prevents excitatory amino acid-induced neuronal death (Sato *et al.* 2008).

4.2. Relation between glial cells and neurons

The communication between the neural and the immune system is obvious. The communication between the two is mediated by soluble factors such as neurotransmitters, neuromodulators, neuropeptides or through cell-cell contact by neuroimmune regulatory molecules that can reduce or inhibit any exacerbated inflammatory response (Tian *et al.* 2012). Glial cells, such as microglia, astrocytes and neurons can express pro- and anti-inflammatory molecules to modulate the injured environment and these molecules play a major role in their communication (Table 2).

Properties	Pro-inflammatory	Anti-inflammatory
Microglia soluble factors	TNF, IFN γ , IL-1 β , CXCL1,2,12, CCL2,5,10,19, Glutamate, NO, ATP, MMPs, Complements, Heat-shock proteins	IL-4, IL-10, IFN β , TGF- β , BDNF, GDNF, TIMPs
Microglia membrane proteins	TLRs, RAGE, LFA-1, MAC-1, FcR β , NCAM	CD45, CD91, CD200R, CD172a, CX3CR1, TREM-2, FasL, Fas
Astrocytes soluble factors	TNF, IFN γ , IL-1 β , CXCL1, 2,12, CCL2,5,10,19, Glutamate, NO, ATP, MMPs, Complements, HMGB1, heat-shock proteins	IL-4, IL-10, IFN β , TGF- β , Proteoglycans, BDNF, GDNF, TIMPs
Astrocytes membrane proteins	TLRs, RAGE, ICAM-1	FasL, Complement inhibitors
Neuronal soluble factors	CXCL10, CCL21, Glutamate, Dopamine, NO, ATP, Substance-P, MMPs, HMGB1, heat-shock proteins	TGF- β , CX3CL1, GABA, VIP, Proteoglycans, NGF, BDNF, NT3, GDNF, CNTF
Neuronal membrane proteins	TLRs	CD22, CD47, CD200, ICAM-5, FasL

Table 2: Soluble factors and membrane proteins expressed by microglia, astrocytes and neurons and their pro- or anti-inflammatory properties (adapted Tian *et al.*, 2012).

4.2.1. Cellular interactions

Neurons possess several membrane molecules to control local immune functions by targeting local immune cells such as microglia, astrocytes and peripheral immune cells, which are present in the CNS. Neurons might indirectly suppress T-cell activation by restricting antigen, presenting properties of glial cells, directly suppressing T-cell activation, favoring a Th2 profile or promoting apoptosis of activated microglia and T cells (Tian *et al.* 2012).

The microglia activation may be beneficial, deleterious or neutral. Neurons express cell surface glycoproteins (CD22, CD47, CD200, NCAM) (Table 1) to prevent microglia activation. A relationship between the nervous and the immune system has been studied this past decade. Indeed, glial cells (microglia and astrocytes) not only serve supportive and nutritive roles for neurons, but serve also to defend the CNS. An excessive and prolonged glial cells activation results in more severe and chronic neuronal damage, which leads to neuroinflammation and neurodegeneration.

The interaction in healthy CNS between neurons and astrocytes allows regulation of blood supply control, neurotransmission, synaptic formation and plasticity and metabolic support. In healthy CNS, neurons-microglia communication allows for debris clearance and immune surveillance. After a CNS injury, the balance is broken which gives way to excitotoxicity, glial scar and inflammatory damage.

4.2.2. Molecular interactions

The neuronal cell adhesion molecule (NCAM/CD56) is expressed on the surface of neurons, astrocytes and microglia (Chang, Hudson, Wilson, Liu, *et al.* 2000; Chang, Hudson, Wilson, Haddon, *et al.* 2000). NCAM is involved in cell-cell adhesion, synaptic plasticity, neurite outgrowth and others processes. The astrocytes-neuronal interactions via NCAM lead to the modulation of glial scar formation by the inhibition of astrocyte proliferation (Krushel *et al.* 1998). Furthermore, NCAM modulate microglial activation by decreasing TNF α and nitric oxide (NO) after glial stimulation with lipopolysaccharides (LPS) (Chang, Hudson, Wilson, Liu, *et al.* 2000; Chang, Hudson, Wilson, Haddon, *et al.* 2000).

CD200 (OX2) is an important molecule which contributes to the anti-inflammatory and regulatory environment (Table 2). CD200 expression has been detected in oligodendrocytes, reactive astrocytes and neurons, but not in astrocytes or microglia (Koning *et al.* 2009). Microglia possess CD200 receptors (CD200R), thus neuronal CD200 down-modulates the activation state of perivascular macrophages and microglia (Hoek *et al.* 2000). Defects in the CD200-CD200R pathway play a critical role in neurodegenerative disease development as Multiple sclerosis and Parkinson's disease (Koning *et al.* 2007; S. Zhang *et al.* 2011).

The expression of chemokine CX3CL1 (fractalkine) and its receptor CX3CR1 is limited to neurons and microglia (Hughes *et al.* 2002). Microglia are characterized by a prominent expression of the chemokine receptor CX3CR1. CX3CR1 is a conventional Gai-coupled seven transmembrane receptor. CX3CL1, the ligand of CX3CR1, is synthesized by a transmembrane protein with the CX3C chemokine domain displayed on an extended highly glycosylated, mucin-like stalk (Bazan *et al.* 1997). Under inflammatory processes, proteolytic cleavage of CX3CL1 occurs by disintegrin-like metalloproteinase ADAM 10 or 17 (Hundhausen *et al.* 2003; Garton *et al.* 2001) (Figure 8).

CX3CR1 receptor expression has also been demonstrated for an NK cell subset and certain T cell populations (Imai *et al.* 1997). Cocultures of neuron-microglia with CX3CL1 exposure reduced inflammatory neuronal death *in vitro* (Mizuno *et al.* 2003). A higher level of microglia activity was observed in mice with a CX3CR1 deficiency in three models of brain diseases, and this was also accompanied by increased neuronal vulnerability (Cardona *et al.* 2006). These studies have shown that in normal mice, neurotoxic microglia activity is suppressed by CX3CL1-CX3CR1 signaling.

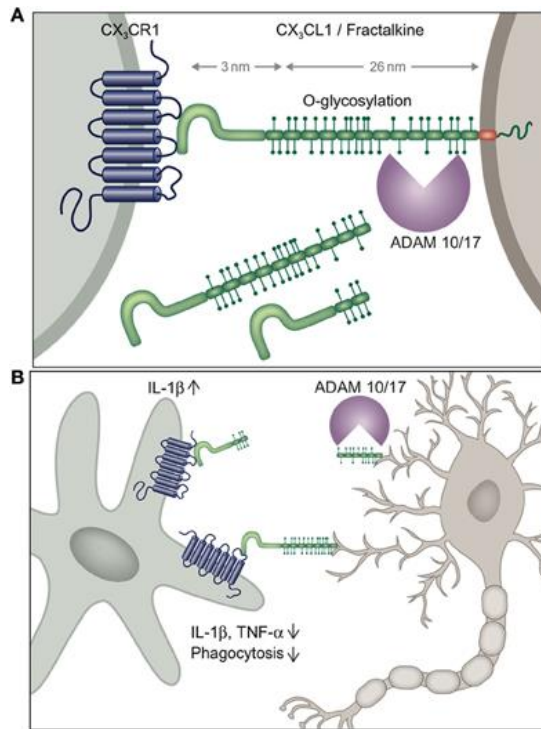


Figure 8: CX3CR1 receptor in microglia and its ligand CX3CL1 expressed by a neuron. A) Fractalkine composition and the proteo cleavage by ADAM10/17. B) Different effects of the cleavage of CX3CL1 on microglia activity (Wolf *et al.* 2013).

Neurons are able to control microglia with two types of signals; “On” or “Off” (Biber *et al.* 2007) (Table 3). Off signals (TGF- β , CD22, CX3CL1, neurotransmitters, CD20) are found in healthy conditions to maintain homeostasis and also restrict microglia activities under inflammatory conditions to prevent damage to healthy tissue. Conversely, “On” signals (CCL21, CXCL10, MMP3 (from apoptotic neurons)) are produced by damaged and impaired neurons to activate microglia (pro- or anti-inflammatory).

Neuron signals	Released signals	Membrane signals
Off signals	TGF- β , CD22, CX3CL1, neurotransmitters, NGF, BDNF, NT-3	CD200, CD22, CD47, CX3CL1?
On signals	CCL21, CXCL10, ATP, UTP, Glutamate, MMP3	TREM2 ligand

Table 3 : Neuron-mediated Off and On signals to modulate microglia activity (Adapted from Biber *et al.*, 2007).

4.3. T cells and innate immune cells

Lymphocytes represent the adaptive cellular arm of the immune system (Figure 9). Lymphocytic infiltration of the injury site occurs during the first week post-injury and is maintained chronically (Beck *et al.* 2010). Some lymphocytes can react with CNS proteins and the activation of CNS-reactive T cells leads to the demyelinating disorder in multiple sclerosis (Martin, McFarland, and McFarlin 1992). Popovich in 1996 demonstrated that CNS-reactive T cells are activated in SCI (P G Popovich, Stokes, and Whitacre 1996).

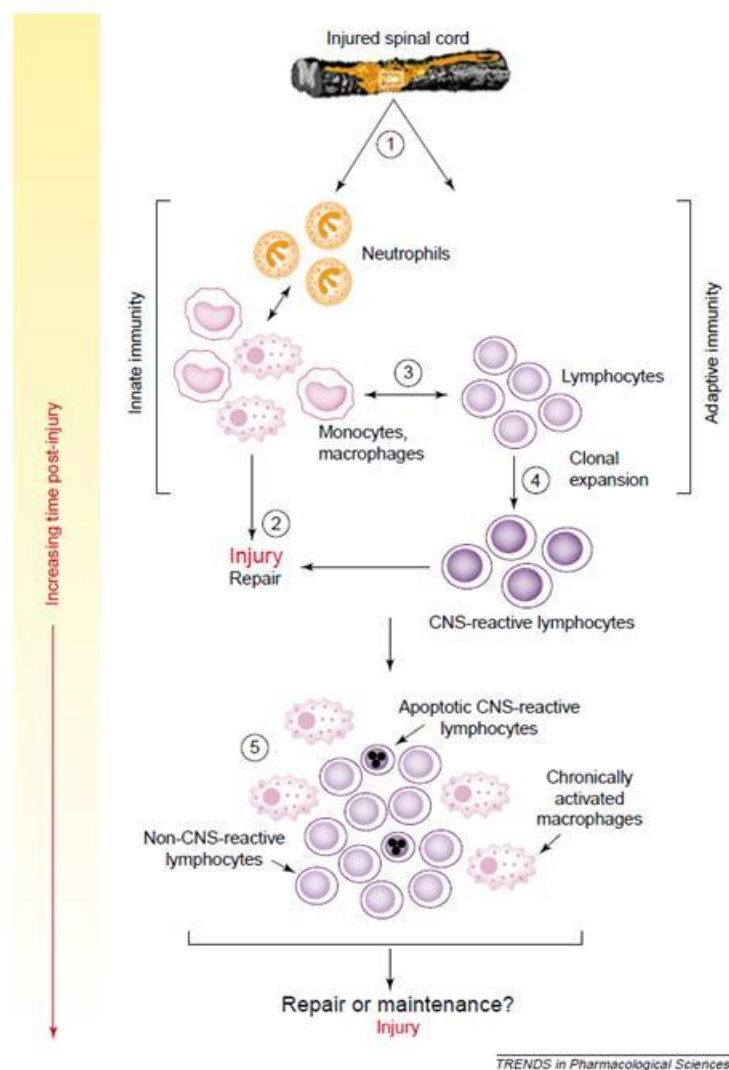


Figure 9: Recruitment of innate immune cells and adaptive immune cells after SCI and the progression to the chronic phase (Phillip G. Popovich and Jones 2003).

Lymphocytes respond to myelin protein after SCI and may contribute to post-traumatic secondary damages. However, there is increasing evidence that autoreactive T-lymphocytes may also convey neuroprotection and promote functional recovery after a CNS injury. Myelin basic protein (MBP)-reactive T cells are increased in SCI and stroke patients, which provides evidence of an association between CNS trauma and the activation of CNS reactive T cells (Kil *et al.* 1999).

In order to explain the effects of MBP-reactive T cells, Lewis rats and transgenic mice enriched in MBP-reactive T cells were used. These studies demonstrated that CNS-reactive T cells can exacerbate axonal injury, demyelination and functional loss after SCI (P G Popovich, Stokes, and Whitacre 1996; T. B. Jones *et al.* 2002). T-cells reactions against CNS proteins exacerbate acute tissue damage while simultaneously triggering the induction of chronic immunoregulatory networks. Surprisingly, autoimmune cells originally considered as pathogenic in autoimmune diseases were shown to be neuroprotective after CNS trauma. In contrast, several studies have suggested that T cells were beneficial to disease progression and survival after amyotrophic lateral sclerosis (Chiu *et al.* 2008; Beers *et al.* 2008). The presence of CD4+ T cells provides supportive neuroprotection by modulating the trophic/cytotoxic balance of glia. These contradictory results may be explained by the distinct roles of each T-lymphocyte subset.

5. Treatments for spinal cord injury

Spinal cord injuries induce several complications; patients suffer from motor and sensory impairments leading to complications in their lives. Over the last two decades, numerous clinical trials have been fully evaluated to restore damaged spinal cords. Despite broad research on animals, only few studies lead to pharmacological therapies due to the side effects that occur, or to the lack of regeneration or functional recovery. After SCI, many molecules are involved in motor and sensory dysfunction. Therefore, therapy should target several points, such as neuroprotection, plasticity, regeneration and replacement of lost cells (Figure 10).

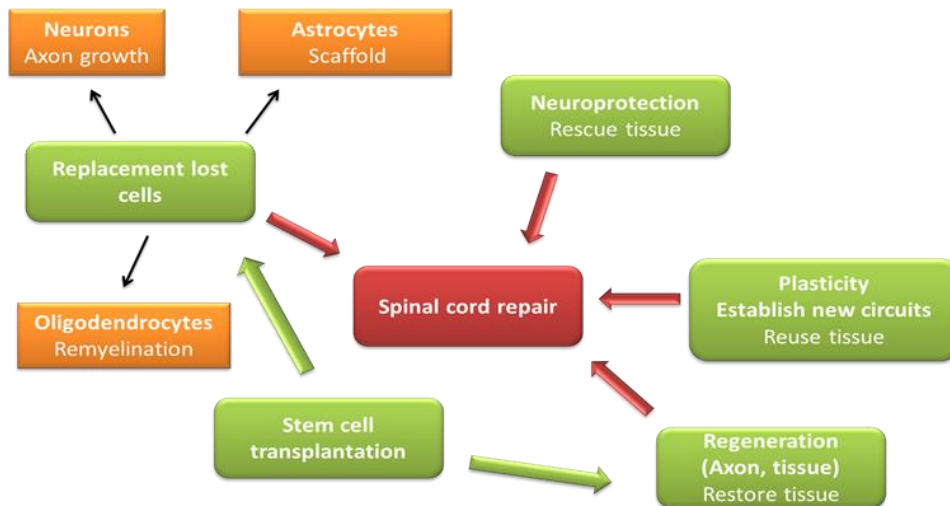


Figure 10: Several parameters are involved in spinal cord repair

Several molecules are studied for their various properties, such as neuroregeneration and the sprouting of spinal tracts (BDNF, GDNF, NT-3), remyelination (Withanoside IV, 4-Aminipyridine), antagonization of inhibitory factors from myelin or glial scar (Cethrin, Chondroitinase ABC, Y27632), protection of neuronal death, inhibition of inflammatory responses in the chronic phase (Minocycline, Estrogen, MPSS), plasticity: rewiring of propriospinal interneurons, and cells and tissue transplantation (OECs, BMSCs, Peripheral nerve cells, hNSCs, nerve grafts).

5.1. Myelin neurite growth inhibitors

Axonal regeneration is one of the important key factors after SCI. Three criteria bring out the crucial role of myelin-associated neurite growth inhibitors in preventing CNS regeneration. The depletion of oligodendrocytes and myelin enhances the regeneration of descending tracts in the differentiated spinal cord of rats (M E Schwab and Bartholdi 1996). Antibodies against Nogo-A enhance regenerative sprouting and long distance elongation (Schnell and Schwab 1990). Finally, the autoimmunization of rats with myelin or spinal cord homogenates allows for regenerative sprouting and axonal growth after SCI (D. W. Huang *et al.* 1999).

Nogo (Martin E Schwab 2004), myelin associated glycoprotein (MAG, (McKerracher *et al.* 1994)) and oligodendrocyte myelin glycoprotein (OMgp, (K. C. Wang *et al.* 2002)) are all neurite growth inhibitory components found in white matter of the CNS. Nogo-A is

principally expressed by CNS oligodendrocytes, whereas Nogo-B is expressed in the central and peripheral nervous system and other peripheral tissues and Nogo-C is found in muscle. By binding to an axonal Nogo-66 receptor (NgR) protein, Nogo, MAG and OMgp cause the collapse of axonal growth cones and stop axonal extension (McKerracher *et al.* 1994; M. S. Chen, Huber, van der Haar, *et al.* 2000; K. C. Wang *et al.* 2002). Diverse studies have used peptides that competitively inhibit Nogo-66 interaction with NgR (S. Li and Strittmatter 2003), anti-Nogo-A antibodies (Schnell and Schwab 1990) and soluble ectodomain fragments of the NgR (Fournier *et al.* 2002). P-75, the receptor for nerve growth factor (NGF), may act as a signal transducing subunit. Nogo-A can interact with different receptors such as nogo-A receptors, NgR, p75 and is similar for MAG and OMgp (Figure 11). Both calcium and RhoA/Rho kinase (ROCK) pathway are linked with Nogo (Bandtlow *et al.* 1993; Fournier, Takizawa, and Strittmatter 2003). The inhibition of one of these components has been shown to prevent myelin and Nogo-A induced growth cone collapse and growth inhibition (Niederost *et al.* 2002).

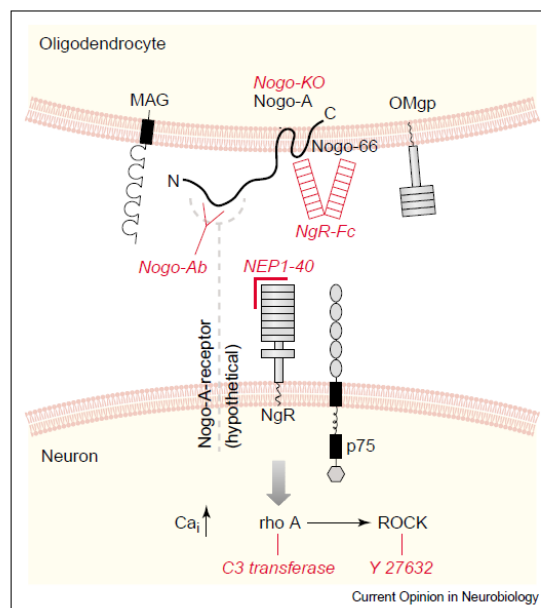


Figure 11: Myelin neurite growth inhibitors Nogo-A, MAG and OMgp and their different receptors NgR, p75. Inhibition of Nogo-A is possible by the different processes in red (Martin E Schwab 2004).

The inhibition effects of Nogo can be prevented by using antibodies against Nogo-A, Nogo gene deletions, soluble NgR fragments, NgR blocking peptides, inhibition of Rho-A,

inhibition of the intracellular calcium rise or through a high concentration of cAMP (Figure 11). Deleting one of the three major myelin inhibitors *i.e.* Nogo, Mag or OMgp, results in an enhancement of corticospinal sprouting in mice. However, no behavioral improvements or synergistic effects occur after the deletion of these three molecules (J. K. Lee *et al.* 2010). This study shows that even if these molecules are involved in axonal growth inhibition and their inhibition allows axonal sprouting, they do not play a central role in CNS injury, and these inhibitors should be used in combination with other drugs or molecules.

A study by David and Aguayo in 1981 showed that components of the CNS environment must inhibit axonal regrowth after injury, and that CNS neurons have the capacity to regenerate their disrupted axons (S David and Aguayo 1981). Two molecules that have reached clinical trials (to inhibit Nogo) are ATI-355 and Cethrin. Oligodendrocytes and their myelin membranes have been demonstrated to be major inhibitors of axonal growth in the CNS (Caroni, Savio, and Schwab 1988; Caroni and Schwab 1988). Caroni and Schwab developed a monoclonal antibody IN-1, after the biochemical separation 35- and 250 kDa inhibitory fraction within CNS myelin (NI-35 and NI-250). This antibody has proven to be effective *in vivo* in rodents, as revealed by axonal sprouting and corticospinal axonal regeneration within the mammalian CNS (Schnell and Schwab 1990). This treatment has also shown some improvement in locomotion, rope climbing and food pellet reaching (Bregman *et al.* 1995; Merkler *et al.* 2001). The target antigen of an IN-1 antibody was analyzed by Spillmann *et al.*, 1998, which is known as Nogo (M. S. Chen, Huber, Van der Haar, *et al.* 2000; GrandPré *et al.* 2000).

The human anti-Nogo antibody (ATI-335) has been shown to promote axonal sprouting and functional recovery following SCI in animal models, including in primates (Freund *et al.* 2006). In May 2006, a human phase I clinical trial was initiated by Novartis in Europe to assess the safety, feasibility and pharmacokinetics of this antibody in patients with complete SCI between C5 and T12, who were 4-14 days post injury. Neutropenia was reported as a severe adverse effect associated with this therapy.

The three myelin inhibitors are known to signal via the activation of the guanosine triphosphate Rho. After activation, Rho binds to Rho kinase (ROCK), a key regulator of axonal growth cone dynamic and cellular apoptosis. C3 transferase, a toxin produced by *Clostridium botulinum*, is a specific inhibitor of Rho. This inhibition is due to the ADP-ribosylation on

asparagines 41 in the effector binding domain of the GTPase interruption of this final common pathway, Rho-ROCK. This thus has the potential to be more potent than efforts to antagonize any single myelin inhibitor. Axonal growth and functional recovery is facilitated by this inhibitor in the mouse model (Dergham *et al.* 2002). Another study of Dubreuil *et al.*, in 2003 demonstrated a reduction in p75-dependent apoptosis in association with their therapy.

McKerracher's group created a recombinant version incorporating a transport sequence to improve cellular permeability. This protein, called BA-210, was commercialized by BioAxone Therapeutic and brought for clinical trial. In the human application, BA-210 is mixed with Tisseal (the combination being called Cethrin), which is applied to the dura at the time of spinal decompression. A phase I/IIa multicenter dose escalation trial in humans was initiated at the University of Toronto. No significant adverse effects were reported with the administration of Cethrin. More importantly, a 27% conversion rate from ASIA Grade A to B, C or D was observed (Fehlings *et al.* 2011).

5.2. Proteoglycan inhibitor

Chondroitin sulfate proteoglycans (CSPGs) are a family of macromolecules consisting of a core protein and one or more covalently attached glycosaminoglycans (GAG). CSPGs are present in glial scar after injury (Fawcett and Asher 1999). CSPGs represent an inhibitory extracellular matrix for axonal growth *in vitro* (McKeon *et al.* 1991; Smith-thomas *et al.* 1994), as well as *in vivo*, and are especially secreted by astrocytes. It is known that CSPGs activate the Rho-Rho kinase pathway, leading to the suppression of axonal growth (Borisoff *et al.* 2003). Chondroitinase ABC, a bacterial enzyme, is able to degrade the CSPGs.

An intrathecal treatment at the injury site allows for an upregulation of regeneration associated proteins in injured neurons and for the promotion of regeneration of both ascending sensory projection and descending corticospinal tract axons (Bradbury *et al.* 2002). Post synaptic activity below the lesion is also restored after ChABC. All of these data have shown that CSPGs are important inhibitory molecules *in vivo*. A study SCI in cats showed that intraspinal cleavage of CSPGs can enhance functional recovery with sophisticated motor behaviors and axonal growth (Tester and Howland 2008). ChABC has been combined

experimentally with nerve or cellular transplantation (Fouad *et al.* 2005; Karimi-Abdolrezaee *et al.* 2010; Houle *et al.* 2006) and rehabilitation (García-Alías *et al.* 2009).

However, even if preclinical essays show evidence that ChABC is beneficial for CNS repair, many obstacles remain in terms of its clinical translation. The first one is the safety and immunogenicity of delivering a bacterial protein to human beings. The second is concerned with dose effects of the treatment, because since the enzymatic activity diminishes over time, multiple doses are required. This repeated administration increases the risk of infection. One study by Bartus *et al.*, 2014 showed that ChABC gene therapy promoted tissue repair and improved hind limb function and spinal conduction in SCI rats. A significant reduction of secondary injury pathology in adult rats after spinal cord contusion injury was observed with reduced cavitation and enhanced preservation of spinal neurons and axons 12 weeks post injury. The gene therapy allowed for a change in the immune response following SCI by increasing the presence of reparative M2 macrophages at the epicenter of the injury, which resulted in neuroprotection (Bartus *et al.* 2014).

Another glycosaminoglycan associated with the glial scar is keratan sulfate (KS). It is composed of repeating disaccharide units of galactose and N-acetylglucosamine (GlcNAc), where a C6 position of GlcNAc is always sulfated. By using mice deficient in N-acetylglucosamine 6-O-sulfotransferase-1 that lack 5D4-reactive KS in the CNS, (Ito *et al.* 2010), an investigation into the role of KS in functional recovery after contusion at thoracic level can be conducted. The level of CSPG and CD11b- positive inflammatory cells recruitment was similar in wild-type and deficient mice. However, motor function recovery and axonal regrowth of both the corticospinal and raphespinal tracts was significantly better in deficient mice. KS has a primordial role in functional disturbance after SCI.

5.3. Cellular therapy

5.3.1. Autologous Schwann cell transplantation

An inhibitory environment is present after injury. One approach is to replace the negative environment by a permissive environment. Schwann cell transplantation emerged to be a candidate for supporting axonal regeneration after SCI. Schwann cell transplantation

research is studied by the Miami Project to Cure Paralysis (Bunge and Wood 2012). Schwann cells support and encourage the growth of new axons and they also repair myelination. Phase 1 trial of autologous Schwann cells for SCI is underway (Guest *et al.* 2013). After nerve injury, nerves are able to recover spontaneously. However, if a graft is depleted of Schwann cells by freezing, then the graft did not support CNS axonal growth, and so viable Schwann cells are essential (Smith and Stevenson 1988). The suspension of Schwann cells cultured from peripheral nerve biopsies can be delivered with less surgical spinal tissue manipulation and has several advantages. Schwann cells can be highly characterized by their phenotype markers, purified to remove fibroblasts, and expanded exponentially to provide the large cell numbers that are necessary for adequate engraftment in SCI. Schwann cells can form bridging tissue and fill the injury region.

5.3.2. Olfactory ensheathing cells (OECs)

OECs are specialized glial cells of the olfactory system. The OECs allow regenerating axons of olfactory receptor neurons from the PNS of the nasal epithelium to the CNS of the olfactory bulb. Several preclinical studies have shown the potential of OECs as a promising cell type for SCI (Y. Li *et al.* 1997; Raisman *et al.* 2012). The main benefits involve the modulation of reactive astrocytes and the reduction of proteoglycan expression, the promotion of neo-angiogenesis, and the release of neurotrophic factors by transplanted OECs. They also promote axonal regeneration after SCI, collateral sprouting and remyelination. A recent study showed the dangers of transplantation with inadequate monitoring and follow-up when a woman who received an autograft of nasal epithelium developed a painful intramedullary mass that required resection 8 years after transplantation (Dlouhy *et al.* 2014), but the transplant was not purified OECs.

Purified OECs were grafted into SCI dogs (Granger *et al.* 2012) with no voluntary locomotion. Human OECs can be autologously isolated and purified and safely transplanted into a human spinal cord as was shown in a 2013 phase 1 clinical trial (Tabakow *et al.* 2013). This group has published a study of one patient with complete transaction SCI and reported functional repair following OEC transplantation combined with peripheral nerve bridges (Tabakow *et al.* 2014).

5.3.3. Human embryonic stem cells, induced pluripotent stem cells

Stem cells are widely studied for their regenerative properties in medicine. Stem cells might bridge the lesion site, produce growth promoting factors and replace lost neurons, glia and other cells. Human embryonic stem cells (hESCs) and human induced pluripotent stem cells (iPSCs) are considered as a renewable source of cells for regenerative medicine because of their potential to differentiate into all cell types found in the adult human body. hESCs are derived from the inner cell mass of developing embryos, whereas hiPSCs are reprogrammed from somatic cells. Several characteristics are common between hiPSCs and hESCs, such as their morphology, expression of pluripotency markers and their ability to differentiate into definitive cell lineage. The first study in rats with transplantation after 10 months post injury with hESC derived oligodendrocyte precursors cells has shown no improvement in functional recovery compared to early injection 7 days post injury, where remyelination and improvement of locomotor ability were observed (Keirstead *et al.* 2005). The second study with human fetal brain neural stem cell transplantation at 30 days after injury reported an improvement in locomotor recovery (Salazar *et al.* 2010).

5.3.4. Neural stem cells

Numerous studies have demonstrated the ability of human neural progenitor cells (NPCs) to promote functional recovery. NPCs derived from human embryonic and induced pluripotent stem cells have shown efficacy (Fujimomto *et al.* 2012). Using iPSCs, ethics points and host immune rejection are limited making these cells ideal resources for transplantation therapy. Neural stem cells have the capacity to self-renew and produce the 3 major cell types of the CNS. Reynolds in 1992 demonstrated that cells could be isolated from the CNS of adult and embryonic mice. In the presence of the EGF, they proliferate to large spheres of cells termed “neurospheres” (Reynolds *et al.* 1992). Neurospheres contain stem cells and progenitor cells with the ability to differentiate into astrocytes, oligodendrocytes and neurons (Reynolds and Weiss 1992). Stem cell mediated repair of the spinal cord is studied by transplanting neural stem cells isolated from the spinal cord of rats or human being into rats with complete transaction SCI (Lu *et al.* 2012). Neural stem cells were co-grafted in a supportive fibrin matrix containing a growth factor cocktail. Axons grew a remarkably long distance (1-2mm per day), and they even grew through inhibitory environments to form connections with host axons. NSC

grafts demonstrated an improvement on hind limb recovery. Three months after the C5 lateral hemisection, iPSCs survived and differentiated into neurons and glia. Several axonal outgrowths and synapses were observed (Lu *et al.* 2014). The first phase I safety trial was approved in 2009 by the FDA for the direct intraspinal transplantation of NSC into patients with amyotrophic lateral sclerosis (Boulis *et al.* 2011).

5.3.5. Bone marrow stromal cells (BMSCs)

BMSCs are non-hematopoietic multipotent progenitor cells with a self-renewing capacity (Caplan 1991; Caplan 1994). In a physiological environment they provide support for developing hematopoietic cells by producing erythropoietin (EPO) and granulocyte-colony stimulating factor (G-CSF). They can differentiate into cells of mesodermal lineage, such as adipocytes, osteocytes, chondrocytes and also cells of other embryonic lineages (Figure 12).

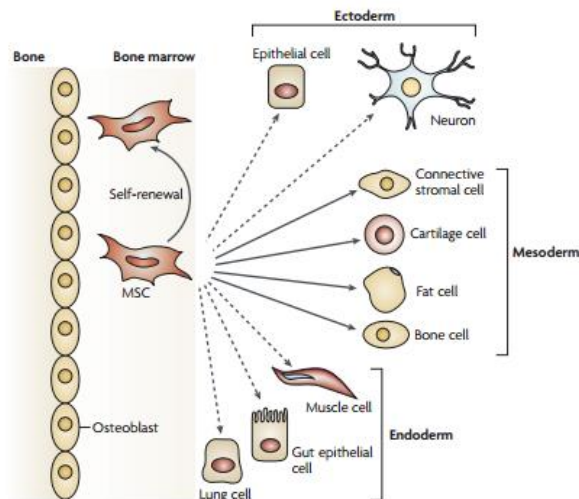


Figure 12: The multi-potentiality of MSCs (Uccelli et al. 2008).

BMSCs have potent immunomodulatory and anti-inflammatory effects. Immunomodulatory effects were described following the observation that BMSCs suppressed T-cell proliferation (Bartholomew *et al.* 2002). BMSCs have the ability to migrate to the lesion site following intravascular or intrathecal administration. A study of Cizkova *et al.*, in 2011 compared the intrathecal administration of BMSCs with three daily injections (3, 4, 5 days or 7, 8, 9 days following SCI) to a single injection (3 or 7 days post injury) (Cížková *et al.* 2011). A non-significant improvement in function and a low survival of grafted BMSCs could be

observed in the rat treated with single injection at 3 or 7 days post injury. In contrast, rats treated with three daily injections 7, 8 and 9 days post SCI showed significantly higher motor function recovery 14-28 days post injury. However, even if cells are able to migrate and incorporate to the lesion site, only a limited number of surviving BMSCs was observed within the damaged white matter.

Recent studies showed that the transplantation of BMSCs in rats 9 days after complete transection elicits an influx and survival of local cells at the injury site. These cells support the axonal regeneration and remyelination after SCI (P. Ding *et al.* 2014). BMSCs have been shown to secrete several growth factors as brain-derived growth factors (BDNF), glial-derived neurotrophic factor (GDNF), vascular endothelial growth factor (VEGF), fibroblast growth factor 2 (FGF-2), nerve growth factor (NGF) and neurotrophin-3 (NT-3). These molecules have various effects. NGF and BDNF increase survival and decrease apoptotic death of neurons and oligodendrocytes. GDNF is involved in the rescue of motor neurons. FGF-2 positively affects tissue sparing and promotes neuronal survival and angiogenesis. VEGF is known to be an angiogenic factor effective in tissue preservation. These factors can also positively affect remyelination and axonal growth.

To improve BMSCs survival, biomaterials are used as scaffolds for BMSC transplants. The materials for transplantation can be hydrogels, fibronectin, agarose scaffolds, fibrin scaffolds or alginate supplemented with growth factors and survival factors.

5.4. Pharmacotherapy

5.4.1. Minocycline

Minocycline is a semi-synthetic tetracycline antibiotic used in dermatological treatment. This molecule has also demonstrated neuroprotective effects in animal models of stroke, Parkinson's disease, Huntington's disease and multiple sclerosis (Yong *et al.* 2004). Minocycline was selected for its multifunctional properties in the hope that it would target several mediators involved in SCI. This molecule is known to inhibit the expression and activity of several mediators of tissue injury, including inflammatory cytokines, free radicals and matrix metalloproteinases. Work from Wells *et al.*, 2003 showed that treatment with minocycline 1h

after injury resulted in an improvement of hindlimb function, a significant reduction of the lesion size and axonal sparing (Wells *et al.* 2003).

5.4.2. Withanoside IV

Withanoside IV is a constituent in Ashwagandha (roots of *Withaniasomnifera Dunal*), an Indian traditional herbal drug that allows for an improvement in locomotor functions in mice which were injured by a contusion at the thoracic level (Nakayama and Tohda 2007). The mice were treated with 10 μ mol/kg 1 hour after SCI and repeatedly administered every day for 21 days (orally) per os. The axonal density and astrocytes increased in the injured center during this treatment. In contrast, accumulated microglia cells were reduced in the lesion site.

5.4.3. Neuroimmunophilin ligand

FK506, an FDA-approved immunosuppressant macrolide drug that is isolated from the bacterium *Streptomyces tsukubaensis*, is used to prevent allograft rejection in organ transplantations. FK506 blocks the activation of calcineurin through the formation of complexes with immunophilins. FK506 binds to a different immunophilin than cyclosporine A (CsA), called FK506 binding protein (FKBP) (Powell and Zheng 2006). Furthermore, it has been demonstrated that the FK506-FKBP complex suppresses the activation of the calcineurin-dependent NF-AT pathway (Figure 13) and calcineurin-independent activation pathway for JNK and p38 (Matsuda *et al.* 2000; Vafadari *et al.* 2012).

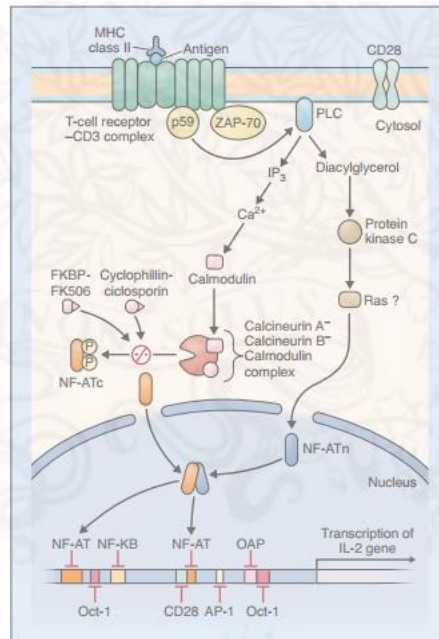


Figure 13: FK506-FKBP complex inhibits NF-AT pathway Elsevier Image 29832.

FK506 has been found to increase nerve regeneration and functional re-innervation after peripheral nerve injury and to prevent axonal damage in toxic neuropathies (Udina *et al.* 2002). FK506 also protects from secondary injury and enhances axonal sprouting and regeneration after SCI in rats (Madsen *et al.* 1998; M. S. Wang and Gold 1999).

In experimental autoimmune encephalomyelitis, FK506 protects against demyelination and axonal loss in the murine model (Gold and Zhong 2004). The timing and dosage administered varied a lot in spinal cord studies (Saganová *et al.* 2012). FK506 had a beneficial effect on the spinal cord parenchyma and axonal sparing rostrally to traumatic lesion. FK506, as a potent inhibitor of activation T-cells that also infiltrates the injured spinal cord, can modulate inflammation within the spinal cord and ameliorate neuroprotection through its immunosuppressive action on immune cells (D P Ankeny and Popovich 2009). The immunosuppressant action of FK506 was proven by the prevention of graft rejection following spinal cord ischemia and SCI (Marsala *et al.* 2004; D Cizkova *et al.* 2007).

5.4.4. Estrogen

Estrogen treatment reduced the COX-2 activity, blocked NF-kB translocation, prevented glial reactivity, attenuated neuron death, inhibited activation and activity of calpain

and caspase-3, decreased axonal damage, reduced myelin loss in the lesion, and improved locomotor function compared with vehicle-treated animals (Eric A Sribnick *et al.* 2010).

Microglia cells are involved in the activation of astrocytes and in the migration of peripheral immune cells in response to injury. Estrogen and estrogen receptor (ER) agonists are able to modulate the activation of many different cell types in the immune system (Straub 2007) and the CNS.

Sribnick's studies suggest that estrogen and ER agonists can protect neurons and inhibit axonal degeneration during the early phase (48h) following SCI in rats (Eric A Sribnick *et al.* 2005). Estrogen can suppresses the activation of microglia and recruits blood-derived monocytes in rat brains after LPS stimulation (Vegeto *et al.* 2003). Inhibition of pro-inflammatory cytokines such as IL-1 β and TNF- α by estrogen occurs in primary astrocytes following LPS exposure (Lewis *et al.* 2008). Estrogen is able to attenuate neuroinflammation and neurodegeneration by inhibiting microglia and astrocytes activation (Figure14).

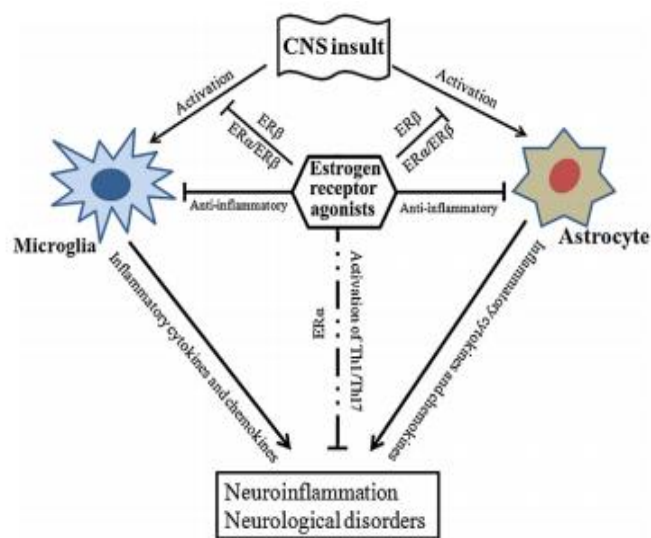


Figure 14: Anti-inflammatory role of estrogen and ER agonists in CNS disorders. Injuries of CNS induce activation of microglia and astrocytes which leads to neuroinflammation with the release of cytokines and chemokines pro-inflammatory. Estrogen and ER agonists induce anti-inflammatory effects and the activation of Th1/Th17 to block neuroinflammation (Chakrabarti *et al.* 2014).

CNS trauma -particularly SCI- is a complex injury associated with different neurodegenerative/regenerative/plasticity processes developed in time and in specific segments that need to be considered. Although many therapeutic strategies are evaluated and tested,

ranging from medical compounds (drugs) capable of blocking inflammation, enhancing axonal growth or treatments using stem cells or biomaterials, there is still no effective therapy available. Therefore, we need to study the spatial and temporal molecular environment after injury in order to distinguish the key factor in treating SCI.

6. Proteomics

The proteome refers to the entire set of proteins produced by an organism. The proteome is dynamic and interacts with the environment. Proteomic allows for the analysis of the total protein content of a cell or tissue in qualitative and quantitative ways during ongoing biological processes. Proteomics is highly used as an approach for biomarkers and therapeutic target discovery by following the type and the concentration of a proteins for a time period and looking at the correlation to healthy tissue. Proteomics take into account the abundance of proteins; proteins of interest are mostly rare compared to the predominant ones. At the beginning of proteomics, researchers focused on one or few proteins to identify quantify and characterize them by chromatography or electrophoresis. However, researchers needed to understand global biological process so laboratory techniques, statistical approaches and softwares were developed to analyze hundreds or thousands of proteins.

6.1. Proteomic approach

Mass spectrometry is becoming the most important of the proteomics technology. The introduction of soft ionization techniques such as matrix assisted laser desorption ionization (MALDI) (Karas *et al.* 1987) and electrospray ionization (ESI) (M. Yamashita and Fenn 1984) allows for the characterization of such biomolecules as proteins and peptides with greater sensitivity and speed than the older technology allowed for. ESI is an ideal ionization source due to its ability to produce multiple charged ions. It can also conveniently be coupled on-line with nano-liquid chromatography. Electrospray ionization with tandem mass spectrometry is one of the techniques used for protein identification.

Two major approaches are used in proteomic studies: the bottom-up (or shot-gun) approach and the top down approach (Figure 15).

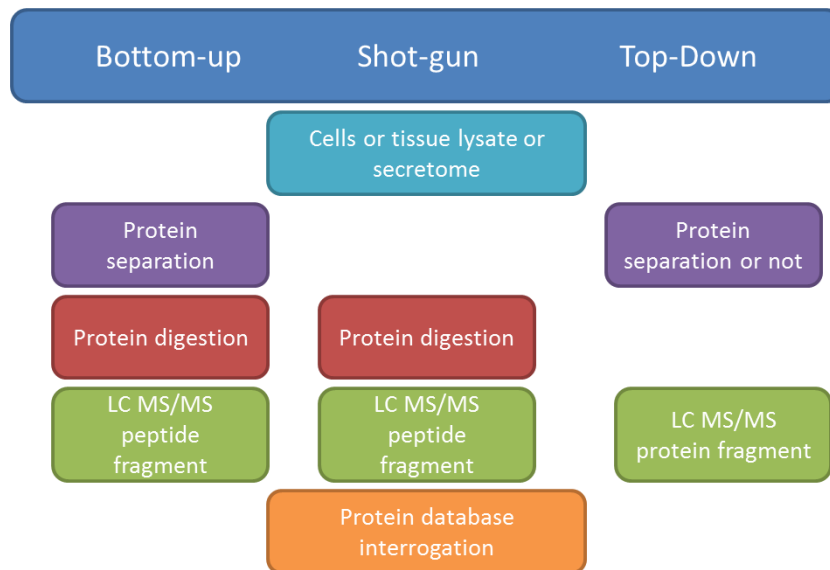


Figure 15: Proteomic strategies: the bottom-up, the shot-gun and the top-down approaches

The bottom-up approach consists of an enzymatic digestion of the biological sample to cleave at the define site in order to get a peptide mixture. This mixture will be analyzed by liquid chromatography coupled with a mass spectrometer. The second approach is the top-down strategy, where intact proteins are first separated using liquid chromatography (Y. Zhang *et al.* 2013).

Several groups studied SCI using 2-D separation, followed by MS/MS to identify proteins after SCI (S. K. Kang *et al.* 2006; Yan *et al.* 2010; Q. Ding *et al.* 2006). For example, Ding *et al.*, (2006) showed the up-regulation of 30 protein spots for whole tissue five days after SCI, which are involved in stress response, lipid and protein degeneration and neural survival and regeneration. They were also able to demonstrate the expression of 11-zinc finger protein and glypican, which may be involved in the neurite and regeneration inhibition. By analyzing tissues from the lesion site 24 hours after injury, Kang *et al.*, (2006) demonstrated an over-expression of 39 proteins such as neurofilament light chain, annexin 5, peripherin, apolipoprotein A and 21 proteins with an under-expression. Similarly, through the analysis of tissue from the lesion site, Yan *et al.*, (2010) described 31 proteins, such as heat shot protein (HSP70-1B) over-expressed at 1 day after SCI, septin-7 up-regulated up to day 5 after SCI. However, even if an in-gel based proteomic study was used, this approach has inherent limitations such as its low reproducibility, poor representation of low abundant proteins,

difficulty with highly acid or basic protein, over sized or hydrophobic proteins. In addition, the co-migration of different protein in the same spot renders the quantification inaccurate. Other studies analyze cerebrospinal fluid (CSF) from rat or human to highlight biomarkers. CSF analyses allow the creation of real time molecular pictures after SCI. Lubieniecka *et al.*, (2011) studied CSF from rats with the aim to find biomarkers of severity after a rat SCI. They identified 10 potential biomarkers by LC-MS/MS, and validated 3 of them by Western-blot: 14-3-3 protein zeta/delta (Ywhaz), Inter-alpha-trypsin inhibitor heavy chain H4 (Itih4), and Glutathione peroxidase 3 (Gpx3) (Lubieniecka *et al.* 2011). In 2014, Sengupta *et al.*, proceeded to proteomics of CSF from secondary phase SCI in humans over two time periods (1-8 days and 15-60 days) after injury. They identified 8 proteins which were differentially abundant among the 2 severity groups (Sengupta *et al.* 2014).

Taken together, all these proteomic studies did not take into account the spatial and temporal processes occurring in the time after SCI neither the cellular dynamic nor the plasticity occurring along the segments. Such information is necessary to better understand the molecular orchestra occurring during inflammation and the neurogenesis reexpression processes occurring after SCI and in time course of regeneration. These points are the main objectives of the thesis:

- To understand the biological processes occurring after a spinal cord injury from a spatial and temporal point of view during the first stage of the injury.
- To promote the regeneration, the neurite outgrowth and the modulation of the inflammation *in vitro* by modulating inflammation
- To stimulate *in vivo* the regeneration process and spinal cord plasticity

PART 1: SPATIAL AND TEMPORAL ANALYSES AFTER SPINAL CORD INJURY

CHAPTER 1: Spatial and temporal analyses after spinal cord injury

One of the major events at the beginning of the SCI is the development of an acute inflammatory process characterized by fluid accumulation and the recruitment of immune cells and microglia. Microglial cells normally function as sentinel immune cells regulating tissue homeostasis in the adult central nervous system (CNS) and participate in pathological processes, orchestrating tissue remodeling. Their functions appear to be complex as they exhibit both neuroprotective and neurotoxic effects. When the CNS is injured or affected by diseases, the resident ramified microglia morphologically transform into activated microglia” or “reactive microglia” with retracted processes and enlarged cell bodies, accumulate at the affected site and release various bioactive substances. Some are cytotoxic or pro-inflammatory and others may aid survival and regeneration. In fact, macrophages are divided in two sub-populations *i.e.* the macrophages M1 and M2 type. The M1 macrophages type produces some pro-inflammatory mediators like TNF- α and nitric oxide (NO), whereas the M2 modulate the immune response through IL-10, IL-4 and IL-13 and is involved in tissues repair. Two sub-populations of monocytes also exist *i.e.* which can be discriminated at the transcriptomic level by the presence of NOS2, CIITA, IL12, IL6 over-expressed genes for M1 cells or CX3CR1, arginase 1, CD206, Ym1, Fizz1 genes for M2 cells. The M1 population is involved in inflammatory response whereas the M2 plays a role in the neuron-glia cross-talk and maintains the microglial cells in physiological conditions to interact with neurons through the fractalkine linker. This data suggests the existence of a sub-population of microglial cells, one sharing a proinflammatory role and another one with an anti-inflammatory function, explaining the balancing effects of these cells when damage occurs. This is the reason why we will focus our attention on these cells during SCI. Thus, in order to understand molecular and cellular events occurring both spatially and temporally, proteomic approaches were undertaken in both tissue and secretome levels 3, 7 and 10 days after SCI at the lesion site and from the rostral to the caudal parts in order to determine the inflammatory profil (Articles 1 & 2).

In this context, we established for the first time that molecular and cellular processes occurring after SCI are altered between the lesion proximity, *i.e.*, rostral and caudal segments

nearby the lesion (R1-C1) whereas segments distant from R1-C1, *i.e.*, R2-C2 and R3-C3 levels co-expressed factors implicated in neurogenesis. M2 orientated factors secretion such as CCL20 or CCL22 are produced 3 days after SCI in both R1 and L segments except in C1 segment, where M1 immune factors (IL6, TNF α , IFN γ , IL15), neurite outgrowth inhibitors in particular brevican, versican, neurocan, aggrecan, which act as scavengers, but also as immunoglobulins (IgG2a, IgH γ 3), or Ras homolog gene family, member A (RhoA) are over-expressed. These results are in line with a quantitative study of the spatial and temporal *in vivo* analysis of immune cells in after SCI. We confirmed that microglia cells with neutrophils are the first ones recruited at the lesion site. Three days after SCI, microglia, neutrophils and macrophages cells are distributed along in both segments surrounding the SCI, whereas T regulator cells are only detected in R1 (FoxP3+) 3 days after SCI at 7 days after in C1, the number of immune cells diminished in both segments, except in C1. Thus, a delay in T regulators recruitment between R1 and C1 favors discrepancies between the two segments. Moreover, the presence of immunoglobulins (IgGs) in neurons at the lesion site at 3 days, validated by mass spectrometry, may present additional factors that contribute to limited regeneration. Treatment *in vivo* with anti-CD20 one hour after SCI did not improve locomotor function and decreased IgGs expression. Tests of collected secretome from each spinal segment *in vitro*, on microglial BV2 cell lines and DRGs explants, confirmed a lesion site-dependent impact on microglia activation and DRGs neurite outgrowth. In addition, while naive BV2 cells exhibited insignificant staining for CX3CR1 receptor, the level of CX3CR1 was strongly enhanced in some BV2 cells after their stimulation by secretome collected from SCI. The molecular data correlate to different polarization of activated microglia and macrophages along the rostro-caudal axis following acute injury. This was partially confirmed *in vivo* with CX3CR1 receptor, revealing higher expression in the R1, with potential neuroprotective action. In addition, the neurotrophic factors released from R1 and lesion segments enhanced outgrowth of DRGs explants. Taken together, we demonstrate that the C1 is the therapeutic target segment due to the fact that it presents all factors favoring the regeneration processes but inflammation occurring in this segment is deleterious and specific neurite outgrowth inhibitors (MEMO1, IgGs, Lectin proteins) are detected. This data is consequences of what's occurring at the tissue level. We thus established the presence of injury-induced gene transcription factors (TF) as well as several neurotrophic and synaptogenesis factors. It is well-known that the expression of

several TFs and co-factors changes after SCI. These play a role in orchestrating a regenerative cell body response. Activation of specific TF pathways is likely to be one of the first steps required to mount a cell-autonomous regenerative response and secreted factor in time course after SCI and reflects the specificity of TF pathways selected activation and synchronization.

Article 1: Alterations of protein composition along the rostro-caudal axis after spinal cord injury: proteomic, *in vitro* and *in vivo* analyses

Authors: Dasa Cizkova, Françoise Le Marrec-Croq, Julien Franck, Lucia Slovinska, Ivana Grulova, Stéphanie Devaux, Christophe Lefebvre, Isabelle Fournier, Michel Salzet

Article Status: published in *Frontiers in cellular neuroscience*, 8: 105, 2014

Summary: Proteomic experiments and procedures were realized by Ms Devaux. She participated in the writing of the manuscript and in the revision.



Alterations of protein composition along the rostro-caudal axis after spinal cord injury: proteomic, *in vitro* and *in vivo* analyses

Dasa Cizkova^{1,2†}, Françoise Le Marrec-Croq^{1†}, Julien Franck², Lucia Slovinska¹, Ivana Grulova², Stéphanie Devaux¹, Christophe Lefebvre¹, Isabelle Fournier¹ and Michel Salzet^{1*}

¹ Laboratoire de Spectrométrie de Masse Biologique Fondamentale et Appliquée, EA 4550, FRE CNRS 3637, Université Lille 1, Villeneuve d'Ascq, France

² Laboratory of Cell and Tissue Culture, Institute of Neurobiology, Center of Excellence for Brain Research, Slovak Academy of Sciences, Košice, Slovakia

Edited by:

Dirk M. Hermann, University Hospital Essen, Germany

Reviewed by:

Stefano Pluchino, University of Cambridge, UK

Andrew Chan, Ruhr University Bochum, Germany

*Correspondence:

Michel Salzet, Laboratoire de Spectrométrie de Masse Biologique Fondamentale et Appliquée, EA 4550, FRE CNRS 3637, Université Lille Nord de France, Université de Lille 1, Bât SN3, 1er étage, F-59655 Villeneuve d'Ascq, France
e-mail: michel.salzet@univ-lille1.fr

[†] These authors have contributed equally to this work.

Based on proteomic analyses we investigated the differences of released molecules in the conditioned media (CM) from the spinal cord central lesion and adjacent rostral and caudal segments at 3, 7, and 10 days after spinal cord injury (SCI), in order to specify the molecular environment within greater extent of tissue damage. Proteins found in CM were analyzed by shot-gun MS using nanoLC coupled to an orbitrap. The results showed some specific proteins at each site of the lesion at 3 days. Among the proteins from rostral and lesion segments, some are related to chemokines, cytokines or to neurogenesis factors. In contrast, proteins from caudal segments are more related to necrosis factors. The CM from each spinal segment were used *in vitro*, on microglial BV2 cell lines and DRGs explants, showing a lesion site-dependent impact on microglia activation and DRGs neurite outgrowth. In addition, while naive BV2 cells exhibited insignificant staining for CX3CR1 receptor, the level of CX3CR1 was strongly enhanced in some BV2 cells after their stimulation by CM collected from SCI. The molecular data might correlate with different polarization of activated microglia and macrophages along the rostro-caudal axis following acute injury. This was partially confirmed *in vivo* with CX3CR1 receptor, revealing higher expression in the rostral segment, with potential neuroprotective action. In addition, the neurotrophic factors released from rostral and lesion segments enhanced outgrowth of DRGs explants. Taken together these data suggest that regionalization in terms of inflammatory and neurotrophic responses may occur between rostral and caudal segments in acute SCI.

Keywords: microglia, proteomic analysis, inflammation, spinal cord injuries, dorsal root ganglion, chemokines, neurotrophic, secreted protein

INTRODUCTION

Spinal cord injury (SCI) represents one of the most devastating forms of trauma, often leading to permanent spastic paralysis in humans (Beattie et al., 2002). After initial primary injury caused by direct mechanical insult, the spinal cord tissue progressively undergoes pathological changes that are associated with secondary damage affecting intact, neighboring tissue (Tator, 1995; Schwab and Bartholdi, 1996). One of the key events of secondary processes is related to the development of acute inflammation characterized by fluid accumulation (edema) and the recruitment of immune cells (neutrophils, T-cells, macrophages, and monocytes) (Schwab and Bartholdi, 1996; Schwartz et al., 1999). In fact, spinal cord microglial cells normally function as a kind of reactive immune cells that begin to respond to signals after pathological stimuli (injury, infection, or tumors) (Ransohoff et al., 2007) and are activated at the lesion epicenter (Kreutzberg, 1996).

Although, it has been suggested that microglia/macrophages can be polarized into M1-neurotoxic or M2-neuroprotective states, and produce a variety of cytokines, chemokines and neurotrophic factors, the mechanisms regulating microglial polarity remain unclear (Aguzzi et al., 2013). In this context recent studies

indicate that macrophages can alter their phenotypes and functions according to changes in the spinal cord microenvironment during sub-acute and chronic phase. Thus, SCI triggers excessive inflammatory response mediated by the invasion of predominantly M2 macrophages into and around the central lesion at sub-acute phase, but not at chronic phase that is involved in the formation of glial scar (Nishimura et al., 2013). These findings correlate with accumulated data pointing to a chronological time line expression of different degeneration and regeneration associated genes that are involved in the pathogenesis and endogenous repair or plasticity during days to months following SCI (Gerin et al., 2011). However, not only microglia/macrophages but also astrocytes, meningeal cells and fibroblasts together with the increased production of inhibitory chondroitin sulfate proteoglycans (CSPGs) are involved in the spinal cord pathogenesis (Fitch and Silver, 1997).

Moreover, it seems that complex changes in gene and protein expression as well as in cellular interactions are taking place not only at the central lesion, but also in adjacent segments (above and below central lesion). However, the exact mechanisms of the proteins involved during secondary damage, inflammation,

recruitment, and polarization of microglia, activation of astrocytes and glial scarring, remyelination, or axonal growth and plasticity, remain to be further explored. Thus, to better understand the secondary damage processes and plasticity, we used a reliable and reproducible balloon-compression technique to produce SCI (Vanicky et al., 2001). Sham operated vs. SCI rat spinal cord tissues were analyzed at 3 days post-lesion; when the polarization of microglia into M2 phenotype seems to transiently (3–7 days) dominate (Kigerl et al., 2009). The collection of tissues from epicenter and both adjacent segments above (rostral) and below (caudal) the lesion allowed to study released molecules.

We have taken advantages of proteomic technology to screen and identify peptides in each spinal cord segment-derived conditioned medium (CM), obtained *in vitro*, to better understand protein composition changes along the rostral-caudal axis after SCI with time (3, 7, 10 days). Afterwards, we have used these CM for *in vitro* tests investigating the BV2 cells activation by chemotaxis assay, western blot, and M1/M2 polarization through CX3CR1 and CD206 expression, based on immunocytochemistry *in vitro* and *in vivo*. Chemotaxis assays showed that BV2 cells were highly responsive to the CM derived from rostral and lesion segments, compared to CM from caudal site. Efficacy of neurotrophic factors released from rostral and lesion segments was confirmed on enhanced outgrowth of DRGs explants.

In summary we demonstrate that at 3 days after SCI, a clear regionalization occurs between the rostral and caudal axes, with expression of neurotrophic and immune modulatory factors in the rostral region, in contrast to inflammatory and apoptotic molecules in the caudal region.

EXPERIMENTAL PROCEDURES

CHEMICALS

All chemicals were of the highest purity obtainable. Water, formic acid (FA), trifluoroacetic acid (TFA), acetonitrile (ACN), and methanol (MeOH) were purchased from Biosolve B.V. (Valkenswaard, the Netherlands). Sequencing grade, modified porcine trypsin was purchased from Promega (Charbonnières, France).

ANIMALS

The study was performed with approval and in accordance to the guidelines of the Institutional Animal Care and Use Committee of the Slovak Academy of Sciences and with the European Communities Council Directive (2010/63/EU) regarding the use of animals in Research, Slovak Law for Animal Protection No. 377/2012 and 436/2012.

SPINAL CORD TRAUMA

The SCI was induced using the modified balloon compression technique in adult male Wistar rats ($n = 16$), according to our previous study (Vanicky et al., 2001). Manual bladder expression was required for 3–10 days after the injury. In the sham group (control, $n = 16$) a 2-French Fogarty catheter was inserted at the same level of spinal cord, but the balloon was not inflated and no lesion was made. SCI animals ($n = 16$) were divided in groups processed for immunohistochemistry ($n = 4$) and for CM production ($n = 12$) with corresponding sham-controls.

TISSUE PROCESSING AND IMMUNOHISTOCHEMISTRY

Rats following SCI ($n = 4$) and sham surgery ($n = 4$) at day 3 were deeply anesthetized and perfused transcardially with saline, followed by 4% paraformaldehyde (PFA) in 0.1M phosphate-buffered saline. Spinal cords were removed, post-fixed in 4% PFA, embedded in gelatin–egg albumin protein matrix (10% ovalbumin, 0.75% gelatin, glutaraldehyde) and soaked overnight in 30% sucrose. Each spinal cord was dissected into 1.0 cm blocks (lesion site, rostral, and caudal segments to the lesion) and 30- μ m thick transverse cryostat (Leica Instruments, Heidelberg, Germany) sections were cut serially (100 μ m interval) ($n = 60$ each segment) and standard immunohistochemistry (IHC) technique was performed. Tissue sections were incubated in the following primary antibodies: anti-Iba1 (a marker for microglia/macrophages, rabbit IgG, 1:1000; Wako Pure Chemical Industries, Osaka, Japan), anti-ED1 (a marker for monocytes, mouse IgG, 1:500; Chemicon, Millipore, Billerica, MA, USA), anti-CX3CR1 receptor and anti-CD206 (a marker for M2 phenotype, rabbit IgG, 1:100; Santa Cruz Biotechnology, Santa Cruz, CA, USA) that after wash in PBS was followed by secondary fluorescent antibodies: goat anti-rabbit IgG conjugated with Texas Red (Alexa Flour 594), goat anti-mouse IgG or goat anti-rabbit IgG conjugated with Oregon Green dye (Alexa Flour 488). Fluorescence conjugated secondary antibodies were purchased from Molecular Probes, Oregon, USA. Omission of the primary antibody served as the negative control. For nuclear staining, we used 4-6-diaminidino-2-phenylindol (DAPI) (1:200). Finally, sections were washed in 0.1M PBS, mounted, and cover slipped with Vectashield mounting medium (Vector Laboratories, Inc.) and observed under a fluorescence microscope (Nikon Eclipse Ti, Japan) and confocal laser scanning microscope (Leica TCS SP5 AOBs, Leica Microsystems, Mannheim, Germany).

IHC QUANTIFICATION

Quantificative analyses of immunofluorescence staining for Iba1, CX3CR1, and CD206 were performed on 8 sections/per animal (rostrally/caudally, $n = 4$ each; captured fluorescence digital images) at 40 \times magnification and were analyzed by Image J software according to the previous protocol (Jones et al., 2002). For each SCI and sham group we analyzed totally 32 transverse sections (Iba1+/CX3CR1+/CD206+ $n = 4$). In the monochrome 8-bit images we have determined the mean gray level number of black and white pixels within five identical sampling fields (250 \times 250 μ m) in following regions: gray matter (summary dorsal + ventral areas), white matter divided into Dorsal, Lateral and Ventral White Matter, and digitally subtracting a background image of a control section from each image. The threshold values were maintained at a constant level for all analyses.

COLLECTION OF CM FROM CONTROL AND LESIONED SPINAL CORD SEGMENTS

Experimental SCI rats ($n = 4$) at 3, 7, and 10 days and sham-operated-control rats ($n = 4$) were sacrificed by isoflurane anesthesia followed by decapitation. The spinal cord was pressure expressed by injecting sterile saline (10 ml) throughout the vertebrate canal, along the caudo-rostral axis. Each spinal cord was macroscopically observed and the central lesion distinguished at

the Th8-Th9 level. Samples (approximately 1.0 cm each) taken from the central lesion (Th7-Th11) rostral (Th2-Th6) and caudal (Th12-L3) segments to the site of injury were additionally chopped into 0.3 cm thick sections/3 per segment and deposited into a 12-well culture plate containing 1 ml DMEM without fetal calf serum (FCS). After 24 h incubation in a humidified atmosphere with 5% CO₂ at 37°C, 1 ml of SCI-derived conditioned media CM (CM-SCI) were collected (rostral, lesion, caudal segments) and centrifuged 30 min at 15,000 rpm at 4°C. The same procedure was performed for obtaining CM from sham spinal cord tissue. From the 1 ml stock 50 µL samples were then taken and subjected to trypsin digestion (24 h, 37°C) followed by desalting using C18 ziptips (Millipore). The solution was dried under vacuum and resuspended in water /5% acetonitrile /0.1% formic acid before injecting into nanoLC. Unused samples were stored at -80°C.

CHEMOTAXIS ASSAYS

The effects of CM obtained from control (CM CTR) or injured spinal cord (CM SCI) along the rostral (CM RSCI), lesion (CM LSCI) or caudal segments (CM CSCI) on microglial recruitment were determined using the Boyden chambers (Cell Biolabs, CytoSelect™ 96-Well Cell Migration Assay, 5 µm) (Smith et al., 2008). The BV2 cells (Species: mouse, C57BL/6; Tissue: brain, microglial cells) were purchased from the IRCCS Azienda Ospedaliera, Università San Martino (Italy) (Bocchini et al., 1992) and initially cultured in Roswell Park Memorial Institute (RPMI) 1640 medium supplemented with 10% FCS and 1% penicillin/streptomycin (P/S), and split twice a week to obtain a sufficient number of BV2 cells. Before experiment, cells were plated in Dulbecco's Modified Eagle's Medium (DMEM) with P/S (all reagents from Invitrogen). Replacement of RPMI with DMEM did not decrease the viability of BV2 cells nor changed their morphological pattern (data not shown). In the first experiment, BV2 cells at a concentration of 50,000 per insert were placed into the upper chamber while the CM from control and from different segments (rostral, lesion and caudal) of the injured spinal cord were filled into the lower one (1:3, CM: DMEM) and then cultured for 3 h. Prior to application, the CM from each spinal segment was centrifuged 10 min at 1500 rpm and sterilized with 0.22 µm filters. The protein concentration (2.15–2.8 µg/10 µl per each CM) was assessed by Bradford protein assay. ATP (10 µM) was used as positive control for microglial cell recruitment. The migrating BV2 cells were detected by Hoechst staining and the number of cells was counted on dissected membranes transferred on glass slides and mounted with Vectashield mounting medium (Vector Laboratories, Inc. on LinkedIn). Three different counts were performed under a Nikon Eclipse Ti microscope with motorized stage.

IMMUNOFLUORESCENCE ANALYSIS OF BV2 CELLS

For detection of CX3CR1 receptor, BV2 cells were grown on Poly-L-Ornithine-Coated Glass Coverslips in DMEM with 10% FBS, 1% P/S, for 24 h and then washed and treated with CM LSCI (1:3, CM LSCI:DMEM lacking FCS) or CM CTR, for 24 h BV2 cells were fixed with 4.0% paraformaldehyde, treated with 0.2% Triton X-100, and blocked with 2% normal goat serum (NGS,

Sigma-Aldrich). Afterwards, they were sequentially incubated with anti-CX3CR1 antibody (1:100, Santa Cruz, USA), followed by FITC-conjugated goat anti-rabbit IgG, and 4,6-diamidino-2 phenylindole (DAPI, Sigma-Aldrich, Germany) solution, and examined using a fluorescence and confocal microscope (Leica, Germany).

WESTERN BLOT ANALYSES

Western Blot analysis was carried out from BV2 cell extracts as previously described (Salzet et al., 1993). Blots were blocked with 5% milk in PBS for 45 min and incubated overnight at 4°C with a rabbit CX3CR1 antibody diluted 1/200. Detection was performed by enhanced chemiluminescence (Amersham, France) after 1h incubation with a peroxidase-conjugated secondary antibody (Aventis, Sanofi Pasteur, France) diluted at 1/20,000.

DORSAL ROOT GANGLION EXPLANTS

DRGs were isolated from the thoracic and lumbar spinal levels of a total of 3 Wistar rats (P2, $n = 50$). Under aseptic conditions, the DRG explants were prepared by trimming nerve roots using microsurgical scissors. Afterwards each explant was transferred to laminin pre-coated glass slides (0.1 mg/ml) in 12-well tissue culture plates (Costar, Corning, USA) with DMEM/F12 culture medium supplemented with: (i) CM CTR, (ii) CM RSCI segment, (iii) CM LSCI, (iv) CM CSCI (1:3, CM: DMEM) during 7 days *in vitro* (7DIV). Control DRGs neurite outgrowth was induced with DMEM-F12 containing epidermal growth factor (EGF) and basic fibroblast growth factor (bFGF) (20 ng/ml/ each factor, 1% B27, 0.5% N2) during 7DIV. For all DRGs we have used standard IHC procedures to visualize neurite outgrowth. Briefly, DRGs were incubated in mouse anti-Neuron-specific class III beta-tubulin (TUJ1) (1:200; Merck) for 24 h at 4°C. Afterwards, they were washed in 0.1 M PBS and incubated for 2 h with goat anti-mouse IgG (Alexa Flour 488). For nuclear staining, we used DAPI (1:200). Finally, they were mounted, and cover slipped with Vectashield mounting medium (Vector Laboratories, Inc.). Digitized images of DRGs/per treatment ($n = 6$) were captured and saved with NIS-Elements Ar Microscope Imaging Software (Nikon). The outgrowth of neurite was analyzed at identical sampling fields, for each CM experiment by Image J software according to the above mentioned method applied for primary antibodies quantification.

STATISTICAL ANALYSIS

All data are reported as the mean \pm s.e.m. One-Way ANOVA followed by the Tukey-Kramer test for multiple comparisons was used in the analyses of the Iba1+/CX3CR1+/CD206 in the spinal sections and for the chemotactic results. Repeated-measures Two-Way ANOVA followed by the Tukey-Kramer test was used for the DRGs/TUJ1+ neurite outgrowth analysis. Statistical significance was set at * $p < 0.05$; ** $p < 0.01$, *** $p < 0.001$.

PROTEOMIC STUDIES

Digestion of CM

Fifty µL of the solution of CM obtained from the control spinal cord and along the lesion or rostral and caudal segments after SCI were added to 20 µL of a solution of DTT (50 mM) in NH₄HCO₃ buffer (50 mM) (pH = 8) and heated for 15 min at 95°C. After

cooling, 20 μ L of a solution of IAA (100 mM) in NH_4HCO_3 buffer (50 mM) were added and the mixture was incubated for 15 min at room temperature in the dark. 10 μ L of a solution of trypsin (20 μ g/mL) in NH_4HCO_3 (50 mM) were then added and the sample was incubated overnight at 37°C.

Tissue protein extraction

Twenty μ m spinal cord tissue sections were mounted on a parafilm covered glass slide and the tissue was microdissected manually using a binocular. The pieces were extracted by incubating in 20 μ L of 50 mM bicarbonate buffer containing 50mM DTT and 1% SDS at 55°C for 15 min. The extracts were then loaded on 12% polyacrylamide gel and separated at 70V for 15 min and then 120V until the dye front reaches the other end of the gel. After migration, the gel was incubated in the gel fixative solution for 30 min and stained with colloidal Comassie brilliant blue overnight. The stain was removed by washing the gel four times with distilled deionized water.

In gel digestion

The gel was cut into ten pieces. Pieces were washed with 300 μ L of distilled deionized water for 15 min, 300 μ L of ACN for 15 min and 300 μ L of NH_4HCO_3 100mM (pH8) for 15 min. Then a mix of 300 μ L of NH_4HCO_3 /ACN (1:1, v/v) for 15 min and 300 μ L of ACN for 5 min. Band pieces were dried in a Speedvac for 5 min. The reduction of cystine residues was made with 50 μ L of 10 mM of DTT in NH_4HCO_3 100 mM (pH8). Pieces were incubated at 56°C for 1 h. Alkylation of cystine was made with 50 μ L of 50 mM of IAA in NH_4HCO_3 100 mM (pH8). Pieces were incubated at room temperature in the dark for 30 min. Band pieces were washed a second time with 300 μ L of NH_4HCO_3 100 mM (pH8) for 15 min. Then a mix of 300 μ L of NH_4HCO_3 /ACN (1:1, v/v) for 15 min and 300 μ L of ACN for 5 min. Band pieces were dried in a Speedvac for 5min. A digestion of band pieces was made with trypsin (12.5 μ g/mL) in NH_4HCO_3 20 mM (pH8), enough to cover pieces. Pieces were incubated at 37°C overnight. Peptides were extracted on shaking platform with 50 μ L of FA 1% two times for 20 min, then 150 μ L of ACN for 10 min. The supernatant was transferred in new tube and dried with Speedvac.

NanoLC-HR-MS/MS

Samples were separated by online reversed-phase chromatography using a Thermo Scientific Proxeon Easy-nLC system equipped with a Proxeon trap column (100 μ m ID \times 2 cm, Thermo Scientific) and a C18 packed-tip column (100 μ m ID \times 15 cm, Nikkyo Technos Co. Ltd.). Peptides were separated using an increasing amount of acetonitrile (5–40% over 110 min) at a flow rate of 300 nL/min. The LC eluent was electrosprayed directly from the analytical column and a voltage of 1.7 kV was applied via the liquid junction of the nanospray source. The chromatography system was coupled to a Thermo Scientific Orbitrap Elite mass spectrometer programmed to acquire in a data-dependent mode. The survey scans were acquired in the Orbitrap mass analyzer operated at 120,000 (FWHM) resolving power. A mass range of 400–2000 m/z and a target of 1E6 ions were used for the survey scans. Precursors observed with an intensity over 500 counts were selected “on the fly” for ion trap collision-induced dissociation (CID) fragmentation with an isolation window of 2 amu and

a normalized collision energy of 35%. A target of 5000 ions and a maximum injection time of 200 ms were used for CID MS² spectra. The method was set to analyze the 20 most intense ions from the survey scan and dynamic exclusion was enabled for 20 s.

Data analyses

Tandem mass spectra were processed with Thermo Scientific Proteome Discoverer software version 1.3. Resultant spectra were searched against the Swiss-Prot® *Rattus norvegicus* database (version January 2012) using the SEQUEST® algorithm. The search was performed choosing trypsin as the enzyme with two missed cleavages allowed. Precursor mass tolerance was 10 ppm, and fragment mass tolerance was 0.5 Da. N-terminal acetylation, methionine oxidation and arginine deamination were set as variable modifications. Peptide validation was performed with the Percolator algorithm. Peptides were filtered based on a *q*-Value below 0.01, which corresponds to a false discovery rate (FDR) of 1%.

Label free quantification with Scaffold 4 software

Scaffold (version Scaffold 4.0.6.1, Proteome Software Inc., Portland, OR) was used to validate MS/MS based peptide and protein identifications and label free quantification (Gstaiger and Aebersold, 2009). Peptide identifications were accepted if they could be established at greater than 50% probability by the Peptide Prophet algorithm (Keller et al., 2002) with Scaffold delta-mass correction. Protein identifications were accepted if they could be established at greater than 90% probability and contained at least 2 identified peptides. Protein probabilities were assigned by the Protein Prophet algorithm (Choi et al., 2008). Proteins that contained similar peptides and could not be differentiated based on MS/MS analysis alone were grouped to satisfy the principles of parsimony. Normalization was done on top 3 total ion current (TIC) in addition to spectral counting.

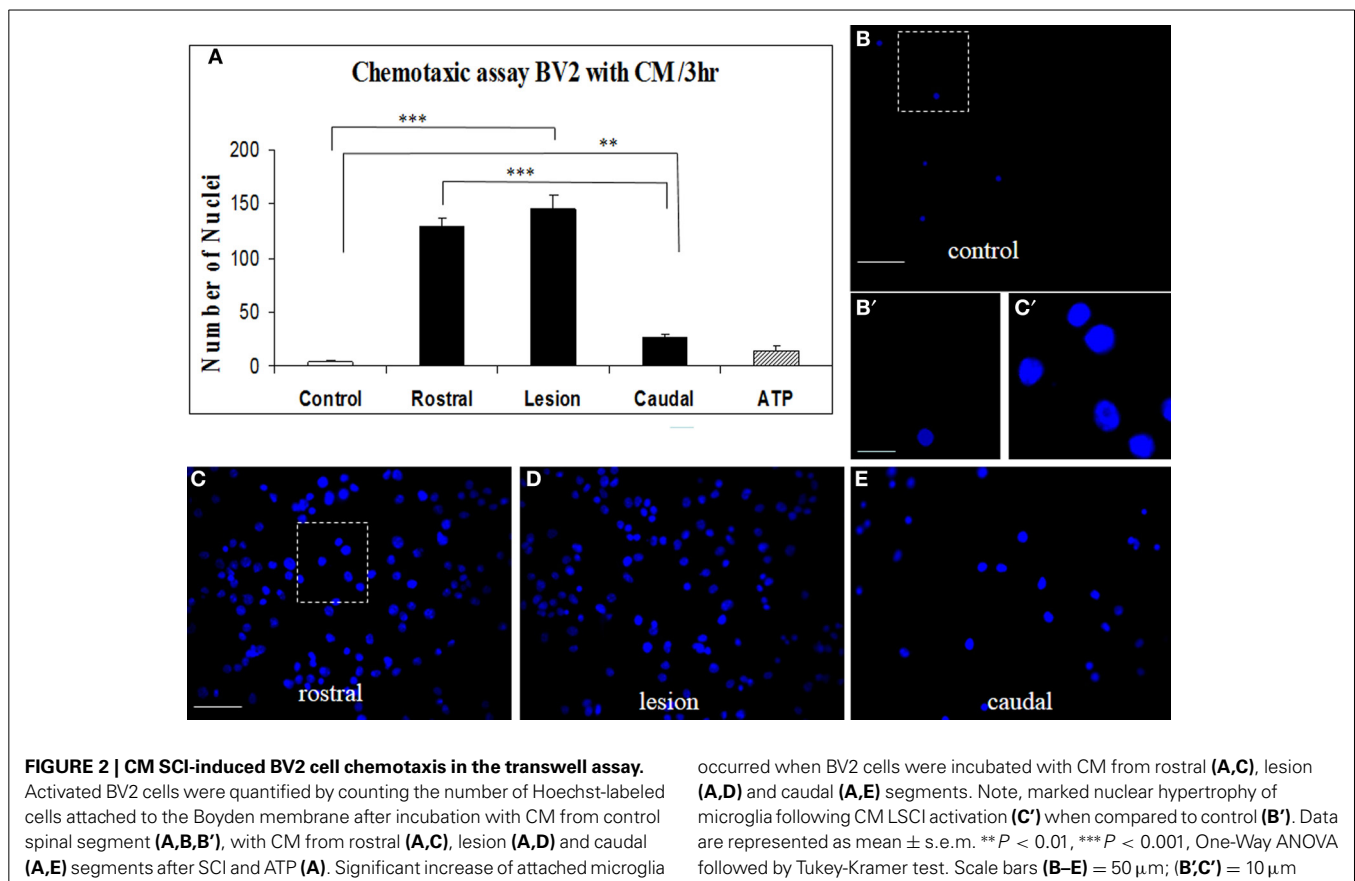
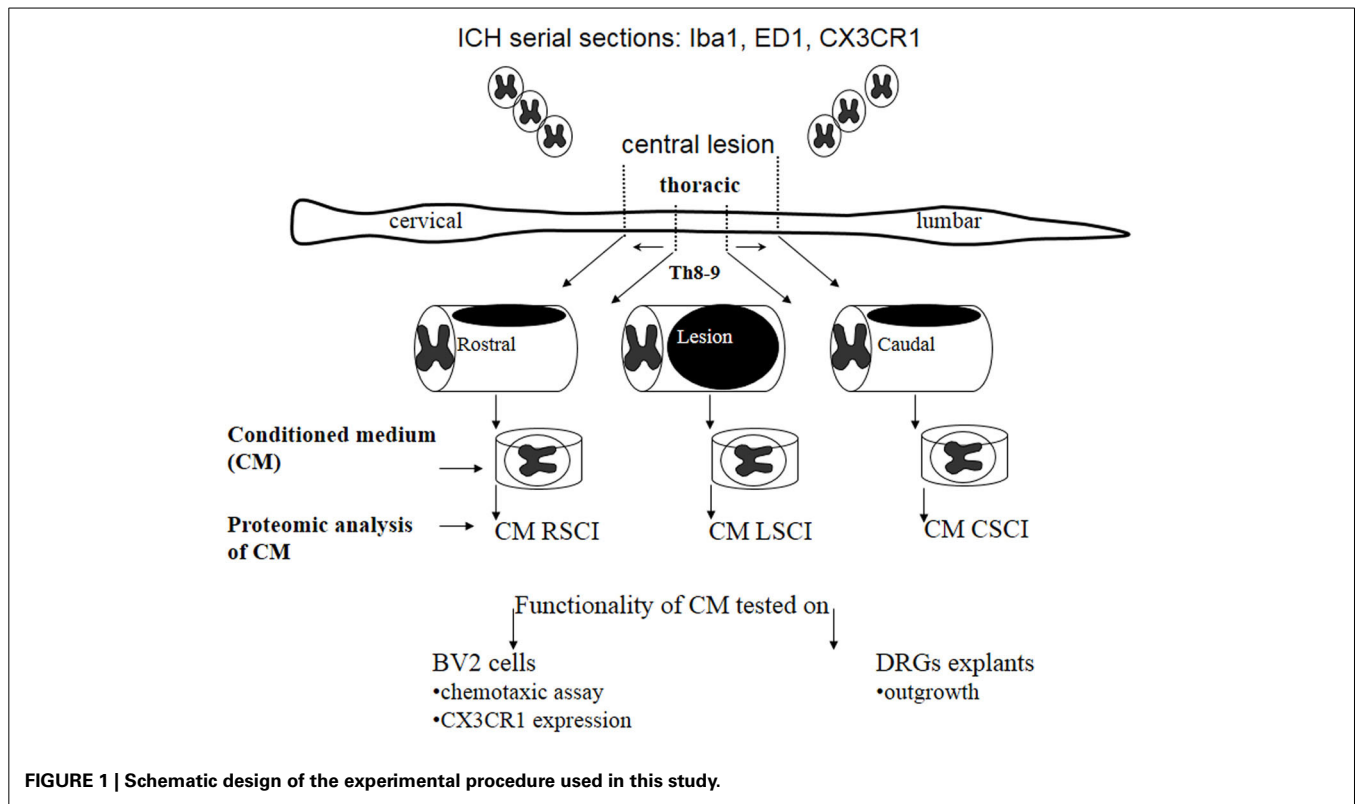
RESULTS

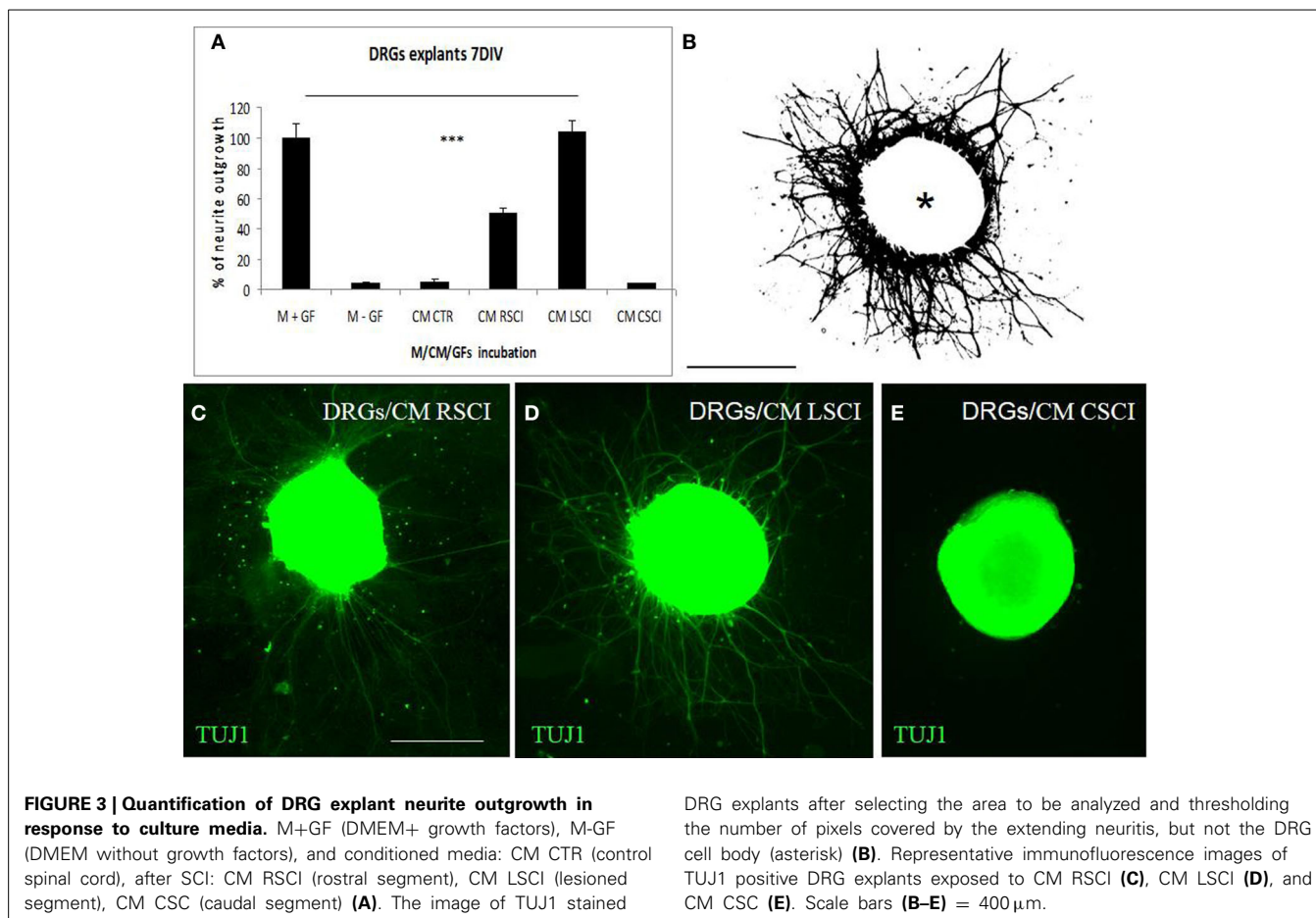
Here, we investigated nature of the factors released in CM derived from three spinal cord segments (rostral, central lesion, caudal) obtained 3, 7, and 10 days after SCI and correlated its molecular composition with the *in vitro* and *in vivo* analyses (Figure 1).

BV2 CELLS ARE STIMULATED WITH CM FROM INJURED SPINAL TISSUE

Microglia recruitment response to CM from SCI

Proteins secreted from segmental fragments of injured and control spinal cords were analyzed after 24 h *in vitro* incubation. The regionalization between rostral and caudal segments from the lesion has been taken into account and each collected CM has been individually tested on microglial BV2 cells using Boyden chambers. BV2 cells were counted by using Hoechst-labeling (Figure 2A). More than a 37-fold increase of attached microglial cells were observed with the CM from the rostral and lesion regions (Figures 2A,C,D), compared to the CM from control or ATP application (number of nuclei in the identical sampling fields: control = 4.2 ± 1.6 , rostral = 129.6 ± 8.5 , lesion = 145 ± 12 , caudal = 27.1 ± 3.8 , ATP = 15.0 ± 5.3) (Figures 2A,B).





In addition, comparison of microglia recruitment showed 5-fold higher activity using lesion and rostral CM when compared to the caudal one (Figures 2A,E). Furthermore, a marked nuclear hypertrophy of microglia was detected following activation, compared to control (Figures 2B',C').

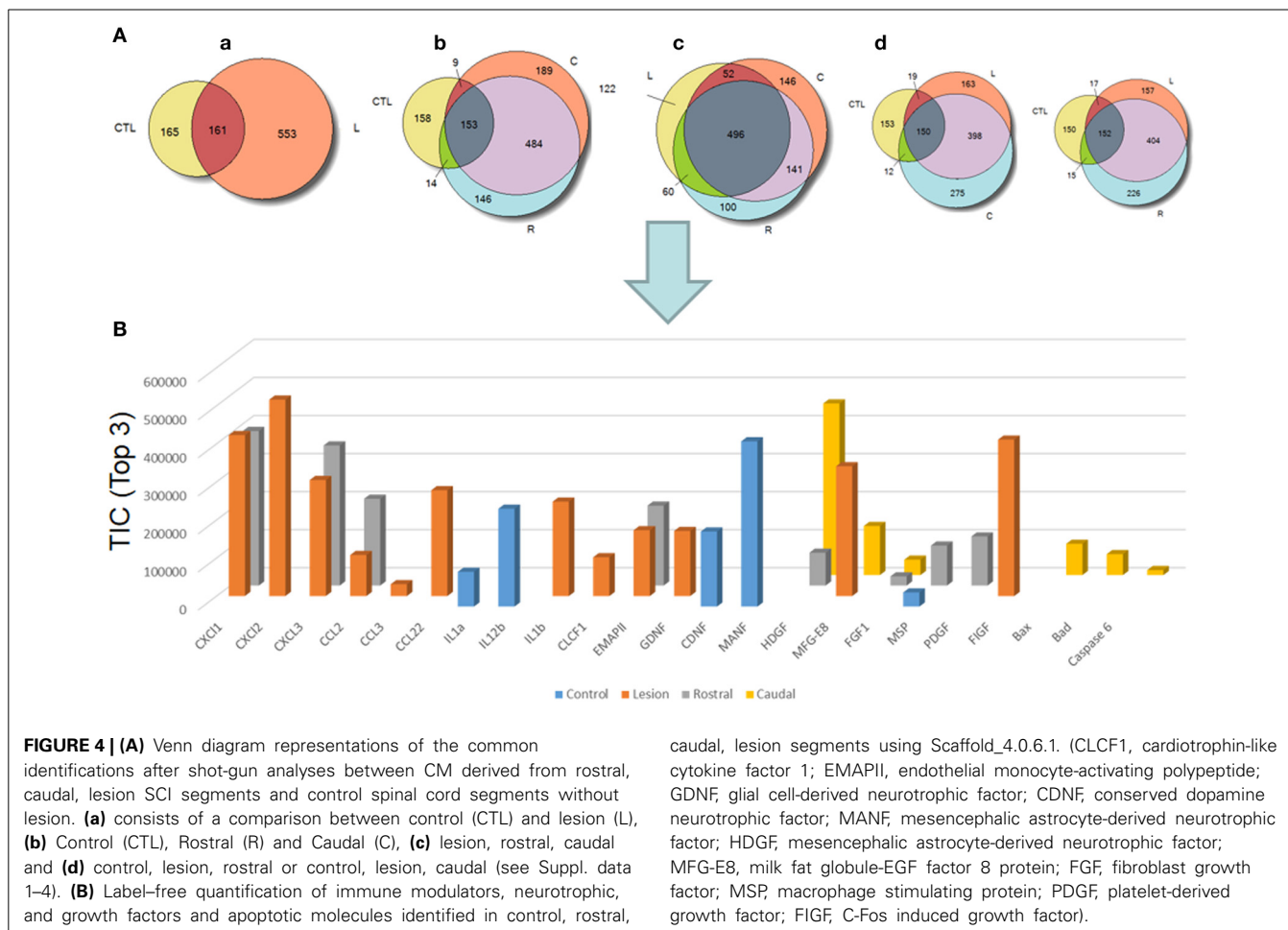
DRGs NEURITE OUTGROWTH

For quantification of neurite growth, the surface area outside the ganglion that was covered with neurites was determined (Figure 3B). This showed that enhanced TUJ1 positive neurite outgrowth from DRG explants was induced with CM LSCI (Figure 3D), and about half the growth was observed after culturing with CM RSCI (Figure 3C), if compared with control (Figure 3A). Conversely, almost no outgrowth from DRG explants was found after incubation with CM CSC (Figure 3E), CM CTR nor with media lacking GFs (M-GFs) (Figure 3A). Thus, the outgrowth induced with CM LSCI was the most pronounced, and DRG explants sent large radial projections to the peripheral area (<500 μm). In addition, bright field images of DRGs confirmed a high number of migrating cells with neuron-like bipolar and fibroblast-like morphology scattered around those explants expressing high neurite outgrowth (CM CTR, CM LSCI) (Suppl. data 1). The mean value % of neurite outgrowth for each group was: 100% ± 9.1 = M + GFs; 4.07% ± 1.28 = M - GFs;

5.42% ± 1.7 = CM CTR; 50.38% ± 3.15 = CM RSCI; 103.9% ± 7.76 = CM LSCI; 4.03% ± 0.76 = CM CSC. (***) $P < 0.001$.

Proteomic studies

We pointed out in our above results that a regionalization occurred between the rostral and the caudal segments in terms of factors secreted, i.e., neurotrophic and chemoattractant from the rostral segment, whereas none were from the caudal one. In this context, we investigated at a proteomic level the content of the SCI CM released from each spinal cord segment in order to identify these secreted factors. These experiments have been done on 4 SCI rats and 4 sham-operated rats per each survival (3, 7, 10 days). Among the identified proteins, those with a score under 5 were removed from subsequent analyses because they were identified from the MS/MS to have less than two peptides. We then evaluated the number of common peptides between the CM of interest. Each accession number, protein description, gene name and relative score associated with the selected proteins is reported in (Suppl. data 2–4). The Venn diagram presented in Figure 4A illustrates the common identifications between rostral, caudal, lesion SCI and control without lesion. Specific proteins have also been detected for each segment after SCI. In fact, 553 specific proteins have been detected in lesion (Figure 4A). 153 ± 3 ($n = 5$) proteins are in common between control, rostral and caudal SCI.



In addition, 14 ± 1 ($n = 5$) proteins are in common between control and rostral SCI whereas only 9 ± 4 ($n = 5$) are found in both caudal SCI and control (**Figure 4Aa–d**). Comparison between caudal and rostral SCI showed 481 ± 3 ($n = 5$) proteins in common. Experiments have been redone 5 times and the number of proteins identified in each condition was very close (± 4). The Venn diagram (between rostral and caudal SCI after elimination of the proteins in common with the ones detected in normal SC) confirmed the chemotaxis data. In fact, not only do the rostral and caudal CM have proteins in common but also some specific proteins compared to each other (**Figure 4A**). As presented in **Table 1**, for the first time in shot-gun analyses from CM, chemokines have been identified and quantified by label-free quantification (Suppl. data 5) in the lesion and rostral segments, e.g., CXCL1; CXCL2; CXCL7, CCL2, CCL3, CCL22, CLCF1, EMAP II. These chemokines and the neurotrophic factors (TGF β , FGF-1, PDGF, and FIGF1) detected in these regions clearly showed the presence of factors that are known to be immune-modulators and are neurotrophic (**Figure 4B**). Together, these factors are known to polarize the macrophages/microglial cells in the M2 phenotype (**Figure 4B**). Thus, three days after SCI, factors secreted by the cells present at the lesion and in the rostral segment (**Table 1**) are in neuroprotective and neurotrophic

environment whereas those from the caudal region are more apoptotic. The complete screening of the CM confirmed such evidence. In fact, more neurotrophic factors have been detected in the lesion and rostral part, i.e., CTGF (Connective tissue growth factor), NOV (Protein NOV homolog), PIGF (Placenta growth factor), FGF-1 (Fibroblast growth factor 1), BMP 2 or BMP3 (Bone morphogenetic proteins (2 or 3)), NGF, PGE, TGF beta (1–3) (Transforming growth factor beta), periostin, GAP-43, neurotrimin, neurofascin, Hepatocyte growth factor-regulated tyrosine kinase substrate (HGS). Also, molecules involved in neuronal development/differentiation/neuronal migration, i.e., CRIP1 (Cysteine-rich protein 1), DRP-5 (Dihydropyrimidinase-related protein 5), Negr1 (Neuronal growth regulator 1), NCAN (Neurocan core protein), CD44, Wnt8, syndecan-4, nexin, Bcl-2, were identified. Specific factors involved in immune cell chemotaxis or cellular adhesion, including complement factors (C1qb, C1qc, factor D, factor I, CD59), tetraspanins (CD9, CD82), and CD14 have also been characterized. In the contrast, proteins from the caudal region are more related to necrosis factors (BAX, BAD, Casapase 6, neogenin), cytoskeleton proteins, synaptic vesicle exocytosis, chemoattractant factors and neuronal postsynaptic density (**Figure 4B**, **Table 1**). Only BMP2, BMP3, and HGS have been detected. Comparison of proteins identified

Table 1 | List of proteins identified by shot-gun issue from CM (24 h) of central lesion, adjacent rostral and caudal segments after SCI at 3 days.

Protein family	Accession number	Protein name	SCI 3D		
			Lesion	Rostra	Cauda
Chemokines	P14095	CXCL1	■	■	■
	P30348	CXCL2	■	■	■
	Q99ME0	CXCL7	■	■	■
	O08565	CXCR4	■	■	■
	P14844	CCL2	■	■	■
	P50229	CCL3	■	■	■
	Q5I0L5	CCL22	■	■	■
Cytokines	Q320X2	EMPAII	■	■	■
	F7EKG3	CLCF1	■	■	■
Lectins	O88201	CLEC11a	■	■	■
	P11762	GAL1	■	■	■
	P08699	GAL3	■	■	■
CD	P40241	CD9	■	■	■
	Q63691	CD14	■	■	■
	P26051-2	CD44 isoform 1	■	■	■
	P27274	CD59	■	■	■
	Q6P9V1	CD81	■	■	■
	O70352	CD82	■	■	■
	D3ZNV9	CD93	■	■	■
	P20786	CD140a	■	■	■
	Complement	P31720	C1qa	■	■
P31721		C1qb	■	■	■
P31722		C1qc	■	■	■
P01026		C3	■	■	■
P08649		C4	■	■	■
P32038		Factor D	■	■	■
Q9WUW3	Factor I	■	■	■	
Growth factors	P07936	GAP-43	■	■	■
	Q9R1E9	CTGF	■	■	■
	Q9QZQ5	NOV	■	■	■
	Q63434	PLGF	■	■	■
	P70521	MSP	■	■	■
	P70490	MFG-E8	■	■	■
	Q63740	PDGF	■	■	■
	O35251	FIGF	■	■	■
	D3ZNW5	Neurofascin	■	■	■
	P17246	TGFb1	■	■	■
	Q07257-2	TGFb2	■	■	■
	Q07258	TGFb3	■	■	■
	P61149	FGF-1	■	■	■
	P49002	BMP2	■	■	■
	P49001	BMP3	■	■	■
	D3ZCR6	Periostin	■	■	■
Q9JJ50-2	HGS	■	■	■	
Q62718	Neurotrimin	■	■	■	

(Continued)

Table 1 | Continued

Protein family	Accession number	Protein name	SCI 3D		
			Lesion	Rostra	Cauda
Response to stress	P04094	proenkephalin	■	■	■
	Q8N729	Neuropeptide W Precursor	■	■	■
Neuronal development/differentiation	P47875	Cysteine-rich protein 1	■	■	■
	P36201	Cysteine-rich protein 2	■	■	■
	Q9JHU0	DRP-5	■	■	■
	Q9Z0J8	Negr1	■	■	■
	P55067	Ncan	■	■	■

The black shade corresponds to the proteins identified in the concerned case.

from the lesion rostral and caudal regions gave 122 proteins specific to the lesion site, 100 to the rostral segment, and 146 to the caudal one (Table 1). Nevertheless, 60 proteins are in common between the rostral and the lesion, and among these proteins, chemokines and neurotrophic factors have been only detected in these segments and never in the caudal part. Thus, 3 days after SCI, a clear regionalization occurs between the rostral and caudal regions (Table 1). These data can explain why initial sprouting and neurite outgrowth occur within the rostral and lesion parts and no regenerative processes can be found in the caudal part, although microglial cells are present and are in an activated state. Tissue proteomic analyses have been performed 3, 7, and 10 days after SCI. 801 common proteins to both 3 conditions have been identified. 58 specific proteins have been identified at 3 days, 446 at 7 days, 62 at 10 days after SCI. 230 proteins are common to both 7 and 10 days after SCI whereas only 41 between 3 and 10 days after SCI. Neurotrophic factors have been identified at 3 days, diminished at 7 days and disappeared at 10 days after SCI. However 10 days after SCI, proteins related to synaptogenesis have been detected, e.g., R-SNARE synaptobrevine, Q-SNAREs (SNAP25), GTPases (Rab proteins family), les synaptogenines, syntaxines, synaptotagmine. This reflected that 10 days after SCI proteins involved in axonal reconnection and synaptic transmission are expressed. This reflects that a neurorepair process has started (Table 2). In contrast, at the caudal segment, the protein profile is always inflammatory and apoptotic whatever the days after SCI (Data not shown).

MICROGLIA EXPRESSION IN CONTROL AND INJURED SPINAL CORD TISSUE

Antibodies against Iba1 exhibited moderate expression of resident microglia (Figures 5A,A',A''). After SCI, microglia changed into an activated phenotype: marked cellular hypertrophy and thick, short and radially projecting processes with fewer ramifications (Figures 5B,B',B'',C,C'). This was confirmed by quantification analyses, which showed some disparities between microglia accumulated in the dorsal white matter of the rostral and caudal spinal cord segments (Figures 5C,C', 6A–D). Significant

Table 2 | Identified proteins from rostral tissue sections in time course after SCI.

Protein family	Accession number	Protein name	3 Days	7 Days	10 Days
Neurotrophic factors	P07936	GAP-43			
	Q9R1E9	Cntf			
	Q9QZQ5	NOV			
	Q63434	Plgf			
	D3ZNW5	Neurofascin			
	Q923W4	HDGR3			
	POC5H9	MANF			
	P17246	TGFb1			
	Q07257-2	TGFb2			
	Q07258	TGFb3			
	P61149	Fgf-1			
	P49002	BMP2			
	P49001	BMP3			
	D3ZCR6	Periostin			
	Q9JJ50-2	HGS			
	Q62718	Neurotrimin			
	Q6P686	Ostf1			
Synaptogenesis factors	P60881	SNAP25			
		SNAP29			
	D4ABK1	SYNGR			
	Q03410	SYCP1			
	Q62910-5	SYNJ-1			
	P09951-2	SYN1			
	Q63537	SYN2			
	P21707	SYT1			
	P29101	SYT2			
	Q02563	SYV2A			
	P07825	SYNPH			
	Q5EGY4	Synpatobrevin			
	P63012	Rab3a			
	A1L1J8	Rab5b			
	P09527	Rab7A			
	P35281	Rab10			
	Q35509	Rab11			
Q6AXT5	Rab23				
Q99P74	Rab27				
Q6GQP4	Rab31				

The gray shade corresponds to the proteins identified in the concerned case.

enhancement of Iba1 positive microglia occurred in the rostral dorsal white matter (**Figure 6B**), while in other areas we did not detect significant differences between the rostral and caudal segments. The spinal cord tissue at the central lesion was severely damaged, losing its typical anatomical architecture (Suppl. data 6). Therefore, we could not quantify Iba1 positive profiles at the lesion site. In addition, the entire dissected central segment (± 5.0 mm) showed dense and homogenous infiltration of Iba1 and ED1 positive macrophages (Suppl. data 7). However, out of

the central lesion, toward the rostral or caudal segments, Iba1 macrophages together with migrated ED1 monocytes occupy mainly the lesion cavity and accumulate at the lesion penumbra (Suppl. data 7). In addition, we could clearly distinguish the monocyte-derived amoeboid Iba1 microglia concentrated within the dorsal WM, while hypertrophied microglia with ramified processes retained at the gray matter tissue (Suppl. data 7). Furthermore, by immunofluorescent double labeling of ED1 and Iba1 we confirm the distribution of macrophages throughout the rostro-caudal extent of spinal contusion lesions (Suppl. data 7). All data are included in **Table 3**. To confirm the key role of inflammation and not gliosis at 3 days after SCI we studied response of astrocytes by GFAP IHC. Here we show that injury resulted into decreased number of GFAP positive profiles, with short processes surrounded by debris. These GFAP+ profiles were impaired, when compared to fine star like astrocyte morphology found in sham spinal cord sections (Suppl. data 8).

EXPRESSION OF CX3CR1 RECEPTOR AND CD206+ PROFILES ALONG THE ROSTRO-CAUDAL AXIS IN SPINAL CORD TISSUE

The proteomic data showed that factors released from the rostral and lesion segments express neuroprotective and immunomodulatory properties, whereas the ones found in the caudal are more inflammatory. In this context, we focus our attention on the CX3CR1 receptor which is known to be expressed in immune cells expressing an M2 profile characterized by production of neurotrophic factors and immune modulators like CXCL1, CXCL2, CXCL3, CCL1, CCL2, CCL22, EMAP II, and CLCF1, factors that were identified in CM derived from rostral and lesion segments. Expression of CX3CR1 in sham spinal cord tissue was low, with homogenous distribution in whole layers of the spinal cord with occasionally labeled microglia (**Figures 7A,A',C,D**). However, SCI after 3 days induced a significant upregulation of CX3CR1 expression in the dorsal, ventral gray and white matter. This upregulation seems to co-localize with spinal microglia and recruited monocytes within damaged tissue (**Figures 7B,B',E**). Higher expression of CX3CR1 was detected in rostral segments (**Figures 7B,B',E**) when compared to the caudal spinal cord tissue at day 3 post-injury which was validated by quantification of CX3CR1 immunohistochemistry in coronal sections (**Figure 8D**). Similarly, CD206+ macrophages significantly increased in both rostral and caudal spinal segments when compared to corresponding areas of sham operated rats. However, we did not find differences along the rostro-caudal axis, thus the white and gray matter were infiltrated with large multipolar macrophages with elongated processes (**Figures 7C,C', 8E**).

In order to evaluate the part of infiltrating macrophage that can also express the CX3CR1 receptor, double labeling using anti-CX3CR1 (red) and anti-ED1 (green) was performed in the dorsal white matter at the level of rostral and caudal segments three days after SCI. Results confirm that a clear labeling for CX3CR1 is found in the rostral segment (**Figure 8A**) and lower in the caudal segment (**Figure 8B**). No co-localization was detected between CX3CR1 and ED1 labeling indicating that macrophages did not express CX3CR1 receptors (**Figure 8C**, arrows indicate the Iba1 labeling distinct from the ED1).

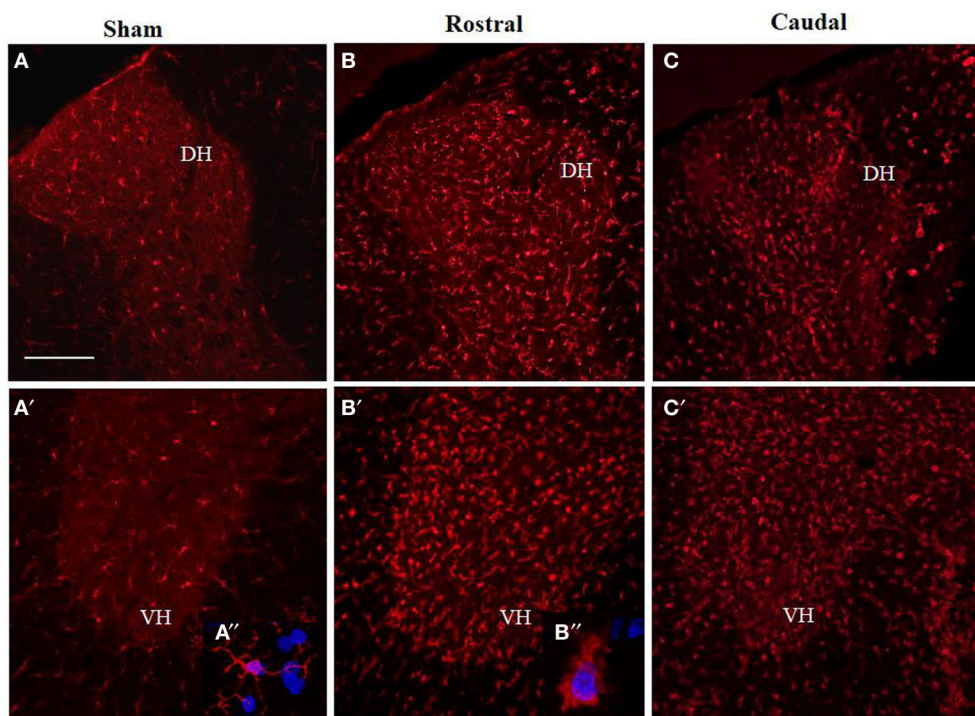


FIGURE 5 | Comparison of Iba1 immunoreactivity (IR) in coronal thoracic spinal cord sections of sham rats (A,A') and rats 3 days after injury in rostral (B,B') and caudal segments (C,C') in the dorsal (upper) and ventral horn (lower panel). Note, significantly

increased number of activated Iba1-positive microglia in both rostral and caudal segments within the dorso-ventral axis of gray matter as well as throughout corresponding white matter. Scale bars (A,A'-C,C') = 150 μ m.

MODULATION OF CX3CR1 IN BV2 CELLS

Naive BV2 cells did not show any signal for CX3CR1 (Figure 9A) similar to the negative control, when using only the secondary antibody (Figure 9B). Following 24 h stimulation of BV2 cells with CM RSCI, multipolar or round cells (arrows) expressed strong CX3CR1 immunofluorescence (Figures 9C,C',D). Interestingly, it can be noticed that the labeling was either vesicular (Figure 9C'), or membranous (Figure 9D), which demonstrates a receptor from Golgi to membrane after activation of the BV2 cells with CM from an injured spinal cord. No labeling using anti-CKR2, a marker for M1 polarization of macrophages and microglial cells, has been found in control nor in BV2 cells stimulated with CM RSCI (data not shown). Western blot analysis showed the presence of a specific band at 34 kDa (Figure 9E) corresponding to the CX3CR1 receptor only in BV2 cells stimulated with CM RSCI.

DISCUSSION

In the present study, we show that the activated Iba1 positive microglia increased in all evaluated areas following SCI, but the significant differences between rostral and caudal segments occurred only within the dorsal white matter, where the impact of damage is most prominent in this SCI animal model. Thus, this discrepancy could be accounted in part to the presence or absence of macrophages derived from CNS-residing microglia or from blood-derived monocytes invading the most damaged regions at the rostral and caudal spinal levels (Mawhinney et al., 2012).

Previous work have shown that after SCI, pro-inflammatory cytokines are upregulated by microglia and macrophages in the first few days after injury. These inflammatory mediators are also produced by other cell types in the lesioned spinal cord (Pineau and Lacroix, 2007; Pineau et al., 2010). Thus, after SCI, a complex array of chemokines and cytokines regulate myelopoiesis and intraspinal trafficking of myeloid cells. As these cells accumulate in the injured spinal cord, the collective actions of diverse cues in the lesion environment help to create an inflammatory response marked by tremendous phenotypic and functional heterogeneity. Indeed, it is difficult to attribute specific reparative or injurious functions to one or more myeloid cells because of convergence of cell function and difficulties in using specific molecular markers to distinguish between subsets of myeloid cell populations (Hawthorne and Popovich, 2011). The temporal activation of the myeloid cell lineage leads within minutes of SCI to the creation of a heterogeneous network of multifunctional cells that could be able of promoting injury and repair of neural tissue. Microglia are among the first myeloid cells to be set in motion, responding to changes in extracellular ions and ATP within minutes to hours post-injury followed by neutrophils (Hawthorne and Popovich, 2011). Neutrophils arrive first between 3 and 24 h post-injury. Then monocytes arrive later, \sim 2 to 3 days post-injury with maximal infiltration occurring 1–2 weeks post-injury. At 3 days post-injury data obtained by cDNA microarray and quantitative real-time PCR analyses, showed that macrophage expressed M1 and M2 markers, but the M1/M2 ratio determines

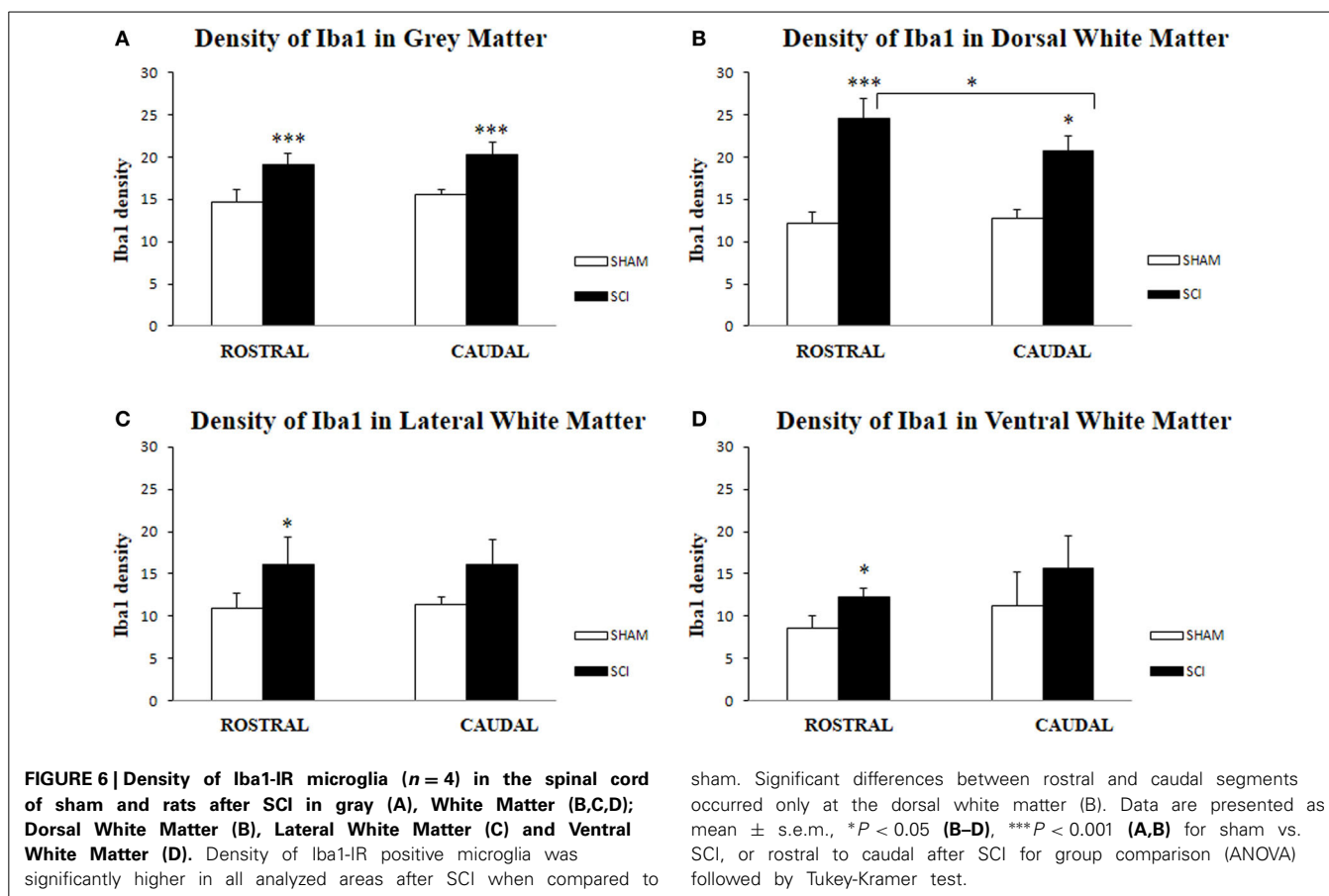


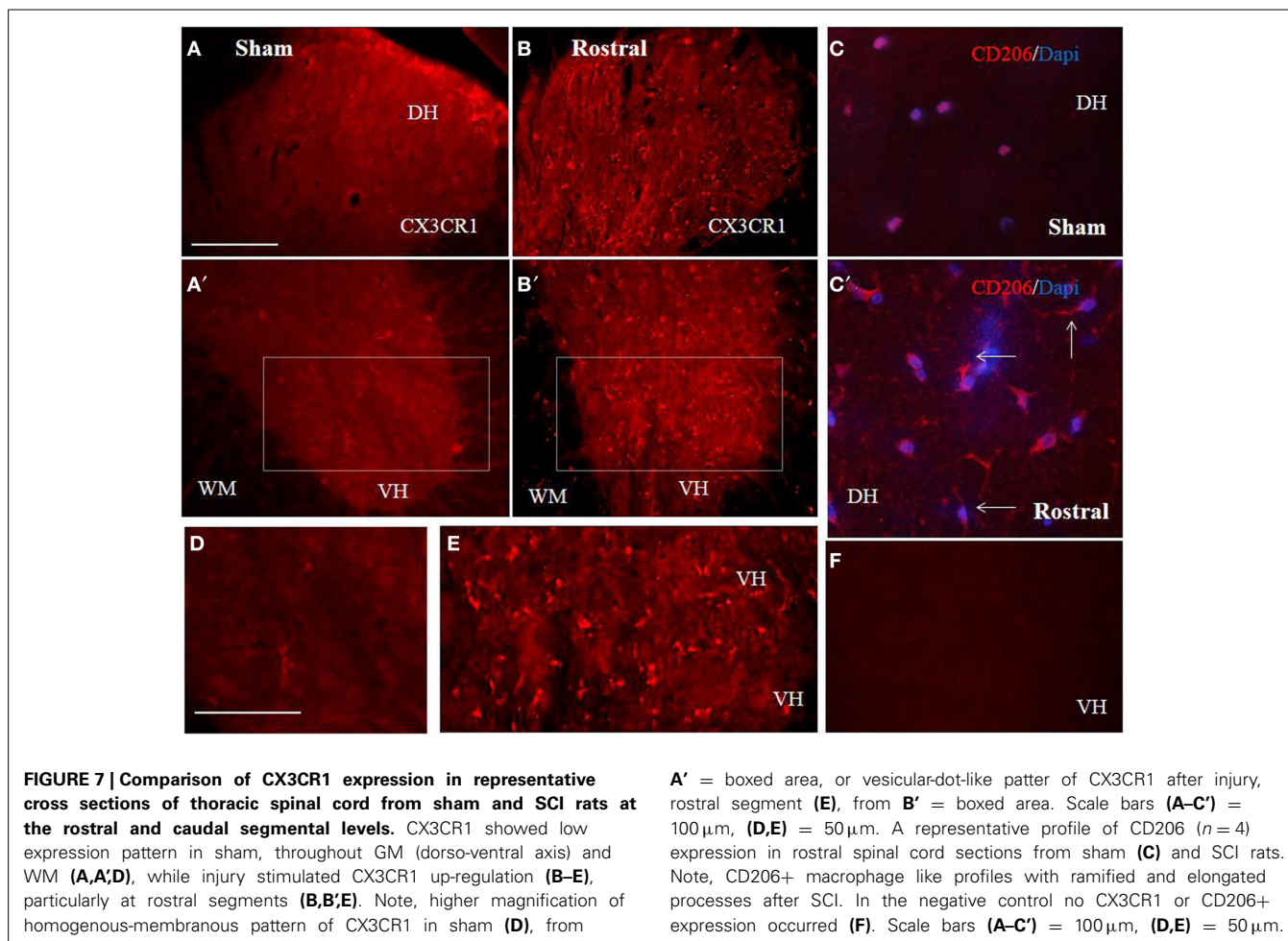
Table 3 | Quantification of Iba1, CX3CR1 and CD206 immunoreactivities in sham, SCI tissue from rostral and caudal segments at 3 days.

	Sham rostral	SCI rostral	Sham caudal	SCI caudal
DENSITY OF Iba1				
GM	14.6 \pm 1.5	9.1 \pm 1.3	15.5 \pm 0.4	20.3 \pm 1.4
WMD	12.1 \pm 1.4	24.6 \pm 6.2	12.8 \pm 0.9	20.7 \pm 3.7
WML	10.8 \pm 1.7	16.1 \pm 6.4	11.3 \pm 0.8	16.1 \pm 3.9
WMV	8.6 \pm 1.4	12.2 \pm 1.3	11.2 \pm 4.6	15.6 \pm 4.8
DENSITY OF CX3CR1				
GM	5.1 \pm 1.07	22.8 \pm 3.2	4.2 \pm 1.8	16.2 \pm 3.8
WM	2.0 \pm 1.32	17.27 \pm 4.4	3.0 \pm 1.6	8.0 \pm 2.6
DENSITY OF CD206				
GM	8.8 \pm 1.1.7	27.8 \pm 4.6	9.2 \pm 1.9	28.2 \pm 2.8
WM	4.8 \pm 1.2.1	28.4 \pm 5.4	5.4 \pm 2.4	26.8 \pm 4.4

whether CNS macrophages contribute to axonal regeneration after SCI (David and Kroner, 2011). Here we also confirm that CX3CR1 immunoreactivity was up-regulated after SCI, revealing most prominent expression within the gray and white matter of rostral spinal segments. This may coincide with both activated intraspinal microglia as well as with monocytes invading the lesion already 3 days post-injury, as confirmed in the present study with ED1 immunoreactivity. It is important to point out that monocyte recruitment after SCI is a dynamic process that initiates within the first days post injury, but is further accelerated

during longer survival (Kullberg et al., 2001; Stanislaus et al., 2001). However, in the present study, co-localization experiments between CX3CR1 and ED1 did not confirm that macrophage expressed an M2 profile, while it seems more likely to be expressed in resident microglia.

Based on advanced proteomic analyses, we were trying to find a correlation between the immune response along the rostro-caudal axis and the content of released molecules 3, 7, and 10 days after injury. This is the first time that chemokines were identified by shot-gun analysis in the CM derived from rostral to caudal



spinal cord segments. In particular, the immune factors (CCL2, CCL3, CCL22, CXCL1, CXCL2, CXCL7, EMPAII, CLCF1) that were detected in the CM from rostral segments with the neurotrophic factors (CTGF, NOV, PIGF, FGF-1 BMP 2, BMP3, NGF, PGE, TGF beta (1–3) periostin, GAP-43, neurotrimin, HGS) favor differentiation of microglia cells toward the M2 rather than the M1 phenotype. These data are in line with our findings showing increased CX3CR1 expression in rostral spinal segments as well as with previous data of M2 microglia polarization at the central lesion 3 days after SCI (Kigerl et al., 2009). In contrast to CX3CR1, the CD206+ profiles revealed similar response at both rostral and caudal segments. Furthermore, *in vitro* chemotaxis assays confirmed that BV2 cells were highly responsive to the cytokine cocktail present in the CM from lesion and rostral sites. Interestingly, the BV2 migratory potency induced by CM derived from rostral and lesion segments was 37-fold higher compared to the ATP or LPS stimulations that increase their migration by close to 3-fold due to the specific factors found in the complex CM (Rahmat et al., 2013). Our immunocytochemical studies prove that activated BV2 cells exposed to CM from the rostral segment over-expressed the CX3CR1 receptor, and this overexpression is known to correspond with the M2 profile. This was strengthened by western blot analysis and lack of labeling with C2KR, an M1 receptor. These data together with *in vivo* CX3CR1 expression

are in close coherence with published transcriptomic experiments showing that in the injured spinal cord M2 gene expression is transiently expressed during 7 days after injury, while the M1 gene expression is maintained for up to 1 month (Kigerl et al., 2009). Moreover, a direct role of CSPG in controlling microglial and macrophage behavior after SCI was demonstrated. It seems that beneficial role of CSPG during the acute stage (regulating their phagocytosis or neurotrophic factor secretion) and its deleterious effect at later stages emphasizes the need to retain the endogenous potential of this molecule for recovery by controlling its levels at different stages of post-injury repair (Rolls et al., 2008).

Our tissue proteomic data also confirm this point. In fact, a temporal-spatial analysis in tissue proteomic has been undertaken at the rostral and caudal segment levels, 3, 7, and 10 days after SCI. Results shown that the proteome pattern is modified in course of time in the rostral segment whereas the caudal segment present the same pattern whatever the time after SCI. Neurotrophic factors are found at 3 and 7 days after lesion and disappeared at 10 days. They are replaced by synaptogenesis factors reflecting the fact that a neurorepair process is taking place after 10 days SCI at the level of the rostral segment. These data are in line with the DRG experiments and our previous *in vivo* results demonstrating that neurite outgrowth takes place from rostral to lesion but never from caudal to lesion (Novotna et al., 2011) Furthermore, the content of

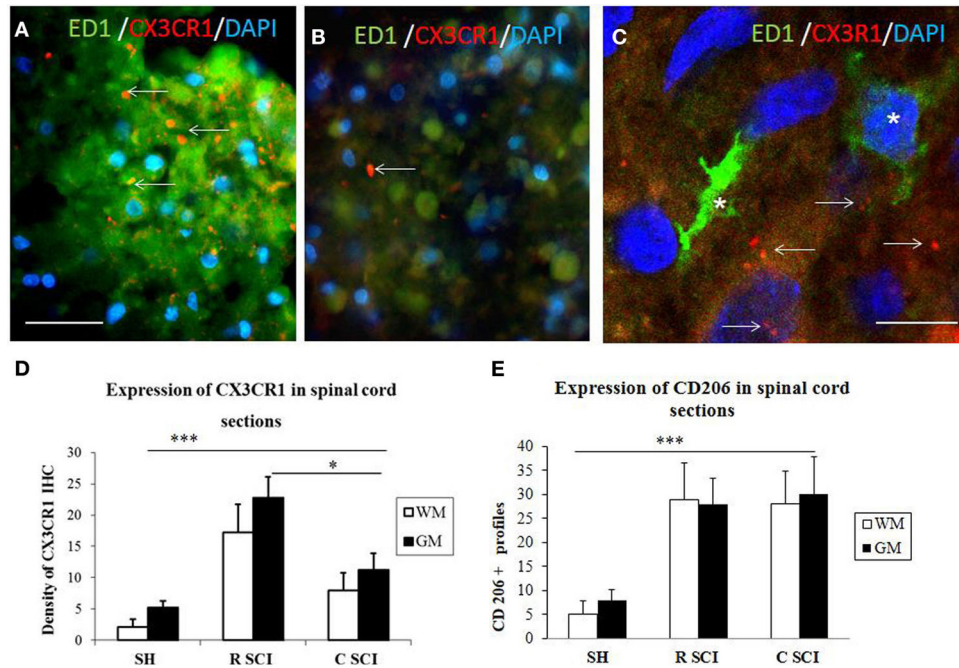


FIGURE 8 | Cross sections through dorsal white matter at the level of rostral (A) and caudal (B) segments of the injured spinal cord stained with CX3CR1 (red) and ED1 (green) antibodies revealing increased expression of CX3CR1 (red) in rostral segment compared to caudal (arrows). Note, no co-localization between CX3CR1 and ED1 labeled macrophages (see arrows indicated red dot for CX3CR1 labeling) (C, confocal image). Density of CX3CR1+ ($n = 4$) and expression of CD206 profiles ($n = 4$) in the spinal cord sections of sham and 3 days after SCI in White /Gray Matter (D,E). (D) Density

of CX3CR1 was significantly higher when comparing Sham (SH) sections with sections from injured spinal cord (SCI), sections from rostral (R SCI) compared with caudal (C SCI) segment within WM/GM. (E) CD206+ profiles significantly increased when compared Sham (SH) sections with sections from injured spinal cord (SCI), not between R SCI and C SCI sections. Data are presented as mean \pm s.e.m., * $P < 0.05$, *** $P < 0.001$ for sham vs. SCI, or rostral to caudal after SCI for group comparison W/G matter (ANOVA) followed by Tukey-Kramer test. Scale bars (A,B) = 50 μ m, (C) = 20 μ m.

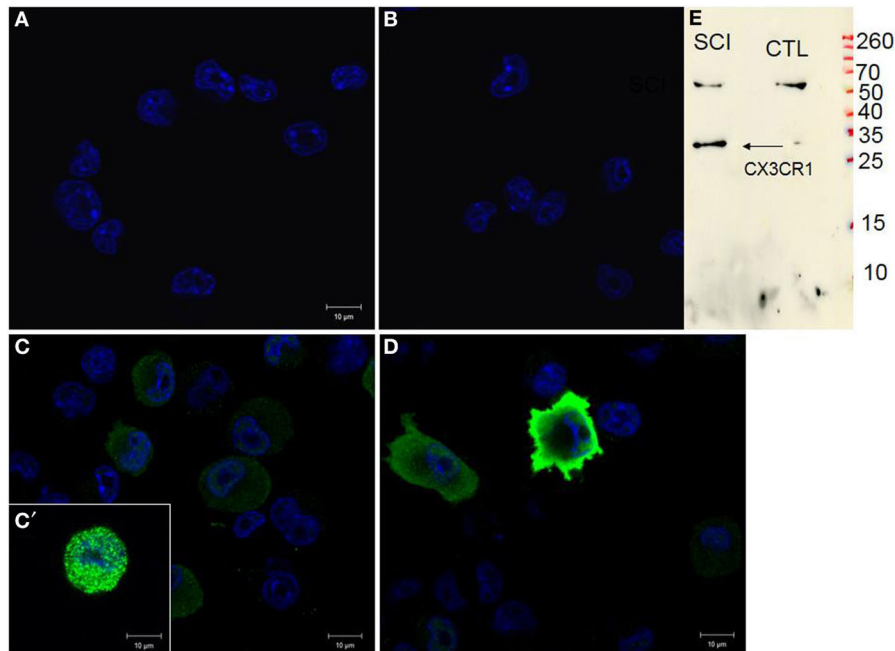


FIGURE 9 | CX3CR1 expression in control BV2 cells (A), stimulated with CM LSCI (C). Spindle shaped, multipolar or round BV2 cells following CM LSCI stimulation expressed intense CX3CR1 IR (C,D). Scale bars (A–D) = 50 μ m. Control (B), only secondary antibody. Inset

picture corresponds to Western blot analyses using anti-CX3CR1 from control or activated BV2 with CM LSCI (E). Note, the band at 34 kDa correspond to the CX3CR1 and the band at 60 kDa is an unspecific band.

chemokines, lectins, and growth factors in the rostral but not in the caudal segment clearly document the immediate inflammatory response together with activity-dependent factors released by neurons and glia.

In order to investigate the neurotrophic role of CM derived from lesioned tissue, we have also undertaken studies of neurite outgrowth in rat DRG explants. Our data validate that pronounced neurite sprouting of DRGs facilitated by CM from rostral and lesion segments are most likely mediated by the content of neurotrophic factors, i.e., FGF-1, NGF, PGE, BMP 2 or BMP3, GAP-43, neurotrophin, neurofascin, and other molecules involved in neuronal development/differentiation/migration. Although the principal role of NGF/TrkA pathways in sensory axon outgrowth have been widely demonstrated, other neurotrophic factors including the BMPs (members of the TGF β superfamily) or GAP-43 have to be taken into account. Particularly, the Smad1-dependent BMP signaling is developmentally regulated and governs axonal growth in the dorsal root ganglion neurons. Similarly, GAP-43, a membrane-bound protein, is expressed in neurons during axonal outgrowth development and is significantly up-regulated in DRGs during regeneration (Tsai et al., 2007; Parikh et al., 2011).

Taken together, these data could have a clear impact in clinics. It will be more important to stimulate neurite sprouting at the caudal region by inhibiting inflammation and polarization of M1 cells to the M2 state. These results demonstrate that each segment of the lesion has to be taken into consideration independently from each other in order to modulate inflammation, stimulate neurite outgrowth and functional reconnection.

ACKNOWLEDGMENTS

This research was supported by a collaboration between the Fundamental and Applied Biology Mass Spectrometry Laboratory (Michel Salzet) and Thermofisher (Bremen, KS) and grants from Ministère de L'Education Nationale, L'Enseignement Supérieur et de la Recherche, Agence Nationale de la Recherche (ANR, MIMIC project), STEFANIK project (to Dasa Cizkova and Michel Salzet), APVV-SK-FR0019-11, Région Nord-Pas de Calais (to Stéphanie Devaux) and Université de Lille 1 (to Michel Salzet), APVV 0472-11 and MVT-COST BH-1002 (Dasa Cizkova). We would like to thank M. Spontakova for IHC analyses, Dr. Christian Slomianny and Professor Natalia Prevarskaya (Inserm, U800, Laboratoire de Physiologie Cellulaire, Université Lille 1) for access to confocal microscopy facilities and Elodie Richard of the CCMIC-Université Lille 1 (BICeL).

SUPPLEMENTARY MATERIAL

The Supplementary Material for this article can be found online at: <http://www.frontiersin.org/journal/10.3389/fncel.2014.00105/abstract>

REFERENCES

Aguzzi, A., Barres, B. A., and Bennett, M. L. (2013). Microglia: scapegoat, saboteur, or something else? *Science* 339, 156–161. doi: 10.1126/science.1227901

Beattie, M. S., Hermann, G. E., Rogers, R. C., and Bresnahan, J. C. (2002). Cell death in models of spinal cord injury. *Prog. Brain Res.* 137, 37–47. doi: 10.1016/S0079-6123(02)37006-7

Bocchini, V., Mazzolla, R., Barluzzi, R., Blasi, E., Sick, P., and Kettenmann, H. (1992). An immortalized cell line expresses properties of activated microglial cells. *J. Neurosci. Res.* 31, 616–621. doi: 10.1002/jnr.490310405

Choi, H., Fermin, D., and Nesvizhskii, A. I. (2008). Significance analysis of spectral count data in label-free shotgun proteomics. *Mol. Cell. Proteomics* 7, 2373–2385. doi: 10.1074/mcp.M800203-MCP200

David, S., and Kroner, A. (2011). Repertoire of microglial and macrophage responses after spinal cord injury. *Nat. Rev. Neurosci.* 12, 388–399. doi: 10.1038/nrn3053

Fitch, M. T., and Silver, J. (1997). Activated macrophages and the blood-brain barrier: inflammation after CNS injury leads to increases in putative inhibitory molecules. *Exp. Neurol.* 148, 587–603. doi: 10.1006/exnr.1997.6701

Gerin, C. G., Madueke, I. C., Perkins, T., Hill, S., Smith, K., Haley, B., et al. (2011). Combination strategies for repair, plasticity, and regeneration using regulation of gene expression during the chronic phase after spinal cord injury. *Synapse* 65, 1255–1281. doi: 10.1002/syn.20903

Gstaiger, M., and Aebersold, R. (2009). Applying mass spectrometry-based proteomics to genetics, genomics and network biology. *Nat. Rev. Genet.* 10, 617–627. doi: 10.1038/nrg2633

Hawthorne, A. L., and Popovich, P. G. (2011). Emerging concepts in myeloid cell biology after spinal cord injury. *Neurotherapeutics* 8, 252–261. doi: 10.1007/s13311-011-0032-6

Jones, L. L., Yamaguchi, Y., Stallcup, W. B., and Tuszynski, M. H. (2002). NG2 is a major chondroitin sulfate proteoglycan produced after spinal cord injury and is expressed by macrophages and oligodendrocyte progenitors. *J. Neurosci.* 22, 2792–2803.

Keller, A., Nesvizhskii, A., Kolker, E., and Aebersold, R. (2002). An explanation of the Peptide Prophet algorithm developed. *Anal. Chem.* 74, 5383–5392. doi: 10.1021/ac025747h

Kigerl, K. A., Gensel, J. C., Ankeny, D. P., Alexander, J. K., Donnelly, D. J., and Popovich, P. G. (2009). Identification of two distinct macrophage subsets with divergent effects causing either neurotoxicity or regeneration in the injured mouse spinal cord. *J. Neurosci.* 29, 13435–13444. doi: 10.1523/JNEUROSCI.3257-09.2009

Kreutzberg, G. W. (1996). Microglia: a sensor for pathological events in the CNS. *Trends Neurosci.* 19, 312–318. doi: 10.1016/0166-2236(96)10049-7

Kullberg, S., Aldskogius, H., and Ulfhake, B. (2001). Microglial activation, emergence of ED1-expressing cells and clusterin upregulation in the aging rat CNS, with special reference to the spinal cord. *Brain Res.* 899, 169–186. doi: 10.1016/S0006-8993(01)02222-3

Mawhinney, L. A., Thawer, S. G., Lu, W. Y., Rooijen, N., Weaver, L. C., Brown, A., et al. (2012). Differential detection and distribution of microglial and hematogenous macrophage populations in the injured spinal cord of lysEGFP-ki transgenic mice. *J. Neuropathol. Exp. Neurol.* 71, 180–197. doi: 10.1097/NEN.0b013e3182479b41

Nishimura, S., Yasuda, A., Iwai, H., Takano, M., Kobayashi, Y., Nori, S., et al. (2013). Time-dependent changes in the microenvironment of injured spinal cord affects the therapeutic potential of neural stem cell transplantation for spinal cord injury. *Mol. Brain* 6:3. doi: 10.1186/1756-6606-6-3

Novotna, I., Slovinska, L., Vanicky, I., Cizek, M., Radonak, J., and Cizkova, D. (2011). IT delivery of ChABC modulates NG2 and promotes GAP-43 axonal regrowth after spinal cord injury. *Cell. Mol. Neurobiol.* 31, 1129–1139. doi: 10.1007/s10571-011-9714-1

Parikh, P., Hao, Y., Hosseinkhani, M., Patil, S. B., Huntley, G. W., Tessier-Lavigne, M., et al. (2011). Regeneration of axons in injured spinal cord by activation of bone morphogenetic protein/Smad1 signaling pathway in adult neurons. *Proc. Natl. Acad. Sci. U.S.A.* 108, E99–E107. doi: 10.1073/pnas.1100426108

Pineau, I., and Lacroix, S. (2007). Proinflammatory cytokine synthesis in the injured mouse spinal cord: multiphasic expression pattern and identification of the cell types involved. *J. Comp. Neurol.* 500, 267–285. doi: 10.1002/cne.21149

Pineau, I., Sun, L., Bastien, D., and Lacroix, S. (2010). Astrocytes initiate inflammation in the injured mouse spinal cord by promoting the entry of neutrophils and inflammatory monocytes in an IL-1 receptor/MyD88-dependent fashion. *Brain Behav. Immun.* 24, 540–553. doi: 10.1016/j.bbi.2009.11.007

Rahmat, Z., Jose, S., Ramasamy, R., and Vidyadaran, S. (2013). Reciprocal interactions of mouse bone marrow-derived mesenchymal stem cells and BV2 microglia following lipopolysaccharide stimulation. *Stem Cell Res. Ther.* 4, 12. doi: 10.1186/scrt160

- Ransohoff, R. M., Liu, L., and Cardona, A. E. (2007). Chemokines and chemokine receptors: multipurpose players in neuroinflammation. *Int. Rev. Neurobiol.* 82, 187–204. doi: 10.1016/S0074-7742(07)82010-1
- Rolls, A., Shechter, R., London, A., Segev, Y., Jacob-Hirsch, J., Amariglio, N., et al. (2008). Two faces of chondroitin sulfate proteoglycan in spinal cord repair: a role in microglia/macrophage activation. *PLoS Med.* 5:e171. doi: 10.1371/journal.pmed.0050171
- Salzet, M., Watzet, C., Baert, J. L., and Malecha, J. (1993). Biochemical evidence of angiotensin II-like peptides and proteins in the brain of the rhynchobdellid leech *Theromyzon tessulatum*. *Brain Res.* 631, 247–255. doi: 10.1016/0006-8993(93)91542-Z
- Schwab, M. E., and Bartholdi, D. (1996). Degeneration and regeneration of axons in the lesioned spinal cord. *Physiol. Rev.* 76, 319–370.
- Schwartz, M., Moalem, G., Leibowitz-Amit, R., and Cohen, I. R. (1999). Innate and adaptive immune responses can be beneficial for CNS repair. *Trends Neurosci.* 22, 295–299. doi: 10.1016/S0166-2236(99)01405-8
- Smith, S. M., Beattie, A. J., Gillings, M. R., Holley, M. P., Stow, A. J., Turnbull, C. L., et al. (2008). An enhanced miniaturized assay for antimicrobial prospecting. *J. Microbiol. Methods* 72, 103–106. doi: 10.1016/j.mimet.2007.10.003
- Stanislaus, R., Singh, A. K., and Singh, I. (2001). Lovastatin treatment decreases mononuclear cell infiltration into the CNS of Lewis rats with experimental allergic encephalomyelitis. *J. Neurosci. Res.* 66, 155–162. doi: 10.1002/jnr.1207
- Tator, C. H. (1995). Update on the pathophysiology and pathology of acute spinal cord injury. *Brain Pathol.* 5, 407–413. doi: 10.1111/j.1750-3639.1995.tb00619.x
- Tsai, S.-Y., Yang, L.-Y., Wu, C.-H., Chang, S.-F., Hsu, C. Y., Wei, C.-P., et al. (2007). Injury-induced Janus kinase/protein kinase Ccalcium dependent phosphorylation of growth-associated protein 43 and signal transducer and activator of transcription 3 for neurite growth in dorsal root ganglion. *J. Neurosci. Res.* 85, 321–331. doi: 10.1002/jnr.21119
- Vanicky, I., Urdzikova, L., Saganova, K., Cizkova, D., and Galik, J. (2001). A simple and reproducible model of spinal cord injury induced by epidural balloon inflation in the rat. *J. Neurotrauma* 18, 1399–1407. doi: 10.1089/08977150152725687

Conflict of Interest Statement: The authors declare that the research was conducted in the absence of any commercial or financial relationships that could be construed as a potential conflict of interest.

Received: 21 November 2013; accepted: 24 March 2014; published online: 17 April 2014.

Citation: Cizkova D, Le Marrec-Croq F, Franck J, Slovinska L, Grulova I, Devaux S, Lefebvre C, Fournier I and Salzet M (2014) Alterations of protein composition along the rostro-caudal axis after spinal cord injury: proteomic, in vitro and in vivo analyses. *Front. Cell. Neurosci.* 8:105. doi: 10.3389/fncel.2014.00105

This article was submitted to the journal *Frontiers in Cellular Neuroscience*. Copyright © 2014 Cizkova, Le Marrec-Croq, Franck, Slovinska, Grulova, Devaux, Lefebvre, Fournier and Salzet. This is an open-access article distributed under the terms of the Creative Commons Attribution License (CC BY). The use, distribution or reproduction in other forums is permitted, provided the original author(s) or licensor are credited and that the original publication in this journal is cited, in accordance with accepted academic practice. No use, distribution or reproduction is permitted which does not comply with these terms.

Article 2: Proteomic analysis of the spatio-temporal based molecular kinetics of acute spinal cord injury identifies a time- and segment-specific window for effective tissue repair


Authors: Stéphanie Devaux*, Dasa Cizkova*, Jusal Quanico, Julien Franck, Serge Nataf, Laurent Pays, Lena Hauberg-Lotte, Peter Maass, Jan H. Kobarg, Firas Kobeissy, Céline Mériaux, Maxence Wisztorski, Lucia Slovinska, Juraj Blasko, Viera Cigankova, Isabelle Fournier, Michel Salzet

Article Status: published in Molecular and Cellular Proteomics, in press

Summary: Experimental manipulation including sample gathering and data analysis were realized by Ms Devaux. In details, my contribution includes:

- Performing experimental spinal cord injury procedure, and collectioning tissue and conditioned media.
- Samples preparation for mass spectrometry analysis prior nanoLC- MS analysis and data analysis.
- Performing MALDI-MS imaging experiments and procedures such as sample preparation, matrix application and image acquisition.
- Performing immunohistochemistry experiments and data analysis.
- In terms of writing the manuscript, Ms Devaux participated in the writing of the manuscript and its revision.

Proteomic Analysis of the Spatio-temporal Based Molecular Kinetics of Acute Spinal Cord Injury Identifies a Time- and Segment-specific Window for Effective Tissue Repair[§]

Stephanie Devaux^{‡§}, Dasa Cizkova^{§§^a}, Jusal Quanicó[‡], Julien Franck[‡], Serge Nataf[¶], Laurent Pays[¶], Lena Hauberg-Lotte^{||}, Peter Maass^{||}, Jan H. Kobarg^{**}, Firas Kobeissy^{‡‡}, Céline Mériaux[‡], Maxence Wisztorski[‡], Lucia Slovinska[§], Juraj Blasko[§], Viera Cigankova^{§§}, Isabelle Fournier[‡], and  Michel Salzet^{**}

Spinal cord injury (SCI) represents a major debilitating health issue with a direct socioeconomic burden on the public and private sectors worldwide. Although several studies have been conducted to identify the molecular progression of injury sequel due from the lesion site, still the exact underlying mechanisms and pathways of injury development have not been fully elucidated. In this work, based on OMICs, 3D matrix-assisted laser desorption ionization (MALDI) imaging, cytokines arrays, confocal imaging we established for the first time that molecular and cellular processes occurring after SCI are altered between the lesion proximity, *i.e.* rostral and caudal segments nearby the lesion (R1-C1) whereas segments distant from R1-C1, *i.e.* R2-C2 and R3-C3 levels coexpressed factors implicated in neurogenesis. Delay in T regulators recruitment between R1 and C1 favor discrepancies between the two segments. This is also reinforced by presence of neurites outgrowth inhibitors in C1, absent in R1.

Moreover, the presence of immunoglobulins (IgGs) in neurons at the lesion site at 3 days, validated by mass spectrometry, may present additional factor that contributes to limited regeneration. Treatment *in vivo* with anti-CD20 one hour after SCI did not improve locomotor function and decrease IgG expression. These results open the door of a novel view of the SCI treatment by considering the C1 as the therapeutic target. *Molecular & Cellular Proteomics* 15: 10.1074/mcp.M115.057794, 2641–2670, 2016.

Spinal cord injury (SCI)¹ belongs to the serious, currently incurable disorders of the central nervous system (CNS), that are often accompanied by a permanent disability (1). Most SCI are related to traumatic spinal cord damages induced by road trauma, falls, or sport injuries (diving). Among the hallmark features of SCI is the axonal disruption in the spinal cord, which is often caused by fractured intervertebral disc or vertebrae. This primary event is followed by a progressive cascade of secondary deleterious reactions spreading to the adjacent spared tissue leading to a worsening of the neurological status (2, 3). Although axonal regeneration is initiated, it is hampered by a combination of local factors that include severe inflammation, lack of trophic support and development of an inhibitory scar-forming environment. In fact, the regenerative capacity of the central nervous system is particularly challenged in SCI as multiple cues converge to act as a chemical and physical barrier for the repair process (4, 5). It is now acknowledged that inflammation is one of the major key player that determines abortive axonal repair in SCI. Thus, although the immune response is recognized as primordial to preserve tissue homeostasis, the spatio-temporal course of inflammation in SCI is not favorable to axonal regeneration.

Acute inflammation develops hours to days following initial spinal cord trauma and is triggered by the axonal damage and

From the [‡]Univ. Lille, Inserm, U-1192 - Laboratoire Protéomique, Réponse Inflammatoire et Spectrométrie de Masse-PRISM, F-59000 Lille, France; [§]Institute of Neurobiology, Slovak Academy of Sciences, Center of Excellence for Brain Research, Soltesovej 4–6 Kosice, Slovakia; [¶]Inserm U-1060, CarMeN Laboratory, Banque de Tissus et de Cellules des Hospices Civils de Lyon, Université Lyon-1, France; ^{||}Center for industrial mathematics, University of Bremen, Bibliothekstraße 1, MZH, Room 2060, 28359 Bremen, Germany; ^{**}Steinbeis Innovation Center SCiLS Research, Fahrenheitstr. 1, 28359 Bremen, Germany; ^{‡‡}Department of Biochemistry and Molecular Genetics, Faculty of Medicine, American University of Beirut. ^{§§}Department of Anatomy, Histology and Physiology, University of Veterinary Medicine and Pharmacy in Kosice, Komenského 73, 041 81 Kosice, Slovakia

Received December 29, 2015, and in revised form, May 31, 2016
 Published, MCP Papers in Press, June 1, 2016, DOI 10.1074/mcp.M115.057794

Author contributions: D.C. and M.S. designed research; S.D., D.C., J.Q., J.F., S.N., L.P., L.H., P.M., J.H.K., F.K., L.S., J.B., V.C., I.F., and M.S. performed research; S.D., D.C., J.Q., J.F., S.N., L.P., L.H., P.M., J.H.K., F.K., C.M., M.W., L.S., J.B., V.C., I.F., and M.S. analyzed data; S.D. D.C. and M.S. wrote the paper; D.C., I.F., and M.S. received funding for this project.

¹ The abbreviations used are: SCI, Spinal cord injury.

neuronal cell death at the lesion site. This is followed by a cellular and molecular inflammatory cascade that initiates the activation of resident glial cells (microglia, astrocytes), infiltration of blood-borne immune cells (lymphocytes, monocytes), and a massive release of chemokines/cytokines by microglia, macrophages and neuronal cells. During the acute inflammatory response, macrophages/microglia phagocytose cell debris and also release neurotoxic factors and stimulate the formation of a glial scar that, on the long-term, prevents axonal regrowth. At this stage, a resolution of acute inflammation and a switch toward a neuroprotective cytokines/chemokines profile would favor tissue repair and limit glial scar extension. Instead, a chronic inflammatory process usually develops weeks after trauma and leads to both an aberrant tissue remodeling and a defective tissue repair. Interestingly, although there is currently no efficient therapy for SCI, one of the approved clinical treatments in the early phase of SCI is the administration of methylprednisolone treatment in order to prevent edema and to modulate inflammation (6). However, high-dose methylprednisolone is often associated with severe immunosuppression and side effects, such as pulmonary or urinary tract infections. Thus, there is an urgent need for identifying and testing novel neuro-therapeutic strategies that could prevent inflammation, limit scar extent, and stimulate tissue repair process.

In this context, a large array of molecules and therapies has been tested experimentally with the goal of targeting the healthy tissue adjacent to spinal cord lesion. Such a strategy is aimed at not only protecting this spared tissue from secondary lesion but also stimulating its regenerative potential in order to promote neuronal networks connectivity and axonal outgrowth. Among these proposed therapeutic strategies, cellular therapy belongs to the promising candidate approaches. Ideally, cell therapy strategies may allow to: (1) bridge spinal cord segments over any cavities or cysts formed at the lesion site, (2) replace lost neurons, oligodendroglia, and (3) create a favorable environment for axonal regeneration (7). Different cell therapy approaches include embryonic stem cells, induced pluripotent stem cells (iPS) and different categories of adult stem cells and progenitors such as olfactory ensheathing stem cells, neural progenitor cells (NPC) and mesenchymal stem cells (MSCs). In addition, graft of activated macrophages and transplantation of peripheral or central nervous tissue have been also proposed as an alternative to these stem cells based treatments (8). Comparative to cell therapy, other approaches including the use of exogenously-delivered neuroprotective molecules that would protect neurons from deleterious secondary processes, promote axonal growth and/or enhance nerve conduction in the preserved or regenerating axons. Different classes of molecules were shown to afford variable levels of clinical recovery in animal models of SCI. These comprise anti-inflammatory compounds such as minocycline, neurotrophic factors (BDNF, GDNF, NGF, erythropoietin) and molecules that alleviate re-

generating axons from the inhibitory effects of extracellular matrix molecules (9, 10). In particular, chondroitinase ABC eliminates chondroitin sulfate proteoglycans (CSPG) that interact with the major membranous component NG2 and inhibit the regeneration of damaged axons (11). Also, Nogo-A is one of several neurite growth inhibitory receptors expressed by axons (12). Thereby Nogo neutralizing antibodies or blockers of the post-receptors components of RhoA are used to improve long-distance axon regeneration and sprouting (13). Of note, Rho pathway is important to control the neuronal response after CNS injury and the RhoA inhibitor cethrin is actually in phase I/II a clinical trial (14). However, although numerous therapies exhibit potentials to foster neuroprotection, stimulate neurite outgrowth and reduce inflammation, the translation to clinical side is still not crowned by success. Reasons for such a failure are multiple and reside notably in our relatively poor knowledge on the spatiotemporal kinetics of secondary molecular events that characterize the post-trauma phase. This holds particularly important with regard to inflammatory mechanisms that may greatly vary depending on the time point and spinal cord segment considered. Defining a time- and segment-specific window for effective treatment is a key knowledge for an appropriate neuro-therapeutic intervention.

In this work, we present the first exhaustive spatio-temporal proteomic and biochemical analysis performed along the entire spinal cord axis in rat model of SCI. We combined this global proteomic analysis with 3D molecular mass spectrometry imaging study, time course analysis of immune cells infiltration and cytokine microarrays quantification. The whole spectrum of the data allowed us to depict a complete scheme along the spinal cord axis of the cellular and molecular sequel of events occurring through the time course of inflammatory process and abortive regeneration. We identified specific markers for each segment at different time points (3, 7, and 10 days) of the biochemical-pathophysiological processes and observed that, surprisingly, segments caudal to the lesion site host a robust inflammatory process accompanied by the local synthesis of neuroprotective and regenerative molecules. In particular, we demonstrated that the caudal segment immediately adjacent to the lesion site possesses, at least temporarily, all the intrinsic components/features that may allow axonal regeneration to occur. Such a caudal-to-rostral altered regenerative potential is likely hampered by inhibitory signals such as glycans that are abundantly detected or even secreted at the lesion site. Finally, we provided evidence that immunoglobulins (IgGs) are present at the lesion site only 3 days after injury and that *in vivo* treatment of anti-CD20 did not diminish the presence of these antibodies and did not ameliorate the BBB score of the treated animals.

EXPERIMENTAL PROCEDURES

Reagents—Dulbecco's modified Eagle's medium (DMEM) media, phosphate buffer saline (PBS), fetal calf serum (FCS) were purchased

from Invitrogen Life Technologies (Milan, Italy). Rat Cytokine Array Panel A was from R&D Systems (Minneapolis, MN). All chemicals were of the highest purity obtainable. Water, formic acid (FA), trifluoroacetic acid (TFA), acetonitrile (AcN) were purchased from Biosolve B.V. (Valkenswaard, The Netherlands). DL-dithiothreitol (DTT), Thiourea and iodoacetamide (IAA) were purchased from SIGMA (Saint-Quentin Fallavier, France). Trypsin/Lys-C Mix, Mass Spec Grade was purchased from Promega (Charbonnières, France) and Dynabeads® Protein A from Novex (Life Technologies, France). Fluorescence conjugated secondary antibodies and DAPI were purchased from MolecularProbes (Eugene, OR).

Animals—The study was performed with approval and in accordance to the guidelines of the Institutional Animal Care and Use Committee of the Slovak Academy of Sciences and with the European Communities Council Directive (2010/63/EU) regarding the use of animals in Research, Slovak Law for Animal Protection No. 377/2012 and 436/2012.

Experimental Design and Statistical Rational—For the collection of the conditioned media $n = 3$ rats control (no balloon inflation, 0 day) were sacrificed, $n = 3$ rats after 3 days SCI, $n = 3$ rats after 7 days post injury and $n = 3$ rats after 10 days post SCI. For the control group all segments are in triplicate. For the group 3 days after SCI, R3 and C3 segments include 2 replicates and $n = 3$ for the other segments. For the group 7 days after SCI R3 and C3 segments include 2 replicates and $n = 3$ for the other segments. For the group 10 days post SCI all segments are in triplicate. For the cytokines arrays experiments $n = 1$ rat were sacrificed per condition. The experiments were performed in experimental replicates. For the IgG purification $n = 3$ rats per condition (control, 3, 7, and 10 days) were sacrificed. The experiments were performed in biological replicates. For the immunohistochemistry experiments $n = 3$ rats per condition were sacrificed. The analyses were performed in biological triplicates. For MALDI imaging experiment $n = 1$ rat was sacrificed 3 days post injury. Twenty-five sections for the complete 3D MALDI imaging experiments have been performed from R1 to C1.

Statistical analysis: For the proteomic statistical analysis of conditioned media, only proteins presenting as significant by the ANOVA test were used with FDR 5%. Normalization was achieved using a Z-score with a matrix access by rows. The immunohistochemistry statistical analyses were based on one-way ANOVA followed by Tukey Kramer test, significant values were marked * $p < 0.05$, ** $p < 0.01$, *** $p < 0.001$. Quantification analyses of immunofluorescence staining for Iba1, FoxP3 and neutrophil elastase were performed on six sections from rostral and caudal/per condition ($n = 3$ each). Error bars represent the S.E. BBB score analysis was based on one-way ANOVA test. Values of $p < 0.05$ were considered statistically significant. For the cytokines array panel, the statistical analyses were performed using Student's t test * $p < 0.05$, ** $p < 0.01$, *** $p < 0.001$. Error bars represent the S.E.

Experimental Spinal Cord Injury Procedure—The SCI was induced using the modified balloon compression technique in adult male Wistar rats, according to our previously published study (15). Manual bladder expression, 2 times a day, was required for 3–10 days after the injury. In the control group a 2-French Fogarty catheter was inserted at the same level of spinal cord, but the balloon was not inflated and no lesion was performed.

Collection of Conditioned Media (CM) from Control and Lesioned Spinal Cord Segments—Experimental SCI rats at 3, 7, and 10 days and sham-operated-control rats were sacrificed by isoflurane anesthesia followed by decapitation. The spinal cord was pressure expressed by injecting sterile saline (10 ml) throughout the vertebrate canal, along the caudo-rostral axis. Each spinal cord was macroscopically observed to check that lesion was well centered at the Th8-Th9 level on the longitudinal axis. Entire spinal cord was divided into

transversally sectioned slides (~1.0 cm thick each) obtained from the lesion site (Th7-Th11) and from the segments rostral (C1-Th6) and caudal (Th12-L6) to the site of injury. Slides were then chopped into 0.5 cm thick sections (2 sections per segment) and deposited into a 12-well culture plate containing 1 ml DMEM without FCS. After 24 h incubation in a humidified atmosphere with 5% CO₂ at 37 °C, 1 ml of SCI-derived conditioned media CM (CM-SCI) were collected (rostral, lesion, caudal segments) and centrifuged 30 min at 15,000 rpm at 4 °C. The same procedure was performed for obtaining CM from control spinal cord tissue. Samples were stored at –80 °C. To address the degree of cell-to cell integrity and viability, additional cryostat sections were cut from incubated segments for 24 h and immersed into tissue-tek®. Afterward cryostat sections were processed to standard IHC with NeuN and GFAP antibodies. The data confirmed the cyto- architecture of neurons and glial cells (supplemental Fig. S1) and confirmed the well preserved neuro-glial integrity within cultured spinal cord segments 24 h *in vitro*. This confirms that the collected molecules are products of vital cells processes.

Conditioned Media Digestion—A volume of 150 μ l of tissue supernatants were denatured with 2 M urea in 10 mM HEPES pH 8 by ultrasonication on ice. Protein reduction is realized by incubation with 10 mM DTT for 40 min at 56 °C followed by alkylation with 55 mM IAA for 40 min in the dark. IAA was quenched with 100 mM thiourea. Protein digestion was performed with 30 μ g/ml LysC/Trypsin mix, overnight, at 37 °C. Digestion was stopped with 0.5% TFA. The solution was dried in a SpeedVac to reduce the volume. Peptides were desalted using C18 ziptips (Millipore). Elution peptides were dried in a SpeedVac and resuspended in 0.1% FA before injecting into nanoLC.

LC MS/MS Analysis of Conditioned Media—Samples were separated by online reversed-phase chromatography using a Thermo Scientific Proxeon Easy-nLC1000 system equipped with a Proxeon trap column (100 μ m ID \times 2 cm, Thermo Scientific) and a C18 packed-tip column (Acclaim PepMap, 75 μ m ID \times 15 cm, Thermo Scientific). Peptides were separated using an increasing amount of acetonitrile (5–35% over 120 min) at a flow rate of 300 nL/min. The LC eluent was electrosprayed directly from the analytical column and a voltage of 1.7 kV was applied via the liquid junction of the nanospray source. The chromatography system was coupled to a Thermo Scientific Q-exactive mass spectrometer programmed to acquire in a data-dependent mode Top 10 most intense ion method. The survey scans were done at a resolving power of 70,000 FWHM (m/z 400), in positive mode and using an AGC target of 3e6. Default charge state was set at 2, unassigned and +1 charge states were rejected and dynamic exclusion was enabled for 25 s. The scan range was set to 300–1600 m/z . For ddMS², the scan range was between 200–2000 m/z , 1 microscan was acquired at 17,500 FWHM and an isolation window of 4.0 m/z was used.

MS Data Analysis—All the MS data were processed with MaxQuant (17) (version 1.5.1.2) using the Andromeda (18) search engine. Proteins were identified by searching MS and MS/MS data against Decoy version of the complete proteome for *Rattus norvegicus* of the UniProt database (19) (Release June 2014, 33,675 entries) combined with 262 commonly detected contaminants. Trypsin specificity was used for the digestion mode with N-terminal acetylation and methionine oxidation selected as the variable. Carbamidomethylation of cysteines was set as a fixed modification, with up to two missed cleavages. For MS spectra, an initial mass accuracy of 6 ppm was selected, and the MS/MS tolerance was set to 20 ppm for HCD data. For identification, the FDR at the peptide spectrum matches (PSMs) and protein level was set to 1%. Relative, label-free quantification of proteins was performed using the MaxLFQ algorithm (20) integrated into MaxQuant with the default parameters. The data sets and the Perseus result files used for analysis were deposited at the ProteomeXchange Consor-

tium (21) (<http://proteomecentral.proteomexchange.org>) via the PRIDE partner repository (22) with the data set identifier PXD003375. Analysis of the proteins identified was performed using Perseus software (<http://www.perseus-framework.org/>) (version 1.5.0.31). The file containing the information from identification was used with hits to the reverse database, and proteins only identified with modified peptides and potential contaminants were removed. Then, the LFQ intensity was logarithmized ($\log_2[x]$). Categorical annotation of rows was used to defined different groups after grouping replicates: (1) Temps (Control, 3, 7 and 10 days), (2) Segments (R3, R2, R1, L, C1, C2, and C3). Multiple-samples tests were performed using ANOVA test with a FDR of 5% and preserving grouping in randomization. Normalization was achieved using a Z-score with a matrix access by rows.

For the statistical analysis, only proteins presenting as significant by the ANOVA test were used for statistical analysis. Hierarchical clustering depending on time or segment was first performed using the Euclidean parameter for distance calculation and average option for linkage in row and column trees using a maximum of 300 clusters. For visualization of the variation of proteins expression depending to the condition, the profile plot tool was used with a reference profile and an automatic selection of the 10 or 15 correlated profiles. To quantify fold changes of proteins across samples, we used MaxLFQ. To visualize these fold changes in the context of individual protein abundances in the proteome, we projected them onto the summed peptide intensities normalized by the number of theoretically observable peptides. Specifically, to compare relative protein abundances between and within samples, protein lengths normalized to \log_2 protein intensities (termed “iBAQ” value in MaxQuant) were added to the MaxLFQ differences. Functional annotation and characterization of identified proteins were obtained using PANTHER software (version 9.0, <http://www.pantherdb.org>) and STRING (version 9.1, <http://string-db.org>). Using the GeneMANIA Cytoscape plugin (23), 4 co-expression networks were generated from the proteomic values obtained by the analysis of control samples and caudal, rostral and lesion segments respectively. Each segment-specific coexpression network was calculated from data obtained at all-time points following SCI. Such an approach allowed then to perform a supervised clustering in order to identify functionally-relevant subnetworks that would constitute a segment-specific and time-independent molecular signature. In particular, to identify “Inflammation” subnetworks, Fibrinogen alpha (FgA) was chosen as a reference protein and, for each group of samples, networks were built that gathered the 100 proteins whose values were the most closely correlated with those of FgA. Lists of proteins and their encoding genes were then submitted to an enrichment analysis based on gene ontology (GO) annotations, using the open source tool EnrichR (24). Finally, coexpressed proteins whose encoding genes were annotated with the same GO term of interest (for instance “complement activation”), were extracted and subnetworks visualized on cytoscape. The same method was applied to identify “axon guidance” and “neuron differentiation regulation” subnetworks from the networks of proteins coexpressed with neurofilament proteins Nfl, Nfm and Nfh in each group of samples. For presentation purposes, nodes were assigned equal weights and subnetworks were slightly distorted to avoid node superimposition.

Subnetwork Enrichment Pathway Analyses and Statistical Testing—The Elsevier’s Pathway Studio version 9.0 (Ariadne Genomics/Elsevier) was used to deduce relationships among differentially expressed proteomics protein candidates using the Ariadne ResNet-database (25, 26). “Subnetwork Enrichment Analysis” (SNEA) algorithm was selected to extract statistically significant altered biological and functional pathways pertaining to each identified set of protein hits (C1, C2, C3, R1, R2, and R3 sets). SNEA utilizes Fisher’s statistical test used to determine if there are non-randomized associations

between two categorical variables organized by specific relationship. SNEA starts by creating a central “seed” from all relevant entities in the database, and retrieving associated entities based on their relationship with the “seed” (i.e. binding partners, expression targets, protein modification targets, regulation). The algorithm compares the subnetwork distribution to the background distribution using one-sided Mann-Whitney U-Test, and calculates a p value indicating the statistical significance of difference between two distributions. In our analysis, “GenBank” ID and gene symbols from each set were imported to the software to form an experimental data set. For the reconstruction of networks of pathways, biological processes and molecular function were evaluated for each single protein hit and its associated targets (networks and pathways) (27, 28). Integrated Venn diagram analysis was performed using “the InteractiVenn”; a web-based tool for the analysis of complex data sets.

Cytokines Profile of Conditioned Medium—Cytokines and chemokines expression of CM from control, 3, 7, and 10 days for the segments R1 and C1 was performed by using a Rat Cytokine Array Panel A according to the manufacturer’s instructions. Briefly, the array membranes were first incubated in the blocking buffer for 1 h. In the meantime, 200 μ l of CM were mixed with the Detection Antibody Mixture and incubated for 1 h at room temperature. Then, after removing the block buffer, the sample/antibody mixture were added to array membranes and incubated overnight at 4 °C. After incubation, the membranes were washed 3 times with the wash buffer and then incubated with the Streptavidin-HRP solution for 30 min at room temperature. The membranes were finally washed with wash buffer for 3 times and the bound antibodies were detected by chemoluminescence using the chemireagent mix. The membranes were quantified by densitometry using ImageJ software. Background staining and spot size were analyzed as recommended by the manufacturer. Normalization was done with control expression.

IgG Purification with Dynabeads Protein A—CM (150 μ l) obtained from lesion site (~1.5 mg of protein in 2 ml) after SCI3, 7 or 10 days after SCI and from the corresponding segment of control spinal cord were bound with 50 μ l of Dynabeads Protein-A 200 μ l of PBS-Tween 20 and incubated 10 min with rotation at room temperature. The beads coupled with IgGs were harvested using a magnet (1 min) and the recovered supernatant solution was removed. The remaining beads-IgG complex was washed with PBS-Tween 20. Afterward, IgGs bound to microbeads were eluted by adding 30 μ l of 0.1 M glycine (pH 3), incubated 10 min at 70 °C temperature to dissociate the beads-IgG complex and then neutralized by adding 30 μ l of 1 M Tris-HCl (pH 8.5). Afterward, a magnet was used to remove the beads from the eluate containing IgGs. The eluate was then separated on SDS-PAGE (12% polyacrylamide gel slabs) followed by silver staining to check the bands corresponding to IgGs of the Mw of 25 kDa, 50 kDa and 75 kDa. Shot-gun mass spectrometry analysis was performed to identify the band corresponding to the appropriate Mw. Silver destaining was performed using 30 mM of potassium ferricyanide and 100 mM sodium thiosulfate (1:1) 200 μ l per band for 20 min in the dark. Bands were washed 2 times for 15 min with Milli-Q water followed by an in-gel digestion as previously described (29). The samples were reconstituted with 10 μ l of 5% AcN/0.1% FA and injected on a UPLC MS instrument. Separation was performed using an EASY-nLC 1000 UPLC (Thermo Scientific) equipped with a 75 μ m \times 2 cm Acclaim PepMap 100 pre-column with nanoViper fittings and a 50 μ m ID \times 150 mm Acclaim PepMap RSLC analytical column (Thermo Scientific). The peptides were eluted using a gradient of AcN starting from 5% to 30% over 1 h at a flow rate of 300 nl/min. The Q-Exactive instrument was set to acquire top 10 MS2. The survey scans were taken at 70,000 FWHM (at m/z 400) resolving power in positive mode and using a target of 1E6 and default charge state of +2. Unassigned and +1 charge states were rejected, and dynamic

exclusion was enabled for 30 s. The scan range was set to m/z 300–1600 m/z . For the MS2, 1 microscan was obtained at 17,500 FWHM and isolation window of 3.0 m/z , using a scan range between m/z 200–2000 m/z . Tandem mass spectra were processed with Thermo Scientific Proteome Discoverer software version 1.3. Spectra were searched against UniprotKB/Swiss-Prot (version March 2014) filtered with *Rattus norvegicus* (25678 sequences) taxonomy using the SEQUEST HT algorithm (version 1.3.0.339). The search was performed choosing trypsin as the enzyme with one missed cleavage allowed. Precursor mass tolerance was 10 ppm, and fragment mass tolerance was 0.1 Da. N-terminal acetylation; and cysteine carbamidomethylation; methionine oxidation was set as variable modifications. Peptide validation was performed with the Percolator algorithm by filtering based on a q -value below 0.01, which corresponds to a false discovery rate (FDR) of 1%. The data sets used for analysis were deposited at the ProteomeXchange Consortium (21) (<http://proteomecentral.proteomexchange.org>) via the PRIDE partner repository (22) with the data set identifier PXD004247.

Tissue Processing and Immunohistochemical Analysis of Immune Cells—Rats following SCI at 3, 7 and 10 days and sham surgery were deeply anesthetized and perfused transcardially with saline followed by 4% paraformaldehyde (PFA) in 0.1 M phosphate buffer saline. Spinal cords were removed post-fixed in 4% PFA, embedded in gelatin-egg albumin protein matrix (10% ovalbumin, 0.75% gelatin and glutaraldehyde) and soaked overnight in 30% sucrose. Each spinal cord was dissected into 1 cm block (rostral and caudal segment) and 40 μ m thick longitudinal cryostat (Leica Instruments, Heidelberg, Germany) sections (sagittal plane) were cut serially and standard immunohistochemistry technique was performed. Before incubation with primary antibodies for FoxP3 and neutrophil elastase, to reduce autofluorescence background, tissue sections were incubated 15 min at room temperature in Sudan Black B and then washed in PBS. Tissue sections were incubated in the following primary antibodies: rabbit anti-Iba1, a marker for microglia/macrophages (1:800; Wako Pure Chemical Industries, Osaka, Japan), rabbit anti-FoxP3, a marker for lymphocyte T regulator (1:200; Abcam, Cambridge, UK), rabbit anti-neutrophil elastase, a marker for neutrophil (1:200; Abcam). Tissues sections were washed in PBS and then incubated in the secondary fluorescent antibody goat anti-rabbit IgG or goat anti-mouse conjugated with AlexaFluor 594, goat anti-mouse IgG or goat anti-rabbit IgG conjugated with AlexaFluor488. Omission of the primary antibody served as the negative control. For nuclear staining, we used 4–6-diaminidino-2-phenylindol (DAPI) (1:10000). Finally, sections were washed in 0.1 M PBS, mounted, and coverslipped with Vectashield mounting medium (VectorLaboratories, Inc., Burlingame, CA) and observed under a fluorescence microscope (NikonEclipseTi, Japan) and confocal laser scanning microscope (Leica TCSSP5 AOBs, Leica Microsystems, Mannheim, Germany).

Quantification analyses of immunofluorescence staining for Iba1, FoxP3 and neutrophil elastase were performed on 6 sections from rostral and caudal/per condition ($n = 3$ each). Captured fluorescence digital images at 40x magnification were analyzed by ImageJ software. Iba1 quantification was determined by randomization counting cells manually with Image J software in gray and white matters of rostral and caudal segments. FoxP3 and neutrophil elastase quantification was determined by the percentage of positive cells compared with DAPI staining by counting cell manually with image J software.

Immunohistochemical Analysis of IgG Deposition—Tissue sections of 40 μ m thickness from rostral and caudal segment adjacent to the lesion at the 3, 7 and 10 days post-injury and corresponding cuts for controls (embedded in gelatin-egg albumin protein matrix, same procedure as for IHC for immune response) were cut. One set of tissue sections were incubated with primary goat anti-rat IgG2a antibody (1:500, Bethyl Laboratories, Inc., Montgomery, TX) overnight at 4 °C.

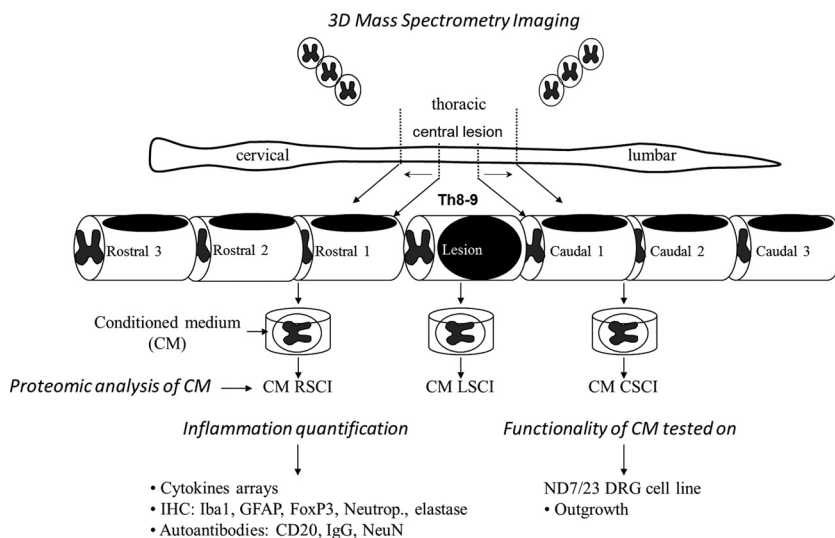
After 3 washing steps in PBS, sections were incubated with secondary fluorescent antibodies: rabbit anti-goat IgG conjugated with AlexaFluor594 or AlexaFluor 488 for one hour at room temperature. For double labeling, we have used the following primary antibodies: mouse anti-GFAP, (1/500; Upstate Biotech Millipore), rabbit anti-Iba1 (1:800), mouse anti-NeuN, marker for neurons, (1/1000; Upstate Biotech Millipore) overnight at 4 °C, followed with corresponding secondary antibodies. Another set of sections were labeled with secondary fluorescent antibody anti-rat IgG conjugated with (AlexaFluor 488), followed by incubation with primary antibodies for NeuN, GFAP and Iba1. Omission of the primary antibody served as the negative control. For nuclear staining, we used DAPI (1:10000). Finally, sections were washed with 0.1 M PBS, mounted, and coverslipped with Vectashield mounting medium and observed under a fluorescence microscope and confocal laser scanning microscope. Fluorescence or confocal images, including orthogonal views, were processed by using 0.5 μ m optical sections at 40x or 60x magnification.

Intraspinal Delivery of CD-20 Antibody—One hour after SCI, in anesthetized rats with 1.5–2% isoflurane we have microinjected intraspinally primary rabbit anti-rat CD-20 antibody (Biorbyt Ltd., Cambridge, United Kingdom), for local depletion of B- lymphocytes IgG production. Intraspinally injections of (1) saline ($n = 3$) and (2) rabbit anti-rat CD-20 antibody, 0.5 μ g/ μ l ($n = 3$) were performed using a 50- μ l Hamilton syringe (30G needle, Cole Parmer, Anjou, Quebec) connected to UltraMicroPump III with Micro4 Controller, 4-Channel (World Precision Instruments, Inc., Sarasota, FL) and stereotactic device, with a delivery rate of 0.5 μ l/min. 3 bilateral intraspinal injections of 1 μ l per injection were performed at the lesion site, whereas one injection of 1 μ l per injection was done at rostral and caudal segments. Each delivery was positioned 1 mm from the spinal cord midline and injected at a depth of 1.8–2 mm from the pial surface of the spinal cord. The distance between injections was 1 mm, avoiding vessels. Intraspinally injections were followed by procedure published in our study (16). After injecting the dose of saline or CD-20 antibody, the needle was maintained in the tissue for an additional 30 s. No antibiotic treatment was performed during animal's survival. All rats survived for 3 days.

Behavioral Testing After CD-20 Antibody Intraspinal Delivery—Animals were evaluated using Basso, Beattie, and Bresnahan (BBB) open-field test to assess motor function after SCI at day 0, 3, 7, 10, 14 and 28. Each rat was tested for 5 min by two blinded examiners. BBB test measures locomotor outcome (hind limb activity, body position, trunk stability, tail position and walking paw placement) of rats utilizing the rating scale ranges from 0 (no observable hind limbs movements) to a maximum of 21 (plantar stepping, coordination and trunk stability similar to control rats). All data are reported as mean \pm S.E. Differences in mean BBB scores between the sham-controls and SCI groups at each survival interval were assessed using one-way ANOVA.

MALDI Imaging Data Analyses—Twelve micrometer tissue sections from the R1, lesion and C1 segments were obtained using a cryostat (Leica Microsystems, Nanterre, France). These were mounted on indium tin oxide (ITO)-coated slides and placed under vacuum in a dessicator for 15 min. 2,5-dihydroxybenzoic acid was used as matrix, and was prepared at a concentration of 20 mg/ml in 70:30 methanol/0.1% TFA in H₂O. The matrix was deposited manually using a sprayer developed in-house at a flow rate of 300 μ l/h for 5 min. Lipid imaging was performed on an UltraFlex II instrument (Bruker Daltonics, Bremen, Germany) equipped with a micro-channel plate (MCP) detector. The instrument was equipped with a Smartbeam™ laser capable of operating up to 200Hz and was controlled using FlexControl 3.3 (Build 108) software (Bruker Daltonics). The data sets were recorded in positive reflector mode and 500 laser shots were accumulated for each raster point. The laser focus was set to medium, and deflection

FIG. 1. Schematic design of the experimental procedure performed in this study.



of masses was deactivated. Spectra were acquired by oversampling at a lateral resolution of 20 μm . External calibration was performed using the PepMix standard (Bruker Daltonics). Spectra were acquired between m/z 60–1000.

The 2D MALDI Imaging data of rostral (R1) caudal (C1) and lesion (L) sections after 3 days of SCI ($n = 1$) were analyzed with SCiLS Lab 2015a (30). The baseline was removed by iterative convolution and the data were normalized based on the total ion count (TIC) method (31). Subsequently, the orthogonal matching pursuit was used to detect peaks. These peaks were aligned to the mean spectrum and the data were smoothed with a strong ($\lambda = 0.5$) Chambolle filter method. Automatic spatial segmentation was performed by using the bisecting k-means algorithm (32). Colocalized m/z values with the lesion region were elucidated by using Pearson's correlation analysis. With component analysis fundamental components of given spectra and m/z images can be discovered unsupervised. Here, the principal component analysis as well as the probabilistic latent semantic analysis were used (33). The PLSA was performed with random initialization with a threshold of 29.0588, maximum interval processing mode, lower m/z range threshold mode and individual spectrum mode. The PCA was performed with no scaling, a threshold of 29.0588, maximum interval processing mode, lower m/z range threshold mode and individual spectrum mode (30).

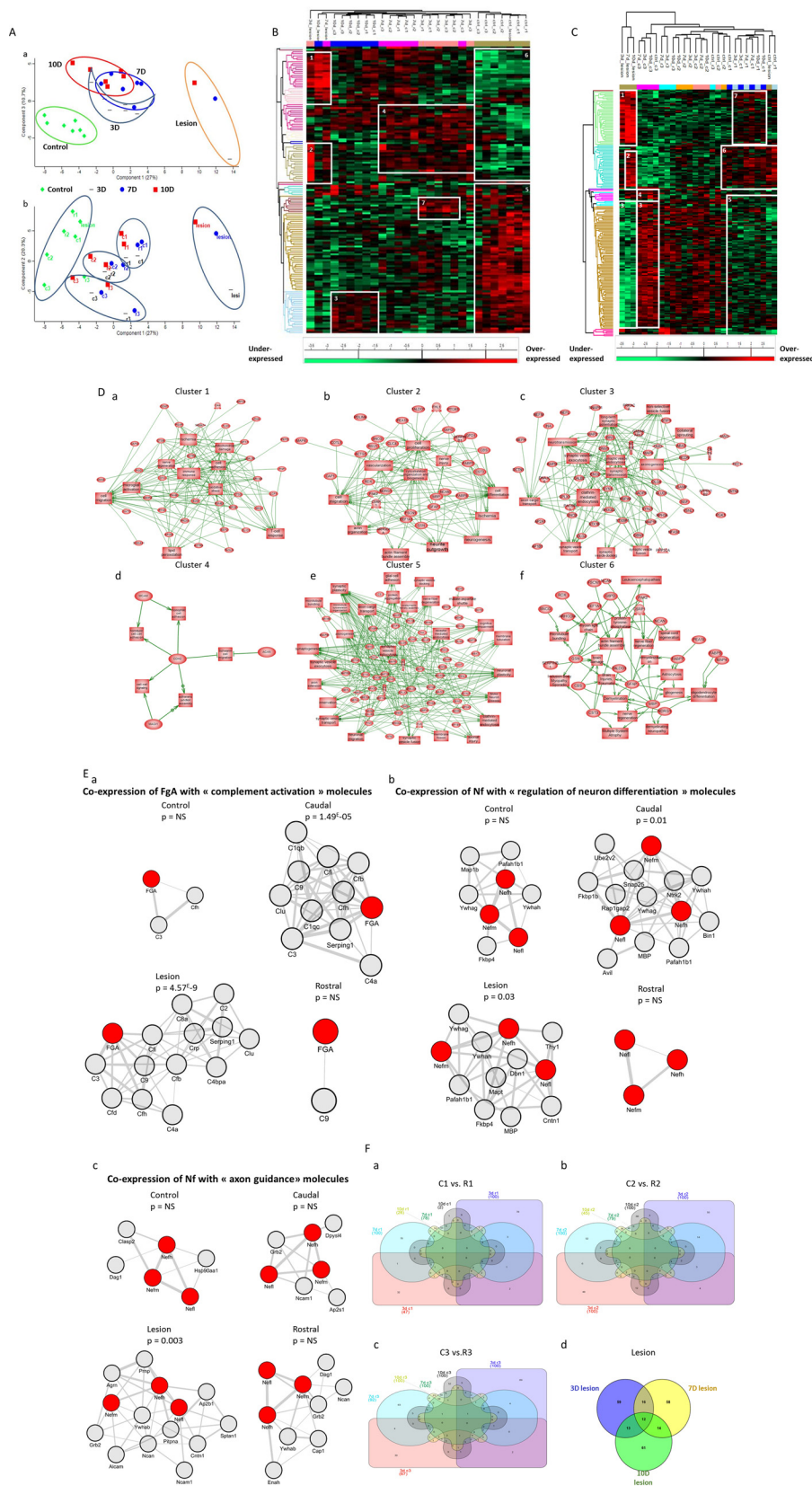
RESULTS

Workflow—Our main goal was to establish a fine mapping of the molecular events that occur in a time- and segment-specific manner during sub-acute SCI. We chose to focus our analysis on the identification of soluble factors that may support intra- or intersegmental communications between distinct cellular compartments. For this purpose, we performed proteomic shot-gun triplicate analyses of the conditioned medium (CM) derived from seven spinal cord segments localized at the lesion site (L) or either caudal to the lesion (C1, C2, C3) or rostral (R1, R2, R3) to the lesion. Each of these analyses were performed on spinal cord segments obtained on days 3, 7, or 10 post-SCI giving rise to a set of 80 proteomic data covering an average of 1500 proteins identified per sample with at least 2 peptides per protein recognized and percentage of false positive (FDR) < 1% (supplemental Data S1).

Proteomic data were then analyzed using complementary bioinformatics approaches that allowed unsupervised or supervised clustering of quantified proteins and the identification of differentially expressed molecules. Thus, both a comprehensive strategy without *a priori* and a focused one were applied to analyze proteomics data. In parallel, cytokine array measurements were performed and the whole of the proteomics data obtained from supernatant analyses was then correlated with immunohistological analyses and functional studies (Fig. 1).

Global Proteomic Study Along the Spinal Cord Axis at Key Time Points of SCI—Principal component analysis of conditioned media proteomics data clearly demonstrated that profiles in SCI samples can be clustered depending on the segment localization, irrespective of the time point considered. In addition, control samples harbor a molecular profile that can be sharply distinguished from any of SCI profiles, including those of segments localized at distance from the lesion site (*i.e.* the R3 and C3 profiles) (Fig. 2A). Time course analyses show that control samples, in one hand, and lesion samples, on the other hand, are clearly distant from all other samples (Fig. 2Aa upper panel). The remaining profiles display a partial overlap, indicating that time point may not be the main parameter allowing discriminating the proteomic profiles of spinal cord segments in this model. In contrast, a clear clustering of profiles was obtained when analyzing samples on the basis of their spatial localization (Fig. 2Ab lower panel). Thus, independently from the time point considered, profiles from each group of segments analyzed (*i.e.* rostral *versus* caudal *versus* lesion) displayed intragroup similarities. This finding provides evidence that in the SCI model, proteomic profiles in spinal cord segments may be discriminated on the basis of spatial localization. This result also demonstrates that with regard to the secretome, spinal cord segments tend to coevolve in function of their distance to the lesion site rather than their caudal *versus* rostral localization. Indeed, in terms of proteins

FIG. 2. Spatio-temporal organization of proteins. **A**, Principal component analysis (PCA) of conditioned media shows the representation of the different samples grouping regarding (a) time after injury and (b) spatial organization of the spinal cord. One point corresponds to all proteins identified according to their label free quantification for each segments and each time point. Heat map of proteins with different secretion profiles in conditioned media from different time after SCI (3D, 7D, 10D, and control) and from different segments (R3, R2, R1, L, C1, C2, C3). **B**, Hierarchical clustering regarding time point. **C**, Hierarchical clustering regarding spatial organization. Distinct clusters are highlighted. **D**, System biology analysis for network identification in each cluster issued from heat map of proteins with different secretion profiles in conditioned media from different time after SCI (3D, 7D, 10D, and control) and from different segment (R3, R2, R1, L, C1, C2, C3) regarding the spatial organization. **E**, Analysis of coexpression networks identify in inflammation, neuro-axonal and axonal guidance in conditioned media. The 100 genes which encoded molecules were the most tightly coregulated with fibrinogen- α (FgA), neurofilament L, M and H (Nf) respectively in conditioned media control, rostral, lesion and caudal were identified and assessed for gene set enrichment. Panel **Ea** shows subnetworks of genes annotated by the GO terms “inflammation”, caudal and lesion segments have significant p value unlike control and rostral segments. Panel **Eb** presents subnetworks of genes annotated by the GO terms “neuro-axonal,” caudal and lesion have significant p value unlike control and rostral segments. Panel **Ec** shows subnetworks of genes annotated by the GO terms “axonal guidance”, only lesion has significant p value unlike caudal, lesion and rostral segments. **F**, Differential distribution of unique and common/intersected biological and functional pathways among the three spinal cord rostral and caudal regions (C1, C2, C3 versus R1, R2, and R3) factored by time of SCI (3, 7, and 10 days). Each pair of spinal cord region (C1 versus R1) was analyzed across the three time points represented utilizing a comprehensive Venn analysis representation extracted from Subnetwork Enrichment Analysis.



patterns, R3 and C3 samples cosegregated and were clearly distinguished from the R2 and C2 patterns, the R1 and C1 patterns and the lesion patterns.

Hierarchical clustering depending on the time course post-injury (Fig. 2B, Table I) or the spatial localization along the spinal cord (Fig. 2C, Table II, [supplemental Data S2](#)) were first performed using the Euclidean parameter for distance calculation and average option for linkage in row and column trees using a maximum of 300 clusters. As a criterion of significance, we applied an ANOVA significance threshold of $p < 0.05$, and heat maps were created. A total of 147 proteins for time-dependent clustering and 193 proteins for segment-dependent clustering were considered reliable based on statistical analysis. In the time-dependent clustering (Fig. 2B, Table I), two major branches of the heat map separated the 3 day lesion segment in one branch from the others in the second branch. This latter was subdivided in two sub-branches: the first one gathering all controls whatever the segments and the second one all the other ones. This branch was itself subdivided in 4 branches, *i.e.* one for the lesion segments and the three other ones regroup all segments per time. Overall, this approach allowed a total of 6 clusters to be retrieved (Fig. 2B, Table I). The proteins in each cluster were then analyzed using PANTHER software (<http://www.pantherdb.org>) to determine the biological functions based on the protein classes. Control group were found to be characterized by two different clusters, *i.e.* *cluster 5* signing an overexpression of tubulins network, enzymatic metabolism network and vesicle-trafficking network and *cluster 6* corresponding to an under-expression of heat shock proteins network, neurofilaments and filamins networks and immune response factors (Table I). Lesion segments showed proteins overexpressed involved in neurogenesis, notably adducin and plectin, and in immune response (*e.g.* galectin 1 and 3, coronin) (*cluster 1*) (Table I). *Cluster 2* corresponds to a clear increased expression of proteins involved in inflammation in the lesion segment after 3 days and a weak overexpression of these proteins at 7 days in the lesion segment as well as in other segments at 3 and 7 days (Table I). By comparison, inflammatory molecules were down-regulated in all segments at 10 days after SCI and in control samples. *Cluster 4* corresponds to an overexpression of proteins in rostral and caudal segments on day 3 and day 7 post-SCI. *Cluster 4* shows an overexpression of proteins involved in neurite outgrowth like SPARC, neurofilament, lamin and the ones involved in regeneration processes, but are underexpressed in control (*cluster 6*). Some proteins involved in these functions are found at 10 days overexpressed as CRMP-3 and transgelin 3, but these proteins are also present in control (Table I).

For the second clustering analysis taking into account the spatial distribution of proteins (Fig. 2C, Table II, [supplemental Data S2](#)), we observed again that the lesion segments were clustered apart from the other groups of samples. The second branch is subdivided in two branches, *i.e.* one separating C3

at each time point from the others which are then subdivided again in two branches, *i.e.* one regrouping R3 (3 and 7 days after SCI) and the other one including segments with 2 major groups (R1 and C1 *versus* R2 and C2). In the lesion segments, proteins overexpressed are related to the immune response (Table II). These proteins are also expressed in R1 and C1 segments at each time point after SCI and under-expressed in the other segments, showing the correlation between lesion and the rostral and caudal adjacent segments. A total of 7 clear clusters were identified. *Clusters 2* and *6* correspond to proteins overexpressed in lesion and in R1, C1, respectively, and include proteins involved in neurite outgrowth but also inhibitors of neurite outgrowth such as neurocan (Table II). These proteins are expressed in lesion after 7 and 10 days and also in segments R1 and C1 for each time point. Some proteins involved in neurite outgrowth are present in C3 segment but some are inhibitory like aggrecan protein. Proteins involved in neurogenesis and synaptogenesis are overexpressed in C3 segments, with lower expression in segments R3, R2, and C2 and under-expressed in lesion, R1 and C1 segments (*cluster 3* and *cluster 5*). However, some neurite inhibitors are also present (Table II). For a more detailed analysis, we performed a systems biology analysis for network identification in each cluster identified in the segment-dependent clustering analysis (Fig. 2D, Table II). Differential pathways were generated using the “direct interaction” algorithm to map the functional relationships linking the identified proteins in each cluster. Regarding clusters identified as overexpressed in the lesion segment, the protein network formed by *cluster 1* is implicated in immune response (*i.e.* cell migration, microglia activation and T cell response) as well as nerve regeneration whereas *cluster 2* forms a protein network involved in neurite outgrowth, nerve regeneration, cell migration and cytoskeleton remodeling (Figs. 2Da and 2Db). By contrast, *cluster 3*, which corresponds to proteins under-expressed in lesion segment, is functionally related to synaptic functions and axonogenesis and collateral sprouting (Fig. 2Dc). *Cluster 4* corresponds to proteins overexpressed in C3 segment and functionally associated with cell-adhesion N-cadherin-related functions involving notably aggrecan, and CD146 (Fig. 2Dd). *Clusters 5* and *6* are formed by overexpressed proteins in both R1 and C1 segments. *Cluster 5* is related to synaptogenesis, axon extension, and neuronal plasticity (Fig. 2De) whereas *cluster 6* is linked to demyelination, oligodendrocytes differentiation, astrogliosis, and nerve regeneration, (Fig. 2Df). Overall, these clustering analysis data confirmed that (1) the lesion site is the most divergent from the other segments in terms of nature and functions of protein networks and (2) secretome profiles of spinal cord segments tend to coevolve depending on their relative distance to the lesion site (*i.e.* R3 with C3, R2 with C2, R1 with C1).

However, besides similarities, differences could be also identified between segments located at equidistance from the

TABLE I

List of proteins identified by cluster after perseus analyses taking into account the time course

Time clustering		
Accession number	Protein name	Gene name
Cluster 1		
O08557	N(G),N(G)-dimethylarginine dimethylaminohydrolase 1	Ddah1
P02650	Apolipoprotein E	ApoE
P06761	78 kDa glucose-regulated protein	Hspa5
P08699	Galectin-3	Lgals3
P09495	Tropomyosin alpha-4 chain	Tpm4
P10960	Sulfated glycoprotein 1	Psap
P11598	Protein disulfide-isomerase A3	Pdia3
P11762	Galectin-1	Lgals1
P30427	Plectin	Plec
P31000	Vimentin	Vim
P31232	Transgelin	Tagln
G3V913	Heat shock 27kDa protein 1	Hspb1
P55051	Fatty acid-binding protein, brain	Fabp7
P85972	Vinculin	Vcl
Q5RK10	WD repeat-containing protein 1	Wdr1
Q5XF0	Transgelin-2	Tagln2
Q63610-2	Tropomyosin alpha-3 chain	Tpm3
Q6JE36	Protein NDRG1	NdrG1
Q9WVW7	Protein phosphatase 1F	Ppm1f
B0K010	Protein Txndc17	Txndc17
C0JPT7	Filamin alpha	Flna
D3ZHA0	Protein FlnC	FlnC
D3ZQP6	Protein Sema7a	Sema7a
G3V852	Protein Tln1	Tln1
G3V8L3	Lamin A, isoform CRA_b	Lmna
G3V940	Coronin	Coro1b
Q5XI38	Lymphocyte cytosolic protein 1	Lcp1
Cluster 2		
B0BNN3	Carbonic anhydrase 1	Ca1
P01048	T-kininogen 1	Map1
P02091	Hemoglobin subunit beta-1	Hbb
P02680-2	Fibrinogen gamma chain	Fgg
P04639	Apolipoprotein A-I	Apoa1
P06238	Alpha-2-macroglobulin	A2m
P06866	Haptoglobin	Hp
P08932	T-kininogen 2	
P14480	Fibrinogen beta chain	Fgb
P17475	Alpha-1-antiproteinase	Serpina1
P20059	Hemopexin	Hpx
Q63041	Alpha-1-macroglobulin	A1m
Q9QX79	Fetuin-B	Fetub
G3V7K3	Ceruloplasmin	Cp
M0RBF1	Complement C3	C3
O54854	Kallikrein 6, isoform CRA_a	Klk6
Q5EBC0	Inter alpha-trypsin inhibitor, heavy chain 4	Itih4
Q5M7T5	Protein Serpinc1	Serpinc1
Q62669	Protein Hbb-b1	Hbb-b1
Q68FY4	Group specific component	Gc
Q7TQ70	Ac1873	Fga
Cluster 3		
B0BNM1	NAD(P)H-hydrate epimerase	Apoa1bp
B2RYG6	Ubiquitin thioesterase OTUB1	Otub1
P05544	Serine protease inhibitor A3L	Serpina3l
P10860	Glutamate dehydrogenase 1, mitochondrial	Glud1
P11030	Acyl-CoA-binding protein	Dbi
P37805	Transgelin-3	Tagln3
P50398	Rab GDP dissociation inhibitor alpha	Gdi1
P62161	Calmodulin	Calm1
P63086	Mitogen-activated protein kinase 1	Mapk1
Q4KM74	Vesicle-trafficking protein SEC22b	Sec22b

TABLE I—continued

Time clustering		
Accession number	Protein name	Gene name
Q4KMA2	UV excision repair protein RAD23 homolog B	Rad23b
Q62952-2	Dihydropyrimidinase-related protein 3	Dpysl3
Q6AY84	Secernin-1	Scrn1
Q7TP98	Interleukin enhancer-binding factor 2	Ilf2
D4A5X8	Protein Ahcy1	Ahcy1
F1M978	Inositol monophosphatase 1	Impa1
F1M9V7	Protein Npepps	Npepps
F1MAQ5	Microtubule-associated protein	Map2
G3V8G4	Brevican, isoform CRA_a	Bcan
M0R686	Protein Irgq	Irgq
M0RE01	Uncharacterized protein	LOC100911107
Cluster 4		
B0BNN3	Carbonic anhydrase 1	Ca1
P01048	T-kininogen 1	Map1
P02091	Hemoglobin subunit beta-1	Hbb
P02680-2	Fibrinogen gamma chain	Fgg
P04639	Apolipoprotein A-I	Apoa1
P04692-5	Tropomyosin alpha-1 chain	Tpm1
P06238	Alpha-2-macroglobulin	A2m
P06866	Haptoglobin	Hp
P08592-2	Amyloid beta A4 protein	App
P08932	T-kininogen 2	
P09606	Glutamine synthetase	Glul
P11348	Dihydropteridine reductase	Qdpr
P12839	Neurofilament medium polypeptide	Nefm
P14480	Fibrinogen beta chain	Fgb
P16975	SPARC	Sparc
P17475	Alpha-1-antiproteinase	Serpina1
P19527	Neurofilament light polypeptide	Nefl
P20059	Hemopexin	Hpx
P21807	Peripherin	Prph
P34058	Heat shock protein HSP 90-beta	Hsp90ab1
P50503	Hsc70-interacting protein	St13
P62703	40S ribosomal protein S4, X isoform	Rps4x
P82995	Heat shock protein HSP 90-alpha	Hsp90aa1
Q63041	Alpha-1-macroglobulin	A1m
Q66HA8	Heat shock protein 105 kDa	Hsph1
Q9QX79	Fetuin-B	Fetub
Q9QZA2	Programmed cell death 6-interacting protein	Pdcd6ip
F1LM84	Nidogen-1	Nid1
F1LRZ7	Neurofilament heavy polypeptide	Nefh
G3V7K3	Ceruloplasmin	Cp
G3V7U4	Lamin-B1	LmnB1
Q6PDW1	40S ribosomal protein S12	Rps12
M0RBF1	Complement C3	C3
O54854	Kallikrein 6, isoform CRA_a	Klk6
Q5EBC0	Inter alpha-trypsin inhibitor, heavy chain 4	Itih4
Q5M7T5	Protein Serpinc1	Serpinc1
Q62669	Protein Hbb-b1	Hbb-b1
Q68FY4	Group specific component	Gc
Q6MGC4	H2-K region expressed gene 2, rat orthologue	Pfdn6
Q7TQ70	Ac1873	Fga
Cluster 5		
B0BNM1	NAD(P)H-hydrate epimerase	Apoa1bp
B2RYG6	Ubiquitin thioesterase OTUB1	Otub1
O08651	D-3-phosphoglycerate dehydrogenase	Phgdh

TABLE I—continued

Time clustering		
Accession number	Protein name	Gene name
O35077	Glycerol-3-phosphate dehydrogenase [NAD(+)], cytoplasmic	Gpd1
O35760	Isopentenyl-diphosphate Delta-isomerase 1	Idi1
O88350	Putative hydrolase RBBP9	Rbbp9
M0R590	Protein LOC685186	LOC685186
P04905	Glutathione S-transferase Mu 1	Gstm1
F1LND7	Farnesyl pyrophosphate synthase	Fdps
P05544	Serine protease inhibitor A3L	Serpina3l
P05708	Hexokinase-1	Hk1
P08009	Glutathione S-transferase Yb-3	Gstm3
P10860	Glutamate dehydrogenase 1, mitochondrial	Glud1
P10959	Carboxylesterase 1C	Ces1c
P11030	Acyl-CoA-binding protein	Dbi
P11980	Pyruvate kinase PKM	Pkm
P12346	Serotransferrin	Tf
P12785	Fatty acid synthase	Fasn
P13233	2',3'-cyclic-nucleotide 3'-phosphodiesterase	Cnp
P13668	Stathmin	Stmn1
G3V9G4	ATP citrate lyase, isoform CRA_b	Acly
P17425	Hydroxymethylglutaryl-CoA synthase, cytoplasmic	Hmgcs1
P24155	Thimet oligopeptidase	Thop1
P24329	Thiosulfate sulfurtransferase	Tst
P28037	Cytosolic 10-formyltetrahydrofolate dehydrogenase	Aldh1l1
P30904	Macrophage migration inhibitory factor	Mif
P32232-2	Cystathionine beta-synthase	Cbs
P37361	Metallothionein-3	Mt3
P37805	Transgelin-3	Tagln3
P50398	Rab GDP dissociation inhibitor alpha	Gdi1
P50408	V-type proton ATPase subunit F	Atp6v1f
P51635	Alcohol dehydrogenase [NADP(+)]	Akr1a1
P84079	ADP-ribosylation factor 1	Arf1
P62161	Calmodulin	Calm1
P62828	GTP-binding nuclear protein Ran	Ran
P63086	Mitogen-activated protein kinase 1	Mapk1
Q3KRE8	Tubulin beta-2B chain	Tubb2b
Q497B0	Omega-amidase NIT2	Nit2
Q4KM74	Vesicle-trafficking protein SEC22b	Sec22b
Q4KMA2	UV excision repair protein RAD23 homolog B	Rad23b
Q4V8C3-2	Echinoderm microtubule-associated protein-like 1	Eml1
Q5BJP9	Phytanoyl-CoA dioxygenase domain-containing protein 1	Phyhd1
Q5PQN7	Protein LZIC	Lzic
Q5XI22	Acetyl-CoA acetyltransferase, cytosolic	Acat2
Q62952-2	Dihydropyrimidinase-related protein 3	Dpysl3
Q66HG4	Aldose 1-epimerase	Galm
Q6AY84	Secernin-1	Scrn1
Q6AYS7	Aminoacylase-1A	Acy1a
Q6P502	T-complex protein 1 subunit gamma	Cct3
Q6P9V9	Tubulin alpha-1B chain	Tuba1b
Q7TP98	Interleukin enhancer-binding factor 2	Ilf2

TABLE I—continued

Time clustering		
Accession number	Protein name	Gene name
Q91XU1	Protein quaking	Qki
Q9JHU0	Dihydropyrimidinase-related protein 5	Dpysl5
Q9QXU9	ProSAAS	Pcsk1n
Q9Z1B2	Glutathione S-transferase Mu 5	Gstm5
B2GUZ9	Fam49b protein	Fam49b
B4F7C2	Protein Tubb4a	Tubb4a
B5DFN4	Prefoldin 5 (Predicted), isoform CRA_a	Pfdn5
D3ZFU9	Protein Mylk	Mylk
D4AD67	Protein Ktn1	Ktn1
D4A5X8	Protein Ahcy1	Ahcy1
D4ACB8	Chaperonin subunit 8 (Theta) (Predicted), isoform CRA_a	Cct8
D4AEH9	Amylo-1, 6-glucosidase, 4-alpha-glucanotransferase (Glycogen debranching enzyme, glycogen storage disease type III)	Ag1
F1LM42	Protein Ank2	Ank2
F1M978	Inositol monophosphatase 1	Impa1
F1M9V7	Protein Npepps	Npepps
F1MAQ5	Microtubule-associated protein	Map2
F7F7H4	Uncharacterized protein	Dock2
G3V721	WW domain binding protein 2, isoform CRA_b	Wbp2
G3V7C6	RCG45400	Tubb4b
G3V8G4	Brevican, isoform CRA_a	Bcan
G3V8V3	Phosphorylase	Pygm
G3V9U0	Acyl-CoA synthetase short-chain family member 2 (Predicted)	Acss2
M0R686	Protein Irgq	Irgq
M0RE01	Uncharacterized protein	LOC100911107
Q4KM55	Protein Vta1	Vta1
Q642E5	Diphosphomevalonate decarboxylase	Mvd
Cluster 6		
B0BNN3	Carbonic anhydrase 1	Ca1
O08557	N(G),N(G)-dimethylarginine dimethylaminohydrolase 1	Ddah1
P01048	T-kininogen 1	Map1
P02091	Hemoglobin subunit beta-1	Hbb
P02650	Apolipoprotein E	Apoe
P02680-2	Fibrinogen gamma chain	Fgg
P04639	Apolipoprotein A-I	Apoa1
P04692-5	Tropomyosin alpha-1 chain	Tpm1
P06238	Alpha-2-macroglobulin	A2m
P06761	78 kDa glucose-regulated protein	Hspa5
P06866	Haptoglobin	Hp
P08592-2	Amyloid beta A4 protein	App
P08699	Galectin-3	Lgals3
P08932	T-kininogen 2	
P09495	Tropomyosin alpha-4 chain	Tpm4
P09606	Glutamine synthetase	Glul
P10960	Sulfated glycoprotein 1	Psap
P11348	Dihydropteridine reductase	Qdpr
P11598	Protein disulfide-isomerase A3	Pdia3
P11762	Galectin-1	Lgals1
P12839	Neurofilament medium polypeptide	Nefm
P14480	Fibrinogen beta chain	Fgb
P16975	SPARC	Sparc
P17475	Alpha-1-antiproteinase	Serpina1
P19527	Neurofilament light polypeptide	Nefl
P20059	Hemopexin	Hpx
P21807	Peripherin	Prph

TABLE I—continued

Time clustering		
Accession number	Protein name	Gene name
P30427	Plectin	Plec
P31000	Vimentin	Vim
P31232	Transgelin	Tagln
P34058	Heat shock protein HSP 90-beta	Hsp90ab1
G3V913	Heat shock 27kDa protein 1	Hspb1
P50503	Hsc70-interacting protein	St13
P55051	Fatty acid-binding protein, brain	Fabp7
P62703	40S ribosomal protein S4, X isoform	Rps4x
P82995	Heat shock protein HSP 90-alpha	Hsp90aa1
P85972	Vinculin	Vcl
Q5RK10	WD repeat-containing protein 1	Wdr1
Q5XF0	Transgelin-2	Tagln2
Q63028	Alpha-adducin	Add1
Q63041	Alpha-1-macroglobulin	A1m
Q63610-2	Tropomyosin alpha-3 chain	Tpm3
Q66HA8	Heat shock protein 105 kDa	Hsph1
Q68FQ2	Junctional adhesion molecule C	Jam3
Q6JE36	Protein NDRG1	Ndr1
Q9QX79	Fetuin-B	Fetub
Q9QZA2	Programmed cell death 6-interacting protein	Pdcd6ip
Q9WVR7	Protein phosphatase 1F	Ppm1f
B0K010	Protein Txndc17	Txndc17
C0JPT7	Filamin alpha	Flna
D3ZHA0	Protein Flncl	Flncl
D3ZQP6	Protein Sema7a	Sema7a
F1LM84	Nidogen-1	Nid1
F1LRZ7	Neurofilament heavy polypeptide	Nefn
G3V7K3	Ceruloplasmin	Cp
G3V7U4	Lamin-B1	Lmnb1
G3V852	Protein Tln1	Tln1
G3V8L3	Lamin A, isoform CRA_b	Lmna
G3V940	Coronin	Coro1b
Q6PDW1	40S ribosomal protein S12	Rps12
M0RBF1	Complement C3	C3
O54854	Kallikrein 6, isoform CRA_a	Klk6
Q5EBC0	Inter alpha-trypsin inhibitor, heavy chain 4	Itih4
Q5M7T5	Protein Serpinc1	Serpinc1
Q5XI38	Lymphocyte cytosolic protein 1	Lcp1
Q62669	Protein Hbb-b1	Hbb-b1
Q68FY4	Group specific component	Gc
Q6MGC4	H2-K region expressed gene 2, rat orthologue	Pfdn6
Q7TQ70	Ac1873	Fga
Cluster 7		
P05708	Hexokinase-1	Hk1
P12346	Serotransferrin	Tf
P30904	Macrophage migration inhibitory factor	Mif
Q6P502	T-complex protein 1 subunit gamma	Cct3
D4ACB8	Chaperonin subunit 8 (Theta) (Predicted), isoform CRA_a	Cct8
D4AEH9	Amylo-1, 6-glucosidase, 4-alpha-glucanotransferase (Glycogen debranching enzyme, glycogen storage disease type III)	Ag1
F7F7H4	Uncharacterized protein	Dock2
G3V721	WW domain binding protein 2, isoform CRA_b	Wbp2

TABLE II

List of proteins identified by cluster after perseus analyses taking into account spatial localization

Segment clustering		
Accession number	Protein name	Gene name
Cluster 1		
P02650	Apolipoprotein E	ApoE
P04041	Glutathioneperoxidase 1	Gpx1
P04642	L-lactate dehydrogenase A chain	Ldha
P04785	Protein disulfide-isomerase	P4hb
P05197	Elongation factor 2	Eef2
P07151	Beta-2-microglobulin	B2m
P08649	Complement C4	C4
P08699	Galectin-3	Lgals3
P10960	Sulfated glycoprotein 1	Psap
P22734-2	Catechol O-methyltransferase	Comt
P23928	Alpha-crystallin B chain	Cryab
Q6P6T6	Cathepsin D	Ctsd
P31232	Transgelin	Tagln
P37397	Calponin-3	Cnn3
P62963	Profilin-1	Pfn1
P85968	6-phosphogluconate dehydrogenase, decarboxylating	Pgd
P85970	Actin-related protein 2/3 complex subunit 2	Arpc2
P85973	Purine nucleoside phosphorylase	Pnp
Q3MIE4	Synaptic vesicle membrane protein VAT-1 homolog	Vat1
Q4V7C7	Actin-related protein 3	Actr3
Q510D7	Xaa-Pro dipeptidase	Pepd
Q5M7U6	Actin-related protein 2	Actr2
Q5XF0	Transgelin-2	Tagln2
Q63716	Peroxisome oxidin-1	Prdx1
Q64119	Myosin light polypeptide 6	Myl6
Q68FS4-2	Cytosol aminopeptidase	Lap3
Q6AYC4	Macrophage-capping protein	Capg
Q6B345	Protein S100-A11	S100a11
Q6MG61	Chloride intracellular channel protein 1	Clic1
Q6QON1	Cytosolic non-specific dipeptidase	Cndp2
D3ZHA0	Protein Flncl	Flncl
D3ZQP6	Protein Sema7a	Sema7a
F1LP60	Moesin	Msn
F1M5X1	Protein Rrbp1	Rrbp1
F1M983	Protein Cfh	Cfh
G3V852	Protein Tln1	Tln1
G3V8V1	Granulin, isoform CRA_c	Grn
M0R4S2	Apolipoprotein D	Apod
Q5XI38	Lymphocyte cytosolic protein 1	Lcp1
Q6IN22	Cathepsin B	Ctsb
Q6P9V7	Proteasome (Prosome, macropain) activator subunit 1	Psme1
Q63798	Proteasome activator complex subunit 2	Psme2
Cluster 2		
O35077	Glycerol-3-phosphate dehydrogenase [NAD(+)], cytoplasmic	Gpd1
P02688	Myelin basic protein	Mbp
P32232-2	Cystathionine beta-synthase	Cbs
P47819	Glial fibrillary acidic protein	Gfap
P85845	Fascin	Fscn1
B0BNA5	Coactosin-like protein	Cotl1
P05370	Glucose-6-phosphate 1-dehydrogenase	G6pdx
P14841	Cystatin-C	Cst3
P47875	Cysteine and glycine-rich protein 1	Csrp1
P55051	Fatty acid-binding protein, brain	Fabp7
P55053	Fatty acid-binding protein, epidermal	Fabp5
P55067	Neurocan core protein	Ncan
P62630	Elongation factor 1-alpha 1	Eef1a1
P63259	Actin, cytoplasmic 2	Actg1
P97584	Prostaglandin reductase 1	Ptgr1
Q08163	Adenylyl cyclase-associated protein 1	Cap1
Q4G075	Leukocyte elastase inhibitor A	Serpinh1a
Q5M7W5	Microtubule-associated protein 4	Map4

TABLE II—continued

Segment clustering		
Accession number	Protein name	Gene name
Q5U318	Astrocyticphosphoprotein PEA-15	Pea15
Q5X173	Rho GDP-dissociation inhibitor 1	Arhgdia
Q63544	Gamma-synuclein	Sncg
Q64303	Serine/threonine-protein kinase PAK 2	Pak2
Q68FP1-2	Gelsolin	Gsn
Q6JE36	Protein NDRG1	Ndr1
Q7TP52	Carboxymethylenebutenolidasehomolog	Cmb1
Q9EQS0	Transaldolase	Taldo1
Q9WUH4	Four and a half LIM domainsprotein 1	Fhl1
D4A8F2	Protein Rsu1	Rsu1
E9PT65	ProteinRdx	Rdx
G3V8C4	Chlorideintracellularchannel 4, isoformCRA_b	Clic4
M0R4H5	PDZ and LIM domainprotein 4	Pdlim4
Cluster 3		
O08838	Amphiphysin	Amph
O08839-2	Myc box-dependent-interactingprotein 1	Bin1
O35095	Neurochondrin	Ncdn
O35179	Endophilin-A1	Sh3gl2
O35264	Platelet-activating factor acetylhydrolase IB subunit beta	Pafah1b2
O35814	Stress-induced-phosphoprotein 1	Stip1
O88989	Malatedehydrogenase, cytoplasmic	Mdh1
P00507	Aspartate aminotransferase, mitochondrial	Got2
P01830	Thy-1 membrane glycoprotein	Thy1
P04636	Malatedehydrogenase, mitochondrial	Mdh2
P07323	Gamma-enolase	Eno2
P07722	Myelin-associatedglycoprotein	Mag
P09951	Synapsin-1	Syn1
P10860	Glutamate dehydrogenase 1, mitochondrial	Glud1
P11348	Dihydropteridinereductase	Qdpr
P12839	Neurofilament medium polypeptide	Nefm
F1LNY3	Neural celladhesionmolecule 1	Ncam1
P14408-2	Fumarate hydratase, mitochondrial	Fh
P16617	Phosphoglycerate kinase 1	Pgk1
P19527	Neurofilament light polypeptide	Nefl
P21575-2	Dynammin-1	Dnm1
P22062	Protein-L-isoaspartate(D-aspartate) O-methyltransferase	Pcmt1
P23565	Alpha-intermexin	Ina
P25113	Phosphoglyceratemutase 1	Pgam1
P27605	Hypoxanthine-guanine phosphoribosyltransferase	Hprt1
P31016	Disks large homolog 4	Dlg4
P39069	Adenylate kinase isoenzyme 1	Ak1
P42123	L-lactate dehydrogenase B chain	Ldhb
P47709	Rabphilin-3A	Rph3a
P47728	Calretinin	Calb2
P47860	6-phosphofructokinase type C	Pf1k
P50554	4-aminobutyrate aminotransferase, mitochondrial	Abat
P53042	Serine/threonine-protein phosphatase 5	Ppp5c
P54690	Branched-chain-amino-acidaminotransferase, cytosolic	Bcat1
P60522	Gamma-aminobutyricacidreceptor-associatedprotein-like 2	Gabarrpl2
P61265	Syntaxin-1B	Stx1b
P61765-2	Syntaxin-binding protein 1	Stxbp1
P61983	14-3-3 protein gamma	Ywhag
P62632	Elongation factor 1-alpha 2	Eef1a2
P62762	Visinin-likeprotein 1	Vsn11
P62815	V-type proton ATPase subunit B, brainisoform	Atp6v1b2
P62959	Histidine triadnucleotide-binding protein 1	Hint1
P62966	Cellular retinoicacid-binding protein 1	Crabp1
P63018	Heatshockcognate 71 kDa protein	Hspa8
P63041	Complexin-1	Cplx1
P63329-2	Serine/threonine-protein phosphatase 2B catalyticsubunit alpha isoform	Ppp3ca

TABLE II—continued

Segment clustering		
Accession number	Protein name	Gene name
P86252	Transcriptionalactivatorprotein Pur-alpha (Fragments)	Pura
Q05140-2	Clathrincoatassemblyprotein AP180	Snap91
Q07266-2	Drebrin	Dbn1
Q07310-14	Neurexin-3	Nrxn3
Q5GFD9	Protein IMPACT	Impact
Q5HZA6-2	Prolylendopeptidase-like	Prepl
Q5XIT1	Microtubule-associatedprotein RP/EB familymember 3	Mapre3
Q62717	Calcium-dependentsecretionactivator 1	Cadps
Q62813	Limbic system-associated membrane protein	Lsamp
Q62910-5	Synaptojanin-1	Synj1
Q63198	Contactin-1	Cntn1
Q63560	Microtubule-associatedprotein 6	Map6
Q63622-3	Disks large homolog 2	Dlg2
Q63754	Beta-synuclein	Sncb
Q7M767	Ubiquitin-conjugating enzyme E2 variant 2	Ube2v2
Q80WA4	RNA-binding protein Nova-1	Nova1
B2GV79	Pdxpprotein	Pdpx
Q9EPH8	Polyadenylate-binding protein 1	Pabpc1
Q9ER34	Aconitate hydratase, mitochondrial	Aco2
Q9QUL6	Vesicle-fusing ATPase	Nsf
Q9QX69	LanC-likeprotein 1	Lanc1
Q9R063-2	Peroxioredoxin-5, mitochondrial	Prdx5
G3V710	Peroxioredoxin 3	Prdx3
F1LPP3	Protein kinase C and casein kinase substrate in neuronsprotein 1	Pacsin1
A1L1M0	Protein kinase, cAMP-dependent, catalytic, alpha	Prkaca
B0BN63	LOC681996 protein	Ahsa1
B0BNL2	Peptidylprolyl cis/transisomerase, NIMA-interacting 1	LOC364561
B4F772	Heatshock 70 kDa protein 4L	Hspa4l
B4F7A3	Galectin	Lgalsl
D3ZC55	Heatshock 70kDa protein 12A (Predicted), isoformCRA_a	Hspa12a
D3ZCA0	Proline synthetaseco-transcribed (Predicted)	Prosc
D3ZD09	Cytochrome c oxidasesubunit 6B1	Cox6b1
D3ZNW5	Neurofascin	Nfasc
D3ZUY8	Adaptorproteincomplex AP-2, alpha 1 subunit (Predicted)	Ap2a1
D4A0I5	DnaJ (Hsp40) homolog, subfamily C, member 6 (Predicted)	Dnajc6
D4A133	Protein Atp6v1a	Atp6v1a
D4A6C9	Protein Tom1l2	Tom1l2
D4A8U7	Dynactin 1, isoformCRA_a	Dctn1
F1LRL9	Microtubule-associatedprotein 1B	Map1b
F1LRZ7	Neurofilament heavy polypeptide	Nefh
F1MAQ5	Microtubule-associatedprotein	Map2
F7EYB9	ProteinOmg	Omg
G3V758	Contactin 2	Cntn2
G3V774	F-box onlyprotein 2	Fbxo2
G3V7L8	ATPase, H+ transporting, V1 subunit E isoform 1, isoformCRA_a	Atp6v1e1
G3V936	Citrate synthase	Cs
G3V964	Neurotrimin	Ntm
G3V9N8	AP-1 complexsubunit beta-1	Ap1b1
M0RC65	Cofilin 2, muscle (Predicted), isoformCRA_b	Cfl2
Q52KS1	6-phosphofructokinase	Pfkm
Q5BJT9	Creatine kinase, mitochondrial 1, ubiquitous	Ckmt1b
Q5PQK2	Fusion, derivedfrom t(1216) malignantliposarcoma (Human)	Fus
Q6AY48	Poly(RC) binding protein 3	Pcbp3
Q6AYU5	Poly(RC) binding protein 2	Pcbp2
Cluster 4		
P51635	Alcoholdehydrogenase [NADP(+)]	Akr1a1
Q4V898	RNA-binding motif protein, X chromosome	Rbmx

TABLE II—continued

Segment clustering		
Accession number	Protein name	Gene name
Q9EPF2-2	Cell surface glycoprotein MUC18	Mcam
Q9QXU9	ProSAAS	Pcsk1n
G3V803	Cadherin-2	Cdh2
B2GUZ9	Fam49b protein	Fam49b
P07897	Aggrecan core protein	Acan
F1M7H7	Membrane-associated guanylate kinase, WW and PDZ domain-containing protein 1	Magi1
Cluster 5		
M0RDM4	Histone H2A	LOC680322
O08838	Amphiphysin	Amph
O08839-2	Myc box-dependent-interacting protein 1	Bin1
O35095	Neurochondrin	Ncdn
O35179	Endophilin-A1	Sh3gl2
O35264	Platelet-activating factor acetylhydrolase IB subunit beta	Pafah1b2
O35814	Stress-induced-phosphoprotein 1	Stip1
O88989	Malate dehydrogenase, cytoplasmic	Mdh1
P00507	Aspartate aminotransferase, mitochondrial	Got2
P01830	Thy-1 membrane glycoprotein	Thy1
P02680-2	Fibrinogen gamma chain	Fgg
P04636	Malate dehydrogenase, mitochondrial	Mdh2
P07323	Gamma-enolase	Eno2
P07722	Myelin-associated glycoprotein	Mag
P07897	Aggrecan core protein	Acan
P09951	Synapsin-1	Syn1
P10860	Glutamate dehydrogenase 1, mitochondrial	Glud1
P11348	Dihydropteridine reductase	Qdpr
P12839	Neurofilament medium polypeptide	Nefn
F1LNY3	Neural cell adhesion molecule 1	Ncam1
P14408-2	Fumarate hydratase, mitochondrial	Fh
P14480	Fibrinogen beta chain	Fgb
P16617	Phosphoglycerate kinase 1	Pgk1
P19527	Neurofilament light polypeptide	Nefl
P21575-2	Dynamin-1	Dnm1
P22062	Protein-L-isospartate(p-aspartate) O-methyltransferase	Pcmt1
P23565	Alpha-internexin	Ina
P25113	Phosphoglycerate mutase 1	Pgam1
P27605	Hypoxanthine-guanine phosphoribosyltransferase	Hprt1
P31016	Disks large homolog 4	Dlg4
P39069	Adenylate kinase isoenzyme 1	Ak1
P42123	L-lactate dehydrogenase B chain	Ldhb
P47709	Rabphilin-3A	Rph3a
P47728	Calretinin	Calb2
P47860	6-phosphofructokinase type C	Pfkm
P50554	4-aminobutyrate aminotransferase, mitochondrial	Abat
P51635	Alcohol dehydrogenase [NADP(+)]	Akr1a1
P53042	Serine/threonine-protein phosphatase 5	Ppp5c
P54690	Branched-chain-amino-acid aminotransferase, cytosolic	Bcat1
P60522	Gamma-aminobutyrate receptor-associated protein-like 2	Gabarapl2
P61265	Syntaxin-1B	Stx1b
P61765-2	Syntaxin-binding protein 1	Stxbp1
P61983	14-3-3 protein gamma	Ywhag
P62632	Elongation factor 1-alpha 2	Eef1a2
P62762	Visinin-like protein 1	Vsnl1
P62815	V-type proton ATPase subunit B, brain isoform	Atp6v1b2
P62959	Histidine triad nucleotide-binding protein 1	Hint1
P62966	Cellular retinoic acid-binding protein 1	Crabp1
P63018	Heat shock cognate 71 kDa protein	Hspa8
P63041	Complexin-1	Cplx1
P63329-2	Serine/threonine-protein phosphatase 2B catalytic subunit alpha isoform	Ppp3ca
P86252	Transcriptional activator protein Pur-alpha (Fragments)	Pura

TABLE II—continued

Segment clustering		
Accession number	Protein name	Gene name
Q05140-2	Clathrin coat assembly protein AP180	Snap91
Q07266-2	Drebrin	Dbn1
Q07310-14	Neurexin-3	Nrxn3
F1M7H7	Membrane-associated guanylate kinase, WW and PDZ domain-containing protein 1	Magi1
Q4V898	RNA-binding motif protein, X chromosome	Rbmx
Q5GFD9	Protein IMPACT	Impact
Q5HZA6-2	Prolyl endopeptidase-like	Prepl
Q5XIT1	Microtubule-associated protein RP/EB family member 3	Mapre3
Q62717	Calcium-dependent secretion activator 1	Cadps
Q62813	Limbic system-associated membrane protein	Lsmp
Q62910-5	Synaptotagmin-1	Synj1
Q63198	Contactin-1	Cntn1
Q63560	Microtubule-associated protein 6	Map6
Q63622-3	Disks large homolog 2	Dlg2
Q63754	Beta-synuclein	Sncb
Q6PCT3	Tumor protein D54	Tpd52l2
Q7M767	Ubiquitin-conjugating enzyme E2 variant 2	Ube2v2
Q80WA4	RNA-binding protein Nova-1	Nova1
B2GV79	Pdxp protein	Pdxp
Q9EPF2-2	Cell surface glycoprotein MUC18	Mcam
Q9EPH8	Polyadenylate-binding protein 1	Pabpc1
Q9ER34	Aconitate hydratase, mitochondrial	Aco2
Q9QUL6	Vesicle-fusing ATPase	Nsf
Q9QX69	LanC-like protein 1	Lanc1
Q9QXU9	ProSAAS	Pcsk1n
Q9R063-2	Peroxisomal protein 5, mitochondrial	Prdx5
G3V710	Peroxisomal protein 3	Prdx3
F1LPP3	Protein kinase C and casein kinase substrate in neurons protein 1	Pacsin1
G3V803	Cadherin-2	Cdh2
A1L1M0	Protein kinase, cAMP-dependent, catalytic, alpha	Prkaca
B0BN63	LOC681996 protein	Ahsa1
B0BNL2	Peptidylprolyl cis/trans isomerase, NIMA-interacting 1	LOC364561
B2GUZ9	Fam49b protein	Fam49b
B4F772	Heat shock 70 kDa protein 4L	Hspa4l
B4F7A3	Galectin	Lgalsl
D3ZC55	Heat shock 70 kDa protein 12A (Predicted), isoform CRA_a	Hspa12a
D3ZCA0	Proline synthetase co-transcribed (Predicted)	Prosc
D3ZD09	Cytochrome c oxidase subunit 6B1	Cox6b1
D3ZFG5	Protein Pmp2	Pmp2
G3V9C7	Histone H2B	Hist1h2bk
D3ZNW5	Neurofascin	Nfasc
D3ZUY8	Adaptor protein complex AP-2, alpha 1 subunit (Predicted)	Ap2a1
D4A015	DnaJ (Hsp40) homolog, subfamily C, member 6 (Predicted)	Dnajc6
D4A133	Protein Atp6v1a	Atp6v1a
D4A6C9	Protein Tom112	Tom112
D4A8U7	Dynactin 1, isoform CRA_a	Dctn1
F1LRL9	Microtubule-associated protein 1B	Map1b
F1LRZ7	Neurofilament heavy polypeptide	Nefh
F1MAQ5	Microtubule-associated protein	Map2
F7EYB9	Protein Omg	Omg
G3V6P7	Myosin, heavy polypeptide 9, non-muscle	LOC100911597
G3V758	Contactin 2	Cntn2
G3V774	F-box only protein 2	Fbxo2
G3V7L8	ATPase, H+ transporting, V1 subunit E isoform 1, isoform CRA_a	Atp6v1e1
G3V936	Citrate synthase	Cs
G3V964	Neurotrimin	Ntm
G3V9N8	AP-1 complex subunit beta-1	Ap1b1
M0RC65	Cofilin 2, muscle (Predicted), isoform CRA_b	Cfl2
Q52KS1	6-phosphofructokinase	Pfkm
Q5BJT9	Creatine kinase, mitochondrial 1, ubiquitous	Ckmt1b

TABLE II—continued

Segment clustering		
Accession number	Protein name	Gene name
Q5PQK2	Fusion, derived from t(1216) malignant liposarcoma (Human)	Fus
Q6AY48	Poly(RC) binding protein 3	Pcbp3
Q6AYU5	Poly(RC) binding protein 2	Pcbp2
Q7TQ70	Ac1873	Fga
Cluster 6		
B0BNA5	Coactosin-like protein	Cotl1
O35077	Glycerol-3-phosphate dehydrogenase [NAD(+)], cytoplasmic	Gpd1
P02688	Myelin basic protein	Mbp
P05370	Glucose-6-phosphate 1-dehydrogenase	G6pdx
P14841	Cystatin-C	Cst3
P32232-2	Cystathionine beta-synthase	Cbs
P47819	Glial fibrillary acidic protein	Gfap
P47875	Cysteine and glycine-rich protein 1	Csrp1
P55051	Fatty acid-binding protein, brain	Fabp7
P55053	Fatty acid-binding protein, epidermal	Fabp5
P55067	Neurocan core protein	Ncan
P62630	Elongation factor 1-alpha 1	Eef1a1
P63259	Actin, cytoplasmic 2	Actg1
P85845	Fascin	Fscn1
P97584	Prostaglandin reductase 1	Ptgr1
Q08163	Adenylyl cyclase-associated protein 1	Cap1
Q4G075	Leukocyte elastase inhibitor A	Serp1b1a
Q5M7W5	Microtubule-associated protein 4	Map4
Q5U318	Astrocytic phosphoprotein PEA-15	Pea15
Q5X173	Rho GDP-dissociation inhibitor 1	Arhgdia
Q63544	Gamma-synuclein	Sncg
Q64303	Serine/threonine-protein kinase PAK 2	Pak2
Q68FP1-2	Gelsolin	Gsn
Q6JE36	Protein NDRG1	Ndrg1
Q7TP52	Carboxymethylglutaminase homolog	Cmb1
D4ABI6	Protein RGD1561252	RGD1561252
Q920J4	Thioredoxin-like protein 1	Txn1l1
Q9EQS0	Transaldolase	Taldo1
Q9WUH4	Four and a half LIM domain protein 1	Fhl1
B0BMX3	Protein S100a16	S100a16
D4A8F2	Protein Rsu1	Rsu1
E9PT65	Protein Rdx	Rdx
Q3V8C4	Chloride intracellular channel 4, isoform CRA_b	Clic4
M0R4H5	PDZ and LIM domain protein 4	Pdlim4

lesion site. This held of particular interest when comparing R1 *versus* C1 segments. Indeed, as compared with the R1 profile, the C1 profile was characterized by the overexpression of inflammation markers such as fibrinogen alpha, proteins involved in demyelination and molecules either favoring axonal regeneration or inhibiting neurite outgrowth. Searching for functionally-grouped networks overrepresented in the proteins obtained from segments C3, C2, to C1, from control to 3 days, 7 days and 10 days after SCI, using ClueGO, identified leading terms mostly related to axon regeneration, synaptogenesis, extracellular matrix organization, processes in time course (Fig. 3), and thus established neuron outgrowth and regeneration processes occurring after lesion in time course. These data confirm that a neurogenesis process occurs from caudal 3 to caudal 1 after SCI in time course.

To complement these unsupervised bioinformatics analyses, we then proceeded to supervised coexpression analyses in order to confirm the unique functional profile of the caudal segments. Data obtained from our time course experiments

were classified in four groups (*i.e.* control, lesion, rostral and caudal) from which coexpression interactions were identified. Starting from these coexpression networks, a supervised clustering was then performed using the pro-inflammatory factor Fibrinogen alpha (FgA) as a reference molecule. Results showed that, in the lesion and caudal segments only, FgA coexpression networks were significantly enriched in molecules annotated with “complement activation” gene ontology term (Fig. 2Ea). When performing a similar supervised clustering using now the axonal Neurofilament (Nf) molecules Nfl, Nfm, and Nfh, we also found in the lesion and caudal segments only, a significant enrichment in molecules involved in the “regulation of neuron differentiation” function (Fig. 2Eb). However, a significant enrichment in molecules involved in the “axon guidance” function was observed in the lesion segments with the exception of all other segments (Fig. 2Ec). These data confirm that, although similarities can be demonstrated between segments centered by the lesion site, the caudal segments express an unexpected pro-inflammatory profile and pro-regenerative profile.

We then sought to identify specific molecules and pathways that would provide a segment and time-specific proteomic signature of SCI. To achieve this goal, we analyzed the differential distribution of unique *versus* common/intersected biological and functional pathways among the three spinal cord rostral and caudal regions (C1, C2, C3 *versus* R1, R2, R3) factored by time points post-SCI (3, 7, and 10 days). Each pair of spinal cord segments (C1 *versus* R1, C2 *versus* R2, C3 *versus* R3) was analyzed across the three time points and a comprehensive Venn analysis diagram extracted from Subnetwork Enrichment Analysis (SEA) was generated. From the C1 *versus* R1 comparisons, unique statistically significant segment- and time-specific pathways were identified that included 32 pathways for C1 on day 3, 78 pathways for R1 on day 3, 53 pathways for C1 on day 7, 78 pathways for R1 on day 7, 14 pathways for R1 on day 10 and a single pathway for C1 on day 10 (Fig. 2Fa); see [supplemental Data S3](#) for the identity of each of the unique pathways. In Fig. 2Fb, C2 *versus* R2 differential pathways were analyzed across the three time points (3, 7 and 10 days). Unique statistical significant pathways were identified including 48 pathways (3days, C2), 55 pathways (3days, R2), 48 pathways (7days, C2), 52 pathways (7days, R2), 66 pathways (10 days, C2) and 36 pathways (10 days, R2); see [supplemental Data S4](#) for the identity of each of the unique pathways. In Fig. 2Fc, C3 *versus* R3 differential pathways were analyzed across the three time points (3, 7 and 10 days). Unique statistical significant pathways were identified including 30 pathways (3days, C3), 69 pathways (3days, R3), 58 pathways (7days, C3); 63 pathways (7days, R3), 52 pathways (10 days, C3) and 63 pathways (10 days, R3); refer to [supplemental Data S5](#) for the identity of each of the unique pathways. In Fig. 2Fd, *Lesion-specific* unique and common/intersected biological and functional pathways are analyzed across the three time points. 59, 58 and 61 unique pathways

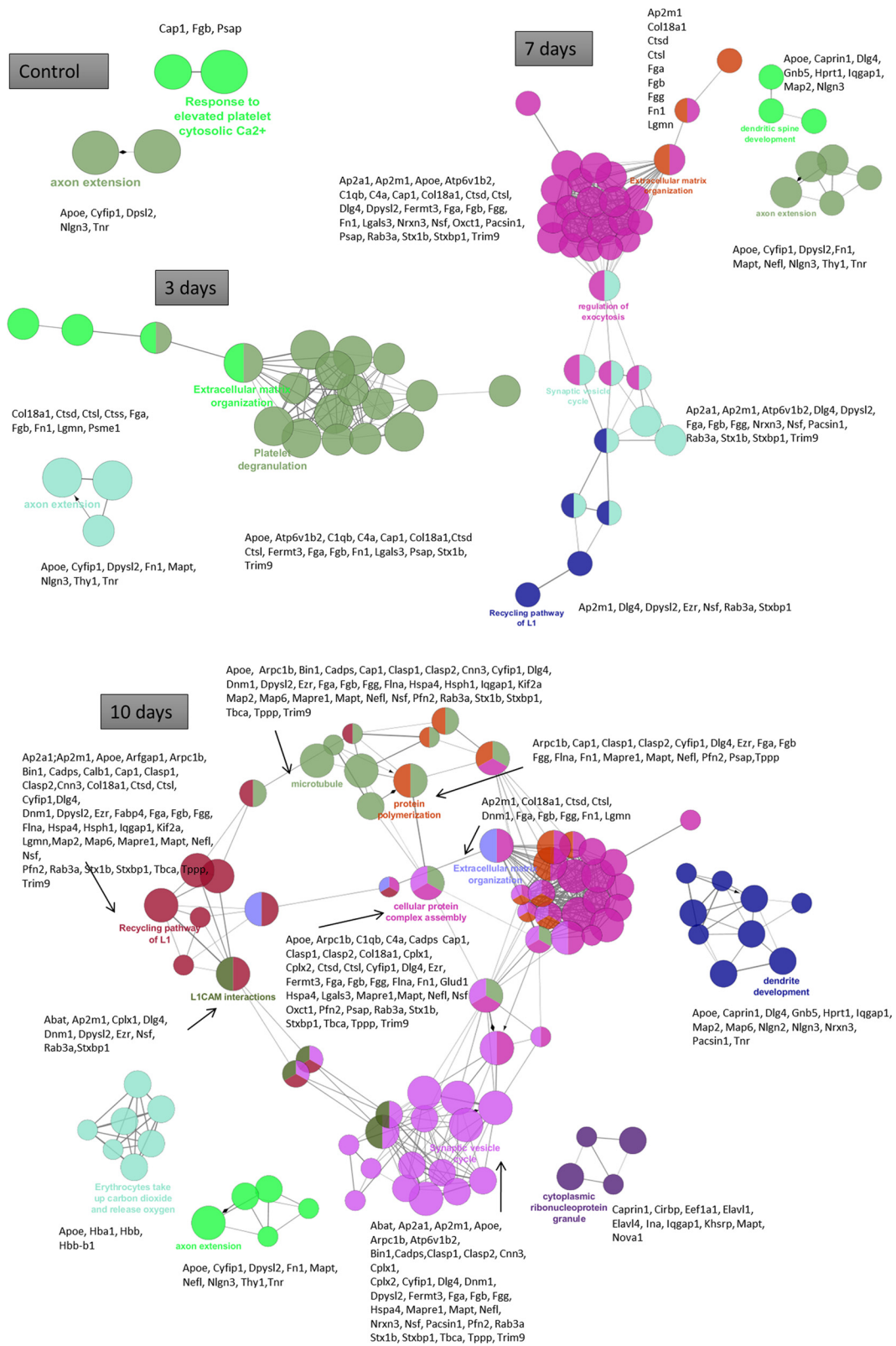


FIG. 3. ClueGo terms involved in proteins overexpressed in C3 compared with C2 and C1.

TABLE III
Specific protein per segments in time course

Segments	Protein ID	Protein Name	Identified per Time	
Lesion	G3V7H3	Cfd	3d/7d	
	P16391	RT1	3d/7d	
	P18331	Inhba	3d/10d	
	Q5FVH2	Pld3	3d/7d	
	Q62632	Fstl1	3d/10d	
	Q6P7C7	Gpnmb	3d/10d	
	B2GVB9	Fermt3	7d/10d	
	B4F7E8	Fam129b	7d/10d	
	E9PSY8	Eps15	7d/10d	
	G3V8L1	Pycard	7d/10d	
	G3V8Q0	Rgs10	7d/10d	
	P97608	Oplah	7d/10d	
	Q5BJY6	Amdhd2	7d/10d	
	Q641X3	Hexa	7d/10d	
	Q66H59	Npl	7d/10d	
	Q66HG3	Cndp1	7d/10d	
	Q6AYF2	Lmcd1	7d/10d	
	Q8K3F3	Ppp1r14b	7d/10d	
	Rostral 1	P30348	Cxcl2	3d/10d
		Q63507	Rpl14	3d/7d
Caudal 1	F1LNE5	Memo1	3d/10d	
	R9PY05	Nfasc	3d/7d	
Rostral 2	Q5U1Z2	Trappc3	7d/10d	
	G3V8D6	Trim3	3d/7d	
	P62836	Rap1a	3d/7d	
Caudal 2	Q68A21	Purb	3d/10d	
	F1LN98	Ewsr1	3d/10d	
	P0DJJ3	Sgip1	3d/7d	
	Q5X181	Fxr1	3d/7d	
	G3V928	Lrp1	ctrl/3d	
Rostral 3	D4ACV3	Hist2h2ac	3d/7d	
	F1LMU0	Myh4	3d/7d	
Caudal 3	B2GV38	Ubl4a	7d/10d	
	P45479	Ppt1	7d/10d	
	P63045	Vamp2	3d/10d	
	Q1M168	Atcay	3d/10d	
	F1LSU5	Defa10	3d/10d	
	Q920J3	Coro6	3d/10d	
	O88902	Ptpn23	3d/7d	
	D3ZH36	LOC100910536	3d/7d	

were identified corresponding to the 3 days, 7 days and 10 days' time points respectively (supplemental Data S6). Moreover, taken into account both the spatial regionalization along the spinal cord and the time course after SCI, we established that R1 versus C1 harbored no common pathways whereas R2 versus C2 shared neurites outgrowth, cell proliferation, cell differentiation, cell death and cytoskeleton organization pathways. In R3 versus C3 analyses, common pathways included cell proliferation and endocytosis pathways were found (supplemental Data S7–S9). In the same way, when taking into account the time course, 40 specific proteins unique of each segment could be retrieved, i.e. 18 specific proteins in lesion segment, 2 in R1, 2 in C1, 3 in R2, 5 in C2, 2 in R3 and 8 in C3 (Table III). Interestingly, the chemokine Cxcl2 was identified as

specific to R1, whereas in C1, Neurofascin and mediator of cell motility-1 (MEMO1). MEMO1 is implicated in a MEMO1-RhoA-DIAPH1 signaling pathway that plays an important role in ErbB2-dependent (34). Neurofascin is related to L1 family immunoglobulin cell adhesion molecule with multiple IgCAM and fibronectin domains. Neurofascin is implicated in neurite outgrowth, neurite fasciculation and organization of the axon initial segment. Importantly, Neurofascin is also targeted by autoantibodies in patients with multiple sclerosis (MS) and its altered expression has been proposed as a contributing factor to axonal pathology in MS (35). Finally, 18 lesion-specific proteins were detected among which: the follistatin-like 1 (Fstl1), a molecule that modulates the action of several growth factors on cell proliferation and differentiation and Niban-like protein 1 (Fam129b), an inhibitor of apoptosis.

Thus, these global proteomic analyses clearly demonstrate that lesion site and the proximal segments (R1 and C1) are different from the distal areas. These results are corroborated by MALDI mass spectrometry imaging (MALDI-MSI) analysis performed on R1, C1, and lesion tissues sections (Fig. 4). In fact, molecular 2D-maps based on metabolites and lipids will allow seeing the molecular regionalization in regards to physiological processes. The molecular imaging studies after SCI (3 days) show a complete disruption of gray matter-specific lipid signals along the lesion site (Fig. 4A). Spatial segmentation of MALDI-MSI data, dividing the spinal cord sections into anatomical regions allowed discriminating between different regions in an unsupervised method. The cluster analyses of rostral, lesion and caudal sections after 3 days of SCI confirm a disrupted structure of lipid distribution along the lesion site whereas the segmentation of rostral and caudal sections is consistently aligned with the spinal cord anatomy (Fig. 4B). The gray matter is shown in red and the white matter in green (Fig. 4B). *m/z* values exclusively localized with the lesion region were automatically elucidated and in Fig. 4C, 18 *m/z* images are shown. With component analysis fundamental components of the spectra and *m/z* images within the SCI MALDI-MSI data set can be discovered unsupervised. By that, the data are decomposed into a pre-specified small number of score images showing the main spatial features and a small set of component spectra showing the main spectral features. Furthermore a Receiver Operating Characteristic (ROC) analysis was performed for detecting *m/z*-values which allow a discrimination of different regions (C1 and R1); see Table IV for discriminating *m/z* values and Fig. 4Cb for a visualization of the spatial distribution of selected *m/z* values. In Fig. 4D, the results of the component analyses for the probabilistic latent semantic analysis (Figs. 4Da and 4Db) with random initialization and for principal component analysis (Fig. 4Dc) with five components are indicated. For verification of the findings obtained above, a second set of MALDI-MSI data was obtained for 24 slices of the caudal region. A 3D-visualization of selected *m/z* values, which were chosen according to the values stated in Table IV, confirms the sig-

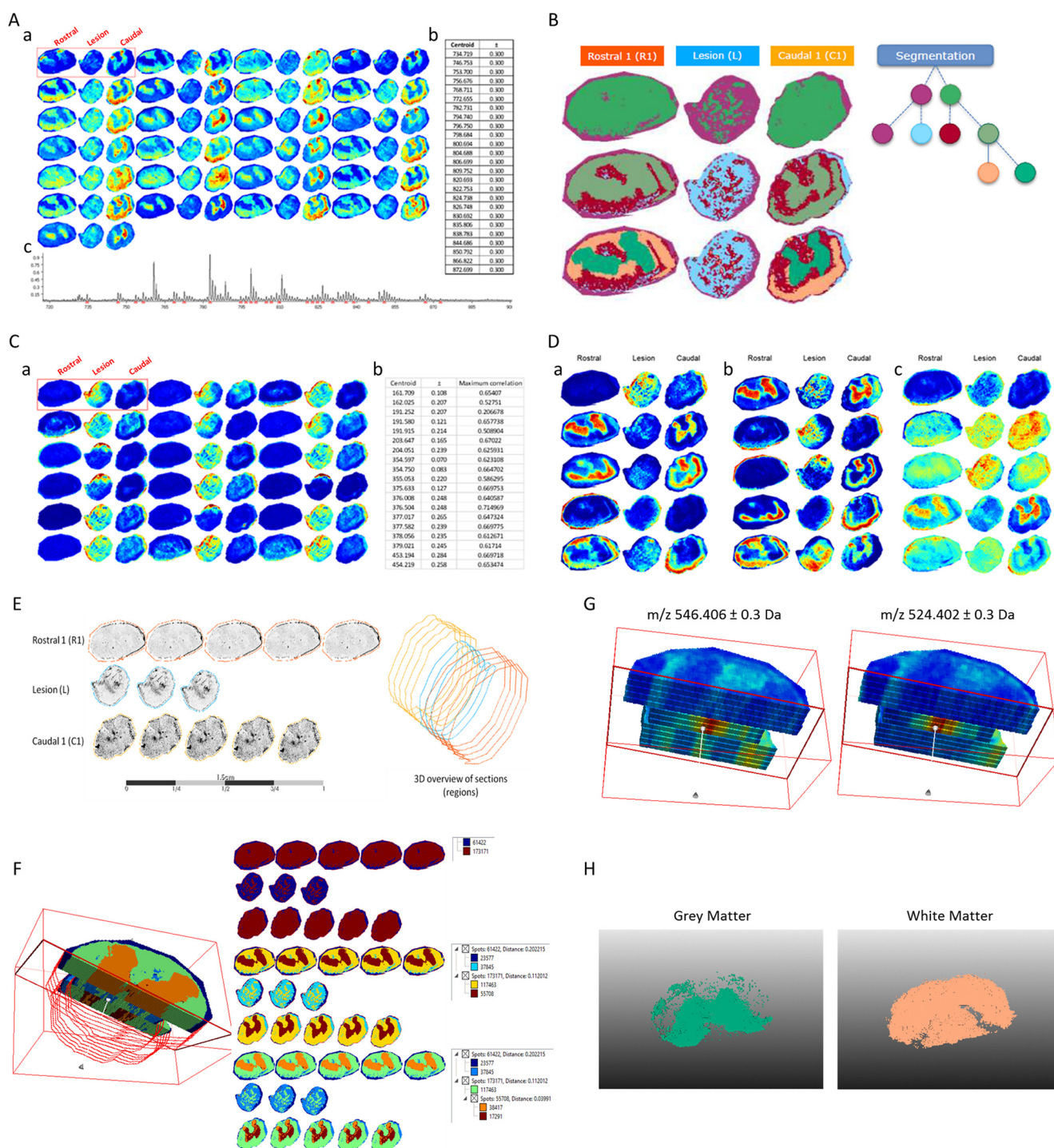


FIG. 4. A, Comparison of signals across different spinal cord segments. (a) 25 m/z image sets (left rostral, middle lesion, right caudal) are shown with ± 0.3 Da and edge-preserving image denoising as well as automatic hot spot removal. (b) The respective m/z values are indicated in the table. (c) The localization of the respective peaks is shown in the mean spectrum below. **B, Hierarchical clustering:** regions which are conjectured to be gray respectively white matter tissue is clearly structured in rostral and caudal regions, no structure visible in lesion region. **C, (a)** Colocalized m/z image sets (left rostral, middle lesion, right caudal) and (b) respective m/z values in the lesion region with the respective Pearson's correlation values. **D, Component analyses** for the probabilistic latent semantic analysis (a and b) with random initialization and principal component analysis (c) with five components. **E, 3D projection** of lipid expression across the length of spinal cord. Initial 3D alignment to follow lipid spatial distribution with imaging. **F, Cluster analyses (segmentation)** for two, four and five clusters with the respective amount of spots per cluster and the distance values to reconstruct spinal cord. **G, 3D projection** of specific signals m/z 524.402 and 546.406 detected at the lesion site. **H, 3D map** at the level of the gray and white matters of the caudal 1 segment based on 24 consecutive sections.

TABLE IV
Discriminating *m/z*-values for lesion vs. rostral/ caudal region obtained by ROC

Centroid	±	Maximum AUC	<i>m/z</i> at maximum
86.005	0.245	0.744975	86.237
86.377	0.127	0.761224	86.263
86.686	0.182	0.674034	86.517
104.076	0.277	0.734237	104.328
104.630	0.277	0.727656	104.353
169.759	0.188	0.397301	169.921
170.055	0.108	0.458626	170.150
170.271	0.108	0.759526	170.278
170.456	0.076	0.691658	170.379
170.720	0.188	0.557438	170.532
174.917	0.258	0.394923	175.163
175.398	0.223	0.739125	175.392
175.885	0.264	0.251686	176.130
184.068	0.300	0.750433	184.322
191.828	0.300	0.239038	192.108
192.352	0.163	0.737723	192.261
192.678	0.163	0.186462	192.821
213.801	0.264	0.299782	214.066
214.244	0.178	0.749835	214.244
214.636	0.214	0.50978	214.422
221.982	0.277	0.721014	222.259
222.536	0.277	0.743943	222.310
240.018	0.300	0.622719	240.298
240.629	0.300	0.755234	240.400
782.731	0.300	0.643802	782.756
783.698	0.300	0.64038	783.748
798.684	0.300	0.61345	798.735
799.702	0.300	0.616393	799.727

nificance of these molecular weights (Fig. 4E). Clustering has been performed through R1, C1, and lesion segments (Fig. 4F) and established that lesion is highly impacted compared with R1. Specific *m/z* at respectively 546.406 and 524.402 which have been retrieved at the lesion site but not in R1 and C1 segments confirm our hypothesis (Fig. 4G). In the same way, clustering analyses also allow to state that C1 is divergent from R1 (Fig. 4G). 3D map performed at the C1 segment from 24 sections showed that gray matter is more impacted compared with the white matter (Fig. 4H) and expressed specific lipids as the ones fully characterized by lipidomic in C1 and in lesion (Table V). In fact, comparison between the lesion and C1 in lipid composition showed difference in the level of expression between the two segments. These 2D- and 3D-molecular maps reinforce the proteomic analyses and point out that C1 is divergent from R1 in term of the molecular contents at different time points.

Time Course Analysis of Inflammatory and modify to regenerative Markers Along the Spinal Cord Axis—To complement the results obtained from our pan-proteomic approaches, we further focused our attention on immune and neurites outgrowth or axon guidance factors along the spinal cord in time course (Table VI). We established that, compared with control samples, immune-related proteins comprising galectins 1 and

3 (Lgals1 and 3), coronin 1b (Coro1b), macrophage migration inhibitory factor (MIF), granulin (Grn), lymphocyte cytosolic protein (Lcp1), complement system components (C3 and B2m) and cathepsins (Ctsb and Ctssd), are overexpressed in the lesion site 3 days after SCI, show further increased levels at 7 days and remain at high levels at 10 days. In contrast, the inflammation peak was observed at 3 days in R1 segments and at 7 days in C1 segments. For axon guidance and neuroprojection represented by microtubule-associated protein Tau (Mapt), Pak proteins (Pak 1 and 2), Ras-related C3 botulinum toxin substrate 1 (Rac1), neural cell adhesion molecule 1 (Ncam1), stathmins (Stmn 1 and 2), semaphorin 7a (Sema7a), dectin 1 (Dctn1), neurofilament light polypeptide (Nefl), profiling 1 (Pfn1), neurofascin (Nfasc), neurotrimin (Ntm), the level of these proteins was low at 3 days, increased at 7 days and stayed stable at 10 days in the lesion segment. At 3 days, the level is the highest in C2 and C3 segments compared with C1 and R1 segments. At 7 days, it increased in C1 to C3 segments. At 10 days, it decreased in lesion, C1 and C2 segments, stayed high in C3 and increased in R1 to R3 segments. For motoneurons degeneration represented by the super dismutase 1 (Sod1), the vesicle-associated membrane protein b (Vapb), dynactin-1 (Dctn1), the highest level is in C1 to C3 segments at 7 days and in R1 to R3 segments at 10 days. For neurites inhibition, *i.e.* RhoA, neurocan (Ncan), amphiphysin (Amph), the overexpression occurs in C1 segment in time course with a peak reaching at 7 days.

In order to extend such proteomic quantitative label free results, cytokines arrays (Figs. 5A–5B) and functional assays (Figs. 5C–5E) that compared the secretome of R1 *versus* C1 segments were performed. Cytokines arrays confirmed the time-dependent and localization-dependent synthesis of chemokines and cytokines in R1 and C1 segments. Compared with control, in R1 segment, CXCL1, CXCL3, CXCL5, CCL20, TIMP-1, and IL6 are overexpressed 3 days after SCI whereas CCL3 and CTNF decrease (Fig. 5A). At 7 days after SCI, some cytokines remain high (*i.e.* CXCL1, CXCL3, and TIMP1), increase (*i.e.* CXCL2, CXCL5, CXCL7, CCL3) or remain constant (*i.e.* IL6 and CCL20) (Fig. 5A). At 10 days, CXCL1, CXCL3, CXCL2, CXCL5, and TIMP 1 fall dramatically, IL6 and CCL20 disappear and CTNF and CXCL7 continue to increase (Fig. 5A). In C1, the evolution is different (Fig. 5B). At 3 days after SCI, level of CXCL3 and TIMP-1 increase but not as registered in R1, the level of CXCL7 and CXCL5 decrease, whereas IL6 and CCL20 are not detected (Fig. 5B). After 7 days, the cytokines pattern changed with an increase of CXCL1, CXCL2, CXCL3, CXCL5, and CXCL7 levels and re-appearance of IL6 together with CCL20. 10 days after SCI, CXCL1, CXCL3, CXCL5, TIMP 1 are even higher than in R1 segment and IL6 is always present in C1 but not in R1 segment. Taken together, these data showed that the cytokines pattern change in time course between R1 and C1. Specific chemokines (CXCL1, CXCL2, CXCL3, CXCL5, CXCL7, CCL3,

TABLE V
Retention time, m/z, and identification of lipids expressed in C1 or lesion segment after lipidomics analyses

Retention time (minutes) / m/z	Compound IDs	Max Fold Change	Highest Mean	Lowest Mean
46.34 / 715.4726	LMGP10010664	11	C1	lesion
	LMGP10010796			
	LMGP10010304			
	LMGP10010502			
52.03 / 876.6130	LMGP01030014	10	lesion	C1
44.95 / 814.5609	LMGP01012192	8	lesion	C1
	LMGP01011838			
	LMGP02010668			
	LMGP02010880			
	LMGP01011560			
	LMGP02010610			
	LMGP01011620			
	LMGP02011076			
	LMGP02010851			
	LMGP01011399			
	LMGP01011530			
	LMGP01010690			
	LMGP02010581			
	LMGP02010806			
LMGP02010502				
LMGP01012127				
48.37 / 848.5810	LMGP02030092	6	lesion	C1
	LMGP01030015			

CCL20, IL6) that are secreted by macrophages or epithelial cells after injury have the ability to attract neutrophils and lymphocytes, activate inflammation and stimulate extracellular matrix synthesis and tissue remodeling. This actually substantiates the hypothesis that the types of immune cells that are attracted along the spinal cord upon injury insult are quite different between rostral and caudal segments in time course, *i.e.* cells start to migrate toward R1 and then C1 segment as shown the proteomic data (Table VI). It has also to be noticed that IL6 and CCL20 are expressed firstly in R1 at 3 days after SCI and secondly appeared in C1 at 7 days. Moreover, CCL20 is also known to attract T regulator lymphocytes through CCR6 binding (36). In that context, it is necessary to correlate the cytokines expression with cellular presence in time course and along the spinal cord.

Fluorescent immunohistochemistry and cell quantification were then performed in order to compare, in C1 *versus* R1, the post-SCI time course of microglial cells, neutrophils and FoxP3 positive T regulator lymphocytes (Tregs) infiltrations (Figs. 6 and 7). Quantification of microglia revealed that the highest density of Iba-1-positive cells could be observed in gray matter areas of caudal regions, at 3 days and 7 days post-SCI (Fig. 6C). No differences are observed between the R1 and C1 segments at 10 days (Fig. 6C). As compared with control samples, Iba-1-positive microglia, in all SCI samples harbor a rounded morphology indicative of an activation state (Fig. 6). Differences between the R1 and C1 segments, with regard to microglial cells density, reach significant levels only in gray matter areas, at 3 and 7 days post-SCI (Fig. 6B–6E). Irrespective of the segment considered, the density of micro-

TABLE V—continued

Retention time (minutes) / m/z	Compound IDs	Max Fold Change	Highest Mean	Lowest Mean
44.35 / 365.3419	LMFA11000455	3	lesion	C1
40.78 / 865.5024	LMGP04010977	3	lesion	C1
	LMGP04010838			
	LMGP04010619			
51.07 / 838.5602	LMGP03010798	3	C1	lesion
	LMGP03010883			
	LMGP03010539			
54.78 / 880.6450	LMGP01090058	3	lesion	C1
	LMGP01030073			
44.35 / 838.5599	LMGP02011114	3	lesion	C1
	LMGP02010652			
	LMGP02011111			
	LMGP02010950			
	LMGP02010589			
	LMGP02010816			
40.54 / 715.5678	LMGL03012630	3	C1	lesion
40.54 / 743.5984	LMGL03012634	3	C1	lesion
45.35 / 826.5611	LMGP02010949	3	lesion	C1
	LMGP02011110			
	LMGP02010785			
	LMGP02010560			
50.09 / 850.5967	LMGP01090049	3	lesion	C1
	LMGP01090048			

glial cells decreases at 7 days but still remains above the basal microglial density observed in control samples (Fig. 6C). Results from cytokine/chemokine arrays urged us to perform a similar immunohistochemical analysis for neutrophils and Tregs. Similar study was performed for neutrophils in regard to chemokines pattern found (Fig. 5D). Neutrophils were abundantly detected in both R1 and C1 segments with a peak reached at 3 days after SCI without any differences in term of amount between each segments. The level decreases in time course. However, immunohistochemistry based on anti-neutrophil elastase marker revealed that the shape of the cells is different in control and after SCI (Fig. 7). In controls, neutrophils are elongated and bipolar (Fig. 7A). Three days after SCI, cells start to make some ramifications and 7 days more cells have ramifications (Fig. 7A and 7C). Ten days later, the num-

ber of cells decreased, but the ones present are still ramified (data not shown). Analyses performed at the level of the blood vessel confirmed that lot of neutrophils are present 3 days (Fig. 7D) after SCI and less at 7 days. At higher magnification, we could discriminate sign of neutrophils extravasation, mimicking movement of cells out of blood vessels toward the injury (Fig. 7E). In comparison, Tregs are present 3 days after SCI, in rostral segment in higher amount than in caudal one. Their levels peak at 7 days for both segments and then decrease at 10 days (Fig. 7E). These results are in line with the cytokine phenotype expressed by the cells (IL6 and CCL20) (Fig. 5). At 3 days after SCI, Tregs presented ramifications (Fig. 7F) whereas at 7 and 10 days, they become round (data not shown). These data are clearly in line with the cytokines pattern observed in Fig. 5 where chemoattractant factors for

TABLE VI

Label free quantification (Intensity-based absolute quantification (iBAQ) value) of identified protein per segments and taking into account time after SCI. the iBAQ values calculated by MaxQuant are proportional to the molar quantities of the proteins

Table with columns for protein names (e.g., axon guidance and neuroprotection, synapse, neuron degeneration, immune response) and rows for segments (C1-C3, D1-D3). Each cell contains numerical iBAQ values for different conditions (e.g., Ctrl R1, Ctrl R2, Ctrl R3).



SCIMICS MOLECULAR & CELLULAR PROTEOMICS





FIG. 5. Chemokines and cytokines array after SCI in CM from R1 and C1 for control and 3, 7, and 10 days post injury. The rat cytokine array assay was performed in SC conditioned media. Blue bars show R1 CM, and orange indicates C1 CM. The bar diagrams represent the ratio of the spot mean pixel densities/reference point pixel densities. A, Comparison of cytokines and chemokines secretion in R1 segment at 3, 7 and 10 days after SCI and control. B, Comparison of cytokines and chemokines secretion in C1 segment at 3, 7, and 10 days after SCI and control. Significant differences were analyzed using Student's *t* test **p* < 0.05, ***p* < 0.01, ****p* < 0.001. Quantification of immune cells recruitment in control and 3, 7, and 10 days post-injury, comparison between R1 rostral and C1 caudal segments. C, Number of Iba1 positive microglia recruited in gray and white matters. D, Percentage of neutrophil elastase-positive neutrophils and E, FoxP3-positive Tregulators recruited in white matter. **p* < 0.05, ***p* < 0.001, ****p* < 0.0001 One-way ANOVA.

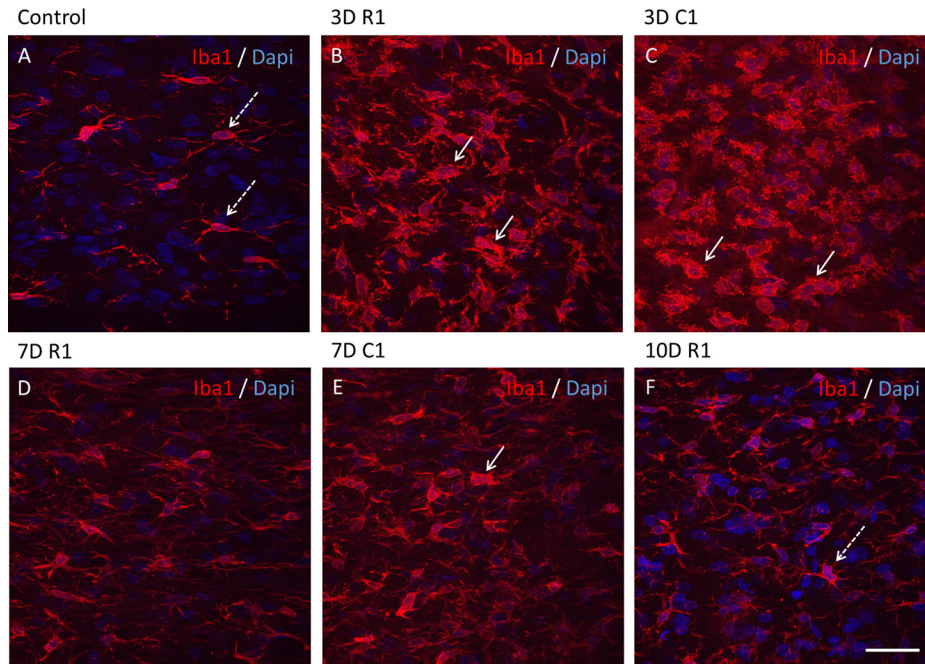


FIG. 6. Representative longitudinal sections of spinal cord revealing Iba1 microglia positive cells rostrally (B, D, E) and caudally (C, F) to the lesion site after SCI (3D, 7D, 10D) in comparison to control (A). Note, activated microglia with hypertrophied cell body and retracted processes at 3 and 7 days at C1 segment (B, C, E arrows-full) in comparison to resting microglia in control (A, arrows-intermitted) or mild activation, re-appearing fine ramification at 10D (F). Scale bar = 25 μ m.

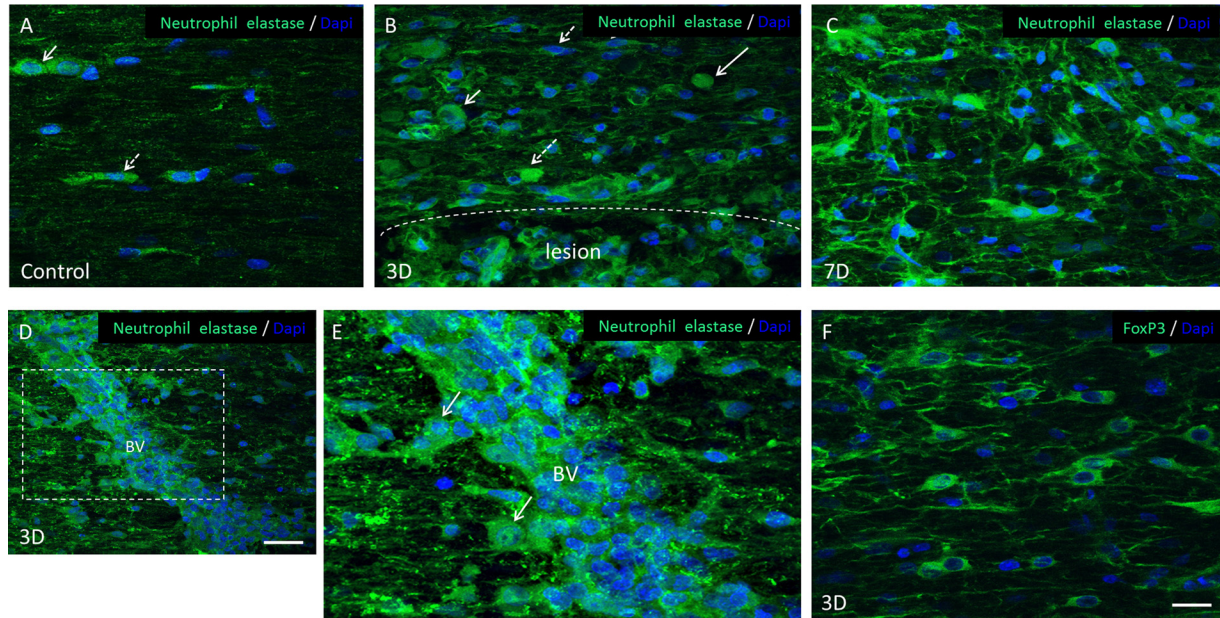


FIG. 7. Fluorescent immunohistochemistry performed on control spinal cord sections and after SCI (3 and 7 days) analyze for neutrophils with neutrophil elastase antibody and lymphocytes Tregulator with FoxP3 antibody. Infiltrated neutrophils showed either elongated (arrow- intermitted) or round shape morphology (arrow-full) at 3 days after SCI (B), whereas at 7 days cellular ramification was apparent in most neutrophils (C). Many blood vessels close to the injury site were filled with neutrophils at 3 and 7 days after SCI (D). At higher magnification, neutrophils extravasation, mimicking movement of cells out of blood vessels toward the injury can be detected (E). Scale bar A-F = 20 μ m, D = 40 μ m, E = 15 μ m. (C3>C2>C1) for control, 3 days, 7 days, and 10 days.

neutrophils and microglia are detected. Neutrophils and microglia are recruited between 0 and 3 days after SCI in caudal segments and their levels decrease at 7 days. Similarly, Tregs

are recruited between 3 and 7 days and peak at 7 days. These data are in line with the presence of CXCL1, CXCL3, CXCL5, CCL20, TIMP-1, and IL6 in R1, at 3 days, which are known to

attract neutrophils and lymphocytes. In C1, a delay is observed for the recruitment of the Tregs, which are recruited 7 days after SCI which correlate with the detection of CCL20 in C1 only at 7 days, whereas neutrophils and microglial cells are already present at 3 days. Taken together the results showed that C1 is clearly different from R1 in term of cell types, molecular content in time course and revealed to be a target segment for therapy.

Focus on C1 Biomarkers for a Targeted Treatment—Because of the presence of neurofascin and MEMO 1 as specific markers of C1 in time course, we investigated the role of these proteins in SCI. Neurofascin could serve as autoantigen. Indeed, in patients sera suffering from inflammatory demyelinating polyneuropathy or multifocal motor neuropathy, specific autoantigens including neurofascin have been found⁶. Moreover, emerging data indicate that pathological sequelae that accompany central nervous system trauma, e.g. SCI, have characteristics of a self-directed immunological disease. Autoantibodies could exacerbate tissue damage impairing neurological recovery and amplify SCI injury. Moreover, the label free quantification (Intensity-based absolute quantification value) of identified protein per segments and taking into account time after SCI have revealed the presence of immunoglobulin (IgG2a) in lesion 3 days after SCI (Table VI). The fact that such cytotoxic immunoglobulin was detected so early after SCI is not in line with a classical adaptive response. In this context, we focused on tracking the occurrence of autoantibodies in time course after SCI. We performed double labeled immunofluorescence on frozen longitudinal sections after 3, 7, and 10 days post-SCI to establish the cell types (neurons, astrocytes and microglia) expressing IgGs. In spinal cord tissue, at 3 days postinjury, IgG-immunoreactivity using both antibodies was found in most neurons (labeled with anti-NeuN), with higher prevalence throughout the layers LV-LIX (Fig. 8A). However, in the case of motor neurons, we could see differences in the double staining expression (Fig. 8A). These IgGs have been characterized (Fig. 8B). In fact, the conditioned media collected at 3, 7, and 10 days post-SCI were incubated with protein A and afterward eluted proteins were separated on SDS-PAGE (Fig. 8B). After silver staining, clear bands are retrieved from the gel at 3 days, but not at 7 or 10 days after SCI. Each selected bands at 25 kDa, 55 kDa, and 75 kDa have been digested in gel before subjected to shot-gun analysis. The identification, performed by MS/MS, of the proteins confirms the presence of the IgGs kappa-chain VJC precursor of fragment (166–218) (Fig. 8B).

Orthogonal views confirmed that anti-IgG (green) and anti-NeuN (red) staining overlap in some, but not all motor neurons (Fig. 8). Thus, some neurons diffusely stained with anti-NeuN were also heavily positive for IgG (Fig. 8C), whereas other neurons were lacking anti-IgG positivity completely, or exhibited labeling only on their surface membrane (Fig. 8D). In few cases we could distinguish also IgG-positive nerve pro-

cesses. Similarly as in neurons, a double anti-GFAP and anti-IgG labeling confirmed positivity in astrocytes (Figs. 9D–9F). Many GFAP-positive astrocytes with hypertrophic appearance and thick processes indicating activated phenotype co-expressed IgG (yellow) primarily at the injury site. These reactive IgG-positive astrocytes were found around neuronal bodies and vessels (Figs. 9D–9F). Baseline expression of GFAP-positive astrocytes with the characteristic round small soma and slender, long processes, but lacking IgG-expression were seen in control spinal cord distributed throughout white and gray matters (Figs. 9A–9C) as well as in the regions out from injury site (Fig. 9G). Furthermore, no GFAP-positive astrocytes expressing IgG were detected in the spinal cord tissue from 7 days and 10 days after SCI. Interestingly, microglia did not express IgG in any of studied groups (data not shown). In addition, to exclude possible effect of B-cells mediated IgG production, we evaluated spinal cord tissue containing multiple *in vivo* injections of rabbit anti-rat CD-20 antibody. In this context, 1 h after SCI, 3 intraspinal injections per animal were applied bilaterally to the lesion site, at the level of the lesion cavity and at rostral and caudal segments. Basso, Beattie and Bresnahan studies at 0, 1, 3, 7, 14, 21 days until 28 days after SCI did not reveal any improvement compared with SCI without anti-CD20 treatment (Fig. 10). In sagittal sections double labeled with primary goat anti-rat IgG2a and mouse anti-NeuN, we did not observe significant attenuation of neurons expressing IgG. The injection tract was occupied with small amount of erythrocytes that were surrounded by neurons with intensely labeled IgGs as well as those farther from injection (Fig. 9H).

DISCUSSION

We have previously investigated the spectrum of released molecules in the conditioned media (CM) from the spinal cord central lesion and adjacent rostral and caudal segments at 3 days after spinal cord injury (SCI) in order to specify the molecular environment within the proximity of the injured tissue. Data suggested that regionalization in terms of inflammatory and neurotrophic responses may occur between rostral and caudal segments in acute SCI. Here, we extended our investigation both spatially and temporally using cellular, biochemical and proteomics techniques. We have shown that the lesion segment is the most divergent from the others ones and is mostly implicated in acute immune response through microglia and neutrophils activation, oxidative stress and lipid peroxidation. R1 and C1 segments present markers for inflammation, axonal regeneration, demyelination and even neurite inhibitors factors. By contrast, segments R3 and C3 and R2 and C2 expressed neurites outgrowth, cell proliferation, cell differentiation, endocytosis and cytoskeleton organization activated pathways. Moreover, these segments are very close in term of the molecular content in time course after lesion and are mostly divergent from R1 and C1 segments. A deeper analysis based on the differential distribution of the

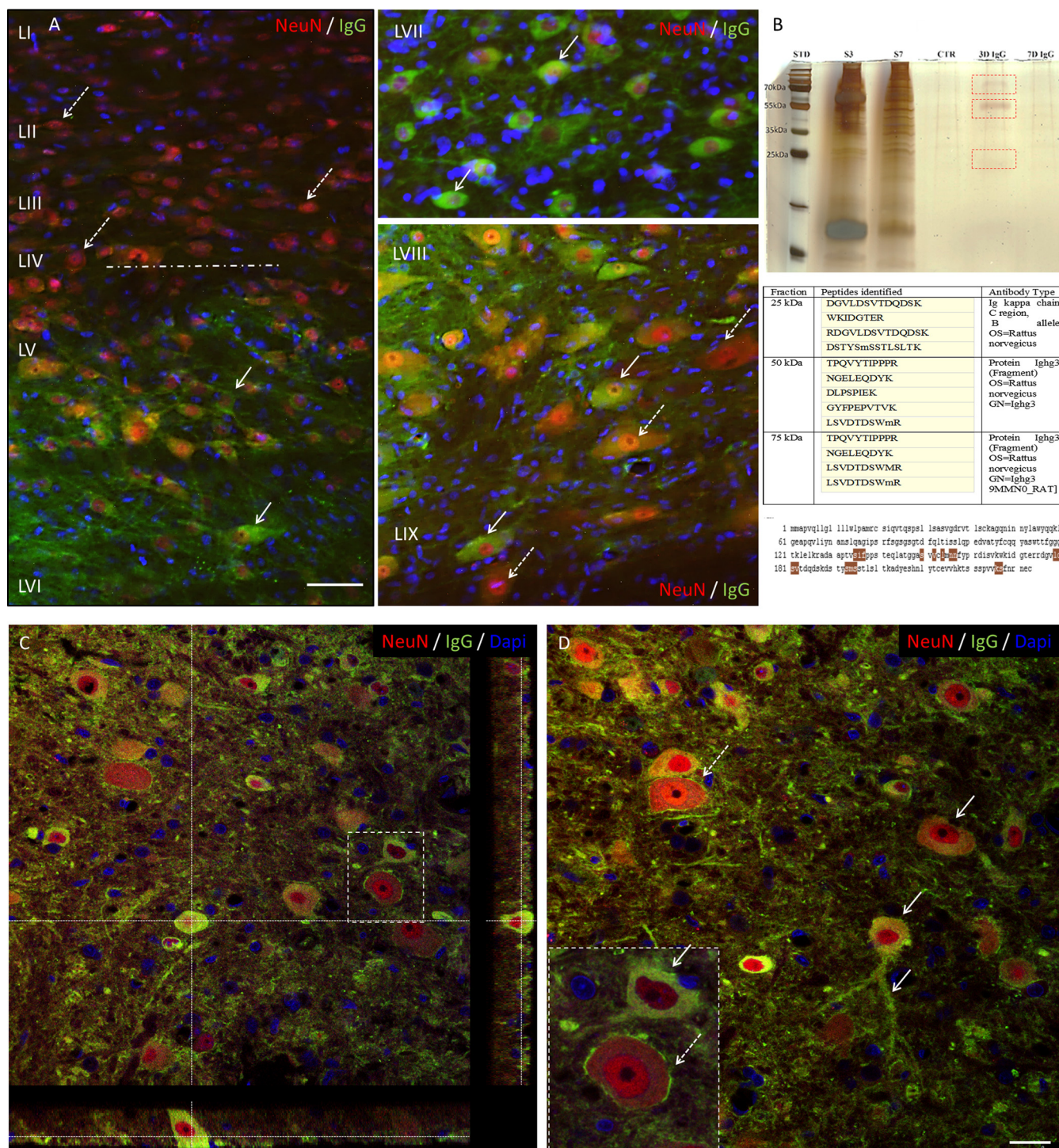


FIG. 8. Specific expression of IgG positivity in neurons through the spinal cord laminae I-IX at 3D. *A*, Double immunofluorescence labeling revealed colocalization of NeuN-positive (red) and IgG-positive (green) cells that were restricted throughout laminae LV-LIX, whereas superficial laminae LI-LIV were IgG-negative. *B*, SDS-PAGE electrophoresis and silver staining confirmed the presence of autoantibodies at 3 days after injury by three bands localized at 70 kDa, 55 kDa and 25 kDa. After in-gel digestion, shot-gun proteomics analysis was performed to confirm the presence of IgGs, for each band (antibody type). BlastP has shown 62% of sequence alignment. Amino acid residues in brown consist of the polypeptide binding sites of the antibody, *i.e.*, sites 135–137, 150, 152, 154, 156–157, 179–182, 193–195, 226–227. Scale bar = 50 μ m. Confocal images demonstrating the presence of IgGs in the spinal cord neurons. *C*, Orthogonal views confirmed that anti-IgG (green) and anti-NeuN (red) stainings overlap in some, but not all motor neurons. *D*, The distribution of IgGs was different across neuronal populations. Although in some neurons intense IgG positivity (green) was homogenously distributed with the cell body and processes (*D*, arrow-full), other neurons exhibited IgG expression limited to their membrane (arrow-intermitted). Scale bar = 25 μ m.

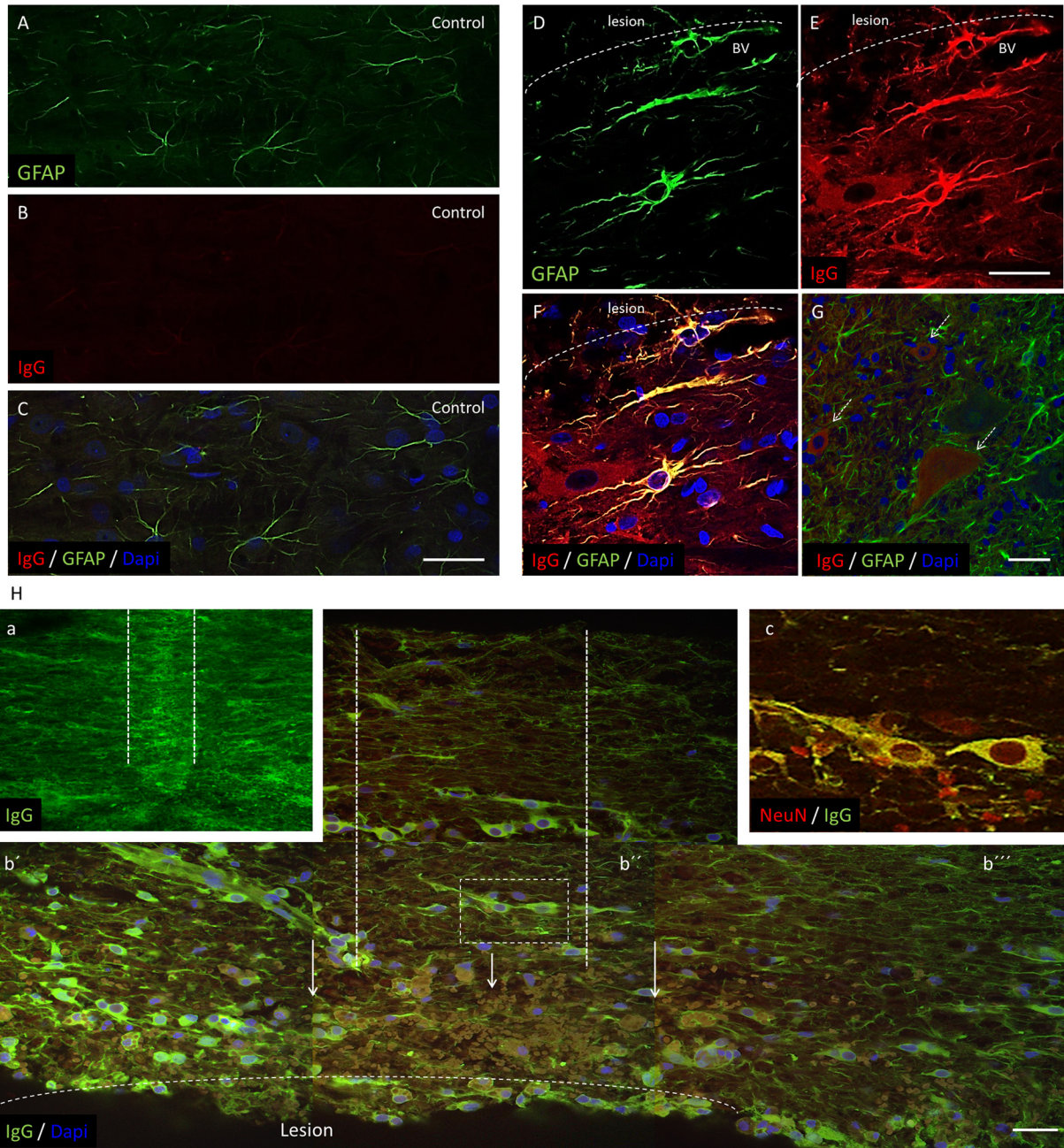


FIG. 9. Representative images of GFAP-positive astrocytes expressing IgG. Control spinal cord sections contained typical astrocytes with star like thin processes (A), lacking IgG (red) expression (B), confirmed by double labeling (C). In contrast, reactive astrocytes with hypertrophic appearance and thick processes, coexpressed IgG (yellow) at the lesion site were found around neuronal bodies and vessels after 3days (D–F). In neighboring rostral and caudal segments, some neurons expressing IgG (red, arrows), but not GFAP-positive astrocytes (green) were detected (G). Scale bar = 25 μ m. H) Intraspinal delivery of anti-CD-20 antibody in rats surviving 3days. (a) Identification of anti-CD-20 delivery tract within the spinal cord tissue labeled with goat-anti rat IgG (green). Note, there is no visible depletion of IgG labeling. (b, b', b'', b''') composite of four detailed figures showing the region adjacent to the lesion, where delivery of CD-20 was performed (outlined by two bars) and is accompanied with infiltrated erythrocytes (arrows) and neurons expressing IgG. At the injections site as well in rostro- caudal axis neurons and their processes expressing IgG were detected. (c) Detail of boxed area from b'' shows double labeling of anti-IgG and anti NeuN confirmed neuronal expression of IgGs. Scale bar = 30 μ m.

unique and common/intersected biological and functional pathways among the three spinal cord rostral and caudal regions (C1,C2, C3 versus R1, R2, R3) factored by time of SCI (3, 7, and 10 days) clearly demonstrate that R1 is different

from C1. The Subnetwork Enrichment Analysis (SEA) showed that only 40 specific proteins unique can be retrieved from each segment taking into account the time course and the spatial localization nearby the lesion (Table III). In this context,

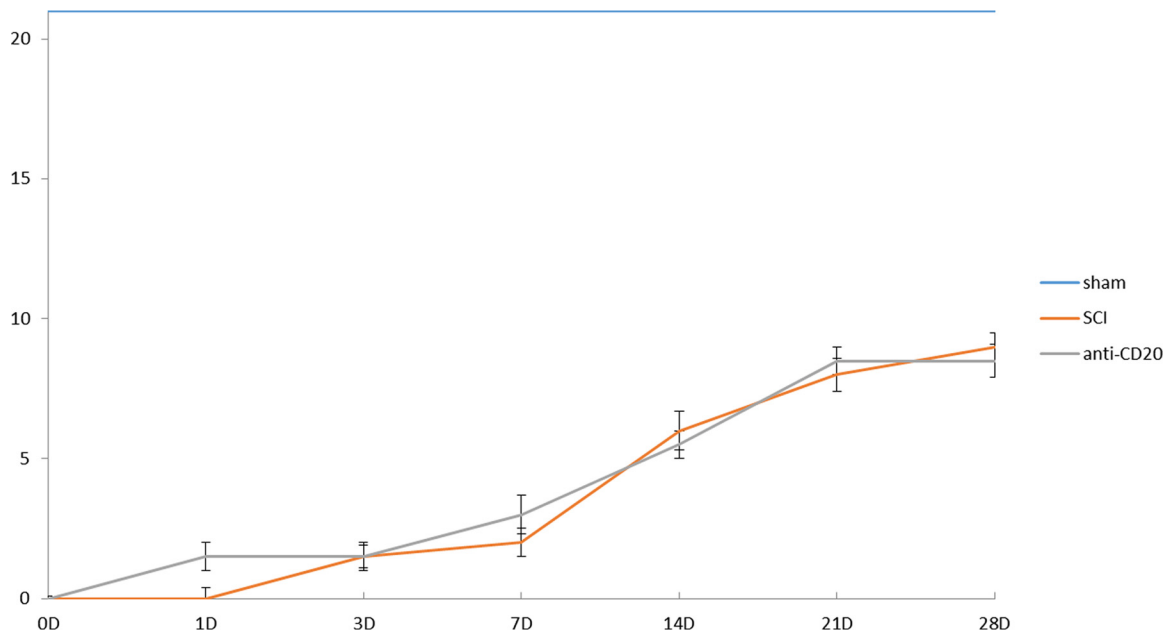


FIG. 10. BBB studies at 0, 1, 3, 7, 10, 14, 21, and 28 days in following experimental groups: in sham, following SCI, and after SCI + anti-CD20 antibody injection. Note, no significant differences in motor function recovery between SCI and SCI+ anti-CD20 treatment during survival.

the chemokine CXCL2 is considered as unique in R1 whereas in C1, the neurofascin and the mediator of cell motility 1 (MEMO 1), which control cell migration by relaying extracellular chemotactic signals to the microtubule cytoskeleton, are detected. The molecular 2D map obtained via MALDI-MSI analysis completed by a lipidomic study in both lesion and C1 (Table V) strengthens these results. The lipid profile detected in lesion is mostly different in term of level of expression to the one detected in C1. The 3D map of the C1 segment at the level of the gray and white matter confirms such differences.

The fine analysis of C1 segments showed, that in time course, C1 segments express neurite inhibitors like MEMO1, neurocan, as well as neurite stimulators such as neurofascin and amphiphysin proteins. MEMO1 is implicated in MEMO1-RHhoA-DIAPH1 signaling pathway which plays an important role in ErbB2-dependence (34). Neurocan is known to inhibit neurites outgrowth (37). After spinal cord injury, neurocan, brevican, and versican expression is increased within days in injured spinal cord parenchyma surrounding the lesion site and peaks at 2 weeks. Neurocan and versican are persistently elevated for 4 weeks post-injury, and brevican expression persisted for at least 2 months (37). On the contrary, neurofascin and amphiphysin, are two proteins known to be implicated in neurites outgrowth, are located at the level of the growth cone. However, these two proteins are also involved in autoimmunity as autoantigens (38–41).

With respect to the proteomic results our next step was to investigate the nature of cellular processes, and identify the cellular content responsible for production of detected molecules. It is well established that injury to the blood-brain barrier facilitates the extravasations of cellular components as

well as immunoglobulins and complement proteins into the neural parenchyma (42, 43). The recruitment of blood-derived cellular components is dependent on inflammatory processes that are orchestrated by secondary damage at the lesion site. Thus, the cytokine environment in the central nervous system (CNS) may determine the phenotype of the inflammatory infiltrate. For example, intra-spinal injections of tumor necrosis factor (TNF)- α induced monocyte infiltration whereas interleukin (IL)-1 β recruited mostly neutrophils (44, 45). Present data confirm that released cytokines and chemokines correlate with the activation of microglia and recruitment of neutrophils in segments anterior and posterior to the lesion site. These cells, along with the soluble mediators/proteins (e.g. cytokines, complement), interact to eliminate pathogenic elements in the affected site, while simultaneously priming the site for repair. Within the spinal cord, microglia are the resident tissue macrophages that primarily control the rate, magnitude and the ultimate fate (supporting regeneration or degeneration) of inflammatory processes at the injury site. However, in our study we have taken into account the cellular microenvironment in which microglia become activated (46). Therefore, we have analyzed response of microglia within the white and gray matters separately in rostro-caudal axis with time.

Present data confirmed striking differences in the number and morphology of microglia cells during injury time. The extent of microglia activation was significantly higher in gray than in white matter tracts in the caudal segments during the time period 3–7 days after injury, whereas at 10 days it dropped down. These discrepancies may be dependent on two factors: i) the metabolic changes in microglial function

that are differentially affected at the gray matter necrotizing injury site and in degenerating white matter tracts, or ii) on the extent of blood-brain barrier injury, which varies between the gray and white matter (42, 47), and on the severity of injury. In this context, gray and white matters microglia express distinct morphologies and levels of cell surface antigens (48, 49), which most likely correspond with unique cell functions (50, 51). Indeed, the microenvironment in which microglia and/or macrophages are activated influences their neurotrophic or neurotoxic effector potential (52, 53) that correspond to M1 and M2 phenotypes. The predominance of microglia activation in caudal segments is in line with our previous and present studies confirming the occurrence of severe inflammation-associated tissue damage taking place in this segment and possibility to switch/or not from M1 to M2 phenotype (29).

In contrast to tissue resident microglia (54), neutrophils are the first inflammatory cells to arrive at the site of injury, with a peak at 24 h post injury. Recruitment of T regulators (Tregs) (Foxp3-positive) firstly occurs at 3 days and mainly at the level of the rostral segment and peaks at 7 days in both rostral and caudal sites. These results are in line with the presence of CCL20 in rostral segment and not in caudal at 3 days and then found at 7 days in both segments. In fact, CCL20 is known to recruit Tregs (55). Presence of recruitment of thymic-derived FoxP3-Tregs was recently suggested (56). Tregs can reduce inflammation and enhance CNS repair (57). Presence of such cells predominantly in rostral segment is in line with the cytokine medium which favor expression of macrophages expressing an M2 phenotype and production of neurotrophic factors (29). Moreover, the time difference of recruitment between rostral and caudal segments of these cells can also contribute to the less enhancement of neurites outgrowth in C1 compared with R1.

Thus, the spinal cord, as a part of CNS has generally been described as having immune privilege, but several facts motivated us to reexamine this principle. Particularly, in a search for presence of antibodies responding to neurofascin found in caudal segment, we have proven via immunohistochemistry that IgGs are expressed by interneurons and motor neurons, 3 days after spinal cord injury suggestive of autoimmunity. Furthermore, in CM from SCI, using biochemical and proteomic analysis, we showed by protein A, gel electrophoresis associated to mass spectrometry analyses, content of spinal IgGs at 3 days, but not at 7 or 10 days after injury. Here, we need to mention few important findings regarding neuronal IgG positivity and IgG sources. Firstly, spinal neurons revealed distinct expression of IgG throughout dorso-ventral axis. Although sensory neurons in laminae I-IV were negative, the neuronal populations corresponding to interneurons and motor neurons of laminae V-IX were most likely positive for IgG, with few discrepancies. The confocal orthogonal views showed that some neurons revealed very clear golgi-like staining of soma and processes, whereas in others the IgG expression was found solely in the neuronal soma, or was

restricted to superficial membrane outlining the neuronal body. We suggest that divergence of neuronal population IgG response may be caused by their different vulnerability to injury or by the extent and severity of impairment *in situ*. Thus, it is more likely that we can see early response of most vulnerable interneurons and motor neurons expressing IgG that are probably behaving to secondary damage processes, similarly as are responding CA1 vulnerable neurons in hippocampus (58). Furthermore, also spinal cord ischemia leads to selective loss of highly vulnerable inhibitory GABAergic interneurons followed by motor neurons resulting to spasticity (59). There are other studies further confirming vulnerability of interneurons, and motor neurons to stress, ischemia, injury or various neurodegenerative diseases. Secondly, it is important to identify the source of IgGs. Because, the motor neurons are projecting outside the CNS, it is assumed that they can take up IgGs from peripheral tissues, by retrograde transport from nerve terminals (60, 61). However, this may not be the case for the interneurons that terminate only within the spinal cord. But, they may have the ability to take up IgGs from the cerebrospinal fluid (CSF) (62).

On other hand, there are studies suggesting productions of IgGs by neurons (63). Present results document specific transient neuronal expression of IgGs, but we do not have proof of their sources, which needs further transcriptomics studies. Another important issue that needs to be mentioned is the functionality of IgGs and their epitopes. There are two contradictory hypotheses that should be taken into account, where IgGs pose as neuroprotective (64) or neurodestructive (60). The first one suggests that neuron-derived IgGs has the ability to protect neurons from early apoptosis and cell death induced by complement. The second one refers to IgGs as detrimental factors of neurons, attacking the regeneration of axons after spinal cord injury (60) (B cells produce pathogenic antibodies and impair recovery after spinal cord injury in mice (65)). Our results are more likely in a favor of the first one, because we identify early, transient expression of IgGs at 3 days. Why we did not see IgGs at 7 or 10 days, we do not have reasonable explanation. Moreover, injection at 1 h after lesion of anti-CD20 did not attenuate the expression of IgGs detected at 3 days post-SCI and Basso, Beattie and Bresnahan motor score of the animals was similar to the one with preliminary treatment. These data tend to reveal that antibodies are not produced by active B cells. Nevertheless, to better understand this interesting finding; we need to follow up with further studies.

Taken together, we described for the first time the molecular and cellular processes occurring after SCI on the temporal and spatial levels. We established that differences in term of molecular pathways occurred between lesion, C1, R1, and the other segments. In fact, R2, C2, and R3, C3 coexpressed the molecules implicated in same physiological pathways. Only 40 specific proteins for each segment and taking into account time after injury have been characterized. Except the

lesion, C1 is the most divergent. The presence of neurites outgrowth inhibitors in C1, with a delay in recruitment of Tregs, favors the lack of regeneration process in C1. Moreover, the presence of IgGs at the lesion site, at 3 days post-SCI, can also be one of the factors that contribute to limitation of the regeneration process. However, treatment of anti-CD20 did not showed any impact *in vivo* in IgGs presence and in enhancement of locomotor function. These results open the door to a novel view of the SCI treatment by considering the C1 as the therapeutic target in order to modulate inflammation and stimulate regeneration process.

* This research was supported by a collaboration between the Fundamental and Applied Biology Mass Spectrometry Laboratory (MS) and grants from Ministère de L'Éducation Nationale, L'Enseignement Supérieur et de la Recherche, INSERM ,Région Nord-Pas de Calais (to S.D.), SIRIC ONCOLille Grant INCa-DGOS-Inserm 6041aa (IF) and Université de Lille 1 (S.D.), VEGA 2/0125/15 (DC), APVV SK-FR-2015-0018 (DC), Stefanic 2016 (MS) and APVV 0472-11 (DC).

☐ This article contains supplemental material.

✉ To whom correspondence should be addressed: University of Lille, INSERM, U1192 - Laboratoire Protéomique, Réponse Inflammatoire et Spectrométrie de Masse-PRISM, F-59000 Lille, France Tel.: +33-320-4194; Fax: +33-320-4354; E-mail: Michel.salzet@univ-lille1.fr.

^a Co-author: The authors declare no competing financial interests.

REFERENCES

- Beattie, M. S., Hermann, G. E., Rogers, R. C., and Bresnahan, J. C. (2002) Cell death in models of spinal cord injury. *Prog. Brain Res.* **137**, 37–47
- Tator, C. H. (1995) Update on the pathophysiology and pathology of acute spinal cord injury. *Brain Pathol.* **5**, 407–413
- Schwab, M. E., and Bartholdi, D. (1996) Degeneration and regeneration of axons in the lesioned spinal cord. *Physiol. Rev.* **76**, 319–370
- Schwab, M. E., and Bartholdi, D. (1996) Degeneration and regeneration of axons in the lesioned spinal cord. *Physiol. Rev.* **76**, 319–370
- Rosignol, S., Schwab, M., Schwartz, M., and Fehlings, M. G. (2007) Spinal cord injury: time to move? *J. Neurosci.* **27**, 11782–11792
- Leybold, B. G., Flanders, A. E., Schwartz, E. D., and Burns, A. S. (2007) The impact of methylprednisolone on lesion severity following spinal cord injury. *Spine* **32**, 373–378; discussion 379–381
- Rowland, J. W., Hawrylyuk, G. W., Kwon, B., and Fehlings, M. G. (2008) Current status of acute spinal cord injury pathophysiology and emerging therapies: promise on the horizon. *Neurosurg Focus* **25**, E2
- Hawrylyuk, G. W., Rowland, J., Kwon, B. K., and Fehlings, M. G. (2008) Protection and repair of the injured spinal cord: a review of completed, ongoing, and planned clinical trials for acute spinal cord injury. *Neurosurg Focus* **25**, E14
- Wells, J. E., Hurlbert, R. J., Fehlings, M. G., and Yong, V. W. (2003) Neuroprotection by minocycline facilitates significant recovery from spinal cord injury in mice. *Brain* **126**, 1628–1637
- Huang, H., Fan, S., Ji, X., Zhang, Y., Bao, F., and Zhang, G. (2009) Recombinant human erythropoietin protects against experimental spinal cord trauma injury by regulating expression of the proteins MKP-1 and p-ERK. *J. Int. Med. Res.* **37**, 511–519
- Bradbury, E. J., Moon, L. D., Popat, R. J., King, V. R., Bennett, G. S., Patel, P. N., Fawcett, J. W., and McMahon, S. B. (2002) Chondroitinase ABC promotes functional recovery after spinal cord injury. *Nature* **416**, 636–640
- Schwab, M. E. (2004) Nogo and axon regeneration. *Curr. Opin. Neurobiol.* **14**, 118–124
- Schwab, M. E. (2002) Repairing the injured spinal cord. *Science* **295**, 1029–1031
- Fehlings, M. G., and Vawda, R. (2011) Cellular treatments for spinal cord injury: the time is right for clinical trials. *Neurotherapeutics* **8**, 704–720
- Vanicky, I., Urdzikova, L., Saganova, K., Cizkova, D., and Galik, J. (2001) A simple and reproducible model of spinal cord injury induced by epidural balloon inflation in the rat. *J. Neurotrauma* **18**, 1399–1407
- Grulova, I., Slovinska, L., Blasko, J., Devaux, S., Wisztorski, M., Salzet, M., Fournier, I., Kryukov, O., Cohen, S., and Cizkova, D. (2015) Delivery of Alginate Scaffold Releasing Two Trophic Factors for Spinal Cord Injury Repair. *Sci. Reports* **5**, 13702
- Cox, J., and Mann, M. (2008) MaxQuant enables high peptide identification rates, individualized p.p.b.-range mass accuracies and proteome-wide protein quantification. *Nat. Biotechnol.* **26**, 1367–1372
- Cox, J., Neuhauser, N., Michalski, A., Scheltema, R. A., Olsen, J. V., and Mann, M. (2011) Andromeda: a peptide search engine integrated into the MaxQuant environment. *J. Proteome Res.* **10**, 1794–1805
- UniProt, C. (2012) Reorganizing the protein space at the Universal Protein Resource (UniProt). *Nucleic Acids Res.* **40**, D71–D75
- Cox, J., Hein, M. Y., Luber, C. A., Paron, I., Nagaraj, N., and Mann, M. (2014) Accurate proteome-wide label-free quantification by delayed normalization and maximal peptide ratio extraction, termed MaxLFQ. *Mol. Cell Proteomics* **13**, 2513–2526
- Vizcaino, J. A., Deutsch, E. W., Wang, R., Csordas, A., Reisinger, F., Rios, D., Dianes, J. A., Sun, Z., Farrah, T., Bandeira, N., Binz, P. A., Xenarios, I., Eisenacher, M., Mayer, G., Gatto, L., Campos, A., Chalkley, R. J., Kraus, H. J., Albar, J. P., Martinez-Bartolome, S., Apweiler, R., Omenn, G. S., Martens, L., Jones, A. R., and Hermjakob, H. (2014) ProteomeX-change provides globally coordinated proteomics data submission and dissemination. *Nat. Biotechnol.* **32**, 223–226
- Vizcaino, J. A., Cote, R. G., Csordas, A., Dianes, J. A., Fabregat, A., Foster, J. M., Griss, J., Alpi, E., Birim, M., Contell, J., O'Kelly, G., Schoenegger, A., Ovelleiro, D., Perez-Riverol, Y., Reisinger, F., Rios, D., Wang, R., and Hermjakob, H. (2013) The PRoteomics IDentifications (PRIDE) database and associated tools: status in 2013. *Nucleic Acids Res.* **41**, D1063–1069
- Montejo, J., Zuberi, K., Rodriguez, H., Bader, G. D., and Morris, Q. (2014) GeneMANIA: Fast gene network construction and function prediction for Cytoscape. *F1000Res* **3**, 153
- Chen, E. Y., Tan, C. M., Kou, Y., Duan, Q., Wang, Z., Meirelles, G. V., Clark, N. R., and Ma'ayan, A. (2013) Enrichr: interactive and collaborative HTML5 gene list enrichment analysis tool. *BMC Bioinformatics* **14**, 128
- Yuryev, A., Kotelnikova, E., and Daraselia, N. (2009) Ariadne's ChemEffect and Pathway Studio knowledge base. *Expert Opin. Drug Discov.* **4**, 1307–1318
- Bonnet, A., Lagarrigue, S., Liaubet, L., Robert-Granie, C., Sancristobal, M., and Tosser-Klopp, G. (2009) Pathway results from the chicken data set using GOTM, Pathway Studio and Ingenuity softwares. *BMC Proc.* **3**, S11
- Pyatnitskiy, M., Mazo, I., Shkrob, M., Schwartz, E., and Kotelnikova, E. (2014) Clustering gene expression regulators: new approach to disease subtyping. *PLoS ONE* **9**, e84955
- Daraselia, N., Wang, Y., Budoff, A., Lituev, A., Potapova, O., Vansant, G., Monforte, J., Mazo, I., and Ossovskaya, V. S. (2012) Molecular signature and pathway analysis of human primary squamous and adenocarcinoma lung cancers. *Am. J. Cancer Res.* **2**, 93–103
- Cizkova, D., Le Marrec-Croq, F., Franck, J., Slovinska, L., Grulova, I., Devaux, S., Lefebvre, C., Fournier, I., and Salzet, M. (2014) Alterations of protein composition along the rostro-caudal axis after spinal cord injury: proteomic, *in vitro* and *in vivo* analyses. *Front. Cell Neurosci.* **8**, 105
- Thiele, H., Heldmann, S., Trede, D., Strehlow, J., Wirtz, S., Dreher, W., Berger, J., Oetjen, J., Kobarg, J. H., Fischer, B., and Maass, P. (2014) 2D and 3D MALDI-imaging: conceptual strategies for visualization and data mining. *Biochim. Biophys. Acta* **1844**, 117–137
- Bonnel, D., Longuespee, R., Franck, J., Roudbaraki, M., Gosset, P., Day, R., Salzet, M., Fournier, I. (2011) Multivariate analyses for biomarkers hunting and validation through on-tissue bottom-up or in-source decay in MALDI-MSI: application to prostate cancer. *Anal. Bioanal. Chem.* **401**(1), 149–165
- Chambolle, A. (2004) An algorithm for total variation minimization and applications. *J. Mathematical Imaging Vision* **20**, 89–97
- Zhang, J., Li, D., Hu, W., Chen, Z., and Yuan, Y. (2014) Multilabel image annotation based on double-layer PLSA model. *ScientificWorldJournal* **2014**, 494387
- Zaoui, K., Honore, S., Isnardon, D., Braguer, D., and Badache, A. (2008) Memo-RhoA-mDia1 signaling controls microtubules, the actin network, and adhesion site formation in migrating cells. *J. Cell Biol.* **183**, 401–408

35. Mathey, E. K., Derfuss, T., Storch, M. K., Williams, K. R., Hales, K., Woolley, D. R., Al-Hayani, A., Davies, S. N., Rasband, M. N., Olsson, T., Moldenhauer, A., Velhin, S., Hohlfeld, R., Meinel, E., and Linington, C. (2007) Neurofascin as a novel target for autoantibody-mediated axonal injury. *J. Exp. Med.* **204**, 2363–2372
36. Han, G., Wu, D., Yang, Y., Li, Z., Zhang, J., and Li, C. (2015) CrkL mediates CCL20/CCR6-induced EMT in gastric cancer. *Cytokine* **76**, 163–169
37. Jones, L. L., Margolis, R. U., and Tuszynski, M. H. (2003) The chondroitin sulfate proteoglycans neurocan, brevican, phosphacan, and versican are differentially regulated following spinal cord injury. *Exp. Neurol.* **182**, 399–411
38. Neshige, S., Hara, N., Takeshima, S., Iwaki, H., Shimoe, Y., Takamatsu, K., and Kuriyama, M. (2014) Anti-amphiphysin antibody-positive paraneoplastic neurological syndrome with a longitudinally extensive spinal cord lesion of the dorsal column. *Clin. Neurol.* **54**, 572–576
39. Levin, M. C., Lee, S., Gardner, L. A., Shin, Y., Douglas, J. N., and Cooper, C. (2013) Autoantibodies to non-myelin antigens as contributors to the pathogenesis of multiple sclerosis. *J. Clin. Cell. Immunol.* **213**, 4–10
40. Huijbers, M. G., Querol, L. A., Niks, E. H., Plomp, J. J., van der Maarel, S. M., Graus, F., Dalmau, J., Illa, I., and Verschuuren, J. J. (2015) The expanding field of IgG4-mediated neurological autoimmune disorders. *Eur. J. Neurol.* **22**, 1151–1161
41. Derfuss, T., Linington, C., Hohlfeld, R., and Meinel, E. (2010) Axo-glial antigens as targets in multiple sclerosis: implications for axonal and grey matter injury. *J. Mol. Med.* **88**, 753–761
42. Popovich, P. G., Horner, P. J., Mullin, B. B., and Stokes, B. T. (1996) A quantitative spatial analysis of the blood-spinal cord barrier. I. Permeability changes after experimental spinal contusion injury. *Exp. Neurol.* **142**, 258–275
43. Noble, L. J., and Wrathall, J. R. (1989) Distribution and time course of protein extravasation in the rat spinal cord after contusive injury. *Brain Res.* **482**, 57–66
44. Schnell, L., Fearn, S., Schwab, M. E., Perry, V. H., and Anthony, D. C. (1999) Cytokine-induced acute inflammation in the brain and spinal cord. *J. Neuropathol Exp. Neurol.* **58**, 245–254
45. Schnell, L., Fearn, S., Klassen, H., Schwab, M. E., and Perry, V. H. (1999) Acute inflammatory responses to mechanical lesions in the CNS: differences between brain and spinal cord. *Eur. J. Neurosci.* **11**, 3648–3658
46. Zhou, X., He, X., and Ren, Y. (2014) Function of microglia and macrophages in secondary damage after spinal cord injury. *Neural Regen Res.* **9**, 1787–1795
47. Horner, P. J., Popovich, P. G., Mullin, B. B., and Stokes, B. T. (1996) A quantitative spatial analysis of the blood-spinal cord barrier. II. Permeability after intraspinal fetal transplantation. *Exp. Neurol.* **142**, 226–243
48. Perry, M. J., and Lawson, S. N. (1993) Neurofilaments in rat and cat spinal cord; a comparative immunocytochemical study of phosphorylated and non-phosphorylated subunits. *Cell Tissue Res.* **272**, 249–256
49. Perry, J. R., Deodhare, S. S., Bilbao, J. M., Murray, D., and Muller, P. (1993) The significance of spinal cord compression as the initial manifestation of lymphoma. *Neurosurgery* **32**, 157–162
50. Popovich, P. G., Wei, P., and Stokes, B. T. (1997) Cellular inflammatory response after spinal cord injury in Sprague-Dawley and Lewis rats. *J. Comp. Neurol.* **377**, 443–464
51. Streit, W. J., Semple-Rowland, S. L., Hurley, S. D., Miller, R. C., Popovich, P. G., and Stokes, B. T. (1998) Cytokine mRNA profiles in contused spinal cord and axotomized facial nucleus suggest a beneficial role for inflammation and gliosis. *Exp. Neurol.* **152**, 74–87
52. Zietlow, R., Dunnett, S. B., and Fawcett, J. W. (1999) The effect of microglia on embryonic dopaminergic neuronal survival in vitro: diffusible signals from neurons and glia change microglia from neurotoxic to neuroprotective. *Eur. J. Neurosci.* **11**, 1657–1667
53. Zhang, S. C., and Fedoroff, S. (1996) Neuron-microglia interactions in vitro. *Acta Neuropathol.* **91**, 385–395
54. Kurihara, D., Ueno, M., Tanaka, T., and Yamashita, T. (2010) Expression of galectin-1 in immune cells and glial cells after spinal cord injury. *Neurosci. Res.* **66**, 265–270
55. Villares, R., Cadenas, V., Lozano, M., Almonacid, L., Zaballos, A., Martinez, A. C., and Varona, R. (2009) CCR6 regulates EAE pathogenesis by controlling regulatory CD4+ T-cell recruitment to target tissues. *Eur. J. Immunol.* **39**, 1671–1681
56. Raposo, C., Graubardt, N., Cohen, M., Eitan, C., London, A., Berkutzki, T., and Schwartz, M. (2014) CNS repair requires both effector and regulatory T cells with distinct temporal and spatial profiles. *J. Neurosci.* **34**, 10141–10155
57. Austin, P. J., Kim, C. F., Perera, C. J., and Moalem-Taylor, G. (2012) Regulatory T cells attenuate neuropathic pain following peripheral nerve injury and experimental autoimmune neuritis. *Pain* **153**, 1916–1931
58. Blanco-Suarez, E., and Hanley, J. G. (2014) Distinct subunit-specific alpha-amino-3-hydroxy-5-methyl-4-isoxazolepropionic acid (AMPA) receptor trafficking mechanisms in cultured cortical and hippocampal neurons in response to oxygen and glucose deprivation. *J. Biol. Chem.* **289**, 4644–4651
59. Cizkova, D., Kakinohana, O., Kucharova, K., Marsala, S., Johe, K., Hazel, T., Hefferan, M. P., and Marsala, M. (2007) Functional recovery in rats with ischemic paraplegia after spinal grafting of human spinal stem cells. *Neuroscience* **147**, 546–560
60. Ankeny, D. P., and Popovich, P. G. (2010) B cells and autoantibodies: complex roles in CNS injury. *Trends Immunol.* **31**, 332–338
61. Ankeny, D. P., Guan, Z., and Popovich, P. G. (2009) B cells produce pathogenic antibodies and impair recovery after spinal cord injury in mice. *J. Clin. Invest.* **119**, 2990–2999
62. Gini, B., Lovato, L., Cianti, R., Cecotti, L., Marconi, S., Anghileri, E., Armini, A., Moretto, G., Bini, L., Ferracci, F., and Bonetti, B. (2008) Novel autoantigens recognized by CSF IgG from Hashimoto's encephalitis revealed by a proteomic approach. *J. Neuroimmunol.* **196**, 153–158
63. Huang, J., Sun, X., Mao, Y., Zhu, X., Zhang, P., Zhang, L., Du, J., and Qiu, X. (2008) Expression of immunoglobulin gene with classical V-(D)-J rearrangement in mouse brain neurons. *Int. J. Biochem. Cell Biol.* **40**, 1604–1615
64. Fehlings, M. G., and Nguyen, D. H. (2010) Immunoglobulin G: a potential treatment to attenuate neuroinflammation following spinal cord injury. *J. Clin. Immunol.* **30 Supplemental 1**, S109–S112
65. Kobeissy, F., and Moshourab, R. A. (2015) Autoantibodies in CNS Trauma and Neuropsychiatric Disorders: A New Generation of Biomarkers. In: Kobeissy, F. H., ed. *Brain Neurotrauma: Molecular, Neuropsychological, and Rehabilitation Aspects*, Boca Raton (FL)

CONCLUSION CHAPTER 1 & 2

The spatio temporal analysis of a spinal cord injury allows us to point out the C1 segment as a possible target for a therapy. Among the factors detected in caudal segments, chondroitin sulfate proteoglycans (CSPG) and immunoglobulins IgG2a have been identified as well as the MEMO1-RHOA-DIAPH1 signaling pathway. The MEMO1-RHOA-DIAPH1 signaling pathway plays an important role in ERBB2-dependent stabilization of microtubules at the cell cortex and inhibits neurites outgrowth. A comparative proteomic approach performed at the caudal segment level has shown the expression of the eukaryotic translation initiation factor 5A1 (eIF5A1) and Rho GDP dissociation inhibitor alpha (RhoGDI α), a member of Rho GDI family (W. Liu *et al.* 2015). *In vitro*, eIF5A1 overexpression in primary neurons increased cell survival and elongated neurite length while eIF5A1 knockdown reversed these results. RhoGDI α up-regulation and down-regulation rescues the effect of eIF5A1 down-regulation and up-regulation both *in vivo* and *in vitro*.

In this context, we have decided to concentrate our efforts on the role of immunoglobulins and the MEMO1-RHOA-DIAPH1 signaling pathway in the inhibition of neurites outgrowth.

IMMUNOGLOBULINS

Among factors highlighted in this part, the high presence of immunoglobulins (Ig) 3 days post injury brought us to study the proteomic profile 24 hours after injury. The aim was to follow the inflammation process at its early stage and to observe the presence of these IgGs. A shot gun proteomic analysis was conducted in the same manner as the previous one, from segments R2 to C2, in order to focus on the adjacent part of the lesion site. 24 hours after injury, the inflammation spread to the adjacent segment (Figure 16).

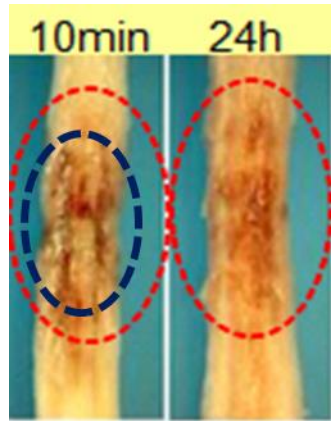


Figure 16: Inflammation expansion in time dependent manner. Blue circle corresponds to the inflammation site 10 min post injury. The red circle corresponds to the spreading of the inflammation 24 hours after SCI.

Proteomic analysis, in triplicate for the segments R1 to C2 and in duplicate for the segment R2, allows for the comparison between these five segments. A venn diagram shows us that among the more than 2000 proteins per condition (Figure 17), 1681 proteins are in common and each condition expresses exclusive proteins, 114, 83, 121, 69 and 126 proteins identified exclusively for R2, R1, L, C1 and C2 respectively.

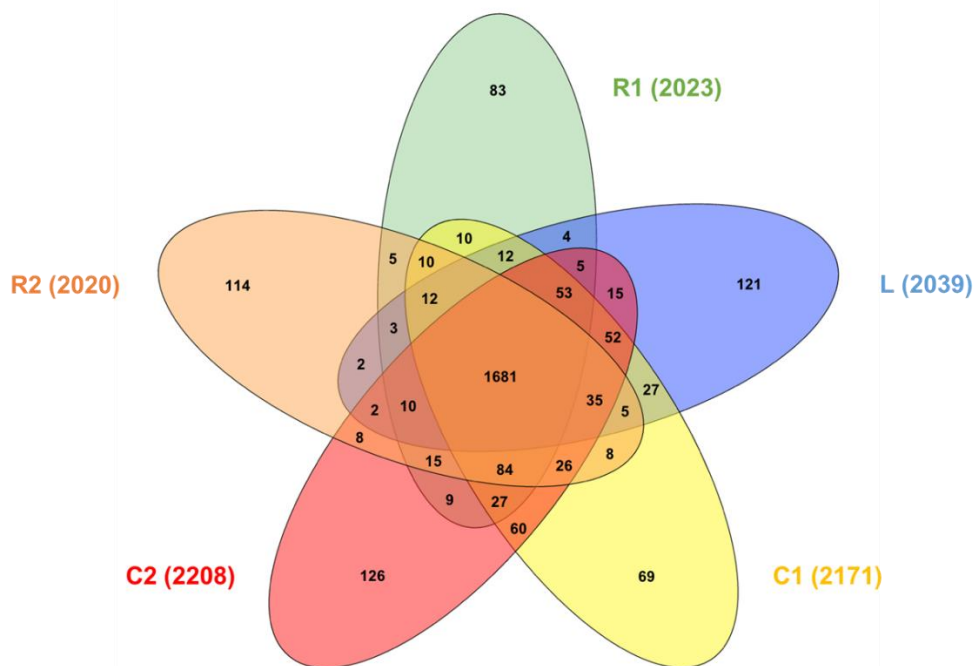


Figure 17: Comparison of proteins identified 24 hours after injury. Venn diagram shows the common and the exclusive proteins for these 5 conditions. 1681 proteins are in common and 114, 83, 121, 69 and 126 exclusives for R2, R1, L, C1 and C2 respectively.

Hierarchical clustering has shown that like in our previous spatio-temporal study, lesions segments are grouped together with a complete difference in protein expression compared to the other segments (Figure 18). With the focus set on the immunoglobulins expression in the conditioned media, we highlighted one cluster. In this cluster, different chains of Igs are identified i.e. heavy chains corresponding to gamma and mu chains and light chains corresponding to kappa and lambda chains. IgM containing mu chain corresponds to primo infection and they will quickly decrease and be replaced by another isotype. Their main roles are the antigen agglutination and the complement activation. IgGs containing gamma chain are the most common antibodies which activate the complement, and are able to go through blood vessels. IgG are mature immunoglobulins. All of these identified chains correspond to the constant part of the immunoglobulins. The main subclass found is related to IgG2. IgG2a is known to be superior to IgG1 in the complement activation. Moreover, it was found that the IgG2a isotype was able to interact very efficiently with Fc γ R. These immunoglobulins are over-expressed in the lesion segment and under-expressed in the R2 and C2 segments. The presence of IgGs one day after lesion is surprising. In fact, IgG2 isotypes need a second infection and more than 21 days after antigen presentation to be produced by the peripheral system. Thus, their presence at such an early stage after lesion remains questionable.

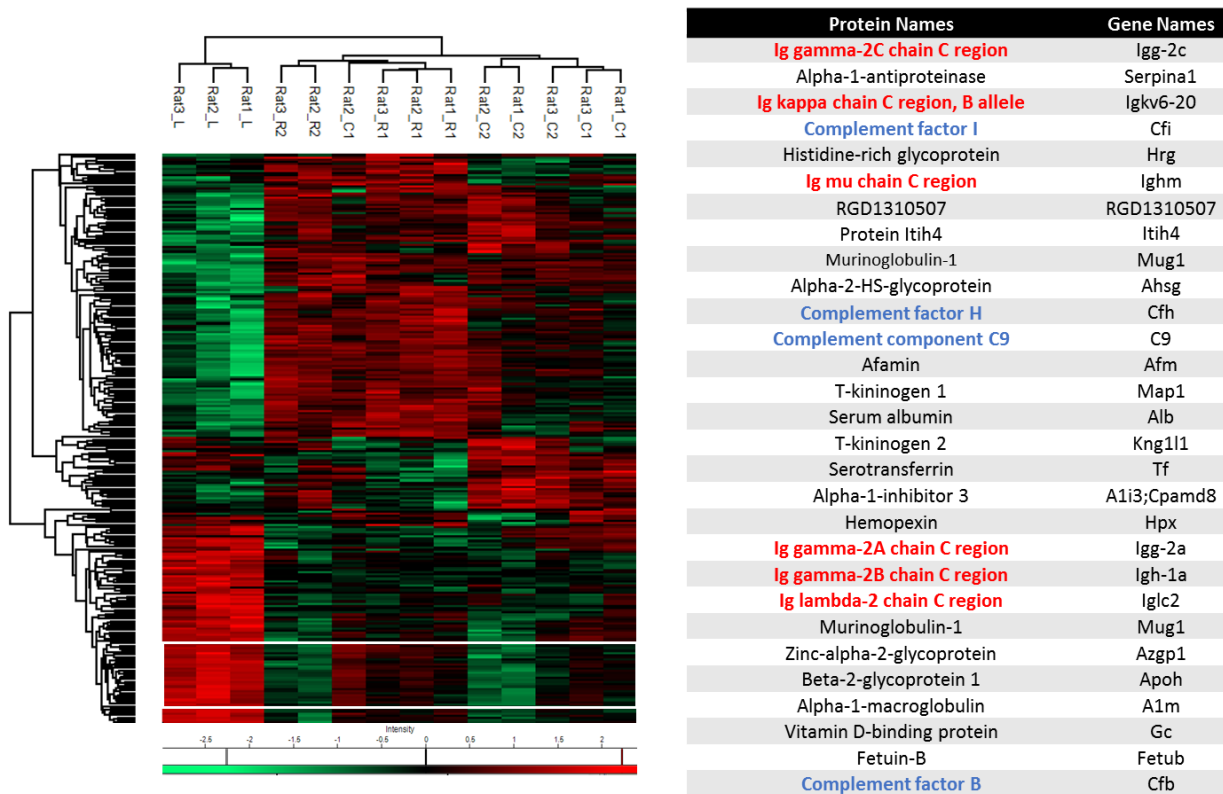


Figure 18: Heat map from the hierarchical clustering of conditioned media 24 hours after injury. Protein under-expression is colored in green and over-expression is in red. Table focus on the cluster shown in white in the heat map, in which Ig and complement factors are expressed.

- Who produce the immunoglobulins?
- Which are their targets?
- What is the effect of these immunoglobulins in the regeneration process?

In this way, thanks to our first results, we have shown the co-expression between IgG and neurons. The central nervous system is protected by the blood brain barrier, and it is considered to be an immune-privileged site where immunocytes and immunoglobulin are excluded from the CNS (Carson *et al.* 2006). It was well known that IgGs could be produced only by lymphocyte B; however, several studies report the presence of Ig in the CNS. In 1991, Chun *et al.*, showed a low level of RAG-1 genes into murine CNS (Chun *et al.* 1991). Further studies demonstrated the presence of Igs in the early generated neurons of rats and cats (Dunn, Kirsch, and Naegle 1995; Henschel and Wahle 1994) and in adult rabbit brain neurons (Yoshimi *et al.* 2002). It was then shown that mouse neurons produced immunoglobulin G at early stage and the adult stage (J. Huang *et al.* 2008). In 2011, Niu *et al.*, have shown that 82.3%

of cells expressing Ig kappa, gamma and lambda chains are neurons in human (Niu, Zhang, Guo, et al. 2011). Brain microglia, glial cells from the spinal cord and ganglia contain Ig gamma. They detect the expressions of RAG-1 and RAG-2 in the brain, the spinal cord and the spinal and sympathetic ganglia. RAG-1 and RAG-2 genes are involved in the V(D)J recombination (Chun *et al.* 1991). Fcγ receptors (FcγR) for IgG were found on the spinal cord (FcγRI (CD64), FcγRII (CD32) and FcγRIII (CD16)) with a variability in the expression on neurons and glial cells. The main role of FcγRIII expressed at the surface of microglia is the induction of chemokines and phagocytosis (Raghavan and Bjorkman 1996). FcγRI is expressed on primary sensory neurons and they are activated during the formation of IgG-antigen complex (Andoh and Kuraishi 2004). The complex formation increased the concentration of intracellular Ca²⁺ in DRG neurons and leads to the release of a neurotransmitter like substance P (Andoh and Kuraishi 2004). CNS resident macrophages express FcγRs, which allow for phagocytosis after the opsonized of invading pathogens by locally produced IgGs which bind to the receptor (Aloisi 2001). IgG production was shown in cortical rat neurons where the injury was mimiced by the presence of complement (J. Zhang, Niu, Li, *et al.* 2013). They demonstrated that the expression of FcγRI in microglia was increased in the presence of neuron-derived IgGs and the concentration of release NO was decreased. Zhang *et al.*, have shown that neuron-derived IgG protects the neurons after complement and microglia activation. The expression of neuron derived IgG has been demonstrated in dopaminergic neurons of human and rat mesencephalon (J. Zhang, Niu, Wang, *et al.* 2013). In the Parkinson's disease model, they showed that a neuron-derived IgG is able to improve the survival and reduce apoptosis of dopaminergic neurons (J. Zhang, Niu, Wang, *et al.* 2013). The neuroprotective phenotype of microglia was expressed by the release of TNFα and Il-10 due to neuron-derived IgG via the FcγRI and TLR4 pathway (J. Zhang, Niu, Wang, *et al.* 2013).

In this context, the communication between the nervous and the immune system is not only bi-directional. The immune system expresses the endocrine phenotype and the nervous system can express the immune phenotype by producing neuronal IgGs (Salzet 2002). Nevertheless, some questions still remain. In fact, we have to precise the main role of RAG genes in neurons, the existence or not of paratope re-arrangement in neurons and the nature of epitopes as well as their roles. These questions will be the main goal of our next studies without closing the door on finding a peripheral origin of such antibodies.

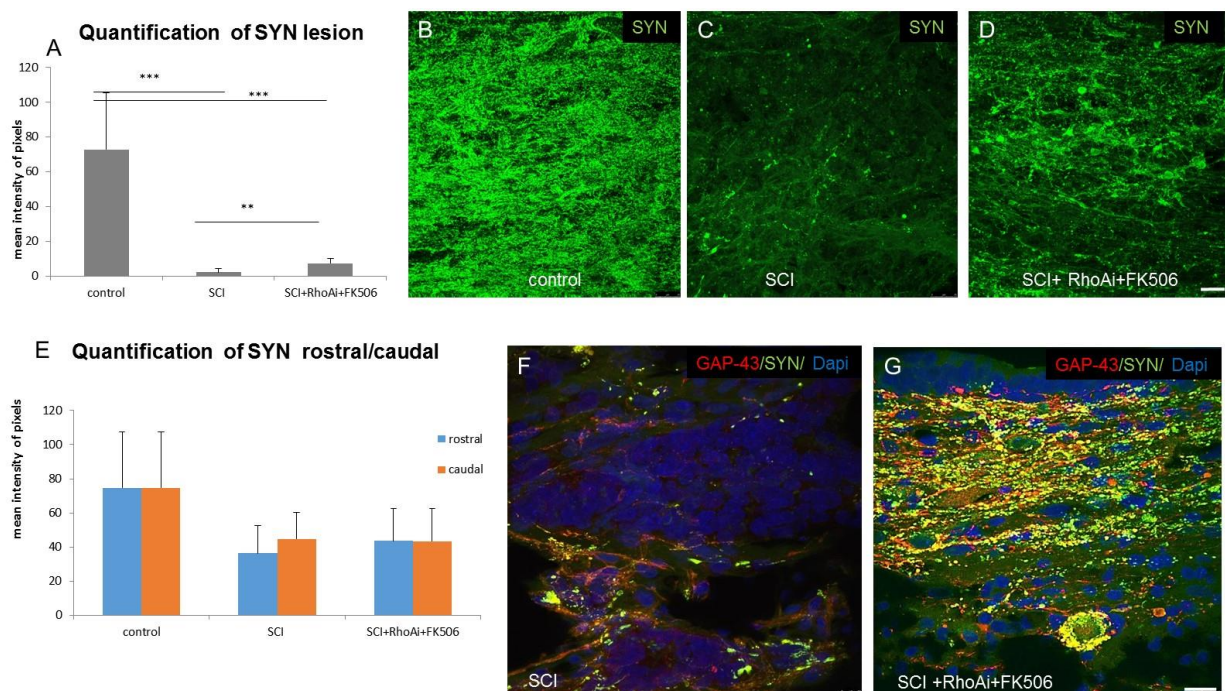
MEMO1-RHOA-DIAPH1 signaling pathway

Among the inhibitory factors implicated in spinal cord injury, the small intracellular GTPase, RhoA is one of the most important. In fact, previous experiments have showed that lysophosphatidic acid causes neurite retraction and cell rounding by activating RhoA (Tigyi *et al.* 1996). The use of C3 transferase to inactivate RhoA in primary neurons culture confirmed the role of RhoA in neurite outgrowth inhibition. Thus blockers of the post-receptors components of RhoA are now used to improve long-distance axon regeneration and sprouting (Martin E Schwab *et al.* 2002). Of note, RhoA pathway is important to control the neuronal response after CNS injury and the RhoA inhibitor cethrin is actually in phase I/II a clinical trial (Fehlings *et al.* 2011). The mechanism by the way that RhoA signaling inhibits neuritis growth has been investigated using p75 neurotrophin receptor– (p75^{NTR}) -null mutant mice (T. Yamashita, Higuchi, and Tohyama 2002). Data shown that RhoA binds to p75^{NTR} and RhoA forms part of the membrane raft receptor complex responsible for growth inhibitory signaling (Ellezam *et al.* 2002; Winton *et al.* 2002; Dergham *et al.* 2002). More recently, several studies have established that activation of RhoA and its downstream effector kinases triggers growth cone collapse and represents a significant barrier to axon regeneration (Forgione and Fehlings 2014). Furthermore, there is evidence that Rho-ROCK signaling mediates the inhibitory effects of chondroitin sulfate proteoglycans (CPSG) on neurons and sustained delivery of RhoA inhibitor and BDNF promote axon growth in CPSG region after SCI (Jain *et al.* 2011). Moreover, novel inhibitors, i.e. cholesterol and sphingomyelin as novel myelin-associated inhibitors, have also demonstrated to operate through a RhoA-dependent mechanism (Mar *et al.* 2016). Thus in order to better understand the mechanism by which RhoA inhibitor can be used for SCI treatment, *in vivo* and *in vitro* studies followed by proteomic approaches based on time course have been undertaken.

Investigate RhoA inhibitor *in vivo*

Based on our previous results in spatio-temporal study, we decided to perform *in vivo* studies using the RhoA inhibitor and an immunosuppressant, calcineurin inhibitor (FK506) in order to diminish the inflammation (Devaux *et al.* 2016). Moreover, these two factors have been used in the presence of functionalized alginate as we previously showed the beneficial impact on neuritis outgrowth (Grulova *et al.* 2015) (Figures 19A). In that context, the RhoAi + FK506

treated group showed significantly higher density of SYN+vesicles at lesion site (Figures 19A, 19D, 19G) in comparison to SCI, but no apparent differences between rostral and caudal segments were detected (Figure 19E). Quantification of GAP-43 immunoreactivity outlining regrowing axons within damaged dorsal and lateral white matter tracts did not show significant differences between treated and not treated RhoAi + FK506 groups (Figure 19H, 19I). Dense network of GAP-43 immunoreactive axons of different thickness oriented in various directions were present in both rostral and caudal segments as well as at the lesion epicenter (Figure 19H). Furthermore, the sections taken from control rats revealed no GAP-43 immunoreactivity, nor in the gray or white matter regions, confirming that GAP-43 positivity strictly corresponds with axonal outgrowth (Figure 19H a, b, 19I). BBB score studies showed that 7 days after treatment with RhoA inhibitor and FK506, the score reached from 1 to 5 whereas the non treated group took 25 days to get the same score level (Figure 19J). Nevertheless, after 7 days of treatment, the BBB score never increased and got a plateau whereas control SCI reached a slightly better one, e.g. around 6. These data clearly show that the beneficial effect of RhoA inhibitor is at the beginning of the treatment but it is not sufficient even in the presence of alginate and anti-inflammatory factors. Thus, in order to better understand the mechanism of RhoA inhibitor *in vivo*, we decided to develop an *in vitro* model to determine the target of this inhibitor in similar conditions than *in vivo* in both a spatially and timely manner.



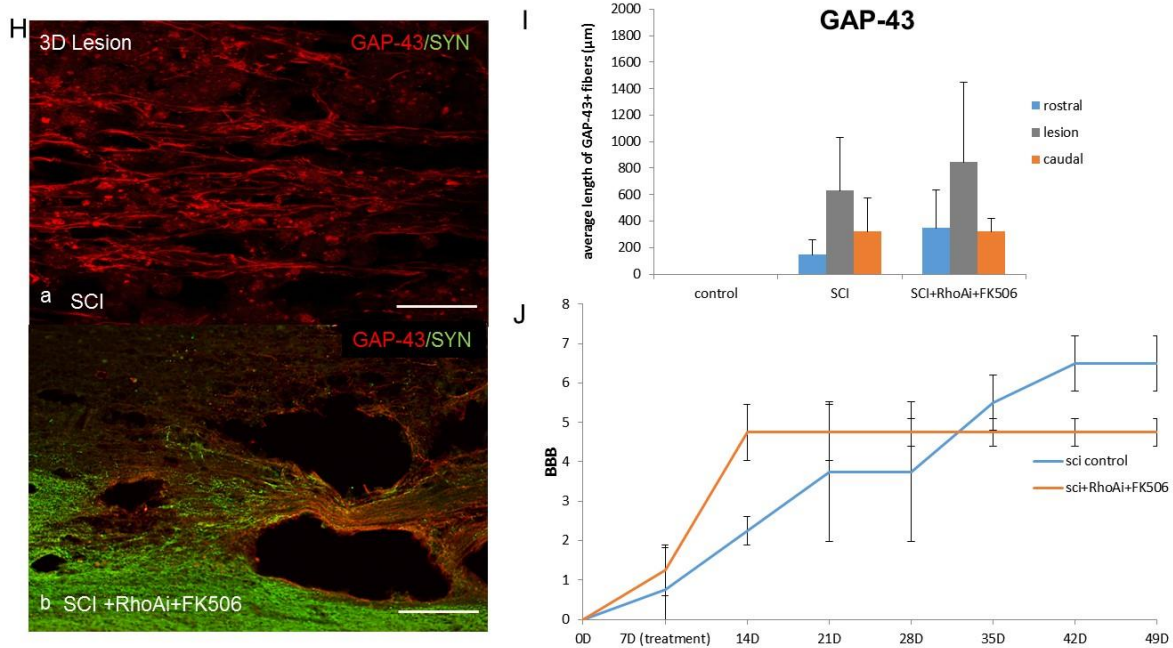


Figure 19: Quantification of synaptophysin (SYN) at the lesion site (A) and rostral-caudal segments (E) showed significant decrease of SYN after injury, while RhoAi + FK506 treatment increased SYN expression significantly at lesion, but not in rostral or caudal segments (E), *P<0.05, ** P<0.001, * P<0.0001 One-way ANOVA. Representative images of synaptophysin immunoreactivity (SYN, green) revealed intensely stained synaptic vesicles – punctate structures within the spinal cord- lesion site in control (B) and treated group (D), not in SCI (C). Confocal images with double labeling of GAP-43 (red) and SYN(green) antibodies, confirmed enhanced growth of axons with dense synaptic vesicles distribution after RhoA inhibitor + FK506 treatment (G). The *in vivo* experiments did not revealed significant differences between SCI and treated RhoAi+ FK506 groups in GAP-43 immunoreactivity (I), outlining growing axons within damaged dorsal and lateral white matter tracts (Ha, Hb). Note, high number of GAP-43 axons penetrating the lesion site. Scale bar =25µm. BBB score study of rat with injury (SCI) and after treatment with RhoAi + FK506 at 0, 7, 14, 21, 28, 35, 42 and 49 days post injury, reveals that with treatment BBB score reached to 5, 14 days after SCI whereas without treatment rats need around 30 days to get score at 5. However, the score does not increase after 14 days (J).**

***In vitro* investigation of RhoA inhibitor on secreted factors from ND7/23 DRGs cell line cultivated in presence of conditioned media from spinal cord injury segments**

In vitro, RhoA inhibitor was added to ND7/23 DRGs cell line cultivated with lesion (L), rostral (R1) and caudal (C1) conditioned media (CM) 3 days post injury to reproduce the injured environment (Figure 20). Combination of 1/3 CM with 2/3 DMEM supplemented media was added to the cells for 24 hours and then 1µg/mL of RhoA inhibitor was added or not in the media. Time course showed that ND7/23 cells in presence of R1, L or C1 conditioned media start to produce neurite outgrowth 24h after cultivation and the results are statistically significant at 48h (Figures 20A, 20B). These results established the ability to block the MEMO1-RHOA-DIAPH1 signaling pathway and stimulate neurogenesis using such RhoA inhibitor.

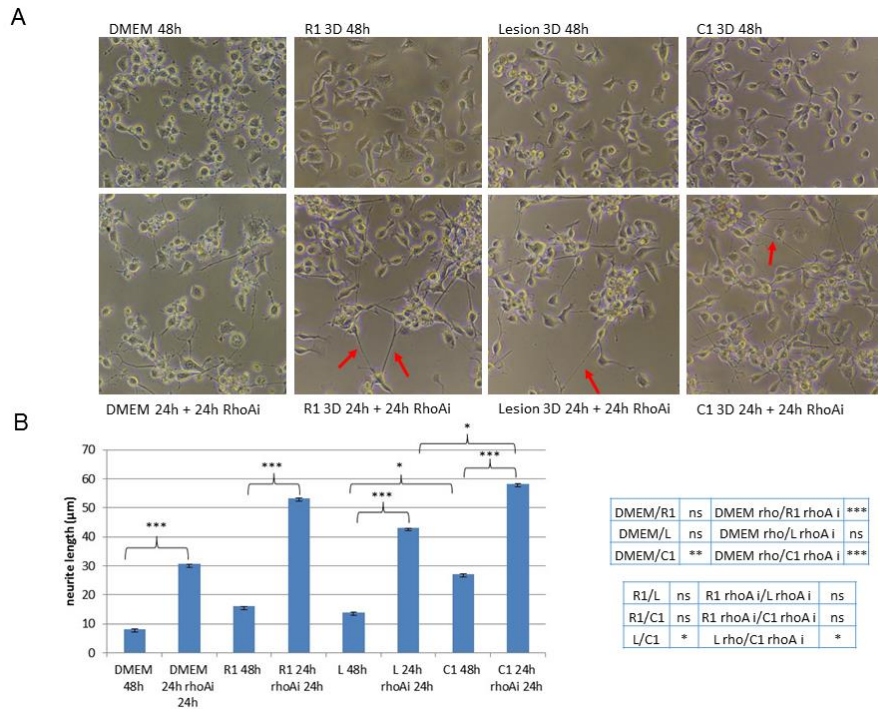


Figure 20: ND7/23 DRG cell line cultured for 24 hours in 1/3 of SCI-CM rostral (R1), lesion (L) or caudal (C1) or DMEM as control, then an addition or not of RhoA inhibitor was applied for 24 hours (A). Quantification of neurite outgrowth by ImageJ demonstrates the effect of RoAi on neurite outgrowth (B) (One Way ANOVA followed by Tukey-Kramer test * $p < 0.05$, ** $p < 0.01$, *** $p < 0.001$, ns= non-significant). Arrows indicate the neurite outgrowth

Shot gun proteomic of secreted factors from ND7/23 DRGs cell line cultivated in presence of conditioned media from spinal cord injury segments

Proteomic approach was then performed with ND7/23 DRGs cell line cultivated with lesion, R1 and C1 conditioned media 3 days post injury in the presence of no RhoA inhibitor (Figure 21). Secretomes collected in each condition have been subjected to shot gun analyses. Proteins with an abundance that was significantly different among the samples were determined according to the MaxQuant and Perseus software. As a criterion of significance, we applied an ANOVA significance threshold of $p\text{-value} < 0.05$, and heat maps were generated (Figure 21). Heat maps were performed and hierarchical clustering indicated two main branches, i.e. one for control (cells in DMEM conditions with or without RhoA inhibitor). The second one is related to the conditioned media (L, R1, or C1) with or without RhoA inhibitor. This branch is then sub-divided between lesion one side from the R1 or C1 in the other side (Figure 21a). From these data clear clusters can be retrieved between the two branches. By contrast, in the second branch, only one main cluster allows to differentiate all conditioned media in the presence or

not of RhoA inhibitor. A zoom of this cluster is presented in Figure 21b and the ibaq quantitative values in Table 4. Main proteins found in this cluster are immunoglobulins (IgG chains light and heavy), AKT proteins (AKT1, AKT2, AKT3), BMP1, syntaxin 12, serpin 3, GMP ganglioside activator, meosin, hemopexin, protein VSP26b, 14-3-3 protein theta, protein disulfide isomerase. The ibaq value showed that most of these proteins are under-expressed in DMEM with a slightly higher expression in some cases in presence of RhoA inhibitor like immunoglobulins, AKT3 or BMP1 except Cthrc1, STX6, VSP26b and 14-3-3 theta protein (Table 4).

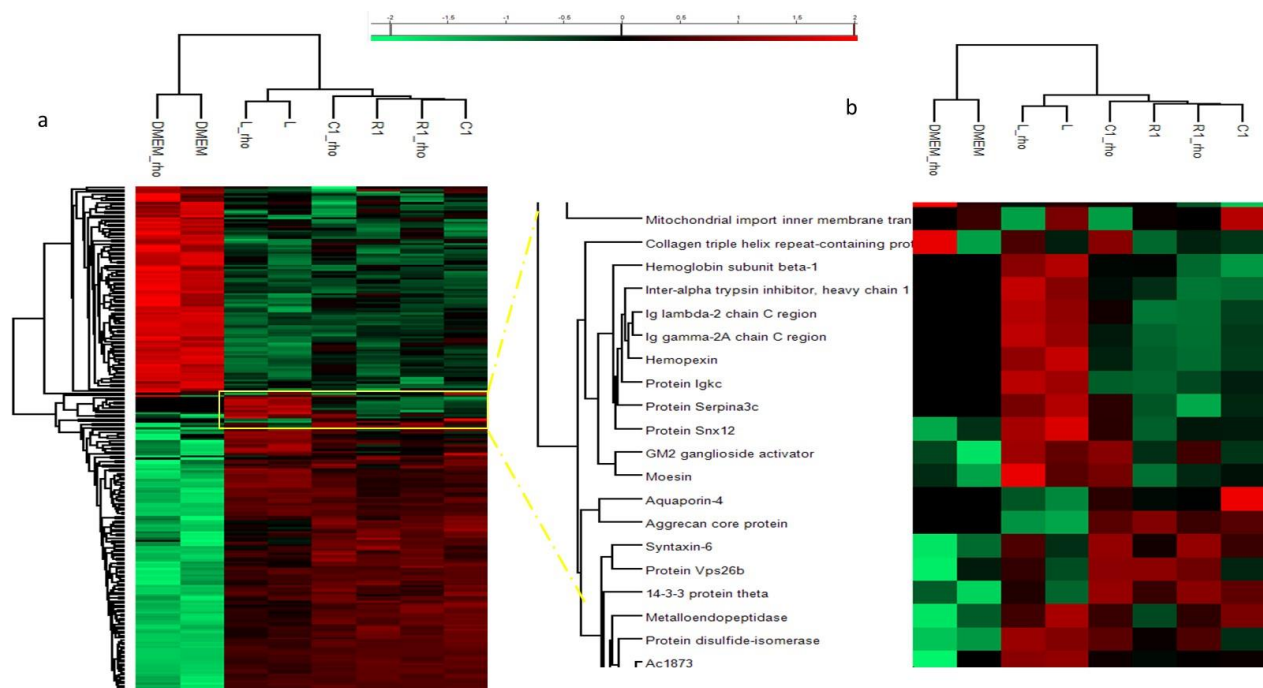


Figure 21: Heat map of proteins from the secretome after different stimulation of ND7/23 DRG cell line. Control (DMEM) or lesion (L), rostral (R1) or caudal (C1) conditioned media from spinal cord 3 days after injury were used to stimulate the cells with or without stimulation of RhoA inhibitor 24 hours after CM stimulation (a). Zoom of the cluster showing a difference between SCI-CM media stimulation with lesion CM and proteins name expressed in this cluster (b).

	DMEM	DMEM_rho	R1	R1_rho	L	L_rho	C1	C1_rho
Ig kappa chain C region, B allele	18.6964	NaN	25.3768	25.2277	26.9871	27.4438	25.6016	25.5407
Ig lambda-2 chain C region	17.9321	16.4463	22.2698	21.8589	23.3483	23.8509	22.0366	22.0278
Ig gamma-1 chain C region	NaN	NaN	22.0093	20.4461	24.4393	22.8095	22.7104	20.9456
Ig gamma-2A chain C region	18.624	17.4331	25.1896	25.1779	27.0487	27.2894	26.02	25.4072
Ig gamma-2B chain C region	15.5964	20.2113	25.1799	24.731	26.7321	27.3434	26.0332	26.1656
Ig gamma-2C chain C region	19.0482	NaN	19.6379	19.3413	21.8845	21.4192	22.532	19.9571
Hemopexin	17.5556	17.6568	24.9554	24.9718	26.501	26.3767	25.2757	25.2145
Akt3	19.3788	18.713	20.2253	18.4289	19.2018	20.113	20.4927	19.8739
Akt1;Akt2	15.0586	17.7401	19.6831	20.2621	20.3283	19.1436	16.7678	NaN
Serpina3c	NaN	NaN	21.9487	21.0965	24.1171	23.3147	22.4255	22.6554
Snx12	22.6267	22.4524	22.975	23.0775	22.4477	23.2473	23.3919	23.7252
Gm2a	21.9105	22.9234	23.095	23.8827	23.9187	24.4643	24.738	24.6447
Moesin	26.5945	26.648	25.8551	26.4947	26.2415	26.9661	26.9044	27.2905
Timm44	19.3845	19.6954	18.1395	16.9738	18.5047	17.9652	18.7997	18.2434
Cthrc1	22.9094	24.5055	22.9746	24.0133	23.7669	23.8026	24.2895	24.6324
Hemoglobin subunit beta-1	21.1296	21.3739	25.3049	25.0801	28.489	28.4313	25.1673	26.6007
Itih1	16.9337	17.7239	19.2479	19.0848	22.3506	21.45	19.9322	19.455
Aqp4	NaN	NaN	24.4126	24.7302	23.8243	23.8015	25.5617	25.3911
Aggrecan core protein	17.4545	NaN	20.3905	20.1099	19.2471	17.804	20.9868	19.9415
Stx6	20.5775	21.3753	21.2685	20.7684	20.4223	21.9301	21.3914	22.1322
Vps26b	20.8545	21.2238	22.5601	21.4776	20.7158	21.0633	21.4782	21.5435
14-3-3 protein theta	27.1402	27.5267	27.8992	27.8027	27.0406	27.6516	27.938	28.2779
Metalloendopeptidase, BMP1	19.3751	18.9169	19.4476	19.8589	21.1409	19.5239	19.8614	20.4628
Protein disulfide-isomerase	23.9259	23.5827	24.2834	24.6904	24.2698	25.1837	24.5249	24.6569

Table 4: Ibaq value of the selected cluster reflecting the more divergent quantitative value of between treatment and conditioned medium from R1, lesion or C1 3 days after SCI.

RhoA inhibitor modulates IgGs levels in ND7/23 DRGs cells line

We confirmed, by western blot based on time course experiments and along the spinal cord segments after SCI, the presence of IgGs related to IgG1 and 2 family (Figure 22a, b) and confirmed by mass spectrometry. Antibodies heavy (Figure 22a) and light (Figure 22b) chains have been detected in tissue extract from rostral, lesion and caudal segments 3, 7 and 10 days post SCI. However, the highest significant statistically amount detected is in lesion 3 days after SCI. This amount decreases at 7 days and increases at 10 days (Figure 22a, b). The lowest amount is in R1 whatever the time considered after SCI (Figure 22a, b).

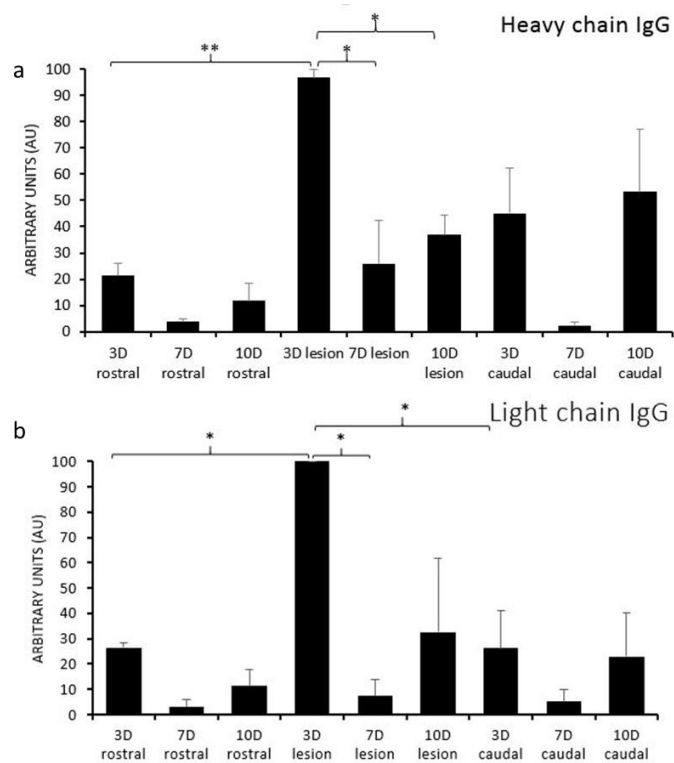


Figure 22: Immunoglobulins in spinal cord injury tissue from rostral, lesion and caudal segments after 3, 7 and 10 days post injury. Expression of heavy chain of IgG (a) and light chain expression (b) were assessed by western blot. Higher expression of IgGs heavy or light chain was observed at 3 days post SCI in the lesion site.

For C1, the amount is higher than in R1 but nosignificant differences are registered in time course. Shot gun studies in the presence of RhoA inhibitor performed on the secreted factors confirmed the presence of IgGs (Figure 21). Studies showed that after R1 and C1 stimulation, globally the level of these antibodies diminished except in lesions where the ibaqa value registered is either constant or slightly higher in the presence of RhoA inhibitor (Table 4). These results can be paralleled with neurite outgrowth tests. In fact, in lesion compared to R1 or C1, in presence of RhoA inhibitor, the neurite outgrowth is less important. These results tend to demonstrate that RhoA inhibitor impact the IgGs level by either diminishing their production by DRG cells or by a neuronal internalization (Congdon *et al.* 2013) by binding to their own receptors that could be present in DRG cells (CD16/CD32, CD64) as recently suggested (Qu *et al.* 2011). This part of the work will be further completed.

Global proteomic analyses of RhoA inhibitor treated ND7/23 DRGs cell line

From table 4 real differences are registered in AKT protein family. With RhoA inhibitor the level of AKT3 is diminished compared to the one registered without treatment. For AKT1 and AKT2, RhoA inhibitor increased the level in R1 and diminished in lesion and C1. Serpina3c, Snx12, Gm2a, moesin, Timm44, Cthrc1, Stx6, vsp26b, Itih1, Aqp4, aggrecan core protein, BMP1 are over-expressed in C1 compared to R1 or lesion with or without treatment. In R1 with RhoA inhibitor only AK1, AKT2 are over-expressed, by contrast Timm44, STX6, Cthrc1, AKT3, STX6 are under-expressed. In lesion, most of proteins present in this cluster are under-expressed or have the same level with RhoA inhibitor treatment except Gm2a, hemopexin, Protein disulfide-isomerase, Stx6 which are over-expressed. Proteomic analysis of secretome from cells after treatment without SCI-CM, means control with DMEM stimulation treated or not with RhoAi, and with SCI-CM treated with RhoAi (RhoAi) or non-treated (NT) have shown common but also exclusive from each condition (Figure 23a).

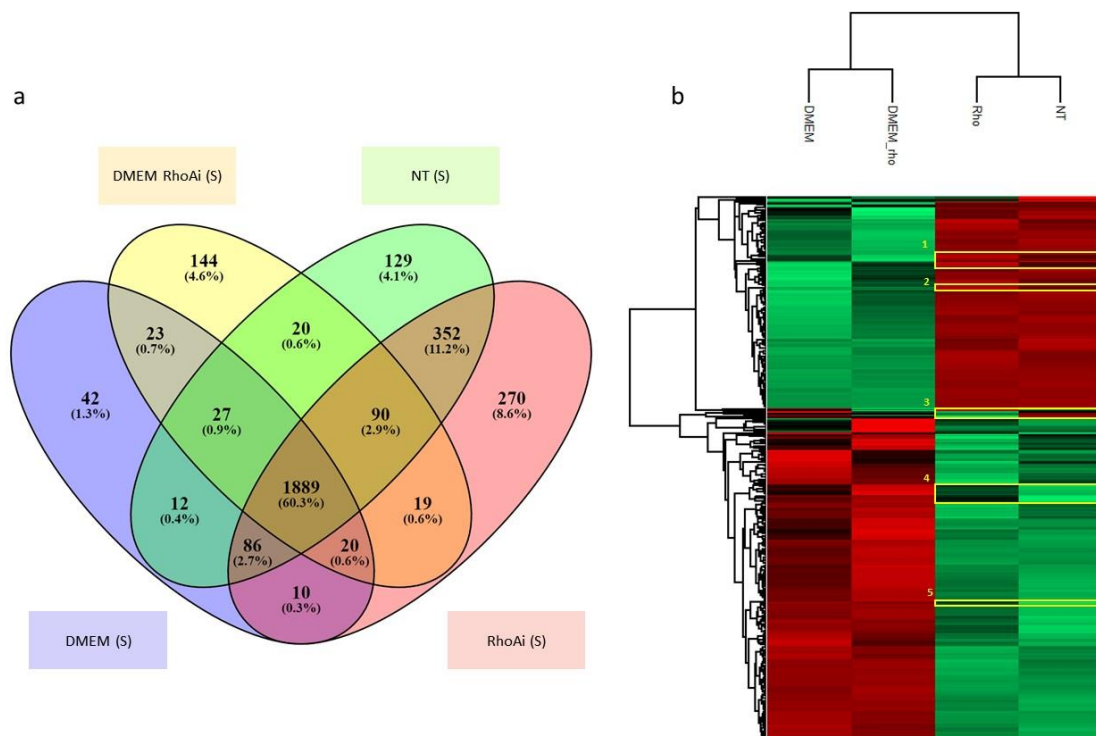


Figure 23: Heat map of proteins secreted by ND7/23 cell line after stimulation with or without RhoAi. Control is cell in DMEM with or without RhoAi, cells stimulated with conditioned media from SCI and RhoAi is named Rho and without RhoAi is called (NT). Venn diagram with the total proteins identified show the presence of exclusive and common proteins for each conditions (a). Heat map of secreted proteins from control versus SCI-CM stimulation with or without RoAi treatment (Rho vs NT) have shown distinct clusters.

A global analysis between control (DMEM treatment) and treated (Rho) or non treated (NT) cells after SCI-CM (R1, L and C1) confirmed that secretome controls are separated from the secretome of cells cultivated with conditioned media (Figure 23b). The second separation confirmed the separation between treated or not with RhoA inhibitor. Five clusters have been identified and again cluster comparisons revealed more proteins under-expressed or absent with RhoA inhibitor treatment (Figure 23b). 16 secreted proteins from ND7/23 DRGs cell line are over-expressed after RhoA inhibitor treatment and 23 are under-expressed (Table 5). Among the 16 over-expressed proteins, some are already known to be implicated in neurite outgrowth or neurogenesis e.g. Pde6d (Tweedie *et al.* 2016), Clip2 (Ota *et al.* 2013), Enah (Doss *et al.* 2012), Vps26b (Chan *et al.* 2015).

Gene name	Protein name	DMEM	DMEM RhoAi	NT	RhoAi
Ctlb	Clathrin light chain B	22,9108	20,9079	24,6101	24,5589
Psmid9	26S proteasome non-ATPase regulatory subunit 9	22,0575	22,5024	23,731	23,3539
Ltbp4	Protein Ltbp4	20,7261	21,3022	21,4152	21,2313
Vegfa	Vascular endothelial growth factor A	22,2847	21,7441	22,6636	22,6461
Ctsz	Cathepsin Z	22,2676	22,4209	23,5532	23,7262
Pde6d	Phosphodiesterase 6D, cGMP-specific, rod, delta	22,9597	22,3894	23,2059	23,9704
Stx6	Syntaxin-6	20,5775	21,3753	21,159	21,6134
Clip2	CAP-Gly domain-containing linker protein 2	18,8133	19,9872	20,7688	20,9273
Ywhaq	14-3-3 protein theta	27,1402	27,5267	27,636	27,8027
Gga1	Golgi associated, gamma adaptin ear containing, ARF binding	21,1791	21,474	21,5419	21,8458
Gm2a	GM2 ganglioside activator	21,9105	22,9234	23,9187	24,059
Clu	Clusterin	21,5919	21,6096	24,059	24,173
Fkbp2	Peptidyl-prolyl cis-trans isomerase	24,2425	25,0884	25,3438	25,2155
Pdxk	Pyridoxal kinase	21,3779	23,0917	23,8266	24,1404
Enah	Protein Enah	21,4766	22,2339	21,0658	22,1981
Vps26b	Protein Vps26b	20,8545	21,2238	21,3013	21,4243
Phax	Phosphorylated adapter RNA export protein	20,6057	21,5545	20,0058	19,9327
	UPF0587 protein C1orf123 homolog	19,8283	21,1305	23,2625	22,6816
Ddt	D-dopachrome decarboxylase	16,4287	NaN	23,5922	22,1647
Minpp1	Multiple inositol polyphosphate phosphatase 1	20,7669	21,2727	20,8248	20,6688
Sar1b	GTP-binding protein SAR1b	21,694	21,3152	22,3763	21,0747
Timm44	Mitochondrial import inner membrane translocase subunit	19,3845	19,6954	18,3148	17,6879
Mvd	Diphosphomevalonate decarboxylase	21,7602	22,097	21,6105	20,9859
Ranbp3	Protein Ranbp3	21,6703	21,842	20,7514	20,5318
Ipo4	Importin 4	21,2689	22,5999	20,5059	21,1659
Gtpbp4	Nucleolar GTP-binding protein 1	20,5677	21,7242	19,3613	19,1347
Fnta	Farnesyltransferase, CAAX box, alpha	20,1966	21,4274	19,902	19,6791
Cul2	Protein Cul2	22,5187	22,6432	21,8199	21,1874
Nae1	NEDD8-activating enzyme E1 regulatory subunit	21,1429	22,6173	21,6993	21,0846
Eif1a	Eukaryotic translation initiation factor 1A	24,6291	24,4566	23,3243	23,0823
Aimp2	Aminoacyl tRNA synthase complex-interacting multifunctional	24,6959	24,8529	24,2577	24,0347
Cstf2	Protein Cstf2	19,0881	19,8525	17,8731	18,7524
Mybbp1a	Myb-binding protein 1A	20,4748	20,2285	20,4614	19,8938
Psmid1	26S proteasome non-ATPase regulatory subunit 1	24,2726	24,1721	23,5677	23,3707
Sf3a2	Splicing factor 3A subunit 2	24,508	24,8563	22,9886	22,9425
Tomm70a	Mitochondrial import receptor subunit TOM70	21,4271	22,0365	20,8489	19,3298
Pcna	Proliferating cell nuclear antigen	25,5532	26,1335	24,8067	25,222
Arpc3	Actin-related protein 2/3 complex subunit 3	24,4744	24,7873	24,3182	24,6005
Ago2	Protein argonaute-2	19,1549	20,7609	18,8243	18,982
Lmnb1	Lamin-B1	25,0612	25,1812	24,723	24,7027
Rps16	40S ribosomal protein S16	27,2324	27,7085	26,8235	26,6169
Khdrbs1	KH domain-containing, RNA-binding, signal transduction	25,7151	25,6983	25,0325	25,056
Bclaf1	BCL2-associated transcription factor 1, isoform CRA_a	24,1191	24,2525	22,9701	23,1659
Rps19l1	Protein Rps19l1	27,747	27,8637	26,4202	26,8181
Snrpd3	Protein Snrpd3	25,7155	26,0016	25,3816	26,0275
Slc39a10	Protein Slc39a10	20,4879	21,6648	19,3242	19,6973
Tcerg1	Protein Tcerg1	22,7216	22,8235	22,1174	22,4468
Sf3a3	Protein Sf3a3	24,4827	24,3498	23,7063	23,5636

Table 5: Ibaq values of the selected cluster reflecting the overexpressed and underexpressed proteins in conditioned media treated or not with RhoA inhibitor. NT regroups all non-treated cells and RhoAi are all treated cells with RhoA inhibitor in presence of SCI-CM.

Secretion of such factors have to be associated with the transcription factors involved after RhoA inhibitor treatment from DRG cells proteins extract (PE). Proteomic data of the cellular proteins extract revealed the presence of 179 modulated proteins between non treated and treated cells (Figure 24).

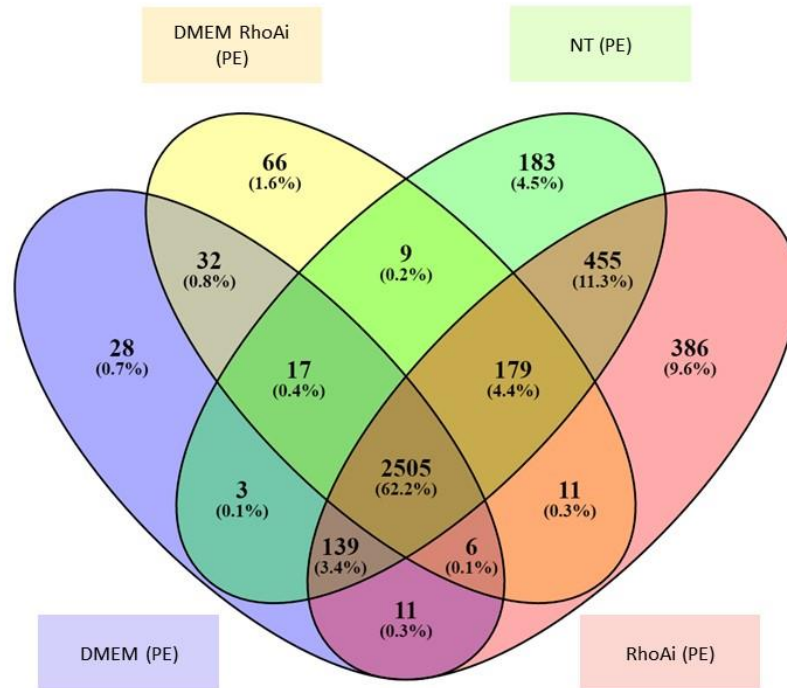


Figure 24: Venn diagram of proteins identified from the cellular protein extract (PE) of ND7/23 cell line. Comparison of control (DMEM) with or without RhoAi and protein extract from cells treated with SCI-CM with (RhoAi) or not treated (NT).

The Ibaq value confirmed the over-expression of Tp53, Stat2, Stat3, Proteins of the Smad family (smad1, smad2, smad3, smad4 and smad5), Smarcc1 and smarcc2, Akt3, rpap3, b-raf and pten (Table 6). The string protein analysis confirms that all these proteins are in the same network (Figure 25). In fact, numerous factors could regulate the intrinsic growth capacity, including certain transcription factors (TF).

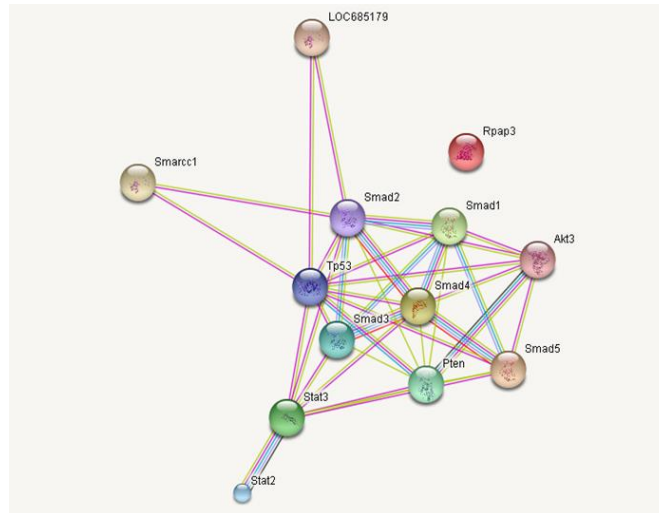


Figure 25: Evidence for protein-protein interaction network of the enriched transcription factors constructed by STRING.

cAMP-responsive element binding protein (CREB), signal transducer and activator of transcription 3 (STAT3), nuclear factor of activated T cell (NFAT), c-Jun activating transcription factor 3 (AFT3), Krüppel-like factors (KLFs), and intracellular signaling proteins, such as PI3 kinase, Akt, phosphatase and tensin homolog (PTEN), suppressor of cytokine signaling 3 (SOCS3), B-RAF, dual leucine zipper kinase (DLK), and insulin/insulin-like growth factor-1 (IGF-1) signaling (Byrne *et al.*, 2014; Lu *et al.*, 2014) are known to be involved in growth capacity.

	DMEM	DMEM RhoA i	NT	RhoA i
Tp53	23.5765	23.6175	23.6662	25.2294
Stat3	18.6756	19.4725	21.8684	21.91
Stat2	17.8025	19.0435	21.0399	21.1396
Smad5;Smad1	17.725	19.2049	17.8188	18.9579
Smad2;Smad3	20.3157	23.2613	21.0561	24.0844
Smad4	17.2251	19.8908	20.3623	17.6374
Smarcc1	21.8454	23.0071	22.0338	22.8988
Smarcc2	19.6602	22.573	17.6423	21.0827
Akt3	14.9283	19.0033	16.8991	22.1317
Rpap3	20.6973	21.7109	20.5903	21.082
B-raf	NaN	NaN	20.6447	20.8239
Pten	18.4462	15.7211	19.5392	20.9376

Table 6: Ibaq values of transcription factors present in protein extract between treated and not treated cells in presence of not the SCI-CM.

Parts of these TF are detected here. Nevertheless, one most intriguing is the presence of PTEN. In fact, it is known that deletion of the tumor suppressor PTEN in conditional knockout (KO) mice appears to result in most dramatic regrowth of CNS axons after injuries (Kevin Kyungsuk Park *et al.* 2008; K. Liu *et al.* 2010), suggesting that PTEN/mammalian target of rapamycin (mTOR) signaling is critical to regulate the intrinsic regenerative ability of young and adult neurons (Kevin K. Park *et al.* 2010). However, other positive factors are over-expressed. Smad proteins family is one of the key players in the regeneration process. Smad1 is known to integrate signals from BMP receptors. Together with Smad4, phosphorylated Smad1 assembles a multi-subunits complex that regulates transcription (Zou *et al.* 2009). In the absence of Smad1, conditioned DRG neurons show impairment in axon elongation *in vitro* (Parikh *et al.* 2011). Blockade of BMP signaling with the BMP antagonist Noggin inhibits axonal growth in both naive and preconditioned DRG neurons (Ma *et al.* 2011). The second player is the tumor suppressor p53. Previous studies have shown that after SCI, transcriptionally active p53 undergoes a series of acetylation events on its C-terminal domain (Di Giovanni *et al.* 2006; A Tedeschi *et al.* 2009; Andrea Tedeschi *et al.* 2009). After injury, active gene transcription is necessary to synthesize new proteins needed for axon growth. Acetylated-p53, together with CBP/p300 and PCAF, selectively occupies regulatory regions upstream to the TSS of pro-neurite and axon-outgrowth genes such as Coronin 1b, Rab13, and GAP-43 during an early regenerative response (P Gaub *et al.* 2010; Perrine Gaub *et al.* 2011; Floriddia, Nguyen, and Di Giovanni 2011). Acetylated-p53 may have a critical role in modulating different transcriptional responses during axonal regeneration (Perrine Gaub *et al.* 2011). For STATs proteins, it is known that in the absence of STAT3, peripheral nerve regeneration is impaired in DRG neurons (Bareyre *et al.* 2011). Interestingly, sustained STAT3 expression promotes terminal and collateral sprouting by controlling initiation of axon growth after dorsal columns injury (Bareyre *et al.* 2011). B-raf is known to be a regulator of RhoA (Klein and Higgins 2011). MAG inhibition is also a positive signal for neurite outgrowth (McKerracher *et al.* 1994). Interestingly is the presence of SWI/SNF complex subunit SMARCC1 and SMARCC2 proteins. These two proteins belong to the neural progenitors-specific chromatin remodeling complex (npBAF complex) and the neuron-specific chromatin remodeling complex (nBAF complex) (Staahl and Crabtree 2013). The npBAF complex is essential for the self-renewal/proliferative capacity of the multipotent neural stem cells. The nBAF complex along

with CREST plays a role regulating the activity of genes essential for dendrite growth (*Wu et al.* 2007). These two proteins are over-expressed after RhoA inhibition treatment.

Taken together, our results suggest a balance between positive and negative signals in TF after RhoA inhibition treatment in DRG cell line. This balance is positive due to a cascade of factors including smad family proteins, SMARCC1&2, P53, STAT3 and secretion of Bmp1 factors. The production of IgG2 isotypes is still in debate and needs further studies. Our next steps will be the time course study of TF expression and neosynthesize proteome after RhoA inhibitor treatment in order to establish which factor activates the other one and the impact in the intracellular trafficking and signaling after RhoA inhibitor treatment. Such informations will allow us to determine when other factors need to be added in order to modify the neuritis media for stimulating reconnection.

For that purpose, we engage the studies about the characterization of bone marrow stromal cell factors in order to evaluate the benefit of the secretome of such cells to counterbalance the medium at the lesion and caudal site in time course after SCI. These studies constitute the part 2 of my thesis.

PART 2: MODULATION OF THE INFLAMMATION AND IMPROVEMENT OF THE REGENERATION PROCESS AND SPINAL CORD PLASTICITY: *IN VITRO* AND *IN VIVO* STUDIES

CHAPTER 2: Properties of factors released by bone marrow stromal cells to modulate microglia cells

Currently, there is no effective treatment for spinal cord injury that can reduce and allow for the modulation of the inflammation and the regeneration. Among all the elements studied for the modulation of the inflammation, stem cells secretome may help in this cause in conjunction with Rho A inhibitor treatment.

Mesenchymal stromal cells (MSCs) are non-hematopoietic cells with multipotent abilities and self-renewable cells. MSCs are known for their immunomodulatory properties. MSCs are also able to modulate the CNS injured environment, to promote repair as they secrete anti-inflammatory and trophic factors which are able to support axonal growth, immunomodulation and to promote angiogenesis and remyelination. Since MSCs have the capacity to differentiate into different types of cells, the first studies worked to engraft the cells into the injured tissue. Despite the fact that *in vivo* studies in which MSCs were injected following SCI have yielded controversial results, overall the results have been rather positive (Ritfeld, Roos, and Oudega 2011; Ritfeld *et al.* 2012). Transplantation of bone marrow derived stromal cells (BMSCs) from rats into the SCI rat model has shown slight improvements in neural regeneration with significant restoration of motor function and attenuation of inflammatory response (Abrams *et al.* 2009; Gu *et al.* 2010; Boido *et al.* 2014). However, engraftment of cells is a rare event, which is difficult to correlate with a possible improvement. Transplantation as a therapeutic approach is limited due to the environment present around the injury site (glial scar, inflammation, inhibitory molecules) rendering the engraftment of the cells, their differentiation and their survival difficult (Mothe *et al.* 2013). Nakano *et al.*, characterized the conditioned media of cultured bone marrow stromal cells by antibody-based protein array analysis and ELISA. They demonstrated the presence of trophic factors such as insulin-like growth factor, hepatocyte growth factor, vascular endothelial growth factors and transforming growth factor- β (Nakano *et al.* 2010). They showed their role in the neuronal

survival and outgrowth *in vitro*. Macrophages / microglia are a key component of the innate immunity. Their role in the primary phase is the defense of the injured tissue to remove the cellular debris (Ransohoff and Perry 2009). Regarding the microenvironment, macrophages are able to change their phenotype in order to adapt specific functional activities relevant to the level of the inflammation. Two main classes of macrophages have been described as pro-inflammatory and anti-inflammatory phenotypes respectively, M1 and M2. M1 macrophages are induced by TLR ligands and IFN γ , and they express a higher level of CD86 and produce several pro-inflammatory molecules such as iNOS, IL-6, TNF α . In contrast, M2 macrophages are induced by cytokines like IL-4 or IL-13 and they express CD206 and arginase I and produce IL-10 and TGF β (Kigerl *et al.* 2009).

In this context, we have taken advantage of the strength of the mass spectrometry analysis to determine factors released by BMSCs without a priori. We first performed a proteomic study of their released molecules to identify factors that can modulate inflammation and allow the switch microglia / macrophages from M1 to M2 phenotype.

We compared conditioned media from either naive or injured rat spinal cord tissue, considered as an agent stimulating inflammation (SC-CM, SCI-CM), with rat bone marrow stromal cells (BMSCs-CM, therapeutic immunomodulation agent). BMSCs produced **growth factors** such as connective tissue growth factor (CTGF), placenta growth factor (PGF), platelet derived growth factor (PDGF), insulin-like growth factor binding protein 7, transforming growth factors beta-1, 2 and 3 (TGF β -1 2 and 3), or **osteogenic factors** like osteopontin, periostin, spondin 2, as well as **differentiating factors** like SPARC, FAM3C, cornifin, or neural migration factors (NOV, neurofascin, neuropilin2, neuroplastin) and immunomodulators such as arginase1, ST2, galectins and metalloproteinase inhibitors. The comparison has shown that SCI-CM produce chemokines (CCL3, CXCL2 and MIF) and neurotrophic factors (GAP-43 and neurotrophin) whereas BMSC-CM contain factors involved in microglia chemoattraction (CCL2) and factors involved in inflammatory regulation (arginase 1, ST2 and galectins). We have shown *in vitro* the attenuation of microglia recruitment of BV2 cell line and primary microglia using Boyden chambers. The combination of BMSC-CM with SCI-CM prevents the recruitment of microglia cells which confirms the involvement of BMSC-CM in the modulation of the immune response after the activation of microglia cells. In order to define the immunomodulatory effect of BMSC-CM, we investigated the morphological changes and the

viability of the microglia. In presence of SCI-CM, microglia cells present a prolonged bipolar or stellar-like shape from 3 hours to 24 hours whereas in the presence of BMSC-CM alone or with SCI-CM lower number of microglia are stimulated and present round to oval or multipolar shape. The production of NO inflammatory mediators decreased in treated primary microglia in the presence of BMSC-CM. Taken together, our proteomics data have shown high modulatory potential of BMSC-CM on inflammation, microglia polarization and neurite outgrowth, which could be used as a cocktail to prevent inflammation after SCI.

Article 3: Modulation properties of factors released by bone marrow stromal cells on activated microglia: an in vitro study

Authors: Stéphanie Devaux*, Dasa Cizkova*, Françoise Le Marrec-Croq, Julien Franck, Lucia Slovinska, Juraj Blasko, Jan Rosocha, Timea Spakova, Christophe Lefebvre, Isabelle Fournier, Michel Salzet

Article Status: published in Scientific Reports 2014 Dec 19; 4: 7514

Summary: Proteomic experiments and procedures were realized by Ms Devaux. She performed BMSC and primary isolation and immunocytochemistry. She participated in the writing of the manuscript and in the revision.



OPEN

SUBJECT AREAS:

SPINAL CORD INJURY
MESENCHYMAL STEM CELLSReceived
19 June 2014Accepted
24 November 2014Published
19 December 2014Correspondence and
requests for materials
should be addressed to
M.S. (Michel.salzet@
univ-lille1.fr)* These authors
contributed equally to
this work.

Modulation properties of factors released by bone marrow stromal cells on activated microglia: an *in vitro* study

Dasa Cizkova^{1,2*}, Stéphanie Devaux^{1*}, Françoise Le Marrec-Croq¹, Julien Franck¹, Lucia Slovinska², Juraj Blasko², Jan Rosocha³, Tímea Spakova³, Christophe Lefebvre¹, Isabelle Fournier¹ & Michel Salzet¹

¹Laboratoire PRISM: Protéomique, Réponse Inflammatoire, Spectrométrie de Masse, U1192 INSERM, Bât SN3, 1^{er} étage, Université de Lille 1, F-59655 Villeneuve d'Ascq, France, ²Institute of Neurobiology, Slovak Academy of Sciences, Center of Excellence for Brain Research, Soltesovej 4-6, 040 01 Kosice, Slovakia, ³Associated Tissue Bank of the Pavol Jozef Safarik University, Faculty of Medicine, University Hospital of. Louis Pasteur in Kosice, Trieda SNP 1, 040 66 Kosice, Slovakia.

In the present paper we develop a new non-cell based (cell-free) therapeutic approach applied to BV2 microglial cells and spinal cord derived primary microglia (PM) using conditioned media from rat bone marrow stromal cells (BMSCs-CM). First we collected conditioned media (CM) from either naive or injured rat spinal cord tissue (SCI-CM, inflammatory stimulation agent) and from rat bone marrow stromal cells (BMSCs-CM, therapeutic immunomodulation agent). They were both subsequently checked for the presence of chemokines and growth, neurotrophic and neural migration factors using proteomics analysis. The data clearly showed that rat BMSCs-CM contain *in vitro* growth factors, neural migration factors, osteogenic factors, differentiating factors and immunomodulators, whereas SCI-CM contain chemokines, chemoattractant factors and neurotrophic factors. Afterwards we determined whether the BMSCs-CM affect chemotactic activity, NO production, morphological and pro-apoptotic changes of either BV2 or PM cells once activated with SCI-CM. Our results confirm the anti-migratory and NO-inhibitory effects of BMSCs-CM on SCI-CM-activated microglia with higher impact on primary microglia. The cytotoxic effect of BMSCs-CM occurred only on SCI-CM-stimulated BV2 cells and PM, not on naive BV2 cells, nor on PM. Taken together, the molecular cocktail found in BMSCs-CM is favorable for immunomodulatory properties.

Bone Marrow Stromal Stem Cells (BMSCs) are a population of heterogeneous cells derived from the non-blood forming fraction of the bone marrow¹. Under physiological conditions they provide stromal support for developing hematopoietic cells² through the continuous release of erythropoietin (EPO) and granulocyte-colony stimulating factor (G-CSF). This continuous release of EPO and G-CSF provides the stromal support for developing hematopoietic cells. Although initially found in the bone marrow, adult stem cells capable of self-renewal and differentiation into various mesodermal cell lineages have been identified in many other organs and tissues including adipose tissue, umbilical cord, blood, skin, teeth, testes, gut, liver and ovarian epithelium³⁻⁵. Unlike other stem cells such as Keratinocyte Stem cells⁶⁻⁸, or pancreatic islet-derived stem cells⁹, BMSCs derived from the bone marrow produce low levels or none of class I and II Major Histocompatibility Complex (MHC) antigens and lack CD40, CD80 and CD86, co-stimulatory molecules required for activation of T cells. Furthermore, BMSCs are able to migrate to the site of inflammation and suppress the function of lymphocytes (T and B)^{10,11}, natural killer cells¹², dendritic cells¹³ and neutrophils¹⁴. The immunosuppressive properties of BMSCs give them a privileged role in ameliorating chronic inflammation-related neuronal damage in various central nervous system (CNS) disease models¹⁵⁻¹⁸. In the case of spinal cord lesion, after initial primary injury caused by direct mechanical insult, the spinal cord tissue progressively undergoes pathological changes that are associated with secondary damage affecting intact, neighboring tissue^{19,20}. One of the key events of secondary processes is related to the development of acute inflammation characterized by fluid accumulation (edema) and the recruitment of immune cells (neutrophils, T-cells, macrophages and monocytes)^{20,21}. The beneficial and detrimental effects of inflammation have been compared to glial scar, which is actively formed after spinal cord injury (SCI)²². Much evidence suggests that glial scar plays an important role in the immediate response to injury, corresponding to the acute phase^{23,24}. Glial scar ensures sealing of the injury site, restoring homeostasis, preserving spared tissue and modulating immunity, however these roles become noxious for the recovery, neurogenesis



and axonal growth in the later phases. Among the immune cells activated during inflammatory processes within the brain and spinal cord, microglia cells are one of the major effectors of immunity²⁵. In response to injury, microglia proliferate and secrete cytotoxic nitric oxide (NO) and pro-inflammatory cytokines such as Tumor Necrosis Factor alpha (TNF- α) and Interleukin 1-beta (IL-1 β)^{26,27} or neuroprotective molecules²⁸. Thus, modulating reactive microglial cells via BMSCs-based therapy may limit chronic inflammation and tissue damage within the CNS^{29–32}.

Moreover, BMSCs have been transplanted into rodent models of SCI by various research groups^{33–36}. Despite considerable variation, a clear functional beneficial effects can be expected after transplantation of BMSCs into the injured spinal cord^{37–40}. These effects include improvements in locomotion, sensorimotor function, promotion of axonal regeneration, and preservation of neural tissue. However, knowledge of the underlying mechanisms is essential to increase the overall outcomes. The question which arise is which molecules and receptors are involved in spinal cord repair? In this context, the content of BMSCs products was investigated at a proteomic level. Furthermore, in order to further understand the mechanism of BMSCs-mediated down-regulation of CNS inflammation, it is important to examine the influence of BMSCs on the activated microglia. Here we have developed a new non-cell based (cell-free) therapeutic approach applied to SCI-CM-stimulated BV2 cells and primary microglia (PM) isolated from rat spinal cord microglia. First we collected conditioned media from injured spinal cord tissue (Spinal Cord Injury Conditioned Media (SCI-CM): inflammatory stimulatory agent) and from rat BMSCs (BMSCs-CM: therapeutic immune-modulating agent) and checked their molecular pattern for the presence of inflammatory cytokines, chemokines and neurotrophic factors using proteomic analysis. Afterwards we evaluated the BMSCs-CM effects on chemotactic activity, and morphological and pathological changes of BV2 cells and PM following stimulation with SCI-CM. Our results confirmed the anti-migratory and cytotoxic effects of BMSCs-CM on BV2 cells and PM, and also Nitric Oxide (NO)-inhibitory effects on PM activated with SCI-CM, but not on control microglia. Furthermore, the molecules found in BMSCs-conditioned media via proteomics are favorable for the pathways involved in their immunomodulatory properties.

Experimental Procedures

Chemicals. All chemicals were of the highest purity obtainable. Water, formic acid (FA), trifluoroacetic acid (TFA), acetonitrile (ACN), and methanol (MeOH) were purchased from Biosolve B.V. (Valkenswaard, the Netherlands). Sequencing grade, modified porcine trypsin was purchased from Promega (Charbonnières, France).

Animals. The study was performed with the approval and according to the guidelines of the Institutional Animal Care and Use Committee of the Slovak Academy of Sciences and with the European Communities Council Directive (2010/63/EU) regarding the use of animals in Research, Slovak Law for Animal Protection No. 377/2012 and 436/2012.

BMSCs culture and conditioned media collection. BMSCs were isolated from the bone marrow of three adult male Wistar rats (300 g), collected from the long bones (femur and tibia)^{36,41}. The bone marrow was dissected into small pieces, gently homogenized, and filtered (70 μ m) to remove bone fragments. Mononuclear cells (MNCs) were isolated by Ficoll density gradient centrifugation (1.077 g/mL; Sigma-Aldrich, Steinheim, Germany) at 400 g for 20 min. MNCs were collected from the interface, washed with alpha-MEM (LONZA, Walkersville Inc.), and centrifuged at 600 g for 10 min. The cell pellet was re-suspended in 1 mL of alpha-MEM, the pooled cells were counted, and their viability was assessed using

the trypan blue dye exclusion method. MNCs were subsequently re-suspended in culture medium composed of alpha-Minimum essential media (MEM) supplemented with 10% of fetal calf serum (FCS)(GIBCO Laboratories, Grand Island, NY) and antibiotics (10,000 units/mL penicillin, 10,000 μ g/mL streptomycin, and 25 μ g/mL amphotericin B; Invitrogen, Carlsbad, CA), and plated at a density of 30.000 cells/cm² in tissue culture flasks. The cells were incubated in a humidified atmosphere with 5% CO₂ at 37°C. Non-adherent cells were removed after 4–5 days by medium change and the remaining cells were fed twice per week. When the cultures reached 80% of confluence, the BMSCs were passaged with 0.25% trypsin/0.53 mM Ethylene diamine tetra acetic (EDTA) (Invitrogen), centrifuged, and re-plated at a density of 5000 cells/cm². The BMSCs were expanded 3 times to achieve the desired cell numbers. Cells at passages 3 cultured in Dulbecco's modification of Eagle's medium (DMEM) with low glucose and without fetal bovine serum were incubated in a humidified atmosphere with 5% CO₂ at 37°C for 24 h and used for BMSCs conditioned media (BMSCs-CM) collection, using a similar protocol as in the previous study⁴².

Characterization of rat bone marrow derived BMSCs. Before experimental use, the ability of BMSCs (from passage 3) to differentiate into adipocytes and osteoblasts was tested. To induce adipogenic differentiation, confluent adherent cells were cultured in alpha-MEM, supplemented with 10% of FCS, 1 μ M dexamethasone (Sigma-Aldrich, Inc., USA), 500 μ M 3-isobutyl-1-methylxanthine (Sigma-Aldrich, Inc., USA), 100 μ M Indomethacin (Sigma-Aldrich, Inc., USA), and 10 μ g/mL insulin (Sanofi-Aventis Deutschland GmbH), and the medium was replaced every 3 days. Oil Red O staining was used to identify adipocyte-differentiated BMSCs. To induce osteogenic differentiation, the alpha-MEM medium was supplemented with 10% of FBS, 0.1 μ M dexamethasone, 10 mM beta-glycerophosphate (Sigma-Aldrich, Inc., USA), and 50 μ M sodium L-ascorbate (Sigma-Aldrich, Inc., USA), and the medium was also replaced every 3 days. Cell differentiation into hydroxyapatite-producing osteoblasts was confirmed by Alizarin Red staining. BMSCs were maintained for 3 passages in alpha-MEM (LONZA, Walkersville Inc.), supplemented with 10% (v/v) FBS (LONZA, Walkersville Inc.) and 1% (v/v) antibiotic/antimycotic solution before being used for further analysis.

Flow cytometry. The phenotypic properties of BMSCs were determined on the basis of the expression of CD90, CD29 and the absence of the pan-hematopoietic marker CD45 at passage 1 and 3. Briefly, BMSCs (0.2×10^6 cells) were incubated with Phycoerythrin (PE)-conjugated antibodies or isotype-matched control immunoglobulin Gs (IgGs, 1 μ g each) diluted in PBS containing 2% FCS, 2 mM EDTA, and 0.01% sodium azide (PFEA buffer) at 4°C for 45 minutes (BD Biosciences). For flow cytometry, the following antibodies were employed according to the supplier's recommendations: PE anti-mouse/rat CD29 (Clone: HM β 1-1, BioLegend); PE anti-rat CD45 (Clone: OX-1, BioLegend), and PE anti-rat CD90 (Clone: OX-7, BioLegend, all from San Diego, CA) and their isotype controls: PE Armenian Hamster IgG (CD29) and PE Mouse IgG1 (CD45, CD90) from BioLegend.

Samples were analyzed using a flow cytometer FACS Calibur (BD Biosciences) operated by CellQuest software and at least 20,000 events were collected per sample. Data were analyzed using WinMDI software (Version 2.8). Forward and side scatter profiles were obtained from the same samples.

Conditioned media collection from spinal cord injury tissue. *Spinal cord trauma.* The spinal cord injury (SCI) was induced using the modified balloon compression technique in adult male Wistar rats ($n = 4$), weighing between 300 and 320 g, according to our previous study⁴³. Manual bladder expression was required for 3 days after the injury. No antibiotic treatment was used. In the sham



group/control (n = 4), a 2-French Fogarty catheter was inserted at the same level of spinal cord, but the balloon was not inflated and no lesion was made. All animals survived three days.

Conditioned media collection from spinal cord injury tissue.

Experimental SCI rats (n = 4) and control rats (n = 4) were sacrificed by isoflurane anesthesia followed by decapitation. The spinal cord was pressure flushed out by injecting sterile saline (10 mL) throughout the vertebral canal, along the caudo-rostral axis. Each spinal cord was macroscopically observed and the central lesion distinguished at Th7–Th10 level. Samples (approximately 1.0 cm) taken from the central lesion (were additionally chopped into 0.3 cm-thick sections/3per segment) and deposited into a 12-well culture plate, containing 2 mL of DMEM without FBS and without antibiotics. After 24 hours incubation in a humidified atmosphere with 5% CO₂ at 37°C, 2 mL samples of SCI-CM were collected and centrifuged 30 min at 15,000 rpm at 4°C. The same procedure was performed for obtaining CM from control spinal cord tissue. A 50-μL aliquot from the 2 mL sample was used for trypsin digestion (24 h, 37°C). The portion was desalted using a solid-phase extraction procedure employing Millipore ZipTips. The solution was then dried again using the SpeedVac and re-suspended in water containing 5% of acetonitrile and 0.1% of formic acid before injection into nano Liquid Chromatography (LC).

Microglia culture. Highly purified spinal cord derived primary microglia cultures (PM) were prepared using post natal day (P) 2–3 Wistar rats (Velaz, CZ) that were anesthetized on ice and afterwards sacrificed by decapitation⁴⁴. The entire spinal cords were removed; meninges were dissected away; spinal cord tissue was minced with a sterile microsurgical scissors and digested with 1 mL trypsin trypsin/EDTA 1 × (Mediatech, Herndon, VA, USA) and 1 mL PBS for 15 min at 37°C. After centrifuging at 300 × g for 3 min, the cells were plated into 75 cm² flasks which had been coated with poly-L-lysine. Mixed glial cells were cultured in DMEM containing 10% FBS at 37°C in 5% CO₂ in air and 95% humidity. The culture medium, one-half of the volume was replaced with an equal volume of fresh growth medium after 6–7 days. After 12–14 days in vitro (DIV 13), the flasks were confluent with astrocytes and microglia. Flasks were agitated on shaker in laminar box (230 rpm, 37°C for 3 hours) supernatants were removed and centrifuged at 300 g for 10 min, plated into 75 cm² flasks, after 30 min the supernatant containing mixed glial population (astrocytes + microglia) was removed and the adherent, highly enriched microglia was cultured with fresh media for 7–10 DIV. Adherent microglia enriched cultures were found to be 98.3 ± 0.52% microglia by staining with Iba1 antibody a marker for the microglia, while mixed glial population contained high percentage of astrocytes 95.8 ± 1.38%. The BV2 cells (Species: mouse, C57BL/6; Tissue: brain, microglial cells) were purchased from the IRCCS Azienda Ospedaliera, Universita San Martino (Italy)⁴⁵.

Experimental groups. The PM and BV2 cells were divided into five experimental groups: 1) Control group, cells were incubated in DMEM containing 2% fetal bovine serum (FBS) and 2) Conditioned media (CM) groups, where cells were incubated in DMEM containing 2% FBS (DMEM) and control spinal cord tissue SC-CM (DMEM: SC-CM (2:1), and 3) DMEM + BMSCs-CM (2:1), and 4) DMEM + SCI-CM (2:1), and 5) DMEM + SCI-CM + BMSCs-CM (1:1:1).

Chemotaxis assays. The effects of conditioned media i) BMSCs-CM, ii) SC-CM (control spinal tissue/Th7–10 segment-conditioned medium), iii) SCI-CM (spinal cord injury tissue central lesion/Th7–10 segment-conditioned medium), and iv) BMSCs-CM + SCI-CM on microglial cell recruitment were determined using Boyden chambers (Cell Biolabs, CytoSelect™ 24-Well Cell

Migration Assay, 5 μm)⁴⁶. The BV2 cells were initially cultured in RPMI medium supplemented with 10% of FBS and 1% of penicillin/streptomycin (P/S), and split twice a week to obtain a sufficient number of BV2 cells. Before the experiment, the cells were replaced in a medium appropriate for the assay, which was DMEM with P/S (all reagents from Invitrogen). BV2 cells and PM at a concentration of 50000 per insert were plated into the upper chamber, while a different combination of CM (SC-CM, SCI-CM, SCI + BMSCs/CM, and BMSCs-CM) was filled into the lower one and then cultured for 3 hours. Each CM (1:2/CM:DMEM) concentration of total protein was measured using the Bradford protein assay (2.2 μg–2.8/10 μL/per each CM), and was centrifuged for 10 min at 1,500 rpm and sterilized through 0.2 μm filters prior to application. As positive control for microglial cell recruitment, ATP (10 μM) together with DMEM, the culture medium for microglia cells (negative control), was used. The migrating BV2 cells and PM were detected by Hoechst staining and the number was counted on dissected membranes transferred on glass slides and mounted with Vectashield mounting medium (Vector Laboratories, Inc. on LinkedIn). Three different counts under Nikon Eclipse Ti microscope with motorized stage were performed. Chemotaxis experiments were carried out in triplicate and their results are expressed as the mean of the microglial cell number ± SEM. *P < 0.01, *** P < 0.001, one-way ANOVA followed by Tukey-Kramer test (SigmaStat 3.11).

Morphology and viability of Microglia. *Morphology.* To analyze the morphological changes of microglia after SCI-CM stimulation (DMEM:SCI-CM/2:1), SCI-CM co-cultured with BMSCs-CM (DMEM:SCI-CM:BMSCs-CM/1:1:1), or only with BMSCs-CM (DMEM:BMSCs-CM/2:1), the BV2 cells and PM were plated in a concentration of 20000 cells per well of 24-well plates. Digital images of BV2 cells were taken at 3 h, 18 h, 24 h and 48 h and of PM at 24 h and 48 h in cultures stimulated with SCI-CM, SCI-CM+BMSCs/CM and BMSCs-CM (Nikon Ti). The percentage of BV2 ramified cells (spindle shaped or multipolar) over the total BV2 cells was calculated by using ImageJ software, at each time period within five sampling fields (500 × 500 μm) for each experimental group in triplicates. To confirm morphological characteristics of BV2 cells and PM after different CM treatment we have defined five following parameters: soma diameter, soma area, process diameter and length, and process length in relation to the soma diameter. Data were collected from measurements of 100 cells per CM treatment (Supplementary data).

Immunohistochemistry. PM and BV2 cells after each CM treatment were fixed with 4% paraformaldehyde in phosphate buffered saline (PBS). After pre-incubation with 10% normal goat serum (NGS) in PBS for 60 min, the cells were washed 3 times with PBS and incubated with the primary antibody anti-Iba1 (a marker for microglia rabbit IgG, 1:1000; Wako Pure Chemical Industries, Osaka, Japan) (1:500) antibodies in PBS containing 2% NGS and 0.1% Triton X for 2 h. Cells were then washed 3 times and incubated with the secondary fluorescent antibody: goat anti-rabbit IgG conjugated with Texas Red (Alexa Flour 594). For nuclear staining, we used 4–6-diaminidino-2-phenylindol (DAPI) (1:200). Finally, cells were washed in 0.1 M PBS, mounted, and cover slipped with Vectashield mounting medium (Vector Laboratories, Inc.) and observed under a fluorescence microscope (Nikon Eclipse Ti, Japan) and confocal laser scanning microscope (Leica TCS SP5 AOBs, Leica Microsystems, Mannheim, Germany). The density analysis of Iba1 positive microglia was enrolled to evaluate possible morphological changes of activation form, based on the fact that hypertrophied/amoeboid microglia and its branched processes occupied larger micro-territory than resting type, in the identical sampling fields. Quantification for Iba1+ cells was performed at 40 × magnification and was analyzed by Image J software



according to the previous protocol (Jones et al. 2002). In the monochrome 8-bit images we have determined the mean gray level number of black and white pixels (value 0–255, when 0 = white pixels, 255 = black pixels) within five identical sampling fields (500 × 500 μm) for each experimental group in triplicate. The threshold values were maintained at a constant level for all analyses. Data are represented as mean pixels ± SEM. *P < 0.1 **P < 0.01, *** P < 0.001, one-way ANOVA followed by Tukey-Kramer test.

Viability and apoptosis. After 48 h incubation (each experimental group), the culture medium was aspirated, and the adherent BV2 cells and PM were harvested by trypsin-EDTA buffer at 37°C (5–7 min) followed by centrifugation. The cell pellets were washed twice in cold PBS (1.4 M NaCl, 27 mM KCl, 100 mM KH₂PO₄/K₂HPO₄, pH 7.2), suspended in 1 × binding buffer at 1 × 10⁶ cells/mL, and stained with Annexin V/Propidium Iodide labeling kit (Apoptosis Detection Kit I, BD Pharmingen, San Jose, CA) to determine dead and apoptotic cells. Labeling was done with 5 μL PI and 5 μL AV (PI, a standard probe used to distinguish viable cells from nonviable ones; AV, recombinant Annexin-V conjugated to green-fluorescent Alexa Fluor® 488 dye recognize the externalization of phosphatidylserine in apoptotic cells, BD Biosciences) at a concentration of 50 μg/mL. After standing for 15 min in the dark, the cells were transferred to cytospin slides by centrifugation of 200 μL sample/10 min 300 g, cover-slipped, mounted with Vectashield mounting medium with 1.5 μg/mL DAPI (Vector Laboratories). The percentage of necrotic AV−/PI+ and late apoptotic AV+/PI+ (BD Bioscience) cells to total DAPI stained nuclei were counted within five sampling fields (500 × 500 μm) for each experimental group in triplicates. The results are expressed as the mean % of ramified microglial cell number. Data are represented as mean ± SEM. *P < 0.1 **P < 0.01, *** P < 0.001, one-way ANOVA followed by Tukey-Kramer test.

Griess assay for nitric oxide production. Nitric oxide production was assessed by using the Griess Assay (Promega, Madison, WI, USA) following the manufacturer's protocol. Detection of nitrite was performed in 96-well plates, BV2 cells and PM (5 × 10⁵ cells/well) were incubated in DMEM containing 2% FBS alone or in combination with SC-CM, and BMSCs-CM, and SCI-CM, and SCI-CM + BMSCs-CM, ratio 2:1/DMEM:CM for 24 hours. NO was detected in the 50 μL of culture supernatant from each sample in triplicate and added with the same volume of Griess reagent (1% sulfanilamide/0.1% N-1-naphthylethylenediaminedihydrochloride/2.5% phosphoric acid; all from Sigma-Aldrich, St. Louis, MO, USA). Absorbance was read at 530 nm (MRX II microplate reader, Dynex Technologies, VA, and USA) after 15 minute incubation. Nitrite concentration was calculated with reference to a standard curve of freshly prepared sodium nitrite (0 to 100 μM). All treatments were completed at least three times and data were expressed as mean μM concentration of NO₂ ± SEM.

Proteomic studies. Three different combinations were applied to the BMSCs-CM before analyzing them using on-line coupling of nanoLC with an ESI MS instrument (ESI-LTQ XL orbitrap, built in 2010) and each experiment was conducted in triplicate.

Bottom-up analyses

- In the first set of analyses, 50 μL of the solution of BMSCs-CM was added to 25 μL of a solution of dithiothreitol (DTT) (50 mM) in ammonium bicarbonate (NH₄HCO₃) buffer (50 mM) (pH = 8) and heated for 15 min at 55°C. After cooling, 25 μL of a solution of IAA (150 mM) in NH₄HCO₃ buffer (50 mM) was added and the mixture was incubated for 15 min at room temperature in the dark. 20 μL of a solution of trypsin (20 μg/mL) in NH₄HCO₃

(50 mM) was then added and the sample was incubated overnight at 37°C.

- In the second set of analyses, 900 μL of the solution of BMSCs-CM was filtered with Sep-Pak Shorty C18 (Waters Corporation, Milford MA, USA), dried under vacuum and then re-suspended in 50 μL of DTT (50 mM) in NH₄HCO₃ buffer (50 mM) (pH = 8), sonicated and heated for 30 min at 93°C. After cooling, 50 μL of a solution of IAA (150 mM) in NH₄HCO₃ buffer (50 mM) was added and the mixture was incubated for 20 min at room temperature in the dark. 50 μL of a solution of trypsin (20 μg/mL) in NH₄HCO₃ (50 mM) was then added and the sample was incubated overnight at 37°C. The digestion was stopped by adding 1 μL of trifluoro acetic acid (TFA), and the product was dried in a vacuum concentrator system.
- In the third set of analyses, 1 mL of the solution of BMSCs-CM was centrifuged at 12000 g for 10 min and the supernatant was collected and dried. 100 μL of Laemmli was used to re-suspend the pellet. The solution was incubated for 30 min at 93°C. The solution was then loaded into a 12% polyacrylamide gel, stacked at 70 V for 15 min and then separated at 120 V until the dye front reaches the other end of the gel. After migration, the gel was incubated in the gel fixative solution for 30 min and stained with Colloidal Coomassie brilliant blue overnight. The stain was removed by washing the gel four times with distilled deionized water. The gel was cut into eight pieces. The pieces were washed with 300 μL of distilled deionized water for 15 min, 300 μL of ACN for 15 min and 300 μL of 100 mM NH₄HCO₃ (pH8) for 15 min. A mix of 300 μL of NH₄HCO₃/ACN (1:1, v/v) was added for 15 min and 300 μL of ACN for 5 min. Band pieces were dried in a vacuum concentrator for 5 min. The reduction of cysteine residues was performed with 50 μL of 10 mM DTT in 100 mM NH₄HCO₃ (pH8) followed by incubation at 56°C for 1 hour. Alkylation of cysteine was obtained by addition of 50 μL of 50 mM IAA in 100 mM NH₄HCO₃ (pH8) followed by incubation at room temperature in the dark for 30 min. Band pieces were then washed once more with 300 μL of 100 mM NH₄HCO₃ (pH8) for 15 min, 300 μL of NH₄HCO₃/ACN (1:1, v/v) for 15 min and 300 μL of ACN for 5 min. Band pieces were dried in a vacuum concentrator for 5 min. Bands were digested by addition of trypsin (12.5 μg/mL) in 20 mM NH₄HCO₃ (pH8) (enough to cover pieces) followed by incubation at 37°C overnight. Peptides were then extracted on a shaking platform with 50 μL of 1% FA two times for 20 min and 150 μL of ACN for 10 min. The supernatant was transferred into the new tube and dried in a vacuum concentrator.

NanoLC-MS & MS/MS. Samples from 3 sets of experiments were re-suspended in 20 μL of TFA 0.1%, then they were desalted on a C-18 Ziptip dried under vacuum and then re-suspended in AcN/0.1% FA, 8:2, v/v). The samples were separated by online reversed-phase chromatography using a Thermo Scientific Proxeon Easy-nLC system equipped with a Proxeon trap column (100 μm ID × 2 cm, Thermo Scientific) and C18 packed tip column (100 μm ID × 10 cm, NikkyoTechnos Co. Ltd). Elution was carried out using an increasing gradient of AcN (5% to 30% over 120 min) at a flow rate of 300 nL/min. A voltage of 1.6 kV was applied via the liquid junction of the nanospray source. The chromatography system was coupled to a Thermo Scientific LTQ-Orbitrap XL mass spectrometer programmed to acquire in data-dependent mode. The survey scans were acquired in the Orbitrap mass analyzer operated at 60,000 (FWHM) resolving power. A mass range of 300 to 2000 m/z and a target of 1E6 ions were used for the survey scans. Precursor ions observed with an intensity over 500 counts were selected “on the fly” for ion trap collision-induced dissociation (CID) fragmentation with an isolation window of 4 a.m.u. and a normalized collision energy of 35%. A target of 5000 ions and a maximum injection time of 200 ms

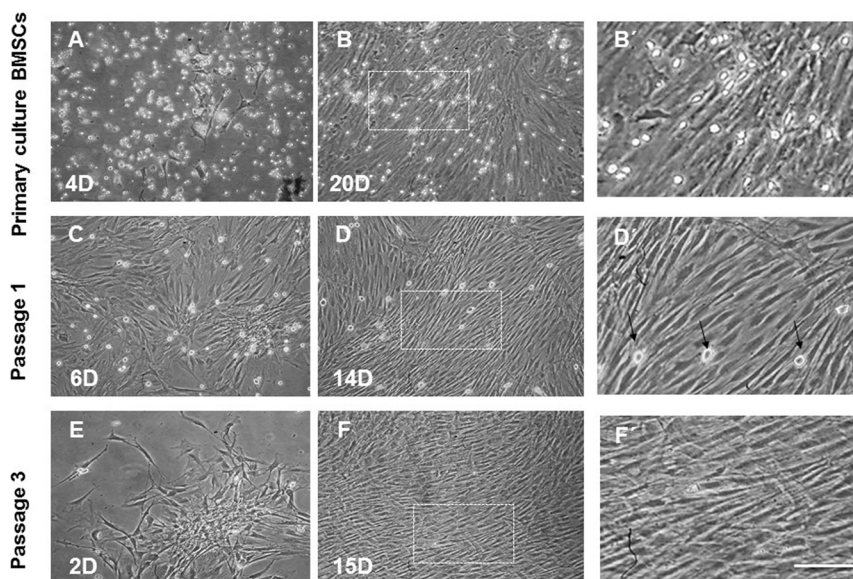


Figure 1 | Representative Fields showing BMSCs morphologies in primary culture and after passaging. BMSCs showed diverse morphologies including ovoid, bipolar and large, flattened cells enriched with a large number of small, round-like floating light cells in the primary culture (A, B, B'). In passage 1, most of the BMSCs exhibited large, flattened or fibroblast-like morphology with sporadically occurring round, bright cells (C, D, D', arrows) that were completely abolished after passage 3 (E, F, F'). Images B', D', F' correspond to boxed areas from B, D, F. Scale bars A–F = 200 μm ; B', D', F' = 50 μm .

were used for MS² spectra. The method was set to analyze the top 20 most intense ions from the survey scan and dynamic exclusion was enabled for 20 s.

Data analyses. All MS/MS samples were analyzed using Sequest (Thermo Fisher Scientific, San Jose, CA, USA; version 1.3.0.339) and X! Tandem (The GPM, thegpm.org; version CYCLONE (2010.12.01.1)). Sequest was set up to search *Rattus norvegicus* Uniprot ref proteome 112011.fasta assuming the digestion enzyme trypsin. X! Tandem was set up to search a subset of the RAT database also assuming trypsin. Sequest and X! Tandem were searched with a fragment ion mass tolerance of 0.50 Da and a parent ion tolerance of 10 ppm. Carbamidomethylation of cysteine was specified in Sequest and X! Tandem as a fixed modification. Glu->pyro-Glu of the n-terminus, ammonia-loss of the n-terminus, gln->pyro-Glu of the n-terminus, amidation of the c-terminus, oxidation of methionine, acetylation of the n-terminus and phosphorylation of tyrosine were specified in X! Tandem as variable modifications. Oxidation of methionine, acetylation of the n-terminus and phosphorylation of tyrosine were specified in Sequest as variable modifications. Scaffold (version Scaffold_4.0.6.1, Proteome Software Inc., Portland, OR) was used to validate MS/MS-based peptide and protein identifications.

Label free quantification. For the validation of protein identifications obtained from Sequest and X! Tandem, the protein identifications were accepted if they could be established at greater than 99% probability and contained at least 2 identified peptides (FDR 0.1%). Protein probabilities were assigned by the Protein Prophet algorithm^{47,48}. Peptide identifications were accepted if they could be established at greater than 95% probability by the Peptide Prophet algorithm⁴⁹ with Scaffold delta-mass correction. Proteins that contained similar peptides and could not be differentiated based on MS/MS analysis alone were grouped to satisfy the principles of parsimony. Normalization followed by quantification was done on top 3 total ion current (TIC) in addition to spectral counting.

Results and Discussion

Characterization of bone marrow stromal stem cells (BMSCs). BMSCs isolated from rat bone marrow were expanded in primary culture and passaged three times. Cultured cells at initial phases of growth contained attached spindle-shaped cells forming colonies and small, bright, round, floating cells (Figures 1A–D), reaching confluence approximately at day 14 (Figures 1B, D, F). The initial high number of bright floating cells in the primary culture of BMSCs

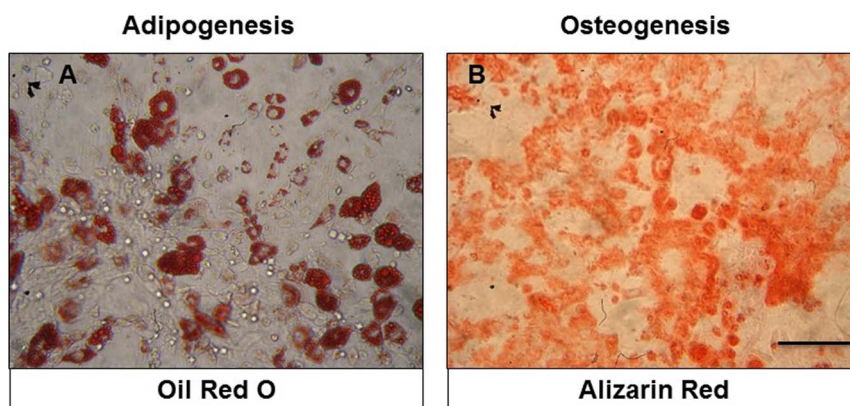


Figure 2 | Micrographs documenting multipotent characteristics of BMSCs, differentiated into adipocytes (A) and osteocytes (B). Scale bars A, B = 100 μm .



Table 1 | Expression of surface markers in BMSCs after Passage 1 and 3

Surface antigens	CD29	CD90	CD45
1 passage	++	++	+
3 passage	+++	+++	–

– no expression (<10%); + weak expression (11–40%); ++ moderate expression (41–70%); +++ strong expression (>71%).

(Figures 1A–B') significantly decreased at passage 1 (Figure 1C–D') or was completely abolished at passage 3 (Figures 1E–F'). To examine the multipotent differentiation potential, we showed that BMSCs generated Oil red-O positive fat cells, while for the osteoblasts, we visualized them with Alizarin Red Solution (Figures 2A and 2B). BMSCs were characterized immunophenotypically and confirmed throughout passages 1–3 using a panel of hematopoietic and non-hematopoietic markers (Table 1).

Immunophenotyping of BMSCs. BMSCs at passage 3 expressed CD29 (94%) and CD90 (96%) but not hematopoietic surface marker CD45 (Table 1, Figure 3) and maintained their typical phenotype throughout passages 4–5 (data not shown). As isotype controls, PE-conjugated Mouse IgG1 (C, C', E, E') was used for CD45 (D, D') and CD90 (F, F'); PE-conjugated Armenian Hamster IgG (A, A') was used for CD29 (B, B').

Proteomic studies: identification of BMSCs–CM content. BMSCs–CM collected after one day culture were centrifuged and the supernatant subjected to different procedures. These were combined (Figure 4A) and subjected to separation using a nano-LC coupled to an ESI-LTQ-Orbitrap XL instrument for LC MS &MS/MS analysis. We identified 658 proteins based on 99% probability and contained at least 2 identified peptides with a false discovery rate (FDR) of 0.1%. Each accession number, protein description, gene name and relative score associated with the selected proteins is reported in Table 2 (Supplementary data 1 & 2). Specific markers of BMSCs were identified *e.g.* osteogenic factors, like osteopontin, periostin, spondin 2 and osteoglycin, differentiating factors (SPARC, FAM3C, cornifin) as well as growth factors *i.e.* Placenta growth factor, Platelet derived growth factor, Insulin-like growth factor-binding protein 7, Transforming growth factor beta-1, 2 & 3, and Matricellular proteins of the CCN

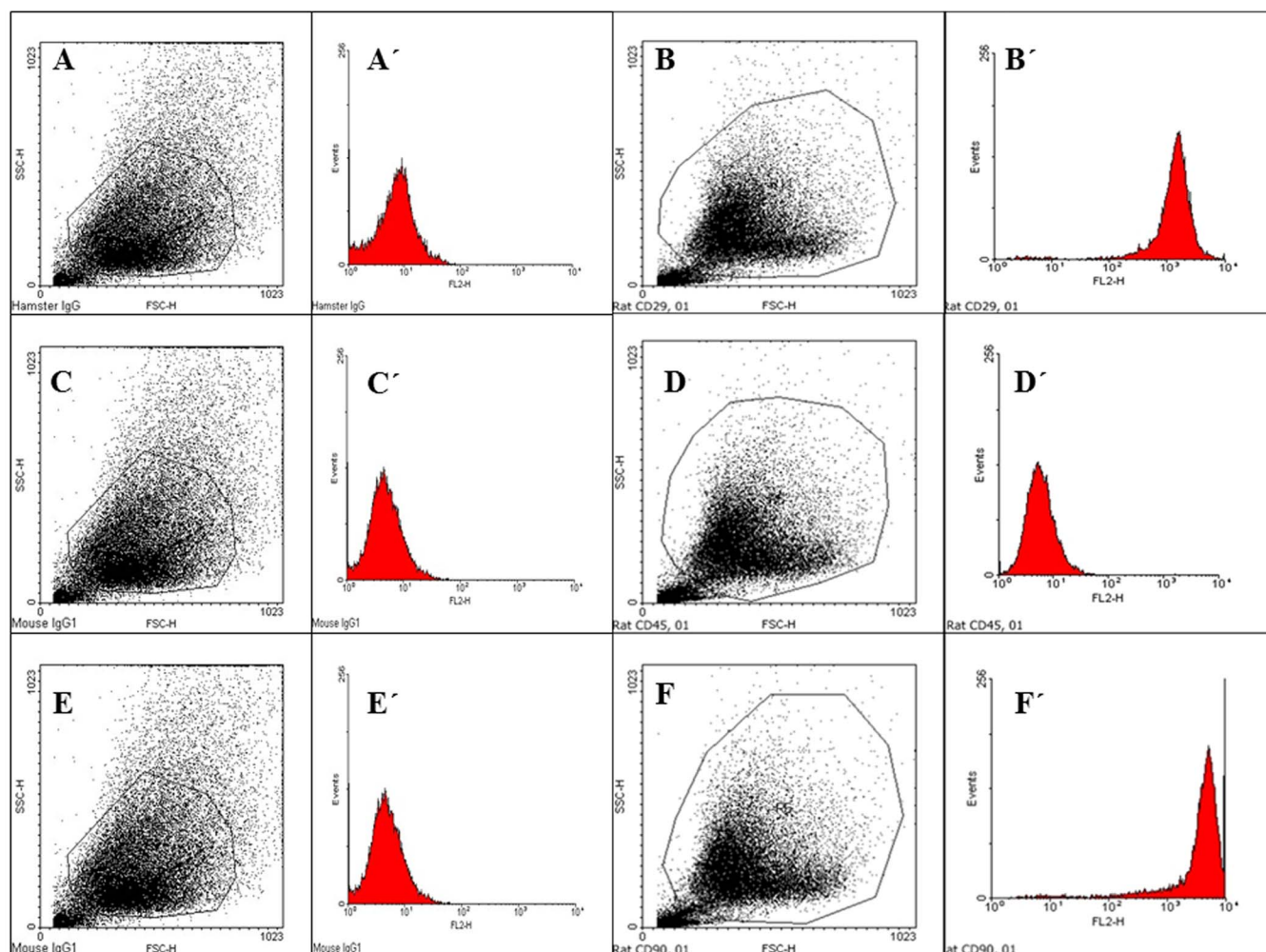


Figure 3 | Representative flow cytometry analysis of cell surface markers (CD29, CD45, and CD90) expressed on BMSCs at passage 3.

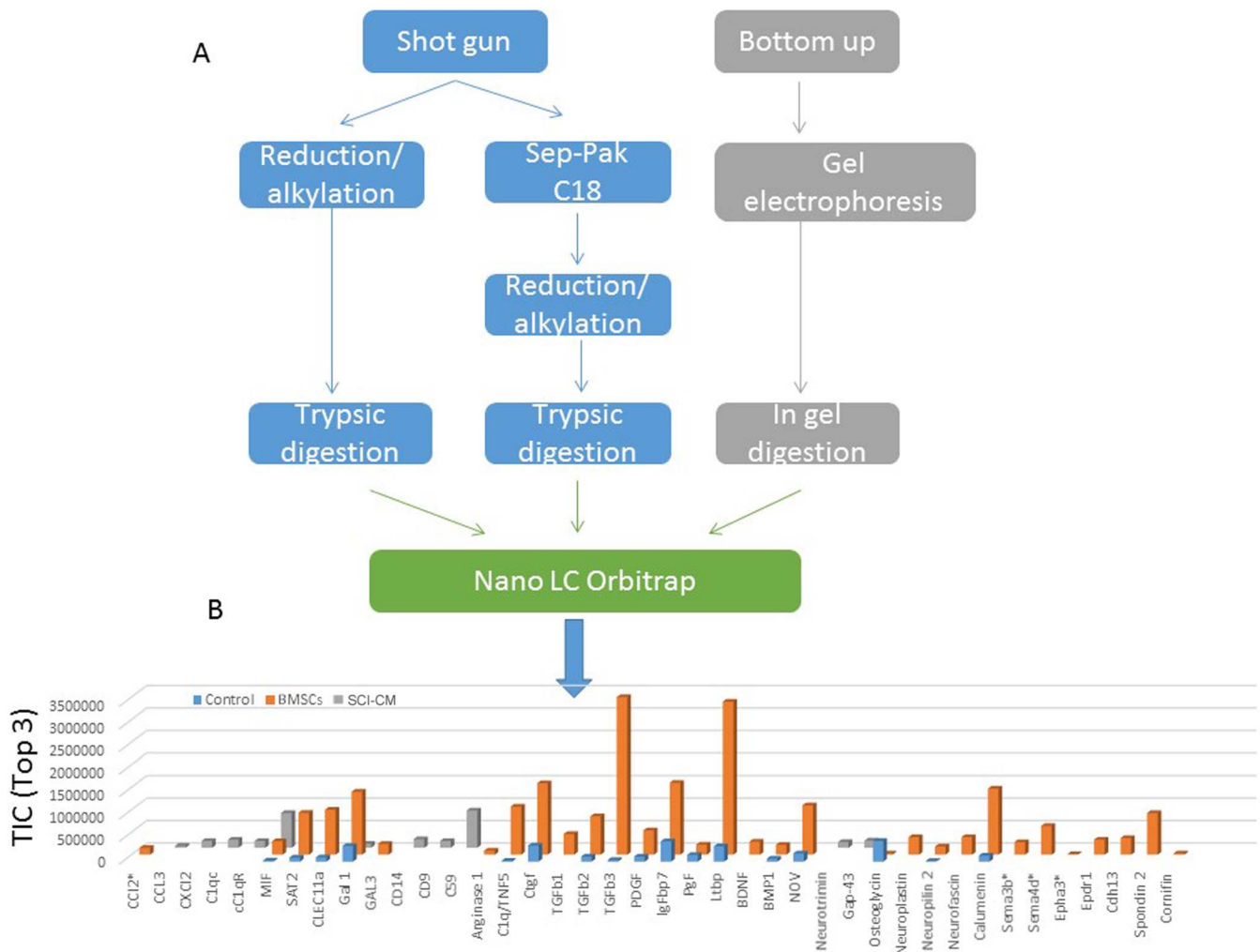


Figure 4 | (A) Scheme of the methods used to analyze BMSCs Proteins identification was done on an orbitrap LTQ XL with a protein threshold of 99% (FDR 0.1%) and peptide threshold of 97% (FDR 0.1%) and contained at least 2 identified peptides as parameters (Supplementary data 1&2). (B) Label free quantification of immune modulators, neurotrophic and growth factors and apoptotic molecules identified in conditioned media obtained from BMSCs, spinal cord lesion (SCI) or control (non injured) using Scaffold_4.0.6.1. Label-free quantification was done on top3 of the total ion current (TIC). (BMP 1: Bone morphogenic protein 1, Cdh13: T-Cadherin, CLEC11a: C-type lectin domain family 11 member A CTGF: connective tissue growth factor, Epha 3: Ephrin A isoform 3, Epdr1: Ependymin related protein 1, FAM3C: family with sequence similarity 3, member C Gal 1: galectin 1; GAP-43: Growth associated protein 43, Ltbp: Latent TGF-beta binding protein, Igfbp 7: Insulin growth factor binding protein 7, MIF: macrophage inhibiting factor, PDGF: Platelet derived growth factor, PGF: placenta growth factor, spondin 2, SPARC, TIMP-1: Tissue inhibitor metalloproteinase 1 & 2).

family (CYR61/CTGF/NOV). Moreover, proteins involved in immunomodulation (arginase 1, ST2, galectins, TIMP-1 and TIMP-2) and in chemotaxis (C-type lectin11a) were identified (supplementary data 1 & 2). The proteins identified in conditioned media obtained either from BMSCs, 3 days injured spinal cord (SCI) or non-injured spinal cord (Control) were compared after shot-gun analyses using scaffold proteome software 4.06. In addition a spectral counting and normalization based on total ion current was done in the three samples. The TOP3 in TIC was used for label-free quantification (Figure 4B). Data clearly reflected that BMSCs produce growth factors (CTGF, PDGF, PGF, TGFβ, IGF binding protein 7, BMP 1, C1q/TNF5), neural migration factors (NOV, neurofascin, neuropilin 2, neuroplastin,) and immunomodulators (arginase 1, ST2, galectins, metalloproteinase inhibitors (supplementary data 1&2)) and chemoattractant factors (CLEC11a) (Table 2). These differences showed that BMSCs produce both factors involved in microglia chemoattraction (CCL2) and factors involved in inflammatory regulation (arginase 1, ST2, galectins), whereas SCI-CM contain chemokines (CCL2, CXCL2, MIF) and neurotrophic

factors (GAP-43 and neurotrimin). According to Riffeld and collaborators⁵⁰, BMSCs have been shown to secrete various growth factors, including brain-derived neurotrophic factor (BDNF), glial-derived neurotrophic factor (GDNF), vascular endothelial growth factor (VEGF), fibroblast growth factor 2 (FGF-2), nerve growth factor (NGF) and neurotrophin-3. Our proteomic data confirm and complete previous work. Thus, based on the secretion profile, BMSCs-CM. may contribute to neuroprotection in a direct manner by rescuing neural cells and switching the microglial cells/macrophages to a M2 polarization³³.

Modulation of stimulated microglia (BV2, PM) using BMSCs-CM. Attenuation of microglia recruitment. Proteins released from the central lesion segment of injured and control spinal cords were analyzed on microglial BV2 cells or PM using Boyden chambers in the presence or absence of BMSCs-CM. Activation of BV2 cells and PM was measured and quantified by counting the number of Hoechst labeled cells attached to the Boyden membrane. More than a 7-fold increase of attached BV2 cells (35.2 ± 2.2) and



Table 2 | Immune and neurotrophic factors identified by shot-gun analyses from MSCs and SCI. Sequence coverage are established from shot gun analyses using LTQ-Orbitrap XL mass spectrometer and based on protein identification with a protein threshold of 99% (FDR 0.1%) and peptide threshold of 97% (0.1%) and contained at least 2 identified peptides (see Supplementary data 2)

ProteinFamily	Protein Name	Accession Number	SequenceCoverage	
Chemokines	CCL3	P50229	35%	
	CXCL2	P303484	49%	
	C1qc	P31722	16%	
	cC1qR	O35796	20%	
	MIF	P30904	36%	
Immune Regulators	ST2(ILRL1)	Q62611	24%	
	CLEC11a	O88201	20%	
	Gal 1	P11762	64%	
	Gal 3	P08699	9%	
	Arginase 1	P07824	9%	
CD	CD9	P40241	15%	
	CD14	Q63691	17%	
	CD59	P27274	30%	
GrowthFactors	CTGF	Q9R1E9	56%	
	BDNF	P23363	12%	
	TGFb1	P17246	16%	
	TGF b2	Q07257-2	18%	
	TGF b3	Q07258	12%	
	PGF	Q63434	22%	
	PDGF	Q5RJP7	19%	
	IGFbp7	F1M9B2	54%	
	BMP1	F1M798	4%	
	Epdr1	Q5XII0	19%	
	C1q/TNF5	Q5FVH0	28%	
	Neurotrophic Factors	Neurotrimin	Q62718	16%
		GAP43	P07936	63%
		Calumenin	O35783	36%
Neural Migration Factor	Neuroplastin	P97546	10%	
	Neuropilin 2	O35276	3.7%	
	Neuromodulin	P07936	63%	
	NOV	Q9QZQ5	30%	
Metalloproteinase	TIMP-1	P30120	71%	
	TIMP-2	P30121	54%	
Osteogenic Factors	Osteoglycin	D3VZB7	13%	
	Osteopontin	PO8721	21%	
	Périostin	D3ZAF5	66%	
Differentiating factors	SPARC	P16975	60%	
	FAM3C	Q10F4	9%	
	Cornifin	Q63532	11%	

8.5-fold increase of PM (42.5 ± 1.9) attached cells were obtained with the conditioned media from SCI (SCI-CM) compared to those from the control spinal cord SC-CM ($5.2-7.5 \pm 1.9$), BMSCs-CM ($5.5-6.2 \pm 2.4$) or DMEM ($3.2-4.1 \pm 1.1$) (Figures 5A, A', B-D). The simultaneous application of BMSCs-CM and SCI-CM (BMSCs-CM + SCI-CM), significantly diminished BV2 cells (31.6 ± 1.3 , * $P < 0.1$) and PM microglial (30.8 ± 1.9 , *** $P < 0.001$) mobility (Figures 5A, 5C) in comparison to SCI-CM alone (Figures 5A, 5B). Whereas, application of BMSCs-CM or DMEM had low influence on BV2 cells and PM migration (Figures 5A, 5D). These data confirmed the involvement of BMSCs in immune response modulation of microglial cells once activated.

Stimulation of microglia: morphological changes and viability. Chemotaxis assays confirmed increased numbers of migrated microglia with significantly enlarged nuclei after SCI-CM treatment (Figure 5B) compared with microglia nuclei after DMEM treatment (Figure 5A'). Our next aim was therefore to investigate the morphological changes in stimulated microglia in a time-dependent manner. We compared the effects of: i) SCI-CM, ii) SCI-CM + BMSCs-CM and iii) BMSCs-CM administration on BV2 cell morphology from 3 h to 24 h (Figures 6 A-E). The first significant changes were observed in the presence of SCI-CM, where most BV2 cells revealed a prolonged bipolar-like or stellate-

like shape (Figures 6A, 7A). Addition of SCI-CM + BMSCs-CM or BMSCs-CM alone stimulated a lower number of BV2 cells, the latter changing cells from round to oval or multipolar cells (Figures 6B, 6C). After further incubation (24 h) significant morphological variability in BV2 cells begins to show, corresponding to different conditioned media exposure. The most significant impact followed after SCI-CM incubation, when the majority of BV2 cells revealed multipolar or prolonged cell shapes with hypertrophied cell bodies and ramified morphology (Figures 6D, 7A'). A similar pattern was seen in SCI-CM + BMSCs-CM, but only in a small number of cells (Figure 6E). In the case of BMSCs-CM, round to oval cells dominated, apart from a few that had a differentiated pattern, similar as at 3 hr (Figure 6C). After 48 h incubation, activated BV2 cells with elongated morphology remained only after SCI-CM stimulation (Figure 7A''). We could follow the time-dependent (3 h-48 h) morphological changes in BV2 cells after SCI-CM stimulation (Figures 7 A-A''). The percentages of ramified (multipolar or spindle-shaped) BV2 cells stimulated with SCI-CM, SCI + BMSCs/CM, BMSCs-CM and SC-CM after 3 h were respectively: 27.4 ± 3.6 , 17.6 ± 2.2 , 21.78 ± 3.1 , 5.2 ± 1.4 ; at 18 h: 49.77 ± 2.7 , 42.9 ± 1.4 , 5 ± 1.8 , 6.7 ± 1.5 ; at 24 h: 67.14 ± 3.8 , 6.01 ± 1.8 , 6.2 ± 0.9 , 7.1 ± 1.1 ; and at 48 h: 64.2 ± 4.9 , 5 ± 1.1 , 5.6 ± 0.8 , 6.4 ± 0.9 (Figure 7B).

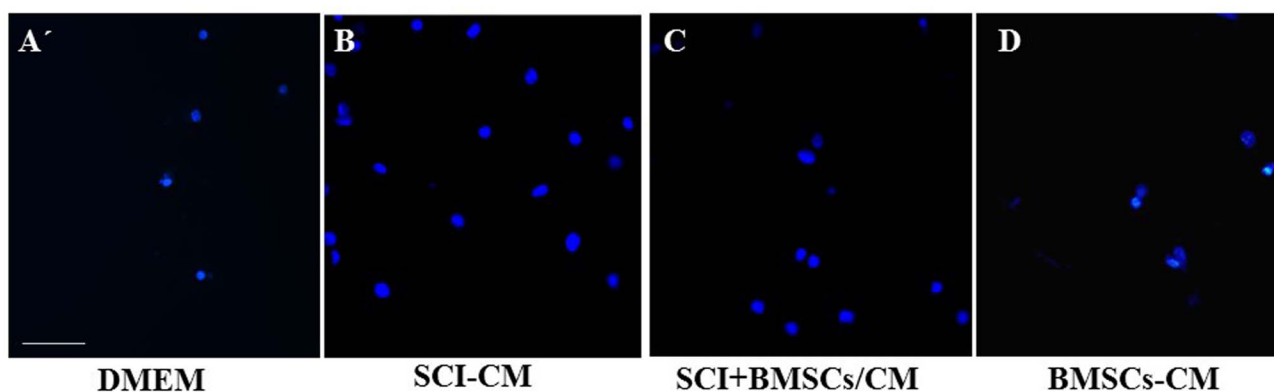
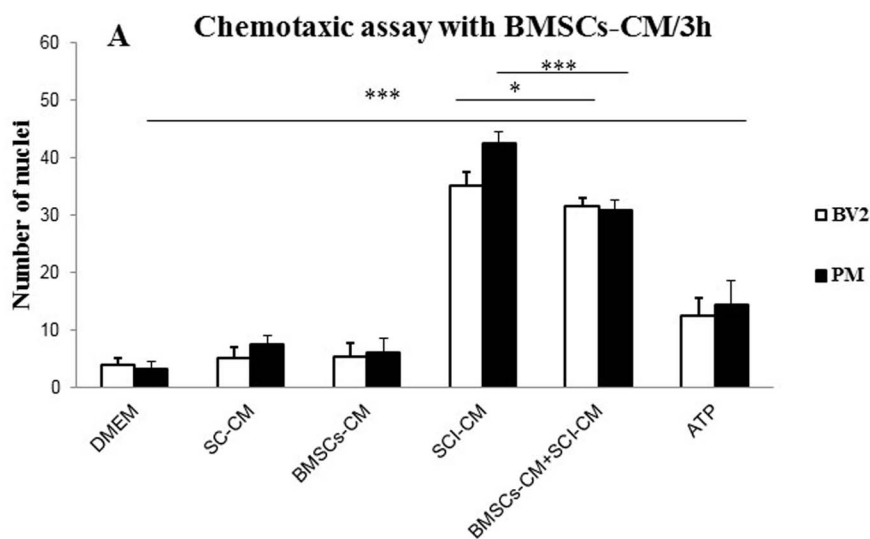


Figure 5 | BMSCs-CM inhibition of BV2 cell and PM chemotaxis in the trans-well assay. Note that the high number of migrated BV2 cells and PM induced by SCI-CM (lesion site) (A, B) was attenuated when they were co-incubated with BMSCs conditioned media (SCI+BMSCs/CM BMSCs/CM) (A, C), as quantified by the number of Hoechst labeled cells. Incubation of BV2 cells and PM with BMSCs-CM or DMEM had low influence on their migration (A, D). Data are represented as mean \pm SEM. * $P < 0.01$, *** $P < 0.001$, one-way ANOVA followed by Tukey-Kramer test. Scale bars A' = 100 μm ; B, C, D = 50 μm .

To further compare the morphological changes in stimulated BV2 cells (Figures 8A–C) and PM (Figures 8E–G'), in each conditioned group we used Iba1 antibody, confirming the positivity in both control and stimulated populations after 24 h. The PM treated with SCI-CM demonstrated a significant shift from resting cells with small soma and ramified, spread-out, thin and long processes, (Figure 8E) to activated forms characterized by marked cellular hypertrophy and thick, short and radially-projecting processes (Figures 8 F'–F''). Similarly, PM incubated in BMSCs-CM and SC-CM showed many hypertrophied microglia with richly-ramified processes (Figures 8 G–G'). Morphological changes were further confirmed using quantification analysis of Iba1+ microglia response (Figure 7), also revealing morphological disparities between BV2 and PM microglia activation. While BV2 cells changed from oval to multipolar or spindle-like forms (Figures 7A,B), a large number of PM transformed from small, less-ramified cells to oval-amoeboid shaped Iba1+ microglia with hypertrophied soma and retracted gross processes with rich branching (Figures 7C–C''). However, in all experimental groups we could detect common intermediate forms of microglia. We therefore quantified the density of all morphological forms of Iba1+ microglia (Figures 7C'–C'') that occurred after treatment with DMEM and different combinations of CM. Thus, the PM with thick processes (Figure 7C'') or enlarged bipolar or multipolar BV2 cells (Figure 7C'') occupied more space (expressed in pixel values within identical fields) after SCI-CM (Figure 7C) than after

the other CM treatments. To confirm morphological characteristics of microglia after different CM treatment we have defined five following parameters: soma diameter, soma area, process diameter and length, and process length in relation to the soma diameter (Supplementary data 3).

The viability test with Propidium iodide (PI) and Annexin-V (AV) confirmed the time-dependent cytotoxic effect of BMSCs-CM when added in combination with SCI-CM ($44 \pm 7\%$ of PI+ and $12 \pm 2.5\%$ of AV+ BV2 cells; $21 \pm 4\%$ of PI+ and $10.1 \pm 3.9\%$ of AV+ PM) (Figures 9B, E), but not alone ($18 \pm 6\%$ of PI+ and $3 \pm 2.3\%$ AV+ BV2 cells; $12.3 \pm 4.4\%$ of PI+ and $5 \pm 2.1\%$ AV+ BV2 cells) (Figure 9C), whereas SCI-CM ($14 \pm 7\%$ of PI+ and $7 \pm 1.9\%$ of AV+ BV2 cells; $12.7 \pm 8.6\%$ of PI+ and $8 \pm 2.9\%$ of AV+ PM) (Figures 9A, D) or DMEM ($11.2 \pm 4.4\%$ of PI+ and $8.6 \pm 1.5\%$ of AV+ BV2 cells; $14.1 \pm 4.2\%$ of PI+ and $5.2 \pm 2.7\%$ of AV+ PM) had a low influence on BV2 cell viability, as revealed by PI+ and AV+ cells. PI is a membrane-impairment dye that is generally excluded from viable cells, while phosphatidylserine cell surface membrane exposure is typical for cell apoptosis and could be detected by its binding to the protein Annexin-V. Thus, in our case it is most probably that PI labeling discriminated necrotic cells PI+/AV– (Figure 9F) that had lost membrane integrity, while Annexin-V and PI labeling distinguished late apoptotic cells (PI+/AV+) (Figure 9G). Only occasional Annexin-V (AV+/PI– < 2%) labeled BV2 and PM cells were detected when cultured with SCI-CM or BMSCs-CM.

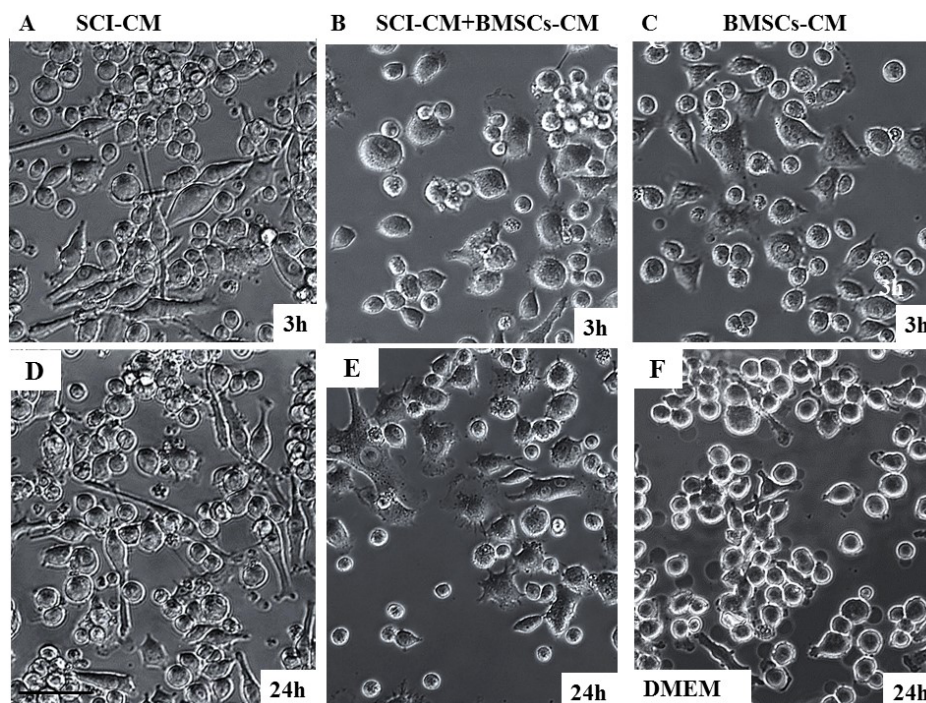


Figure 6 | Representative images depicting morphological changes of BV2 microglial cells incubated with SCI-CM, SCI-CM + BMSCs-CM or BMSCs-CM from 3 h (A–C) to 24 h (D–E). Note the prolonged, bipolar-like morphology of BV2 cells after SCI-CM (A), while after SCI-CM + BMSCs-CM (B, E) or BMSCs-CM (C) incubation only few cells changed their shape into oval or stellate types during 3 h treatment. Most significant morphological changes of BV2 cells were observed after incubation with SCI-CM and SCI-CM + BMSCs-CM at 24 h, when BV2 cells revealed multipolar or prolonged cell shapes with hypertrophied cell bodies and ramified morphology (D,E), while treatment with BMSCs-CM resemble the same pattern as 3 h (C). BV2 cells incubated with DMEM during 24 h revealed oval shape, but occasional ramified cells occurred (F) Scale bars A–F = 50 μm .

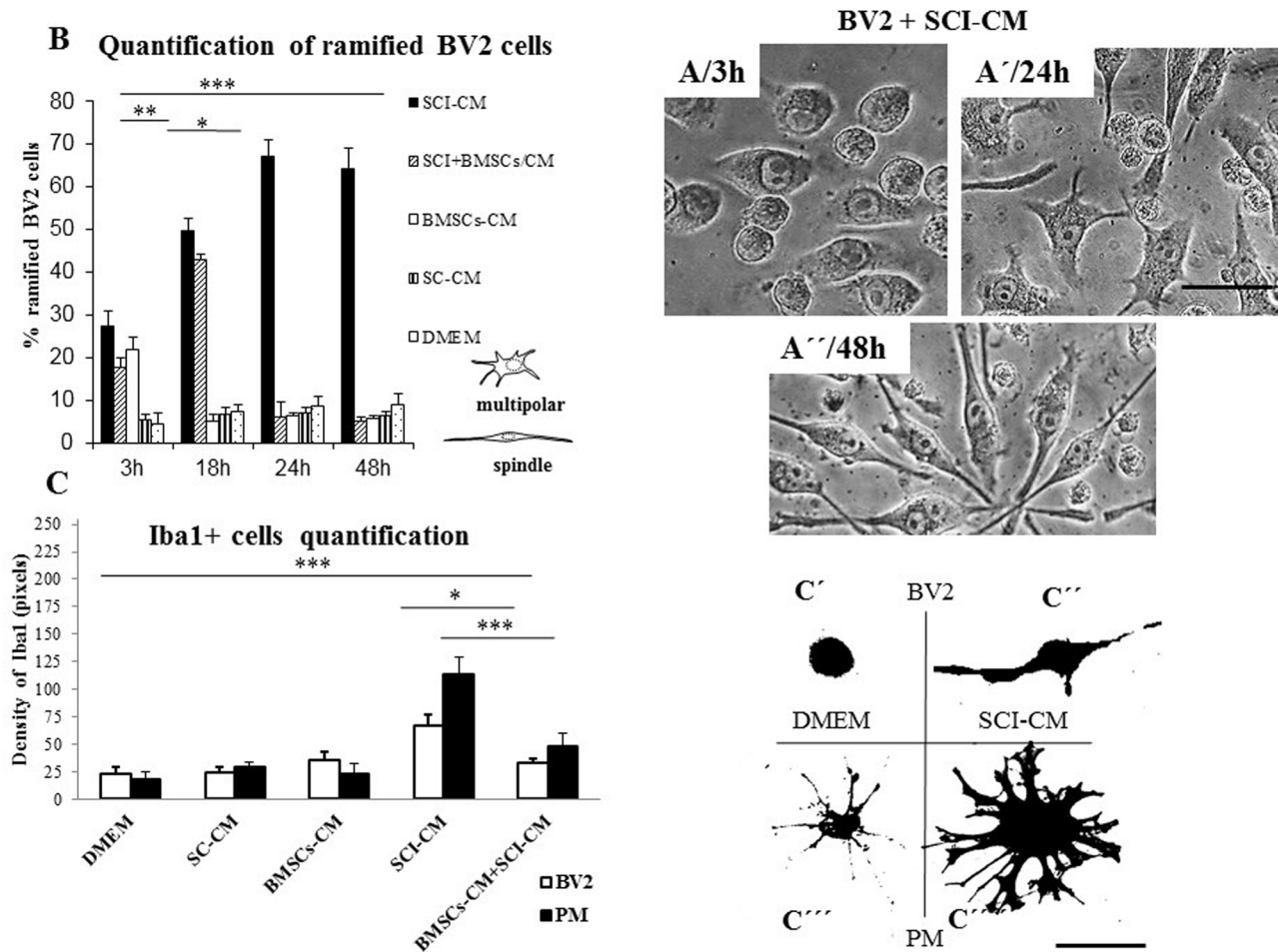
Inhibition of NO with BMSCs-CM. BV2 cells and PM robustly increased NO release into the culture media after SCI-CM treatment. Peak release of $9.98 \pm 0.17 \mu\text{M}$ ($p < 0.001$) NO from BV2 cells and $8.5 \pm 0.27 \mu\text{M}$ ($p < 0.001$) NO from PM at 24 h was significantly decreased in PM to $4.86 \pm 0.13 \mu\text{M}$ ($p < 0.001$) after BMSCs-CM-SCI-CM treatment, but not in BV2 cells, which released $9.6 \pm 0.2 \mu\text{M}$ ($p < 0.001$) NO. DMEM, SCI-CM and BMSCs-CM induced low levels of NO in BV2 cells and PM respectively (0.91 ± 0.2 , 1.82 ± 0.06 , $1.41 \pm 0.3 \mu\text{M}$ and 0.92 ± 0.12 , 2.14 ± 0.21 , $0.69 \pm 0.1 \mu\text{M}$) (Figure 10).

Discussion

The early phase of cellular inflammation is comprised principally of neutrophils (peaking 1 day post-injury), macrophages/microglia (peaking 7 days post-injury) and T cells (peaking 9 days post-injury)⁵¹. This acute phase is decomposed by the production of pro-inflammatory mediators produced by resting microglia, and neutrophils (0 to 1 days), which is correlated to necrosis, followed by apoptosis processes (peaking 3 days post-injury) then demyelination (peaking 7 days post-injury). Anti-inflammatory cytokines are produced rapidly and peaking at 3 days. The late phase of cellular inflammation was detected after 14 days post-injury, peaked after 60 days post-injury and remained detectable throughout 180 days post-injury for macrophages/activated microglial cells and neutrophils⁵¹. Understanding this role is complicated by the observations that while some aspects of post-traumatic inflammation in the spinal cord are clearly detrimental, other delayed inflammatory aspects may facilitate repair mechanisms⁵². For example, the inflammatory response is critical for the clearance of cellular debris, which can prevent the regeneration of surviving neurons. However, over-activation of the inflammatory response can damage healthy tissue and exacerbate the injury^{53,54}. Thus in this context, a therapeutic approach that has to

be designed needs to be focused more on the secondary injury process where the chronic phase of inflammation occurs and needs to be controlled. Previously, it was proposed that, BMSCs could be potentially transplanted during both acute and chronic phases of SCI, because they modify the inflammatory response in the acute setting and may reduce the inhibitory effects of scar tissue in the subacute/chronic phase to provide a permissive environment for axonal extension. However, recently the main attention is focused on their delivery during acute inflammatory processes. Pre-clinical studies showed that acute transplantation of human BMSCs after SCI in rats increases axonal growth and improved locomotor function⁵⁵. Similarly, in clinical trials using BMSCs (alone or in combination with granulocyte-macrophage colony stimulating factor) with over 10 weeks of follow-up moderate functional recovery was noticed in acute and subacute SCI groups^{56–58}, while no improvement was detected in chronically treated patients⁵⁹. On the other hand some experimental studies showed that chronically injured spinal cord axons can regenerate through the gliotic scar only in the presence of local growth-stimulating factors. For example, genetically modified BMSCs secreting neurotrophin-3 (NT-3) injected into the central lesion site were able to induce penetration of modest number of axons through the scar tissue⁶⁰. In general, BMSCs represent a safe, feasible, and reliable method of cellular transplantation for SCI with no fear of tumor formation.

In this context, we focus our attention on factors that can be produced by BMSCs. BMSCs factors are known to ameliorate disease in various animal models of neuroinflammation could control *in vitro* SCI-CM-induced BV2 chemotaxis^{29,58}, NO release, as well as morphological changes in activated microglia. Similarly to microglia, BMSCs are attracted towards areas of tissue damage, indicating that microglia may primarily serve as a homing signal⁶¹. Here we show that BMSCs-soluble factors significantly down-regulated SCI-CM-induced BV2 and PM migration, which confirms their modulatory



properties^{58,60}. Because the chemotactic response was associated with enlarged nuclei as well, we also examined temporal changes in BV2 cell morphology and PM. Our results provide further evidence of a link between migratory response and morphological changes in microglial cells upon exposure to different conditioned media. SCI-CM (lesion site) served as a strong trigger for microglia migration and also caused BV2 cell transformation from round-shaped, semi-adherent cell lines into adherent, stellate-like or long bipolar cells with filopodia production⁶¹, revealing typical inflammatory response during the entire time period. However, BMSCs that clearly attenuated microglia migration showed time-dependent cytotoxic effects on BV2 cells. A similar study has confirmed that BMSCs inhibit the proliferation of lipopolysaccharide (LPS)-activated BV2 microglia by various effects, which may correlate with our cytotoxic findings⁵⁸. It is well known that BMSCs and microglia cells modulate SCI inflammation and regeneration processes.

The proteomic analysis of BMSCs-CM clearly shows that these cells can produce both immune modulator, neurogenic factors and osteogenic factors as well as differentiating molecules. In fact, using a shot-gun proteomic approach we identified several immune modulators (arginase 1, ST2, galectins) and chemoattractant factors (CLEC11a) known to act towards microglia⁶². The different

immune-modulators present in BMSCs-CM *i.e.* arginase, ST2, CCL2 have the ability to shift the polarization of the microglial cells into M2 phenotype which is neuroprotective. Moreover, PDGF, PGF and TGF β are known to increase survival and proliferation of oligodendrocytes⁶³. BDNF also increases oligodendrocyte proliferation and BMP 1 signaling mediates astrocyte differentiation of oligodendrocyte progenitor cells⁶⁴. SPARC has been shown to modulate several growth factor signaling cascades (*i.e.*, VEGF (vascular endothelial growth factor), PDGF (platelet-derived growth factor), FGF2 (fibroblast growth factor-2), and TGF (transforming growth factor beta)) and can regulate integrin-mediated adhesion^{65,66}. The matricellular protein family CCN, which stands for CYR61/CTGF/NOV are suggested to be important players in the modulation of inflammatory cytokines and chemokines production⁶⁷. CCN proteins act alone or in concert with their specific partners in order to regulate the production of cytokines and chemokines. CCN2/CTGF is currently the only CCN family member in which expression has been demonstrated *in vivo* in CNS astrocytes⁶⁸. CCN2 has been demonstrated to bind to TrkA (neurotrophic tyrosine kinase receptor type 1) and p75NTR (p75 neurotrophin receptor), receptors which transduce neurotrophin signals⁶⁹. Similarly, the C1q/TNF-related protein (CTRP) family are also important immune modula-

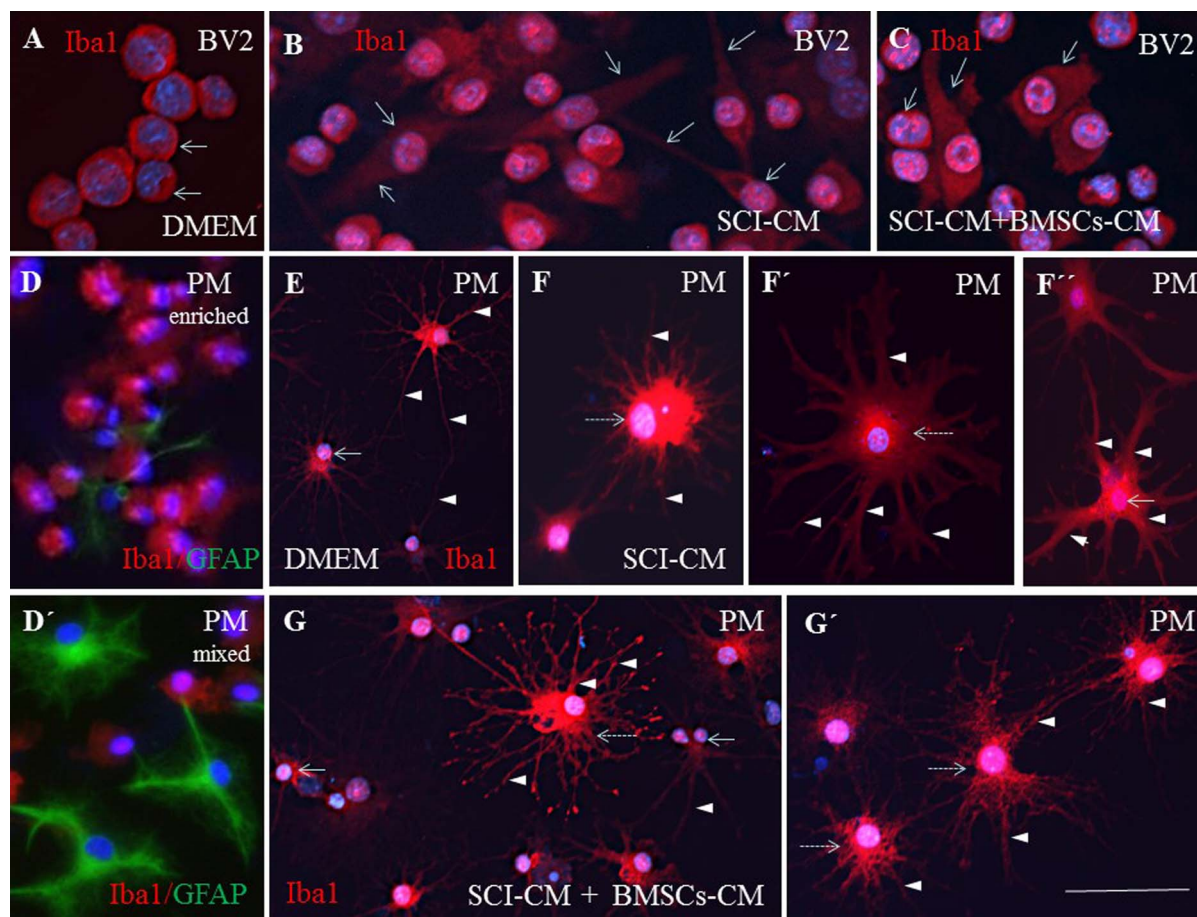


Figure 8 | Immunohistochemistry of Iba1 + BV2 cells (A–C) and PM (E–G′) corresponding to different conditioned media exposure. The round BV2 cells treated with DMEM (A, arrows) changed after SCI-CM exposure to bipolar cells with thin processes (B, arrows), while after BMSCs-CM + SCI-CM cells were round or with partial elongated cell body, but the processes had disappeared (C, arrows). The PM treated with SCI-CM demonstrated a significant shift from resting microglia with a small soma and ramified spread out thin and long processes (E, arrowheads), to activated forms characterized by marked cellular and nuclear hypertrophy (F, dashed arrow) with retracted and thickened radially projecting processes (F′–F′′, arrowheads). Note, following BMSCs-CM + SCI-CM incubation, many hypertrophied microglia (G,G′, intermitted arrows) with ramified processes retained (G–G′), while rich fine branches, closest to the cell soma, began to thicken. Evaluation of PM purity with Iba1 and GFAP antibodies (D, D′). Scale bars A–G′ = 50 μm.

tors⁷⁰. The presence of ST2, a receptor of IL-33, confirms previous data showing that IL-33 is known to induce proliferation of microglia and enhances the production of pro-inflammatory cytokines, such as IL-1 β and TNF α , as well as the anti-inflammatory cytokine IL-10⁶². Galectins were recently shown to be produced by BMSCs with high immunosuppressive activity as well as tissue-inhibitor metalloproteinases^{64–66}. Chang et al⁷⁰ have shown that BMSCs release TIMP-1, which would exert an immune modulatory effect on BV2 LPS-activated microglial cells. The authors have shown that in co-culture between BMSCs and BV2 after LPS activation, TIMP-1 secretion downregulates MMP-9 expression in microglial cells. At the same time, BMSCs produce growth and neurotrophic factors⁷⁰. The CLEC11A, also known as stem cell growth factor^{64,67}, act in conjunction with insulin-like growth-factor binding protein 10^{65,66}, transforming growth factor beta-1⁷¹, and SPARC^{69,70}. Some recent data show moreover that SPARC seems to act as a novel regulator of microglial proliferation, and may play an important role in differently regulating the gray and white matter microglial responses to CNS lesion⁴⁵. Concerning the osteogenic factors produced by BMSCs, these molecules act like osteopontin towards microglial cells in the same way as cytokines, and stimulate their proliferation. Tambuyzer et al⁷¹ have demonstrated that osteopontin shifts

microglia to an alternative functional profile more suited to the immune-balanced microenvironment of the CNS.

Here we confirm that SCI-CM triggers morphological changes in microglia and production of NO inflammatory mediators, while incubation with BMSCs-CM leads to partial attenuation of these processes. The use of morphological change as a readout of microglia activation was supported also by our previous experiment comparing the number of microglia processes to the expression level of P2Y12 (a metabotropic purinergic receptor) under activating conditions⁷¹. In this study the authors clearly demonstrate a positive correlation between decreased process number (amoeboid morphology) and P2Y12 down-regulation. The present data are consistent with these findings and provide fundamental information on the morphological features of BV2 cells and PM upon SCI-CM activation. Based on Iba1 expression or light microscopy image analysis, we present clear morphological differences between microglia cell lines and primary microglia in terms of soma shape, size and extending processes evaluated following induced activation and BMSCs-CM treatment. Unlike other automated or manual quantification methods of microglia morphology based on various parameters^{72,73}, we have used simple ImageJ software to quantify the 2D area occupied by each Iba1 positive cell. Thus, hypertrophied microglia and their extended processes

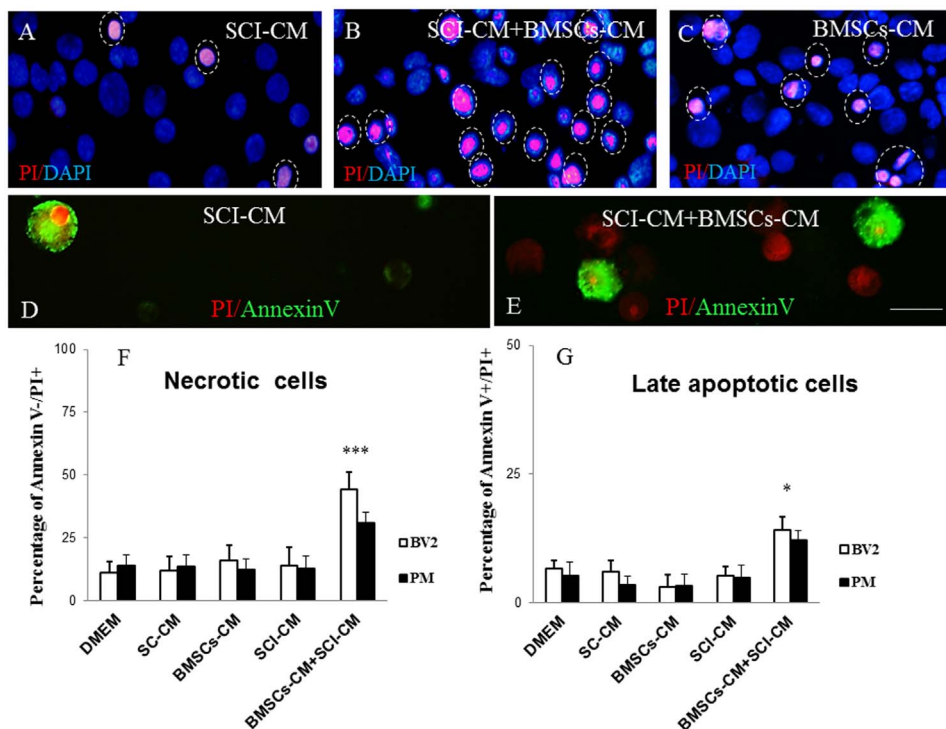


Figure 9 | PI and Annexin V (AV) labeling of BV2 cells (D, E) counterstained with Dapi (A–C). Note, the highest number of late apoptotic or necrotic (PI+/AV+, PI+/AV–) BV2 cells exposed to SCI + BMSCs/CM (B, E) when compared to incubation with SCI-CM with occasional late apoptotic (PI+/AV+) and early apoptotic cells (PI–/AV+) (A,D) or BMSCs-CM (C) (purple, indicated by dashed circles) at 48 h. PI/red, Annexin V/green labeled BV2 cells (D,E). Bar graph reporting the percentage of necrotic and late apoptotic microglia cells after different CM treatment after 48h in vitro incubation. Data are represented as mean \pm SEM. * $P < 0.1$ ** $P < 0.01$, *** $P < 0.001$, one-way ANOVA followed by Tukey-Kramer test (F,G). Scale bars A–E = 20 μ m.

Nitrite release inhibition with BMSCs-CM/24h

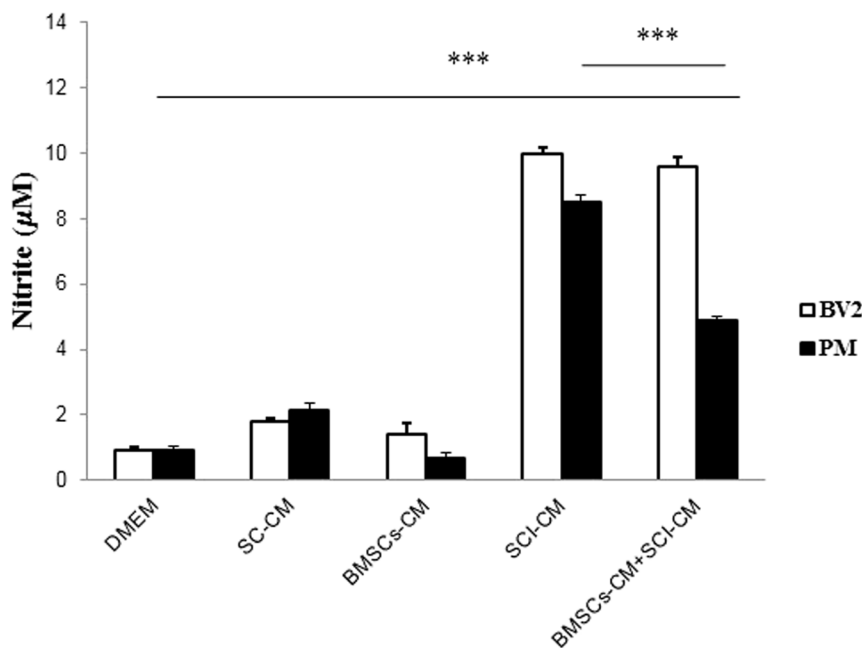


Figure 10 | NO release from BV2 (A) cells and PM (B) into the culture media after different conditioned media exposure after 24 h. Note, significant increase of NO in BV2 cells and PM after SCI-CM when compared to DMEM, SC-CM, and BMSCs-CM incubation, while significant NO decrease in PM, not in BV2 cells occurred after BMSCs-CM + SCI-CM treatment. Data are represented as mean μ M \pm SEM. * $P < 0.01$, *** $P < 0.001$, one-way ANOVA followed by Tukey-Kramer test.



that fill larger micro-territory than the resting type proved to be effective enough as a method of capturing microglia in activated state.

Furthermore, we demonstrate that factors released from BMSCs-CM significantly decreased NO levels in SCI-CM treated PM cultures. Although some studies have indicated that MSCs increase NO when exposed to soluble factors from LPS-activated microglia or when co-cultured with stimulated T lymphocytes, we document the opposite effect^{10,74}. The inhibition of NO levels in activated PM was most likely attributed to the molecule composition of cell-free BMSCs-conditioned medium which unlike mesenchymal cells is unable to produce additional NO. However, the levels of NO were significantly higher in both stimulated microglia cells treated with BMSCs. That may be caused by factors released from SCI-CM, but this needs to be confirmed in further experiments.

Taken together, our preliminary proteomic data obtained with BMSCs-CM confirm the high modulatory potential of these cells on inflammation, microglia polarization and neurite outgrowth activity and could be used as a therapeutic cocktail to prevent the chronic phase of inflammation.

- Luria, E. A., Panasyuk, A. F. & Friedenstein, A. Y. Fibroblast colony formation from monolayer cultures of blood cells. *Transfusion* **11**, 345–349 (1971).
- Uccelli, A., Moretta, L. & Pistoia, V. Mesenchymal stem cells in health and disease. *Nat Rev Immunol* **8**, 726–736 (2008).
- da Silva Meirelles, L., Chagastelles, P. C. & Nardi, N. B. Mesenchymal stem cells reside in virtually all post-natal organs and tissues. *J Cell Sci* **119**, 2204–2213 (2006).
- Kern, S., Eichler, H., Stoeve, J., Kluter, H. & Bieback, K. Comparative analysis of mesenchymal stem cells from bone marrow, umbilical cord blood, or adipose tissue. *Stem Cells* **24**, 1294–1301 (2006).
- Zuk, P. A. *et al.* Human adipose tissue is a source of multipotent stem cells. *Mol Biol Cell* **13**, 4279–4295 (2002).
- Lei, J., Cheng, J., Li, Y., Li, S. & Zhang, L. CD80, but not CD86, express on cultured murine keratinocyte stem cells. *Transplant Proc* **37**, 289–291 (2005).
- Gotherstrom, C. *et al.* Difference in gene expression between human fetal liver and adult bone marrow mesenchymal stem cells. *Haematol.* **90**, 1017–1026 (2005).
- Tani, H., Morris, R. J. & Kaur, P. Enrichment for murine keratinocyte stem cells based on cell surface phenotype. *Proc Natl Acad Sci U S A* **97**, 10960–10965 (2000).
- Karaoz, E. *et al.* Pancreatic islet derived stem cells can express co-stimulatory molecules of antigen-presenting cells. *Transplant Proc* **42**, 3663–3670 (2010).
- Corcione, A. *et al.* Human mesenchymal stem cells modulate B-cell functions. *Blood* **107**, 367–372 (2006).
- Krampera, M. *et al.* Bone marrow mesenchymal stem cells inhibit the response of naive and memory antigen-specific T cells to their cognate peptide. *Blood* **101**, 3722–3729 (2003).
- Spaggiari, G. M., Capobianco, A., Becchetti, S., Mingari, M. C. & Moretta, L. Mesenchymal stem cell-natural killer cell interactions: evidence that activated NK cells are capable of killing MSCs, whereas MSCs can inhibit IL-2-induced NK-cell proliferation. *Blood* **107**, 1484–1490 (2006).
- Jiang, X. X. *et al.* Human mesenchymal stem cells inhibit differentiation and function of monocyte-derived dendritic cells. *Blood* **105**, 4120–4126 (2005).
- Raffaghello, L. *et al.* Human mesenchymal stem cells inhibit neutrophil apoptosis: a model for neutrophil preservation in the bone marrow niche. *Stem Cells* **26**, 151–162 (2008).
- Chen, J. *et al.* Intravenous bone marrow stromal cell therapy reduces apoptosis and promotes endogenous cell proliferation after stroke in female rat. *J Neurosci Res* **73**, 778–786 (2003).
- Park, H. J., Lee, P. H., Bang, O. Y., Lee, G. & Ahn, Y. H. Mesenchymal stem cells therapy exerts neuroprotection in a progressive animal model of Parkinson's disease. *J Neurochem* **107**, 141–151 (2008).
- Wu, D. C. *et al.* Blockade of microglial activation is neuroprotective in the 1-methyl-4-phenyl-1,2,3,6-tetrahydropyridine mouse model of Parkinson disease. *J Neurosci* **22**, 1763–1771 (2002).
- van Velthoven, C. T., Kavelaars, A., van Bel, F. & Heijnen, C. J. Mesenchymal stem cell treatment after neonatal hypoxic-ischemic brain injury improves behavioral outcome and induces neuronal and oligodendrocyte regeneration. *Brain Behav Immun* **24**, 387–393 (2010).
- Tator, C. H. Update on the pathophysiology and pathology of acute spinal cord injury. *Brain Pathol* **5**, 407–413 (1995).
- Schwab, M. E. & Bartholdi, D. Degeneration and regeneration of axons in the lesioned spinal cord. *Physiological Rev* **76**, 319–370 (1996).
- Schwartz, M., Moalem, G., Leibowitz-Amit, R. & Cohen, I. R. Innate and adaptive immune responses can be beneficial for CNS repair. *Trends in Neurosci.* **22**, 295–299 (1999).
- Schwab, J. M., Zhang, Y., Kopp, M. A., Brommer, B. & Popovich, P. G. The paradox of chronic neuroinflammation, systemic immune suppression, autoimmunity after traumatic chronic spinal cord injury. *Exp Neurol* **258C**, 121–129 (2014).
- Rolls, A., Shechter, R. & Schwartz, M. The bright side of the glial scar in CNS repair. *Nat Rev Neurosci* **10**, 235–241 (2009).
- Lalancette-Hebert, M., Gowing, G., Simard, A., Weng, Y. C. & Kriz, J. Selective ablation of proliferating microglial cells exacerbates ischemic injury in the brain. *J Neurosci* **27**, 2596–2605 (2007).
- Ransohoff, R. M., Liu, L. & Cardona, A. E. Chemokines and chemokine receptors: multipurpose players in neuroinflammation. *Int Rev Neurobiol* **82**, 187–204 (2007).
- Aloisi, F. Immune function of microglia. *Glia* **36**, 165–179 (2001).
- Block, M. L. & Hong, J. S. Microglia and inflammation-mediated neurodegeneration: multiple triggers with a common mechanism. *Prog Neurobiol* **76**, 77–98 (2005).
- Ransohoff, R. M. & Cardona, A. E. The myeloid cells of the central nervous system parenchyma. *Nature* **468**, 253–262 (2010).
- Zhou, C. *et al.* Effects of human marrow stromal cells on activation of microglial cells and production of inflammatory factors induced by lipopolysaccharide. *Brain Res* **1269**, 23–30 (2009).
- Lee, H. J. *et al.* Human umbilical cord blood-derived mesenchymal stem cells improve neuropathology and cognitive impairment in an Alzheimer's disease mouse model through modulation of neuroinflammation. *Neurobiol Aging* **33**, 588–602 (2012).
- Kim, Y. J. *et al.* Neuroprotective effects of human mesenchymal stem cells on dopaminergic neurons through anti-inflammatory action. *Glia* **57**, 13–23 (2009).
- Yan, K. *et al.* Bone marrow-derived mesenchymal stem cells maintain the resting phenotype of microglia and inhibit microglial activation. *PLoS One* **8**, e84116 (2013).
- Cizkova, D. *et al.* Alterations of protein composition along the rostral-caudal axis after spinal cord injury: proteomic, in vitro and in vivo analyses. *Front Cell Neurosci* **8**, 105 (2014).
- Filip, S. *et al.* Splenectomy influences homing of transplanted stem cells in bone marrow-ablated mice. *Stem Cells Dev* **21**, 702–709 (2012).
- Cizkova, D. *et al.* Induction of mesenchymal stem cells leads to HSP72 synthesis and higher resistance to oxidative stress. *Neurochem Res* **31**, 1011–1020 (2006).
- Cizkova, D., Rosocha, J., Vanicky, I., Jergova, S. & Cizek, M. Transplants of human mesenchymal stem cells improve functional recovery after spinal cord injury in the rat. *Cell Mol Neurobiol* **26**, 1167–1180 (2006).
- Ritfeld, G. J. *et al.* Bone marrow stromal cell-mediated tissue sparing enhances functional repair after spinal cord contusion in adult rats. *Cell Transplant* **21**, 1561–1575 (2012).
- Nandoe Tewarie, R. D., Hurtado, A., Bartels, R. H., Grotenhuis, J. A. & Oudega, M. A clinical perspective of spinal cord injury. *NeuroRehabilitation* **27**, 129–139 (2010).
- Nandoe Tewarie, R. S., Hurtado, A., Bartels, R. H., Grotenhuis, A. & Oudega, M. Stem cell-based therapies for spinal cord injury. *J Spinal Cord Med* **32**, 105–114 (2009).
- Nandoe Tewarie, R. D., Hurtado, A., Levi, A. D., Grotenhuis, J. A. & Oudega, M. Bone marrow stromal cells for repair of the spinal cord: towards clinical application. *Cell Transplant* **15**, 563–577 (2006).
- Cizkova, D. *et al.* Role of transplanted bone marrow cells in response to skeletal muscle injury. *Folia Biol (Praha)* **57**, 232–241 (2011).
- Cizkova, D. *et al.* Repetitive intrathecal catheter delivery of bone marrow mesenchymal stromal cells improves functional recovery in a rat model of contusive spinal cord injury. *J Neurotrauma* **28**, 1951–1961 (2011).
- Vanicky, I., Urdzikova, L., Saganova, K., Cizkova, D. & Galik, J. A simple and reproducible model of spinal cord injury induced by epidural balloon inflation in the rat. *J Neurotrauma* **18**, 1399–1407 (2001).
- Giulian, D. & Baker, T. J. Characterization of ameboid microglia isolated from developing mammalian brain. *J Neurosci* **6**, 2163–2178 (1986).
- Bocchini, V. *et al.* An immortalized cell line expresses properties of activated microglial cells. *Journal of Neurosci. Res.* **31**, 616–621 (1992).
- Smith, S. M. *et al.* An enhanced miniaturized assay for antimicrobial prospecting. *J Microbiol Methods* **72**, 103–106 (2008).
- Choi, H., Fermin, D. & Nesvizhskii, A. I. Significance analysis of spectral count data in label-free shotgun proteomics. *Mol Cell Proteomics* **7**, 2373–2385 (2008).
- Nesvizhskii, A., Keller, A., Kolker, E. & Abersold, R. A statistical model for identifying proteins by tandem mass spectrometry. *Anal Chem* **75** (2003).
- Keller, A., Nesvizhskii, A. I., Kolker, E. & Abersold, R. An explanation of the Peptide Prophet algorithm developed. *Anal Chem* **74**, 5383–5392 (2002).
- Ritfeld, G. J., Roos, R. A. & Oudega, M. Stem cells for central nervous system repair and rehabilitation. *PM R* **3**, S117–122 (2011).
- Beck, K. D. *et al.* Quantitative analysis of cellular inflammation after traumatic spinal cord injury: evidence for a multiphasic inflammatory response in the acute to chronic environment. *Brain* **133**, 433–447 (2010).
- Popovich, P. G. & Jones, T. B. Manipulating neuroinflammatory reactions in the injured spinal cord: back to basics. *Trends Pharmacol Sci* **24**, 13–17 (2003).
- Fleming, J. C. *et al.* The cellular inflammatory response in human spinal cords after injury. *Brain* **129**, 3249–3269 (2006).



54. Keane, R. W., Davis, A. R. & Dietrich, W. D. Inflammatory and apoptotic signaling after spinal cord injury. *J Neurotrauma* **23**, 335–344 (2006).
55. Nakajima, H. *et al.* Transplantation of mesenchymal stem cells promotes an alternative pathway of macrophage activation and functional recovery after spinal cord injury. *J Neurotrauma* **29**, 1614–1625 (2012).
56. Geffner, L. F. *et al.* Administration of autologous bone marrow stem cells into spinal cord injury patients via multiple routes is safe and improves their quality of life: comprehensive case studies. *Cell Transplant* **17**, 1277–1293 (2008).
57. Yoon, S. H. *et al.* Complete spinal cord injury treatment using autologous bone marrow cell transplantation and bone marrow stimulation with granulocyte macrophage-colony stimulating factor: Phase I/II clinical trial. *Stem Cells* **25**, 2066–2073 (2007).
58. Park, H. C. *et al.* Treatment of complete spinal cord injury patients by autologous bone marrow cell transplantation and administration of granulocyte-macrophage colony stimulating factor. *Tissue Eng* **11**, 913–922 (2005).
59. Sykova, E. *et al.* Autologous bone marrow transplantation in patients with subacute and chronic spinal cord injury. *Cell Transplant* **15**, 675–687 (2006).
60. Lu, P., Jones, L. L. & Tuszynski, M. H. Axon regeneration through scars and into sites of chronic spinal cord injury. *Exp Neurol* **203**, 8–21 (2007).
61. Carney, B. J. & Shah, K. Migration and fate of therapeutic stem cells in different brain disease models. *Neurosci* **197**, 37–47 (2011).
62. Tambuyzer, B. R., Ponsaerts, P. & Nouwen, E. J. Microglia: gatekeepers of central nervous system immunology. *J. of leukocyte biol* **85**, 352–370 (2009).
63. Watzlawik, J. O., Warrington, A. E. & Rodriguez, M. PDGF is required for remyelination-promoting IgM stimulation of oligodendrocyte progenitor cell proliferation. *PLoS One* **8**, e55149 (2013).
64. Robinson, A. P., Foraker, J. E., Ylostalo, J. & Prockop, D. J. Human stem/progenitor cells from bone marrow enhance glial differentiation of rat neural stem cells: a role for transforming growth factor beta and Notch signaling. *Stem Cells Dev* **20**, 289–300 (2011).
65. Au, E. *et al.* SPARC from olfactory ensheathing cells stimulates Schwann cells to promote neurite outgrowth and enhances spinal cord repair. *J Neurosci* **27**, 7208–7221 (2007).
66. Rivera, L. B., Bradshaw, A. D. & Brekken, R. A. The regulatory function of SPARC in vascular biology. *Cell Mol Life Sci* **68**, 3165–3173 (2011).
67. Kular, L., Pakradouni, J., Kitabgi, P., Laurent, M. & Martinierie, C. The CCN family: a new class of inflammation modulators? *Biochimie* **93**, 377–388 (2011).
68. Kondo, Y., Nakanishi, T., Takigawa, M. & Ogawa, N. Immunohistochemical localization of connective tissue growth factor in the rat central nervous system. *Brain Res* **834**, 146–151 (1999).
69. Wahab, N. A., Weston, B. S. & Mason, R. M. Connective tissue growth factor CCN2 interacts with and activates the tyrosine kinase receptor TrkA. *J Am Soc Nephrol* **16**, 340–351 (2005).
70. Schaffler, A. & Buechler, C. CTRP family: linking immunity to metabolism. *Trends Endocrinol Metab* **23**, 194–204 (2012).
71. Siegenthaler, J. A. & Miller, M. W. Transforming growth factor beta 1 promotes cell cycle exit through the cyclin-dependent kinase inhibitor p21 in the developing cerebral cortex. *J Neurosci* **25**, 8627–8636 (2005).
72. Kozlowski, C. & Weimer, R. M. An automated method to quantify microglia morphology and application to monitor activation state longitudinally in vivo. *PLoS One* **7**, e31814 (2012).
73. Karperien, A., Ahamme, H. & Jelinek, H. F. Quantitating the subtleties of microglial morphology with fractal analysis. *Front Cell Neurosci* **7**, 3 (2013).
74. Rahmat, Z., Jose, S., Ramasamy, R. & Vidyadaran, S. Reciprocal interactions of mouse bone marrow-derived mesenchymal stem cells and BV2 microglia after lipopolysaccharide stimulation. *Stem Cell Res Ther* **4**, 12 (2013).

Acknowledgments

This research was supported by a collaboration between the PRISM (MS) and ThermoFisher (Bremen, KS) and grants from Ministère de L'Éducation Nationale, L'Enseignement Supérieur et de la Recherche, Agence Nationale de la Recherche (ANR, MIMIC project, CL), Région Nord-Pas de Calais (to SD), SIRIC ONCOLille (IF), Grant INCa-DGOS-Inserm 6041aa and Université de Lille 1 (to DC), APVV 0472-11(DC), MVTS-COST BH-1002.

Author contributions

D.C. and M.S. conceived of the study, participated in the data collection, performed the statistical analysis and wrote the main manuscript. S.D., F.L.M., J.F., L.S., J.B., J.R. and T.S. participated in the data collection. J.R., C.L. and I.F. participated in the design of the study and helped to write the manuscript. All authors have reviewed the manuscript.

Additional information

Supplementary information accompanies this paper at <http://www.nature.com/scientificreports>

Competing financial interests: The authors declare no competing financial interests.

How to cite this article: Cizkova, D. *et al.* Modulation properties of factors released by bone marrow stromal cells on activated microglia: an *in vitro* study. *Sci. Rep.* **4**, 7514; DOI:10.1038/srep07514 (2014).



This work is licensed under a Creative Commons Attribution 4.0 International License. The images or other third party material in this article are included in the article's Creative Commons license, unless indicated otherwise in the credit line; if the material is not included under the Creative Commons license, users will need to obtain permission from the license holder in order to reproduce the material. To view a copy of this license, visit <http://creativecommons.org/licenses/by/4.0/>

CONCLUSION CHAPTER 2

Inflammation at the acute phase of SCI is necessary in order to clear the debris of the apoptotic cells which could prevent regeneration. However, at the chronic phase, inflammation becomes a barrier for remyelination, axon outgrowth and regeneration. Our study of the released proteins by BMSC has pointed out that these cells are able to produce immune modulators such as arginase 1, ST2 and galectins and chemoattractant factors such as CLEC11a and CCL2. These factors are known to switch the polarization of microglia cells into M2 phenotype which is neuroprotective and anti-inflammatory. Moreover, the presence of BMSC conditioned media reduces the chemoattractivity of the SCI conditioned media to modulate the inflammation and diminishes the activation of the microglia cell line and primary microglia. The production of NO is reduced in presence of BMSC-CM, which is correlated with the decrease of the cells activation. BMSCs-CM stimulate the M2 polarization of macrophages. The expression of M2 macrophages in the injured environment proves the interest of using BMSC-CM for wound healing spinal cord injury. In our study, we reinforced this theory in which local injection of the cocktail containing multiple factors will act directly on several mechanisms.

We highlighted the beneficial effects of secreted factors from BMSC-CM to modulate inflammation and to improve regeneration. By using a cocktail of molecules instead of targeting only one factor, the efficiency of the therapy will be more complete and efficient. In general, stem cell therapies are used for their differentiation properties and are then be involved in tissue repair and in the immune system function (Akiyama *et al.* 2012). The advantage of conditioned-media is that healing actions occur through the paracrine and autocrine pathways to modulate the vascular genesis, the tissue regeneration and the immune modulation (Maguire *et al.* 2013; Pluchino and Cossetti 2013).

Future work will be oriented to couple the BMSC-CM with an alginate, a biomaterial which has the propriety to create a scaffold able to fill the cyst cavity formed after SCI. Different factors can be bound and released progressively into the lesion microenvironment. However, further studies need to be carried out for the affinity-binding alginate scaffold allowing the release of a cocktail of molecules as released by BMSC-CM.

Among growth factors identified in the conditioned media from BMSC, fibroblast growth factor 2 (FGF2) is known to promote angiogenesis (Montesano *et al.* 1986), and be neuroprotective if secreted by neurons to induce microglia activation and phagocytosis of debris (Noda *et al.* 2014). Kang *et al.*, have shown that delivery of FGF2 can reduce the permeability of the blood-spinal cord barrier (C. E. Kang *et al.* 2010). Moreover, another growth factor, epidermal growth factor (EGF), is known to preserve the blood-spinal cord barrier integrity and improves functional recovery after SCI (Zheng *et al.* 2016). The combination of FGF2 and EGF enhances the neuroprotective and the cell proliferative effects (Martens, Seaberg, and van der Kooy 2002; Kojima and Tator 2002). In this way, after an *in vitro* point of view, the third chapter of my thesis will discuss the delivery of FGF2 and EGF coupled with the alginate biomaterial, in order to enhance spinal repair.

CHAPTER 3: Alginate biomaterial coupled with growth factors to promote *in vivo* regeneration

After *in vitro* studies to promote the neurite outgrowth via RhoA inhibitor and to modulate the inflammation through the microglia activation using factors released by BMSC, the third chapter of my thesis will be dedicated to the *in vivo* study by taking advantages of both elements.

SCI leads to the formation of a cavity which does not allow the neurons and cells to adhere in a physical matrix to support their growing and repairing. Hydrogel is one biomaterial with appropriate physical properties that can mimic the environment and architecture of the CNS. Hydrogel has been used to fill cavities in SCI (Nomura, Tator, and Shoichet 2006) and to provide a substrate for axon attachment and regrowth (N. Zhang, Yan, and Wen 2005; Piantino *et al.* 2006; Prang *et al.* 2006). Moreover, the biocompatibility with the host tissue is primordial. It will not be toxic nor induce immune response during injection and degradation (M. Wang *et al.* 2011). The alginate is a natural hydrogel obtained from a brown algae. It is an anionic polymer used for many biomedical applications and mild gelation through the addition of divalent cations such as Ca^{2+} (Gombotz and Wee 1998; K. Y. Lee and Mooney 2012). Hydrogels retain a significant fraction >20% of water which allows them to mimic the aqueous environment of the extracellular matrix (Pego *et al.* 2012). The methods of drug delivery to treat spinal cord injuries such as injection, or several injections, implantation of pump or intrathecal catheter are often highly invasive and uncontrolled method, causing scarring and compression for the intrathecal infusions (L. L. Jones and Tuszynski 2001). Hydrogel can be directly injected into the lesion site, where it will polymerize and will be used as a cell-delivery vehicle. Alginate will acquire the shape of the cavity and function as an extracellular matrix (Taylor and Sakiyama-Elbert 2006). It has been shown that alginate enhances cell resistance to oxidative stress, and increases neuronal regeneration (Matyash *et al.* 2012). A scaffold made of alginate-sulphate/alginate was developed by Smadar Cohen group in 2008 (Freeman, Kedem, and Cohen 2008). They have shown *in vitro* that alginates coupled, with FGF2 and EGF promote neural progenitor cell proliferation, survival and differentiation (Dasa Cizkova *et al.* 2015). FGF2 is present in the nervous system and was shown to support survival and growth of neurons and NPS *in vitro* (Mayer *et al.* 1993). FGF2 has a neuroprotective role (Lee *et al.* 1999).

EGF has been shown to attenuate the blood-spinal cord barrier permeability (Zheng *et al.* 2016). The scaffold releases GFs in time to avoid repetition of GF delivery in cell media. FGF2 and EGF have strong but reversible binding to alginate-sulphate (Freeman, Kedem, and Cohen 2008) which exhibited continuous release of the factors for over 21 days (Dasa Cizkova *et al.* 2015).

Our data obtained from *in vitro* BMSC-CM studies showed the presence of neurotrophic factors such as BDNF, TGF β , CTGF, PGF, PDGF and IGF (Dasa Cizkova *et al.* 2014). The previous work related to alginate coupled with EGF and FGF2 (Dasa Cizkova *et al.* 2015) leads us to inject alginate, releasing identical GFs into the lesion site seven days after SCI. We focus first on the delivery of only two factors to get an overview of the beneficial effects of alginate alone and coupled with these GFs injections, before starting with a more complex cocktail of molecules. The aim is to see *in vivo* the potential of this hydrogel injection with or without GFs on the locomotor behavior recovery, the cavity size, the motor neurons survival, the synaptic alterations, the impact on sensory fibers as well as on the immune response via microglia activation.

We conducted a tissue shot gun proteomic analysis in order to define the main molecular profile expressed at different times and locations, such as in a control spinal cord without injury and after 7 and 10 days in rostral and caudal adjacent segments, and the lesion segment grouping 7 and 10 days together. A totally different profile of tissue control has been highlighted compared to the injured tissue. Moreover, rostral and caudal tissues from each time condition are grouped together with a different branch for the lesion segments. We have shown at 7 and 10 days in the caudal segment the over-expression of neurotrophic and adhesion molecules and signaling proteins (neurofascin, radixin, NDRG2, glia maturation factor b, NCAM1). In rostral segments, proteins involved in mitochondrial and cytoplasm metabolisms in intracellular signaling were over-expressed (amphiphysin, microtubule associated protein 1A, hydroxyacyl glutathione hydrolase, inositol monophosphatase, superoxide dismutase). These proteomics data demonstrated a clear difference between rostral and caudal segments adjacent to the lesion in terms of physiological and molecular processes through time after injury, which is in line with the spatio temporal study performed at the level of the secreted factors (Devaux *et al.* 2016). Important factors for neurogenesis are present in the caudal segment, but they are

repressed by the expression of proteoglycans as we previously found in secretome (Devaux *et al.* 2016).

In this way, we used alginate to link the rostral and caudal segments in order to build a scaffold where cells will be able to grow and communicate via a structure similar to the extracellular matrix. From these analyses, the other studies will focus on the physiological and regenerative differences along the rostro-caudal axis after biomaterial treatment. Regarding the locomotor recovery, the BBB score was assessed from 0 to 49 days. Significant differences were observed 12 and 14 days post injury between SCI + saline (SCI+SAL) and SCI + alginate + GFs (SCI+ALG+GFs) /SCI + alginate (SCI+ALG). The sensitivity to a normal non-painful cold stimulus was assessed after SCI. SCI results into adverse pain behavior with development of cold allodynia. Low increase in sensitivity to a normally innocuous stimulus was observed in the entire survival in SCI+ALG+GF compared to sham. 16 days post injury, a significant difference was observed between SCI+SAL and SCI+ALG+GFs. The cavity formation is one of the elements which takes place after the acute phase corresponding to high inflammation around 7 days post SCI. We filled the cavity 7 days after injury with alginate directly into the lesion site to create a favorable environment for regeneration. 42 days post treatment, a histological assessment was performed in the rostro-caudal axis with Luxol Fast Blue staining to measure the cavity length and size. The cavity length and size decreased with SCI+ALG or SCI+ALG+GFs compared to SCI+SAL. SCI+ALG+GFs is more efficient than SCI+ALG in reducing the cavitation. The loss of neurons occurs after SCI. Among neurons present in the spinal cord, motor neurons are present in the ventral horn and sensory neurons are present in the dorsal horn. We first have shown that after the injury and with the saline treatment, the number of neurons decreased significantly. However, with alginate and GFs, the number of neurons NeuN positive increased significantly compared to saline treatment, to get a similar number to the sham group. We then focused on motoneurons using ChAT antibody in rostral and caudal ventral horns. A significantly higher number of ChAT positive neurons were detected after the delivery of alginate and GFs in both segments. A higher decrease of ChAT positive motoneurons is observed in the caudal ventral horn after injury and saline treatment. Treatment with alginate and GFs supports the survival of ChAT positive motoneurons. In order to assess the synaptic response of the motoneurons, we looked at the distribution of synaptophysin positive vesicles in the area of ChAT positive neurons of the ventral horns 42

days after treatment. Numerous fine dots were distributed along the motoneurons surface and the proximal dendrites. The alginate coupled to GFs treatment revealed a significant increase of the synaptic vesicles in the motoneurons area. However, no difference was observed between rostral and caudal segments. We then investigated the reponse of the sensory fibers determined by the CGRP expression in the dorsal horn. All treatment groups have shown a significant increase of the length of the CGRP fibers compared to the sham. However, no difference was observed between treatment conditions, the delivery means of alginate alone or with GFs. SCI leads to disruption of long projection axons, therefore here we have analyzed the axonal sprouting via BDA tracing after alginate treatment. The corticospinal tract (CST) projections are very important for the voluntary motor function. We delivered BDA to the sensorimotor cortex to label the descending CST axons of the spinal cord. The treatment with alginate and GFs significantly increased the BDA label fibers compared to the saline treatment. Another point of view for the efficacy of the alginate is to point out the treatment effect on the immune response by focusing on the microglia cells. Rostral and caudal sections were stained with Iba1 antibody to show their activation and the morphology after the different treatments. Basal microglia expression was present in the sham group. For each segment, a high increase in microglia activation was observed in the saline group; however, the alginate + GFs treatment allowed a significant attenuation of microglia compared to saline. The delivery of injectable alginate biomaterial coupled with EGF and FGF2 into the lesion site 7 days post injury demonstrates the improvement of the spinal cord repair through different aspects: the reduction of the cavitation, an increase of the motoneurons and their synaptic connections, the enhancement of the CST axons outgrowth and the attenuation of the inflammation. Moreover, biomaterial treatment enhanced changes in CGRP fibers, but without behavioural adverse sensory response.

Article 4: Delivery of Alginate Scaffold Releasing Two Trophic Factors for Spinal Cord Injury Repair

Authors: Ivana Grulova, Lucia Slovinska, Juraj Blasko, Stéphanie Devaux, Maxence Wisztorski, Michel Salzet, Isabelle Fournier, Olga Kryukov, Smadar Cohen & Dasa Cizkova

Article Status: published in Scientific Reports 2015 Sep 8; 5: 13702

Summary: Proteomic experiments, procedures and data analyses were realized by Ms Devaux. She participated in the writing of the manuscript and in the revision.

SCIENTIFIC REPORTS



OPEN

Delivery of Alginate Scaffold Releasing Two Trophic Factors for Spinal Cord Injury Repair

I. Grulova¹, L. Slovinska¹, J. Blaško¹, S. Devaux^{1,2}, M. Wisztorski², M. Salzet², I. Fournier², O. Kryukov³, S. Cohen³ & D. Cizkova^{1,2}

Received: 14 May 2015

Accepted: 04 August 2015

Published: 08 September 2015

Spinal cord injury (SCI) has been implicated in neural cell loss and consequently functional motor and sensory impairment. In this study, we propose an alginate-based neurobridge enriched with/without trophic growth factors (GFs) that can be utilized as a therapeutic approach for spinal cord repair. The bioavailability of key GFs, such as Epidermal Growth factor (EGF) and basic Fibroblast Growth Factor (bFGF) released from injected alginate biomaterial to the central lesion site significantly enhanced the sparing of spinal cord tissue and increased the number of surviving neurons (choline acetyltransferase positive motoneurons) and sensory fibres. In addition, we document enhanced outgrowth of corticospinal tract axons and presence of blood vessels at the central lesion. Tissue proteomics was performed at 3, 7 and 10 days after SCI in rats indicated the presence of anti-inflammatory factors in segments above the central lesion site, whereas in segments below, neurite outgrowth factors, inflammatory cytokines and chondroitin sulfate proteoglycan of the lectican protein family were overexpressed. Collectively, based on our data, we confirm that functional recovery was significantly improved in SCI groups receiving alginate scaffold with affinity-bound growth factors (ALG +GFs), compared to SCI animals without biomaterial treatment.

Spinal cord injury (SCI) involves a multifactorial process that initiates pathological cellular and molecular responses resulting in limited spontaneous axonal regeneration¹. Clinical symptoms following trauma can vary in severity, but usually lead to complete paralysis and spasticity¹⁻⁴. The development of a safe and efficient treatment for spinal cord injuries is greatly complicated by the existence of a highly complex injury environment. Over the past decades various strategies have been proposed including inflammatory processes and suppression of edema^{5,6}, promotion of axonal regeneration through the decrease of inhibitory molecules⁷⁻⁹, transplantation of stem cells to replace lost tissue, or enhancement of endogenous repair with trophic factor support and rehabilitative training¹⁰⁻¹². All these strategies were developed to target specific pathological players during secondary damage, whereas nowadays a combinatorial approach integrating biomaterial scaffolds, cell transplantation and molecule delivery seems to be more promising for regeneration and functional recovery¹³⁻¹⁶.

An attractive strategy for repairing injured spinal cord is to incorporate multiple neurotrophic factors in biodegradable and biocompatible microspheres, or injectable matrices that allow controlled, sustained and localized delivery of those factors^{17,18}. The alginate scaffold is a suitable biomaterial construct providing a cellular mechanical framework of polysaccharide chains that gels by ionic cross linking after mixing aqueous alginate solution with divalent cations such as Ca²⁺¹⁹. Natural substrate isolated from the wall

¹Institute of Neurobiology, Center of Excellence for Brain Research, Department of Regenerative Medicine and Stem Cell Therapy, Slovak Academy of Sciences, Soltesovej 4-6, 040 01 Kosice, Slovakia. ²Laboratoire PRISM: Protéomique, Réponse Inflammatoire, Spectrométrie de Masse, INSERM U1192, Bât SN3, 1er étage, Université de Lille 1, F-59655 Villeneuve d'Ascq, France. ³The Center of Regenerative Medicine and Stem Cell Research and The Avram and Stella Goldstein-Goren Department of Biotechnology Engineering, Ben-Gurion University of the Negev, Beer Sheva, Israel. Correspondence and requests for materials should be addressed to D.C. (email: cizkova.dasa@gmail.com)

of brown seaweed represents a non-toxic/non-inflammatory, highly porous scaffold with relatively low cost²⁰. Alginate hydrogel has been widely used for drug or cell delivery as an injectable vehicle capable of filling cavities in the injured spinal cord^{21–23}, and of providing the substrate for axon attachment and re-growth^{15,20,24}.

Along these lines, we have recently reported that an affinity-binding alginate scaffold which sustains the release and presentation of both epidermal growth factor (EGF) and fibroblast growth factor-2 (bFGF) is capable of supporting the viability, expansion and lineage differentiation of neural progenitor cells (NPCs) *in vitro*²⁵. Following these findings, our next goal was to test this scaffold with its affinity-bound growth factors (GFs) for treatment of spinal cord compression in rats. Although increasing evidence demonstrates that the adult spinal cord harbours a population of multipotent neural precursor cells (NPCs), which is further increased by injury, their ability to replace lost neuroglia populations has been shown to be insufficient. Optimizing the SCI environment, therefore, by enhancing the presence and longevity of EGF and bFGF may provide an appropriate supportive microenvironment for the survival, and integration of endogenous NPCs into functional neural circuitry *in situ*^{14,26–28}. The GFs selected for this study share important roles in regulating NPC proliferation and differentiation: bFGF is a known mitogen for stem cell self-renewal, while EGF induces both proliferation and differentiation in many mammalian stem cells²⁹ including NPCs. Furthermore, both GFs accelerate neovascularisation, necessary for supporting and rebuilding the damaged tissue.

In the present study, we performed biomaterial treatment at 7 days after SCI followed by tissue micro-proteomics and immunocytochemistry. Our microproteomic data based on high-resolution (HR) MS/MS shot-gun procedures and statistical analyses³⁰ indicated that the caudal region 7–10 days post SCI compared to that of 3 days post SCI is able to initiate neurogenesis if trophic and inflammatory inhibitors factors are present on-site. We therefore addressed the therapeutic efficacy of the affinity-binding alginate scaffold as described herein in terms of functional recovery and nerve tissue repair. Specifically, we investigated its influence on: (i) tissue sparing *via* reduction of the central cavity and enhanced survival of neuronal populations, (ii) neurite outgrowth, (iii) angiogenesis, (iv) response of astrocytes and microglia involved in inflammation and scarring, and (v) functional recovery of sensory-motor pathways during a period of 49 days after SCI in rats.

Materials and Methods

Experimental groups. Male Wistar albino rats weighing 290–320 g were divided into 5 groups: 1) sham-operated SCI group (n = 6), 2) sham-operated and SCI rats (ALG+ALG+GFs) after biotinylated dextran amines (BDA) tracing (n = 10), 3) SCI group receiving saline injection (SCI+SAL) (n = 8), 4) SCI group receiving an injection of alginate scaffold/lacking growth factors (SCI+ALG) (n = 8), and 5) SCI group receiving an injection of alginate scaffold with affinity-bound EGF and bFGF (SCI+ALG+GFs) (n = 8). During the survival, rats were behaviourally tested and after 49 day post-injury, all groups were sacrificed and spinal cord tissue was processed for immunohistochemistry and tracing analysis. A set of 12 animals subjected to SCI at 3, 7, 10 days (n = 4 for each time point) was used for proteomic analyses.

Animals. The study was performed with the approval and according to the guidelines of the Institutional Animal Care and Use Committee of the Slovak Academy of Sciences and with the European Communities Council Directive (2010/63/EU) regarding the use of animals in Research, Slovak Law for Animal Protection No. 377/2012 and 436/2012. In present study we used a total of 40 rats, and 34 survived.

Spinal cord injury. The SCI was induced using the modified balloon-compression technique according to our previous study³¹. Briefly, 2-French Fogarty catheter was inserted epidurally at Th8–9 level and the balloon was inflated with 12.5 µl of saline for 5 min. After compression of spinal cord tissue, catheter was deflated and removed from epidural space. In the sham group (n = 4), the catheter was inserted at the same level of spinal cord, but balloon was not inflated and no lesion was performed. Manual bladder expression was required for 7–14 days after the injury until the bladder reflex was established. No antibiotic treatment was used.

Tissue protein extraction. Fresh frozen spinal cord collected after 3, 7 and 10 days after lesion and controls were embedded (n = 4, each group) on optimal cutting temperature polymer before sectioned using a cryomicrotome (Leica Microsystems, Nanterre, France) and subjected to trypsin digestion. Spinal cord tissue sections (20 µm thick) were mounted on a parafilm covered glass slide and the tissue was microdissected manually using a binocular. The pieces were extracted by incubating in 20 µL of 50 mM bicarbonate buffer containing 50 mM dithiothreitol and 1% SDS at 55 °C for 15 min. The extracts were then loaded on 12% polyacrylamide gel and separated at 70 V for 15 min and then 120 V until the dye front reaches the other end of the gel. After migration, the gel was incubated in the gel fixative solution for 30 min and stained with colloidal Coomassie brilliant blue overnight. The stain was removed by washing the gel four times with distilled deionized water³⁰.

In gel digestion. The gel was cut into ten pieces. Pieces were washed with 300 µL of distilled deionized water for 15 min, 300 µL of ACN for 15 min and 300 µL of NH₄HCO₃ (100 mM; pH8) for 15 min

followed by incubation of 300 μ L of NH_4HCO_3 /acetonitrile (ACN) (1:1, v/v) for 15 min and 300 μ L of ACN for 5 min. Band pieces were dried in a Speedvac for 5 min. The reduction of cystine residues was made with 50 μ L of 10 mM of DTT in NH_4HCO_3 100 mM (pH8). Pieces were incubated at 56 °C for 1 hour. Alkylation of cystine was made with 50 μ L of iodoacetamide IAA (50 mM) in NH_4HCO_3 (100 mM; pH8). Pieces were incubated at room temperature in the dark for 30 min. Band pieces were washed a second time with 300 μ L of NH_4HCO_3 100 mM (pH8) for 15 min, then with a mix of 300 μ L of NH_4HCO_3 /ACN (1:1, v/v) for 15 min and 300 μ L of ACN for 5 min. Band pieces were dried in a Speedvac for 5 min. A digestion of band pieces was made with trypsin (12.5 μ g/mL) in NH_4HCO_3 20 mM (pH8), enough to cover pieces. Pieces were incubated at 37 °C overnight. Peptides were extracted on shaking platform with 50 μ L of formic acid (FA) 1% two times for 20 min, then 150 μ L of ACN for 10 min. The supernatant was transferred in new tube and dried with Speedvac. Samples were resuspended in 20 μ L of 0.1% trifluoro acetic acid (TFA) and then desalted with Ziptip C18 and eluted with 10 μ L of ACN/0.1% TFA (8:2, v/v). Samples were dried in a Speedvac and resuspended in 15 μ L of ACN/0.1% FA (2:98, v/v).

NanoLiquid Chromatography –High Resolution-MS/MS (NanoLC-HR- MS/MS). Samples were separated by online reversed-phase chromatography using a Thermo Scientific Proxeon Easy-nLC system equipped with a Proxeon trap column (100 μ m ID \times 2 cm, Thermo Scientific) and a C18 packed-tip column (100 μ m ID \times 10 cm, Nikkyo Technos Co. Ltd). Peptides were separated using an increasing amount of acetonitrile (5%–30% over 120 minutes) at a flow rate of 300 nL/min. The LC eluent was electrosprayed directly from the analytical column and a voltage of 1.6 kV was applied via the liquid junction of the nanospray source. The chromatography system was coupled to a Thermo Scientific LTQ-Orbitrap XL mass spectrometer. The LTQ-Orbitrap XL instrument was set to acquire top 20 MS/MS in data-dependent mode. The survey scans were taken at 70,000 full width at half maximum (FWHM) (at m/z 400) resolving power in positive mode and using a target of 3E6 and default charge state of 2. Unassigned and +1 charge states were rejected, and dynamic exclusion was enabled for 20 s. The scan range was set to 300–1600 m/z. For the MS/MS, 1 microscan was obtained at 17,500 FWHM and isolation window of 4.0 m/z, using a scan range between 200–2000 m/z^{30,32}.

Mass Spectra Data Analysis. Tandem mass spectra were processed with Thermo Scientific Proteome Discoverer software version 1.3. Resultant spectra were searched against the Swiss-Prot[®] *Rattus norvegicus* database (version January 2012) using the SEQUEST[®] algorithm. The search was performed choosing trypsin as the enzyme with two missed cleavages allowed. Precursor mass tolerance was 10 ppm, and fragment mass tolerance was 0.5 Da. N-terminal acetylation, methionine oxidation and arginine deamination were set as variable modifications. Peptide validation was performed with the Percolator algorithm. Peptides were filtered based on a q-Value below 0.01, which corresponds to a false discovery rate (FDR) of 1%. All the MS data were processed with MaxQuant³³ (version 1.5.1.2) using Andromeda³⁴ search engine. Proteins were identified by searching MS and MS/MS data against Decoy version of the complete proteome for *Rattus norvegicus* of the UniProt database [UniProt Consortium. Reorganizing the protein space at the Universal Protein Resource (UniProt). *Nucleic Acids Res.* 2012, 40 (Database issue), D71–5.] (Release June 2014, 33675 entries) combined with 262 commonly detected contaminants. Trypsin specificity was used for digestion mode, with N-terminal acetylation and methionine oxidation selected as variable, carbamidomethylation of cysteines was set as a fixed modification and we allow up to two missed cleavages. For MS spectra an initial mass accuracy of 6 ppm was selected and the MS/MS tolerance was set to 0.5 Th for CID data. For identification, the FDR at the peptide spectrum matches (PSM) and protein level was set to 0.01. Relative, label-free quantification of proteins was done using the MaxLFQ algorithm³⁵ integrated into MaxQuant with the default parameters.

The data sets used for analysis are deposited at the ProteomeXchange Consortium³⁶ (<http://proteomecentral.proteomexchange.org>) via the PRIDE partner repository³⁷ with the dataset identifier.

Analysis of the proteins identified was done using Perseus software (<http://www.perseus-framework.org/>) (version 1.5.0.31). The file containing the information from identification was used and hits to the reverse database, proteins only identified with modified peptides and potential contaminants were removed. Then the LFQ intensity were logarithmized ($\log_2(x)$). A normalization was achieved using a Z-score with a matrix access by rows. Data coming from control samples were average as the one coming from the lesion part. Six conditions were then analyzed: control (ctrl), lesion part (lesion), segment R1 or C1 seven days (respectively r1_7D and C1_7D) or ten days (r1_10D and C1_10D) after lesion. Only proteins presenting a valid value of LFQ intensity for these six conditions were used for statistical analysis. A Hierarchical clustering was first performed using a Pearson correlation for distance calculation and average option for linkage in row and column trees using a maximum of 300 clusters. For visualization of the variation of proteins expression depending to the segment/time parameter, the profile plot tool was used with a reference profile and an automatic selection of the 10 or 15 correlated profiles.

Preparation of alginate scaffold with affinity-bound factors. Fabrication of the scaffold with the affinity-bound dual growth factors (ALG+GFs) involved preparing bioconjugates of bFGF and EGF with alginate-sulfate and then mixing both bioconjugate solutions with the solution of a partially calcium-cross-linked alginate. The bioconjugates were prepared by mixing bFGF or EGF with alginate-sulfate solution (1%, w/v) and incubating for 1.5 h at 37 °C, to allow equilibrium binding. The

partially calcium-cross-linked alginate solution was prepared as previously described³⁸. Briefly, stock solutions of sodium alginate (VLVG, 30–50 kDa, >65% guluronic acid content, NovaMatrix FMC Biopolymers, Drammen, Norway) and D-gluconic acid/hemi calcium salt were prepared by dissolving the materials in DDW and stirring at room temperature. Each solution was filtered separately through a sterile 0.2 µm filter membrane into a sterile container in a laminar flow cabinet. Equal volumes from each stock solution (2.08% and 0.68% (w/v) for VLVG alginate and D-gluconic acid, respectively) were combined by extensive homogenization for several minutes to facilitate homogenous distribution of the calcium ions and cross linking of alginate chains. Finally, the bFGF and EGF alginate-sulfate bioconjugates were mixed with the partially cross-linked alginate to yield an bFGF/EGF-containing, affinity-binding alginate scaffold (0.1% alginate-sulfate, 0.9% alginate, 0.3% D-gluconic acid, w/v) (ALG+GFs). For the control system- lacking GFs, the scaffold was prepared with no affinity-bound factors (ALG).

Intraspinal delivery of alginate scaffold. Seven days after SCI, animals were anesthetized with 1.5–2% halothane and partial laminectomy at Th6–12 level was performed. Using a 50-µl Hamilton syringe (30G needle, Cole Parmer, Anjou, Quebec) connected to UltraMicroPump III with Micro4 Controller, 4-Channel (World Precious Instruments, Inc., Sarasota FL) and stereotactic device, 4 intraspinal injections/per animal were applied at the lesion site that showed discreet signs of haemorrhage and slight atrophy. In most cases the lesion cavity was apparent through the dorsal site of spinal cord. Bilateral delivery of i) saline, ii) ALG, or iii) ALG+GFs (2 injections of 2 µl/per injection/on left and 2 injections of 2 µl/per injection/on right side with delivery rate of 0.5 µl/min, loaded with 200 ng/ml of each GF) was performed. Based on our *in vitro* study results, an affinity-binding alginate scaffold loaded with 200 ng of bFGF/EGF confirmed long term release of GFs²⁵. Each delivery was positioned 1 mm from the spinal cord midline and injected at the depth of 1.8–2 mm from the pial surface of the spinal cord. The distance between injections was 1 mm, avoiding vessels. After injecting the dose of alginate scaffold, the needle was maintained in the tissue for an additional 30 seconds. No antibiotic treatment was performed during animal's survival.

Anterograde biotinilated dextran amine (BDA) motor corticospinal tract (CST) axon tracing. Sham rats (n = 4) and SCI rats (ALG (n = 3), and ALG+GFs (n = 3)) at 3 weeks post-injury were anesthetized with 2% halothane and placed in a stereotaxic device. The halothane level was maintained at 2–3% throughout the surgery. An incision was made to expose the skull and to identify the bregma and lambda landmarks. Rats received injections of 10% solution of BDA (biotinilated dextran amine 10,000 MW; Molecular Probes, Eugene, OR) in sterile 10 mM sodium phosphate buffer, pH 7.4, injected via glass micropipettes (inner tip diameter of 60–80 µm) using a controlled pressure device (PicoPump; World Precision Instruments). The injection site was positioned into right and left motor cortex performed at anatomical coordinates: 1.0 mm lateral to bregma, 1.5 mm anterior/posterior to the bregma and 1.5 mm deep to the cortical surface from the pial surface of the brain based on the Stereotaxic Coordinates (Paxinos and Franklin, 2001) (Supplementary Figure 1). A total 8 injections with approximately 0.5 µl of BDA was injected at each of the four sites at a rate of 80 nl/min during 6–7 min/per injection. The micropipette remained in place for 3 minutes following each injection. After the delivery was completed, the skin overlying the skull was sutured and rats returned to their cages.

Behavioral Testing. *BBB scoring.* Animals were behaviourally tested for 5 min using BBB open-field locomotor test³⁹ after SCI at day 1, 3, 5, 7, and then in weekly intervals. Each rat was tested for 5 min by two blinded examiners. BBB test measuring locomotor outcome (hindlimb activity, body position, trunk stability, tail position and walking paw placement) of rats by BBB rating scale ranges from 0 - no observable hindlimbs movements to a maximum 21 - plantar stepping, coordination and trunk stability like healthy rats.

Cold allodynia. Cold sensitivity of the hindpaws to the acetone was quantified by foot withdrawal frequency. All animals were tested at day 3 post-injury and then in weekly intervals at day 16, 25, 32 and 49 after SCI. Before testing, the rats were left to acclimatize inside acrylic-plastic cages during the 10–15 min. A drop of acetone (50–100 µl) was applied to the left and right hindpaws using a plastic syringe, 5 times, with at least 5 min recovery between administrations. The number of brisk foot withdrawals or flinching were considered to be positive behaviour. Data are presented as mean response duration (in seconds). Statistical differences between groups were determined with an unpaired Student's t test.

The sequence of surgical and behavioural procedures performed in time are described in Supplementary Figure 2.

Tissue Processing and Immunohistochemistry. After a 49 day survival period, animals were deeply anesthetized by intraperitoneal thiopental injection (50 mg/kg) and perfused transcardially with 500 ml saline, followed by 500 ml of 4% paraformaldehyde (PFA) in 0.1 M phosphate-buffered. Spinal cords were removed, postfixed in 4% PFA at 4 °C overnight, embedded in gelatin–egg albumin protein matrix (10% ovalbumin, 0.75% gelatine) polymerized by glutaraldehyde (albumin from chicken egg white, grade II, Sigma–Aldrich) subsequently fixed in 4% PFA, and cryoprotected with 30% sucrose in 0.1 M PB at 4 °C. Cryostat transversal and sagittal spinal cord sections (40 µm) were cut from rostral, central or

caudal blocks (each 0.5 cm thick) (Supplementary Figure 3) and collected in 24-well plates with 0.1 M PBS containing 0.1% sodium aside. For immunohistochemistry, free floating sections (40 μ m) were immersed in PBS (0.1 M; pH 7.4) containing 10% normal goat or normal rabbit serum (NGS, NRS), 0.2% Triton X-100 for 2 h at room temperature to block non-specific protein activity. This was followed by overnight incubation at 4 °C with primary antibodies: mouse anti-neuronal nuclei antigen (NeuN; 1:500, Merck-Millipore), goat anti-Choline acetyltransferase (ChAT; 1:5000, Merck-Millipore), rabbit anti-calcitonine gene related protein (CGRP; 1:100, Merck-Millipore), rabbit anti- ionized calcium-binding adapter molecule 1 (Iba1; 1:500, Wako), mouse anti- glial fibrillary acidic protein (GFAP; 1:1000, Merck-Millipore) rabbit anti-vWF (1:200, Chemicon) and mouse anti-synaptophysin (SYN; 1:500, Merck-Millipore) for 24 h. Afterwards sections were washed in 0.1 M PBS and incubated with secondary fluorescent antibodies goat anti-mouse, goat anti-rabbit, rabbit anti-goat conjugated with Texas Red (Alexa Flour 594) and fluorescein isothiocyanate (FITC) (Alexa Flour 488) at room temperature for 2 hours. For general nuclear staining 4-6-diaminidino-2-phenylindol (DAPI) (1:200) was added to the final secondary antibody solutions. Finally, sections were mounted and coverslipped with Vectashield mounting medium (Vector Laboratories).

Serial sagittal sections from each animal were stained for BDA to determine labelled CST axons through the lesion site. Sections were washed in TBS (50 mM Tris/HCl, 150 mM NaCl, pH = 7.6) and subsequently incubated overnight at 4 °C with ABC kit (ABC Vectastain Ellite kit; Vector Laboratories) diluted in TBS. After rinsing 3 times for 10 minutes in TBS, sections were reacted with DAB (consisting of DAB substrate, DAB buffer and 0.6% NiSO_4) for 20 minutes. Sections were finally washed in TBS and coverslipped in Entellan. Similarly serial sagittal sections (n = 5) were stained with Luxol Fast Blue to determine the length and cavity size area⁴⁰. Schematic concept of dissected spinal cord segments consisting of rostral (Th5-7), central (Th8-9), caudal (Th10-12) segments processed for immunohistochemical analyses is included in (Supplementary Figure 3).

Quantification analysis. Immunochemically stained sections were analyzed using Olympus BX-50 fluorescent microscope at 4x, 10x 20x and 40x magnifications, captured with digital camera HP Olympus and analyzed by Image J software according to the previous protocol⁴¹⁻⁴³. Quantification of NeuN, ChAT, Iba1, CGRP, GFAP and SYN positive cells was performed on five transverse sections from rostral and caudal segments of each spinal cord treatment and from sham tissue. Similarly, for quantification of BDA tracing, GFAP, Iba1, vWF expression and cavity size in sagittal sections from lesion epicentre, five sections per each experimental animal were analyzed. Number of NeuN positive cells was evaluated through sample field of 200 μ m \times 200 μ m, bilaterally positioned at Laminae I-IV (DH = area 1), IV-V (deep dorsal horn = area 2) and VIII-IX (ventral horn = area 3). Analysis of ChAT labelling was performed by using the identical field positioned in Laminae VIII-IX, bilaterally. Number of Iba1+ cells rostrally and caudally from injury epicenter was measured at the identical field in the Lamina VII gray matter (GM = area 1), lateral white matter (LWM = area 2) and ventral white matter (VWM = area 3) (Supplementary Figures 4 A,B). Quantification of immunofluorescence intensity (CGRP, Iba1, SYN) rostrally/caudally from lesion site and GFAP, Iba1 also at the site of central lesion) was performed by using ImageJ software. Captured digital images were transformed into monochrome 8-bit images and determined the mean grey level number of black and white pixels within the tissue (value 0–255, when 0 = black pixels, 255 = white pixels). The final result yields the mean ratio of black and white pixels expressed by the histogram. Length of BDA were equally evaluated by Image J and expressed in mm. Morphometric analyses of cavity size were performed on five 1.6 cm sagittal sections from the lesion site of each experimental and sham tissue. Modified Luxol Fast Blue labelling was performed to evaluate cavity area in spinal cord sections⁴⁰. Mean number of cavitation of experimental groups was expressed by mm relative to Sham spinal cord, which was without cavitation's and represent zero (no cavity).

Data and statistical analysis. Obtained data from tissue analyses and behavioural testing were reported as mean \pm SEM. Mean values among different experimental groups were statistically compared by one-way ANOVA and Tukey's post hoc tests using Graph pad PRISM software. Values of $P < 0.05$ were considered statistically significant (* P value of < 0.05 , ** P value of < 0.01 , *** $P < 0.001$).

Results

Spatiotemporal proteomic study of spinal cord tissue after injury. Spinal cord tissues, the rostral, lesion and caudal segments, were collected at 7 and 10 days after lesion and were subjected to tissue microproteomic, MaxQuant proteins analyses followed by Perseus allowed to statistically validate the identification and performed clustering. Figure 1 clearly shows that the control tissue is on a separate branch from lesion, rostral and caudal segments. The time course study reflected that 7 and 10 days are separated from each other. Comparison of the data obtained at 7 days between rostral and caudal segments clearly shows a common cluster of over-expressed groups of proteins (Fig. 1a) and four different clusters between the rostral and caudal of over- or sub-expressed protein groups (Fig. 1b–e). Proteins overexpressed at 7 days (Fig. 1a) are sub-expressed at 10 days (Fig. 1f). Only a cluster of proteins is differentially overexpressed at the caudal level (Fig. 1g). Specific proteins overexpressed in lesion, rostral and caudal segments are presented in Table 1. Radixin, Neural cell adhesion molecule, COP9 signalosome complex (CSN); Cofilin 2; AP-2, dynamin-like, Rab-7a, GST_P are specific proteins that

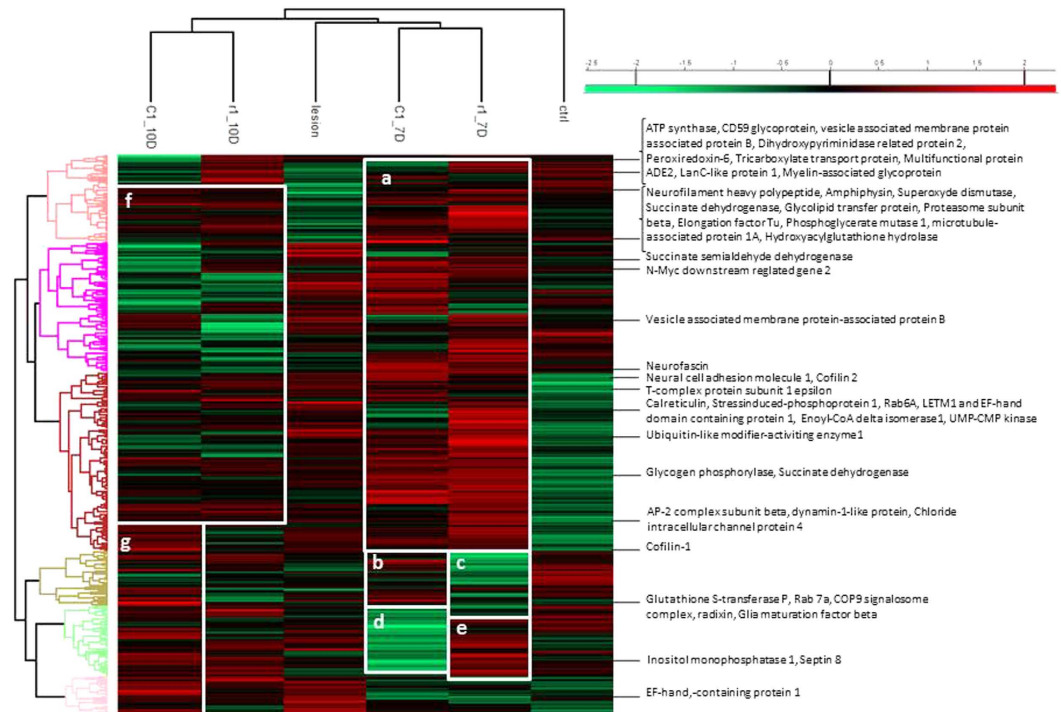


Figure 1. Heat Map of proteins from control, lesion, R1 (rostral segment adjacent to central lesion) at 7 and 10 days (7D and 10D), and C1 (caudal segment adjacent to central lesion) at 7 and 10 days. Green-subexpression, red-overexpression. (a) Protein cluster overexpressed at 7 days compared to 10 days. (b) Protein cluster overexpressed in C1 at 7 days compared to R1 at 7D. (c) Protein cluster subexpressed in R1 at 7D compared to C1 at 7D. (d) Protein cluster subexpressed in C1 at 7D compared to R1 at 7D. (e) Protein cluster overexpressed in R1 at 7D compared to C1 at 7D. (f) Protein cluster subexpressed at 10D compared to 7D. (g) Protein cluster overexpressed at 10D in C1.

are overexpressed only in caudal regions at 7 and 10 days. In rostral segment 7 and 10 days after SCI, amphiphysin, hydroxyacyl glutathione hydrolase, inositol monophosphatase, Neurofilament heavy polypeptide, Glycogen phosphorylase, Superoxide dismutase [Cu-Zn], phosphoglycerate mutase 1, septin 8, microtubule-associated protein 1A, CD59 glycoprotein, LETM1 and EF-hand domain-containing protein 1, Elongation factor Tu, Succinate dehydrogenase [ubiquinone] flavoprotein subunit, Vesicle-associated membrane protein-associated protein B are the ones specifically overexpressed.

Locomotor function recovery. During the initial days post-injury, the compression caused hindlimb paralysis with slight movement in one or two joints in all experimental groups. On following days, the animals in the SCI+ALG and SCI+ALG+GFs biomaterial treatment groups showed a similar gradual recovery of hindlimb locomotion up to 21D after SCI; greater than the recovery in the SCI+SAL group, where only limited recovery of motor function was noted. The significant locomotor improvement ($*p < 0.05$) between SCI+SAL and SCI+ALG/SCI+ALG+GFs was detected at 12 and 14 days post-injury with the final BBB scores $7.3 \pm 2.5/12D$, $8.4 \pm 2.7/14D$ (SCI+ALG+GFs), $6.9 \pm 2.1/12D$, $7.8 \pm 2.9/14D$ (SCI+ALG) and $4 \pm 2.4/12D$, $4.5 \pm 2.7/14D$ (SCI+SAL) (Fig. 2A). The BBB score of hindlimb motor function gradually increased in all experimental groups with the survival (21, 28, 35, 42 and 49 days post-surgery), however the highest scores were observed in SCI+ALG+GFs (10.8 ± 3 , 12.9 ± 3.6 , 13.1 ± 1.2 , 13.8 ± 3.1 , 14.0 ± 3), which closely correlated with SCI+ALG (10.5 ± 2.5 , 11.5 ± 1.4 , 12.4 ± 0.9 , 12.7 ± 0.9 , 12.9 ± 1.9) but the increase was less prominent. The SCI+SAL group following initial gradual motor function improvement at 8 to 28 days, showed only limited recovery during further survival ($7.4 \pm 3.6/21D$, $9.5 \pm 3.6/28D$, $10 \pm 3.1/35D$, $10.6 \pm 2.9/42D$, $11.4 \pm 3/49D$) (Fig. 2A).

Cold allodynia. Increased sensitivity to normally non-painful cold stimulus is a characteristic feature of clinical neuropathic pain states. In our experiments, spinal cord injury result into adverse pain behaviour - development of cold allodynia with positive responses to cold stimulus as paw withdrawal, licking, lifting and shaking of the hindpaw. Increased sensitivity to the acetone application developed mainly at 10D post-injury in the saline ($9.6 \pm 6.2/SCI+SAL$) and alginate ($8.7 \pm 7.8/SCI+ALG$) treated groups. Low increase in sensitivity to a normally innocuous stimulus was observed in SCI+ALG+GFs during entire survival ($4.6 \pm 3.1/10D$, $4.7 \pm 3.8/16D$, $4.6 \pm 2.1/25D$, $6 \pm 2.7/32D$, $6.1 \pm 3.2/49D$), compared to sham ($4 \pm 1.8/10$, 16, 25, 32, 49D). Frequent and more severely aversive responses to the acetone stimulus

Number Accession	Protein Name	Lesion	Rostral 7D	Rostral 10D	Caudal 7D	Caudal 10D
P11505-5	Plasma membrane 1, isoform CRA_b	X				
D4A5×7	Ganglioside-induced differentiation-associated-protein 1	X				
F1LMW7	Myristoylated alanine-rich C-kinase substrate	X				
F1LXA0	NADH dehydrogenase 1 alpha subcomplex	X				
Q64591	2,4-dienoyl-CoA reductase, CRA_a	X				
M0R4S2	Apolipoprotein D	X				
M0R655	Protein Fmnl2	X				
P04904	Glutathione S-transferase alpha-3 protein	X				
P31647	Sodium- and chloride-dependent GABA transporter 3	X				
P35213	14-3-3 protein beta/alpha	X				
P62747	Rho-related GTP-binding protein RhoB	X				
P97532	3-mercaptopyruvate sulfurtransferase	X				
Q02563	Synapticvesicleglycoprotein 2A	X				
Q04462	Valine-tRNA ligase	X				
B0BNM9	Glycolipidtransferprotein		X			
D3ZDK7	ProteinPgp		X			
M0R5K9	40S ribosomal protein S18		X			
D4ACB8	Chaperonin subunit 8, isoform CRA_a		X			
O35814	Stress-induced-phosphoprotein 1		X			
P18418	Calreticulin		X			
Q6PDW4	Proteasomesubunit beta type-1		X			
Q68G41	Dodecenoyl-Coenzyme A delta isomerase		X			
P31399	ATP synthase subunit d, mitochondrial		X			
P39069	Adenylate kinase isoenzyme 1		X			
Q4KM73	UMP-CMP kinase		X			
Q5U300	Ubiquitin-like modifier-activatingenzyme 1		X			
Q5XIN6	LETM1 and EF-hand domain protein 1		X			
Q920L2	Succinatedehydrogenaseflavoprotein		X			
Q9WVB1	Ras-relatedprotein Rab-6A		X			
B0BNM9	Glycolipidtransferprotein		X			
F1LM47	Protein Sucla2			X		
O35244	Peroxiredoxin-6			X		
P07722	Myelin-associatedglycoprotein			X		
P32089	Tricarboxylate transport protein			X		
P51583	Multifunctionalprotein ADE2			X		
Q66H18	Protein Sypl1			X		
Q68FQ0	T-complexprotein 1 subunit epsilon			X		
Q9QUL6	Vesicle-fusing ATPase			X		
Q9QX69	LanC-likeprotein 1			X		
Q9QZR6	Septin-9			X		
F1LM47	Protein Sucla2			X		
B0BNK1	Protein Rab5c				X	
P47942	Dihydropyrimidinaserelatedprotein2				X	
B2GUZ5	F-actin-capping protein subunit alpha-1				X	
D3ZNW5	Neurofascin				X	
P62986	Ubiquitin-60S ribosomal protein L40				X	
G3V9L3	MAGUK p55 subfamily member 3				X	
P19234	NADH dehydrogenaseflavoprotein 2				X	
Continued						

Number Accession	Protein Name	Lesion	Rostral 7D	Rostral 10D	Caudal 7D	Caudal 10D
D4A8U7	Dynactin subunit 1					X
E2RUH2	Ribonuclease inhibitor					X
E9PT65	Protein Rdx					X
G3V8A5	Vacuolar protein sorting protein 35					X
G3V8C4	Chloride intracellular channel protein 4					X
Q63228	Glia maturation factor beta					X
P18484	AP-2 complex subunit alpha-2					X
P97852	Peroxisomal multifunctional enzyme type 2					X
Q510D7	Xaa-Pro dipeptidase					X
Q7TMC7	Ab2-417					X
Q8VBU2	NDRG2					X

Table 1. Specific proteins present in tissue in lesion, rostral at 7 days, rostral at 10 days, caudal at 7 days or in caudal at 10 days.

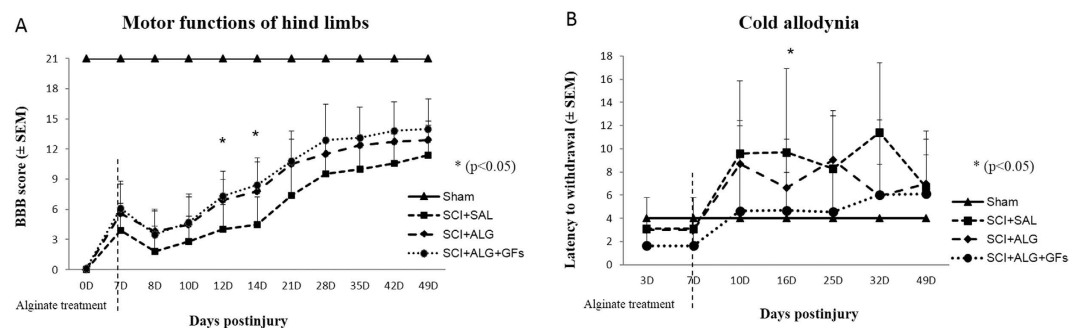


Figure 2. Functional recovery of hindlimb motor (A) and sensory functions (B) following SCI in Sham, SCI+SAL, SCI+ALG and SCI+ALG+GFs experimental groups. (A) * $P < 0.05$ indicates significant differences among the experimental groups.

retained in SCI+ALG group at 10D, 16D, 25D ($8.7 \pm 7.8/10D$, $6.6 \pm 3.3/16D$, $9 \pm 8.3/25D$, $5.9 \pm 2.6/32D$) and SCI+SAL group until 49D post injury ($9.6 \pm 6.4/10D$, $9.7 \pm 7.2/16D$, $8.3 \pm 5/25D$, $11.4 \pm 6/32D$, $6.7 \pm 4.8/49D$). Significant differences (* $p < 0.05$) were observed among SCI+SAL (9.7 ± 7.2) and SCI+ALG+GFs (4.7 ± 3.8) groups at 16D post-injury (Fig. 2B).

Cavity size. During the first week post-injury, a severe inflammatory response occurs at the central lesion. The secondary damage processes lead to cell death and development of cavitations at the epicenter and along the rostrocaudal axis of the spinal cord⁴⁰. In order to fill the cavity and create a permissive environment for regeneration, we administered the liquid form of alginate scaffold directly to the lesion cavity at 7D post injury. Histological assessment of spinal cord sections stained with Luxol Fast Blue revealed cavity area reduction in SCI+ALG+GFs and SCI+ALG groups compared to SCI+SAL at 42 day post-implantation (Fig. 3). Quantitative stereological analyses of tissue fenestration in 1.6 cm segment revealed significant (** $P < 0.01$, *** $P < 0.001$) reduction of cavitation (analysing length and area of cavity) after application of ALG+GFs (cavity length/ 3.3 ± 1.5 mm/area/ 0.56 ± 0.2 mm²) and ALG (cavity length/ 5.4 ± 1.2 mm/area/ 1.13 ± 0.2 mm²) compared to the saline treatment (cavity length/ 7.7 ± 1.4 mm/area/ 1.96 ± 0.3 mm²) (Fig. 3).

Quantification of NeuN. Quantification analyses of representative transverse sections were processed bilaterally in dorsal (Laminae I–IV), ventral horns (Laminae VIII–IX) and Laminae IV–V, rostrally and caudally from the lesion site (Fig. 4). The higher number of NeuN-positive cells was documented rostrally from the injury site in all studied groups SCI+ALG+GFs, SCI+ALG and SCI+SAL. The most profound neuronal loss was observed in the SCI+SAL group (Rostral/Laminae I–IV 69.5 ± 8.1 ; Laminae VIII–IX 13 ± 1.5 ; Caudal/Laminae I–IV 68.8 ± 17.7 ; Laminae VIII–IX 11.8 ± 5.8). The delivery of ALG or ALG+GFs promoted the survival of neuronal cells, resulting in a significant increase in number of NeuN-positive cells SCI+ALG: Rostral/Laminae I–IV 103.1 ± 26.6 ; Laminae VIII–IX 22 ± 5.5 ; Caudal/Laminae I–IV 103.3 ± 16.8 ; Laminae VIII–IX 15.8 ± 2.7 ; SCI+ALG+GFs: Rostral/Laminae I–IV

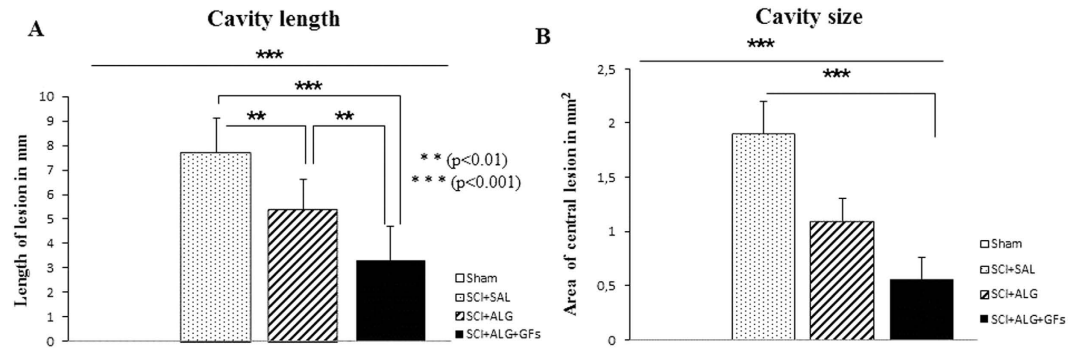


Figure 3. Morphometric analyses of cavity length (A) and size (B) in experimental groups showed significant reduction after intraspinal injection of biomaterial alginate (** $P < 0.01$, *** $P < 0.001$). Cavity size was expressed by mm in injured experimental groups (SCI+SAL, SCI+ALG and SCI+ALG+GFs) relative to Sham spinal cord without cavitations represent by zero.

110 ± 5.3 ; Laminae VIII–IX 27.3 ± 4.4 ; Caudal/Laminae I–IV 125.5 ± 4.2 ; Laminae VIII–IX 23.6 ± 6.4). Moreover, the number of NeuN positive cells in the SCI+ALG+GFs group closely correlated with the NeuN numbers observed in Sham group (Rostral/Laminae I–IV 122 ± 5.2 ; Laminae VIII–IX 23.1 ± 5 ; Caudal/Laminae I–IV 120.7 ± 12.7 ; Laminae VIII–IX 24 ± 3.8) (Fig. 4). The differences in NeuN positive profiles show a statistical significance between individual experimental groups: Sham, SCI+SAL, SCI+ALG, SCI+ALG+GFs *** $P < 0.001$, ** $P < 0.01$, * $P < 0.05$.

ChAT labeled motoneurons. The average number of ChAT positive cells in the SCI+SAL, SCI+ALG and SCI+ALG+GFs groups was compared to confirm the hypothesis whether neuronal sparing has included motor neurons of ventral horns. Rostral to the lesion site, the number of spared ChAT+ neurons within the ventral horns significantly increased (* $P < 0.05$) following alginate biomaterial treatment (10 ± 2.1 /SCI+ALG; 10.9 ± 1.7 /SCI+ALG+GFs) when compared to the control saline group (7.4 ± 0.9) (Figs 5 and 6). Significant differences in sparing of motor neurons (* $P < 0.05$, *** $P < 0.001$) were also recorded among experimental groups caudal to the injury site, although the average number of positive cells had declined (6.9 ± 1.5 /SCI+ALG+GFs, 5.4 ± 0.9 /SCI+ALG, 2.8 ± 0.8 /SCI+SAL, 11.9 ± 1.9 /Sham) compared to spinal rostral part (Figs 5 and 6). Our results demonstrate that alginate biomaterial implantation resulted not only in common NeuN positive neurons sparing, but also in the specific sparing of endogenous ChAT+ motor neurons.

Synaptic vesicles alterations. In the spinal cord of Sham and both SCI-SAL and SCI-ALG groups of treated rats, synaptophysin immunoreactivity (SYN+IR) appeared as numerous diffusely distributed fine dots along the surface of motor neurons and their proximal dendrites, and delineated their polygonal contours (Fig. 7A,B). However, after ALG+GFs treatment, the density of SYN+ vesicles around remaining CHAT+ motor neurons of the anterior horns strikingly increased when compared to all experimental groups (Fig. 7C,D). The immunoreactive profiles appeared as coarse granules of different size that were also distributed on motor neuron surface. Quantitative analysis of SYN+ vesicle expressed as % of SYN+ positive vesicles within identical fields of anterior horns in all experimental groups confirmed significant increase in ALG+GFs treated group, particularly caudally to the epicentre of injury (Fig. 7D). Interestingly, we did not see any differences in the density of SYN+ positive vesicles within segments above the lesion site (data not shown).

CGRP positive fibres. CGRP immunoreactivity was observed in all experimental groups (SCI+ALG+GFs, SCI+ALG, SCI+SAL) in fibres and punctuate terminals of superficial dorsal horn (Laminae I–III) and LT (LT-Lissauer's tract) area⁴⁴ located along the lateral edge of the dorsal horn and medial grey mater (Fig. 8). Moreover, depending on the experimental group, few individual CGRP positive fibres extending from Lamina III toward Laminae V (0.226 ± 0.099 mm/SCI+SAL) and VII (Figs 8 and 9) were detected. The longest CGRP+ fibres with the average of length 0.301 ± 0.103 mm were observed after administration of alginate biomaterial alone and alginate biomaterial with affinity-bound GFs to the injured spinal cord (0.301 ± 0.103 mm/SCI+ALG; 0.27 ± 0.053 mm/SCI+ALG+GFs). Sham spinal cord didn't contain CGRP positive fibres extended into the intermedia spinal cord layers; however CGRP terminals within superficial dorsal horn were frequently observed. The differences associated with length of fibres show statistical significance (** $P < 0.01$, * $P < 0.05$) only between Sham and other experimental groups (SCI+SAL, SCI+ALG, SCI+ALG+GFs) (Fig. 9).

The number of immunolabeled CGRP fibres varied among individual experimental groups and areas of spinal cord. The most numerous CGRP positive fibres, forming bundles-like structures were observed in rostral segments from the lesion site after the delivery of alginate biomaterial with the affinity-bound

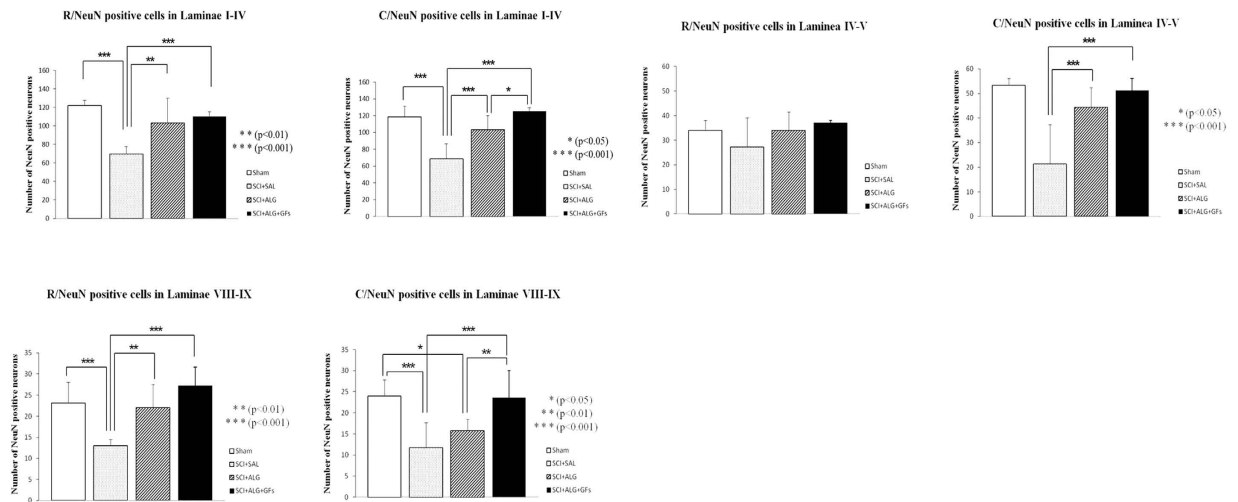


Figure 4. Stereological analyses of NeuN positive cells in Laminae I–IV, Laminae IV–V and Laminae VIII–IX after SCI and treatment. Number of NeuN labeled neurons in all studied areas increased after pure and enriched alginate administration compared to saline. Among the experimental groups we observed statistical differences (** $P < 0.001$, ** $P < 0.01$, * $P < 0.05$).

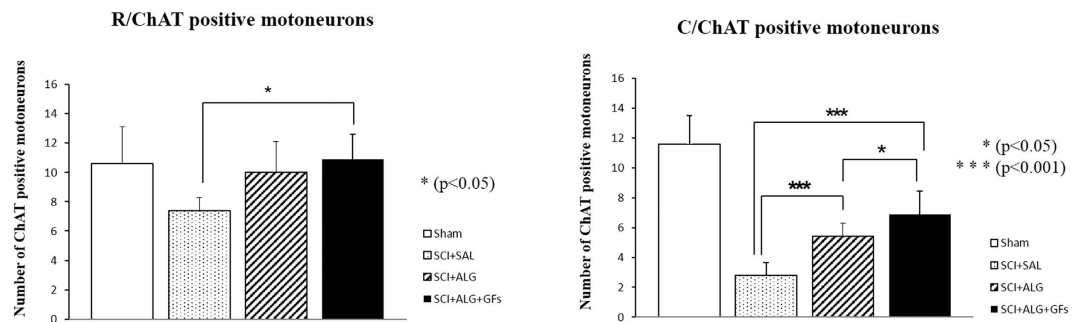


Figure 5. Quantification of ChAT labeled motoneurons in the Laminae VIII–IX. Marked depletion of motoneurons was observed caudally to the lesion site when compared with segment located rostrally. Significantly higher number of ChAT positive neurons was detected after delivery of enriched alginate in both studied segments (rostral, caudal) (** $P < 0.001$, * $P < 0.05$).

GFs (6.7 ± 2.3 /SCI+ALG+GFs, 4.5 ± 4 /SCI+ALG, 4.2 ± 3.3 /SCI+SAL, 1 ± 1 /Sham). Average number of positive fibres was slightly decreased caudally to the epicentre of injury (5.9 ± 4 /SCI+ALG+GFs, 4.8 ± 4.5 /SCI+ALG, 4.1 ± 3 /SCI+SAL, 1 ± 1 /Sham) (Figs 8 and 9). Among the individual experimental groups in both studied parameters we did not observe statistical differences (Fig. 9).

Axonal sprouting via BDA tracing. BDA delivery to the sensorimotor cortex served to label descending CST axons of spinal cord. In sham animals, BDA-labelled CST axons were detected along the entire length of sagittal sections (16 mm) of the spinal cord; more specifically in the ventral part of the dorsal column, where stripe of organized BDA positive axons occurred ($16 \text{ mm} \pm 0$) (Figs 10 and 11). After spinal cord injury, CST axons appeared disorganized, ended above the lesion site and many cut BDA axons formed terminal structures like buttons. Re-growth of CST fibres into denervated areas of spinal cord was monitored following alginate administration. Moreover, the alginate biomaterial alone and with affinity-bound EGF/bFGF promoted increased re-growth of few BDA positive fibres through the central lesion with occasional innervations below the lesion site ($2.9 \text{ mm} \pm 0.7$ from a total 16 mm length of section) compared to saline treatment ($0.6 \text{ mm} \pm 0.1$) (Figs 10 and 11) (* $P < 0.05$).

Iba1 immunohistochemistry. In order to monitor the immune response of host tissue, particularly the presence of microglia cells after alginate biomaterial treatment, Iba1 immunoreactivity in lesion site and also in the adjacent segments located 0.8 cm rostrally/caudally to the epicenter, were used. Enhancement of the microglia responsiveness and subsequent density was observed mainly after injury with injection of saline (SCI+SAL: Ros/17 \pm 3, Ros-Centre/23.3 \pm 3.4, Centre-Caud/22.3 \pm 4.4, Caud/21.3 \pm 4.9), while the decreased tendency of Iba1 expression was seen after treatment with alginate biomaterial

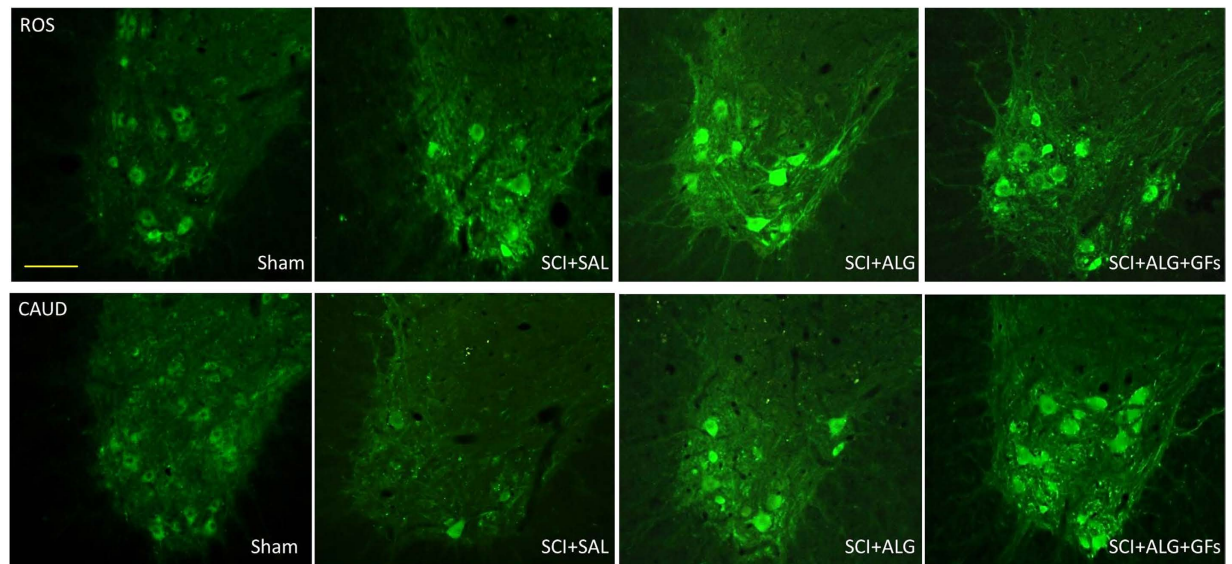
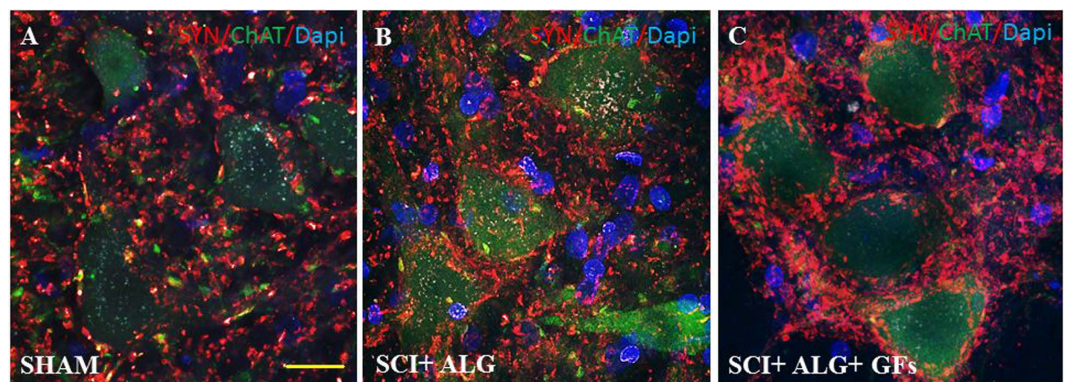


Figure 6. Representative transverse sections revealing ChAT positive motoneurons located rostrally and caudally to the lesion site following SCI in Sham, SCI+SAL, SCI+ALG and SCI+ALG+GFs experimental groups. Significant decrease of ChAT immunohistochemical staining was observed in ventral horns caudally to the lesion site (lower panel) following SCI and saline delivery. Injected alginate supports survival of ChAT positive motoneurons. Scale bar = 500 μ m.



D Quantification of SYN+ vesicles

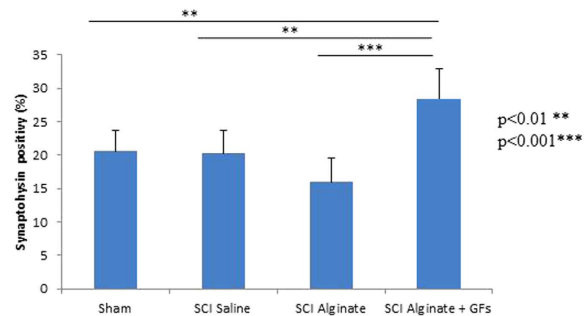


Figure 7. Distribution of synaptophysin positive vesicles (red) in the area of ChAT positive motoneurons (green) of the ventral horns. The density of vesicles after ALG+GFs treatment (C) is increased compared to both sham (A) and ALG without GFs group (B). (D) Quantification has revealed statistical significance only between ALG+GFs group and other experimental groups (SHAM, SCI+SAL, SCI+ALG). (** $P < 0.01$, *** $P < 0.001$). Scale bar = 50 μ m.

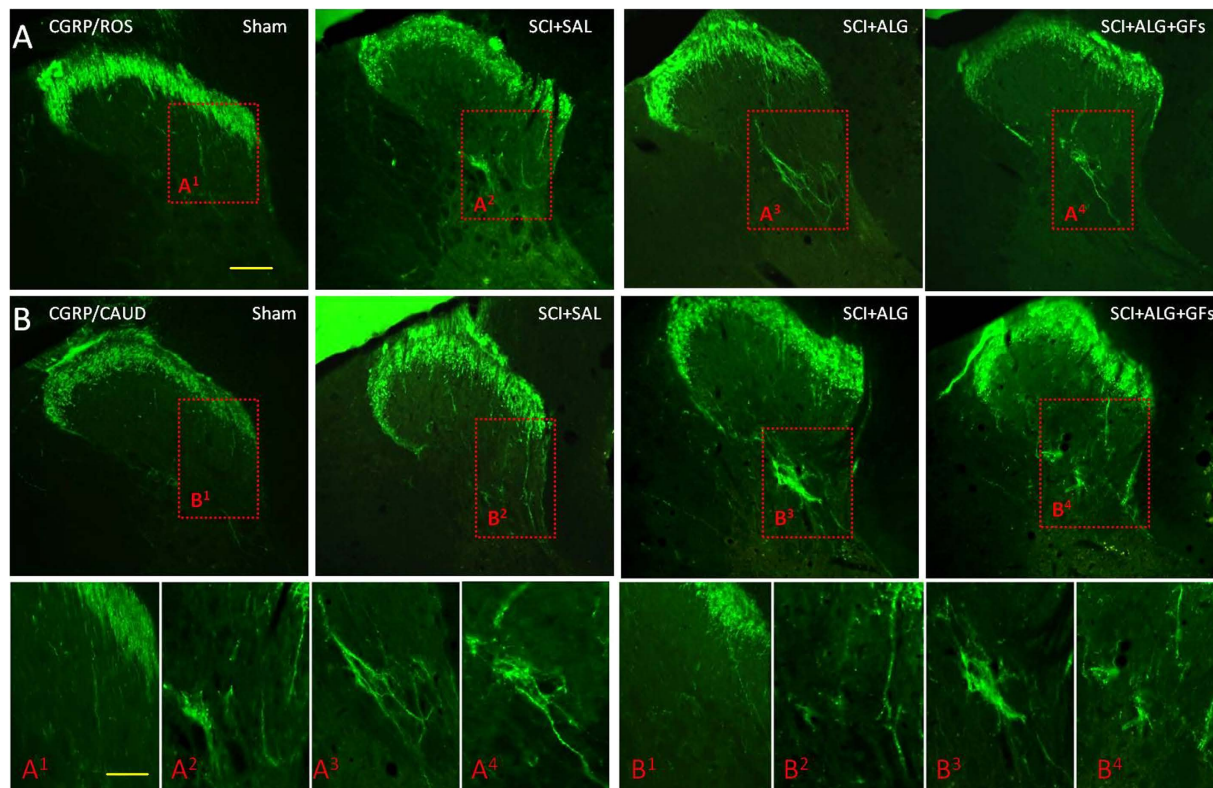


Figure 8. CGRP expression in transverse sections of dorsal horn/thoracic spinal cords from Sham, SCI+SAL, SCI+ALG and SCI+ALG+GFs groups 49D post-injury. Representative pictures demonstrate differences in CGRP expression, particularly in number and length of CGRP positive fibers among the experimental groups. Note, enhanced growth and branching of CGRP fibers from dorsal horn to Laminae III–V and VII in SCI+ALG and SCI+ALG+GFs groups (A^3 , B^3 , A^4 , B^4) when compared to sham and saline rats (A^1 , B^1 , A^2 , B^2). Scale bar = 500 μm . Lower panel shows higher magnification from corresponding regions. Scale bar = 250 μm .

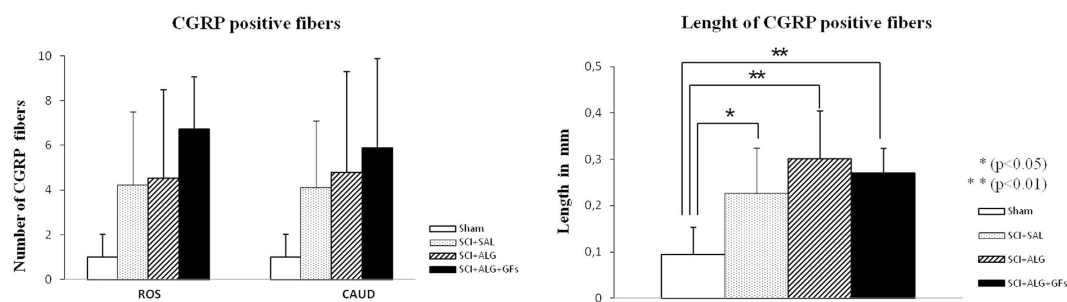


Figure 9. Number and length of CGRP positive fibers. (A) Quantitative analyses of CGRP positive fibers number showed no significant differences between individual experimental groups. (B) Statistical significance was observed only in the length of CGRP positive fibers between Sham and other experimental groups (SCI+SAL, SCI+ALG, SCI+ALG+GFs) (* $P < 0.05$, ** $P < 0.01$, *** $P < 0.001$).

(SCI+ALG+GFs: Ros/ 14.8 ± 2.1 , Ros-Centre/ 17.3 ± 4.3 , Centre-Caud/ 18.1 ± 3 , Caud/ 17.4 ± 2.9 ; SCI+ALG: Ros/ 16.4 ± 2.5 , Ros-Centre/ 20.5 ± 3.2 , Centre-Caud/ 17.6 ± 4.2 , Caud/ 14.2 ± 4.3) (Fig. 12, Supplementary Figure 5). Positivity of Iba1 expression in Sham animals revealed baseline levels (Ros/ 9.4 ± 1.5 , Ros-Centre/ 9.3 ± 0.8 , Centre-Caud/ 9.3 ± 1.6 , Caud/ 9.8 ± 1.6). Among experimental groups and individual parts of spinal cord significant differences were detected (*** $P < 0.001$, ** $P < 0.01$, * $P < 0.05$, Supplementary Figure 5).

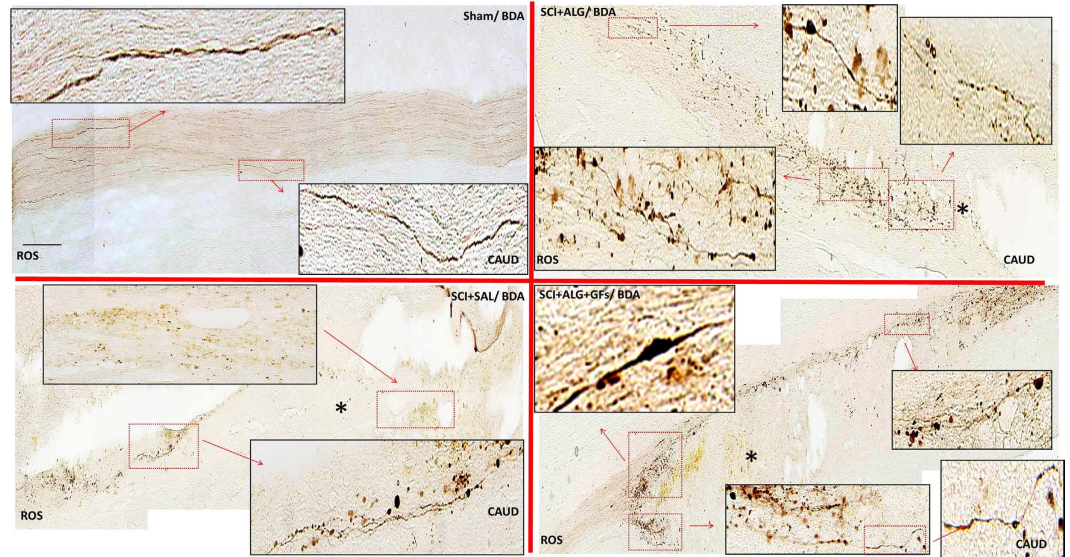


Figure 10. BDA labeling in the representative sagittal sections in Sham, SCI+SAL, SCI+ALG and SCI+ALG+GFs groups 49D post injury. Representative pictures and corresponding details (boxed areas) illustrate growth potential of CST fibers after SCI and individual treatments. Increased positivity of BDA was seen after alginate administration (SCI+ALG and SCI+ALG+GFs groups) where CST axons were growing around the lesion site towards disconnected caudal segment. Scale bar = 500 μ m.

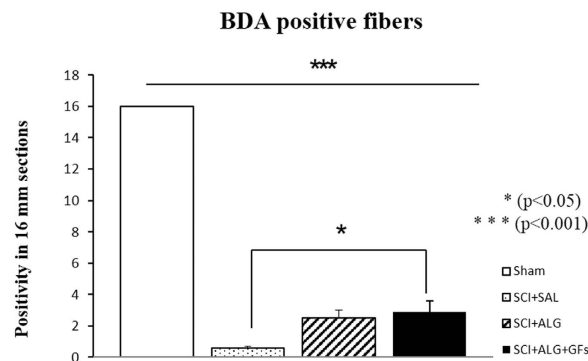


Figure 11. Quantification of BDA positivity in sagittal section of spinal cord. Administration of alginate enriched with growth factors leads to the significant (* $P < 0.05$) increase of BDA labeled fibers when compared to saline treatment.

Glial scar modulation (GFAP immunoreactivity). Baseline expression of GFAP-positive astrocytes with the characteristic round small soma and slender, long processes were seen in Sham spinal cord distributed throughout white and grey matter (Ros/ 11 ± 1.8 , Ros-Centre/ 10.81 ± 1.41 , Centre-Caud/ 10.81 ± 1.41 , Caud/ 12.6 ± 1.6) (Fig. 13). The significant response of astrocytes that resulted in increased density and change of cellular morphology was observed following SCI and saline delivery (** $P < 0.001$, ** $P < 0.01$, * $P < 0.05$). Astrocytes assumed increased GFAP staining with subsequent cellular transformation into swollen hypertrophic appearance and short, thick processes indicating activated phenotype (Fig. 13). Similarly, alginate biomaterial treatment alone or with affinity-bound bFGF/EGF induced appearance of activated astrocytes, but with poorer ramification as seen after saline delivery (Fig. 13). The densitometry analysis revealed differences between the individual parts of 1.6 cm sections (Ros, Ros/Central, Central/Caudal, Caudal) of spinal cord. The highest positivity of GFAP was measured within Centro-Caudal site in all experimental groups (SCI+ALG+GFs: Ros/ 11 ± 1.8 , Ros-Centre/ 10.81 ± 1.41 , Centre-caud/ 10.81 ± 1.41 , Caud/ 12.6 ± 1.6 ; SCI+ALG: Ros/ 14.9 ± 4.1 , Ros-Centre/ 13.4 ± 3.6 , Centre-Caud/ 16 ± 3.5 , Caud/ 13.8 ± 3.1 ; SCI+SAL: Ros/ 17.9 ± 2.2 , Ros-Centre/ 18 ± 3.7 , Centre-Caud/ 21.5 ± 3.9 , Caud/ 21.4 ± 1.6) (Supplementary Figure 6). The quantification of GFAP immunoreactivity on transverse sections from rostral and caudal segments of spinal cord also confirmed an increase in immunoreactivity caudally to the lesion site especially after saline delivery (Rostrally: 14.8 ± 4.2 /SCI+ALG+GFs, 14.9 ± 4.9 /SCI+ALG, 18.11 ± 1.6 /SCI+SAL,

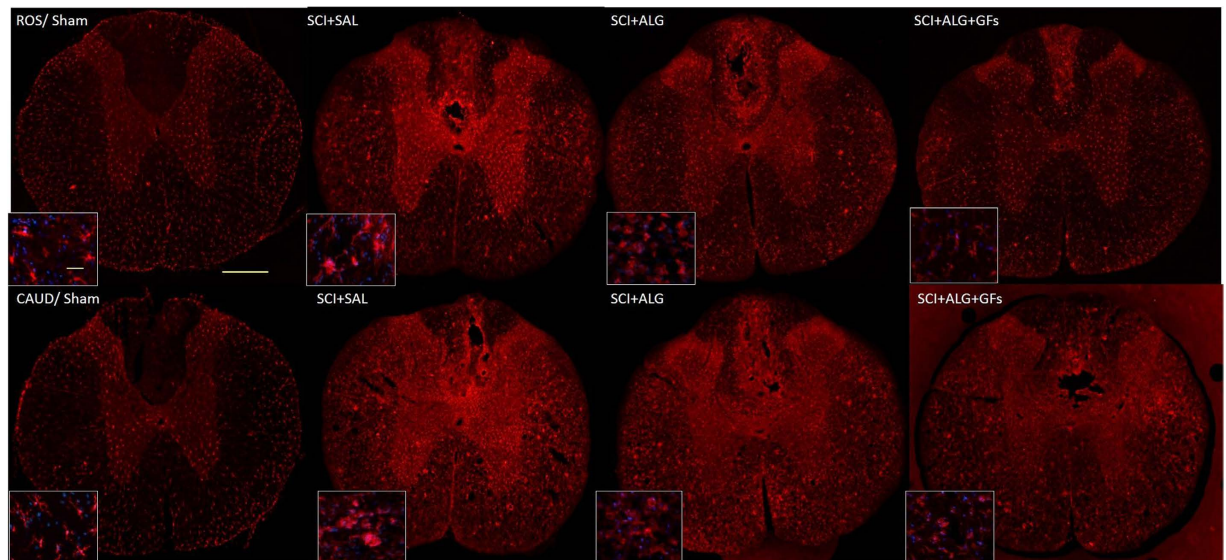


Figure 12. Representative transverse sections of Iba1 expression from caudal and rostral segments of spinal cord. Sections illustrate changes in activation and cell morphology after saline and alginate treatment. Baseline expression of non-active microglia in gray and white matter was observed in Sham animals. Strong activation of microglia characterized by enlarged round-shaped perikaryon with truncated, thick and ramified processes was detected in SCI+SAL group. Alginate treatment (SCI+ALG and SCI+ALG+GFs groups) inhibited activation of Iba1 positive cells. Scale bars = 500 μ m, 10 μ m (higher magnification of boxed area).

13.6 \pm 1.6/Sham; Caudally: 16.3 \pm 3/SCI+ALG+GFs, 15.3 \pm 3.4/SCI+ALG, 17.6 \pm 2.4/SCI+SAL, 13.2 \pm 0.5/Sham). Differences in GFAP density between experimental groups in rostro-caudal segments were without observed significant differences (Supplementary Figure 6).

Angiogenesis. For visualization of the vascular structures, the endothelial cell marker von Willebrand Factor (vWF) was used (Supplementary Figure 7). Numerous positive blood vessels were observed in the Sham group, mainly in the white matter compared to the injured spinal cord groups (SCI+SAL or SCI+ALG), where the density of blood vessels decreased in close vicinity of the lesion site (Supplementary Figure 7). Treatment with alginate biomaterial with the affinity-bound GFs resulted in an increase of vWF positive blood vessels in the white matter and in grey matter as well, at lesion site. Results obtained from immunohistochemical analyses suggest that GFs-enriched alginate biomaterial created a suitable environment for blood vessels survival or reconstruction, but without significant differences between treatment groups (data not shown).

Discussion

Currently, the field of SCI neurotherapeutics is still in its infancy and there are no effective and approved therapies for SCI in humans. A contributing factor for such failed neuroregenerative processes has been attributed partly to the development of the optimal regeneration-supportive microenvironment that can initiate a neurobridge connecting disconnected spinal cord segments.

The present study clearly demonstrates that the local delivery of injectable alginate biomaterial capable of increasing the bioavailability of key growth factors such as bFGF and EGF and their appropriate presentation improve the repair of SCI through multiple mechanisms, such as: i) reducing the central lesion cavity, ii) increasing the number of surviving neurons including ChAT+ motor neurons and their synaptic connections, iii) enhancing outgrowth of CST axons, iv) preserving or stimulating formation of new blood vessels, and v) attenuating inflammation; which altogether enhance the functional recovery after SCI without sensory impairments.

Here we applied a well-characterized compression model of spinal cord injury leading to overall impairment of motor and sensory functions associated with loss of corresponding neuronal pools, overreaction of microglia/astrocytes and inability of axonal regrowth through the lesion site⁴⁵. Using a tissue micro-proteomic approach, we established that in the time period after lesion, the nature of proteins varied throughout the spinal rostro-caudal axis. Particularly, the proteins found in caudal and rostral segments at 7 and 10 days after SCI were different compared to 3 days post injury⁴⁰. Previous data clearly show that three days after lesion, the factors secreted in the lesion and rostral segments are anti-inflammatory and neurotrophic, while in the caudal region a cocktail of apoptotic and neurotoxic

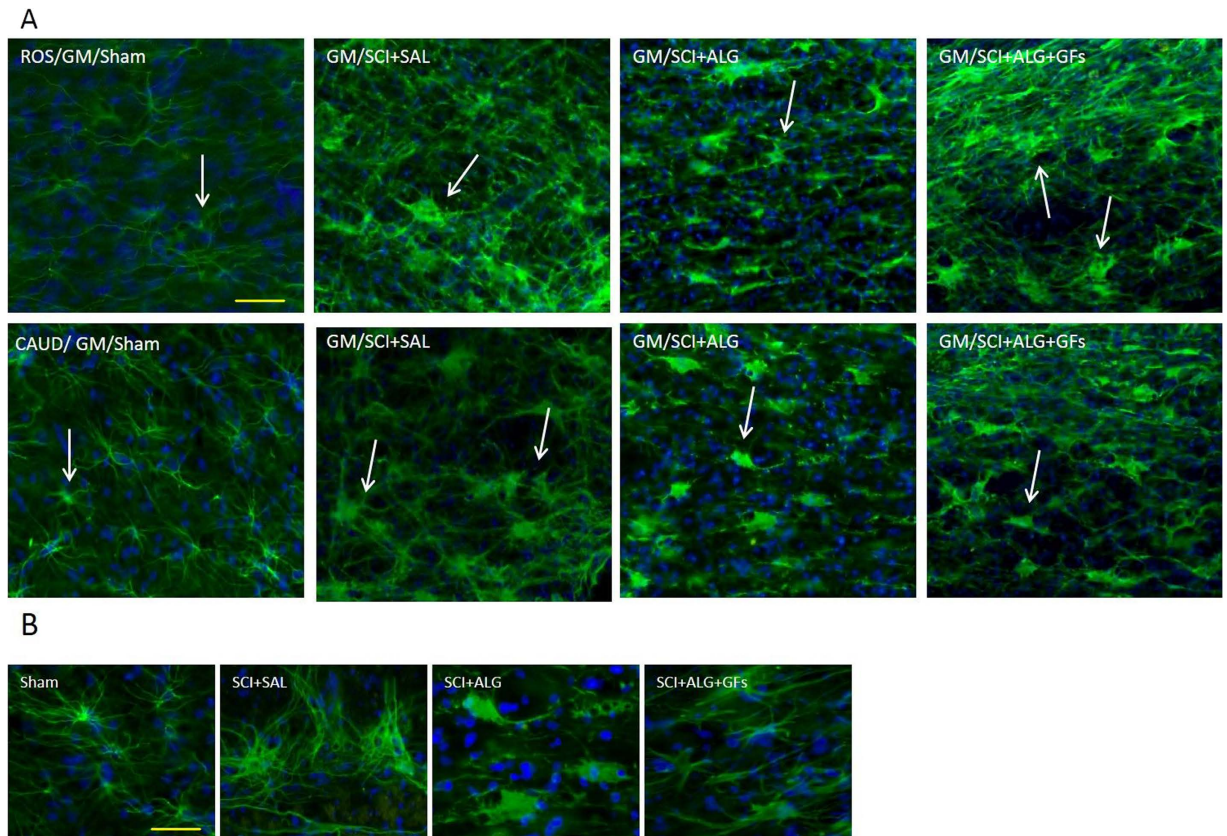


Figure 13. Baseline expression of GFAP-positive astrocytes with the characteristic round nuclei and slender, long processes distributed throughout both white and gray matter was revealed in Sham animals 49D post-injury. SCI and vehicle/saline treatment induced increase in GFAP immunohistochemical staining associated with cellular transformation; swollen hypertrophic appearance and short, thick processes indicating activated phenotype. Similarly alginate slightly increased the GFAP density but positive cells were without hypertrophic appearance. Scale bars = 100 μ m (A), 50 μ m (B).

proteins predominate³⁰. The present study shows that on days 7 and 10 after SCI, in the caudal segments neurotrophic factors are overexpressed, as well as adhesion molecules and signalling proteins. In contrast, in rostral segments the proteins overexpressed are involved in metabolism at the level of the mitochondria or the cytoplasm, as well as in intracellular signalling. This clearly indicates that real differences exist between the rostral and caudal segments in terms of physiological and molecular processes, and that these differences are dynamic in time. Importantly, the results indicate that the caudal region possesses all the factors that can stimulate neurite outgrowth, but these seem to be insufficient in amount and are blocked by proteoglycans. Taking into account these *ex vivo* data, we attempted to connect the rostral and caudal segments through the lesion by constructing an alginate biomaterial bridge loaded with GFs. Thus all immunohistochemical and tracing analyses were performed along the rostro-caudal axis, to better understand and define differences in pathological or regenerative processes above and below the lesion site after biomaterial treatment.

Our strategy is in line with recent pre-clinical studies performed after incomplete/complete injuries, and attempting to reconnect links with the tissue below the injury site, either bypassing the central lesion or rebuilding tissue in a cyst mediated via the application of biomaterials^{46–50}. The novelty of our strategy is the combination of biomaterial used as a bridge together with sustained delivery of key growth factors for SCI repair. *In vitro*, this combination was found to be effective in promoting cell retention and expansion, while also enabling neural progenitor lineage differentiation *in situ*²⁵. In continuity with these findings, our *in vivo* results document significant spinal cord tissue sparing, resulting in neuronal sparing that may lead to enhanced plasticity and reorganization of preserved neuronal circuits. Furthermore, the sparing of ChAT positive motor neurons may correlate with the trend of motor function improvement observed during the whole survival period in SCI rats treated with the alginate scaffold with or without GFs, in comparison to animals treated with saline.

Physiological locomotion is governed by motoneurons that receive synaptic inputs from local interneurons, descending pathways and proprioceptive sensory neurons. The convergence of proper excitatory and inhibitory inputs on motoneurons mediated by synaptic connections is required for motor control,

reflexes and tonic firing of the motoneurons. Disruption of the cellular components and/or synaptic connectivity in this spinal circuitry has been implicated in motoneuron spasticity and various motoneuron disorders⁴⁵. For this reason in this study we followed the response of ChAT motor neuron-related synaptic vesicles in segments above and below the central lesion using synaptophysin immunohistochemistry (SYN+IR). Synaptophysin is the most abundant integral membrane protein of synaptic vesicles⁵¹ and can be used as a marker protein of synaptic vesicles in the central and peripheral nervous systems⁵². The present data document that SYN+IR around motor neurons in the anterior horns showed similar patterns in most experimental groups, except for the group receiving ALG+GFs. In these rats, we observed more intense SYN+IR in the caudal compared to the rostral segments. These results may be linked with our proteomic data, confirming the higher expression of neurotrophic and synaptogenetic factors in the caudal segment, thus producing a favourable environment for synaptic rebuilding reflected by increased SYN+IR after ALG+GF delivery. Although our proteomic findings respond to 10 days survival following SCI, the higher level of synaptogenetic factors may be further potentiated with a GF-enriched environment, as most likely seen in the present study with ALG+GF delivery. The mechanisms mediating increase in SYN+IR may reflect several processes such as: i) up-regulation of synaptic functions after SCI, which is more likely related to the release of excitatory amino acids, or ii) may indicate plastic changes associated with formation of new synapses. Thus, to further understand changes in motoneuron synaptic connectivity after SCI treatment, the transporter systems such as vesicular glutamate and glycine transporters (VGluT1/VGluT2, GlyT2) need to be further studied.

Furthermore, SCI-induced secondary pathological processes also cause interruption of the CST tract^{53,54}, leading to partial or complete impairment of descending motor pathways for skilled movements below the injury^{2,55}. The compression model used in the present experimental study carried out at thoracic levels caused interruption of axon fibres corresponding to both hindpaws with some degree of spontaneous regeneration and behavioural improvements⁵⁶. The behavioural outcome can be enhanced by promoting the axonal integrity and plasticity of the corticospinal tract and descending serotonergic pathways via GF delivery⁵⁷. In according with these finding, our data confirm significant re-growth of BDA positive fibres observed after intraspinal injection of GF-enriched alginate biomaterial at the central lesion⁵⁸. In contrast, delivery of alginate biomaterial alone did not induce the same effect as the GF-enriched biomaterial. The neuroprotective effect of biomaterial on axon regrowth has been described in many other *in vitro* and *in vivo* studies, where *in vitro* studies demonstrate that biomaterial promotes neural cell attachment and neurite outgrowth^{59–61} while *in vivo* studies show only partial regeneration after gel is implanted in the injured spinal cord^{23,62,63}. The explanation for differences in axonal outgrowth seen between *in vitro* and *in vivo* may be given by multiple factors associated with inhibitory, immune, endocrine processes that are typical for the complex *in vivo* environment^{21,64,65}. In addition, optimal regeneration of axons requires preserved vascular supply. Our data indicate that an alginate scaffold may provide an appropriate substrate also for the survival and re-growth of blood vessels. Furthermore, growth factors affinity-bound to the alginate scaffold promote the survival, proliferation and differentiation of microvascular cells^{66,67}, which results in extensive collateral branching of damaged vessels and thickening of vessels within the lesion site.

Another important issue in damaged spinal cord pathology is the development of central sensitization, which often contributes to hyperalgesia and allodynia typically associated with inflammatory pain⁶⁸. In the present study therefore we addressed the response of sensory fibres expressing calcitonin gene-related peptide (CGRP) following treatment with alginate biomaterial. Our data show that significant increase in CGRP+ fibres occurred in the dorsal horns and lateral grey matter after ALG+GF delivery. These most likely represent unmyelinated pelvic afferent fibres that convey thermal and nociceptive information⁶⁹. Plastic re-organization of spinal neural circuitry and morphological changes in the spinal reflex pathway (primary afferent fibres and spinal interneurons) may be responsible for serious post-injury complications that could lead to uncontrolled excitatory activity of glutamate-driven sympathetic preganglionic neurons, and similarly to loss of inhibitory GABAergic/glycinergic interneurons that could have an impact on increased bilateral hind limb sensitivity to cold. Although the administration of GF-enriched alginate biomaterial promoted extending of CGRP positive fibres, we did not observe adverse sensory response to cold, such as observed after saline or pure alginate delivery. Responses of the hind limbs were relatively stable in the SCI+ALG+GF treated group during the whole survival period, with intensity similar to that in the sham controls. From our results we can speculate that alginate biomaterial with affinity-bound growth factors enhanced changes in CGRP fibres, but without behavioural adverse sensory response.

Central sensitization of spinal neurons or neuronal hyper-responsiveness and alterations in behavioural pain thresholds may be also in close correlation with microglial activation, as pointed out in some recent studies^{70–72}. It is known that release of excitatory amino acids⁷³, interleukin-1⁷⁴, and prostaglandin E2⁷⁵ by microglia actively participate in the generation of central sensitization after SCI. On the basis of this hypothesis we can conclude that significant microglia response after saline delivery could induce an increase in central sensitization of spinal neurons and promote the kind of adverse sensory response to cold detected in the present study. However, ALG+GF treatment causing attenuation of microglia may lead to normalization of sensory behaviour.

Reactive astrocytes together with microglia and meningeal fibroblasts are known to participate in scar formation, representing a mechanical and chemical barrier for nerve tissue regeneration⁷⁶. Significant

differences in GFAP+IR between the experimental groups were observed spatially, mainly in the central and caudal segments. However, treatment with ALG and ALG+GFs did not attenuate the activation and proliferation of astrocytes after SCI, which may ultimately contribute to glia scarring at the central lesion site.

In the present experimental study we tried to define the efficacy of usage of alginate itself as well as alginate enriched with GFs for spinal cord repair. EGF and bFGF were selected due to their stable and high binding properties, as well as long-term sustained GF release from alginates, confirmed *in vitro*²⁵. Although these factors are important for their mitotic and partially differential properties for endogenous neural progenitors and their ability to accelerate neovascularisation, they may also contribute to astrogliosis and tissue scarring. In future experiments therefore, other neurotrophins such as BDNF, GDNF, NT-3 with neuroprotective action, or VEGF, PDGF with angiogenic properties should be considered for incorporation into one alginate device. In addition, simultaneous digestion of Chondroitin Sulfate Proteoglycans by chondroitinase ABC (ChABC) should be considered as well^{8,9,43}. From the surgical point of view, the alginate scaffold described herein was injected into irregular spinal cord cavities, where it adjusted itself into the cavity shape and in the presence of calcium ions could undergo gelation *in situ*. This type of non-invasive technique for vehicle administration is potentially advantageous in particular when considering the fragility of the spinal cord site.

Conclusions

We describe here that an affinity-binding alginate scaffold with sustained presentation of bFGF/EGF has the potential to serve as a useful delivery vehicle in a certain model of SCI damage, with proven capability to promote neuronal sparing, modulate motoneuron synapses, enhance regrowth of BDA-positive CST fibres and the presence of vWF positive vessels at the injury site, as well as enhancing changes in CGRP fibres, but without behavioural adverse sensory response.

Furthermore, combinatory-based local therapy using a biomaterial scaffold with neurotrophic factors, inhibitory molecules, enzymes that could digest deposits of extracellular matrix, e.g. chondroitin sulphate proteoglycans, as well as stem cells, may provide more advanced therapy for spinal cord repair.

References

- Rowland, J. W., Hawryluk, G. W., Kwon, B. & Fehlings, M. G. Current status of acute spinal cord injury pathophysiology and emerging therapies: promise on the horizon. *Neurosurg Focus* **25**, E2 (2008).
- Kakulas, B. A. A review of the neuropathology of human spinal cord injury with emphasis on special features. *J Spinal Cord Med* **22**, 119–124 (1999).
- Kwon, B. K., Tetzlaff, W., Grauer, J. N., Beiner, J. & Vaccaro, A. R. Pathophysiology and pharmacologic treatment of acute spinal cord injury. *Spine J* **4**, 451–464 (2004).
- Norenberg, M. D., Smith, J. & Marcillo, A. The pathology of human spinal cord injury: defining the problems. *J Neurotrauma* **21**, 429–440 (2004).
- Fitch, M. T. & Silver, J. CNS injury, glial scars, and inflammation: Inhibitory extracellular matrices and regeneration failure. *Exp Neurol* **209**, 294–301 (2008).
- Ha, K. Y. & Kim, Y. H. Neuroprotective effect of moderate epidural hypothermia after spinal cord injury in rats. *Spine (Phila Pa 1976)* **33**, 2059–2065 (2008).
- Cafferty, W. B. *et al.* Chondroitinase ABC-mediated plasticity of spinal sensory function. *J Neurosci* **28**, 11998–12009 (2008).
- Galtrey, C. M., Asher, R. A., Nothias, F. & Fawcett, J. W. Promoting plasticity in the spinal cord with chondroitinase improves functional recovery after peripheral nerve repair. *Brain* **130**, 926–939 (2007).
- Galtrey, C. M. & Fawcett, J. W. The role of chondroitin sulfate proteoglycans in regeneration and plasticity in the central nervous system. *Brain Res Rev* **54**, 1–18 (2007).
- Andrade, M. S., Mendonca, L. M. & Chadi, G. Treadmill running protects spinal cord contusion from secondary degeneration. *Brain Res* **1346**, 266–278 (2010).
- Cizkova, D. *et al.* Response of ependymal progenitors to spinal cord injury or enhanced physical activity in adult rat. *Cell Mol Neurobiol* **29**, 999–1013 (2009).
- Thuret, S., Moon, L. D. & Gage, F. H. Therapeutic interventions after spinal cord injury. *Nat Rev Neurosci* **7**, 628–643 (2006).
- Gupta, D., Tator, C. H. & Shoichet, M. S. Fast-gelling injectable blend of hyaluronan and methylcellulose for intrathecal, localized delivery to the injured spinal cord. *Biomaterials* **27**, 2370–2379 (2006).
- Jain, A., Kim, Y. T., McKeon, R. J. & Bellamkonda, R. V. *In situ* gelling hydrogels for conformal repair of spinal cord defects, and local delivery of BDNF after spinal cord injury. *Biomaterials* **27**, 497–504 (2006).
- Piantino, J., Burdick, J. A., Goldberg, D., Langer, R. & Benowitz, L. I. An injectable, biodegradable hydrogel for trophic factor delivery enhances axonal rewiring and improves performance after spinal cord injury. *Exp Neurol* **201**, 359–367 (2006).
- Williams, D. F. On the nature of biomaterials. *Biomaterials* **30**, 5897–5909 (2009).
- Garbayo, E. *et al.* Effective GDNF brain delivery using microspheres—a promising strategy for Parkinson's disease. *J Control Release* **135**, 119–126 (2009).
- Wang, Y. C. *et al.* Sustained intraspinal delivery of neurotrophic factor encapsulated in biodegradable nanoparticles following contusive spinal cord injury. *Biomaterials* **29**, 4546–4553 (2008).
- Gutowska, A., Jeong, B. & Jasionowski, M. Injectable gels for tissue engineering. *Anat Rec* **263**, 342–349 (2001).
- Tan, L. P., Hidayat, A., Lao, L. L. & Quah, L. F. Release of hydrophilic drug from biodegradable polymer blends. *J Biomater Sci Polym Ed* **20**, 1381–1392 (2009).
- Nomura, H., Tator, C. H. & Shoichet, M. S. Bioengineered strategies for spinal cord repair. *J Neurotrauma* **23**, 496–507 (2006).
- Sugahara, K. *et al.* Structural studies on the chondroitinase ABC-resistant sulfated tetrasaccharides isolated from various chondroitin sulfate isomers. *Carbohydr Res* **255**, 145–163 (1994).
- Suzuki, Y. *et al.* Electrophysiological and horseradish peroxidase-tracing studies of nerve regeneration through alginate-filled gap in adult rat spinal cord. *Neurosci Lett* **318**, 121–124 (2002).
- Prang, P. *et al.* The promotion of oriented axonal regrowth in the injured spinal cord by alginate-based anisotropic capillary hydrogels. *Biomaterials* **27**, 3560–3569 (2006).

25. Cizkova, D. *et al.* The influence of sustained dual-factor presentation on the expansion and differentiation of neural progenitors in affinity-binding alginate scaffolds. *J Tissue Eng Regen Med* doi: 10.1002/term.1797 (2013).
26. Lee, K., Silva, E. A. & Mooney, D. J. Growth factor delivery-based tissue engineering: general approaches and a review of recent developments. *J R Soc Interface* **8**, 153–170 (2011).
27. Perale, G. *et al.* Hydrogels in spinal cord injury repair strategies. *ACS Chem Neurosci* **2**, 336–345 (2011).
28. Shanbhag, M. S. *et al.* Neural progenitor cells grown on hydrogel surfaces respond to the product of the transgene of encapsulated genetically engineered fibroblasts. *Biomacromolecules* **11**, 2936–2943 (2010).
29. Lam, H. J., Patel, S., Wang, A., Chu, J. & Li, S. *In vitro* regulation of neural differentiation and axon growth by growth factors and bioactive nanofibers. *Tissue Eng Part A* **16**, 2641–2648 (2010).
30. Cizkova, D. *et al.* Alterations of protein composition along the rostral-caudal axis after spinal cord injury: proteomic, *in vitro* and *in vivo* analyses. *Front Cell Neurosci* **8**, 105 (2014).
31. Vanicky, I., Urdzikova, L., Saganova, K., Cizkova, D. & Galik, J. A simple and reproducible model of spinal cord injury induced by epidural balloon inflation in the rat. *J Neurotrauma* **18**, 1399–1407 (2001).
32. Cizkova, D. *et al.* Modulation properties of factors released by bone marrow stromal cells on activated microglia: an *in vitro* study. *Sci Rep* **4**, 7514 (2014).
33. Cox, J. & Mann, M. MaxQuant enables high peptide identification rates, individualized p.p.b.-range mass accuracies and proteome-wide protein quantification. *Nat Biotechnol* **26**, 1367–1372 (2008).
34. Cox, J. N. N., Michalski, A., Scheltema, R. A., Olsen, J. V., Mann, M. Andromeda: a peptide search engine integrated into the MaxQuant environment. *J. Proteome Res.* **10**, 1794–1805 (2011).
35. Cox, J. *et al.* Accurate proteome-wide label-free quantification by delayed normalization and maximal peptide ratio extraction, termed MaxLFQ. *Mol Cell Proteomics* **13**, 2513–2526 (2014).
36. Vizcaino, J. A. *et al.* ProteomeXchange provides globally coordinated proteomics data submission and dissemination. *Nat Biotechnol* **32**, 223–226 (2014).
37. Vizcaino, J. A. *et al.* The PRoteomics IDentifications (PRIDE) database and associated tools: status in 2013. *Nucleic Acids Res* **41**, D1063–1069 (2013).
38. Tsur-Gang, O. *et al.* The effects of peptide-based modification of alginate on left ventricular remodeling and function after myocardial infarction. *Biomaterials* **30**, 189–195 (2009).
39. Basso, D. M., Beattie, M. S. & Bresnahan, J. C. A sensitive and reliable locomotor rating scale for open field testing in rats. *J Neurotrauma* **12**, 1–21 (1995).
40. Grulova, I., Slovinska, L., Nagyova, M., Cizek, M. & Cizkova, D. The effect of hypothermia on sensory-motor function and tissue sparing after spinal cord injury. *Spine J* **13**, 1881–1891 (2013).
41. Cizkova, D. *et al.* Enrichment of rat oligodendrocyte progenitor cells by magnetic cell sorting. *J Neurosci Methods* **184**, 88–94 (2009).
42. Jones, L. L. & Tuszynski, M. H. Spinal cord injury elicits expression of keratan sulfate proteoglycans by macrophages, reactive microglia, and oligodendrocyte progenitors. *J Neurosci* **22**, 4611–4624 (2002).
43. Novotna, I. *et al.* IT delivery of ChABC modulates NG2 and promotes GAP-43 axonal regrowth after spinal cord injury. *Cell Mol Neurobiol* **31**, 1129–1139 (2011).
44. Nadelhaft, I. & Booth, A. M. The location and morphology of preganglionic neurons and the distribution of visceral afferents from the rat pelvic nerve: a horseradish peroxidase study. *J Comp Neurol* **226**, 238–245 (1984).
45. Cizkova, D. *et al.* Functional recovery in rats with ischemic paraplegia after spinal grafting of human spinal stem cells. *Neuroscience* **147**, 546–560 (2007).
46. Bareyre, F. M. Neuronal repair and replacement in spinal cord injury. *J Neurol Sci* **265**, 63–72 (2008).
47. Hejcl, A. *et al.* Acute and delayed implantation of positively charged 2-hydroxyethyl methacrylate scaffolds in spinal cord injury in the rat. *J Neurosurg Spine* **8**, 67–73 (2008).
48. Pachence, J. M. Collagen-based devices for soft tissue repair. *J Biomed Mater Res* **33**, 35–40 (1996).
49. Schwab, M. E. Repairing the injured spinal cord. *Science* **295**, 1029–1031 (2002).
50. Urdzikova, L. M. *et al.* Human mesenchymal stem cells modulate inflammatory cytokines after spinal cord injury in rat. *Int J Mol Sci* **15**, 11275–11293.
51. Jahn, R., Schiebler, W., Ouimet, C. & Greengard, P. A 38,000-dalton membrane protein (p38) present in synaptic vesicles. *Proc Natl Acad Sci USA* **82**, 4137–4141 (1985).
52. Wiedenmann, B. & Franke, W. W. Identification and localization of synaptophysin, an integral membrane glycoprotein of Mr 38,000 characteristic of presynaptic vesicles. *Cell* **41**, 1017–1028 (1985).
53. Nudo, R. J. & Masterton, R. B. Descending pathways to the spinal cord: a comparative study of 22 mammals. *J Comp Neurol* **277**, 53–79 (1988).
54. Nudo, R. J. & Masterton, R. B. Descending pathways to the spinal cord, IV: Some factors related to the amount of cortex devoted to the corticospinal tract. *J Comp Neurol* **296**, 584–597 (1990).
55. Bareyre, F. M. *et al.* The injured spinal cord spontaneously forms a new intraspinal circuit in adult rats. *Nat Neurosci* **7**, 269–277 (2004).
56. Cizkova, D. *et al.* Repetitive intrathecal catheter delivery of bone marrow mesenchymal stromal cells improves functional recovery in a rat model of contusive spinal cord injury. *J Neurotrauma* **9**, 1951–1961 (2011).
57. Karimi-Abdolrezaee, S., Eftekharpour, E., Wang, J., Schut, D. & Fehlings, M. G. Synergistic effects of transplanted adult neural stem/progenitor cells, chondroitinase, and growth factors promote functional repair and plasticity of the chronically injured spinal cord. *J Neurosci* **30**, 1657–1676 (2010).
58. Maier, I. C. *et al.* Constraint-induced movement therapy in the adult rat after unilateral corticospinal tract injury. *J Neurosci* **28**, 9386–9403 (2008).
59. Carbonetto, S., Gruver, M. M. & Turner, D. C. Nerve fiber growth in culture on fibronectin, collagen, and glycosaminoglycan substrates. *J Neurosci* **3**, 2324–2335 (1983).
60. Carbonetto, S. T., Gruver, M. M. & Turner, D. C. Nerve fiber growth on defined hydrogel substrates. *Science* **216**, 897–899 (1982).
61. Zhong, Y., Yu, X., Gilbert, R. & Bellamkonda, R. V. Stabilizing electrode-host interfaces: a tissue engineering approach. *J Rehabil Res Dev* **38**, 627–632 (2001).
62. Kataoka, K. *et al.* Alginate, a bioresorbable material derived from brown seaweed, enhances elongation of amputated axons of spinal cord in infant rats. *J Biomed Mater Res* **54**, 373–384 (2001).
63. Suzuki, K. *et al.* Regeneration of transected spinal cord in young adult rats using freeze-dried alginate gel. *Neuroreport* **10**, 2891–2894 (1999).
64. Joosten, E. A., Bar, P. R. & Gispén, W. H. Collagen implants and cortico-spinal axonal growth after mid-thoracic spinal cord lesion in the adult rat. *J Neurosci Res* **41**, 481–490 (1995).
65. Olson, H. E. *et al.* Neural stem cell- and Schwann cell-loaded biodegradable polymer scaffolds support axonal regeneration in the transected spinal cord. *Tissue Eng Part A* **15**, 1797–1805 (2009).
66. Plate, K. H. Mechanisms of angiogenesis in the brain. *J Neuropathol Exp Neurol* **58**, 313–320 (1999).

67. Sobue, K. *et al.* Induction of blood-brain barrier properties in immortalized bovine brain endothelial cells by astrocytic factors. *Neurosci Res* **35**, 155–164 (1999).
68. Bird, G. C. *et al.* Pain-related synaptic plasticity in spinal dorsal horn neurons: role of CGRP. *Mol Pain* **2**, 31 (2006).
69. Keast, J. R. & De Groat, W. C. Segmental distribution and peptide content of primary afferent neurons innervating the urogenital organs and colon of male rats. *J Comp Neurol* **319**, 615–623 (1992).
70. Ji, R. R., Kohno, T., Moore, K. A. & Woolf, C. J. Central sensitization and LTP: do pain and memory share similar mechanisms? *Trends Neurosci* **26**, 696–705 (2003).
71. Minami, T. *et al.* Involvement of primary afferent C-fibres in touch-evoked pain (allodynia) induced by prostaglandin E2. *Eur J Neurosci* **11**, 1849–1856 (1999).
72. Samad, T. A. *et al.* Interleukin-1beta-mediated induction of Cox-2 in the CNS contributes to inflammatory pain hypersensitivity. *Nature* **410**, 471–475 (2001).
73. Hua, X. Y., Chen, P., Marsala, M. & Yaksh, T. L. Intrathecal substance P-induced thermal hyperalgesia and spinal release of prostaglandin E2 and amino acids. *Neuroscience* **89**, 525–534 (1999).
74. Ferrari, D. *et al.* Extracellular ATP triggers IL-1 beta release by activating the purinergic P2Z receptor of human macrophages. *J Immunol* **159**, 1451–1458 (1997).
75. Svensson, C. I. *et al.* Prostaglandin E2 release evoked by intrathecal dynorphin is dependent on spinal p38 mitogen activated protein kinase. *Neuropeptides* **39**, 485–494 (2005).
76. Silver, J. & Miller, J. H. Regeneration beyond the glial scar. *Nat Rev Neurosci* **5**, 146–156 (2004).

Acknowledgements

This research was supported by APVV 0472-11 (DC), VEGA 2/0125/15, PRISM (INSERM U1192) (MS) and Thermofisher (Bremen) and grants from Ministère de L'Education Nationale, L'Enseignement Supérieur et de la Recherche, Agence Stefanick PHC (MS, DC) Région Nord-Pas de Calais (to SD), SIRIC ONCOLille (IF), Grant INCa-DGOS-Inserm 6041aa and Université de Lille 1 (SD, DC). Professor Cohen holds the Clair and Harold Oshry Professor Chair in Biotechnology. The authors gratefully thank Maria Spontakova (Institute of Neurobiology) for technical assistance with immunocytochemical analyses.

Author Contributions

D.C., I.G., S.C. and M.S. have written the paper. I.G., L.S., J.B., S.D., M.W., M.S., I.F., O.K., S.C., V.C., D.C. have done the experiments. All authors have reviewed the manuscript.

Additional Information

Supplementary information accompanies this paper at <http://www.nature.com/srep>

Competing financial interests: The authors declare no competing financial interests.

How to cite this article: Grulova, I. *et al.* Delivery of Alginate Scaffold Releasing Two Trophic Factors for Spinal Cord Injury Repair. *Sci. Rep.* **5**, 13702; doi: 10.1038/srep13702 (2015).



This work is licensed under a Creative Commons Attribution 4.0 International License. The images or other third party material in this article are included in the article's Creative Commons license, unless indicated otherwise in the credit line; if the material is not included under the Creative Commons license, users will need to obtain permission from the license holder to reproduce the material. To view a copy of this license, visit <http://creativecommons.org/licenses/by/4.0/>

CONCLUSION CHAPTER 3

Alginate biomaterial can be enriched with factors to allow their delivery directly into the lesion site over time. These factors could be neurotrophic factors, enzymes, or stem cells to improve the repair process. The biomaterial by itself built a scaffold that is able to fill the gap and make a bridge between rostral and caudal segments adjacent to the lesion. The scaffold allows neurons to get a support for the axonal guidance and the neurite outgrowth.

Further studies will need to be conducted to bind different molecules to the alginate, for example the conditioned media from bone marrow stromal cells to modulate the microglia activation or others drugs to promote neurite outgrowth, as we already started to conduct. First results with RhoA inhibitor were shown in the first part of my thesis. The treatment at 7 days after SCI with alginate coupled with RhoA inhibitor demonstrated an increase of the synaptic vesicles in the lesion area compared to the rats without treatment at 49 days after injury. However, this study needs to be continued to determine the appropriate concentration of RhoAi and the most suitable period to treat the rats. We will probably need to combine it with other multifactorial molecules in order to enhance the axonal repair.

Regarding the stem cell therapy and the beneficial effect of their released molecules, we begin to focus our interest on adipose stem cells and their secretomes. Adipose stem cells (ASC) are abundant, accessible, easily expanded *in vitro* and rich of adult stem cells. In 1964, initial methods for the isolation of mature adipocytes and adipogenic progenitors from rat fat tissue were described by Rodbell *et al.*, (Rodbell 1964). ASC are multipotent and are able to differentiate into adipocytes, chondrocytes, osteoblasts and neural lineages (Gimble and Guilak 2003; Zuk *et al.* 2001). The conditioned media from ASC will be analyzed by mass spectrometry without a priori to identify the proteomic profile of these cells to assess the possibility incorporating them into alginate.

The repair of the spinal cord needs to be addressed from different points of view and at different times after injury. The first step of the inflammation is crucial to phagocytize and to clean cellular debris after the injury (Donnelly and Popovich 2008). Macrophages and microglia can synthesize pro- or anti-inflammatory cytokines such as TNF- α and IL-6 or TGF- β and IL-10 respectively (Aloisi 2001; Kigerl *et al.* 2009). With the intention of modulating the

inflammation, we have to always have in mind the role of microglia in the acute stage of SCI and their capacity to express a ratio of M1/M2 phenotype in order to modulate them in the neuroprotective way. Once the inflammation is regulated, the second point will be to fill the cavity to allow the axon guidance and the neurite outgrowth in order to reconnect disconnected tissue due to the injury. Moreover, we have shown that in the C1 segment, inhibitor molecules such as NCAM and aggrecan are present and they prevent the action of molecules involved in neurite outgrowth or neurogenesis. There are two possibilities that lead to axonal regeneration: the first one is to remove the inhibitory molecules and the second is to introduce molecules to promote neurogenesis. Biomaterials can deliver factors which will affect the growth inhibition balance to promote axonal regeneration.

Taken together, thanks to our spatio-temporal analysis, we will be able to take into account all the elements as microenvironment in the entire spinal cord during the acute phase and the cellular recruitment. The C1 segment seems to be a potential target for the future therapy. We also showed that alginate + GFs treatment associated with RhoAi + FK506 improves the regeneration processes, but it is still insufficient for a complete functional repair. We will start to include in the scaffold microvesicles (ectosomes and exosomes) from stem cells secretome in order to increase the neurogenesis and decrease the inflammation. We are analysing the proteomic and the physiological profiles of microvesicles from bone marrow stem cells, adipocytes stem cells and from neuroprogenitors. These tasks will help us to define the best association that is necessary.

Discussion

In the previous parts, we have demonstrated a spatio-temporal evolution of proteins released after the spinal cord injury. Currently, surgeons only take care of the rostral segment following injury. However, we showed that the caudal segment has to be taken into consideration as a potential therapeutic target. We established that both segments have the ability to regenerate but the inflammation occurring in each part is different due to the nature of recruited cells in both sides of the lesion. T regulator cells migrate first at the rostral region before moving to the caudal one a couple of days later. This provokes a discrepancy in the nature of inflammatory molecules produced as well as the neurotrophic factors. The C1 segment contains neurite inhibitor factors such as MEMO1, CSPGs and immunoglobulins. A complementary study of SCI conditioned media at one-day post injury clearly confirmed the presence of immunoglobulins at an early stage after injury. The presence of such immunoglobulins is an interesting point. Their presence at one day leads to the question of their origins, i.e. neuronal or peripheral. In fact, the production of IgG subtypes needs a second infection and more than 21 days by B lymphocytes. Recent studies have demonstrated that non-lymphoid cells are able to express IgGs in such cells as cancer cells, neurons and in the eye, which is protected by a blood-ocular barrier (Niu *et al.* 2011). They detected the presence of IgGs and its receptors in an intraocular structure. The role of these IgGs has been started to be studied and two contradictory hypotheses are highlighted: the neuroprotective effects (Arumugam *et al.* 2007; Hulse *et al.* 2008; Gok *et al.* 2009; Fehlings and Nguyen 2010) or the neurodestructive effects (Daniel P. Ankeny *et al.* 2009; Daniel P Ankeny and Popovich 2010). The protective effects of IgGs have been demonstrated in the brain by preventing complement mediated neuronal cell death (Arumugam *et al.* 2007) and via the enhancement of microglia recycling endocytosis and TNF α (Hulse *et al.* 2008). Moreover, it is also well known that the nature of glycans on IgG can modulate the immune response (Novokmet *et al.* 2014). The presence of specific sugar moieties on the glycan modifies the implications of Fc effector functions. The addition of terminal sialic acid to the glycan reduces Fc γ R binding and converts IgG antibodies to anti-inflammatory mediators (Anthony and Ravetch 2010). In this context, in our next perspective we will engage in such glycomic study in order to see in a spatio-temporal

manner the nature of glycans present on the secreted IgG. In the same way, we have also started to elucidate the origin of such antibodies.

Transcriptomic studies on different neurons cell lines, such as dopaminergic neurons or neurons derived rat DRG, will be conducted in order to prove the presence or not of mRNA of recombination activated gene (RAG1 and RAG2) involved in the V(D)J recombination and IgG mRNA previously identified by mass spectrometry. This transcriptomic analysis will validate our cell lines for future experiments based on IgG analysis. The dopaminergic system is known to promote the recovery of the locomotor function after SCI (Sharples *et al.* 2014), whereas the neurons DRG derived are involved in the sensory system. RAG1 and RAG2 are expressed and translated in a subset of zebrafish olfactory sensory neurons (Jessen *et al.* 2001; Feng *et al.* 2005). Previous experiments on transgenic mice were designed to determine whether cells of the CNS can perform a site-specific recombination reaction similar to that of lymphocytes (Kawaichi *et al.* 1991; Matsuoka *et al.* 1991). Two questions have emerged and are still open, ie. is the site-specific recombination reaction in neurons different to the one found in B cells or do other site-specific recombination processes occur in the brain?

We thus need to demonstrate the presence of a complete functional RAG1 and RAG2 V(D)J recombination system in line with the neuronal production of IgG. Moreover, due to the fact that it is known that neurons and glial cells such as microglia are able to express Fcγ receptors (Raghavan and Bjorkman 1996), it is necessary to understand the functional role of these neuronal IgGs in line with the spinal cord injury. For this purpose, we need to identify the epitopes towards these antibodies are directed.

The studies concerning traumatic brain injury (TBI) and autoimmunity have shown that in serum from patients with TBI, autoantibodies directed against GFAP and its breakdown products were identified (Z. Zhang *et al.* 2014). In this way, the possibility that GFAP and its breakdown could be targeted by IgGs in the spinal cord will be considered. Immunohistochemistry on astrocytes cell line with SCI-CM 1 or 3 days after injury as antibodies could prove the link between GFAP and IgGs. The calpain enzyme used to induce the breakdown of GFAP could allow us to study the ability of IgGs to bind to the breakdown products. In the optic system, immunohistochemistry will proceed to check if IgGs are only present on the cellular soma or if they are also present on the axon and on the axonal synapse.

Our hypothesis is if IgGs are also present on axons and on axonal synapses, they could be involved in axonal guidance. The use of an antibody against GFAP could prevent the binding between IgG-GFAP, if it is proven that GFAP can be an autoantigen. The neurite outgrowth *in vitro* analysis will be one element to bring out the neuroprotective role of IgGs.

FcγRI is expressed on sensory neurons and the formation of the IgG-antigen complex induces the increase of intracellular Ca²⁺ in DRG neurons (Andoh and Kuraishi 2004). Neuronal voltage-gated calcium channels are very important for the depolarization-evoked release of neurotransmitters (Simms and Zamponi 2014). The study of calcium channels will probably allow us to further understand the mechanisms involved in the IgG-antigen complex after a combination treatment of the RhoA inhibitor and IgGs present in SCI-CM. IgG internalization by neurons has been shown through a clatherin-mediated endocytic pathway via FcγRII/III for acute clearance of Tau in neuronal cultures (Congdon *et al.* 2013). The antibodies anti-CD32 to block FcγRII or CD16 for FcγRIII will be used in the presence of SCI-CM 1 or 3 days after SCI from the lesion site, in which we identified several IgGs, to prevent the possible internalization of IgGs and to analyze the effect on neurons and on the neurite outgrowth. An addition, the RhoA inhibitor will be added in the culture media to follow if these different factors promote the neurite elongation. The possible internalization of IgGs will be quantified by mass spectrometry by following their concentration into the culture media.

Taken together, our next step will be to find out the involvement of IgGs in SCI and to try to understand the origin of these antibodies, their functions and the nature of their epitopes while keeping in mind that these molecules can be a clear target for SCI therapy.

References

- Abrams, M Birdsall, Cecilia Dominguez, Karin Pernold, Roxanne Reger, Zsuzsanna Wiesenfeld-Hallin, Lars Olson, and Darwin Prockop. 2009. "Multipotent Mesenchymal Stromal Cells Attenuate Chronic Inflammation and Injury-Induced Sensitivity to Mechanical Stimuli in Experimental Spinal Cord Injury." *Restorative Neurology and Neuroscience* 27 (4): 307–21. doi:10.3233/RNN-2009-0480.
- Akiyama, Kentaro, Chider Chen, DanDan Wang, Xingtian Xu, Cunye Qu, Takayoshi Yamaza, Tao Cai, WanJun Chen, Lingyun Sun, and Songtao Shi. 2012. "Mesenchymal-Stem-Cell-Induced Immunoregulation Involves FAS-Ligand-/FAS-Mediated T Cell Apoptosis." *Cell Stem Cell* 10 (5): 544–55. doi:10.1016/j.stem.2012.03.007.
- Albert, T, and J-F Ravaud. 2005. "Rehabilitation of Spinal Cord Injury in France: A Nationwide Multicentre Study of Incidence and Regional Disparities." *Spinal Cord: The Official Journal of the International Medical Society of Paraplegia* 43 (6): 357–65. doi:10.1038/sj.sc.3101717.
- Aloisi, F. 2001. "Immune Function of Microglia." *Glia* 36 (2): 165–79. doi:10.1002/glia.1106.
- Andoh, Tsugunobu, and Yasushi Kuraishi. 2004. "Direct Action of Immunoglobulin G on Primary Sensory Neurons through Fc Gamma Receptor I." *FASEB Journal: Official Publication of the Federation of American Societies for Experimental Biology* 18 (1): 182–84. doi:10.1096/fj.02-1169fje.
- Ankeny, D P, and P G Popovich. 2009. "Mechanisms and Implications of Adaptive Immune Responses after Traumatic Spinal Cord Injury." *Neuroscience* 158 (3): 1112–21. doi:10.1016/j.neuroscience.2008.07.001.
- Ankeny, Daniel P, and Phillip G Popovich. 2010. "B Cells and Autoantibodies: Complex Roles in CNS Injury." *Trends in Immunology* 31 (9): 332–38. doi:10.1016/j.it.2010.06.006.
- Ankeny, Daniel P., Zhen Guan, Phillip G. Popovich, K.A. Kigerl, V.M. McGaughy, P.G. Popovich, P.G. Popovich, et al. 2009. "B Cells Produce Pathogenic Antibodies and Impair Recovery after Spinal Cord Injury in Mice." *Journal of Clinical Investigation* 119 (10). American Society for Clinical Investigation: 2990–99. doi:10.1172/JCI39780.
- Anthony, Robert M, and Jeffrey V Ravetch. 2010. "A Novel Role for the IgG Fc Glycan: The Anti-Inflammatory Activity of Sialylated IgG Fcs." *Journal of Clinical Immunology* 30 Suppl 1 (May): S9–14. doi:10.1007/s10875-010-9405-6.
- Arumugam, T. V., S.-C. Tang, J. D. Lathia, A. Cheng, M. R. Mughal, S. Chigurupati, T. Magnus, et al. 2007. "Intravenous Immunoglobulin (IVIG) Protects the Brain against Experimental Stroke by Preventing Complement-Mediated Neuronal Cell Death." *Proceedings of the National Academy of Sciences* 104 (35). National Academy of Sciences: 14104–9. doi:10.1073/pnas.0700506104.
- Bandtlow, C E, M F Schmidt, T D Hassinger, M E Schwab, and S B Kater. 1993. "Role of

- Intracellular Calcium in NI-35-Evoked Collapse of Neuronal Growth Cones.” *Science (New York, N.Y.)* 259 (5091): 80–83. <http://www.ncbi.nlm.nih.gov/pubmed/8418499>.
- Bareyre, F. M., N. Garzorz, C. Lang, T. Misgeld, H. Buning, and M. Kerschensteiner. 2011. “In Vivo Imaging Reveals a Phase-Specific Role of STAT3 during Central and Peripheral Nervous System Axon Regeneration.” *Proceedings of the National Academy of Sciences* 108 (15). National Acad Sciences: 6282–87. doi:10.1073/pnas.1015239108.
- Bartholomew, Amelia, Cord Sturgeon, Mandy Siatskas, Karen Ferrer, Kevin McIntosh, Sheila Patil, Wayne Hardy, et al. 2002. “Mesenchymal Stem Cells Suppress Lymphocyte Proliferation in Vitro and Prolong Skin Graft Survival in Vivo.” *Experimental Hematology* 30 (1): 42–48. doi:10.1016/S0301-472X(01)00769-X.
- Bartus, Katalin, Nicholas D James, Athanasios Didangelos, Karen D Bosch, Joost Verhaagen, Rafael J Yáñez-Muñoz, John H Rogers, Bernard L Schneider, Elizabeth M Muir, and Elizabeth J Bradbury. 2014. “Large-Scale Chondroitin Sulfate Proteoglycan Digestion with Chondroitinase Gene Therapy Leads to Reduced Pathology and Modulates Macrophage Phenotype Following Spinal Cord Contusion Injury.” *The Journal of Neuroscience : The Official Journal of the Society for Neuroscience* 34 (14): 4822–36. doi:10.1523/JNEUROSCI.4369-13.2014.
- Basso, D. Michele, Michael S. Beattie, and Jacqueline C. Bresnahan. 1995. “A Sensitive and Reliable Locomotor Rating Scale for Open Field Testing in Rats.” *Journal of Neurotrauma* 12 (1): 1–21. doi:10.1089/neu.1995.12.1.
- Bazan, J F, K B Bacon, G Hardiman, W Wang, K Soo, D Rossi, D R Greaves, A Zlotnik, and T J Schall. 1997. “A New Class of Membrane-Bound Chemokine with a CX3C Motif.” *Nature* 385 (6617): 640–44. doi:10.1038/385640a0.
- Beck, Kevin D, Hal X Nguyen, Manuel D Galvan, Desirée L Salazar, Trent M Woodruff, and Aileen J Anderson. 2010. “Quantitative Analysis of Cellular Inflammation after Traumatic Spinal Cord Injury: Evidence for a Multiphasic Inflammatory Response in the Acute to Chronic Environment.” *Brain: A Journal of Neurology* 133 (Pt 2): 433–47. doi:10.1093/brain/awp322.
- Beers, David R, Jenny S Henkel, Weihua Zhao, Jinghong Wang, and Stanley H Appel. 2008. “CD4+ T Cells Support Glial Neuroprotection, Slow Disease Progression, and Modify Glial Morphology in an Animal Model of Inherited ALS.” *Proceedings of the National Academy of Sciences of the United States of America* 105 (40): 15558–63. doi:10.1073/pnas.0807419105.
- Biber, Knut, Harald Neumann, Kazuhide Inoue, Hendrikus W G M Boddeke, G.W. Kreutzberg, W.J. Streit, A. Nimmerjahn, et al. 2007. “Neuronal ‘On’ and ‘Off’ Signals Control Microglia.” *Trends in Neurosciences* 30 (11). Elsevier: 596–602. doi:10.1016/j.tins.2007.08.007.
- Boido, Marina, Diego Garbossa, Marco Fontanella, Alessandro Ducati, and Alessandro Vercelli. 2014. “Mesenchymal Stem Cell Transplantation Reduces Glial Cyst and Improves Functional Outcome after Spinal Cord Compression.” *World Neurosurgery* 81

(1): 183–90. doi:10.1016/j.wneu.2012.08.014.

- Borisoff, Jaimie F, Carmen C.M Chan, Gordon W Hiebert, Loren Oschipok, George S Robertson, R Zamboni, John D Steeves, and Wolfram Tetzlaff. 2003. “Suppression of Rho-Kinase Activity Promotes Axonal Growth on Inhibitory CNS Substrates.” *Molecular and Cellular Neuroscience* 22 (3): 405–16. doi:10.1016/S1044-7431(02)00032-5.
- Boulis, Nicholas M, Thais Federici, Jonathan D Glass, J Simon Lunn, Stacey A Sakowski, and Eva L Feldman. 2011. “Translational Stem Cell Therapy for Amyotrophic Lateral Sclerosis.” *Nature Reviews. Neurology* 8 (3): 172–76. doi:10.1038/nrneuro.2011.191.
- Bradbury, Elizabeth J, Lawrence D F Moon, Reena J Popat, Von R King, Gavin S Bennett, Preena N Patel, James W Fawcett, and Stephen B McMahon. 2002. “Chondroitinase ABC Promotes Functional Recovery after Spinal Cord Injury.” *Nature* 416 (6881): 636–40. doi:10.1038/416636a.
- Bregman, B S, E Kunkel-Bagden, L Schnell, H N Dai, D Gao, and M E Schwab. 1995. “Recovery from Spinal Cord Injury Mediated by Antibodies to Neurite Growth Inhibitors.” *Nature* 378 (6556): 498–501. doi:10.1038/378498a0.
- Bruce, Jamie C., Mark a. Oatway, and Lynne C. Weaver. 2002. “Chronic Pain after Clip-Compression Injury of the Rat Spinal Cord.” *Experimental Neurology* 178 (1): 33–48. doi:10.1006/exnr.2002.8026.
- Bunge, Mary Bartlett, and Patrick McGhee Wood. 2012. “Realizing the Maximum Potential of Schwann Cells to Promote Recovery from Spinal Cord Injury.” *Handbook of Clinical Neurology* 109 (January): 523–40. doi:10.1016/B978-0-444-52137-8.00032-2.
- Caggiano, Anthony O, Michael P Zimmer, Anindita Ganguly, Andrew R Blight, and Elliott A Gruskin. 2005. “Chondroitinase ABCI Improves Locomotion and Bladder Function Following Contusion Injury of the Rat Spinal Cord.” *Journal of Neurotrauma* 22 (2): 226–39. doi:10.1089/neu.2005.22.226.
- Caplan, A I. 1991. “Mesenchymal Stem Cells.” *Journal of Orthopaedic Research : Official Publication of the Orthopaedic Research Society* 9 (5): 641–50. doi:10.1002/jor.1100090504.
- . 1994. “The Mesengenic Process.” *Clinics in Plastic Surgery* 21 (3): 429–35. <http://www.ncbi.nlm.nih.gov/pubmed/7924141>.
- Cardona, Astrid E, Erik P Pioro, Margaret E Sasse, Volodymyr Kostenko, Sandra M Cardona, Ineke M Dijkstra, Deren Huang, et al. 2006. “Control of Microglial Neurotoxicity by the Fractalkine Receptor.” *Nature Neuroscience* 9 (7): 917–24. doi:10.1038/nn1715.
- Caroni, P, T Savio, and M E Schwab. 1988. “Central Nervous System Regeneration: Oligodendrocytes and Myelin as Non-Permissive Substrates for Neurite Growth.” *Progress in Brain Research* 78 (January): 363–70. <http://www.ncbi.nlm.nih.gov/pubmed/3073419>.
- Caroni, P, and M E Schwab. 1988. “Antibody against Myelin-Associated Inhibitor of Neurite

- Growth Neutralizes Nonpermissive Substrate Properties of CNS White Matter.” *Neuron* 1 (1): 85–96. <http://www.ncbi.nlm.nih.gov/pubmed/3272156>.
- Carson, Monica J, Jonathan M Doose, Benoit Melchior, Christoph D Schmid, and Corinne C Ploix. 2006. “CNS Immune Privilege: Hiding in Plain Sight.” *Immunological Reviews* 213 (October): 48–65. doi:10.1111/j.1600-065X.2006.00441.x.
- Cassatella, Marco A. 1995. “The Production of Cytokines by Polymorphonuclear Neutrophils.” *Immunology Today* 16 (1): 21–26. doi:10.1016/0167-5699(95)80066-2.
- Chakrabarti, Mrinmay, Azizul Haque, Naren L Banik, Prakash Nagarkatti, Mitzi Nagarkatti, and Swapan K Ray. 2014. “Estrogen Receptor Agonists for Attenuation of Neuroinflammation and Neurodegeneration.” *Brain Research Bulletin* 109C (October): 22–31. doi:10.1016/j.brainresbull.2014.09.004.
- Chan, Shing Fai, Xiayu Huang, Scott R McKercher, Rameez Zaidi, Shu-Ichi Okamoto, Nobuki Nakanishi, and Stuart A Lipton. 2015. “Transcriptional Profiling of MEF2-Regulated Genes in Human Neural Progenitor Cells Derived from Embryonic Stem Cells.” *Genomics Data* 3 (March): 24–27. doi:10.1016/j.gdata.2014.10.022.
- Chang, Raymond C.C, Pearlie Hudson, Belinda Wilson, Bin Liu, Heidi Abel, John Hemperly, and Jau-Shyong Hong. 2000. “Immune Modulatory Effects of Neural Cell Adhesion Molecules on Lipopolysaccharide-Induced Nitric Oxide Production by Cultured Glia.” *Molecular Brain Research* 81 (1-2): 197–201. doi:10.1016/S0169-328X(00)00175-3.
- Chang, Raymond C.C., Pearlie Hudson, Belinda Wilson, Lisa Haddon, and Jau-Shyong Hong. 2000. “Influence of Neurons on Lipopolysaccharide-Stimulated Production of Nitric Oxide and Tumor Necrosis Factor- α by Cultured Glia.” *Brain Research* 853 (2): 236–44. doi:10.1016/S0006-8993(99)02255-6.
- Chen, M S, A B Huber, M E van der Haar, M Frank, L Schnell, A A Spillmann, F Christ, and M E Schwab. 2000. “Nogo-A Is a Myelin-Associated Neurite Outgrowth Inhibitor and an Antigen for Monoclonal Antibody IN-1.” *Nature* 403 (6768): 434–39. doi:10.1038/35000219.
- Chen, M S, A B Huber, M E Van der Haar, Marcus Frank, Lisa Schnell, Adrian A Spillmann, Franziska Christ, and Martin E Schwab. 2000. “Nogo-A Is a Myelin-Associated Neurite Outgrowth Inhibitor and an Antigen for Monoclonal Antibody IN-1.” *Nature* 403 (January): 1–6.
- Chen, Yongmei, Nina E. Vartiainen, Weihai Ying, Pak H. Chan, Jari Koistinaho, and Raymond A. Swanson. 2001. “Astrocytes Protect Neurons from Nitric Oxide Toxicity by a Glutathione-Dependent Mechanism.” *Journal of Neurochemistry* 77 (6): 1601–10. doi:10.1046/j.1471-4159.2001.00374.x.
- Chiu, Isaac M, Adam Chen, Yi Zheng, Bela Kosaras, Stefanos A Tsiftoglou, Timothy K Vartanian, Robert H Brown, and Michael C Carroll. 2008. “T Lymphocytes Potentiate Endogenous Neuroprotective Inflammation in a Mouse Model of ALS.” *Proceedings of the National Academy of Sciences of the United States of America* 105 (46): 17913–18.

doi:10.1073/pnas.0804610105.

- Chun, Jerold J.M., David G. Schatz, Marjorie A. Oettinger, Rudolf Jaenisch, and David Baltimore. 1991. "The Recombination Activating Gene-1 (RAG-1) Transcript Is Present in the Murine Central Nervous System." *Cell* 64 (1). Cell Press: 189–200. doi:10.1016/0092-8674(91)90220-S.
- Cizkova, D, O Kakinohana, K Kucharova, S Marsala, K Johe, T Hazel, M P Hefferan, and M Marsala. 2007. "Functional Recovery in Rats with Ischemic Paraplegia after Spinal Grafting of Human Spinal Stem Cells." *Neuroscience* 147 (2): 546–60. doi:10.1016/j.neuroscience.2007.02.065.
- Cížková, D, J Vávrová, S Mičuda, S Filip, E Brčáková, L Brůčková, and J Mokry. 2011. "Role of Transplanted Bone Marrow Cells in Response to Skeletal Muscle Injury." *Folia Biologica* 57 (6): 232–41. <http://www.ncbi.nlm.nih.gov/pubmed/22264717>.
- Cizkova, Dasa, Stéphanie Devaux, Françoise Le Marrec-Croq, Julien Franck, Lucia Slovinska, Juraj Blasko, Jan Rosocha, et al. 2014. "Modulation Properties of Factors Released by Bone Marrow Stromal Cells on Activated Microglia: An in Vitro Study." *Scientific Reports* 4 (January): 7514. doi:10.1038/srep07514.
- Cizkova, Dasa, Lucia Slovinska, Ivana Grulova, Michel Salzet, Stefan Cikos, Olga Kryukov, and Smadar Cohen. 2015. "The Influence of Sustained Dual-Factor Presentation on the Expansion and Differentiation of Neural Progenitors in Affinity-Binding Alginate Scaffolds." *Journal of Tissue Engineering and Regenerative Medicine* 9 (8): 918–29. doi:10.1002/term.1797.
- Congdon, Erin E, Jiaping Gu, Hameetha B R Sait, and Einar M Sigurdsson. 2013. "Antibody Uptake into Neurons Occurs Primarily via Clathrin-Dependent Fcγ Receptor Endocytosis and Is a Prerequisite for Acute Tau Protein Clearance." *The Journal of Biological Chemistry* 288 (49): 35452–65. doi:10.1074/jbc.M113.491001.
- David, S, and A J Aguayo. 1981. "Axonal Elongation into Peripheral Nervous System 'bridges' after Central Nervous System Injury in Adult Rats." *Science (New York, N.Y.)* 214 (4523): 931–33. <http://www.ncbi.nlm.nih.gov/pubmed/6171034>.
- David, Samuel, and Antje Kroner. 2011. "Repertoire of Microglial and Macrophage Responses after Spinal Cord Injury." *Nature Reviews. Neuroscience* 12 (7). Nature Publishing Group: 388–99. doi:10.1038/nrn3053.
- Dergham, Pauline, Benjamin Ellezam, Charles Essagian, Hovsep Avedissian, William D Lubell, and Lisa Mckerracher. 2002. "Rho Signaling Pathway Targeted to Promote Spinal Cord Repair." *The Journal of Neuroscience: The Official Journal of the Society for Neuroscience* 22 (15): 6570–77.
- Devaux, Stephanie, Dasa Cizkova, Jusul Quanico, Julien Franck, Serge Nataf, Laurent Pays, Lena Hauberg-Lotte, et al. 2016. "Proteomic Analysis of the Spatio-Temporal Based Molecular Kinetics of Acute Spinal Cord Injury Identifies a Time- and Segment-Specific Window for Effective Tissue Repair." *Molecular & Cellular Proteomics: MCP*, June.

doi:10.1074/mcp.M115.057794.

- Di Giovanni, Simone, Chad D Knights, Mahadev Rao, Alexander Yakovlev, Jeannette Beers, Jason Catania, Maria Laura Avantaggiati, et al. 2006. "The Tumor Suppressor Protein p53 Is Required for Neurite Outgrowth and Axon Regeneration." *The EMBO Journal* 25 (17). EMBO Press: 4084–96. doi:10.1038/sj.emboj.7601292.
- Ding, Peng, Zhiyong Yang, Weimin Wang, Jinkun Wang, and Liping Xue. 2014. "Transplantation of Bone Marrow Stromal Cells Enhances Infiltration and Survival of CNP and Schwann Cells to Promote Axonal Sprouting Following Complete Transection of Spinal Cord in Adult Rats." *American Journal of Translational Research* 6 (3): 224–35.
- Ding, Qinxue, Zhe Wu, Yaojun Guo, Congjian Zhao, Yufeng Jia, Fanwen Kong, Bingyao Chen, et al. 2006. "Proteome Analysis of up-Regulated Proteins in the Rat Spinal Cord Induced by Transection Injury." *Proteomics* 6 (2): 505–18. doi:10.1002/pmic.200500296.
- Dlouhy, B J, Awe O, R C Rao, P A Kirby, and P W Hitchon. 2014. "Autograft-Derived Spinal Cord Mass Following Olfactory Mucosal Cell Transplantation in a Spinal Cord Injury Patient." *Journal of Neurosurgery* 21 (October): 618–22.
- Donnelly, Dustin J, and Phillip G Popovich. 2008. "Inflammation and Its Role in Neuroprotection, Axonal Regeneration and Functional Recovery after Spinal Cord Injury." *Experimental Neurology* 209 (2): 378–88. doi:10.1016/j.expneurol.2007.06.009.
- Doss, Michael Xavier, John Antonydas Gaspar, Johannes Winkler, Jürgen Hescheler, Herbert Schulz, and Agapios Sachinidis. 2012. "Specific Gene Signatures and Pathways in Mesodermal Cells and Their Derivatives Derived from Embryonic Stem Cells." *Stem Cell Reviews* 8 (1): 43–54. doi:10.1007/s12015-011-9263-5.
- Dubreuil, Catherine I, Matthew J Winton, and Lisa McKerracher. 2003. "Rho Activation Patterns after Spinal Cord Injury and the Role of Activated Rho in Apoptosis in the Central Nervous System." *The Journal of Cell Biology* 162 (2): 233–43. doi:10.1083/jcb.200301080.
- Dunn, J A, J D Kirsch, and J R Naegele. 1995. "Transient Immunoglobulin-like Molecules Are Present in the Subplate Zone and Cerebral Cortex during Postnatal Development." *Cerebral Cortex (New York, N.Y. : 1991)* 5 (6): 494–505. <http://www.ncbi.nlm.nih.gov/pubmed/8590823>.
- Eddleston, M., and L. Mucke. 1993. "Molecular Profile of Reactive astrocytes—Implications for Their Role in Neurologic Disease." *Neuroscience* 54 (1): 15–36. doi:10.1016/0306-4522(93)90380-X.
- Ellezam, Benjamin, Catherine Dubreuil, Matthew Winton, Leanna Loy, Pauline Dergham, Inmaculada Sellés-Navarro, and Lisa McKerracher. 2002. "Inactivation of Intracellular Rho to Stimulate Axon Growth and Regeneration." *Progress in Brain Research* 137: 371–80. <http://www.ncbi.nlm.nih.gov/pubmed/12440379>.

- Faulkner, Jill R, Julia E Herrmann, Michael J Woo, Keith E Tansey, Ngan B Doan, and Michael V Sofroniew. 2004. "Reactive Astrocytes Protect Tissue and Preserve Function after Spinal Cord Injury." *The Journal of Neuroscience : The Official Journal of the Society for Neuroscience* 24 (9): 2143–55. doi:10.1523/JNEUROSCI.3547-03.2004.
- Fawcett, James W, and Richard.A Asher. 1999. "The Glial Scar and Central Nervous System Repair." *Brain Research Bulletin* 49 (6): 377–91. doi:10.1016/S0361-9230(99)00072-6.
- Fehlings, Michael G, Nicholas Theodore, James Harrop, Gilles Maurais, Charles Kuntz, Chris I Shaffrey, Brian K Kwon, et al. 2011. "A Phase I/IIa Clinical Trial of a Recombinant Rho Protein Antagonist in Acute Spinal Cord Injury." *Journal of Neurotrauma* 28 (5): 787–96. doi:10.1089/neu.2011.1765.
- Fehlings, Michael G., and Dung H. Nguyen. 2010. "Immunoglobulin G: A Potential Treatment to Attenuate Neuroinflammation Following Spinal Cord Injury." *Journal of Clinical Immunology* 30 (S1). Springer US: 109–12. doi:10.1007/s10875-010-9404-7.
- Feng, Bo, Sarada Bulchand, Emre Yaksi, Rainer W Friedrich, and Suresh Jesuthasan. 2005. "The Recombination Activation Gene 1 (Rag1) Is Expressed in a Subset of Zebrafish Olfactory Neurons but Is Not Essential for Axon Targeting or Amino Acid Detection." *BMC Neuroscience* 6. BioMed Central: 46. doi:10.1186/1471-2202-6-46.
- Fidler, Penny S, Katrin Schuette, Richard A Asher, Alexandre Dobbertin, Suzanne R Thornton, Yolanda Calle-patino, Elizabeth Muir, et al. 1999. "Comparing Astrocytic Cell Lines That Are Inhibitory or Permissive for Axon Growth : The Major Axon-Inhibitory Proteoglycan Is NG2." *The Journal of Neuroscience : The Official Journal of the Society for Neuroscience* 19 (20): 8778–88.
- Floriddia, Elisa, Tuan Nguyen, and Simone Di Giovanni. 2011. "Chromatin Immunoprecipitation from Dorsal Root Ganglia Tissue Following Axonal Injury." *Journal of Visualized Experiments*, no. 53 (July): e2803–e2803. doi:10.3791/2803.
- Forgione, Nicole, and Michael G Fehlings. 2014. "Rho-ROCK Inhibition in the Treatment of Spinal Cord Injury." *World Neurosurgery* 82 (3-4): e535–39. doi:10.1016/j.wneu.2013.01.009.
- Fouad, Karim, Lisa Schnell, Mary B Bunge, Martin E Schwab, Thomas Liebscher, and Damien D Pearse. 2005. "Combining Schwann Cell Bridges and Olfactory-Ensheathing Glia Grafts with Chondroitinase Promotes Locomotor Recovery after Complete Transection of the Spinal Cord." *The Journal of Neuroscience : The Official Journal of the Society for Neuroscience* 25 (5): 1169–78. doi:10.1523/JNEUROSCI.3562-04.2005.
- Fournier, Alyson E, Graham C Gould, Betty P Liu, and Stephen M Strittmatter. 2002. "Truncated Soluble Nogo Receptor Binds Nogo-66 and Blocks Inhibition of Axon Growth by Myelin." *The Journal of Neuroscience : The Official Journal of the Society for Neuroscience* 22 (20): 8876–83.
- Fournier, Alyson E, Bayan T Takizawa, and Stephen M Strittmatter. 2003. "Rho Kinase Inhibition Enhances Axonal Regeneration in the Injured CNS." *The Journal of*

Neuroscience : The Official Journal of the Society for Neuroscience 23 (4): 1416–23.

- Freeman, Inbar, Alon Kedem, and Smadar Cohen. 2008. “The Effect of Sulfation of Alginate Hydrogels on the Specific Binding and Controlled Release of Heparin-Binding Proteins.” *Biomaterials* 29 (22): 3260–68. doi:10.1016/j.biomaterials.2008.04.025.
- Freund, Patrick, Eric Schmidlin, Thierry Wannier, Jocelyne Bloch, Anis Mir, Martin E Schwab, and Eric M Rouiller. 2006. “Nogo-A-Specific Antibody Treatment Enhances Sprouting and Functional Recovery after Cervical Lesion in Adult Primates.” *Nature Medicine* 12 (7): 790–92. doi:10.1038/nm1436.
- Fujimomto, Yusuke, Masahiko Abematsu, Anna Falk, Keita Tsujimura, Tsukasa Sanosaka, Berry Juliandi, Katsunori Semi, et al. 2012. “Treatment of a Mouse Model of Spinal Cord Injury by Transplantation of Human Induced Pluripotent Stem Cell-Derived Long-Term Self-Renewing Neuroepithelial-Like Stem Cells.” *Stem Cells* 30: 1163–73. doi:10.1002/stem.1083.
- García-Alías, Guillermo, Stanley Barkhuysen, Miranda Buckle, and James W Fawcett. 2009. “Chondroitinase ABC Treatment Opens a Window of Opportunity for Task-Specific Rehabilitation.” *Nature Neuroscience* 12 (9): 1145–51. doi:10.1038/nn.2377.
- Garton, K J, P J Gough, C P Blobel, G Murphy, D R Greaves, P J Dempsey, and E W Raines. 2001. “Tumor Necrosis Factor-Alpha-Converting Enzyme (ADAM17) Mediates the Cleavage and Shedding of Fractalkine (CX3CL1).” *The Journal of Biological Chemistry* 276 (41): 37993–1. doi:10.1074/jbc.M106434200.
- Gaub, P, A Tedeschi, R Puttagunta, T Nguyen, A Schmandke, and S Di Giovanni. 2010. “HDAC Inhibition Promotes Neuronal Outgrowth and Counteracts Growth Cone Collapse through CBP/p300 and p53 Acetylation.” *Cell Death & Differentiation* 17 (9). Nature Publishing Group: 1392. doi:10.1038/CDD.2009.216.
- Gaub, Perrine, Yashashree Joshi, Anja Wuttke, Ulrike Naumann, Sven Schnichels, Peter Heiduschka, and Simone Di Giovanni. 2011. “The Histone Acetyltransferase p300 Promotes Intrinsic Axonal Regeneration.” *Brain : A Journal of Neurology* 134 (Pt 7). Oxford University Press: 2134–48. doi:10.1093/brain/awr142.
- Gimble, J.M., and F. Guilak. 2003. “Adipose-Derived Adult Stem Cells: Isolation, Characterization, and Differentiation Potential.” *Cytotherapy* 5 (5): 362–69. doi:10.1080/14653240310003026.
- Gok, Beril, Daniel M. Sciubba, Ozerk Okutan, Etem Beskonakli, Selcuk Palaoglu, Husamettin Erdamar, and Mustafa F. Sargon. 2009. *Immunomodulation of Acute Experimental Spinal Cord Injury with Human Immunoglobulin G*. *Journal of Clinical Neuroscience*. Vol. 16. doi:10.1016/j.jocn.2008.04.024.
- Gold, Bruce G, and Yong-Ping Zhong. 2004. “FK506 Requires Stimulation of the Extracellular Signal-Regulated Kinase 1/2 and the Steroid Receptor Chaperone Protein p23 for Neurite Elongation.” *Neuro-Signals* 13 (3). Karger Publishers: 122–29. doi:10.1159/000076565.

- Gombotz, Wayne R, and SiowFong Wee. 1998. "Protein Release from Alginate Matrices." *Advanced Drug Delivery Reviews* 31 (3): 267–85. doi:10.1016/S0169-409X(97)00124-5.
- GrandPré, T, F Nakamura, T Vartanian, and S M Strittmatter. 2000. "Identification of the Nogo Inhibitor of Axon Regeneration as a Reticulon Protein." *Nature* 403 (6768): 439–44. doi:10.1038/35000226.
- Granger, Nicolas, Helen Blamires, Robin J M Franklin, and Nick D Jeffery. 2012. "Autologous Olfactory Mucosal Cell Transplants in Clinical Spinal Cord Injury: A Randomized Double-Blinded Trial in a Canine Translational Model." *Brain : A Journal of Neurology* 135 (Pt 11): 3227–37. doi:10.1093/brain/aws268.
- Grulova, I., L. Slovinska, J. Blaško, S. Devaux, M. Wisztorski, M. Salzet, I. Fournier, O. Kryukov, S. Cohen, and D. Cizkova. 2015. "Delivery of Alginate Scaffold Releasing Two Trophic Factors for Spinal Cord Injury Repair." *Scientific Reports* 5 (September): 13702. doi:10.1038/srep13702.
- Gu, Weidong, Fujun Zhang, Qingsheng Xue, Zhengwen Ma, Peihua Lu, and Buwei Yu. 2010. "Transplantation of Bone Marrow Mesenchymal Stem Cells Reduces Lesion Volume and Induces Axonal Regrowth of Injured Spinal Cord." *Neuropathology : Official Journal of the Japanese Society of Neuropathology* 30 (3): 205–17. doi:10.1111/j.1440-1789.2009.01063.x.
- Guest, James, Andrea J Santamaria, and Francisco D Benavides. 2013. "Clinical Translation of Autologous Schwann Cell Transplantation for the Treatment of Spinal Cord Injury." *Current Opinion in Organ Transplantation* 18 (6): 682–89. doi:10.1097/MOT.0000000000000026.
- Hamers, F P, A J Lankhorst, T J van Laar, W B Veldhuis, and W H Gispen. 2001. "Automated Quantitative Gait Analysis during Overground Locomotion in the Rat: Its Application to Spinal Cord Contusion and Transection Injuries." *Journal of Neurotrauma* 18 (2): 187–201. doi:10.1089/08977150150502613.
- Henschel, Reinhard, and Petra Wahle. 1994. "The SP1 Antigen in Subplate Neurons of the Developing Cat Cortex Is an Immunoglobulin-like Molecule." *European Journal of Neuroscience* 6 (8). Blackwell Publishing Ltd: 1239–46. doi:10.1111/j.1460-9568.1994.tb00313.x.
- Hoek, R M, S R Ruuls, C A Murphy, G J Wright, R Goddard, S M Zurawski, B Blom, et al. 2000. "Down-Regulation of the Macrophage Lineage through Interaction with OX2 (CD200)." *Science (New York, N.Y.)* 290 (5497): 1768–71. <http://www.ncbi.nlm.nih.gov/pubmed/11099416>.
- Horn, Kevin P, Sarah a Busch, Alicia L Hawthorne, Nico van Rooijen, and Jerry Silver. 2008. "Another Barrier to Regeneration in the CNS: Activated Macrophages Induce Extensive Retraction of Dystrophic Axons through Direct Physical Interactions." *The Journal of Neuroscience : The Official Journal of the Society for Neuroscience* 28 (38): 9330–41. doi:10.1523/JNEUROSCI.2488-08.2008.

- Houle, John D, Veronica J Tom, Debra Mayes, Gail Wagoner, Napoleon Phillips, and Jerry Silver. 2006. "Combining an Autologous Peripheral Nervous System 'bridge' and Matrix Modification by Chondroitinase Allows Robust, Functional Regeneration beyond a Hemisection Lesion of the Adult Rat Spinal Cord." *The Journal of Neuroscience : The Official Journal of the Society for Neuroscience* 26 (28): 7405–15. doi:10.1523/JNEUROSCI.1166-06.2006.
- Huang, D W, L Mckerracher, P E Braun, S David, and Departement De Pathologie. 1999. "To Stimulate Axon Regeneration in the Adult Mammalian Spinal Cord." *Neuron* 24: 639–47.
- Huang, Jing, Xin Sun, Yuntao Mao, Xiaohui Zhu, Pei Zhang, Li Zhang, Jin Du, and Xiaoyan Qiu. 2008. "Expression of Immunoglobulin Gene with Classical V-(D)-J Rearrangement in Mouse Brain Neurons." *The International Journal of Biochemistry & Cell Biology* 40 (8): 1604–15. doi:10.1016/j.biocel.2007.12.004.
- Hughes, Paula Marie, Michelle Sandra Botham, Stefan Frentzel, Anis Mir, and Victor Hugh Perry. 2002. "Expression of Fractalkine (CX3CL1) and Its Receptor, CX3CR1, during Acute and Chronic Inflammation in the Rodent CNS." *Glia* 37 (4): 314–27. <http://www.ncbi.nlm.nih.gov/pubmed/11870871>.
- Hulse, Raymond E, Wade G Swenson, Phillip E Kunkler, David M White, and Richard P Kraig. 2008. "Monomeric IgG Is Neuroprotective via Enhancing Microglial Recycling Endocytosis and TNF-Alpha." *The Journal of Neuroscience : The Official Journal of the Society for Neuroscience* 28 (47): 12199–211. doi:10.1523/JNEUROSCI.3856-08.2008.
- Hundhausen, Christian, Dominika Misztela, Theo A Berkhout, Neil Broadway, Paul Saftig, Karina Reiss, Dieter Hartmann, et al. 2003. "The Disintegrin-like Metalloproteinase ADAM10 Is Involved in Constitutive Cleavage of CX3CL1 (Fractalkine) and Regulates CX3CL1-Mediated Cell-Cell Adhesion." *Blood* 102 (4): 1186–95. doi:10.1182/blood-2002-12-3775.
- Imai, Toshio, Kunio Hieshima, Christopher Haskell, Masataka Baba, Morio Nagira, Miyuki Nishimura, Mayumi Kakizaki, et al. 1997. "Identification and Molecular Characterization of Fractalkine Receptor CX3CR1, Which Mediates Both Leukocyte Migration and Adhesion." *Cell* 91 (4). Elsevier: 521–30. doi:10.1016/S0092-8674(00)80438-9.
- Ito, Zenya, Kazuma Sakamoto, Shiro Imagama, Yukihiro Matsuyama, Haoqian Zhang, Kenichi Hirano, Kei Ando, Toshihide Yamashita, Naoki Ishiguro, and Kenji Kadomatsu. 2010. "N-Acetylglucosamine 6-O-Sulfotransferase-1-Deficient Mice Show Better Functional Recovery after Spinal Cord Injury." *The Journal of Neuroscience : The Official Journal of the Society for Neuroscience* 30 (17): 5937–47. doi:10.1523/JNEUROSCI.2570-09.2010.
- Jain, Anjana, Robert J McKeon, Susann M Brady-Kalnay, and Ravi V Bellamkonda. 2011. "Sustained Delivery of Activated Rho GTPases and BDNF Promotes Axon Growth in CSPG-Rich Regions Following Spinal Cord Injury." *PloS One* 6 (1): e16135. doi:10.1371/journal.pone.0016135.
- Jessen, J R, T N Jessen, S S Vogel, and S Lin. 2001. "Concurrent Expression of Recombination

- Activating Genes 1 and 2 in Zebrafish Olfactory Sensory Neurons.” *Genesis (New York, N.Y. : 2000)* 29 (4): 156–62. <http://www.ncbi.nlm.nih.gov/pubmed/11309848>.
- Jones, L L, and M H Tuszynski. 2001. “Chronic Intrathecal Infusions after Spinal Cord Injury Cause Scarring and Compression.” *Microscopy Research and Technique* 54 (5): 317–24. doi:10.1002/jemt.1144.
- Jones, T Bucky, D Michele Basso, Ajeet Sodhi, Jonathan Z Pan, Ronald P Hart, Robert C MacCallum, Sunhee Lee, Caroline C Whitacre, and Phillip G Popovich. 2002. “Pathological CNS Autoimmune Disease Triggered by Traumatic Spinal Cord Injury: Implications for Autoimmune Vaccine Therapy.” *The Journal of Neuroscience : The Official Journal of the Society for Neuroscience* 22 (7): 2690–2700. doi:20026267.
- Kang, Catherine E, Richard Clarkson, Charles H Tator, Ivan W T Yeung, and Molly S Shoichet. 2010. “Spinal Cord Blood Flow and Blood Vessel Permeability Measured by Dynamic Computed Tomography Imaging in Rats after Localized Delivery of Fibroblast Growth Factor.” *Journal of Neurotrauma* 27: 1–12. doi:10.1089/neu.2010.1345.
- Kang, Soo Kyung, Hyeun Hwa So, Yo Seup Moon, and Cheul Hong Kim. 2006. “Proteomic Analysis of Injured Spinal Cord Tissue Proteins Using 2-DE and MALDI-TOF MS.” *Proteomics* 6 (9): 2797–2812. doi:10.1002/pmic.200500621.
- Karas, M., D. Bachmann, U. Bahr, and F. Hillenkamp. 1987. “Matrix-Assisted Ultraviolet Laser Desorption of Non-Volatile Compounds.” *International Journal of Mass Spectrometry and Ion Processes* 78 (September): 53–68. doi:10.1016/0168-1176(87)87041-6.
- Karimi-Abdolrezaee, Soheila, Eftekhar Eftekharpour, Jian Wang, Desiree Schut, and Michael G Fehlings. 2010. “Synergistic Effects of Transplanted Adult Neural Stem/progenitor Cells, Chondroitinase, and Growth Factors Promote Functional Repair and Plasticity of the Chronically Injured Spinal Cord.” *The Journal of Neuroscience : The Official Journal of the Society for Neuroscience* 30 (5): 1657–76. doi:10.1523/JNEUROSCI.3111-09.2010.
- Kawaichi, M, C Oka, R Reeves, M Kinoshita, and T Honjo. 1991. “Recombination of Exogenous Interleukin 2 Receptor Gene Flanked by Immunoglobulin Recombination Signal Sequences in a Pre-B Cell Line and Transgenic Mice.” *The Journal of Biological Chemistry* 266 (27). American Society for Biochemistry and Molecular Biology: 18387–94. <http://www.ncbi.nlm.nih.gov/pubmed/1917962>.
- Keirstead, Hans S, Gabriel Nistor, Giovanna Bernal, Minodora Totoiu, Frank Cloutier, Kelly Sharp, and Oswald Steward. 2005. “Human Embryonic Stem Cell-Derived Oligodendrocyte Progenitor Cell Transplants Remyelinate and Restore Locomotion after Spinal Cord Injury.” *The Journal of Neuroscience* 25 (19): 4694–4705. doi:10.1523/JNEUROSCI.0311-05.2005.
- Kigerl, Kristina A, John C Gensel, Daniel P Ankeny, Jessica K Alexander, Dustin J Donnelly, and Phillip G Popovich. 2009. “Identification of Two Distinct Macrophage Subsets with Divergent Effects Causing Either Neurotoxicity or Regeneration in the Injured Mouse Spinal Cord.” *The Journal of Neuroscience : The Official Journal of the Society for Neuroscience* 29 (43): 13435–44. doi:10.1523/JNEUROSCI.3257-09.2009.

- Kil, Kisoo, Ying C.Q Zang, Deye Yang, Jon Markowski, Glenn S Fuoco, Gina C Vendetti, Victor M Rivera, and Jingwu Z Zhang. 1999. "T Cell Responses to Myelin Basic Protein in Patients with Spinal Cord Injury and Multiple Sclerosis." *Journal of Neuroimmunology* 98 (2). Elsevier: 201–7. doi:10.1016/S0165-5728(99)00057-0.
- Klein, R Matthew, and Paul J Higgins. 2011. "A Switch in RND3-RHOA Signaling Is Critical for Melanoma Cell Invasion Following Mutant-BRAF Inhibition." *Molecular Cancer* 10: 114. doi:10.1186/1476-4598-10-114.
- Kojima, Atsuhiko, and Charles H. Tator. 2002. "Intrathecal Administration of Epidermal Growth Factor and Fibroblast Growth Factor 2 Promotes Ependymal Proliferation and Functional Recovery after Spinal Cord Injury in Adult Rats." *Journal of Neurotrauma* 19 (2): 223–38. doi:10.1089/08977150252806974.
- Koning, Nathalie, Lars Bö, Robert M Hoek, and Inge Huitinga. 2007. "Downregulation of Macrophage Inhibitory Molecules in Multiple Sclerosis Lesions." *Annals of Neurology* 62 (5): 504–14. doi:10.1002/ana.21220.
- Koning, Nathalie, Dick F Swaab, Robert M Hoek, and Inge Huitinga. 2009. "Distribution of the Immune Inhibitory Molecules CD200 and CD200R in the Normal Central Nervous System and Multiple Sclerosis Lesions Suggests Neuron-Glia and Glia-Glia Interactions." *Journal of Neuropathology and Experimental Neurology* 68 (2): 159–67. doi:10.1097/NEN.0b013e3181964113.
- Krushel, L A, M H Tai, B A Cunningham, G M Edelman, and K L Crossin. 1998. "Neural Cell Adhesion Molecule (N-CAM) Domains and Intracellular Signaling Pathways Involved in the Inhibition of Astrocyte Proliferation." *Proceedings of the National Academy of Sciences of the United States of America* 95 (5): 2592–96. <http://www.pubmedcentral.nih.gov/articlerender.fcgi?artid=19425&tool=pmcentrez&rendertype=abstract>.
- LARNER, ANDREW J., ALAN R. JOHNSON, and ROGER J. KEYNES. 1995. "REGENERATION IN THE VERTEBRATE CENTRAL NERVOUS SYSTEM: PHYLOGENY, ONTOGENY, AND MECHANISMS." *Biological Reviews* 70 (4): 597–619. doi:10.1111/j.1469-185X.1995.tb01653.x.
- Lee, Jae K, Cédric G Geoffroy, Andrea F Chan, Kristine E Tolentino, Michael J Crawford, Marisa A Leal, Brian Kang, and Binhai Zheng. 2010. "Assessing Spinal Axon Regeneration and Sprouting in Nogo, MAG and OMgp Deficient Mice." *Neuron* 66 (5): 663–70. doi:10.1016/j.neuron.2010.05.002.Assessing.
- Lee, Kuen Yong, and David J Mooney. 2012. "Alginate: Properties and Biomedical Applications." *Progress in Polymer Science* 37 (1). NIH Public Access: 106–26. doi:10.1016/j.progpolymsci.2011.06.003.
- LEE, THOMAS T., BARTH A. GREEN, W. DALTON DIETRICH, and ROBERT P. YEZIERSKI. 1999. "Neuroprotective Effects of Basic Fibroblast Growth Factor Following Spinal Cord Contusion Injury in the Rat." *Journal of Neurotrauma* 16 (5): 347–56. doi:10.1089/neu.1999.16.347.

- Lewis, Danielle K, Adam B Johnson, Shannon Stohlgren, Ashley Harms, and Farida Sohrabji. 2008. "Effects of Estrogen Receptor Agonists on Regulation of the Inflammatory Response in Astrocytes from Young Adult and Middle-Aged Female Rats." *Journal of Neuroimmunology* 195 (1-2): 47–59. doi:10.1016/j.jneuroim.2008.01.006.
- Li, Shuxin, and Stephen M Strittmatter. 2003. "Delayed Systemic Nogo-66 Receptor Antagonist Promotes Recovery from Spinal Cord Injury." *The Journal of Neuroscience : The Official Journal of the Society for Neuroscience* 23 (10): 4219–27.
- Li, Y, P M Field, and G Raisman. 1997. "Repair of Adult Rat Corticospinal Tract by Transplants of Olfactory Ensheathing Cells." *Science (New York, N.Y.)* 277 (5334): 2000–2002. <http://www.ncbi.nlm.nih.gov/pubmed/9302296>.
- Liu, Kai, Yi Lu, Jae K Lee, Ramsey Samara, Rafer Willenberg, Ilse Sears-Kraxberger, Andrea Tedeschi, et al. 2010. "PTEN Deletion Enhances the Regenerative Ability of Adult Corticospinal Neurons." *Nature Neuroscience* 13 (9): 1075–81. doi:10.1038/nn.2603.
- Liu, Wei, Fei-Fei Shang, Yang Xu, Visar Belegu, Lei Xia, Wei Zhao, Ran Liu, et al. 2015. "eIF5A1/RhoGDI α Pathway: A Novel Therapeutic Target for Treatment of Spinal Cord Injury Identified by a Proteomics Approach." *Scientific Reports* 5. Nature Publishing Group: 16911. doi:10.1038/srep16911.
- Lu, Paul, Yaozhi Wang, Lori Graham, Karla Mchale, Mingyong Gao, Di Wu, Armin Blesch, et al. 2012. "Long-Distance Growth and Connectivity of Neural Stem Cells After Severe Spinal Cord Injury." *Cell* 150 (6): 1264–73. doi:10.1016/j.cell.2012.08.020.Long-Distance.
- Lu, Paul, Grace Woodruff, Yaozhi Wang, Lori Graham, Matt Hunt, Di Wu, Eileen Boehle, et al. 2014. "Long-Distance Axonal Growth from Human Induced Pluripotent Stem Cells after Spinal Cord Injury." *Neuron* 83 (4). NIH Public Access: 789–96. doi:10.1016/j.neuron.2014.07.014.
- Lubieniecka, Joanna M, Femke Streijger, Jae H T Lee, Nikolay Stoyanov, Jie Liu, Randy Mottus, Tom Pfeifer, et al. 2011. "Biomarkers for Severity of Spinal Cord Injury in the Cerebrospinal Fluid of Rats." *PloS One* 6 (4): e19247. doi:10.1371/journal.pone.0019247.
- Ma, Chi Him Eddie, Takao Omura, Enrique J. Cobos, Alban Latrémolière, Nader Ghasemlou, Gary J. Brenner, Ed van Veen, et al. 2011. "Accelerating Axonal Growth Promotes Motor Recovery after Peripheral Nerve Injury in Mice." *Journal of Clinical Investigation* 121 (11). American Society for Clinical Investigation: 4332–47. doi:10.1172/JCI58675.
- Madsen, J R, P MacDonald, N Irwin, D E Goldberg, G L Yao, K F Meiri, I J Rimm, P E Stieg, and L I Benowitz. 1998. "Tacrolimus (FK506) Increases Neuronal Expression of GAP-43 and Improves Functional Recovery after Spinal Cord Injury in Rats." *Experimental Neurology* 154 (2): 673–83. doi:10.1006/exnr.1998.6974.
- Maguire, Greg, Peter Friedman, Greg Maguire, and Peter Friedman. 2013. "The Systems Biology of Stem Cell Released Molecules—Based Therapeutics." *ISRN Stem Cells* 2013. Hindawi Publishing Corporation: 1–12. doi:10.1155/2013/784541.

- Mar, Fernando M, Tiago F da Silva, Marlene M Morgado, Lorena G Rodrigues, Daniel Rodrigues, Marta I L Pereira, Ana Marques, et al. 2016. "Myelin Lipids Inhibit Axon Regeneration Following Spinal Cord Injury: A Novel Perspective for Therapy." *Molecular Neurobiology* 53 (2): 1052–64. doi:10.1007/s12035-014-9072-3.
- Marsala, Martin, Osamu Kakinohana, Tony L Yaksh, Zoltan Tomori, Silvia Marsala, and Dasa Cizkova. 2004. "Spinal Implantation of hNT Neurons and Neuronal Precursors: Graft Survival and Functional Effects in Rats with Ischemic Spastic Paraplegia." *The European Journal of Neuroscience* 20 (9): 2401–14. doi:10.1111/j.1460-9568.2004.03702.x.
- Martens, David J, Raewyn M Seaberg, and Derek van der Kooy. 2002. "In Vivo Infusions of Exogenous Growth Factors into the Fourth Ventricle of the Adult Mouse Brain Increase the Proliferation of Neural Progenitors around the Fourth Ventricle and the Central Canal of the Spinal Cord." *The European Journal of Neuroscience* 16 (6): 1045–57. <http://www.ncbi.nlm.nih.gov/pubmed/12383233>.
- Martin, R, H F McFarland, and D E McFarlin. 1992. "Immunological Aspects of Demyelinating Diseases." *Annual Review of Immunology* 10 (January). Annual Reviews 4139 El Camino Way, P.O. Box 10139, Palo Alto, CA 94303-0139, USA: 153–87. doi:10.1146/annurev.iy.10.040192.001101.
- Matsuda, S, F Shibasaki, K Takehana, H Mori, E Nishida, and S Koyasu. 2000. "Two Distinct Action Mechanisms of Immunophilin-Ligand Complexes for the Blockade of T-Cell Activation." *EMBO Reports* 1 (5): 428–34. doi:10.1093/embo-reports/kvd090.
- Matsuoka, M, F Nagawa, K Okazaki, L Kingsbury, K Yoshida, U Müller, D T Larue, J A Winer, and H Sakano. 1991. "Detection of Somatic DNA Recombination in the Transgenic Mouse Brain." *Science (New York, N.Y.)* 254 (5028): 81–86. <http://www.ncbi.nlm.nih.gov/pubmed/1925563>.
- Matyash, Marina, Florian Despang, Rakesh Mandal, Diccon Fiore, Michael Gelinsky, and Chrysanthy Ikonomidou. 2012. "Novel Soft Alginate Hydrogel Strongly Supports Neurite Growth and Protects Neurons against Oxidative Stress." *Tissue Engineering. Part A* 18 (1-2): 55–66. doi:10.1089/ten.TEA.2011.0097.
- Mayer, E., S.B. Dunnett, R. Pellitteri, and J.W. Fawcett. 1993. "Basic Fibroblast Growth Factor Promotes the Survival of Embryonic Ventral Mesencephalic Dopaminergic Neurons—i. Effects in Vitro." *Neuroscience* 56 (2): 379–88. doi:10.1016/0306-4522(93)90339-H.
- McDonald, Patrick P, and Marco A Cassatella. 1997. "Activation of Transcription Factor NF- κ B by Phagocytic Stimuli in Human Neutrophils." *FEBS Letters* 412 (3): 583–86. doi:10.1016/S0014-5793(97)00857-0.
- McKeon, R J; Schreiber, R C; Rudge, J S; Silver, J. 1991. "Reduction of Neurite Outgrowth in a Model of Glial Scarring CNS Injury Is Correlated with the Expression of Inhibitory Molecules on Reactive Astrocytes." *The Journal of Neuroscience: The Official Journal of the Society for Neuroscience* 7 (November): 3398–3411.
- McKerracher, L, S David, D Jackson, V Kottis, R Dunn, and P E Braunt. 1994. "Identification

- of Myelin-Associated Glycoprotein as a Major Myelin-Derived Inhibitor * of Neurite Growth." *Neuron* 13: 805–11.
- Means, E D, and D K Anderson. 1983. "Neuronophagia by Leukocytes in Experimental Spinal Cord Injury." *Journal of Neuropathology and Experimental Neurology* 42 (6): 707–19. <http://www.ncbi.nlm.nih.gov/pubmed/6631457>.
- Meissner, Felix, Richard A Scheltema, Hans-Joachim Mollenkopf, Matthias Mann, L. A. O'Neill, P. Mallick, B. Kuster, et al. 2013. "Direct Proteomic Quantification of the Secretome of Activated Immune Cells." *Science (New York, N.Y.)* 340 (6131). American Association for the Advancement of Science: 475–78. doi:10.1126/science.1232578.
- Merkler, Doron, Gerlinde A S Metz, Olivier Raineteau, Volker Dietz, Martin E Schwab, and Karim Fouad. 2001. "Locomotor Recovery in Spinal Cord-Injured Rats Treated with an Antibody Neutralizing the Myelin-Associated Neurite Growth Inhibitor Nogo-A." *The Journal of Neuroscience : The Official Journal of the Society for Neuroscience* 21 (10): 3665–73.
- Mizuno, Tetsuya, Jun Kawanokuchi, Kenji Numata, and Akio Suzumura. 2003. "Production and Neuroprotective Functions of Fractalkine in the Central Nervous System." *Brain Research* 979 (1-2): 65–70. doi:10.1016/S0006-8993(03)02867-1.
- Montesano, R, J D Vassalli, A Baird, R Guillemin, and L Orci. 1986. "Basic Fibroblast Growth Factor Induces Angiogenesis in Vitro." *Proceedings of the National Academy of Sciences of the United States of America* 83 (19): 7297–7301. <http://www.ncbi.nlm.nih.gov/pubmed/2429303>.
- Mothe, Andrea J., Roger Y. Tam, Tasneem Zahir, Charles H. Tator, and Molly S. Shoichet. 2013. "Repair of the Injured Spinal Cord by Transplantation of Neural Stem Cells in a Hyaluronan-Based Hydrogel." *Biomaterials* 34 (15): 3775–83. doi:10.1016/j.biomaterials.2013.02.002.
- Nakae, Aya, Kunihiro Nakai, Kenji Yano, Ko Hosokawa, Masahiko Shibata, and Takashi Mashimo. 2011. "The Animal Model of Spinal Cord Injury as an Experimental Pain Model." *Journal of Biomedicine & Biotechnology* 2011 (January): 939023. doi:10.1155/2011/939023.
- Nakano, Norihiko, Yoshiyasu Nakai, Tae-Boem Seo, Yoshihiro Yamada, Takayuki Ohno, Atsuo Yamanaka, Yoji Nagai, et al. 2010. *Characterization of Conditioned Medium of Cultured Bone Marrow Stromal Cells. Neuroscience Letters*. Vol. 483. doi:10.1016/j.neulet.2010.07.062.
- Nakayama, Natsuki, and Chihiro Tohda. 2007. "Withanoside IV Improves Hindlimb Function by Facilitating Axonal Growth and Increase in Peripheral Nervous System Myelin Level after Spinal Cord Injury." *Neuroscience Research* 58: 176–82. doi:10.1016/j.neures.2007.02.014.
- Neirinckx, Virginie, Cécile Coste, Rachelle Franzen, André Gothot, Bernard Rogister, and Sabine Wislet. 2014. "Neutrophil Contribution to Spinal Cord Injury and Repair." *Journal*

of Neuroinflammation 11 (150): 1–9.

- Niederost, B, Thomas Oertle, Jens Fritsche, R Anne Mckinney, and Christine E Bandtlow. 2002. “Nogo-A and Myelin-Associated Glycoprotein Mediate Neurite Growth Inhibition by Antagonistic Regulation of RhoA and Rac1.” *The Journal of Neuroscience: The Official Journal of the Society for Neuroscience* 22 (23): 10368–76.
- Niu, Na, Jie Zhang, Yong Guo, Yingying Zhao, Christine Korteweg, and Jiang Gu. 2011. “Expression and Distribution of Immunoglobulin G and Its Receptors in the Human Nervous System.” *The International Journal of Biochemistry & Cell Biology* 43 (4): 556–63. doi:10.1016/j.biocel.2010.12.012.
- Niu, Na, Jie Zhang, Yingui Sun, Shuna Wang, Yonghong Sun, Christine Korteweg, Weiwei Gao, and Jiang Gu. 2011. “Expression and Distribution of Immunoglobulin G and Its Receptors in an Immune Privileged Site: The Eye.” *Cellular and Molecular Life Sciences: CMLS* 68 (14): 2481–92. doi:10.1007/s00018-010-0572-7.
- Noda, Mariko, Kento Takii, Bijay Parajuli, Jun Kawanokuchi, Yoshifumi Sonobe, Hideyuki Takeuchi, Tetsuya Mizuno, and Akio Suzumura. 2014. “FGF-2 Released from Degenerating Neurons Exerts Microglial-Induced Neuroprotection via FGFR3-ERK Signaling Pathway.” *Journal of Neuroinflammation* 11: 76. doi:10.1186/1742-2094-11-76.
- Nomura, Hiroshi, Charles H Tator, and Molly S Shoichet. 2006. “Bioengineered Strategies for Spinal Cord Repair.” *Journal of Neurotrauma* 23 (3-4): 496–507. doi:10.1089/neu.2006.23.496.
- Novokmet, Mislav, Edita Lukić, Frano Vučković, Željko Đurić, Toma Keser, Katarina Rajšl, Daniel Remondini, et al. 2014. “Changes in IgG and Total Plasma Protein Glycomes in Acute Systemic Inflammation.” *Scientific Reports* 4. Nature Publishing Group: 4347. doi:10.1038/srep04347.
- Ota, Haruko, Takao Hikita, Tomoki Nishioka, Mami Matsumoto, Jun Ito, Naoya Asai, Atsushi Enomoto, et al. 2013. *Proteomic Analysis of Girdin-Interacting Proteins in Migrating New Neurons in the Postnatal Mouse Brain. Biochemical and Biophysical Research Communications*. Vol. 442. doi:10.1016/j.bbrc.2013.10.126.
- Parikh, P., Y. Hao, M. Hosseinkhani, S. B. Patil, G. W. Huntley, M. Tessier-Lavigne, and H. Zou. 2011. “Regeneration of Axons in Injured Spinal Cord by Activation of Bone Morphogenetic protein/Smad1 Signaling Pathway in Adult Neurons.” *Proceedings of the National Academy of Sciences* 108 (19). National Acad Sciences: E99–107. doi:10.1073/pnas.1100426108.
- Park, Kevin K., Kai Liu, Yang Hu, Jennifer L. Kanter, and Zhigang He. 2010. “PTEN/mTOR and Axon Regeneration.” *Experimental Neurology* 223 (1): 45–50. doi:10.1016/j.expneurol.2009.12.032.
- Park, Kevin Kyungsuk, Kai Liu, Yang Hu, Patrice D Smith, Chen Wang, Bin Cai, Bengang Xu, et al. 2008. “Promoting Axon Regeneration in the Adult CNS by Modulation of the

- PTEN/mTOR Pathway.” *Science (New York, N.Y.)* 322 (5903). American Association for the Advancement of Science: 963–66. doi:10.1126/science.1161566.
- Parri, Rheinallt, and Vincenzo Crunelli. 2003. “An Astrocyte Bridge from Synapse to Blood Flow.” *Nature Neuroscience* 6 (1): 5–6. doi:10.1038/nn0103-5.
- Pego, Ana Paula, Sarka Kubinova, Dasa Cizkova, Ivo Vanicky, Fernando Milhazes, Monica Mendes, and Eva Sykova. 2012. “Regenerative Medicine for the Treatment of Spinal Cord Injury : More than Just Promises ? Aspects of Stem Cell-Based Therapy for Spinal Cord Injury.” *Journal of Cellular and Molecular Medicine* 16 (11): 2564–82. doi:10.1111/j.1582-4934.2012.01603.x.
- Piantino, J., J.A. Burdick, D. Goldberg, R. Langer, and L.I. Benowitz. 2006. “An Injectable, Biodegradable Hydrogel for Trophic Factor Delivery Enhances Axonal Rewiring and Improves Performance after Spinal Cord Injury.” *Experimental Neurology* 201 (2): 359–67. doi:10.1016/j.expneurol.2006.04.020.
- Pluchino, Stefano, and Chiara Cossetti. 2013. “How Stem Cells Speak with Host Immune Cells in Inflammatory Brain Diseases.” *Glia* 61 (9): 1379–1401. doi:10.1002/glia.22500.
- Poon, Peter C, Dimpay Gupta, Molly S Shoichet, and Charles H Tator. 2007. “Clip Compression Model Is Useful for Thoracic Spinal Cord Injuries Histologic and Functional Correlates.” *Spine* 32 (25): 2853–59.
- Popovich, P G, B T Stokes, and C C Whitacre. 1996. “Concept of Autoimmunity Following Spinal Cord Injury: Possible Roles for T Lymphocytes in the Traumatized Central Nervous System.” *Journal of Neuroscience Research* 45 (4): 349–63. doi:10.1002/(SICI)1097-4547(19960815)45:4<349::AID-JNR4>3.0.CO;2-9.
- Popovich, Phillip G, Ping Wei, and Bradford T Stokes. 1997. “After Spinal Cord Injury in Sprague-Dawley and Lewis Rats.” *The Journal of Comparative Neurology* 464 (April 1996): 443–64.
- Popovich, Phillip G., and T.Bucky Jones. 2003. “Manipulating Neuroinflammatory Reactions in the Injured Spinal Cord: Back to Basics.” *Trends in Pharmacological Sciences* 24 (1): 13–17. doi:10.1016/S0165-6147(02)00006-8.
- Powell, Jonathan D, and Yan Zheng. 2006. “Dissecting the Mechanism of T-Cell Anergy with Immunophilin Ligands.” *Current Opinion in Investigational Drugs (London, England : 2000)* 7 (11): 1002–7. <http://www.ncbi.nlm.nih.gov/pubmed/17117589>.
- Prang, Peter, Rainer Müller, Ahmed Eljaouhari, Klaus Heckmann, Werner Kunz, Thomas Weber, Cornelius Faber, Maurice Vroemen, Ulrich Bogdahn, and Norbert Weidner. 2006. “The Promotion of Oriented Axonal Regrowth in the Injured Spinal Cord by Alginate-Based Anisotropic Capillary Hydrogels.” *Biomaterials* 27 (19): 3560–69. doi:10.1016/j.biomaterials.2006.01.053.
- Qu, Lintao, Pu Zhang, Robert H. LaMotte, and Chao Ma. 2011. “Neuronal Fc-Gamma Receptor I Mediated Excitatory Effects of IgG Immune Complex on Rat Dorsal Root Ganglion

- Neurons.” *Brain, Behavior, and Immunity* 25 (7): 1399–1407. doi:10.1016/j.bbi.2011.04.008.
- Raghavan, M, and P J Bjorkman. 1996. “Fc Receptors and Their Interactions with Immunoglobulins.” *Annual Review of Cell and Developmental Biology* 12: 181–220. doi:10.1146/annurev.cellbio.12.1.181.
- Raisman, Geoffrey, S C Barnett, and Almudena Ramón-Cueto. 2012. “Repair of Central Nervous System Lesions by Transplantation of Olfactory Ensheathing Cells.” *Handbook of Clinical Neurology* 109 (January): 541–49. doi:10.1016/B978-0-444-52137-8.00033-4.
- Ransohoff, Richard M, and Astrid E Cardona. 2010. “The Myeloid Cells of the Central Nervous System Parenchyma.” *Nature* 468 (7321). Nature Publishing Group, a division of Macmillan Publishers Limited. All Rights Reserved.: 253–62. doi:10.1038/nature09615.
- Ransohoff, Richard M, and V Hugh Perry. 2009. “Microglial Physiology: Unique Stimuli, Specialized Responses.” *Annual Review of Immunology* 27: 119–45. doi:10.1146/annurev.immunol.021908.132528.
- Reynolds, Brent A, W Tetzlaff, and S Weiss. 1992. “A Multipotent EGF-Responsive Striatal Embryonic Produces Neurons and Astrocytes.” *The Journal of Neuroscience : The Official Journal of the Society for Neuroscience* 12 (November): 4565–74.
- Reynolds, Brent A, and S Weiss. 1992. “Generation of Neurons and Astrocytes from Isolated Cells of the Adult Mammalian Central Nervous System.” *Science*, no. October 1991: 1–4.
- Riegger, Tino, Sabine Conrad, Kai Liu, Hermann J Schluesener, Mahdi Adibzahdeh, and Jan M Schwab. 2007. “Spinal Cord Injury-Induced Immune Depression Syndrome (SCI-IDS).” *The European Journal of Neuroscience* 25 (6): 1743–47. doi:10.1111/j.1460-9568.2007.05447.x.
- Ritfeld, Gaby J, Rishi D S Nandoe Tewarie, Katarina Vajn, Sahar T Rahiem, Andres Hurtado, Dane F Wendell, Raymund A C Roos, and Martin Oudega. 2012. “Bone Marrow Stromal Cell-Mediated Tissue Sparing Enhances Functional Repair after Spinal Cord Contusion in Adult Rats.” *Cell Transplantation* 21 (7): 1561–75. doi:10.3727/096368912X640484.
- Ritfeld, Gaby J, Raymund A C Roos, and Martin Oudega. 2011. “Stem Cells for Central Nervous System Repair and Rehabilitation.” *PM & R : The Journal of Injury, Function, and Rehabilitation* 3 (6 Suppl 1): S117–22. doi:10.1016/j.pmrj.2011.02.011.
- RODBELL, M. 1964. “METABOLISM OF ISOLATED FAT CELLS. I. EFFECTS OF HORMONES ON GLUCOSE METABOLISM AND LIPOLYSIS.” *The Journal of Biological Chemistry* 239 (February): 375–80. <http://www.ncbi.nlm.nih.gov/pubmed/14169133>.
- Roitbak, T, and E Syková. 1999. “Diffusion Barriers Evoked in the Rat Cortex by Reactive Astrogliosis.” *Glia* 28 (1): 40–48. <http://www.ncbi.nlm.nih.gov/pubmed/10498821>.
- Rowland, James W, Gregory W J Hawryluk, Brian Kwon, and Michael G Fehlings. 2008. “Current Status of Acute Spinal Cord Injury Pathophysiology and Emerging Therapies:

- Promise on the Horizon.” *Neurosurgical Focus* 25 (5): E2. doi:10.3171/FOC.2008.25.11.E2.
- Rudge, J S, and J Silver. 1990. “Inhibition of Neurite Outgrowth on Astroglial Scars in Vitro.” *The Journal of Neuroscience : The Official Journal of the Society for Neuroscience* 10 (11): 3594–3603. <http://www.ncbi.nlm.nih.gov/pubmed/2230948>.
- Saganová, Kamila, Ján Gálik, Juraj Bla, Andrea Korimová, Eniko Ra, and Ivo Vanický. 2012. “Immunosuppressant FK506 : Focusing on Neuroprotective Effects Following Brain and Spinal Cord Injury.” *Life Sciences* 91: 77–82. doi:10.1016/j.lfs.2012.06.022.
- Salazar, L, Nobuko Uchida, Frank P T Hamers, Brian J Cummings, and J Aileen. 2010. “Human Neural Stem Cells Differentiate and Promote Locomotor Recovery in an Early Chronic Spinal cord Injury NOD-Scid Mouse Model.” *PlosOne* 5 (8). doi:10.1371/journal.pone.0012272.
- Salzet, Michel. 2002. “Immune Cells Express Endocrine Markers.” *Neuro Endocrinology Letters* 23 (1): 8–9. <http://www.ncbi.nlm.nih.gov/pubmed/11880855>.
- Sato, Yoshiaki, Keiko Nakanishi, Yoshihito Tokita, Hiroko Kakizawa, Michiru Ida, Hiroshi Maeda, Fumiko Matsui, et al. 2008. “A Highly Sulfated Chondroitin Sulfate Preparation, CS-E, Prevents Excitatory Amino Acid-Induced Neuronal Cell Death.” *Journal of Neurochemistry* 104 (6): 1565–76. doi:10.1111/j.1471-4159.2007.05107.x.
- Schnell, Lisa, and Martin E Schwab. 1990. “Axonal Regeneration in the Rat Spinal Cord Produced by an Antibody against Myelin-Associated Neurite Growth Inhibitors.” *Nature* 343: 269–72.
- Schwab, M E, and D Bartholdi. 1996. “Degeneration and Regeneration of Axons in the Lesioned Spinal Cord.” *Physiological Reviews* 76 (2): 319–70. <http://www.ncbi.nlm.nih.gov/pubmed/8618960>.
- Schwab, Martin E. 2004. “Nogo and Axon Regeneration.” *Current Opinion in Neurobiology* 14 (1): 118–24. doi:10.1016/j.conb.2004.01.004.
- Schwab, Martin E, R. J. Dumont, M. E. Schwab, D. Bartholdi, B. A. Kakulas, P. Caroni, M. E. Schwab, et al. 2002. “Repairing the Injured Spinal Cord.” *Science (New York, N.Y.)* 295 (5557). American Association for the Advancement of Science: 1029–31. doi:10.1126/science.1067840.
- Schwartz, Joan P., and Nobuyoshi Nishiyama. 1994. “Neurotrophic Factor Gene Expression in Astrocytes during Development and Following Injury.” *Brain Research Bulletin* 35 (5-6): 403–7. doi:10.1016/0361-9230(94)90151-1.
- Sekhon, L H, and M G Fehlings. 2001. “Epidemiology, Demographics, and Pathophysiology of Acute Spinal Cord Injury.” *Spine* 26 (24 Suppl): S2–12. <http://www.ncbi.nlm.nih.gov/pubmed/11805601>.
- Sengupta, Mohor Biplab, Mahashweta Basu, Sourav Iswarari, Kiran Kumar Mukhopadhyay, Krishna Pada Sardar, Biplab Acharyya, Pradeep K Mohanty, and Debashis

- Mukhopadhyay. 2014. "CSF Proteomics of Secondary Phase Spinal Cord Injury in Human Subjects: Perturbed Molecular Pathways Post Injury." *PloS One* 9 (10): e110885. doi:10.1371/journal.pone.0110885.
- Sharples, Simon A, Kathrin Koblinger, Jennifer M Humphreys, and Patrick J Whelan. 2014. "Dopamine: A Parallel Pathway for the Modulation of Spinal Locomotor Networks." *Frontiers in Neural Circuits* 8. Frontiers Media SA: 55. doi:10.3389/fncir.2014.00055.
- Sica, Antonio, Tiziana Schioppa, Alberto Mantovani, and Paola Allavena. 2006. "Tumour-Associated Macrophages Are a Distinct M2 Polarised Population Promoting Tumour Progression: Potential Targets of Anti-Cancer Therapy." *European Journal of Cancer (Oxford, England : 1990)* 42 (6). Elsevier: 717–27. doi:10.1016/j.ejca.2006.01.003.
- Silver, Jerry, and Jared H Miller. 2004. "Regeneration beyond the Glial Scar." *Nature Reviews. Neuroscience* 5 (2): 146–56. doi:10.1038/nrn1326.
- Simms, Brett A., and Gerald W. Zamponi. 2014. "Neuronal Voltage-Gated Calcium Channels: Structure, Function, and Dysfunction." *Neuron* 82 (1). Elsevier: 24–45. doi:10.1016/j.neuron.2014.03.016.
- Singh, Vaibhav, Rogier Q Hintzen, Theo M Luider, and Marcel P Stoop. 2012. "Proteomics Technologies for Biomarker Discovery in Multiple Sclerosis." *Journal of Neuroimmunology* 248 (1-2): 40–47. doi:10.1016/j.jneuroim.2011.11.004.
- Smith, G V, and J A Stevenson. 1988. "Peripheral Nerve Grafts Lacking Viable Schwann Cells Fail to Support Central Nervous System Axonal Regeneration." *Experimental Brain Research* 69 (2): 299–306. <http://www.ncbi.nlm.nih.gov/pubmed/3278916>.
- Smith-thomas, Linda C, Juin Fok-seang, James Stevens, Jian-sheng Du, Elizabeth Muir, Herbert M Geller, John H Rogers, and James W Fawcett. 1994. "An Inhibitor of Neurite Outgrowth Produced by Astrocytes." *Journal of Cell Science* 1695: 1687–95.
- Smith-thomas, Linda C, James Stevens, Juin Fok-seang, Andreas Faissner, John H Rogers, and James W Fawcett. 1995. "Increased Axon Regeneration in Astrocytes Grown in the Presence of Proteoglycan Synthesis Inhibitors." *Journal of Cell Science* 1315: 1307–15.
- Spillmann, A A, C E Bandtlow, F Lottspeich, F Keller, and M E Schwab. 1998. "Identification and Characterization of a Bovine Neurite Growth Inhibitor (bNI-220)." *The Journal of Biological Chemistry* 273 (30): 19283–93. <http://www.ncbi.nlm.nih.gov/pubmed/9668118>.
- Sribnick, Eric A, Supriti Samantaray, Arabinda Das, Joshua Smith, D Denise Matzelle, Swapan K Ray, and Naren L Banik. 2010. "Postinjury Estrogen Treatment of Chronic Spinal Cord Injury Improves Locomotor Function in Rats." *Journal of Neuroscience Research* 88 (8): 1738–50. doi:10.1002/jnr.22337.
- Sribnick, Eric Anthony, James Michael Wingrave, Deborah Denise Matzelle, Gloria Gant Wilford, Swapan Kumar Ray, and Naren Lal Banik. 2005. "Estrogen Attenuated Markers of Inflammation and Decreased Lesion Volume in Acute Spinal Cord Injury in Rats."

Journal of Neuroscience Research 82 (2): 283–93. doi:10.1002/jnr.20622.

- Staaht, Brett T, and Gerald R Crabtree. 2013. “Creating a Neural Specific Chromatin Landscape by npBAF and nBAF Complexes.” *Current Opinion in Neurobiology* 23 (6). NIH Public Access: 903–13. doi:10.1016/j.conb.2013.09.003.
- Stokes, B T, D H Noyes, and D L Behrmann. 1992. “An Electromechanical Spinal Injury Technique with Dynamic Sensitivity.” *Journal of Neurotrauma* 9 (3): 187–95. <http://www.ncbi.nlm.nih.gov/pubmed/1474607>.
- Straub, Rainer H. 2007. “The Complex Role of Estrogens in Inflammation.” *Endocrine Reviews* 28 (5): 521–74. doi:10.1210/er.2007-0001.
- Tabakow, Pawel, Wlodzimierz Jarmundowicz, Bogdan Czapiga, Wojciech Fortuna, Ryszard Miedzybrodzki, Marcin Czyz, Juliusz Huber, et al. 2013. “Transplantation of Autologous Olfactory Ensheathing Cells in Complete Human Spinal Cord Injury.” *Cell Transplantation*, April. doi:10.3727/096368913X663532.
- Tabakow, Pawel, Geoffrey Raisman, Wojciech Fortuna, Marcin Czyz, Juliusz Huber, Daqing Li, Pawel Szewczyk, et al. 2014. “Functional Regeneration of Supraspinal Connections in a Patient with Transected Spinal Cord Following Transplantation of Bulbar Olfactory Ensheathing Cells with Peripheral Nerve Bridging.” *Cell Transplantation*, October, 1–70. doi:10.3727/096368914X685131.
- Tambuyzer, Bart R, Peter Ponsaerts, and Etienne J Nouwen. 2009. “Microglia: Gatekeepers of Central Nervous System Immunology.” *Journal of Leukocyte Biology* 85 (3): 352–70. doi:10.1189/jlb.0608385.
- Taoka, Y, K Okajima, M Uchiba, K Murakami, S Kushimoto, M Johno, M Naruo, H Okabe, and K Takatsuki. 1997. “Role of Neutrophils in Spinal Cord Injury in the Rat.” *Neuroscience* 79 (4): 1177–82. doi:10.1016/S0306-4522(97)00011-0.
- TARLOV, I M, H KLINGER, and S VITALE. 1953. “Spinal Cord Compression Studies. I. Experimental Techniques to Produce Acute and Gradual Compression.” *A.M.A. Archives of Neurology and Psychiatry* 70 (6): 813–19. <http://www.ncbi.nlm.nih.gov/pubmed/13103865>.
- Taylor, Sara J., and Shelly E. Sakiyama-Elbert. 2006. “Effect of Controlled Delivery of Neurotrophin-3 from Fibrin on Spinal Cord Injury in a Long Term Model.” *Journal of Controlled Release* 116 (2): 204–10. doi:10.1016/j.jconrel.2006.07.005.
- Tedeschi, A, T Nguyen, R Puttagunta, P Gaub, and S Di Giovanni. 2009. “A p53-CBP/p300 Transcription Module Is Required for GAP-43 Expression, Axon Outgrowth, and Regeneration.” *Cell Death and Differentiation* 16 (4). Nature Publishing Group: 543–54. doi:10.1038/cdd.2008.175.
- Tedeschi, Andrea, Simone Di Giovanni, RS. Aloyz, SX. Bamji, CD. Pozniak, JG. Toma, J. Atwal, et al. 2009. “The Non-Apoptotic Role of p53 in Neuronal Biology: Enlightening the Dark Side of the Moon.” *EMBO Reports* 10 (6). EMBO Press: 576–83.

doi:10.1038/embor.2009.89.

- Tester, N J, and D R Howland. 2008. "Chondroitinase ABC Improves Basic and Skilled Locomotion in Spinal Cord Injured Cats." *Experimental Neurology* 209 (2): 483–96. doi:10.1016/j.expneurol.2007.07.019.Chondroitinase.
- Thuret, Sandrine, Lawrence D F Moon, and Fred H Gage. 2006. "Therapeutic Interventions after Spinal Cord Injury." *Nature Reviews. Neuroscience* 7 (8): 628–43. doi:10.1038/nrn1955.
- Tian, Li, Li Ma, Tiina Kaarela, and Zhilin Li. 2012. "Neuroimmune Crosstalk in the Central Nervous System and Its Significance for Neurological Diseases." *Journal of Neuroinflammation* 9 (155): 1–10. doi:10.1186/1742-2094-9-155.
- Tigyi, G, D J Fischer, A Sebök, F Marshall, D L Dyer, and R Miledi. 1996. "Lysophosphatidic Acid-Induced Neurite Retraction in PC12 Cells: Neurite-Protective Effects of Cyclic AMP Signaling." *Journal of Neurochemistry* 66 (2): 549–58. <http://www.ncbi.nlm.nih.gov/pubmed/8592124>.
- Tom, Veronica J, and John D Houllé. 2008. "Intraspinal Microinjection of Chondroitinase ABC Following Injury Promotes Axonal Regeneration out of a Peripheral Nerve Graft Bridge." *Experimental Neurology* 211 (1): 315–19. doi:10.1016/j.expneurol.2008.01.021.
- Tonai, Takeharu, Kei-ichiro Shiba, Yutaka Taketani, Yasukazu Ohmoto, Kaori Murata, Masahiro Muraguchi, Hiroyuki Ohsaki, Eiji Takeda, and Takehiko Nishisho. 2001. "A Neutrophil Elastase Inhibitor (ONO-5046) Reduces Neurologic Damage after Spinal Cord Injury in Rats." *Journal of Neurochemistry* 78 (5): 1064–72. doi:10.1046/j.1471-4159.2001.00488.x.
- Tweedie, David, Lital Rachmany, Dong Seok Kim, Vardit Rubovitch, Elin Lehrmann, Yongqing Zhang, Kevin G. Becker, Evelyn Perez, Chaim G. Pick, and Nigel H. Greig. 2016. "Mild Traumatic Brain Injury-Induced Hippocampal Gene Expressions: The Identification of Target Cellular Processes for Drug Development." *Journal of Neuroscience Methods*. doi:10.1016/j.jneumeth.2016.02.003.
- Uccelli, Antonio, Lorenzo Moretta, and Vito Pistoia. 2008. "Mesenchymal Stem Cells in Health and Disease." *Nature Reviews. Immunology* 8 (9): 726–36. doi:10.1038/nri2395.
- Udina, Esther, Dolores Ceballos, Enrique Verdú, Bruce G Gold, and Xavier Navarro. 2002. "Bimodal Dose-Dependence of FK506 on the Rate of Axonal Regeneration in Mouse Peripheral Nerve." *Muscle & Nerve* 26 (3): 348–55. doi:10.1002/mus.10195.
- Vafadari, Ramin, Dennis A Hesselink, Monique M Cadogan, Willem Weimar, and Carla C Baan. 2012. "Inhibitory Effect of Tacrolimus on p38 Mitogen-Activated Protein Kinase Signaling in Kidney Transplant Recipients Measured by Whole-Blood Phosphospecific Flow Cytometry." *Transplantation* 93 (12): 1245–51. doi:10.1097/TP.0b013e318250fc62.
- Vanicky, Ivo, Lucia Urdzíkóvá, and Kamila Saganová. 2001. "A Simple and Reproducible Model of Spinal Cord Injury Induced by Epidural Balloon Inflation in the Rat." *Journal*

of Neurotrauma 18 (12): 1399–1407.

- Vegeto, Elisabetta, Silvia Belcredito, Sabrina Etteri, Serena Ghisletti, Alessia Brusadelli, Clara Meda, Andrée Krust, et al. 2003. “Estrogen Receptor-Alpha Mediates the Brain Antiinflammatory Activity of Estradiol.” *Proceedings of the National Academy of Sciences of the United States of America* 100 (16): 9614–19. doi:10.1073/pnas.1531957100.
- Voríšek, I, M Hájek, J Tintera, K Nicolay, and E Syková. 2002. “Water ADC, Extracellular Space Volume, and Tortuosity in the Rat Cortex after Traumatic Injury.” *Magnetic Resonance in Medicine: Official Journal of the Society of Magnetic Resonance in Medicine / Society of Magnetic Resonance in Medicine* 48 (6): 994–1003. doi:10.1002/mrm.10305.
- Wang, Kevin C, Vuk Koprivica, Jieun A Kim, Rajeev Sivasankaran, Yong Guo, Rachel L Neve, and Zhigang He. 2002. “Oligodendrocyte-Myelin Glycoprotein Is a Nogo Receptor Ligand That Inhibits Neurite Outgrowth.” *Nature*, 941–44. doi:10.1038/nature00834.1.
- Wang, M S, and B G Gold. 1999. “FK506 Increases the Regeneration of Spinal Cord Axons in a Predegenerated Peripheral Nerve Autograft.” *The Journal of Spinal Cord Medicine* 22 (4): 287–96. <http://europepmc.org/abstract/med/10751133>.
- Wang, Mindan, Peng Zhai, Xiongbiao Chen, David J Schreyer, Xiaodan Sun, and Fuzhai Cui. 2011. “Bioengineered Scaffolds for Spinal Cord Repair.” *Tissue Engineering. Part B, Reviews* 17 (3): 177–94. doi:10.1089/ten.TEB.2010.0648.
- Watanabe, T, T Yamamoto, Y Abe, N Saito, T Kumagai, and H Kayama. 1999. “Differential Activation of Microglia after Experimental Spinal Cord Injury.” *Journal of Neurotrauma* 16 (3): 255–65. <http://www.ncbi.nlm.nih.gov/pubmed/10195473>.
- Wells, Jennifer E a, R John Hurlbert, Michael G Fehlings, and V Wee Yong. 2003. “Neuroprotection by Minocycline Facilitates Significant Recovery from Spinal Cord Injury in Mice.” *Brain: A Journal of Neurology* 126 (Pt 7): 1628–37. doi:10.1093/brain/awg178.
- White, Robin E, Feng Qin Yin, and Lyn B Jakeman. 2008. “TGF-Alpha Increases Astrocyte Invasion and Promotes Axonal Growth into the Lesion Following Spinal Cord Injury in Mice.” *Experimental Neurology* 214 (1): 10–24. doi:10.1016/j.expneurol.2008.06.012.
- Winton, M. J., Catherine I. Dubreuil, Dana Lasko, Nicole Leclerc, and Lisa McKerracher. 2002. “Characterization of New Cell Permeable C3-like Proteins That Inactivate Rho and Stimulate Neurite Outgrowth on Inhibitory Substrates.” *Journal of Biological Chemistry* 277 (36): 32820–29. doi:10.1074/jbc.M201195200.
- Wolf, Yochai, Simon Yona, Ki-Wook Kim, and Steffen Jung. 2013. “Microglia, Seen from the CX3CR1 Angle.” *Frontiers in Cellular Neuroscience* 7 (January). Frontiers: 26. doi:10.3389/fncel.2013.00026.
- Wu, Jiang I, Julie Lessard, Ivan A Olave, Zilong Qiu, Anirvan Ghosh, Isabella A Graef, Gerald

- R Crabtree, et al. 2007. "Regulation of Dendritic Development by Neuron-Specific Chromatin Remodeling Complexes." *Neuron* 56 (1). Elsevier: 94–108. doi:10.1016/j.neuron.2007.08.021.
- Yamashita, Masamichi, and John B. Fenn. 1984. "Electrospray Ion Source. Another Variation on the Free-Jet Theme." *The Journal of Physical Chemistry* 88 (20). American Chemical Society: 4451–59. doi:10.1021/j150664a002.
- Yamashita, Toshihide, Haruhisa Higuchi, and Masaya Tohyama. 2002. "The p75 Receptor Transduces the Signal from Myelin-Associated Glycoprotein to Rho." *The Journal of Cell Biology* 157 (4): 565–70. doi:10.1083/jcb.200202010.
- Yan, Xiaodong, Juanfang Liu, Zhanpeng Luo, Qinxue Ding, Xinggong Mao, Ming Yan, Shuguang Yang, Xueyu Hu, Jinghui Huang, and Zhuojing Luo. 2010. "Proteomic Profiling of Proteins in Rat Spinal Cord Induced by Contusion Injury." *Neurochemistry International* 56 (8): 971–83. doi:10.1016/j.neuint.2010.04.007.
- Yong, V Wee, Jennifer Wells, Fabrizio Giuliani, Steven Casha, Christopher Power, and Luanne M Metz. 2004. "Minocycline and Neurological Diseases The Promise of Minocycline in Neurology." *Lancet Neurology* 3 (December): 744–51.
- Yoshimi, Kenji, Monica Woo, Yubei Son, Michel Baudry, and Richard F Thompson. 2002. "IgG-Immunostaining in the Intact Rabbit Brain: Variable but Significant Staining of Hippocampal and Cerebellar Neurons with Anti-IgG." *Brain Research* 956 (1): 53–66. doi:10.1016/S0006-8993(02)03479-0.
- Zhang, Jie, Na Niu, Bingjie Li, and Michael A McNutt. 2013. "Neuron-Derived IgG Protects Neurons from Complement-Dependent Cytotoxicity." *The Journal of Histochemistry and Cytochemistry: Official Journal of the Histochemistry Society* 61 (12): 869–79. doi:10.1369/0022155413504196.
- Zhang, Jie, Na Niu, Mingyu Wang, Michael A. McNutt, Donghong Zhang, Baogang Zhang, Shijun Lu, Yuqing Liu, and Zhihui Liu. 2013. "Neuron-Derived IgG Protects Dopaminergic Neurons from Insult by 6-OHDA and Activates Microglia through the FcγR I and TLR4 Pathways." *The International Journal of Biochemistry & Cell Biology* 45 (8): 1911–20. doi:10.1016/j.biocel.2013.06.005.
- Zhang, Ning, Honghai Yan, and Xuejun Wen. 2005. "Tissue-Engineering Approaches for Axonal Guidance." *Brain Research Reviews* 49 (1): 48–64. doi:10.1016/j.brainresrev.2004.11.002.
- Zhang, Shi, Xi-Jin Wang, Li-Peng Tian, Jing Pan, Guo-Qiang Lu, Ying-Jie Zhang, Jian-Qing Ding, and Sheng-Di Chen. 2011. "CD200-CD200R Dysfunction Exacerbates Microglial Activation and Dopaminergic Neurodegeneration in a Rat Model of Parkinson's Disease." *Journal of Neuroinflammation* 8 (January): 154. doi:10.1186/1742-2094-8-154.
- Zhang, Yaoyang, Bryan R Fonslow, Bing Shan, Moon-Chang Baek, and John R Yates. 2013. "Protein Analysis by Shotgun/bottom-up Proteomics." *Chemical Reviews* 113 (4). American Chemical Society: 2343–94. doi:10.1021/cr3003533.

- Zhang, Zhiqun, J. Susie Zoltewicz, Stefania Mondello, Kimberly J. Newsom, Zhihui Yang, Boxuan Yang, Firas Kobeissy, et al. 2014. "Human Traumatic Brain Injury Induces Autoantibody Response against Glial Fibrillary Acidic Protein and Its Breakdown Products." Edited by Irun R. Cohen. *PLoS ONE* 9 (3). Public Library of Science: e92698. doi:10.1371/journal.pone.0092698.
- Zheng, Binbin, Libing Ye, Yulong Zhou, Sipin Zhu, Qingqing Wang, Hongxue Shi, Daqing Chen, et al. 2016. "Epidermal Growth Factor Attenuates Blood-Spinal Cord Barrier Disruption via PI3K/Akt/Rac1 Pathway after Acute Spinal Cord Injury." *Journal of Cellular and Molecular Medicine* 20 (6): 1062–75. doi:10.1111/jcmm.12761.
- Zou, H., C. Ho, K. Wong, and M. Tessier-Lavigne. 2009. "Axotomy-Induced Smad1 Activation Promotes Axonal Growth in Adult Sensory Neurons." *Journal of Neuroscience* 29 (22): 7116–23. doi:10.1523/JNEUROSCI.5397-08.2009.
- Zuk, P A, M Zhu, H Mizuno, J Huang, J W Futrell, A J Katz, P Benhaim, H P Lorenz, and M H Hedrick. 2001. "Multilineage Cells from Human Adipose Tissue: Implications for Cell-Based Therapies." *Tissue Engineering* 7 (2): 211–28. doi:10.1089/107632701300062859.

Annex

Comparison of dynamic behavior and maturation of neural multipotent cells derived from different spinal cord developmental stages: an *in vitro* study

Lucia Slovinska^{1*}, Eva Szekiova¹, Juraj Blasko¹, Stéphanie Devaux¹, Michel Salzet², and Dasa Cizkova^{1,2}

¹Institute of Neurobiology, Slovak Academy of Sciences, Kosice, Slovak Republic, *Email: slovinska@saske.sk; ²U-1192 INSERM, Laboratoire PRISM (Protéomique, Réponse Inflammatoire, Spirométrie de masse), Université Lille, Villeneuve d'Ascq, France

Neural progenitor cells (NPCs) are characterized as undifferentiated cells with the ability of self-renewal and multipotency to give rise to other cells of the nervous system. In our *in vitro* study we demonstrate the proliferative and differentiative potential of NPCs isolated from the spinal cord at different developmental stages (embryonal, early postnatal, adult), maintained and expanded within neurospheres (NSs). Using the NSs culture system, we examined the size, number of NSs and their fate when exposed to differentiation conditions. Based on immunocytochemical analyses for cell markers (MAP 2, GFAP, RIP) we evaluated the occurrence of various cell types: neurons, astrocytes and oligodendrocytes. The results show that NSs increased in size during cultivation time *via* NPC proliferation, but proliferation potential decreased during maturation stages. In addition, NPCs derived from spinal cord developmentally different stages gave rise to a consistent ratio of glial and neuronal progeny (3:1), and adult tissues represent a comparable source of NPCs compared to embryonal and early postnatal tissues. These data provide useful information for large-scale *in vitro* expansion of NPCs required for potential cell therapy after spinal cord injury.

Key words: neural progenitor cells, neurospheres, *in vitro* cultivation

The terms neural stem cells and progenitors NSCs/NPCs (herein collectively termed neural progenitor cells – NPCs) refer to the multipotent cells that give rise to other cells of the nervous system. NPCs characterized by multilineage potency and self-renewal capacity are present during embryonic development, as well as in certain regions of the adult central nervous system (CNS), brain and spinal cord (SC) (Reynolds et al. 1992, Palmer et al. 1997, Chiasson et al. 1999, Gage 2000, Alvarez-Buylla et al. 2001, Okano and Sawamoto 2008, Skup et al. 2014). NPCs have been identified in the adult mammalian CNS along with the entire neuroaxis from the forebrain to the spinal cord. There are two constitutive neurogenic sites in the adult CNS, the subventricular zone and

subgranular zone (Weiss et al. 1996, Shihabuddin et al. 1997, Temple and Alvarez-Buylla 1999). The adult SC has also been shown to contain progenitors for neurons and glia with proven localization of NPCs in: the white matter parenchyma (Horner et al. 2000, Yamamoto et al. 2001), the region around the central canal (Kulbatski et al. 2007, Mothe et al. 2011), either in the ependyma (Meletis et al. 2008), or subependymally (Martens et al. 2002). The central canal extends into the terminal part of the SC, the filum terminale (FT) (Varghese et al. 2010). The filum terminale is the rudimentary, most caudal part of the spinal cord and it develops as a consequence of the unequal growth rate of the vertebral canal vs. spinal cord. For a long time it was considered that the FT consisted of a fibrous strand bonding the caudal end of the spinal cord to the vertebral canal and played no functional role in the postnatal nervous system. Traditionally, the FT has been regarded as a fibrovascular tag of clinical significance only if it resulted

Correspondence should be addressed to L. Slovinska
Email: slovinska@saske.sk

Received 30 September 2014, accepted 19 February 2015

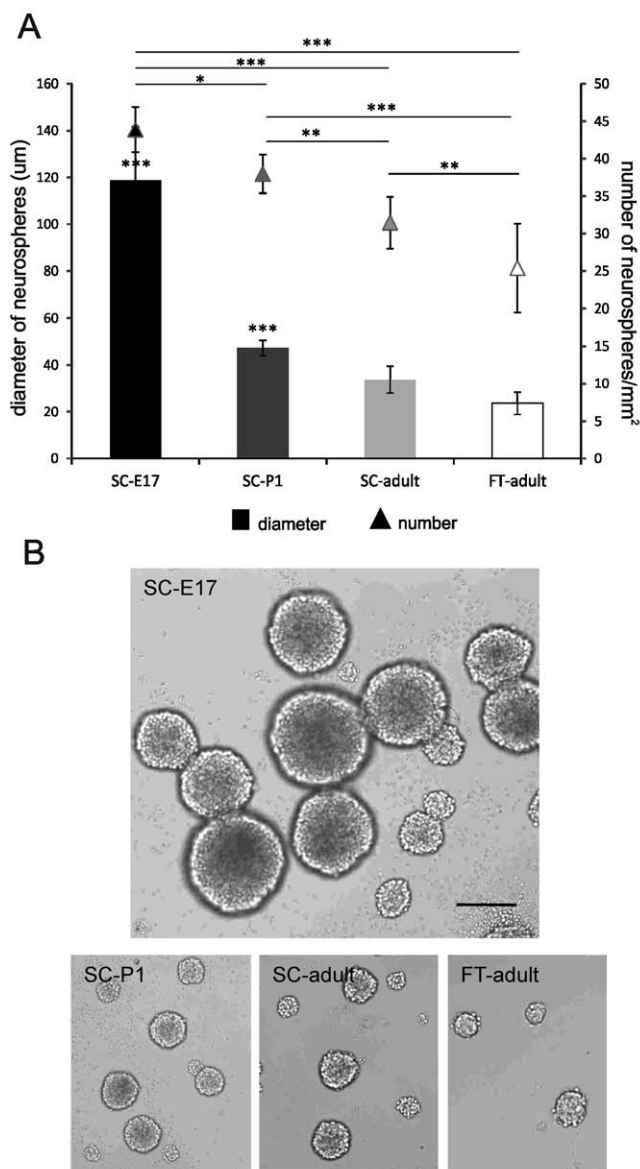


Fig. 1. Number and size of neurospheres (NSs) derived from individual spinal cord tissues of embryonal/SC- E17, postnatal day 1/SC-P1, adult/SC-adult and filum terminale/FT-adult during cultivation in proliferation media on the tenth day *in vitro*. The number of NSs was counted in 10 different fields/each group and calculated *per* mm². The number of NSs ranged from 28 to 46 spheres/mm² with the required statistical significance (* $P < 0.05$, ** $P < 0.01$, *** $P < 0.001$). The measured diameter of formed NSs in ten random fields/each group was in the interval of 29–104 µm, with the vast majority of the largest spheres occurring in culture derived from SC-E17 (*** $P < 0.001$) (A). Brightfield images of neurospheres obtained from individual spinal cord tissues illustrating the size and amount of cultivated NSs. Scale bar is 100 µm (B).

in the overstretching or compression of the SC, giving rise to the tethered cord syndrome (Yamada et al. 2004). Treatment often includes surgical removal of the FT with beneficial outcomes for patients (Garces-Ambrossi et al. 2009). Subsequent findings produced evidence controverting this opinion, and recent histological studies have shown that the FT contains an ependymal-lined canal, glial and neuronal cell bodies, as well as stem/progenitor cells in rats (Rethelyi et al. 2004, 2008, Boros et al. 2008), and also in humans (Varghese et al. 2009, Arvidsson et al. 2011).

NPCs can be isolated and expanded *in vitro* to study their characteristics. The possibility to cultivate NPCs through the assay of neurospheres (NSs) was first described by Reynolds and coworkers (1992) and is now widely used for determining the presence of NPCs *in vitro*. NPCs can be expanded in serum-free medium supplemented with epidermal growth factor and fibroblast growth factor, which act as mitogens for these cells both *in vitro* (Reynolds et al. 1992, Gritti et al. 1996, 1999) and *in vivo* (Craig et al. 1996). Generally, NSs are derived from a single-cell suspension of neural stem and progenitor cells isolated from the adult or fetal CNS, but NSs culture can also be established from embryonic stem cells (ESCs) (Tropepe et al. 2001, Jensen and Parmar 2006). NSs are spheroid, free-floating cultures, 3D structures that consist of cells with a rich extra-cellular matrix, composed of a heterogenous mix of neural stem cells, neural progenitor cells and more differentiated cells at different stages of mitotic division (Alam et al. 2004) with varying capability to form NSs. Although both neural stem cells and neural progenitor cells are able to give rise to NSs, only neural stem cells can retain the ability to form NSs over long periods of the time in culture (Reynolds and Rietze 2005). Until recently, no specific markers were available to explicitly identify NPCs, because of their paucity and primitive nature (Kim and Morshead 2003), so these cells were identified by their self-renewal capacity. The ability to form NSs is still a good indicator of the presence of NPCs (Louis et al. 2008). When floating NSs are plated on adhesive substrate and the mitogens are removed, progenitor cells migrate out of the spheres and differentiate into neurons and glia (Gage et al. 1995).

In our *in vitro* study using rats, we demonstrate and compare the proliferative and differentiating potential of NPCs isolated from embryonic day 17 (SC-E17), postnatal day one (SC-P1) and adult spinal cord (SC-adult) and filum terminale (FT-adult).

All experiments conformed to the Slovak Law for Animal Protection No. 23/2009, which is transposed from Directive 86/609/EEC on the protection of animals used for experimental and other scientific purposes, and were approved by the Institutional Ethical Committee for animal research.

Neural progenitor cells were harvested from embryonic day 17 (E17) ($n=12$), postnatal day one (P1) ($n=12$) spinal cord, adult spinal cord (SC) ($n=6$) and filum terminale (FT) ($n=6$) of male Wistar rats. The overlying meninges of spinal cords were removed, the dissected individual tissues were cut into small pieces and transferred into a solution (Worthington Biochemicals, New Jersey) containing 0.01% papain and 0.01% DNase for 1.5 hour at 37°C and then mechanically dissociated into a cell suspension which was centrifuged using a discontinuous density gradient to remove cell membrane fragments. Harvested single cells were cultivated in Nunc T25 culture flasks (5000 cells/cm²), grown in proliferation culture medium composed of Dulbecco's Modified Eagle Medium (DMEM) and Ham's F12 (1/1 v/v) (Biowest, Nuaille, France) supplemented with 5 mg/ml streptomycin, 5 IU/ml penicillin (Biochrom AG, Berlin, DE), B27, N2 (Gibco; Invitrogen, Carlsbad, CA) and growth factors: basic fibroblast growth factor-2 (bFGF-2) and epidermal growth factor (EGF) (both 20 ng/ml) (AppliChem GmbH, Darmstadt, Germany) to allow the formation of neurospheres (37°C, 5% CO₂). Using the NSs culture, we investigated the qualities of NSs: the number of NSs/mm² and the size of NSs (µm) on the tenth day of cultivation (10DIV-day *in vitro*). We counted the number of neurospheres in 10 different fields/each group and calculated the number of NSs *per* mm². Considering NSs size, we measured the diameter of formed NSs in ten random fields/each group. After analysis, these neurospheres were dissociated by means of mechanical trituration and cultured in growth factors free and 3% foetal calf serum (FCS) (Biowest, Nuaille, France) enriched differentiation medium on laminin-coated (Gibco; Invitrogen, Carlsbad, CA) plates for an additional 14 days to induce final differentiation. Using immunocytochemistry and applying specific antibodies, the populations of neurons (MAP 2 1:200), astrocytes (GFAP 1:500) and oligodendrocytes (RIP 1:1 000) were analyzed. The number of cells positive for each specific marker was counted as a percentage of total DAPI + nuclei in 10 random visual fields of cells (400–600 cells)/tissue/per each marker. In subsequent

NSs passages the self-renewal was determined as the number of secondary neurospheres/number of seeded cells ×100, i.e how many precursors capable of generating a “daughter” neurosphere were contained in each “mother” neurosphere (Lu et al. 2010). Data are presented as mean ± SEM. Statistical differences between groups were evaluated with one-way analysis of variance (ANOVA). Values of * $P<0.05$, ** $P<0.01$, *** $P<0.001$ were considered to be statistically significant.

After 2–3 DIV of cultivation in proliferation media, the first NSs were observed, mainly in cultures derived from SC- E17, SC-P1 and SC-adult tissues. In FT-adult derived culture, the NSs developed after 3–5 DIV. The NSs initially appeared as smaller clusters of 2–4 cells and later grew into larger NSs. The NSs were free-floating and were identified by their spherical structure and bright phase appearance. During the cultivation we observed time-dependent changes in the neurospheres. During cultivation time NSs increased in size *via* NPCs proliferation, but proliferation potential decreased with maturation and no obvious differences were observed in the morphologies of types of NSs, e.g. shape, density. The number of NSs *per* primary culture varied depending on the tissues they were derived from. The highest number of NSs was found in culture derived from embryonic tissue (45 NSs/ mm² on average), and during maturation the proliferation activity of NPCs expressed by NS formation ability

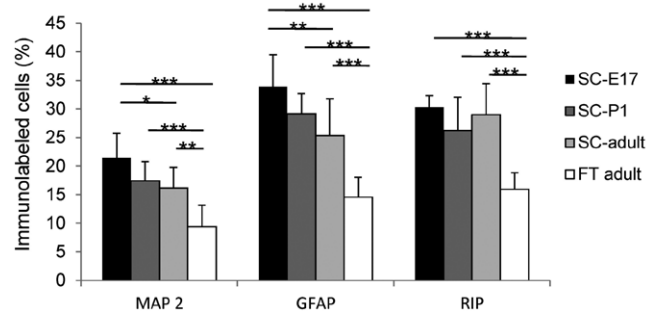


Fig. 2. Phenotype of neural progenitor cells (NPCs) obtained by mechanical dissociation of neurospheres and cultivated in differentiation medium for 14 days. Based on immunocytochemical analyses, the occurrence of neurons (MAP 2), astrocytes (GFAP) and oligodendrocytes (RIP) was counted as a percentage of total DAPI+ nuclei in 10 random visual fields of cells (400–600 cells)/tissue *per* each marker. Percentages of phenotypes changed during the developmental stages, with preservation of glia:neuron ratio 3:1 (* $P<0.05$, ** $P<0.01$, *** $P<0.001$).

went into decline (see Fig. 1). The same pattern was observed in NSs size (see Fig. 1). Moreover the self-renewal capacity of NPCs decreased during the developmental stages (SC-E17=3.4; SC-P1=2.5; SC-adult=1.7; SC-FT=1.3). So the most and the largest NSs were formed in culture derived from SC-E17, which means that NPCs derived from embryonic tissue are the most potent. Interesting findings were that the FT exhibited similar characteristics in NSs formation and proliferation, while the number of neurospheres from the FT is almost half the number of SC-E17, and the NSs of the FT are six times smaller than the embryonic NSs.

After ten days of NPC cultivation and NSs formation, these NSs were dissociated and the final differentiation was induced. After replacing growth factors with FCS in the cultivation media, the dissociated cells

started to attach to the laminin-coated surface and underwent differentiation into neurons, astrocytes and oligodendrocytes at different rates, because not only proliferation, but also differentiation of NPCs is mediated by the effects of external stimuli coming from medium components (Cameron et al. 1998, Hung and Young 2006). NPCs derived from all tissue began to differentiate in the same manner, but occurrence of different neural cell types changed during the developmental stages (see Fig. 2). No morphological differences in neurons, astrocytes and oligodendrocytes were seen between any experimental groups (see Fig. 3). In our FT cultures, and in fact in all cultures (E17, P1, SC-adult), the glia:neuron ratio 3:1 was preserved. Although in younger stages (E17, P1) in the glia population the astrocytes predominated over the oligoden-

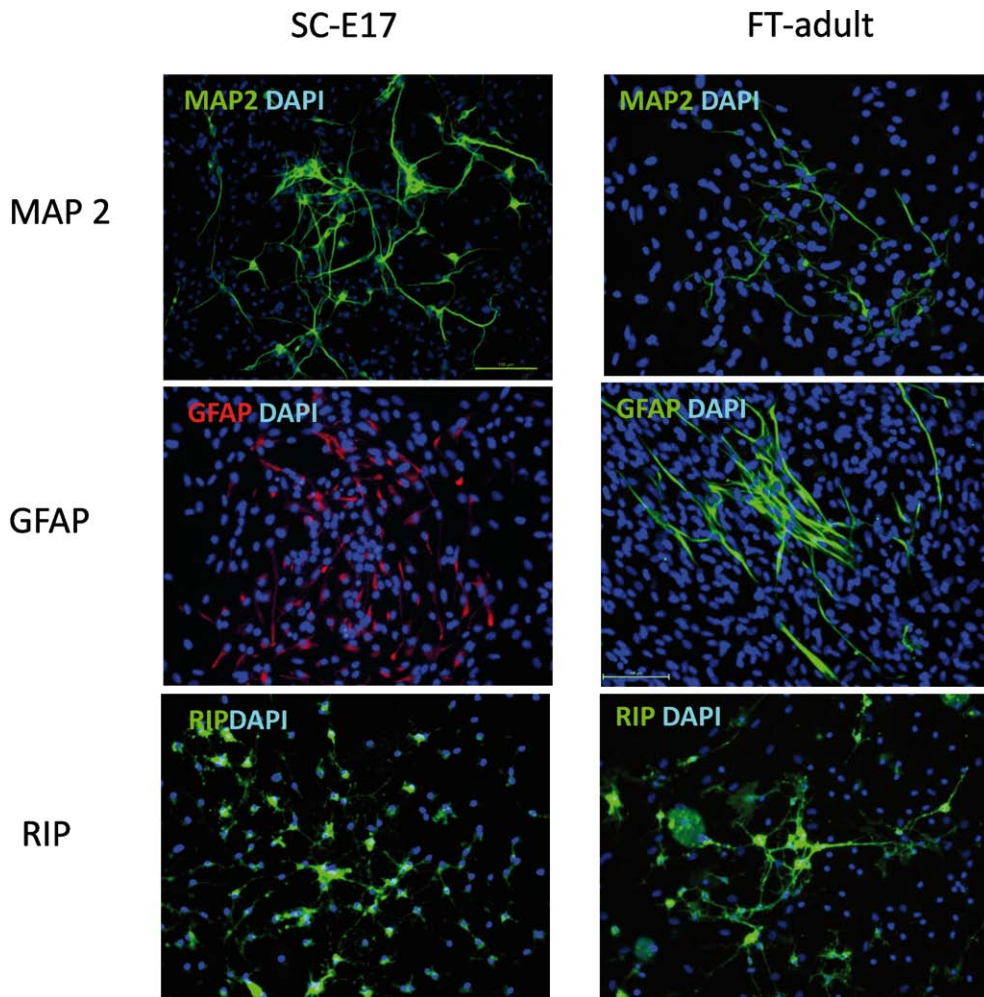


Fig. 3. Immunocytochemical identification of the phenotype of neural progenitor cells (NPCs) obtained from embryonal (SC-E17) and adult (FT-adult) filum terminale that were cultivated in differentiation medium for 14 days. Expression of neuronal (MAP2), astroglial (GFAP) and oligodendroglial (RIP) markers. Scale bar equals to 100 μ m.

drocytes, in adult stages the representation of glia converted in favor of oligodendrocytes with preservation of the total volume of glia vs. neurons. This may reflect some internal programming of progenitors specific for their region of origin. In studying NPCs from the human FT, Varghese and colleagues (2009) came to similar results, obtaining a 2:1 glia:neuron ratio. However, not all NPCs are identical since the proliferative and differentiation capacity of NPCs is dependent upon the location and developmental stage from which these cells are derived. *In vitro* experiments with NPCs originating from different CNS regions have revealed that the original NPCs were indeed regionally specified; for example in cultures obtained from brain, a 2:7 glia: neuron ratio was found (Hitoshi et al. 2002, Moe et al. 2005, Sypecka et al. 2013). Cells derived from NSs are plastic in their differentiation, and by changing the media composition the proportion of the three neural cell types can be altered. But in our experiment, all cells derived from different tissues were cultivated under the same conditions.

The discovery of NPCs, followed by deeper understanding of their characteristics and behaviour, opens up the potential for new treatments of devastating neurodegenerative diseases and damage such as stroke and spinal cord injuries. Currently there are several treatments available for these diseases involving the preferential use of ESCs (Nistor et al. 2005). ESCs probably have greater plastic potential than adult stem cells; however, ethical concerns and their potential for unwanted and possibly dangerous continued growth and tumor formation limit their application (Nussbaum et al. 2007). An alternative for ESCs are stem cells obtained from tissue after birth. NPCs have been harvested from the adult brain (Lois and Alvarez-Buylla 1993, Nunes et al. 2003) and spinal cord (Mayer-Proschel et al. 1997). However, adult stem cells are less plastic than ESCs and divide less frequently in culture (Doetsch et al. 1999). On the other hand, they offer the advantage that they can be transplanted without genetic modifications. Moreover, adult stem cells show a high degree of genomic stability during culture (Feroni et al. 2007). Finally, there is much less moral concern surrounding the use of adult stem cells because they can be harvested from patients, so they can be used in an autologous fashion (Nandoe Tewarie et al. 2009).

In our study, putative NPCs were isolated from FT samples using both mechanical and enzymatical dissociation. The neurosphere culture system remains an

extremely useful tool to analyze the behavior of NPCs, self-renewal capacity and multipotency of neural stem and progenitor cells, and represents a potential source for cell replacement therapy (Hung and Young 2006, Jensen and Parmar 2006, Mothe et al. 2008, Parr et al. 2008, Sulla et al. 2010)

Our results support the suggestion that NPCs derived from the FT are easy to obtain, proliferate readily, and are able to differentiate into the cells of gliogenic lineages and neurogenic (motor neurons) *in vitro* (Jha et al. 2013), which represents a promising way for their utilization in cell-based therapies for CNS injuries and diseases. FT-derived NPCs could be utilized for their next purpose immediately after their isolation, or could be stored by freezing, because cryopreservation does not affect the proliferation and multipotency of NPCs (Milosevic et al. 2005). The FT is an excellent candidate as a source of autologous multipotent cells with putative biological and clinical implication. Because the FT is abundant, reproducible and easily accessed without moral concern, FT-derived NPCs offer a more clinically feasible source than embryonal stem cells.

In conclusion, our findings add further evidence for the existence of cells with neural progenitor nature within the filum terminale. In all tissues, SC-E17, SC-P1, SC-adult, FT-adult, the presence of neural progenitor cells was determined *via* neurosphere formation, as a good indicator of NPCs proliferation. Another indicator of NPCs proliferation in culture is the increase in neurosphere size with cultivation time. NPCs from SC-E17 were more potent, producing the largest neurospheres, but the NPCs proliferation potential decreased during subsequent developmental stages. The NPCs' ability of terminal differentiation into neurons, astrocytes and oligodendrocytes decreased during maturation, while the glia:neuron ratio 3:1 was preserved, which may reflect some internal programming specific for cells isolated from the spinal cord. The FT exhibits the same features in neurosphere formation, proliferation and terminal differentiation as other parts of the adult spinal cord, which suggests that the FT is an equivalent part of the spinal cord and not just a problematic remnant; in fact it may be a potential source of NPCs with promising biological and clinical implications.

This study was supported by: VEGA 2/0169/13, APVV-0472-11, the Center of Excellence for Brain Research, by Region Nord Pas de Calais, and University of Lille1.

- Alam S, Sen A, Behie LA, Kallos MS (2004) Cell cycle kinetics of expanding populations of neural stem and progenitor cells in vitro. *Biotechnol Bioeng* 88: 332–347.
- Alvarez-Buylla A, Garcia-Verdugo JM, Tramontin AD (2001) A unified hypothesis on the lineage of neural stem cells. *Nat Rev Neurosci* 2: 287–293.
- Arvidsson L, Fagerlund M, Jaff N, Ossoinak A, Jansson K, Hagerstrand A, Johansson CB, Brundin L, Svensson M (2011) Distribution and characterization of progenitor cells within the human filum terminale. *PLoS One* 6: e27393.
- Boros C, Lukacs E, Horvath-Oszwald E, Rethelyi M (2008) Neurochemical architecture of the filum terminale in the rat. *Brain Res* 1209: 105–114.
- Cameron HA, Hazel TG, McKay RD (1998) Regulation of neurogenesis by growth factors and neurotransmitters. *J Neurobiol* 36: 287–306.
- Chiasson BJ, Tropepe V, Morshead CM, van der Kooy D (1999) Adult mammalian forebrain ependymal and subependymal cells demonstrate proliferative potential, but only subependymal cells have neural stem cell characteristics. *J Neurosci* 19: 4462–4471.
- Craig CG, Tropepe V, Morshead CM, Reynolds BA, Weiss S, van der Kooy D (1996) In vivo growth factor expansion of endogenous subependymal neural precursor cell populations in the adult mouse brain. *J Neurosci* 16: 2649–2658.
- Doetsch F, Caille I, Lim DA, Garcia-Verdugo JM, Alvarez-Buylla A (1999) Subventricular zone astrocytes are neural stem cells in the adult mammalian brain. *Cell* 97: 703–716.
- Foroni C, Galli R, Cipelletti B, Caumo A, Alberti S, Fiocco R, Vescovi A (2007) Resilience to transformation and inherent genetic and functional stability of adult neural stem cells ex vivo. *Cancer Res* 67: 3725–3733.
- Gage FH (2000) Mammalian neural stem cells. *Science* 287: 1433–1438.
- Gage FH, Ray J, Fisher LJ (1995) Isolation, characterization, and use of stem cells from the CNS. *Annu Rev Neurosci* 18: 159–192.
- Garces-Ambrossi GL, McGirt MJ, Samuels R, Sciubba DM, Bydon A, Gokaslan ZL, Jallo GI (2009) Neurological outcome after surgical management of adult tethered cord syndrome. *J Neurosurg Spine* 11: 304–309.
- Gritti A, Parati EA, Cova L, Frolichsthal P, Galli R, Wanke E, Faravelli L, Morassutti DJ, Roisen F, Nickel DD, Vescovi AL (1996) Multipotential stem cells from the adult mouse brain proliferate and self-renew in response to basic fibroblast growth factor. *J Neurosci* 16: 1091–1100.
- Gritti A, Frolichsthal-Schoeller P, Galli R, Parati EA, Cova L, Pagano SF, Bjornson CR, Vescovi AL (1999) Epidermal and fibroblast growth factors behave as mitogenic regulators for a single multipotent stem cell-like population from the subventricular region of the adult mouse forebrain. *J Neurosci* 19: 3287–3297.
- Hitoshi S, Tropepe V, Ekker M, van der Kooy D (2002) Neural stem cell lineages are regionally specified, but not committed, within distinct compartments of the developing brain. *Development* 129: 233–244.
- Horner PJ, Power AE, Kempermann G, Kuhn HG, Palmer TD, Winkler J, Thal LJ, Gage FH (2000) Proliferation and differentiation of progenitor cells throughout the intact adult rat spinal cord. *J Neurosci* 20: 2218–2228.
- Hung CH, Young TH (2006) Differences in the effect on neural stem cells of fetal bovine serum in substrate-coated and soluble form. *Biomaterials* 27: 5901–5908.
- Jensen JB, Parmar M (2006) Strengths and limitations of the neurosphere culture system. *Mol Neurobiol* 34: 153–161.
- Jha RM, Chrenek R, Magnotti LM, Cardozo DL (2013) The isolation, differentiation, and survival in vivo of multipotent cells from the postnatal rat filum terminale. *PLoS One* 8: e65974.
- Kim M, Morshead CM (2003) Distinct populations of forebrain neural stem and progenitor cells can be isolated using side-population analysis. *J Neurosci* 23: 10703–10709.
- Kulbatski I, Mothe AJ, Keating A, Hakamata Y, Kobayashi E, Tator CH (2007) Oligodendrocytes and radial glia derived from adult rat spinal cord progenitors: morphological and immunocytochemical characterization. *J Histochem Cytochem* 55: 209–222.
- Lois C, Alvarez-Buylla A (1993) Proliferating subventricular zone cells in the adult mammalian forebrain can differentiate into neurons and glia. *Proc Natl Acad Sci U S A* 90: 2074–2077.
- Louis SA, Rietze RL, Deleyrolle L, Wagey RE, Thomas TE, Eaves AC, Reynolds BA (2008) Enumeration of neural stem and progenitor cells in the neural colony-forming cell assay. *Stem Cells* 26: 988–996.
- Lu Z, Kipnis J (2010) Thrombospondin 1-a key astrocyte-derived neurogenic factor. *FASEB J* 24: 1925–1934.
- Martens DJ, Seaberg RM, van der Kooy D (2002) In vivo infusions of exogenous growth factors into the fourth ventricle of the adult mouse brain increase the proliferation of neural progenitors around the fourth ventricle and the central canal of the spinal cord. *Eur J Neurosci* 16: 1045–1057.

- Mayer-Proschel M, Kalyani AJ, Mujtaba T, Rao MS (1997) Isolation of lineage-restricted neuronal precursors from multipotent neuroepithelial stem cells. *Neuron* 19: 773–785.
- Meletis K, Barnabe-Heider F, Carlen M, Evergren E, Tomilin N, Shupliakov O, Frisen J (2008) Spinal cord injury reveals multilineage differentiation of ependymal cells. *PLoS Biol* 6: e182.
- Milosevic J, Storch A, Schwarz J (2005) Cryopreservation does not affect proliferation and multipotency of murine neural precursor cells. *Stem Cells* 23: 681–688.
- Moe MC, Varghese M, Danilov AI, Westerlund U, Ramm-Petersen J, Brundin L, Svensson M, Berg-Johnsen J, Langmoen IA (2005) Multipotent progenitor cells from the adult human brain: neurophysiological differentiation to mature neurons. *Brain* 128: 2189–2199.
- Mothe AJ, Kulbatski I, Parr A, Mohareb M, Tator CH (2008) Adult spinal cord stem/progenitor cells transplanted as neurospheres preferentially differentiate into oligodendrocytes in the adult rat spinal cord. *Cell Transplant* 17: 735–751.
- Mothe AJ, Zahir T, Santaguida C, Cook D, Tator CH (2011) Neural stem/progenitor cells from the adult human spinal cord are multipotent and self-renewing and differentiate after transplantation. *PLoS One* 6: e27079.
- Nandoe Tewarie RS, Hurtado A, Bartels RH, Grotenhuis A, Oudega M (2009) Stem cell-based therapies for spinal cord injury. *J Spinal Cord Med* 32: 105–114.
- Nistor GI, Totoiu MO, Haque N, Carpenter MK, Keirstead HS (2005) Human embryonic stem cells differentiate into oligodendrocytes in high purity and myelinate after spinal cord transplantation. *Glia* 49: 385–396.
- Nunes MC, Roy NS, Keyoung HM, Goodman RR, McKhann G, 2nd, Jiang L, Kang J, Nedergaard M, Goldman SA (2003) Identification and isolation of multipotential neural progenitor cells from the subcortical white matter of the adult human brain. *Nat Med* 9: 439–447.
- Nussbaum J, Minami E, Laflamme MA, Virag JA, Ware CB, Masino A, Muskheili V, Pabon L, Reinecke H, Murry CE (2007) Transplantation of undifferentiated murine embryonic stem cells in the heart: teratoma formation and immune response. *Faseb J* 21: 1345–1357.
- Okano H, Sawamoto K (2008) Neural stem cells: involvement in adult neurogenesis and CNS repair. *Philos Trans R Soc Lond B Biol Sci* 363: 2111–2122.
- Palmer TD, Takahashi J, Gage FH (1997) The adult rat hippocampus contains primordial neural stem cells. *Mol Cell Neurosci* 8: 389–404.
- Parr AM, Kulbatski I, Zahir T, Wang X, Yue C, Keating A, Tator CH (2008) Transplanted adult spinal cord-derived neural stem/progenitor cells promote early functional recovery after rat spinal cord injury. *Neuroscience* 155: 760–770.
- Rethelyi M, Lukacs E, Boros C (2004) The caudal end of the rat spinal cord: transformation to and ultrastructure of the filum terminale. *Brain Res* 1028: 133–139.
- Rethelyi M, Horvath-Oszwald E, Boros C (2008) Caudal end of the rat spinal dorsal horn. *Neurosci Lett* 445: 153–157.
- Reynolds BA, Rietze RL (2005) Neural stem cells and neurospheres—re-evaluating the relationship. *Nat Methods* 2: 333–336.
- Reynolds BA, Tetzlaff W, Weiss S (1992) A multipotent EGF-responsive striatal embryonic progenitor cell produces neurons and astrocytes. *J Neurosci* 12: 4565–4574.
- Shihabuddin LS, Ray J, Gage FH (1997) FGF-2 is sufficient to isolate progenitors found in the adult mammalian spinal cord. *Exp Neurol* 148: 577–586.
- Skup M, Ziemińska E, Gajewska-Wozniak O, Platek R, Maciejewska A, Czarkowska-Bauch J (2014) The impact of training and neurotrophins on functional recovery after complete spinal cord transection: cellular and molecular mechanisms contributing to motor improvement. *Acta Neurobiol Exp (Wars)* 74: 121–141.
- Sulla I, Balik V, Sarissky M (2010) A preliminary report on time dependent changes of some immunophenotypic characteristics of adult rat bone marrow derived stem/progenitor cells. *Folia Veterinaria* 54: 191–195.
- Sypecka J, Sarnowska A, Gadomska-Szabłowska I, Lukomska B, Domanska-Janik K (2013) Differentiation of glia-committed NG2 cells: The role of factors released from hippocampus and spinal cord. *Acta Neurobiol Exp (Wars)* 73: 116–129.
- Temple S, Alvarez-Buylla A (1999) Stem cells in the adult mammalian central nervous system. *Curr Opin Neurobiol* 9: 135–141.
- Tropepe V, Hitoshi S, Sirard C, Mak TW, Rossant J, van der Kooy D (2001) Direct neural fate specification from embryonic stem cells: a primitive mammalian neural stem cell stage acquired through a default mechanism. *Neuron* 30: 65–78.
- Varghese M, Olstorn H, Berg-Johnsen J, Moe MC, Murrell W, Langmoen IA (2009) Isolation of human multipotent neural progenitors from adult filum terminale. *Stem Cells Dev* 18: 603–613.

- Varghese M, Olstorn H, Murrell W, Langmoen IA (2010) Exploring atypical locations of mammalian neural stem cells: the human filum terminale. *Arch Ital Biol* 148: 85–94.
- Weiss S, Dunne C, Hewson J, Wohl C, Wheatley M, Peterson AC, Reynolds BA (1996) Multipotent CNS stem cells are present in the adult mammalian spinal cord and ventricular neuroaxis. *J Neurosci* 16: 7599–609.
- Yamada S, Knerium DS, Mandybur GM, Schultz RL, Yamada BS (2004) Pathophysiology of tethered cord syndrome and other complex factors. *Neurol Res* 26: 722–726.
- Yamamoto S, Yamamoto N, Kitamura T, Nakamura K, Nakafuku M (2001) Proliferation of parenchymal neural progenitors in response to injury in the adult rat spinal cord. *Exp Neurol* 172: 115–127.

**ELSEVIER LICENSE
TERMS AND CONDITIONS**

Jun 20, 2016

This Agreement between Stéphanie Devaux ("You") and Elsevier ("Elsevier") consists of your license details and the terms and conditions provided by Elsevier and Copyright Clearance Center.

License Number	3893070354471
License date	Jun 20, 2016
Licensed Content Publisher	Elsevier
Licensed Content Publication	Brain Research Bulletin
Licensed Content Title	Estrogen receptor agonists for attenuation of neuroinflammation and neurodegeneration
Licensed Content Author	Mrinmay Chakrabarti,Azizul Haque,Naren L. Banik,Prakash Nagarkatti,Mitzi Nagarkatti,Swapan K. Ray
Licensed Content Date	October 2014
Licensed Content Volume Number	109
Licensed Content Issue Number	n/a
Licensed Content Pages	10
Start Page	22
End Page	31
Type of Use	reuse in a thesis/dissertation
Intended publisher of new work	other
Portion	figures/tables/illustrations
Number of figures/tables/illustrations	1
Format	both print and electronic
Are you the author of this Elsevier article?	No
Will you be translating?	No
Order reference number	
Original figure numbers	figure 1
Title of your thesis/dissertation	Proteomic analysis of spinal cord after injury and regeneration
Expected completion date	Jul 2016
Estimated size (number of pages)	300
Elsevier VAT number	GB 494 6272 12
Requestor Location	Stéphanie Devaux INSERM U1192 Université Lille1

Villeneuve d'Ascq, 59650
France
Attn: Stéphanie Devaux

Total 0.00 EUR

[Terms and Conditions](#)

INTRODUCTION

1. The publisher for this copyrighted material is Elsevier. By clicking "accept" in connection with completing this licensing transaction, you agree that the following terms and conditions apply to this transaction (along with the Billing and Payment terms and conditions established by Copyright Clearance Center, Inc. ("CCC"), at the time that you opened your Rightslink account and that are available at any time at <http://myaccount.copyright.com>).

GENERAL TERMS

2. Elsevier hereby grants you permission to reproduce the aforementioned material subject to the terms and conditions indicated.

3. Acknowledgement: If any part of the material to be used (for example, figures) has appeared in our publication with credit or acknowledgement to another source, permission must also be sought from that source. If such permission is not obtained then that material may not be included in your publication/copies. Suitable acknowledgement to the source must be made, either as a footnote or in a reference list at the end of your publication, as follows:

"Reprinted from Publication title, Vol /edition number, Author(s), Title of article / title of chapter, Pages No., Copyright (Year), with permission from Elsevier [OR APPLICABLE SOCIETY COPYRIGHT OWNER]." Also Lancet special credit - "Reprinted from The Lancet, Vol. number, Author(s), Title of article, Pages No., Copyright (Year), with permission from Elsevier."

4. Reproduction of this material is confined to the purpose and/or media for which permission is hereby given.

5. Altering/Modifying Material: Not Permitted. However figures and illustrations may be altered/adapted minimally to serve your work. Any other abbreviations, additions, deletions and/or any other alterations shall be made only with prior written authorization of Elsevier Ltd. (Please contact Elsevier at permissions@elsevier.com)

6. If the permission fee for the requested use of our material is waived in this instance, please be advised that your future requests for Elsevier materials may attract a fee.

7. Reservation of Rights: Publisher reserves all rights not specifically granted in the combination of (i) the license details provided by you and accepted in the course of this licensing transaction, (ii) these terms and conditions and (iii) CCC's Billing and Payment terms and conditions.

8. License Contingent Upon Payment: While you may exercise the rights licensed immediately upon issuance of the license at the end of the licensing process for the transaction, provided that you have disclosed complete and accurate details of your proposed use, no license is finally effective unless and until full payment is received from you (either by publisher or by CCC) as provided in CCC's Billing and Payment terms and conditions. If full payment is not received on a timely basis, then any license preliminarily granted shall be deemed automatically revoked and shall be void as if never granted. Further, in the event that you breach any of these terms and conditions or any of CCC's Billing and Payment terms and conditions, the license is automatically revoked and shall be void as if never granted. Use of materials as described in a revoked license, as well as any use of the materials beyond the scope of an unrevoked license, may constitute copyright infringement and publisher reserves the right to take any and all action to protect its copyright in the materials.

9. Warranties: Publisher makes no representations or warranties with respect to the licensed material.

10. Indemnity: You hereby indemnify and agree to hold harmless publisher and CCC, and

their respective officers, directors, employees and agents, from and against any and all claims arising out of your use of the licensed material other than as specifically authorized pursuant to this license.

11. **No Transfer of License:** This license is personal to you and may not be sublicensed, assigned, or transferred by you to any other person without publisher's written permission.

12. **No Amendment Except in Writing:** This license may not be amended except in a writing signed by both parties (or, in the case of publisher, by CCC on publisher's behalf).

13. **Objection to Contrary Terms:** Publisher hereby objects to any terms contained in any purchase order, acknowledgment, check endorsement or other writing prepared by you, which terms are inconsistent with these terms and conditions or CCC's Billing and Payment terms and conditions. These terms and conditions, together with CCC's Billing and Payment terms and conditions (which are incorporated herein), comprise the entire agreement between you and publisher (and CCC) concerning this licensing transaction. In the event of any conflict between your obligations established by these terms and conditions and those established by CCC's Billing and Payment terms and conditions, these terms and conditions shall control.

14. **Revocation:** Elsevier or Copyright Clearance Center may deny the permissions described in this License at their sole discretion, for any reason or no reason, with a full refund payable to you. Notice of such denial will be made using the contact information provided by you. Failure to receive such notice will not alter or invalidate the denial. In no event will Elsevier or Copyright Clearance Center be responsible or liable for any costs, expenses or damage incurred by you as a result of a denial of your permission request, other than a refund of the amount(s) paid by you to Elsevier and/or Copyright Clearance Center for denied permissions.

LIMITED LICENSE

The following terms and conditions apply only to specific license types:

15. **Translation:** This permission is granted for non-exclusive world **English** rights only unless your license was granted for translation rights. If you licensed translation rights you may only translate this content into the languages you requested. A professional translator must perform all translations and reproduce the content word for word preserving the integrity of the article.

16. **Posting licensed content on any Website:** The following terms and conditions apply as follows: Licensing material from an Elsevier journal: All content posted to the web site must maintain the copyright information line on the bottom of each image; A hyper-text must be included to the Homepage of the journal from which you are licensing at <http://www.sciencedirect.com/science/journal/xxxxx> or the Elsevier homepage for books at <http://www.elsevier.com>; Central Storage: This license does not include permission for a scanned version of the material to be stored in a central repository such as that provided by Heron/XanEdu.

Licensing material from an Elsevier book: A hyper-text link must be included to the Elsevier homepage at <http://www.elsevier.com>. All content posted to the web site must maintain the copyright information line on the bottom of each image.

Posting licensed content on Electronic reserve: In addition to the above the following clauses are applicable: The web site must be password-protected and made available only to bona fide students registered on a relevant course. This permission is granted for 1 year only. You may obtain a new license for future website posting.

17. **For journal authors:** the following clauses are applicable in addition to the above:

Preprints:

A preprint is an author's own write-up of research results and analysis, it has not been peer-reviewed, nor has it had any other value added to it by a publisher (such as formatting, copyright, technical enhancement etc.).

Authors can share their preprints anywhere at any time. Preprints should not be added to or enhanced in any way in order to appear more like, or to substitute for, the final versions of

articles however authors can update their preprints on arXiv or RePEc with their Accepted Author Manuscript (see below).

If accepted for publication, we encourage authors to link from the preprint to their formal publication via its DOI. Millions of researchers have access to the formal publications on ScienceDirect, and so links will help users to find, access, cite and use the best available version. Please note that Cell Press, The Lancet and some society-owned have different preprint policies. Information on these policies is available on the journal homepage.

Accepted Author Manuscripts: An accepted author manuscript is the manuscript of an article that has been accepted for publication and which typically includes author-incorporated changes suggested during submission, peer review and editor-author communications.

Authors can share their accepted author manuscript:

- immediately
 - via their non-commercial person homepage or blog
 - by updating a preprint in arXiv or RePEc with the accepted manuscript
 - via their research institute or institutional repository for internal institutional uses or as part of an invitation-only research collaboration work-group
 - directly by providing copies to their students or to research collaborators for their personal use
 - for private scholarly sharing as part of an invitation-only work group on commercial sites with which Elsevier has an agreement
- after the embargo period
 - via non-commercial hosting platforms such as their institutional repository
 - via commercial sites with which Elsevier has an agreement

In all cases accepted manuscripts should:

- link to the formal publication via its DOI
- bear a CC-BY-NC-ND license - this is easy to do
- if aggregated with other manuscripts, for example in a repository or other site, be shared in alignment with our hosting policy not be added to or enhanced in any way to appear more like, or to substitute for, the published journal article.

Published journal article (JPA): A published journal article (PJA) is the definitive final record of published research that appears or will appear in the journal and embodies all value-adding publishing activities including peer review co-ordination, copy-editing, formatting, (if relevant) pagination and online enrichment.

Policies for sharing publishing journal articles differ for subscription and gold open access articles:

Subscription Articles: If you are an author, please share a link to your article rather than the full-text. Millions of researchers have access to the formal publications on ScienceDirect, and so links will help your users to find, access, cite, and use the best available version. Theses and dissertations which contain embedded PJAs as part of the formal submission can be posted publicly by the awarding institution with DOI links back to the formal publications on ScienceDirect.

If you are affiliated with a library that subscribes to ScienceDirect you have additional private sharing rights for others' research accessed under that agreement. This includes use for classroom teaching and internal training at the institution (including use in course packs and courseware programs), and inclusion of the article for grant funding purposes.

Gold Open Access Articles: May be shared according to the author-selected end-user license and should contain a [CrossMark logo](#), the end user license, and a DOI link to the formal publication on ScienceDirect.

Please refer to Elsevier's [posting policy](#) for further information.

18. **For book authors** the following clauses are applicable in addition to the above: Authors are permitted to place a brief summary of their work online only. You are not allowed to download and post the published electronic version of your chapter, nor may you scan the printed edition to create an electronic version. **Posting to a repository:** Authors are permitted to post a summary of their chapter only in their institution's repository.

19. **Thesis/Dissertation:** If your license is for use in a thesis/dissertation your thesis may be submitted to your institution in either print or electronic form. Should your thesis be published commercially, please reapply for permission. These requirements include permission for the Library and Archives of Canada to supply single copies, on demand, of the complete thesis and include permission for Proquest/UMI to supply single copies, on demand, of the complete thesis. Should your thesis be published commercially, please reapply for permission. Theses and dissertations which contain embedded PJAs as part of the formal submission can be posted publicly by the awarding institution with DOI links back to the formal publications on ScienceDirect.

Elsevier Open Access Terms and Conditions

You can publish open access with Elsevier in hundreds of open access journals or in nearly 2000 established subscription journals that support open access publishing. Permitted third party re-use of these open access articles is defined by the author's choice of Creative Commons user license. See our [open access license policy](#) for more information.

Terms & Conditions applicable to all Open Access articles published with Elsevier:

Any reuse of the article must not represent the author as endorsing the adaptation of the article nor should the article be modified in such a way as to damage the author's honour or reputation. If any changes have been made, such changes must be clearly indicated.

The author(s) must be appropriately credited and we ask that you include the end user license and a DOI link to the formal publication on ScienceDirect.

If any part of the material to be used (for example, figures) has appeared in our publication with credit or acknowledgement to another source it is the responsibility of the user to ensure their reuse complies with the terms and conditions determined by the rights holder.

Additional Terms & Conditions applicable to each Creative Commons user license:

CC BY: The CC-BY license allows users to copy, to create extracts, abstracts and new works from the Article, to alter and revise the Article and to make commercial use of the Article (including reuse and/or resale of the Article by commercial entities), provided the user gives appropriate credit (with a link to the formal publication through the relevant DOI), provides a link to the license, indicates if changes were made and the licensor is not represented as endorsing the use made of the work. The full details of the license are available at <http://creativecommons.org/licenses/by/4.0>.

CC BY NC SA: The CC BY-NC-SA license allows users to copy, to create extracts, abstracts and new works from the Article, to alter and revise the Article, provided this is not done for commercial purposes, and that the user gives appropriate credit (with a link to the formal publication through the relevant DOI), provides a link to the license, indicates if changes were made and the licensor is not represented as endorsing the use made of the work. Further, any new works must be made available on the same conditions. The full details of the license are available at <http://creativecommons.org/licenses/by-nc-sa/4.0>.

CC BY NC ND: The CC BY-NC-ND license allows users to copy and distribute the Article, provided this is not done for commercial purposes and further does not permit distribution of the Article if it is changed or edited in any way, and provided the user gives appropriate credit (with a link to the formal publication through the relevant DOI), provides a link to the license, and that the licensor is not represented as endorsing the use made of the work. The full details of the license are available at <http://creativecommons.org/licenses/by-nc-nd/4.0>.

Any commercial reuse of Open Access articles published with a CC BY NC SA or CC BY NC ND license requires permission from Elsevier and will be subject to a fee.

Commercial reuse includes:

- Associating advertising with the full text of the Article
- Charging fees for document delivery or access
- Article aggregation
- Systematic distribution via e-mail lists or share buttons

Posting or linking by commercial companies for use by customers of those companies.

20. Other Conditions:

v1.8

Questions? customer care@copyright.com or +1-855-239-3415 (toll free in the US) or +1-978-646-2777.

NATURE PUBLISHING GROUP LICENSE TERMS AND CONDITIONS

Jun 20, 2016

This Agreement between Stéphanie Devaux ("You") and Nature Publishing Group ("Nature Publishing Group") consists of your license details and the terms and conditions provided by Nature Publishing Group and Copyright Clearance Center.

License Number	3893061003197
License date	Jun 20, 2016
Licensed Content Publisher	Nature Publishing Group
Licensed Content Publication	Nature Reviews Neuroscience
Licensed Content Title	Repertoire of microglial and macrophage responses after spinal cord injury
Licensed Content Author	Samuel David and Antje Kroner
Licensed Content Date	Jul 1, 2011
Licensed Content Volume Number	12
Licensed Content Issue Number	7
Type of Use	reuse in a dissertation / thesis
Requestor type	academic/educational
Format	print and electronic
Portion	figures/tables/illustrations
Number of figures/tables/illustrations	1
High-res required	no
Figures	figure2
Author of this NPG article	no
Your reference number	
Title of your thesis / dissertation	Proteomic analysis of spinal cord after injury and regeneration
Expected completion date	Jul 2016
Estimated size (number of pages)	300
Requestor Location	Stéphanie Devaux INSERM U1192 Université Lille1 Villeneuve d'Ascq, 59650 France Attn: Stéphanie Devaux
Billing Type	Invoice
Billing Address	Stéphanie Devaux INSERM U1192 Université Lille1

Villeneuve d'Ascq, France 59650
Attn: Stéphanie Devaux

Total 0.00 EUR

Terms and Conditions

Terms and Conditions for Permissions

Nature Publishing Group hereby grants you a non-exclusive license to reproduce this material for this purpose, and for no other use, subject to the conditions below:

1. NPG warrants that it has, to the best of its knowledge, the rights to license reuse of this material. However, you should ensure that the material you are requesting is original to Nature Publishing Group and does not carry the copyright of another entity (as credited in the published version). If the credit line on any part of the material you have requested indicates that it was reprinted or adapted by NPG with permission from another source, then you should also seek permission from that source to reuse the material.
2. Permission granted free of charge for material in print is also usually granted for any electronic version of that work, provided that the material is incidental to the work as a whole and that the electronic version is essentially equivalent to, or substitutes for, the print version. Where print permission has been granted for a fee, separate permission must be obtained for any additional, electronic re-use (unless, as in the case of a full paper, this has already been accounted for during your initial request in the calculation of a print run). NB: In all cases, web-based use of full-text articles must be authorized separately through the 'Use on a Web Site' option when requesting permission.
3. Permission granted for a first edition does not apply to second and subsequent editions and for editions in other languages (except for signatories to the STM Permissions Guidelines, or where the first edition permission was granted for free).
4. Nature Publishing Group's permission must be acknowledged next to the figure, table or abstract in print. In electronic form, this acknowledgement must be visible at the same time as the figure/table/abstract, and must be hyperlinked to the journal's homepage.
5. The credit line should read:
Reprinted by permission from Macmillan Publishers Ltd: [JOURNAL NAME] (reference citation), copyright (year of publication)
For AOP papers, the credit line should read:
Reprinted by permission from Macmillan Publishers Ltd: [JOURNAL NAME], advance online publication, day month year (doi: 10.1038/sj.[JOURNAL ACRONYM].XXXXX)

Note: For republication from the *British Journal of Cancer*, the following credit lines apply.

Reprinted by permission from Macmillan Publishers Ltd on behalf of Cancer Research UK: [JOURNAL NAME] (reference citation), copyright (year of publication) For AOP papers, the credit line should read:

Reprinted by permission from Macmillan Publishers Ltd on behalf of Cancer Research UK: [JOURNAL NAME], advance online publication, day month year (doi: 10.1038/sj.[JOURNAL ACRONYM].XXXXX)

6. Adaptations of single figures do not require NPG approval. However, the adaptation should be credited as follows:

Adapted by permission from Macmillan Publishers Ltd: [JOURNAL NAME] (reference citation), copyright (year of publication)

Note: For adaptation from the *British Journal of Cancer*, the following credit line applies.

Adapted by permission from Macmillan Publishers Ltd on behalf of Cancer Research UK: [JOURNAL NAME] (reference citation), copyright (year of publication)

7. Translations of 401 words up to a whole article require NPG approval. Please visit <http://www.macmillanmedicalcommunications.com> for more information. Translations of up

to a 400 words do not require NPG approval. The translation should be credited as follows:

Translated by permission from Macmillan Publishers Ltd: [JOURNAL NAME] (reference citation), copyright (year of publication).

Note: For translation from the *British Journal of Cancer*, the following credit line applies.

Translated by permission from Macmillan Publishers Ltd on behalf of Cancer Research UK: [JOURNAL NAME] (reference citation), copyright (year of publication)

We are certain that all parties will benefit from this agreement and wish you the best in the use of this material. Thank you.

Special Terms:

v1.1

Questions? customercare@copyright.com or +1-855-239-3415 (toll free in the US) or +1-978-646-2777.

**WOLTERS KLUWER HEALTH, INC. LICENSE
TERMS AND CONDITIONS**

Jun 20, 2016

This Agreement between Stéphanie Devaux ("You") and Wolters Kluwer Health, Inc. ("Wolters Kluwer Health, Inc.") consists of your license details and the terms and conditions provided by Wolters Kluwer Health, Inc. and Copyright Clearance Center.

License Number	3893040542557
License date	Jun 20, 2016
Licensed Content Publisher	Wolters Kluwer Health, Inc.
Licensed Content Publication	Spine
Licensed Content Title	Clip Compression Model Is Useful for Thoracic Spinal Cord Injuries: Histologic and Functional Correlates
Licensed Content Author	Peter Poon, Dimpy Gupta, Molly Shoichet, et al
Licensed Content Date	Jan 1, 2007
Licensed Content Volume Number	32
Licensed Content Issue Number	25
Type of Use	Dissertation/Thesis
Requestor type	Individual
Portion	Figures/table/illustration
Number of figures/tables/illustrations	1
Figures/tables/illustrations used	Figure 1
Author of this Wolters Kluwer article	No
Title of your thesis / dissertation	Proteomic analysis of spinal cord after injury and regeneration
Expected completion date	Jul 2016
Estimated size(pages)	300
Requestor Location	Stéphanie Devaux INSERM U1192 Université Lille1 Villeneuve d'Ascq, 59650 France Attn: Stéphanie Devaux
Publisher Tax ID	EU826013006
Billing Type	Invoice
Billing Address	Stéphanie Devaux INSERM U1192 Université Lille1 Villeneuve d'Ascq, France 59650 Attn: Stéphanie Devaux

Total 0.00 EUR

[Terms and Conditions](#)

Wolters Kluwer Terms and Conditions

1. **Transfer of License:** Wolters Kluwer hereby grants you a non-exclusive license to reproduce this material for this purpose, and for no other use, subject to the conditions herein.
2. **Credit Line:** will be prominently placed and include: For books – the author(s), title of book, editor, copyright holder, year of publication; For journals – the author(s), title of article, title of journal, volume number, issue number and inclusive pages.
3. **Warranties:** The requestor warrants that the material shall not be used in any manner which may be considered derogatory to the title, content, or authors of the material, or to Wolters Kluwer.
4. **Indemnity:** You hereby indemnify and hold harmless Wolters Kluwer and their respective officers, directors, employees and agents, from and against any and all claims, costs, proceeding or demands arising out of your unauthorized use of the Licensed Material.
5. **Geographical Scope:** Permission granted is non-exclusive, and is valid throughout the world in the English language and the languages specified in your original request.
6. Wolters Kluwer cannot supply the requestor with the original artwork, electronic files or a "clean copy."
7. Permission is valid if the borrowed material is original to a Wolters Kluwer imprint (Lippincott-Raven Publishers, Williams & Wilkins, Lea & Febiger, Harwal, Rapid Science, Little Brown & Company, Harper & Row Medical, American Journal of Nursing Co, and Urban & Schwarzenberg - English Language, Raven Press, Paul Hoeber, Springhouse, Ovid).
8. **Termination of contract:** If you opt not to use the material requested above please notify RightsLink or Wolters Kluwer within 90 days of the original invoice date.
9. This permission does not apply to images that are credited to publications other than Wolters Kluwer books/journals or its Societies. For images credited to non-Wolters Kluwer books or journals, you will need to obtain permission from the source referenced in the figure or table legend or credit line before making any use of the image(s) or table(s).
10. **Modifications:** With the exception of text size or color, no Wolters Kluwer material is permitted to be modified or adapted without publisher approval.
11. **Third party material:** Adaptations are protected by copyright, so if you would like to reuse material that we have adapted from another source, you will need not only our permission, but the permission of the rights holder of the original material. Similarly, if you want to reuse an adaptation of original LWW content that appears in another publishers work, you will need our permission and that of the next publisher. The adaptation should be credited as follows: Adapted with permission from Wolters Kluwer: Book author, title, year of publication or Journal name, article author, title, reference citation, year of publication. Modifications are permitted on an occasional basis only and permission must be sought by Wolters Kluwer.
12. **Duration of the license:** Permission is granted for a one-time use only within 12 months from the date of this invoice. Rights herein do not apply to future reproductions, editors, revisions, or other derivative works. Once the 12 - month term has expired, permission to renew must be submitted in writing.
 - i. For content reused in another journal or book, in print or electronic format, the license is one-time use and lasts for the 1st edition of a book or for the life of the edition in case of journals.
 - ii. If your Permission Request is for use on a website (which is not a journal or a book), internet, intranet, or any publicly accessible site, you agree to remove the material from such site after 12 months or else renew your permission request.
13. **Contingent on payment:** While you may exercise the rights licensed immediately upon issuance of the license at the end of the licensing process for the transaction, provided that you have disclosed complete and accurate details of your proposed use, no license is finally effective unless and until full payment is received from you (either by publisher or by CCC) as provided in CCC's Billing and Payment terms and conditions. If full payment is not received on a timely basis, then any license preliminarily granted shall be deemed automatically revoked and shall be void as if never granted. Further, in the event that you breach any of these terms and conditions or any of CCC's Billing and Payment terms and conditions, the license is automatically revoked and shall be void as if never granted. Use of materials as described in a revoked license, as well as any use of the materials beyond the scope of an unrevoked license, may constitute copyright infringement and publisher reserves the right to take any and all action to protect its copyright in the materials.

14. **Waived permission fee:** If the permission fee for the requested use of our material has been waived in this instance, please be advised that your future requests for Wolters Kluwer materials may incur a fee.
15. **Service Description for Content Services:** Subject to these terms of use, any terms set forth on the particular order, and payment of the applicable fee, you may make the following uses of the ordered materials:
 - i. **Content Rental:** You may access and view a single electronic copy of the materials ordered for the time period designated at the time the order is placed. Access to the materials will be provided through a dedicated content viewer or other portal, and access will be discontinued upon expiration of the designated time period. An order for Content Rental does not include any rights to print, download, save, create additional copies, to distribute or to reuse in any way the full text or parts of the materials.
 - ii. **Content Purchase:** You may access and download a single electronic copy of the materials ordered. Copies will be provided by email or by such other means as publisher may make available from time to time. An order for Content Purchase does not include any rights to create additional copies or to distribute copies of the materials.

For Journals Only:

1. Please note that articles in the **ahead-of-print stage** of publication can be cited and the content may be re-used by including the date of access and the unique DOI number. Any final changes in manuscripts will be made at the time of print publication and will be reflected in the final electronic version of the issue. Disclaimer: Articles appearing in the Published Ahead-of-Print section have been peer-reviewed and accepted for publication in the relevant journal and posted online before print publication. Articles appearing as publish ahead-of-print may contain statements, opinions, and information that have errors in facts, figures, or interpretation. Accordingly, Wolters Kluwer, the editors and authors and their respective employees are not responsible or liable for the use of any such inaccurate or misleading data, opinion or information contained in the articles in this section.
2. Where a journal is being published by a learned society, the details of that society must be included in the credit line.
 - i. **For Open Access journals:** The following statement needs to be added when reprinting the material in Open Access journals only: "promotional and commercial use of the material in print, digital or mobile device format is prohibited without the permission from the publisher Wolters Kluwer. Please contact healthpermissions@wolterskluwer.com for further information."
 - ii. **Exceptions:** In case of **Disease Colon Rectum, Plastic Reconstructive Surgery, The Green Journal, Critical Care Medicine, Pediatric Critical Care Medicine, the American Heart Publications, the American Academy of Neurology** the following guideline applies: no drug/ trade name or logo can be included in the same page as the material re-used. .
3. **Translations:** If granted permissions to republish a full text article in another language, Wolters Kluwer should be sent a copy of the translated PDF. Please include disclaimer below on all translated copies:
 - i. ***Wolters Kluwer and its Societies take no responsibility for the accuracy of the translation from the published English original and are not liable for any errors which may occur.***
4. **Full Text Articles:** Reuse of full text articles in English is prohibited.

STM Signatories Only:

1. Any permission granted for a particular edition will apply also to subsequent editions and for editions in other languages, provided such editions are for the work as a whole in situ and does not involve the separate exploitation of the permitted illustrations or excerpts. Please click [here](#) to view the STM guidelines.

Other Terms and Conditions:

v1.3

Questions? customercare@copyright.com or +1-855-239-3415 (toll free in the US) or +1-978-646-2777.



ELSEVIER LICENSE TERMS AND CONDITIONS

Jun 20, 2016

This Agreement between Stéphanie Devaux ("You") and Elsevier ("Elsevier") consists of your license details and the terms and conditions provided by Elsevier and Copyright Clearance Center.

License Number	3893070016298
License date	Jun 20, 2016
Licensed Content Publisher	Elsevier
Licensed Content Publication	Trends in Pharmacological Sciences
Licensed Content Title	Manipulating neuroinflammatory reactions in the injured spinal cord: back to basics
Licensed Content Author	Phillip G. Popovich, T. Bucky Jones
Licensed Content Date	January 2003
Licensed Content Volume Number	24
Licensed Content Issue Number	1
Licensed Content Pages	5
Start Page	13
End Page	17
Type of Use	reuse in a thesis/dissertation
Intended publisher of new work	other
Portion	figures/tables/illustrations
Number of figures/tables/illustrations	1
Format	both print and electronic
Are you the author of this Elsevier article?	No
Will you be translating?	No
Order reference number	
Original figure numbers	figure 1
Title of your thesis/dissertation	Proteomic analysis of spinal cord after injury and regeneration
Expected completion date	Jul 2016
Estimated size (number of pages)	300
Elsevier VAT number	GB 494 6272 12
Requestor Location	Stéphanie Devaux INSERM U1192 Université Lille1

Villeneuve d'Ascq, 59650

France
Attn: Stéphanie Devaux

Total 0.00 EUR

[Terms and Conditions](#)

INTRODUCTION

1. The publisher for this copyrighted material is Elsevier. By clicking "accept" in connection with completing this licensing transaction, you agree that the following terms and conditions apply to this transaction (along with the Billing and Payment terms and conditions established by Copyright Clearance Center, Inc. ("CCC"), at the time that you opened your Rightslink account and that are available at any time at <http://myaccount.copyright.com>).

GENERAL TERMS

2. Elsevier hereby grants you permission to reproduce the aforementioned material subject to the terms and conditions indicated.

3. Acknowledgement: If any part of the material to be used (for example, figures) has appeared in our publication with credit or acknowledgement to another source, permission must also be sought from that source. If such permission is not obtained then that material may not be included in your publication/copies. Suitable acknowledgement to the source must be made, either as a footnote or in a reference list at the end of your publication, as follows:

"Reprinted from Publication title, Vol /edition number, Author(s), Title of article / title of chapter, Pages No., Copyright (Year), with permission from Elsevier [OR APPLICABLE SOCIETY COPYRIGHT OWNER]." Also Lancet special credit - "Reprinted from The Lancet, Vol. number, Author(s), Title of article, Pages No., Copyright (Year), with permission from Elsevier."

4. Reproduction of this material is confined to the purpose and/or media for which permission is hereby given.

5. Altering/Modifying Material: Not Permitted. However figures and illustrations may be altered/adapted minimally to serve your work. Any other abbreviations, additions, deletions and/or any other alterations shall be made only with prior written authorization of Elsevier Ltd. (Please contact Elsevier at permissions@elsevier.com)

6. If the permission fee for the requested use of our material is waived in this instance, please be advised that your future requests for Elsevier materials may attract a fee.

7. Reservation of Rights: Publisher reserves all rights not specifically granted in the combination of (i) the license details provided by you and accepted in the course of this licensing transaction, (ii) these terms and conditions and (iii) CCC's Billing and Payment terms and conditions.

8. License Contingent Upon Payment: While you may exercise the rights licensed immediately upon issuance of the license at the end of the licensing process for the transaction, provided that you have disclosed complete and accurate details of your proposed use, no license is finally effective unless and until full payment is received from you (either by publisher or by CCC) as provided in CCC's Billing and Payment terms and conditions. If full payment is not received on a timely basis, then any license preliminarily granted shall be deemed automatically revoked and shall be void as if never granted. Further, in the event that you breach any of these terms and conditions or any of CCC's Billing and Payment terms and conditions, the license is automatically revoked and shall be void as if never granted. Use of materials as described in a revoked license, as well as any use of the materials beyond the scope of an unrevoked license, may constitute copyright infringement and publisher reserves the right to take any and all action to protect its copyright in the materials.

9. Warranties: Publisher makes no representations or warranties with respect to the licensed material.

10. Indemnity: You hereby indemnify and agree to hold harmless publisher and CCC, and their respective officers, directors, employees and agents, from and against any and all

claims arising out of your use of the licensed material other than as specifically authorized pursuant to this license.

11. **No Transfer of License:** This license is personal to you and may not be sublicensed, assigned, or transferred by you to any other person without publisher's written permission.

12. **No Amendment Except in Writing:** This license may not be amended except in a writing signed by both parties (or, in the case of publisher, by CCC on publisher's behalf).

13. **Objection to Contrary Terms:** Publisher hereby objects to any terms contained in any purchase order, acknowledgment, check endorsement or other writing prepared by you, which terms are inconsistent with these terms and conditions or CCC's Billing and Payment terms and conditions. These terms and conditions, together with CCC's Billing and Payment terms and conditions (which are incorporated herein), comprise the entire agreement between you and publisher (and CCC) concerning this licensing transaction. In the event of any conflict between your obligations established by these terms and conditions and those established by CCC's Billing and Payment terms and conditions, these terms and conditions shall control.

14. **Revocation:** Elsevier or Copyright Clearance Center may deny the permissions described in this License at their sole discretion, for any reason or no reason, with a full refund payable to you. Notice of such denial will be made using the contact information provided by you. Failure to receive such notice will not alter or invalidate the denial. In no event will Elsevier or Copyright Clearance Center be responsible or liable for any costs, expenses or damage incurred by you as a result of a denial of your permission request, other than a refund of the amount(s) paid by you to Elsevier and/or Copyright Clearance Center for denied permissions.

LIMITED LICENSE

The following terms and conditions apply only to specific license types:

15. **Translation:** This permission is granted for non-exclusive world **English** rights only unless your license was granted for translation rights. If you licensed translation rights you may only translate this content into the languages you requested. A professional translator must perform all translations and reproduce the content word for word preserving the integrity of the article.

16. **Posting licensed content on any Website:** The following terms and conditions apply as follows: Licensing material from an Elsevier journal: All content posted to the web site must maintain the copyright information line on the bottom of each image; A hyper-text must be included to the Homepage of the journal from which you are licensing at <http://www.sciencedirect.com/science/journal/xxxxx> or the Elsevier homepage for books at <http://www.elsevier.com>; Central Storage: This license does not include permission for a scanned version of the material to be stored in a central repository such as that provided by Heron/XanEdu.

Licensing material from an Elsevier book: A hyper-text link must be included to the Elsevier homepage at <http://www.elsevier.com>. All content posted to the web site must maintain the copyright information line on the bottom of each image.

Posting licensed content on Electronic reserve: In addition to the above the following clauses are applicable: The web site must be password-protected and made available only to bona fide students registered on a relevant course. This permission is granted for 1 year only. You may obtain a new license for future website posting.

17. **For journal authors:** the following clauses are applicable in addition to the above:

Preprints:

A preprint is an author's own write-up of research results and analysis, it has not been peer-reviewed, nor has it had any other value added to it by a publisher (such as formatting, copyright, technical enhancement etc.).

Authors can share their preprints anywhere at any time. Preprints should not be added to or enhanced in any way in order to appear more like, or to substitute for, the final versions of articles however authors can update their preprints on arXiv or RePEc with their Accepted

Author Manuscript (see below).

If accepted for publication, we encourage authors to link from the preprint to their formal publication via its DOI. Millions of researchers have access to the formal publications on ScienceDirect, and so links will help users to find, access, cite and use the best available version. Please note that Cell Press, The Lancet and some society-owned have different preprint policies. Information on these policies is available on the journal homepage.

Accepted Author Manuscripts: An accepted author manuscript is the manuscript of an article that has been accepted for publication and which typically includes author-incorporated changes suggested during submission, peer review and editor-author communications.

Authors can share their accepted author manuscript:

- immediately
 - via their non-commercial person homepage or blog
 - by updating a preprint in arXiv or RePEc with the accepted manuscript
 - via their research institute or institutional repository for internal institutional uses or as part of an invitation-only research collaboration work-group
 - directly by providing copies to their students or to research collaborators for their personal use
 - for private scholarly sharing as part of an invitation-only work group on commercial sites with which Elsevier has an agreement
- after the embargo period
 - via non-commercial hosting platforms such as their institutional repository
 - via commercial sites with which Elsevier has an agreement

In all cases accepted manuscripts should:

- link to the formal publication via its DOI
- bear a CC-BY-NC-ND license - this is easy to do
- if aggregated with other manuscripts, for example in a repository or other site, be shared in alignment with our hosting policy not be added to or enhanced in any way to appear more like, or to substitute for, the published journal article.

Published journal article (JPA): A published journal article (PJA) is the definitive final record of published research that appears or will appear in the journal and embodies all value-adding publishing activities including peer review co-ordination, copy-editing, formatting, (if relevant) pagination and online enrichment.

Policies for sharing publishing journal articles differ for subscription and gold open access articles:

Subscription Articles: If you are an author, please share a link to your article rather than the full-text. Millions of researchers have access to the formal publications on ScienceDirect, and so links will help your users to find, access, cite, and use the best available version.

Theses and dissertations which contain embedded PJAs as part of the formal submission can be posted publicly by the awarding institution with DOI links back to the formal publications on ScienceDirect.

If you are affiliated with a library that subscribes to ScienceDirect you have additional private sharing rights for others' research accessed under that agreement. This includes use for classroom teaching and internal training at the institution (including use in course packs and courseware programs), and inclusion of the article for grant funding purposes.

Gold Open Access Articles: May be shared according to the author-selected end-user license and should contain a [CrossMark logo](#), the end user license, and a DOI link to the formal publication on ScienceDirect.

Please refer to Elsevier's [posting policy](#) for further information.

18. **For book authors** the following clauses are applicable in addition to the above:

Authors are permitted to place a brief summary of their work online only. You are not allowed to download and post the published electronic version of your chapter, nor may you scan the printed edition to create an electronic version. **Posting to a repository:** Authors are permitted to post a summary of their chapter only in their institution's repository.

19. **Thesis/Dissertation:** If your license is for use in a thesis/dissertation your thesis may be submitted to your institution in either print or electronic form. Should your thesis be published commercially, please reapply for permission. These requirements include permission for the Library and Archives of Canada to supply single copies, on demand, of the complete thesis and include permission for Proquest/UMI to supply single copies, on demand, of the complete thesis. Should your thesis be published commercially, please reapply for permission. Theses and dissertations which contain embedded PJAs as part of the formal submission can be posted publicly by the awarding institution with DOI links back to the formal publications on ScienceDirect.

Elsevier Open Access Terms and Conditions

You can publish open access with Elsevier in hundreds of open access journals or in nearly 2000 established subscription journals that support open access publishing. Permitted third party re-use of these open access articles is defined by the author's choice of Creative Commons user license. See our [open access license policy](#) for more information.

Terms & Conditions applicable to all Open Access articles published with Elsevier:

Any reuse of the article must not represent the author as endorsing the adaptation of the article nor should the article be modified in such a way as to damage the author's honour or reputation. If any changes have been made, such changes must be clearly indicated.

The author(s) must be appropriately credited and we ask that you include the end user license and a DOI link to the formal publication on ScienceDirect.

If any part of the material to be used (for example, figures) has appeared in our publication with credit or acknowledgement to another source it is the responsibility of the user to ensure their reuse complies with the terms and conditions determined by the rights holder.

Additional Terms & Conditions applicable to each Creative Commons user license:

CC BY: The CC-BY license allows users to copy, to create extracts, abstracts and new works from the Article, to alter and revise the Article and to make commercial use of the Article (including reuse and/or resale of the Article by commercial entities), provided the user gives appropriate credit (with a link to the formal publication through the relevant DOI), provides a link to the license, indicates if changes were made and the licensor is not represented as endorsing the use made of the work. The full details of the license are available at <http://creativecommons.org/licenses/by/4.0>.

CC BY NC SA: The CC BY-NC-SA license allows users to copy, to create extracts, abstracts and new works from the Article, to alter and revise the Article, provided this is not done for commercial purposes, and that the user gives appropriate credit (with a link to the formal publication through the relevant DOI), provides a link to the license, indicates if changes were made and the licensor is not represented as endorsing the use made of the work. Further, any new works must be made available on the same conditions. The full details of the license are available at <http://creativecommons.org/licenses/by-nc-sa/4.0>.

CC BY NC ND: The CC BY-NC-ND license allows users to copy and distribute the Article, provided this is not done for commercial purposes and further does not permit distribution of the Article if it is changed or edited in any way, and provided the user gives appropriate credit (with a link to the formal publication through the relevant DOI), provides a link to the license, and that the licensor is not represented as endorsing the use made of the work. The full details of the license are available at <http://creativecommons.org/licenses/by-nc-nd/4.0>.

Any commercial reuse of Open Access articles published with a CC BY NC SA or CC BY NC ND license requires permission from Elsevier and will be subject to a fee.

Commercial reuse includes:

- Associating advertising with the full text of the Article

- Charging fees for document delivery or access
- Article aggregation
- Systematic distribution via e-mail lists or share buttons

Posting or linking by commercial companies for use by customers of those companies.

20. Other Conditions:

v1.8

Questions? customercare@copyright.com or +1-855-239-3415 (toll free in the US) or +1-978-646-2777.

NATURE PUBLISHING GROUP LICENSE TERMS AND CONDITIONS

Jun 20, 2016

This Agreement between Stéphanie Devaux ("You") and Nature Publishing Group ("Nature Publishing Group") consists of your license details and the terms and conditions provided by Nature Publishing Group and Copyright Clearance Center.

License Number	3893060823799
License date	Jun 20, 2016
Licensed Content Publisher	Nature Publishing Group
Licensed Content Publication	Nature
Licensed Content Title	The myeloid cells of the central nervous system parenchyma
Licensed Content Author	Richard M. Ransohoff, Astrid E. Cardona
Licensed Content Date	Nov 10, 2010
Licensed Content Volume Number	468
Licensed Content Issue Number	7321
Type of Use	reuse in a dissertation / thesis
Requestor type	academic/educational
Format	print and electronic
Portion	figures/tables/illustrations
Number of figures/tables/illustrations	1
High-res required	no
Figures	figure1
Author of this NPG article	no
Your reference number	
Title of your thesis / dissertation	Proteomic analysis of spinal cord after injury and regeneration
Expected completion date	Jul 2016
Estimated size (number of pages)	300
Requestor Location	Stéphanie Devaux INSERM U1192 Université Lille1 Villeneuve d'Ascq, 59650 France Attn: Stéphanie Devaux
Billing Type	Invoice
Billing Address	Stéphanie Devaux INSERM U1192 Université Lille1 Villeneuve d'Ascq, France 59650

Attn: Stéphanie Devaux

Total

0.00 EUR

[Terms and Conditions](#)

Terms and Conditions for Permissions

Nature Publishing Group hereby grants you a non-exclusive license to reproduce this material for this purpose, and for no other use, subject to the conditions below:

1. NPG warrants that it has, to the best of its knowledge, the rights to license reuse of this material. However, you should ensure that the material you are requesting is original to Nature Publishing Group and does not carry the copyright of another entity (as credited in the published version). If the credit line on any part of the material you have requested indicates that it was reprinted or adapted by NPG with permission from another source, then you should also seek permission from that source to reuse the material.
2. Permission granted free of charge for material in print is also usually granted for any electronic version of that work, provided that the material is incidental to the work as a whole and that the electronic version is essentially equivalent to, or substitutes for, the print version. Where print permission has been granted for a fee, separate permission must be obtained for any additional, electronic re-use (unless, as in the case of a full paper, this has already been accounted for during your initial request in the calculation of a print run). NB: In all cases, web-based use of full-text articles must be authorized separately through the 'Use on a Web Site' option when requesting permission.
3. Permission granted for a first edition does not apply to second and subsequent editions and for editions in other languages (except for signatories to the STM Permissions Guidelines, or where the first edition permission was granted for free).
4. Nature Publishing Group's permission must be acknowledged next to the figure, table or abstract in print. In electronic form, this acknowledgement must be visible at the same time as the figure/table/abstract, and must be hyperlinked to the journal's homepage.
5. The credit line should read:
Reprinted by permission from Macmillan Publishers Ltd: [JOURNAL NAME] (reference citation), copyright (year of publication)
For AOP papers, the credit line should read:
Reprinted by permission from Macmillan Publishers Ltd: [JOURNAL NAME], advance online publication, day month year (doi: 10.1038/sj.[JOURNAL ACRONYM].XXXXX)

Note: For republication from the *British Journal of Cancer*, the following credit lines apply.

Reprinted by permission from Macmillan Publishers Ltd on behalf of Cancer Research UK: [JOURNAL NAME] (reference citation), copyright (year of publication) For AOP papers, the credit line should read:

Reprinted by permission from Macmillan Publishers Ltd on behalf of Cancer Research UK: [JOURNAL NAME], advance online publication, day month year (doi: 10.1038/sj.[JOURNAL ACRONYM].XXXXX)

6. Adaptations of single figures do not require NPG approval. However, the adaptation should be credited as follows:

Adapted by permission from Macmillan Publishers Ltd: [JOURNAL NAME] (reference citation), copyright (year of publication)

Note: For adaptation from the *British Journal of Cancer*, the following credit line applies.

Adapted by permission from Macmillan Publishers Ltd on behalf of Cancer Research UK: [JOURNAL NAME] (reference citation), copyright (year of publication)

7. Translations of 401 words up to a whole article require NPG approval. Please visit <http://www.macmillanmedicalcommunications.com> for more information. Translations of up to a 400 words do not require NPG approval. The translation should be credited as follows:

Translated by permission from Macmillan Publishers Ltd: [JOURNAL NAME] (reference citation), copyright (year of publication).

Note: For translation from the *British Journal of Cancer*, the following credit line applies.

Translated by permission from Macmillan Publishers Ltd on behalf of Cancer Research UK: [JOURNAL NAME] (reference citation), copyright (year of publication)

We are certain that all parties will benefit from this agreement and wish you the best in the use of this material. Thank you.

Special Terms:

v1.1

Questions? customercare@copyright.com or +1-855-239-3415 (toll free in the US) or +1-978-646-2777.

ELSEVIER LICENSE TERMS AND CONDITIONS

Jun 20, 2016

This Agreement between Stéphanie Devaux ("You") and Elsevier ("Elsevier") consists of your license details and the terms and conditions provided by Elsevier and Copyright Clearance Center.

License Number	3893070196150
License date	Jun 20, 2016
Licensed Content Publisher	Elsevier
Licensed Content Publication	Current Opinion in Neurobiology
Licensed Content Title	Nogo and axon regeneration
Licensed Content Author	Martin E Schwab
Licensed Content Date	February 2004
Licensed Content Volume Number	14
Licensed Content Issue Number	1
Licensed Content Pages	7
Start Page	118
End Page	124
Type of Use	reuse in a thesis/dissertation
Intended publisher of new work	other
Portion	figures/tables/illustrations
Number of figures/tables/illustrations	1
Format	both print and electronic
Are you the author of this Elsevier article?	No
Will you be translating?	No
Order reference number	
Original figure numbers	figure 1
Title of your thesis/dissertation	Proteomic analysis of spinal cord after injury and regeneration
Expected completion date	Jul 2016
Estimated size (number of pages)	300
Elsevier VAT number	GB 494 6272 12
Requestor Location	Stéphanie Devaux INSERM U1192 Université Lille1

Villeneuve d'Ascq, 59650
France

Attn: Stéphanie Devaux

Total

0.00 EUR

[Terms and Conditions](#)

INTRODUCTION

1. The publisher for this copyrighted material is Elsevier. By clicking "accept" in connection with completing this licensing transaction, you agree that the following terms and conditions apply to this transaction (along with the Billing and Payment terms and conditions established by Copyright Clearance Center, Inc. ("CCC"), at the time that you opened your Rightslink account and that are available at any time at <http://myaccount.copyright.com>).

GENERAL TERMS

2. Elsevier hereby grants you permission to reproduce the aforementioned material subject to the terms and conditions indicated.

3. Acknowledgement: If any part of the material to be used (for example, figures) has appeared in our publication with credit or acknowledgement to another source, permission must also be sought from that source. If such permission is not obtained then that material may not be included in your publication/copies. Suitable acknowledgement to the source must be made, either as a footnote or in a reference list at the end of your publication, as follows:

"Reprinted from Publication title, Vol /edition number, Author(s), Title of article / title of chapter, Pages No., Copyright (Year), with permission from Elsevier [OR APPLICABLE SOCIETY COPYRIGHT OWNER]." Also Lancet special credit - "Reprinted from The Lancet, Vol. number, Author(s), Title of article, Pages No., Copyright (Year), with permission from Elsevier."

4. Reproduction of this material is confined to the purpose and/or media for which permission is hereby given.

5. Altering/Modifying Material: Not Permitted. However figures and illustrations may be altered/adapted minimally to serve your work. Any other abbreviations, additions, deletions and/or any other alterations shall be made only with prior written authorization of Elsevier Ltd. (Please contact Elsevier at permissions@elsevier.com)

6. If the permission fee for the requested use of our material is waived in this instance, please be advised that your future requests for Elsevier materials may attract a fee.

7. Reservation of Rights: Publisher reserves all rights not specifically granted in the combination of (i) the license details provided by you and accepted in the course of this licensing transaction, (ii) these terms and conditions and (iii) CCC's Billing and Payment terms and conditions.

8. License Contingent Upon Payment: While you may exercise the rights licensed immediately upon issuance of the license at the end of the licensing process for the transaction, provided that you have disclosed complete and accurate details of your proposed use, no license is finally effective unless and until full payment is received from you (either by publisher or by CCC) as provided in CCC's Billing and Payment terms and conditions. If full payment is not received on a timely basis, then any license preliminarily granted shall be deemed automatically revoked and shall be void as if never granted. Further, in the event that you breach any of these terms and conditions or any of CCC's Billing and Payment terms and conditions, the license is automatically revoked and shall be void as if never granted. Use of materials as described in a revoked license, as well as any use of the materials beyond the scope of an unrevoked license, may constitute copyright infringement and publisher reserves the right to take any and all action to protect its copyright in the materials.

9. Warranties: Publisher makes no representations or warranties with respect to the licensed material.

10. Indemnity: You hereby indemnify and agree to hold harmless publisher and CCC, and their respective officers, directors, employees and agents, from and against any and all claims arising out of your use of the licensed material other than as specifically authorized

pursuant to this license.

11. **No Transfer of License:** This license is personal to you and may not be sublicensed, assigned, or transferred by you to any other person without publisher's written permission.

12. **No Amendment Except in Writing:** This license may not be amended except in a writing signed by both parties (or, in the case of publisher, by CCC on publisher's behalf).

13. **Objection to Contrary Terms:** Publisher hereby objects to any terms contained in any purchase order, acknowledgment, check endorsement or other writing prepared by you, which terms are inconsistent with these terms and conditions or CCC's Billing and Payment terms and conditions. These terms and conditions, together with CCC's Billing and Payment terms and conditions (which are incorporated herein), comprise the entire agreement between you and publisher (and CCC) concerning this licensing transaction. In the event of any conflict between your obligations established by these terms and conditions and those established by CCC's Billing and Payment terms and conditions, these terms and conditions shall control.

14. **Revocation:** Elsevier or Copyright Clearance Center may deny the permissions described in this License at their sole discretion, for any reason or no reason, with a full refund payable to you. Notice of such denial will be made using the contact information provided by you. Failure to receive such notice will not alter or invalidate the denial. In no event will Elsevier or Copyright Clearance Center be responsible or liable for any costs, expenses or damage incurred by you as a result of a denial of your permission request, other than a refund of the amount(s) paid by you to Elsevier and/or Copyright Clearance Center for denied permissions.

LIMITED LICENSE

The following terms and conditions apply only to specific license types:

15. **Translation:** This permission is granted for non-exclusive world **English** rights only unless your license was granted for translation rights. If you licensed translation rights you may only translate this content into the languages you requested. A professional translator must perform all translations and reproduce the content word for word preserving the integrity of the article.

16. **Posting licensed content on any Website:** The following terms and conditions apply as follows: Licensing material from an Elsevier journal: All content posted to the web site must maintain the copyright information line on the bottom of each image; A hyper-text must be included to the Homepage of the journal from which you are licensing at <http://www.sciencedirect.com/science/journal/xxxxx> or the Elsevier homepage for books at <http://www.elsevier.com>; Central Storage: This license does not include permission for a scanned version of the material to be stored in a central repository such as that provided by Heron/XanEdu.

Licensing material from an Elsevier book: A hyper-text link must be included to the Elsevier homepage at <http://www.elsevier.com>. All content posted to the web site must maintain the copyright information line on the bottom of each image.

Posting licensed content on Electronic reserve: In addition to the above the following clauses are applicable: The web site must be password-protected and made available only to bona fide students registered on a relevant course. This permission is granted for 1 year only. You may obtain a new license for future website posting.

17. **For journal authors:** the following clauses are applicable in addition to the above:

Preprints:

A preprint is an author's own write-up of research results and analysis, it has not been peer-reviewed, nor has it had any other value added to it by a publisher (such as formatting, copyright, technical enhancement etc.).

Authors can share their preprints anywhere at any time. Preprints should not be added to or enhanced in any way in order to appear more like, or to substitute for, the final versions of articles however authors can update their preprints on arXiv or RePEc with their Accepted Author Manuscript (see below).

If accepted for publication, we encourage authors to link from the preprint to their formal publication via its DOI. Millions of researchers have access to the formal publications on ScienceDirect, and so links will help users to find, access, cite and use the best available version. Please note that Cell Press, The Lancet and some society-owned have different preprint policies. Information on these policies is available on the journal homepage.

Accepted Author Manuscripts: An accepted author manuscript is the manuscript of an article that has been accepted for publication and which typically includes author-incorporated changes suggested during submission, peer review and editor-author communications.

Authors can share their accepted author manuscript:

- immediately
 - via their non-commercial person homepage or blog
 - by updating a preprint in arXiv or RePEc with the accepted manuscript
 - via their research institute or institutional repository for internal institutional uses or as part of an invitation-only research collaboration work-group
 - directly by providing copies to their students or to research collaborators for their personal use
 - for private scholarly sharing as part of an invitation-only work group on commercial sites with which Elsevier has an agreement
- after the embargo period
 - via non-commercial hosting platforms such as their institutional repository
 - via commercial sites with which Elsevier has an agreement

In all cases accepted manuscripts should:

- link to the formal publication via its DOI
- bear a CC-BY-NC-ND license - this is easy to do
- if aggregated with other manuscripts, for example in a repository or other site, be shared in alignment with our hosting policy not be added to or enhanced in any way to appear more like, or to substitute for, the published journal article.

Published journal article (JPA): A published journal article (PJA) is the definitive final record of published research that appears or will appear in the journal and embodies all value-adding publishing activities including peer review co-ordination, copy-editing, formatting, (if relevant) pagination and online enrichment.

Policies for sharing publishing journal articles differ for subscription and gold open access articles:

Subscription Articles: If you are an author, please share a link to your article rather than the full-text. Millions of researchers have access to the formal publications on ScienceDirect, and so links will help your users to find, access, cite, and use the best available version.

Theses and dissertations which contain embedded PJAs as part of the formal submission can be posted publicly by the awarding institution with DOI links back to the formal publications on ScienceDirect.

If you are affiliated with a library that subscribes to ScienceDirect you have additional private sharing rights for others' research accessed under that agreement. This includes use for classroom teaching and internal training at the institution (including use in course packs and courseware programs), and inclusion of the article for grant funding purposes.

Gold Open Access Articles: May be shared according to the author-selected end-user license and should contain a [CrossMark logo](#), the end user license, and a DOI link to the formal publication on ScienceDirect.

Please refer to Elsevier's [posting policy](#) for further information.

18. **For book authors** the following clauses are applicable in addition to the above:

Authors are permitted to place a brief summary of their work online only. You are not

allowed to download and post the published electronic version of your chapter, nor may you scan the printed edition to create an electronic version. **Posting to a repository:** Authors are permitted to post a summary of their chapter only in their institution's repository.

19. **Thesis/Dissertation:** If your license is for use in a thesis/dissertation your thesis may be submitted to your institution in either print or electronic form. Should your thesis be published commercially, please reapply for permission. These requirements include permission for the Library and Archives of Canada to supply single copies, on demand, of the complete thesis and include permission for Proquest/UMI to supply single copies, on demand, of the complete thesis. Should your thesis be published commercially, please reapply for permission. Theses and dissertations which contain embedded PJAs as part of the formal submission can be posted publicly by the awarding institution with DOI links back to the formal publications on ScienceDirect.

Elsevier Open Access Terms and Conditions

You can publish open access with Elsevier in hundreds of open access journals or in nearly 2000 established subscription journals that support open access publishing. Permitted third party re-use of these open access articles is defined by the author's choice of Creative Commons user license. See our [open access license policy](#) for more information.

Terms & Conditions applicable to all Open Access articles published with Elsevier:

Any reuse of the article must not represent the author as endorsing the adaptation of the article nor should the article be modified in such a way as to damage the author's honour or reputation. If any changes have been made, such changes must be clearly indicated.

The author(s) must be appropriately credited and we ask that you include the end user license and a DOI link to the formal publication on ScienceDirect.

If any part of the material to be used (for example, figures) has appeared in our publication with credit or acknowledgement to another source it is the responsibility of the user to ensure their reuse complies with the terms and conditions determined by the rights holder.

Additional Terms & Conditions applicable to each Creative Commons user license:

CC BY: The CC-BY license allows users to copy, to create extracts, abstracts and new works from the Article, to alter and revise the Article and to make commercial use of the Article (including reuse and/or resale of the Article by commercial entities), provided the user gives appropriate credit (with a link to the formal publication through the relevant DOI), provides a link to the license, indicates if changes were made and the licensor is not represented as endorsing the use made of the work. The full details of the license are available at <http://creativecommons.org/licenses/by/4.0>.

CC BY NC SA: The CC BY-NC-SA license allows users to copy, to create extracts, abstracts and new works from the Article, to alter and revise the Article, provided this is not done for commercial purposes, and that the user gives appropriate credit (with a link to the formal publication through the relevant DOI), provides a link to the license, indicates if changes were made and the licensor is not represented as endorsing the use made of the work. Further, any new works must be made available on the same conditions. The full details of the license are available at <http://creativecommons.org/licenses/by-nc-sa/4.0>.

CC BY NC ND: The CC BY-NC-ND license allows users to copy and distribute the Article, provided this is not done for commercial purposes and further does not permit distribution of the Article if it is changed or edited in any way, and provided the user gives appropriate credit (with a link to the formal publication through the relevant DOI), provides a link to the license, and that the licensor is not represented as endorsing the use made of the work. The full details of the license are available at <http://creativecommons.org/licenses/by-nc-nd/4.0>.

Any commercial reuse of Open Access articles published with a CC BY NC SA or CC BY NC ND license requires permission from Elsevier and will be subject to a fee.

Commercial reuse includes:

- Associating advertising with the full text of the Article
- Charging fees for document delivery or access

- Article aggregation
- Systematic distribution via e-mail lists or share buttons

Posting or linking by commercial companies for use by customers of those companies.

20. Other Conditions:

v1.8

Questions? customercare@copyright.com or +1-855-239-3415 (toll free in the US) or +1-978-646-2777.



NATURE PUBLISHING GROUP LICENSE TERMS AND CONDITIONS

Jun 20, 2016

This Agreement between Stéphanie Devaux ("You") and Nature Publishing Group ("Nature Publishing Group") consists of your license details and the terms and conditions provided by Nature Publishing Group and Copyright Clearance Center.

License Number	3893061153698
License date	Jun 20, 2016
Licensed Content Publisher	Nature Publishing Group
Licensed Content Publication	Nature Reviews Immunology
Licensed Content Title	Mesenchymal stem cells in health and disease
Licensed Content Author	Antonio Uccelli, Lorenzo Moretta and Vito Pistoia
Licensed Content Date	Sep 1, 2008
Licensed Content Volume Number	8
Licensed Content Issue Number	9
Type of Use	reuse in a dissertation / thesis
Requestor type	academic/educational
Format	print and electronic
Portion	figures/tables/illustrations
Number of figures/tables/illustrations	1
High-res required	no
Figures	figure1
Author of this NPG article	no
Your reference number	
Title of your thesis / dissertation	Proteomic analysis of spinal cord after injury and regeneration
Expected completion date	Jul 2016
Estimated size (number of pages)	300
Requestor Location	Stéphanie Devaux INSERM U1192 Université Lille1 Villeneuve d'Ascq, 59650 France Attn: Stéphanie Devaux
Billing Type	Invoice
Billing Address	Stéphanie Devaux INSERM U1192 Université Lille1 Villeneuve d'Ascq, France 59650

Attn: Stéphanie Devaux

Total

0.00 EUR

[Terms and Conditions](#)

Terms and Conditions for Permissions

Nature Publishing Group hereby grants you a non-exclusive license to reproduce this material for this purpose, and for no other use, subject to the conditions below:

1. NPG warrants that it has, to the best of its knowledge, the rights to license reuse of this material. However, you should ensure that the material you are requesting is original to Nature Publishing Group and does not carry the copyright of another entity (as credited in the published version). If the credit line on any part of the material you have requested indicates that it was reprinted or adapted by NPG with permission from another source, then you should also seek permission from that source to reuse the material.
2. Permission granted free of charge for material in print is also usually granted for any electronic version of that work, provided that the material is incidental to the work as a whole and that the electronic version is essentially equivalent to, or substitutes for, the print version. Where print permission has been granted for a fee, separate permission must be obtained for any additional, electronic re-use (unless, as in the case of a full paper, this has already been accounted for during your initial request in the calculation of a print run). NB: In all cases, web-based use of full-text articles must be authorized separately through the 'Use on a Web Site' option when requesting permission.
3. Permission granted for a first edition does not apply to second and subsequent editions and for editions in other languages (except for signatories to the STM Permissions Guidelines, or where the first edition permission was granted for free).
4. Nature Publishing Group's permission must be acknowledged next to the figure, table or abstract in print. In electronic form, this acknowledgement must be visible at the same time as the figure/table/abstract, and must be hyperlinked to the journal's homepage.
5. The credit line should read:
Reprinted by permission from Macmillan Publishers Ltd: [JOURNAL NAME] (reference citation), copyright (year of publication)
For AOP papers, the credit line should read:
Reprinted by permission from Macmillan Publishers Ltd: [JOURNAL NAME], advance online publication, day month year (doi: 10.1038/sj.[JOURNAL ACRONYM].XXXXX)

Note: For republication from the *British Journal of Cancer*, the following credit lines apply.

Reprinted by permission from Macmillan Publishers Ltd on behalf of Cancer Research UK: [JOURNAL NAME] (reference citation), copyright (year of publication) For AOP papers, the credit line should read:

Reprinted by permission from Macmillan Publishers Ltd on behalf of Cancer Research UK: [JOURNAL NAME], advance online publication, day month year (doi: 10.1038/sj.[JOURNAL ACRONYM].XXXXX)

6. Adaptations of single figures do not require NPG approval. However, the adaptation should be credited as follows:

Adapted by permission from Macmillan Publishers Ltd: [JOURNAL NAME] (reference citation), copyright (year of publication)

Note: For adaptation from the *British Journal of Cancer*, the following credit line applies.

Adapted by permission from Macmillan Publishers Ltd on behalf of Cancer Research UK: [JOURNAL NAME] (reference citation), copyright (year of publication)

7. Translations of 401 words up to a whole article require NPG approval. Please visit <http://www.macmillanmedicalcommunications.com> for more information. Translations of up to a 400 words do not require NPG approval. The translation should be credited as follows:

Translated by permission from Macmillan Publishers Ltd: [JOURNAL NAME] (reference citation), copyright (year of publication).

Note: For translation from the *British Journal of Cancer*, the following credit line applies.

Translated by permission from Macmillan Publishers Ltd on behalf of Cancer Research UK: [JOURNAL NAME] (reference citation), copyright (year of publication)

We are certain that all parties will benefit from this agreement and wish you the best in the use of this material. Thank you.

Special Terms:

v1.1

Questions? customercare@copyright.com or +1-855-239-3415 (toll free in the US) or +1-978-646-2777.

Abstract

Spinal cord injury (SCI) belongs to currently incurable disorders of the CNS. Primary damage and axonal disruption are followed by progressive cascade of secondary deleterious reactions. Although axonal regeneration is initiated, it is quickly repressed due to severe inflammation, lack of trophic support and inhibitory environment. Despite several researches, current treatments do not allow recovery in motor and sensory function. A balloon-compressive technique was used to produce SCI at thoracic Th8-9 level in adult rat. Secretomes of the lesion segment and adjacent segments 3 days after SCI were studied in order to determine the molecular environment around the injury. The first results were used to highlight regionalization of inflammatory and neurotrophic response between the rostral and caudal segments. These results were then complemented by spatial and temporal study of the SCI. The rostral and caudal segments of the injury had shown the ability to regenerate due to the presence of immune cells (microglia, macrophages, regulatory T cells) with an anti-inflammatory and neurotrophic phenotype. However, a time lag occurs between the two types of segments, with a caudal segment near the lesion expressing the inflammatory and apoptotic phenotype. This segment appears to be a potential target for future treatment. Indeed, this segment further shows the presence of lectin proteins (aggrecan, brevican, neurocan), protein RhoA activation path (which is a path apoptotic) but also the presence of antibodies colocalized with neurons. Therapeutic strategies have therefore focused on the inhibition of these factors by the use of anti-RhoA in addition to the use of biomaterials. Indeed, it seemed sensible to use biomaterials to initially fill the cavity and thus create a network facilitating axonal regrowth and use their ability to release factors then modulate inflammation and stimulate regeneration within an inhibitor environment. Secretome from mesenchymal stem cell has been embedded for their anti-inflammatory and neurotrophic properties. The first results *in vivo* injections of inhibitors only allowed to show a positive effect on neurite regrowth regarding inhibitor RhoA. The results with alginates such biomaterials are also very promising. These data established spatiotemporal evolution and indicate that we can initiate regenerative processes in the disconnected caudal spinal cord segments if trophic and inflammatory inhibitors factors are added and if a bridge is formed on either side of the lesion.

Keywords: spinal cord injury, proteomics, regeneration, microglia cells, immunoglobulins, neurotrophins, stem cells.

Résumé

Les lésions de la moelle épinière (SCI) appartiennent aux graves troubles du système nerveux central (SNC). Incurables, ils sont souvent accompagnés d'invalidité permanente. Les symptômes cliniques sont la conséquence des modifications dégénératives liées principalement à une inflammation aiguë qui se manifeste par la perte de cellules, la démyélinisation des neurones et la formation d'une cicatrice gliale qui perturbe les voies axonales ascendantes et descendantes. Il est nécessaire de trouver un traitement permettant de restaurer les fonctions motrices, la sensation et de soulager la douleur associée, en vue d'améliorer la qualité de vie des patients. Les lésions de la moelle épinière par compression sont réalisées par la technique de ballon compression au niveau thoracique Th8-9 chez le rat adulte. Une première étude a montré une régionalisation des protéines sécrétées 3 jours après lésion avec au niveau rostral un profil neuroprotecteur alors qu'au niveau caudal le profil est neuroinflammatoire et apoptotique. Une étude spatiale et temporelle a ensuite été menée pour compléter ces premiers résultats. De cette étude nous avons mis en évidence une symétrie entre les segments rostral et caudal par rapport à la lésion avec la présence à la fois de facteurs neurotrophiques mais également d'inhibiteur de la croissance neuritique au niveau caudal. Le segment caudal semblerait être une cible pour une future thérapie. Ce segment montre d'une part la présence de molécules inhibitrices telles que aggrecan, neurocan, brevican mais aussi la protéine RhoA. La présence d'immunoglobulines 3 jours après lésion colocalisées avec les neurones rentrera dans nos cibles potentielles de traitement. L'utilisation de biomatériaux injectés directement au niveau de la lésion permet d'une part de combler la cavité et d'autre part de servir de réseau pour une future croissance axonale. De plus les alginates ont la capacité de libérer des facteurs qui permettront de moduler l'inflammation et de promouvoir la repousse neuritique. Dans cet optique, le sécrétome de cellules souches mésenchymateuses a été étudié par spectrométrie de masse pour identifier les molécules à caractères anti-inflammatoire et neurotrophiques pour une future utilisation avec les alginates. Les premiers résultats concernant l'injection de l'inhibiteur de RhoA tendent à montrer une augmentation de la repousse neuritique et des vésicules synaptiques au sein de la lésion. L'ensemble de ces résultats ont clairement démontré une évolution spatiale et temporelle du profil moléculaire et ont défini le segment caudal comme étant une potentielle cible de traitement pour reconnecter les segments adjacents à la lésion et permettre une repousse neuritique et une reconnexion axonale.

Mots clés : lésion de la moelle épinière, protéomique, régénération, cellules microgliales, immunoglobulines, neurotrophines, cellules souches